

NOAA Technical Memorandum ERL ARL-190



---

VORTEX CHARACTERISTICS OF C5A/B, C141B AND C130E AIRCRAFT  
APPLICABLE TO ATC TERMINAL FLIGHT OPERATIONS  
TOWER FLY-BY DATA

Leo J. Garodz  
Kirk L. Clawson

Air Resources Laboratory  
Silver Spring, Maryland  
August 1991

---

**noaa**

NATIONAL OCEANIC AND  
ATMOSPHERIC ADMINISTRATION

Environmental Research  
Laboratories

NOAA Technical Memorandum ERL ARL-190

VORTEX CHARACTERISTICS OF C5A/B, C141B AND C130E AIRCRAFT  
APPLICABLE TO ATC TERMINAL FLIGHT OPERATIONS  
TOWER FLY-BY DATA

Leo J. Garodz  
Kirk L. Clawson

Field Research Division  
Idaho Falls, Idaho

Air Resources Laboratory  
Silver Spring, Maryland  
August 1991



**UNITED STATES  
DEPARTMENT OF COMMERCE**

**Robert A. Mosbacher  
Secretary**

NATIONAL OCEANIC AND  
ATMOSPHERIC ADMINISTRATION

John A. Knauss  
Under Secretary for Oceans  
and Atmosphere/Administrator

Environmental Research  
Laboratories

Joseph O. Fletcher  
Director

## NOTICE

Mention of a commercial company or product does not constitute an endorsement by NOAA/ERL. Use of information from this publication concerning proprietary products or the tests of such products for publicity or advertising purposes is not authorized.

---

For sale by the National Technical Information Service, 5285 Port Royal Road  
Springfield, VA 22161

## ACKNOWLEDGEMENTS

As with any project of this magnitude, there are many people who deserve recognition. We acknowledge the United States Air Force for their permission to use the data and Major David Johnson as the USAF test manager. We thank Mr. Rick Page for his support and patience during the entire analysis-report writing phases of this document. We thank Mrs. Dianne Hoover and Lynelle Simmons for their typographical efforts. Of course we recognize the many hours spent by NOAA personnel in the data collection effort; among those are: C. Ray Dickson, G. E. Start, G. Russ Ackermann, Randy Johnson, Jerry Sagendorf, Neil Hukari, and Joyce Silvester.

**This page intentionally left blank.**

# TABLE OF CONTENTS

	<u>Page</u>
NOTICE and DISCLAIMER .....	ii
ACKNOWLEDGEMENTS .....	iii
ABSTRACT .....	iv
LIST OF FIGURES .....	vii
LIST OF SYMBOLS .....	xi
INTRODUCTION .....	1
BACKGROUND .....	3
FAA Effort .....	3
NOAA/Air Force Effort .....	4
Previous Flight Tests .....	8
TEST AIRCRAFT AND EQUIPMENT .....	11
TEST SITE AND INSTRUMENTATION .....	13
TEST DESCRIPTION .....	21
RESULTS AND DISCUSSION .....	25
Graphical Presentations .....	25
Discussion .....	54
CONCLUSIONS .....	59
RECOMMENDATIONS .....	61
REFERENCES .....	63
APPENDICES	
A. Test Aircraft Specifications .....	65
B. Temperature and Wind Velocity Profiles at Start and Termination of Each Flight Test Period .....	69

	<u>Page</u>
C. Vortex Tangential Velocity Distributions . . . . .	83
1. C141B . . . . .	84
2. C130E . . . . .	137
3. C5A/B . . . . .	190

## LIST OF FIGURES

	<u>Page</u>
Figure 1. Three-view drawing of the Lockheed C5A/B Galaxy . . . . .	5
Figure 2. Three-view drawing of the Lockheed C141B Starlifter . . . . .	6
Figure 3. Three-view drawing of the Lockheed C130E Hercules . . . . .	7
Figure 4A. Schematic of the aircraft vortex measurement system using the tower fly-by technique . . . . .	8
Figure 4B. C141B with corvus oil smoke generators in operation as it passes upwind of the 200 ft. instrumentation tower in preparation for a vortex data acquisition run . . . . .	8
Figure 5A. Plan view of the Idaho National Engineering Laboratory (INEL) and vicinity located in southeastern Idaho . . . . .	14
Figure 5B. Plan view (expanded) of the INEL and vicinity . . . . .	15
Figure 5C. Plan view (close-up) of the NOAA aircraft vortex test site located on the INEL complex . . . . .	16
Figure 6A. NOAA aircraft vortex test site with instrumented 200 ft. tower . . . . .	17
Figure 6B. NOAA ground array vortex sensing system at the base of the 200 ft. test tower . . . . .	18
Figure 7. Schematic of the primary test tower illustrating the mounted instrumentation and the vortex flow visualization system . . . . .	19
Figure 8. Schematic of orientation and spacing of the secondary towers (ground array) employed to measure vortex ground-effect characteristics . . . . .	20
Figure 9. Vortex trajectory in space with the aircraft positioned in close proximity to the test tower . . . . .	21
Figure 10A. General shape of the sinusoidal instability of vortices (after Crow). The vortices are view from above, and the generating airplane lies beyond the upper left-hand corner of the figure . . . . .	22
Figure 10B. C130E airplane trailing vortex system showing extreme sinusoidal type instability . . . . .	24
Figure 11. C5A/B peak recorded vortex tangential velocity ( $V_\theta$ ) vs. age, all configurations, $\delta_F=15$ to 100% with leading edge slats always extended, upwind and downwind vortices . . . . .	25
Figure 12. C141B peak recorded vortex tangential velocity ( $V_\theta$ ) vs. age, all configurations, $\delta_F=11$ to 70% (one at 0%), upwind and downwind vortices . . . . .	26
Figure 13. C130E peak recorded vortex tangential velocity ( $V_\theta$ ) vs. age, all configurations, $\delta_F=0$ to 50%, upwind and downwind vortices . . . . .	26
Figure 14. C5A/B peak recorded vortex tangential velocity ( $V_\theta$ ) vs. ambient wind speed, all configurations, $\delta_F=15$ to 100%, upwind and downwind vortices, 0 to 30 seconds age . . . . .	28
Figure 15. C5A/B peak recorded vortex tangential velocity ( $V_\theta$ ) vs. ambient wind speed, all configurations, $\delta_F=15$ to 100%, upwind and downwind vortices, 30 to 60 seconds age . . . . .	28

	<u>Page</u>
Figure 16. C5A/B peak recorded vortex tangential velocity ( $V_\theta$ ) vs. ambient wind speed, all configurations, $\delta_F=15$ to 100%, upwind and downwind vortices, >60 seconds age	29
Figure 17. C141B peak recorded vortex tangential velocity ( $V_\theta$ ) vs. ambient wind speed, all configurations, $\delta_F=11$ to 70% (one at 0%), upwind and downwind vortices, 0 to 30 seconds age	29
Figure 18. C141B peak recorded vortex tangential velocity ( $V_\theta$ ) vs. ambient wind speed, all configurations, $\delta_F=11$ to 70% (one at 0%), upwind and downwind vortices, 30 to 60 seconds age	30
Figure 19. C141B peak recorded vortex tangential velocity ( $V_\theta$ ) vs. ambient wind speed, all configurations, $\delta_F=11$ to 70% (one at 0%), upwind and downwind vortices, >60 seconds age	30
Figure 20. C130E peak recorded vortex tangential velocity ( $V_\theta$ ) vs. ambient wind speed, all configurations, $\delta_F=0$ to 50%, upwind and downwind vortices, 0 to 30 seconds age	31
Figure 21. C130E peak recorded vortex tangential velocity ( $V_\theta$ ) vs. ambient wind speed, all configurations, $\delta_F=0$ to 50%, upwind and downwind vortices, 30 to 60 seconds age	31
Figure 22. C130E peak recorded vortex tangential velocity ( $V_\theta$ ) vs. ambient wind speed, all configurations, $\delta_F=0$ to 50%, upwind and downwind vortices, >60 seconds age	32
Figure 23. C5A/B peak recorded vortex tangential velocity ( $V_\theta$ ) vs. Richardson Number (Ri), all configurations, $\delta_F=15$ to 100%, upwind and downwind vortices, 0 to 30 seconds age	32
Figure 24. C5A/B peak recorded vortex tangential velocity ( $V_\theta$ ) vs. Richardson Number (Ri), all configurations, $\delta_F=15$ to 100%, upwind and downwind vortices, 30 to 60 seconds age	33
Figure 25. C5A/B peak recorded vortex tangential velocity ( $V_\theta$ ) vs. Richardson Number (Ri), all configurations, $\delta_F=15$ to 100%, upwind and downwind vortices, >60 seconds age	33
Figure 26. C141B peak recorded vortex tangential velocity ( $V_\theta$ ) vs. Richardson Number (Ri), all configurations, $\delta_F=11$ to 70% (one at 0%), upwind and downwind vortices, 0 to 30 seconds age	34
Figure 27. C141B peak recorded vortex tangential velocity ( $V_\theta$ ) vs. Richardson Number (Ri), all configurations, $\delta_F=11$ to 70% (one at 0%), upwind and downwind vortices, 30 to 60 seconds age	34
Figure 28. C141B peak recorded vortex tangential velocity ( $V_\theta$ ) vs. Richardson Number (Ri), all configurations, $\delta_F=11$ to 70% (one at 0%), upwind and downwind vortices, >60 seconds age	35
Figure 29. C130E peak recorded vortex tangential velocity ( $V_\theta$ ) vs. Richardson Number (Ri), all configurations, $\delta_F=0$ to 50%, upwind and downwind vortices, 0 to 30 seconds age	35

	<u>Page</u>
Figure 30. C130E peak recorded vortex tangential velocity ( $V_{\theta}$ ) vs. Richardson Number (Ri), all configurations, $\delta_F=0$ to 50%, upwind and downwind vortices, 30 to 60 seconds age	36
Figure 31. C130E peak recorded vortex tangential velocity ( $V_{\theta}$ ) vs. Richardson Number (Ri), all configurations, $\delta_F=0$ to 50%, upwind and downwind vortices, > 60 seconds age	36
Figure 32. C5A/B peak recorded vortex tangential velocity ( $V_{\theta}$ ) vs. vertical air temperature difference, all configurations, $\delta_F=15$ to 100%, upwind and downwind vortices, 0 to 30 seconds age	38
Figure 33. C5A/B peak recorded vortex tangential velocity ( $V_{\theta}$ ) vs. vertical air temperature difference, all configurations, $\delta_F=15$ to 100%, upwind and downwind vortices, 30 to 60 seconds age	38
Figure 34. C5A/B peak recorded vortex tangential velocity ( $V_{\theta}$ ) vs. vertical air temperature difference, all configurations, $\delta_F=15$ to 100%, upwind and downwind vortices, > 60 seconds age	39
Figure 35. C141B peak recorded vortex tangential velocity ( $V_{\theta}$ ) vs. vertical air temperature difference, all configurations, $\delta_F=11$ to 70% (one at 0%), upwind and downwind vortices, 0 to 30 seconds age	39
Figure 36. C141B peak recorded vortex tangential velocity ( $V_{\theta}$ ) vs. vertical air temperature difference, all configurations, $\delta_F=11$ to 70% (one at 0%), upwind and downwind vortices, 30 to 60 seconds age	40
Figure 37. C141B peak recorded vortex tangential velocity ( $V_{\theta}$ ) vs. vertical air temperature difference, all configurations, $\delta_F=11$ to 70% (one at 0%), upwind and downwind vortices, > 60 seconds age	40
Figure 38. C130E peak recorded vortex tangential velocity ( $V_{\theta}$ ) vs. vertical air temperature difference, all configurations, $\delta_F=0$ to 50%, upwind and downwind vortices, 0 to 30 seconds age	41
Figure 39. C130E peak recorded vortex tangential velocity ( $V_{\theta}$ ) vs. vertical air temperature difference, all configurations, $\delta_F=0$ to 50%, upwind and downwind vortices, 30 to 60 seconds age	41
Figure 40. C130E peak recorded vortex tangential velocity ( $V_{\theta}$ ) vs. vertical air temperature difference, all configurations, $\delta_F=0$ to 50%, upwind and downwind vortices, > 60 seconds age	42
Figure 41. C5A/B vortex descent velocity ( $\dot{z}_v$ ) vs. vortex/tower intercept height, all configurations, $\delta_F=80$ to 100%, upwind and downwind vortices. The vertical dashed line represents a calculated $h_{vge}$ of 87.5 ft. while the horizontal dashed line represents an initial calculated $\dot{z}_v$ of 7.0 f/s	42
Figure 42. C141B vortex descent velocity ( $\dot{z}_v$ ) vs. vortex/tower intercept height, all configurations, $\delta_F=80$ to 100%, upwind and downwind vortices. The vertical dashed line represents a calculated $h_{vge}$ of 62.8 ft. while the horizontal dashed line represents an initial calculated $\dot{z}_v$ of 4.9 f/s	43

	<u>Page</u>
Figure 43. C130E vortex descent velocity ( $\dot{z}_v$ ) vs. vortex/tower intercept height, all configurations, $\delta_F=80$ to $100\%$ , upwind and downwind vortices. The vertical dashed line represents a calculated $h_{vge}$ of 52.1 ft. while the horizontal dashed line represents an initial calculated $\dot{z}_v$ of 4.8 fps . . . . .	43
Figure 44. Vortex persistence as a function of ambient wind speed and height above the ground . . . . .	44
Figure 45A. C5A/B upwind (top) and downwind (bottom) vortex tangential velocity profile at maximum intensity from Test 13, Run 3, ambient wind speed= $31.1$ fps, $\delta_F=100\%$ , IAS= $150$ knots, GW= $689$ k lb. Ages, radii, and velocities of the vortex cores are 12 and 8 sec., 2.6 and 1.4 ft., and 69 and 79 fps, respectively . . . . .	45
Figure 45B. C5A/B upwind (top) and downwind (bottom) vortex tangential velocity profile at maximum intensity from Test 13, Run 5, ambient wind speed= $24.5$ fps, $\delta_F=15\%$ , IAS= $180$ knots, GW= $682$ k lb. Ages, radii, and velocities of the vortex cores are 14 and 7 sec., 0.7 and 0.6 ft., and 218 and 259 fps, respectively. Arrows and values above data points indicate an off-scale value . . . . .	46
Figure 45C. C5A/B upwind (top) and downwind (bottom) vortex tangential velocity profile at maximum intensity from Test 13, Run 8, ambient wind speed= $24.7$ fps, $\delta_F=15\%$ , IAS= $175$ knots, GW= $670$ k lb. Ages, radii, and velocities of the vortex cores are 23 and 13 sec., 0.2 (measured) and 0.1 ft. (estimated), and 208 and 268 fps, respectively. Arrows and values above data points indicate an off-scale value . . . . .	47
Figure 46A. C141B upwind (top) and downwind (bottom) vortex tangential velocity profile at maximum intensity from Test 2, Run 4, ambient wind speed= $11.7$ fps, $\delta_F=39\%$ , IAS= $150$ knots, GW= $225$ k lb. Ages, radii, and velocities of the vortex cores are 38 and 19 sec., 2.7 and 0.7 ft., and 82 and 63 fps, respectively . . . . .	48
Figure 46B. C141B upwind (top) and downwind (bottom) vortex tangential velocity profile at maximum intensity from Test 2, Run 5, ambient wind speed= $12.7$ fps, $\delta_F=39\%$ , IAS= $150$ knots, GW= $223$ k lb. Ages, radii, and velocities of the vortex cores are 28 and 14 sec., 1.1 (measured) and 0.7 ft. (estimated), and 57 and 85 fps, respectively . . . . .	49
Figure 46C. C141B upwind (top) and downwind (bottom) vortex tangential velocity profile at maximum intensity from Test 4, Run 7, ambient wind speed= $5.8$ fps, $\delta_F=11\%$ , IAS= $180$ knots, GW= $257$ k lb. Ages, radii, and velocities of the vortex cores are 39 and 17 sec., 1.0 (estimated) and 0.7 ft. (measured), and 72 and 142 fps, respectively . . . . .	50
Figure 47A. C130E upwind (top) and downwind (bottom) vortex tangential velocity profile at maximum intensity from Test 6, Run 2, ambient wind speed= $6.3$ fps, $\delta_F=27\%$ , IAS= $130$ knots, GW= $145$ k lb. Ages, radii, and velocities of the vortex cores are 35 and 20 sec., 1.0 and 0.4 ft., and 92 and 84 fps, respectively . . . . .	51
Figure 47B. C130E upwind (top) and downwind (bottom) vortex tangential velocity profile at maximum intensity from Test 6, Run 3, ambient wind speed= $6.3$ fps, $\delta_F=27\%$ , IAS= $130$ knots, GW= $144$ k lb. Ages, radii, and velocities of the vortex cores are 25 and 17 sec., 1.0 (measured) and 0.9 ft. (estimated), and 65 and 57 fps, respectively . . . . .	52
Figure 47C. C130E upwind (top) and downwind (bottom) vortex tangential velocity profile at maximum intensity from Test 6, Run 4, ambient wind speed= $6.2$ fps, $\delta_F=0\%$ , IAS= $180$ knots, GW= $143$ k lb. Ages, radii, and velocities of the vortex cores are 35 and 19 sec., 0.5 and 0.2 ft., and 68 and 97 fps, respectively . . . . .	53

## LIST OF SYMBOLS

- AR = wing aspect ratio, i.e.,  $\frac{b^2}{S}$  (unitless)
- b = aircraft wingspan (feet)
- b' = separation of vortex pair, i.e.,  $\frac{\pi b}{4}$  (feet)
- $C_L$  = airplane lift coefficient, i.e.,  $\frac{L}{\frac{1}{2}\rho V^2 S} = \frac{L}{qS}$  (unitless)
- h = height above ground level (AGL, feet)
- IAS = indicated airspeed (knots)
- c = wing mean aerodynamic chord (feet)
- d = distance (feet)
- g = acceleration due to gravity (feet/second<sup>2</sup> or meters/second<sup>2</sup>)
- L = lift, i.e., nW (pounds)
- n = normal load factor (unitless)
- p = port, in relation to airplane's longitudinal axis
- q = dynamic pressure, i.e.,  $\frac{1}{2}\rho V^2$  (pounds/feet<sup>2</sup>)
- r = distance from vortex center (feet)
- $r_c$  = vortex core radius where  $V_\theta$  is a maximum (feet)
- Ri = Richardson Number (unitless)
- S = wing area (feet<sup>2</sup>)

- s = starboard, in relation to airplane's longitudinal axis
- t = vortex age (seconds)
- TAS = true airspeed (knots)
- T = ambient air temperature, ( $^{\circ}\text{C}$ ,  $^{\circ}\text{F}$ , or  $^{\circ}\text{K}$ , as specified)
- u = ambient wind speed (knots or miles/hour or feet/second, as applicable)
- V = true airspeed (knots or feet/second)
- $\hat{V}_{\theta}$  = absolute recorded vortex tangential velocity (feet/second)
- $V_{\theta}$  = vortex tangential velocity (feet/second)
- W = gross weight of aircraft (pounds)
- y = lateral distance from aircraft flight path or centerline (feet)
- $\dot{y}$  = lateral velocity, (feet/second)
- z = height above ground when discussing earth's boundary layer (feet)
- $\dot{z}$  = downward vertical velocity (feet/second)
- Z = vertical distance measured downward from aircraft flight path (feet)
- $\delta_{\text{F}}$  = flap deflection (% or degrees)
- $\Gamma$  = midspan vortex circulation, i.e.,  $\frac{4}{\pi} \frac{nW}{\rho V b}$  (feet<sup>2</sup>/second)
- $\rho$  = air density (slugs/foot<sup>3</sup> or grams/meter<sup>3</sup>)

Subscripts:

- ge = ground-effect
- ind = induced
- max = maximum
- o = initial conditions
- v = vortex
- w = wind
- a/c = aircraft

## ABSTRACT

During the spring of 1987, the National Oceanic and Atmospheric Administration (NOAA) conducted a full-scale flight test program to investigate the vortex wake characteristics of the 3 primary U. S. Air Force (USAF) Military Airlift Command (MAC) jet transport aircraft, namely, the Lockheed C5A/B Galaxy, the C141B Starlifter, and the C130E Hercules. The test program required vortex data at low airspeeds and low altitudes to meet certain operational considerations. The tower fly-by technique was employed for vortex data acquisition purposes. The study was successful in that the objectives of the study were completely fulfilled.

The Federal Aviation Administration (FAA) subsequently commissioned NOAA to reexamine the data with the objective of extending the existing knowledge of vortex behavior in terminal area flight operations. The FAA was particularly interested in the application of the data to Air Traffic Control (ATC) separation standards. The data had not previously been analyzed with this goal in mind. This report describes the results of that effort.

Of significance in the reexamination of the USAF data was the length of vortex persistence even under somewhat turbulent or unstable atmospheric conditions. Although no vortex ages older than 2 minutes were observed in the anemometer data, visual observations of vortex-entrained smoke indicated that C5A/B vortices persisted for as long as 3 minutes. Correlation of the Richardson Number ( $Ri$ ) with vortex persistence indicated the difficulty of using this atmospheric turbulence index as an indicator of vortex decay. The effect of the high wing configuration of all three aircraft and the T-tail configuration of two of the aircraft on trailing vortex system characteristics is also discussed.

**This page intentionally left blank.**

## INTRODUCTION

The primary purpose of this particular effort is to examine newly acquired military transport aircraft vortex wake data for application to existing Air Traffic Control (ATC) terminal area flight operations. The effort also includes examination of the data for application to simultaneous parallel runway operations. The full-scale vortex flight test data were obtained by the National Oceanic and Atmospheric Administration (NOAA) Air Resources Laboratory Field Research Division using the tower fly-by technique (Clawson, 1988). The aircraft studied were U. S. Air Force (USAF) large jet transports from the Military Airlift Command (MAC), namely, the Lockheed C5A/B Galaxy, the C141B Starlifter, and the C130E Hercules. The data were collected and analyzed for military purposes. However, the type of data that was collected permitted further analysis, including vortex persistence and transport at low altitudes.

A secondary purpose was to attempt to determine a correlation parameter(s), other than ambient wind velocity, for vortex persistence (age). The plan was to correlate vortex persistence with atmospheric conditions existing during the time the flight tests were conducted. This was, of course, dependent on appropriate supporting flight test data.

This report is structured to meet the primary and secondary objectives cited above. Some effort has also been devoted, where data permitted, to vortex modeling or existing model validation. This validation includes 1) vortex tangential velocity distribution, 2) vortex ground-effect onset, and 3) aircraft model and configuration effects on vortex characteristics.

**This page intentionally left blank.**

## BACKGROUND

### FAA EFFORT

The Federal Aviation Administration (FAA) currently has underway a high priority aircraft vortex wake program. The primary objective of the program is to reduce or minimize the effects of the aircraft trailing vortex hazard on the flow of air traffic in terminal area flight operations. The program includes the study of both arrivals and departures. The desired outcome of the program is to safely increase airport capacity.

The current program is separate and distinct from an earlier vortex wake program initiated and pursued by the FAA in the early 1970's. That earlier program was motivated by the planned introduction of the so-called jumbo or wide-bodied jet transport aircraft (i.e., Lockheed C5A Galaxy and Boeing 747-100) into the National Airspace System (NAS) in early 1970. Considerable concern was expressed at that time by aviation oriented organizations regarding the vortex wake hazard of these and other large jet transport airplanes, e.g., B707-300 and DC-8-63 series airplanes with a maximum permissible take-off gross weight of greater than 300,000 pounds. It subsequently became imperative to investigate the vortex wake characteristics of these relatively large and heavy aircraft and their potential or actual effects on other aircraft encountering these trailing vortices. The flight tests and analyses were performed by various government agencies and private industry. The results of the tests were used to establish the present set of ATC aircraft separation standards. The many flight tests and associated investigations are well documented and are covered in numerous reports, e.g., Garodz and Miller (1975), Garodz et. al. (1976), and Kurkowski et. al. (1976). These reports will not, with rare exceptions, be discussed in detail herein but are cited mainly for the reader's convenience. This early wake vortex program, for all practical purposes, was terminated in late 1979.

The presently established ATC aircraft separation criteria based on the vortex hazard have proven to be safe, but they are not necessarily very efficient with regard to air traffic flow rates. This suggests the necessity of re-evaluating the separation criteria when new, reliable, and applicable vortex flight test data become available. This is precisely the impetus behind this report. Very little, if any, valid full-scale flight test data have been acquired on the far downstream vortex wake characteristics of the C5A/B, C141B and C130E series aircraft. This is the case for all jet transport aircraft with a high-wing (a design characteristic of all three of these airplanes). Two of the three airplanes are T-tail aircraft. Wing/T-tail vortex interaction is another area of study of which very little is known.

With this in mind, the FAA requested NOAA, via an Interagency Agreement (IA), to re-examine the recently acquired vortex data on the C5A/B, C141B, AND C130E. The data had been collected and analyzed by NOAA to support military purposes, which were quite different from the goals of the FAA vortex wake program. Considerable time and money had been

expended to conduct the full-scale flight tests for the USAF to meet their objectives. However, the data were collected in such a manner as to permit a reanalysis which could be readily used to fill certain FAA knowledge gaps in aircraft vortex wake characteristics. It became apparent that a re-examination of the data in light of the FAA's vortex program objectives would be very cost-effective.

## **NOAA/AIR FORCE EFFORT**

During the spring of 1987, the USAF entered into an IA with NOAA to conduct full-scale flight tests to acquire data on the vortex wake characteristics of its major MAC jet transport aircraft. The flight tests were required to determine the potential effects of trailing vortices on air drop operations conducted during formation flight at low altitudes. The specific aircraft included in the study were the C5A/B, C141B, and C130E. Three-view drawings of these aircraft are shown in Figs. 1, 2 and 3. Additional pertinent aircraft specifications are given in Appendix A.

The flight tests were conducted at the NOAA flight test facility located at the Idaho National Engineering Laboratory (INEL) complex near Idaho Falls ID. The test site selection was based on: 1) the requirement to conduct flight tests at very low altitudes, nominally below 300 feet above ground level (AGL), 2) the capability of the NOAA facility to acquire reliable data on trailing vortices using a specially configured and instrumented 200 foot tall meteorological tower, and 3) the requirement to use the well-recognized tower fly-by technique previously developed by the FAA/NOAA for reliable vortex measurements. Figure 4A illustrates a schematic depiction of the tower fly-by technique. Figure 4B is a photograph of the C141B with active wingtip smoke generators on a tower fly-by approach. One hundred sixty-four tower fly-bys were flown, the majority of which were performed with the airplanes at or close to the maximum permissible take-off gross weight. This was achieved by loading a huge amount of ballast into the cargo bays of the test airplanes. The aircraft take-off gross weights during the flight tests were approximately 700, 261, and 148 thousand pounds for the C5A/B, the C141B, and the C130E, respectively.

The immediate USAF requirement was to acquire raw data on vortex size, intensity (tangential velocities), and persistence. Short, intermediate, and long time-history data were acquired on the vortex wake characteristics of the test aircraft, both in and out of ground-effect, as a function of aircraft configuration, performance, and existing atmospheric conditions (primarily wind speed). The test flights were conducted as planned and were considered a success by both NOAA and the USAF.

Following the completion of these flight tests, it was the intent of FAA to have NOAA further process and analyze the USAF data. The FAA desired to depict the aircraft vortex intensity, movement, persistence, and decay mode, as a function of the ambient atmospheric characteristics in which the vortices were generated and transported. It was felt at the time, that a re-examination of the flight test data could provide an important input into the FAA's Vortex Wake Program elements. One of these elements calls for the correlation (if possible) of vortex

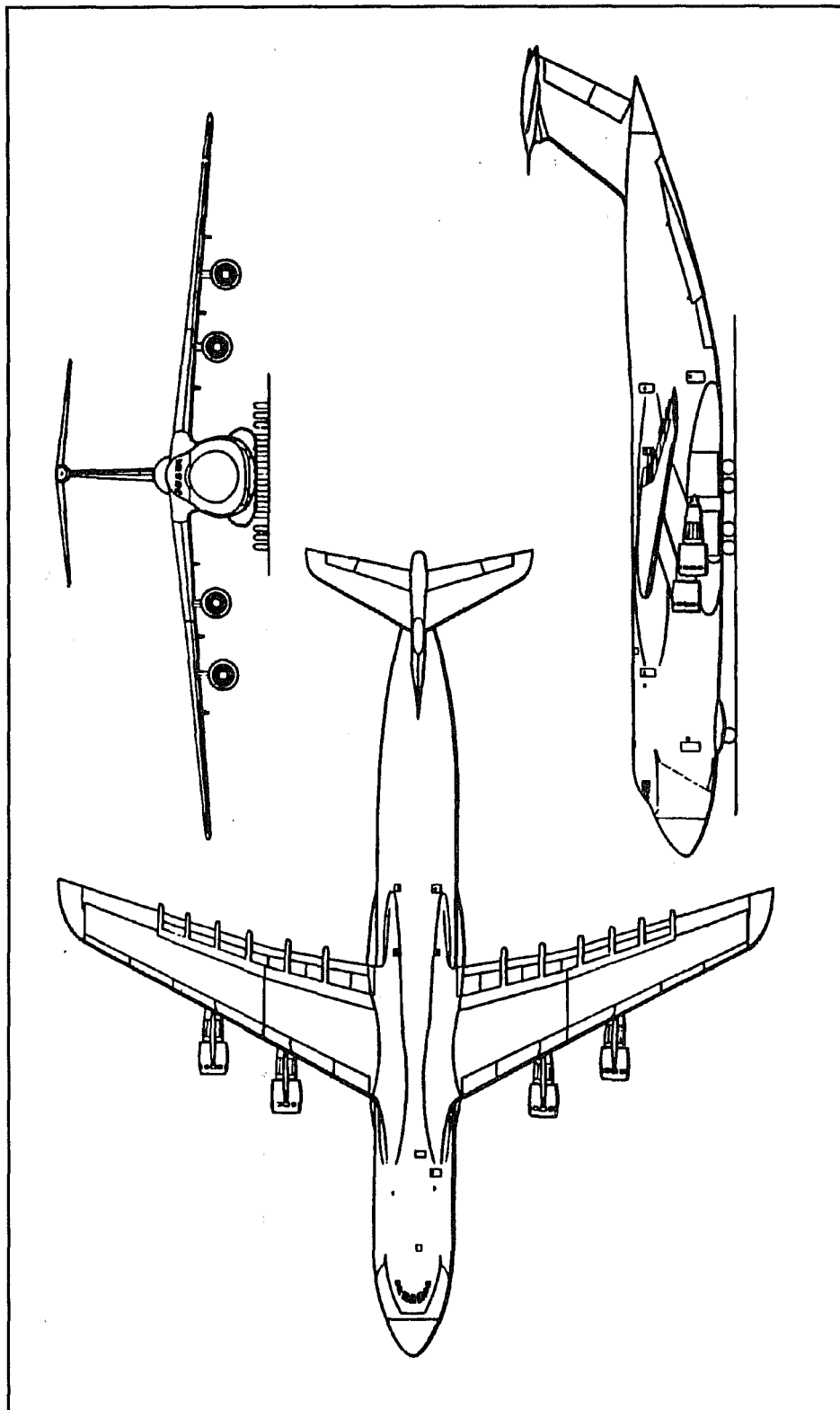


**Figure 1.** Three-view drawing of the Lockheed C5A/B Galaxy.

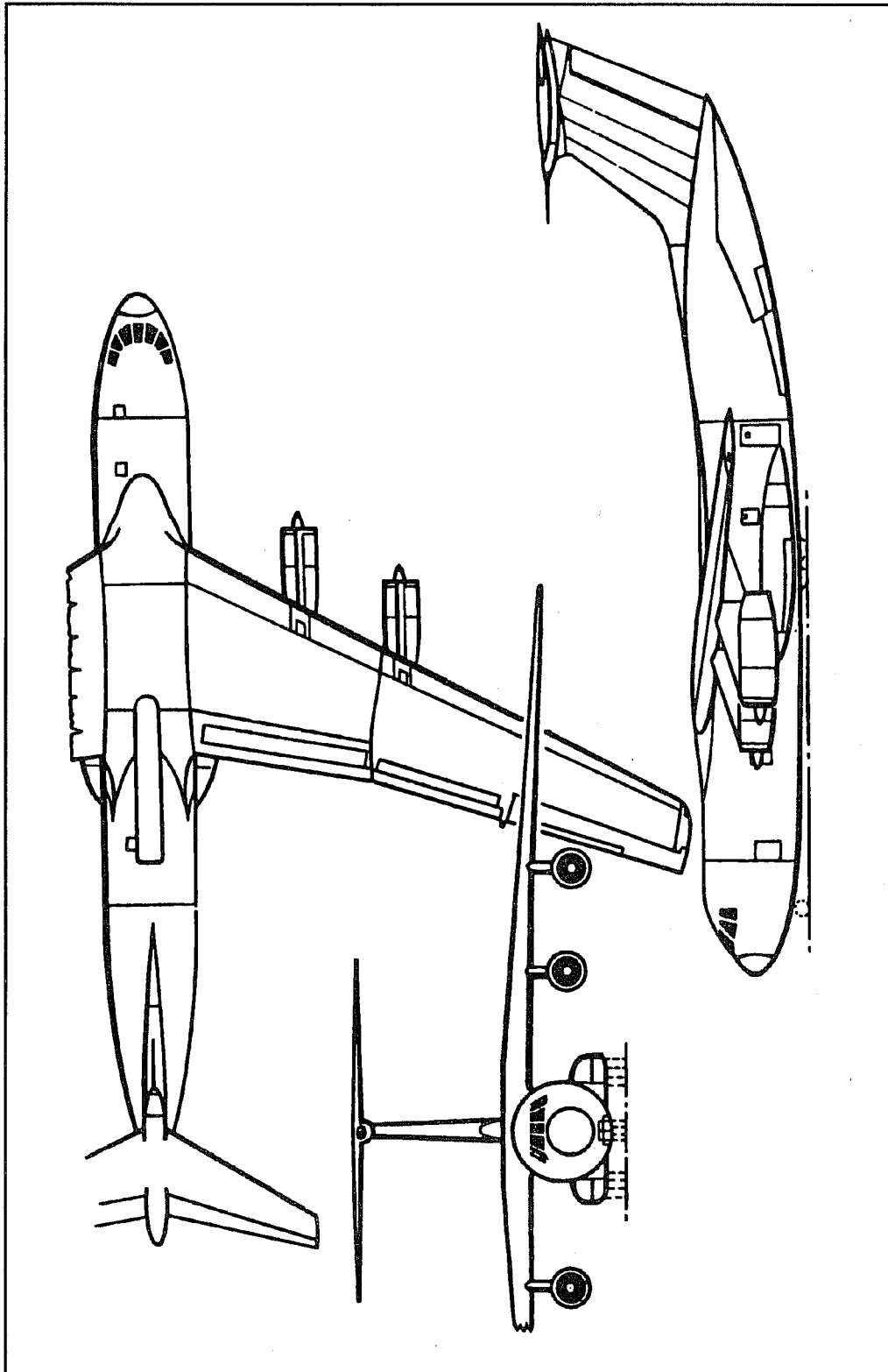
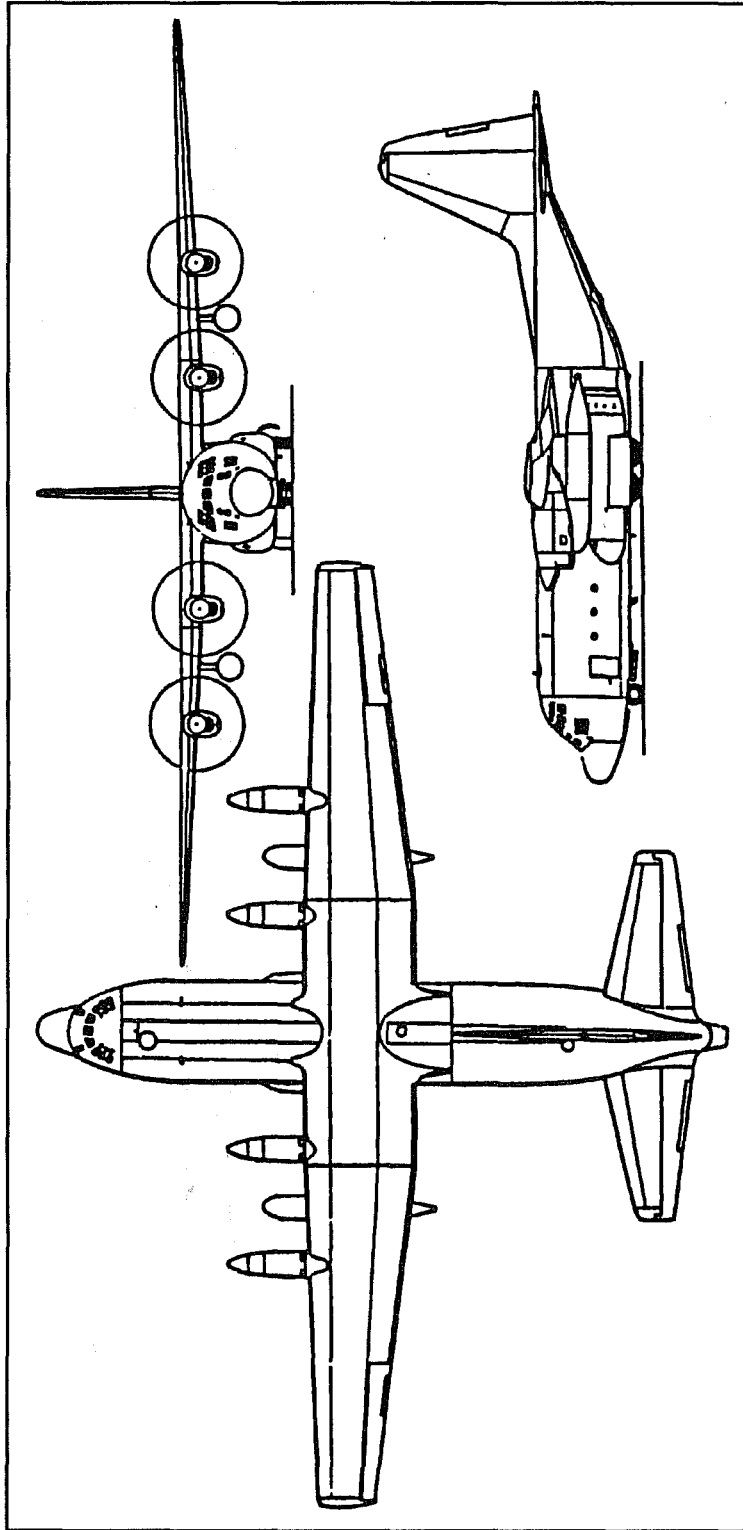


Figure 2. Three-view drawing of the Lockheed C141B Starlifter.



**Figure 3.** Three-view drawing of the Lockheed C130E Hercules.

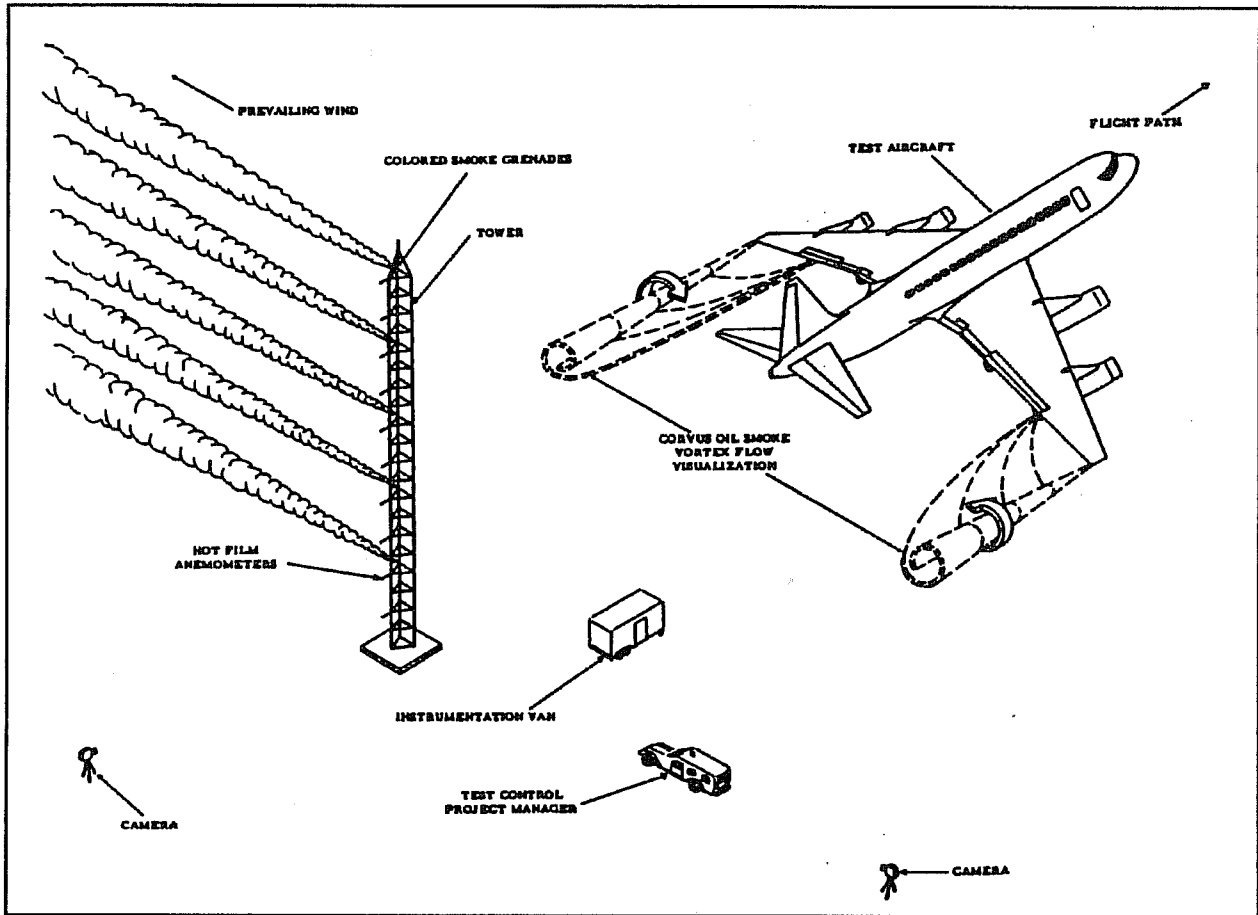
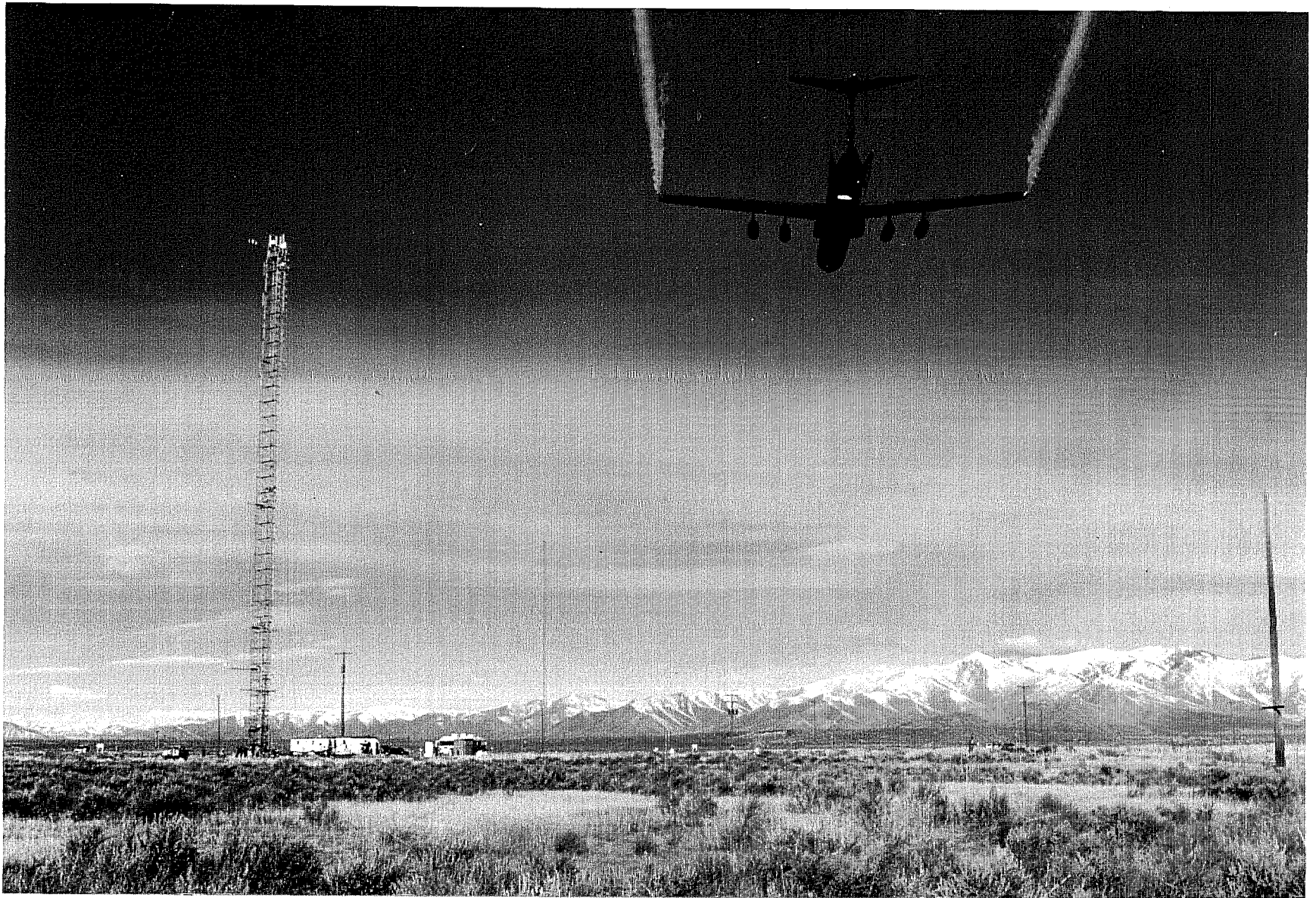


Figure 4A. Schematic of the aircraft vortex measurement system using the tower fly-by technique.

persistence and movement, both in and out of ground-effect, with some reliable index of the atmospheric characteristics within the earth's planetary boundary layer in which the trailing vortices are being transported.

## PREVIOUS FLIGHT TESTS

During the summer of 1970, the FAA initiated a high priority project at its Technical Center (then called NAFEC) to investigate the long time-history vortex wake characteristics of large jet transport aircraft at low altitudes using the tower fly-by technique. The objective of the flight tests was to gather reliable data on vortex persistence and movement close to the ground and within ground-effect. The goal was to establish ATC aircraft separation standards for simultaneous parallel runway operations based on the vortex hazard. Specifically, the FAA desired to establish a minimum lateral separation distance between parallel runways beyond which the ATC controllers could perform arrivals and departures as independent runway operations. If runways could be separated further than the minimum distance, the controllers



6

**Figure 4B.** C141B with corvus oil smoke generators in operation as it passes upwind of the 200 ft. instrumentation tower in preparation for a vortex data acquisition run.

would not need to be concerned about vortices from aircraft operating on one runway drifting laterally on to an adjacent runway or into its respective final approach corridor. Conversely, within this established minimum lateral separation distance limit between parallel runways, the ATC would be required to control departures and arrivals as a single runway operation.

The NAFEC data acquisition tower was specially instrumented by the FAA and NOAA with: 1) hot-film anemometers for vortex flow measurements, 2) meteorological instrumentation for atmospheric characterizations, and 3) colored smoke generators for further vortex characterization as well as data correlation. The data from these flight tests and data from concurrent flight tests performed by others formed the basis for the FAA minimum parallel runway separation distance (for vortex considerations). A separation of 2500 feet was ultimately established which is still in use today.

Garodz (1970) also used the flight test data in an attempt to correlate various atmospheric turbulence parameters with vortex persistence, movement, and the decay mode. The two indices considered were the Richardson Number (Ri) and a Power Spectral Density (PSD) analysis of atmospheric turbulence. However, due to insufficient meteorological instrumentation and the resulting lack of data covering the range and depth of ambient atmospheric conditions, consideration of these two indices had to be abandoned. As a result, surface wind velocity (approximately 100 feet above ground level) was used as the primary indicator of vortex persistence along with temperature gradients measured along the vertical span of the tower. Temperature gradients were very useful for the determination of inversion type conditions close to the ground during flight testing, but were not of sufficient quality for valid Ri determinations.

## TEST AIRCRAFT AND EQUIPMENT

The Lockheed C5A/B, C141B, and C130E were the specific aircraft used for the flight tests (Figures 1, 2 and 3). The C5A/B is simply a C5A with minor wing geometry modifications. All 3 aircraft were provided by the USAF Military Airlift Command and flown by USAF crews. The only special equipment required for the flight tests was ballast and wingtip smoke generators. The ballast was loaded in the cargo bay to achieve the maximum permissible take off gross weight. This resulted in higher wing lift distributions and vortex intensities. The smoke generators provided vortex flow visualization and were installed only on the C130E and the C141B. It was not possible to install the system on the C5A/B airplane for tactical aircraft operational reasons. The USAF objectives were realized without the use of the system on the C5A/B because of an alternate vortex flow visualization system installed on the data acquisition tower. Use of the airplane mounted system and/or the tower based system permitted precise vortex movement calculations and flight path control of the test airplane which insured vortex passage through the instrumented tower.

The vortex marking system used on the C130E and the C141B aircraft consisted of two self-contained smoke generator pods manufactured specifically for these type of flight tests by Frank Sanders Aircraft of Chino, CA. This type of smoke generator has been used successfully by the FAA and NOAA in vortex studies involving the Boeing B727 and B747 aircraft and the Sikorsky S-76 helicopter. The smoke is generated by vaporizing CORVUS smoke oil in a heated chamber inside the pod. The smoke is conspicuous, persistent, non-toxic, non-corrosive, and neutrally buoyant when dispersed within the atmosphere. The smoke generators are good for ten minutes total continuous operation. However, they are usually operated intermittently to extend on-site flight test time.

The smoke generating pods were mounted close to the wing tip on the underside of the wing on each airplane (Fig. 4B). Results from previous vortex flight test investigations conducted with other airplanes have shown that, when the wing landing flaps are extended (deflected), multiple vortices are generated by the wing. The wing flap vortex can, under certain conditions, become the predominant vortex with the wing tip vortex becoming a pseudo satellite vortex around the flap vortex. Accordingly, it would have been most useful to have mounted an additional smoke generator on each wing at the outboard end of the deflected landing flaps. This would have been useful not only for vortex flow field visualization and characterization but for flap vortex/wing-tip vortex interaction observations during and after the roll-up process. However, lack of these additional smoke generating pods did not diminish the quality nor the quantity of acquired vortex data to any significant extent.

Pilot "knee-pad" data was recorded at the time the aircraft was abreast of the tower. These data included the following: 1) time the aircraft was abreast of the tower, 2) aircraft configuration, 3) gross weight, 4) indicated airspeed, 5) radar altitude above the ground, 6)

pressure altitude, 7) magnetic track, 8) estimated lateral distance from tower (actual distance was obtained from ground personnel), 9) engine performance, and 10) flight test altitude atmospheric turbulence according to subjective pilot opinion (none, light, moderate, or severe). These data were also used for data correlation and analysis.

## TEST SITE AND INSTRUMENTATION

The test site and associated instrumentation have been more than adequately described by Clawson (1988). For the benefit of the reader who does not have access to that report, the significant highlights are covered here.

The test site is located on the Idaho National Engineering (INEL) complex, which is approximately 45 miles west of Idaho Falls, ID. The INEL is on the western edge of the Eastern Snake River Plain as shown in Fig. 5A. Figures 5B and 5C present expanded plan views of the INEL complex and the NOAA test site, respectively. Major landmarks used by the test flight pilots for flight path orientation are the Big Southern Butte, Middle Butte, and East Butte. The floor of the Snake River Plain is a broad, rolling land mass with an average elevation of 5000 feet above mean sea level (MSL). The Bitterroot and Centennial Mountain Ranges, which border the INEL complex on the west (approximately 10-12 miles away) rise to approximately 11,000 feet MSL.

At the test site proper, the terrain is fairly level with no significant vegetation (height-wise). In addition, there are no other protuberances or manmade structures which would cause generation of undesirable atmospheric turbulence in the vicinity of the flight test area (Fig. 6A). The test site is a high security area and is free of transient aircraft. The site is also fairly unpopulated, particularly with regard to the projected surface area of the aircraft's flight path over the ground. This helps to minimize any unwanted outside test interference.

The 200 foot tall meteorological tower was the focal point for the flight tests and data acquisition systems including meteorological sensors, data recording and processing systems, flow visualization system (ground-based), video and still photography, and ground-to-ground and ground-to-air communication networks. The base of the test tower is at 4900 feet MSL. A ground-based vortex sensing system/array of towers, was located at the base of the 200 foot tower and extended outward radially as shown in Fig. 6B.

The tower data acquisition and vortex flow visualization systems consisted of hot-film anemometers, conventional meteorological sensors, and colored smoke generators. The complete system is shown in Fig. 7 and each component is described below.

Fifty hot-film anemometers were distributed vertically on the 200-foot tower. They were spaced at three (3) foot intervals vertically from the tower top down to a height of 101 feet AGL. Below this level the vertical spacing was increased to six (6) feet. The closer sensor spacing in the upper half of the test tower permitted more precise measurements of the vortices. This was the portion of the tower through which a higher proportion of the out of ground-effect vortex cores would pass. This out of ground-effect vortex was the type of vortex most desired by the USAF.

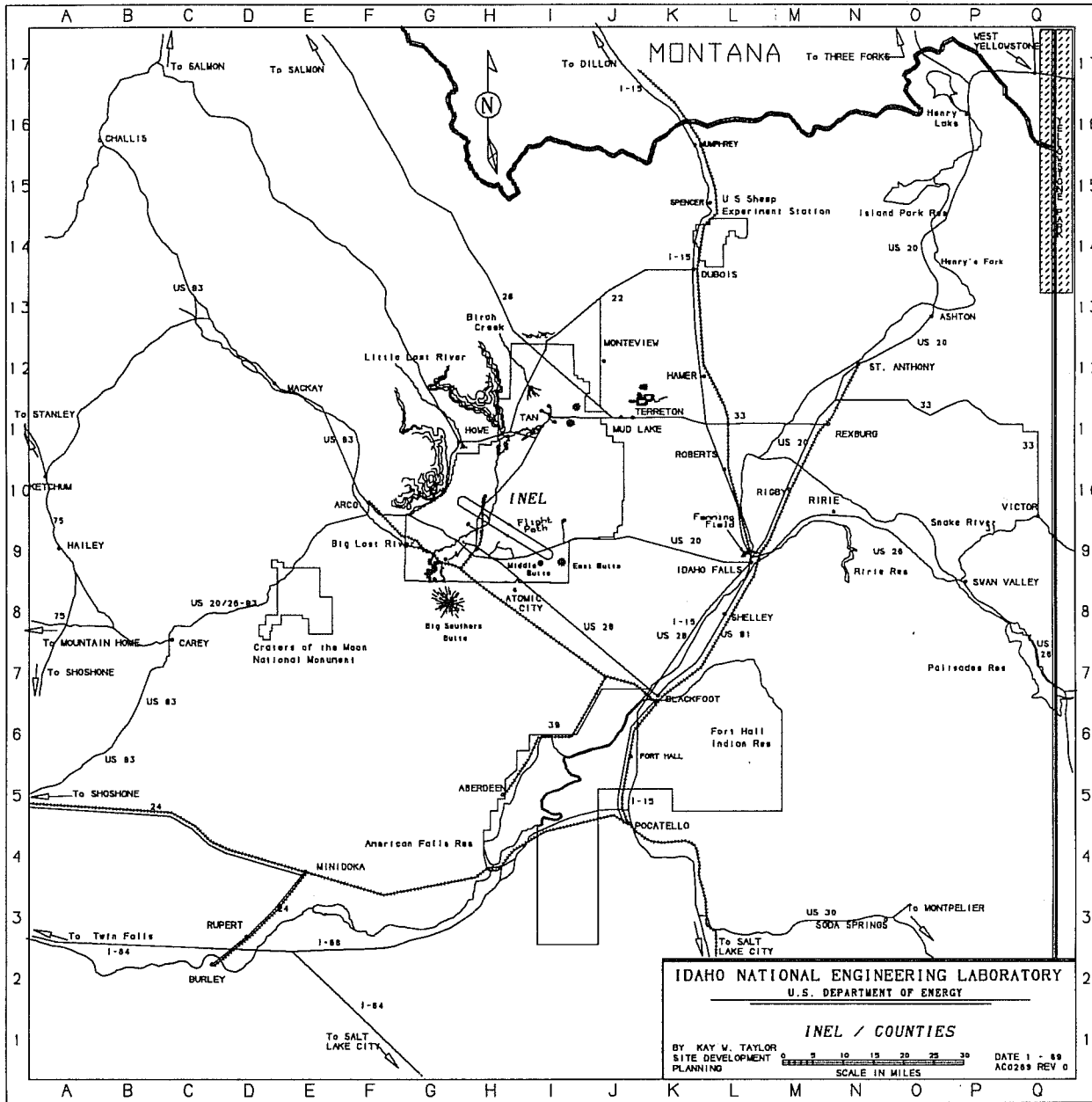


**Figure 5A.** Plan view of the Idaho National Engineering Laboratory (INEL) and vicinity located in southeastern Idaho.

The altitude at which the vortex begins to be involved in ground-effect (according to McGowan, 1971) can initially be calculated assuming an elliptical lift distribution over the wing, i.e.,

$$\Gamma = \frac{4}{\pi} \frac{nW}{\rho Vb} \quad (1)$$

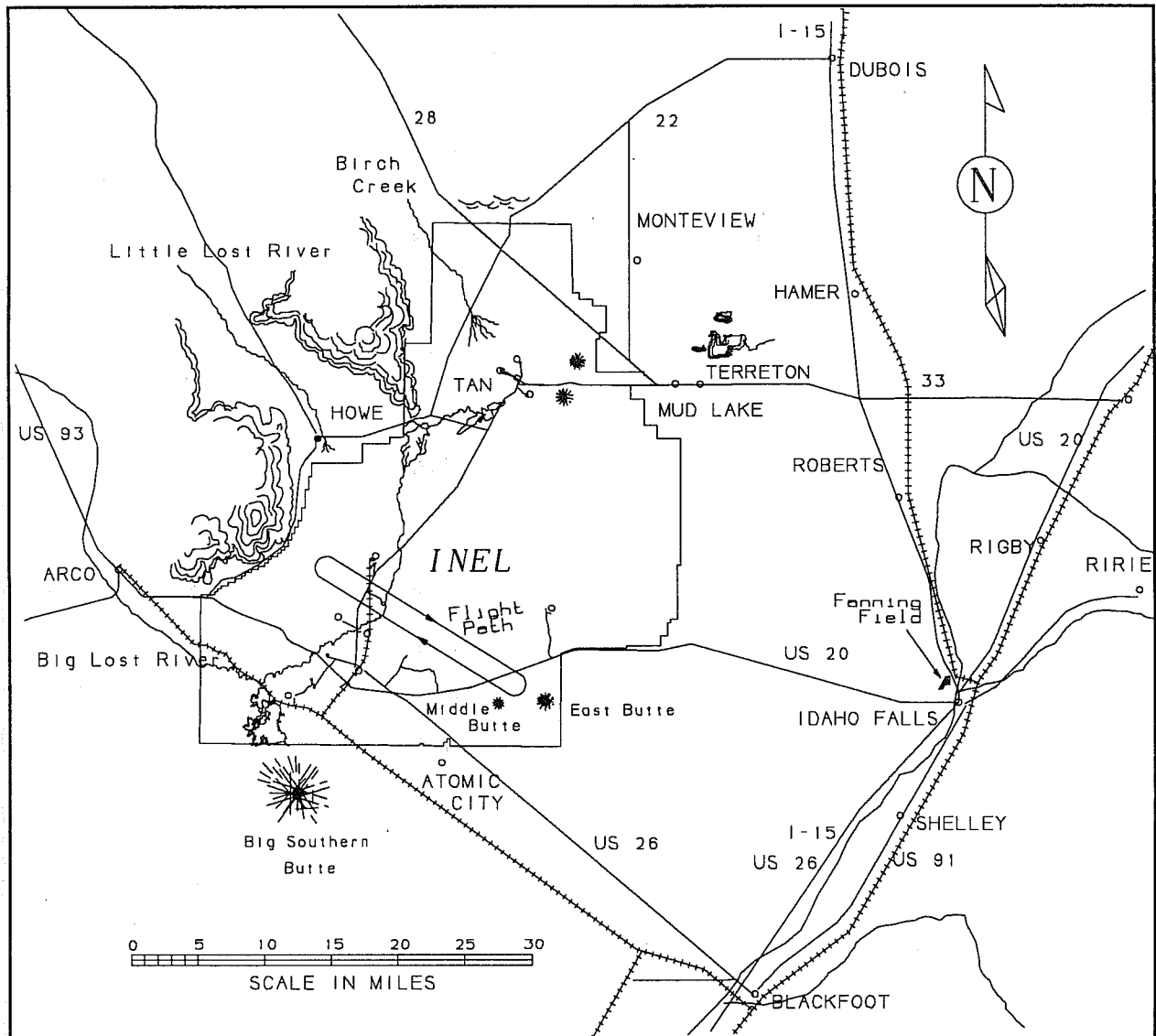
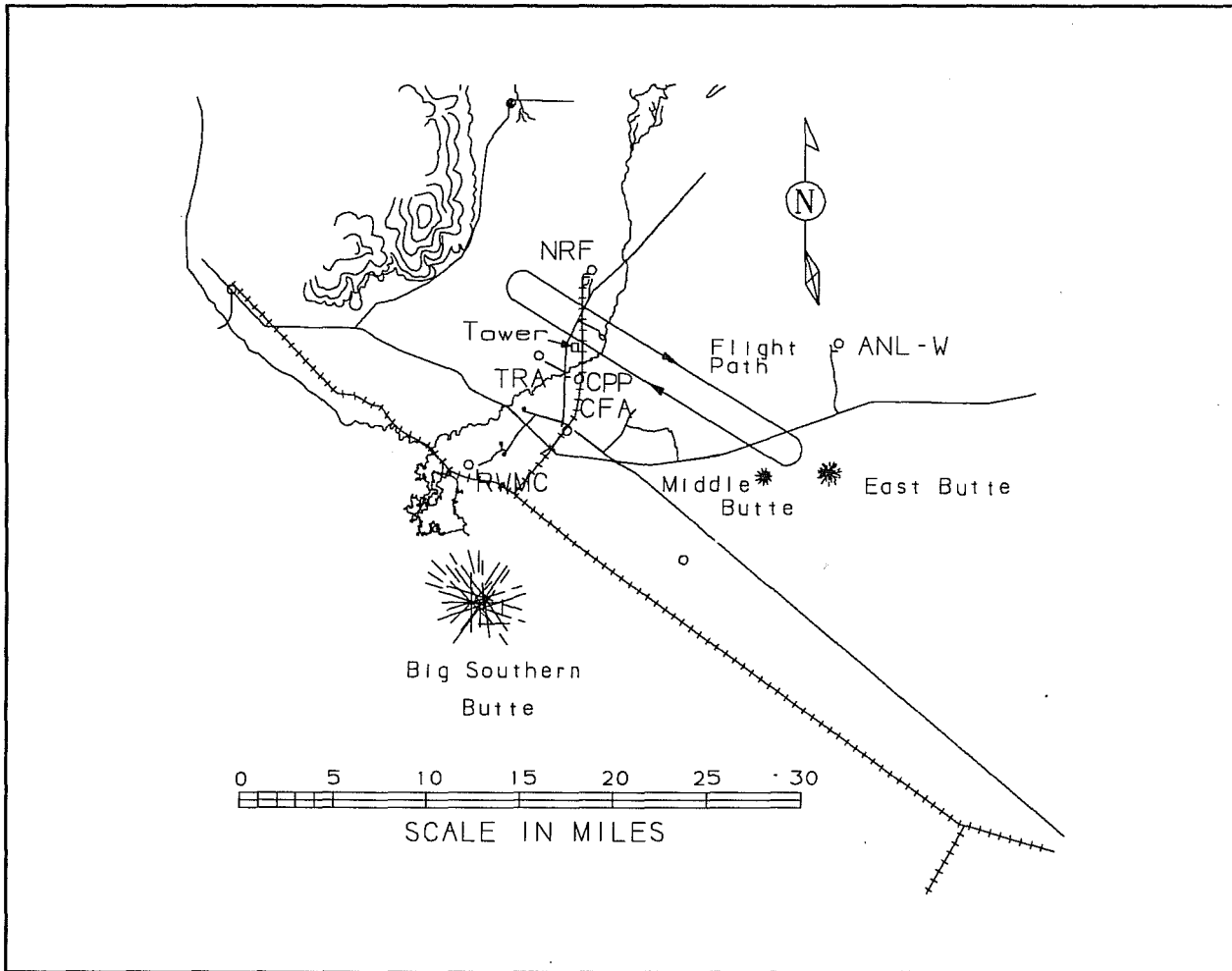


Figure 5B. Plan view (expanded) of the INEL and vicinity.

where  $\Gamma$  is the midspan vortex circulation,  $n$  is the normal load factor,  $W$  is the aircraft gross weight,  $\rho$  is air density,  $V$  is the aircraft true airspeed, and  $b$  is the aircraft wingspan. Ground-effect in relation to vortex movement through space, as a first approximation, begins to be most pronounced at a vortex altitude ( $h_{vge}$ ) of

$$h_{vge} = \frac{\pi}{8} b \quad (2)$$



**Figure 5C.** Plan view (close-up) of the NOAA aircraft vortex test site located on the INEL complex.

For the test aircraft involved,  $h_{vge}$  is:

- 87.5 feet AGL for the C5A/B
- 62.8 feet AGL for the C141B
- 52.1 feet AGL for the C130E

The hot-film sensors provided tangential vortex velocity data for air flows across each probe. They did not provide flow direction. This was determined by careful analysis of the recorded hot-film data as well as video and photographic coverage. These data were used to determine, as closely as possible, vortex core passage height (AGL) through the hot-film array on the tower. This data analysis task becomes more demanding and time-consuming as one approaches the vortex core itself. Use of split-film type hot-film anemometers in place of the single-film probes used in these tests would have resolved a 180 degree flow direction ambiguity



Figure 6A. NOAA aircraft vortex test site with instrumented 200 ft. tower.

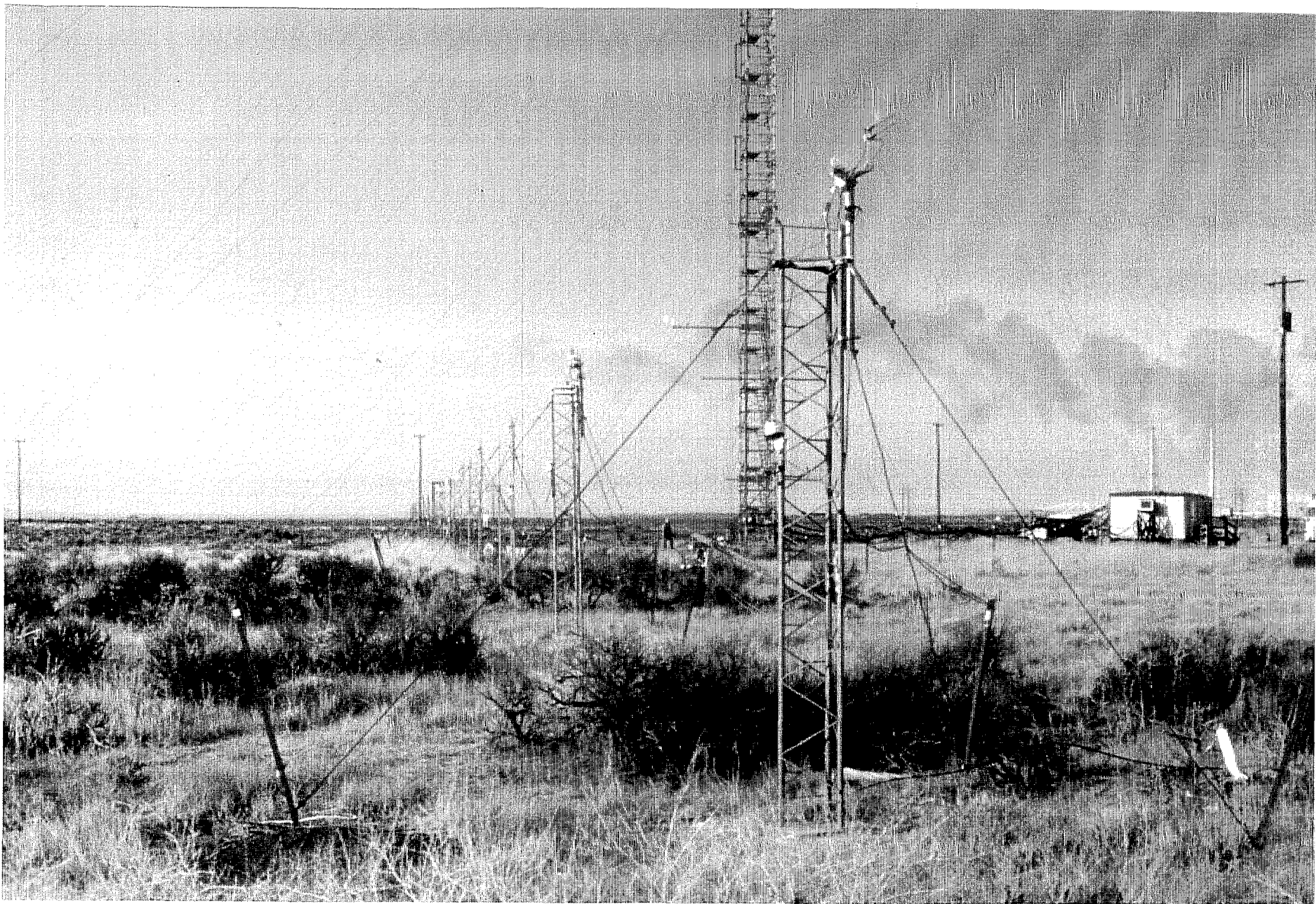


**Figure 6B.** NOAA ground array vortex sensing system at the base of the 200 ft. tower.

problem. Costs associated with analysis processes would have been reduced with their use. However, significantly higher costs would have been associated with the calibration and data processing procedures. Increased data acquisition system design complexity would also have been required. Overall, the costs associated with a split-film anemometer system would have been much greater.

Conventional meteorological sensors were installed in order to measure ambient wind velocity (speed and direction) and ambient temperature. These sensors were placed at seven geometrically spaced levels along the vertical span of the tower, as depicted in Fig. 7.

Colored smoke generators provided vortex flow visualization as the vortex passed through and downwind of the tower. They were installed at ten levels along the vertical span of the test tower and were spaced at fifteen foot intervals starting from the top of the tower downwards. The smoke generators had an operational period of approximately 90 seconds. Ignition time of the smoke generating system had to be judiciously determined for any particular fly-by depending on the desired age of the vortex to be visualized.

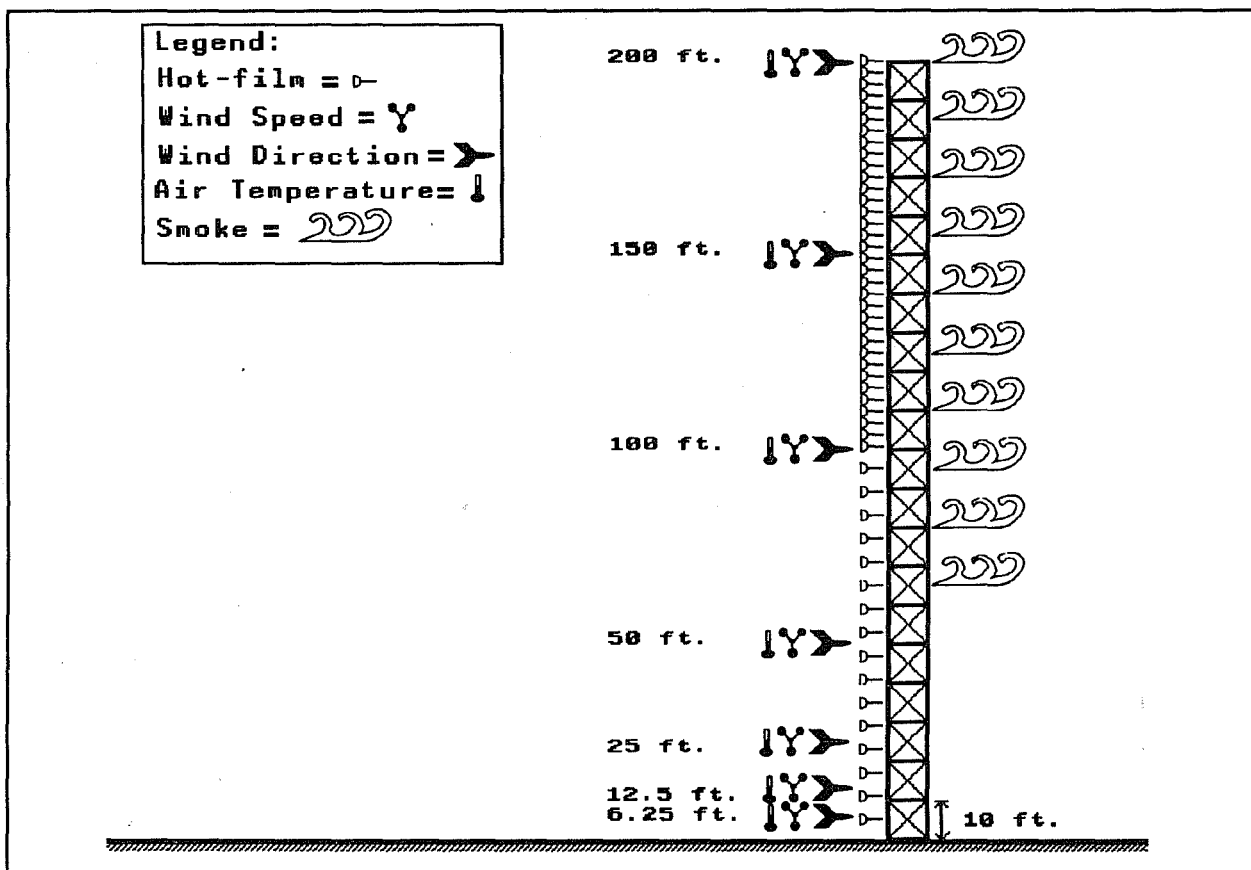
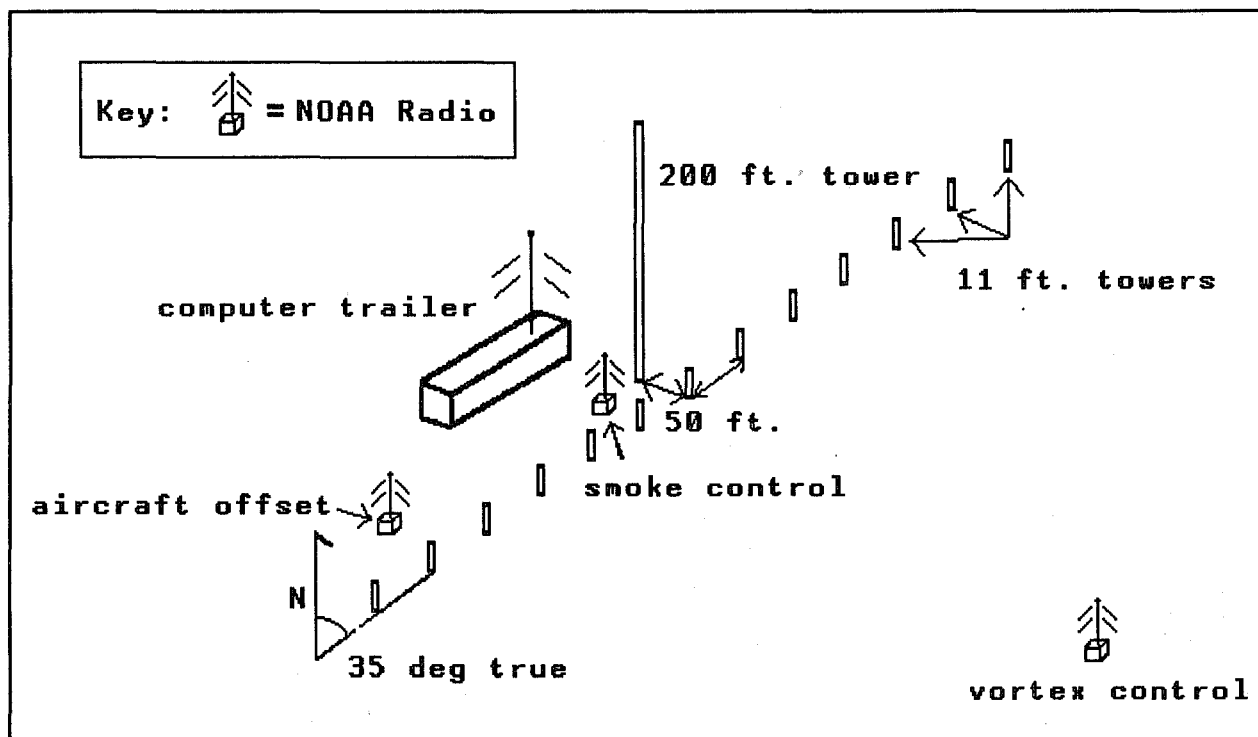


Figure 7. Schematic of the primary test tower illustrating the mounted instrumentation and the vortex flow visualization system.

The radially extended ground-based tower array was installed to measure lateral vortex movement characteristics. The instrumentation system layout or array is shown in Fig. 8 and consisted of thirteen eleven-foot tall towers. Each of the towers were instrumented with two hot-film anemometers mounted at the same height at the tower top. The axes of the two sensors were placed orthogonal to the prevailing wind direction. One sensor was oriented horizontally and the other was oriented vertically. This particular system was designed to gather data on any aircraft generated vortices which descended into ground-effect. Such an approach permitted the calculation of the additive or subtractive effect the vortex flow field exerted on the ambient surface wind. If additive, such an effect could limit USAF parachute drop operations because of the relatively high surface winds thus generated in the drop zone.



**Figure 8.** Schematic of the orientation and spacing of the secondary towers (ground array) employed to measure vortex ground-effect characteristics.

The data acquisition system was operated for a period of about 3 minutes duration. Approximately 1 minute of the beginning of each scan cycle was devoted to the measurement of the ambient wind speed. The remainder of the data contained the vortex flow field. The scan rate was adjusted to measure all sensors (both hot-film and conventional meteorological sensors) 100 times each second.

## TEST DESCRIPTION

The tower fly-by technique was used for the vortex characteristics flight tests. The technique basically consists of flying the test aircraft perpendicular to the ambient surface wind direction. The aircraft is flown at an appropriate altitude and distance upwind from the tower to permit the aircraft wake turbulence to pass through the tower. The tests are conducted under relatively low-ambient wind speed conditions. By manipulating the vertical and lateral positioning of the test aircraft, the age of the vortex system and the tower intercept height can be varied so as to achieve a set of flight test objectives. Miscalculating the wind velocity, the vortex descent velocities (first approximations are made on initial flight tests), or mis-positioning the airplane, can easily result in unsuitable vortex trajectories. For example, the trailing vortex system could float over the tower or settle prematurely into ground-effect. Figure 9 illustrates a general depiction of a vortex pair trajectory obtained with the test airplane slightly above the

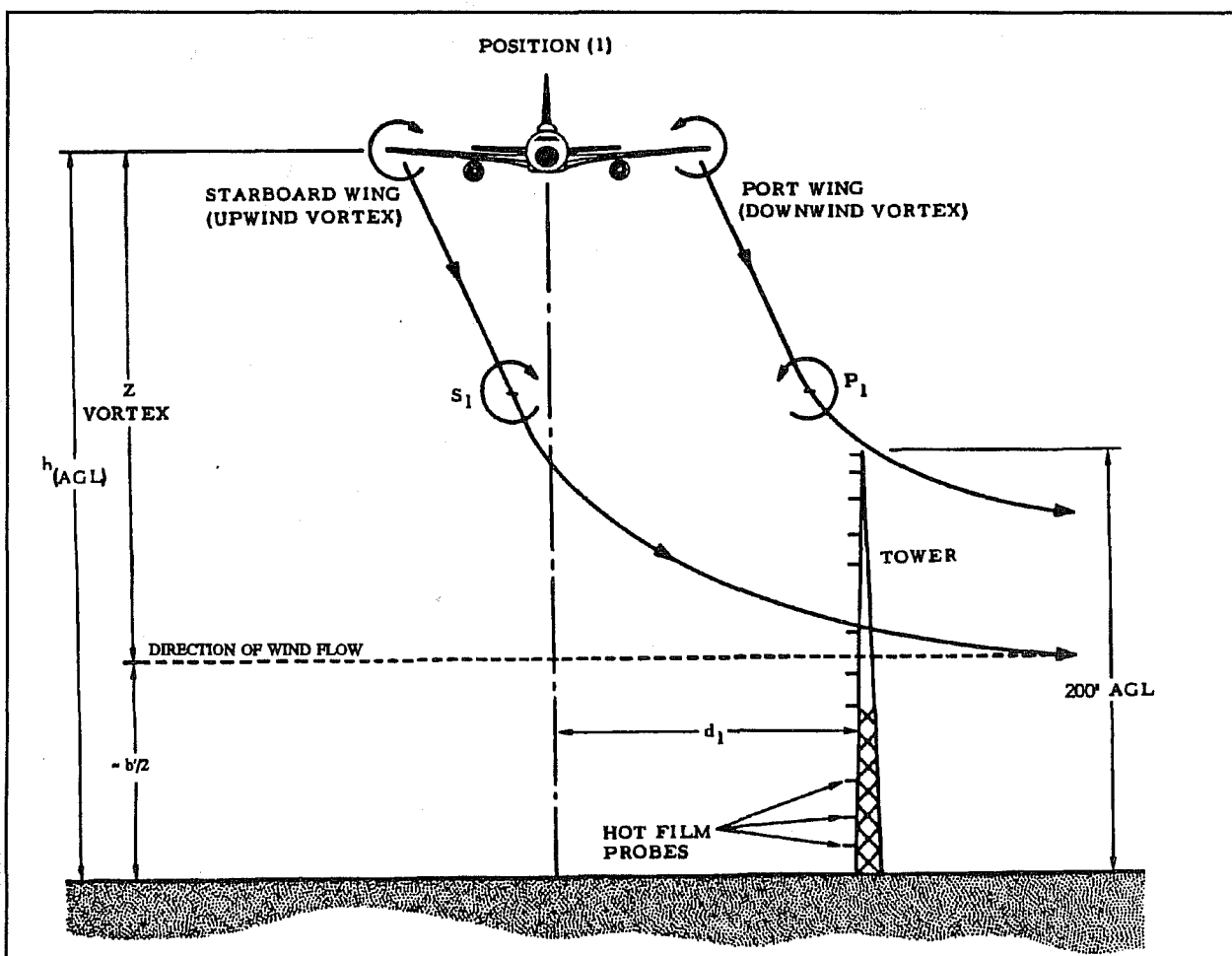
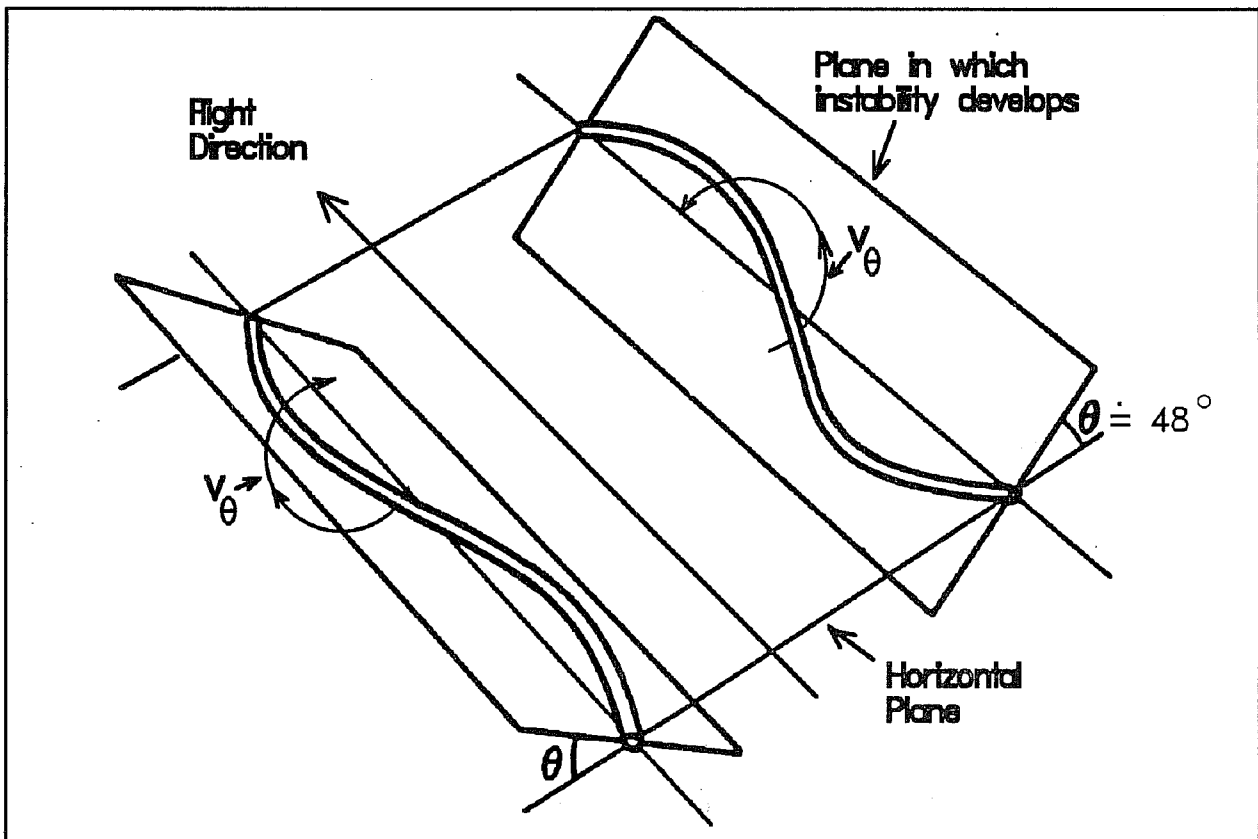


Figure 9. Vortex trajectory in space with the aircraft positioned in close proximity to the test tower.

top of and in close proximity to the tower. Other vortex trajectories can be obtained using other aircraft positions.

The test aircraft is preferably configured with a vortex flow field visualization system when the tower fly-by technique is employed. This helps to determine the precise height at which the vortex passed through the tower. Classical theory on vortex settling rates is still somewhat incomplete, in spite of the large amount of vortex data acquired to date. Many variables can influence settling rates such as: 1) different propulsion systems, i.e. prop or jet, 2) engine location, 3) configuration, e.g., flaps, slats, landing gear positions, and 4) atmospheric stability and buoyancy effects. An airborne visualization system can also aid considerably in determining the vortex decay mode.

In addition to the causes of vortex movement uncertainties cited above, the vortices themselves often exhibit a sinusoidal type oscillation (also called Crow instability after Crow, 1970). This type of phenomenon is covered extensively in Garodz (1970), Garodz and Miller (1975), and Garodz et al. (1976). Figure 10A illustrates Crow instability. The task of accurately calculating the required aircraft position abeam of the tower to insure proper vortex



**Figure 10A.** General shape of the sinusoidal instability of vortices (after Crow). The vortices are viewed from above, and the generating airplane lies beyond the upper left-hand corner of the figure.

intercept with the tower can be very difficult if the oscillations are of a sufficient amplitude. On one pass, the top segment of the oscillating sinuous vortex may float over the tower. On the next pass, the bottom segment of the oscillating vortex may drift appropriately through the tower. This may occur even when initial conditions for both passes are, for all practical purposes, identical.

This oscillatory type vortex motion was most predominant with the C130E aircraft as visually observed during the flight tests. A photo of this type of instability for the C130E is shown in Fig. 10B. Without an aircraft mounted vortex flow visualization system, the flight test team would never have known what was occurring to the trailing vortex system from the time it was generated by and shed from the C130E until it subsequently impacted the test tower. Whether the oscillations were due to atmospheric turbulence or instability, or due to the fact that the C130E is a turboprop airplane is not certain. The latter is the likely cause in that the prop-wash probably became imbedded in the wing vortex sheet during roll-up. The C130E pilot reported no turbulence at flight altitude, making atmospheric turbulence a less likely candidate for the cause of Crow instability.

A minimum of eight (8) minutes per tower pass was established to allow adequate time for proper data acquisition, processing, and storage. Also considered in this minimum time interval are pilot workload and stabilization of the atmosphere after being disturbed by the airplane vortex flow fields. Appropriate visual aids located on the ground were provided to enable the pilot to maintain the desired magnetic track or course over the ground. These aids also helped to ensure safe aircraft offset distance (wing-tip clearance) from the tower when abeam of the tower.

The majority of the test flights were conducted at the airspeeds and in the configurations considered by the USAF to meet operational requirements regarding low altitude airdrop operations. The flight tests were conducted under the following conditions: 1) low airspeeds, 2) extended landing flaps and, where installed, leading edge slats, 3) landing gear up, and 4) open aft cargo doors. The effect of the latter item on vortex characterizations is beyond the scope of this investigation and is not known at this time.

The first test period of each day was planned so that the tower fly-by tests commenced at or just before sunrise. This was done because the ambient atmosphere normally is fairly stable during this time of day. These atmospheric conditions are most conducive to vortex persistence and maintenance of initial relatively high vortex tangential velocities after vortex generation. Subsequent test periods during the day obviously were conducted during periods of increasing atmospheric instability caused by solar insolation and associated convective action.



**Figure 10B.** C130E airplane trailing vortex system showing extreme sinusoidal type instability.

# RESULTS AND DISCUSSION

## GRAPHICAL PRESENTATIONS

A total of 164 flight test data runs were made past the vortex measurement tower during the test program. Fifty-two passes were made by the C130E during 4 days of testing. An additional 52 passes were made by the C141B during three days of testing. The C5A/B made 60 passes during four more days of testing. Approximately 80% of the possible 328 vortex "hits" (two vortex hits per run) provided useful information. This high data recovery percentage was deemed outstanding, considering all of the variables involved which affect vortex transport and decay.

The types of analyses and the summary graphs prepared for this report are presented in the paragraphs and illustrations that follow. The discussion of the results is presented in a subsequent section.

The maximum ages and strengths of the vortices generated by the various aircraft was of primary concern for this report. Graphs of peak recorded vortex tangential velocity ( $V_\theta$ ) versus

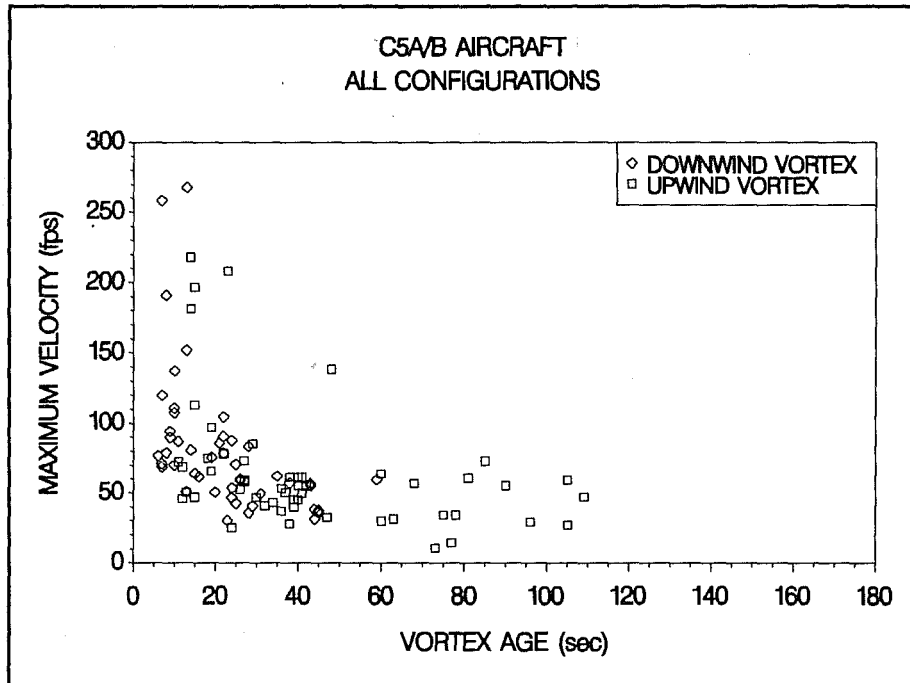
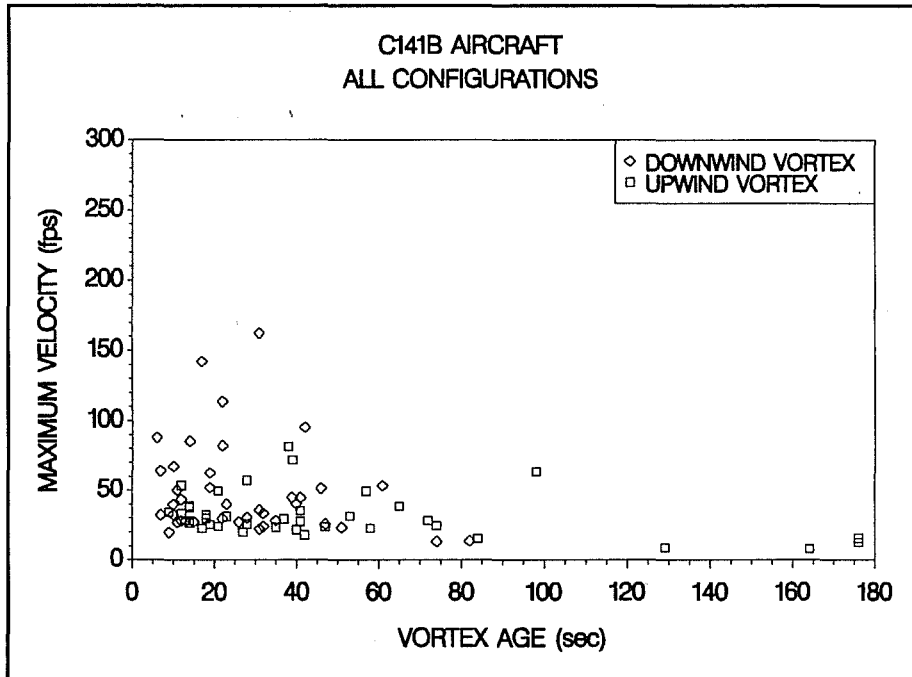
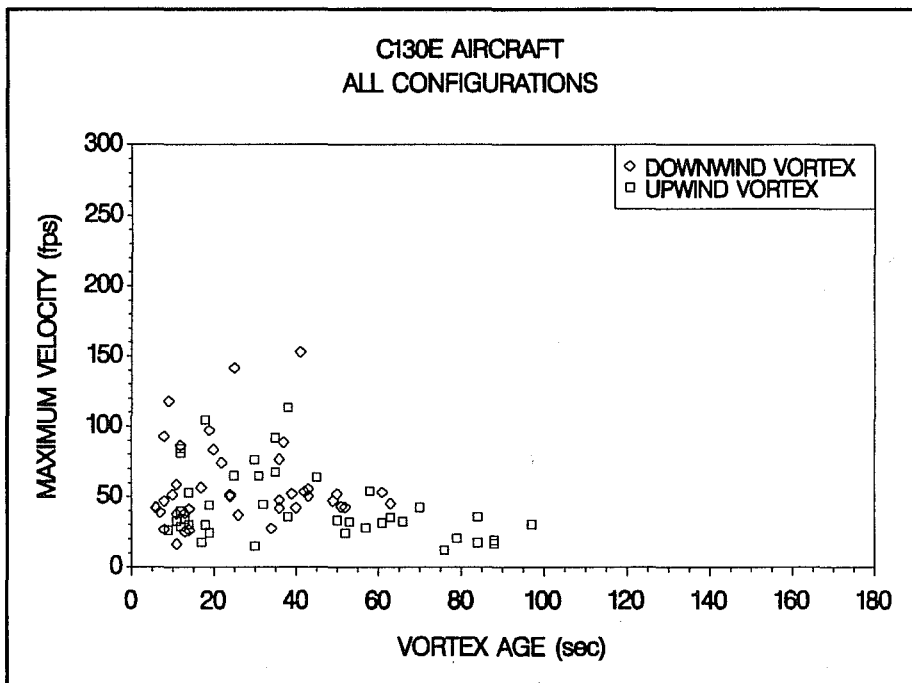


Figure 11. C5A/B peak recorded vortex tangential velocity ( $V_\theta$ ) vs. age, all configurations,  $\delta_F = 15$  to 100% with leading edge slats always extended, upwind and downwind vortices.



**Figure 12.** C141B peak recorded vortex tangential velocity ( $V_{\theta}$ ) vs. age, all configurations,  $\delta_F=11$  to 70% (one at 0%), upwind and downwind vortices.



**Figure 13.** C130E peak recorded vortex tangential velocity ( $V_{\theta}$ ) vs. age, all configurations,  $\delta_F=0$  to 50%, upwind and downwind vortices.

age are presented in Figs. 11-13, for the C5A/B, C141B, and C130E, in order. The graphs include both upwind and downwind vortices obtained from all configurations of the aircraft.

The correlation of  $V_\theta$  with ambient wind speed was examined. Graphs of  $V_\theta$  versus ambient wind speed for the three airplanes are presented in a series of figures. The graphs include both upwind and downwind vortices for all configurations of the aircraft. The graphs are subdivided into aircraft model and vortex age groups, i.e., 0-30, 30-60, and greater than 60 seconds. Figures 14-16 are for the C5A/B, Figs. 17-19 are for the C141B, and Figs. 20-22 are for the C130E.

Correlations were also examined for  $V_\theta$  and Richardson Number (Ri). Ri has been used to characterize the turbulence level of the atmosphere. Graphs with identical categories as those in Figs 14-22 were developed for  $V_\theta$  versus Ri as illustrated in Figs 23-31. Richardson Number is an expression of the ratio of buoyancy to inertia forces and is defined by the following equation (Rosenberg, 1970):

$$Ri = \frac{g \left( \frac{d\theta}{dz} \right)}{\bar{\theta} \left( \frac{du}{dz} \right)^2} \quad (3)$$

where  $g$  is acceleration due to gravity,  $\theta$  is potential temperature,  $z$  is height above the ground, and  $u$  is wind speed. However, for the first few meters AGL, Ri may be calculated with the atmospheric dry bulb temperature ( $T$ ). This substitution was effected for the calculated data presented here. The sign of Ri is determined by the temperature lapse rate. Normally, an Ri at or near zero is indicative of neutral conditions in the atmospheric boundary layer. Outside of this region, stable conditions are indicated for positive values while instability is indicated for negative values.

The plots of vortex tangential velocity versus Ri are based on wind speed and air temperature from 6 feet (1.8 meters) to 200 feet (60.6 meters) AGL. These heights were selected to facilitate data processing. The levels could very well have been from 100 (30.5 meters) to 200 feet, or from 6 to 50 feet (15.2 meters) AGL, or some combination thereof. The larger distance was selected in order to span the rather larger cross-sectional area of the C5A/B vortices. Should Ri be found to be reliable and useful indicator of vortex persistence, an airport installation would most likely preclude the installation of tall meteorological towers. Shorter towers would be required in close proximity to the runway Middle Marker (MM) or threshold area because of concern regarding aircraft obstruction clearance limits. For example, for the Low Level Wind Shear Alert System (LLWSAS), the meteorological towers normally are only 20 feet above the runway surface level. Hence, Ri would need to be calculated from sensors placed at lower heights.

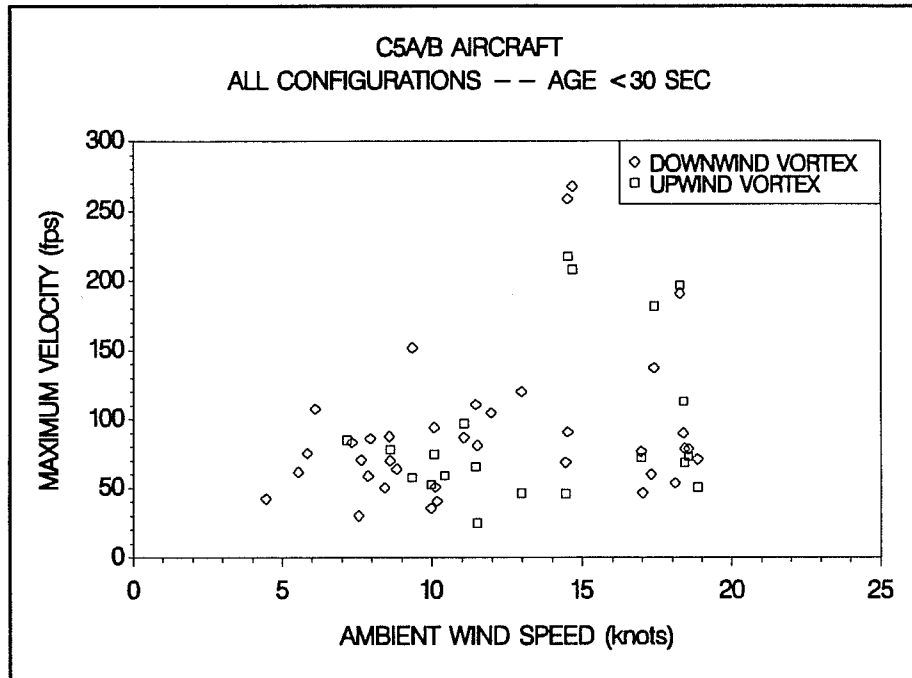


Figure 14. C5A/B peak recorded vortex tangential velocity ( $V_{\theta}$ ) vs. ambient wind speed, all configurations,  $\delta_F=15$  to 100%, upwind and downwind vortices, 0 to 30 seconds age.

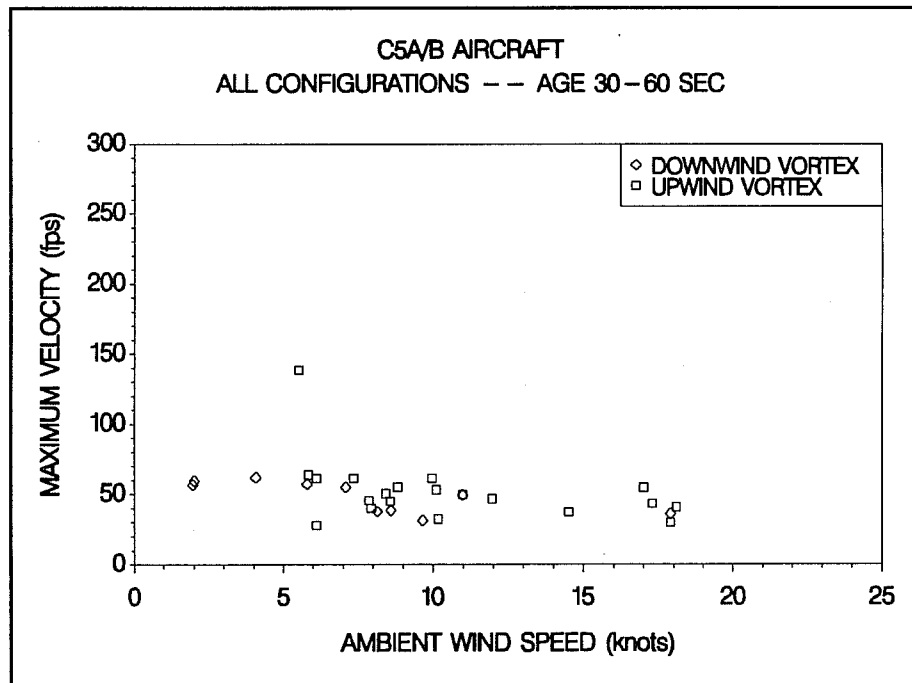


Figure 15. C5A/B peak recorded vortex tangential velocity ( $V_{\theta}$ ) vs. ambient wind speed, all configurations,  $\delta_F=15$  to 100%, upwind and downwind vortices, 30 to 60 seconds age.

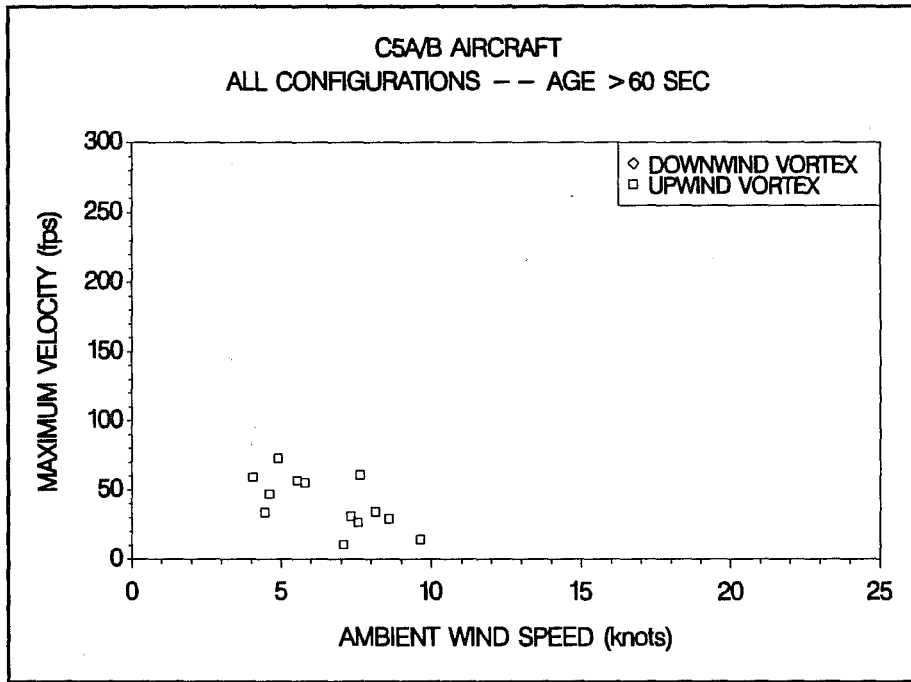


Figure 16. C5A/B peak recorded vortex tangential velocity ( $V_{\theta}$ ) vs. ambient wind speed, all configurations,  $\delta_F=15$  to 100%, upwind and downwind vortices, > 60 seconds age.

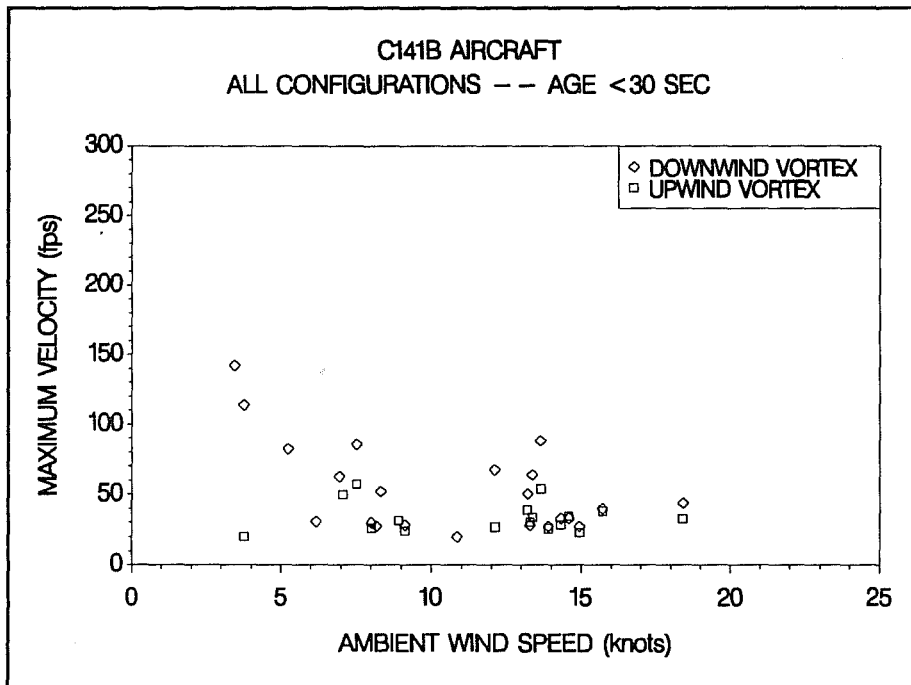


Figure 17. C141B peak recorded vortex tangential velocity ( $V_{\theta}$ ) vs. ambient wind speed, all configurations,  $\delta_F=11$  to 70% (one at 0%), upwind and downwind vortices, 0 to 30 seconds age.

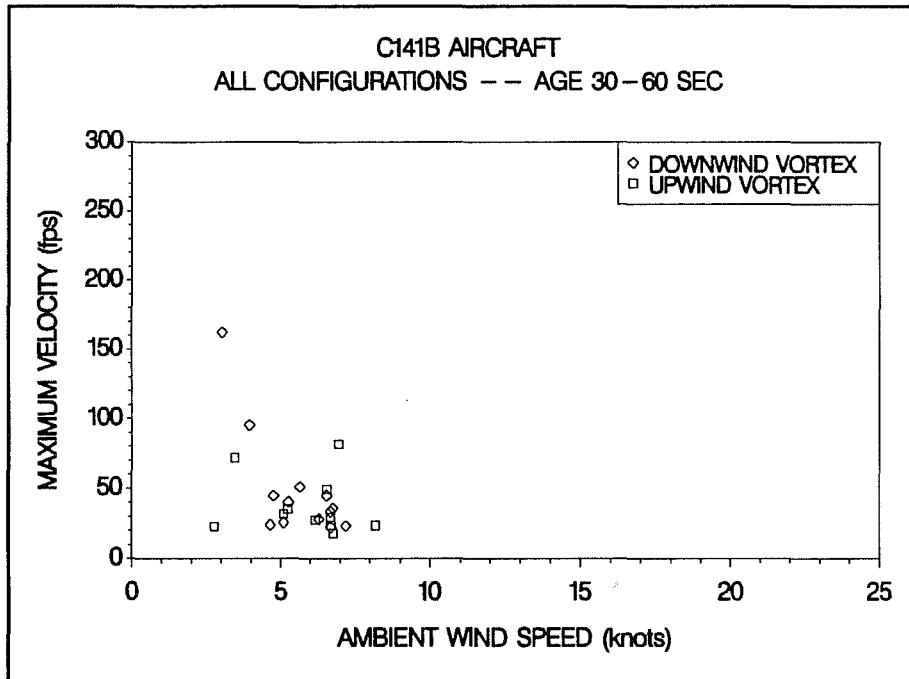


Figure 18. C141B peak recorded vortex tangential velocity ( $V_{\theta}$ ) vs. ambient wind speed, all configurations,  $\delta_F=11$  to 70% (one at 0%), upwind and downwind vortices, 30 to 60 seconds age.

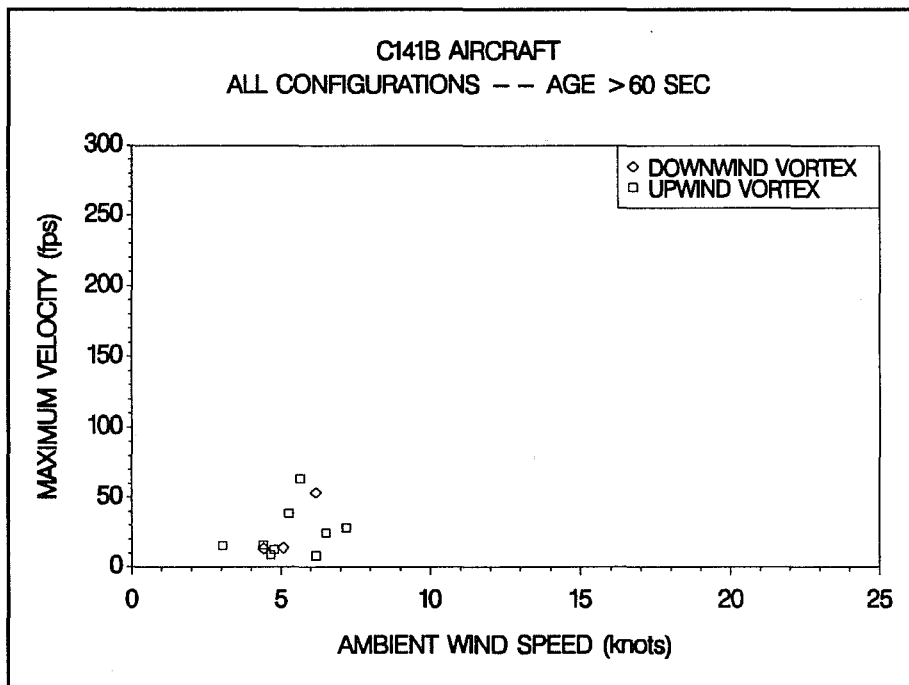


Figure 19. C141B peak recorded vortex tangential velocity ( $V_{\theta}$ ) vs. ambient wind speed, all configurations,  $\delta_F=11$  to 70% (one at 0%), upwind and downwind vortices, > 60 seconds age.

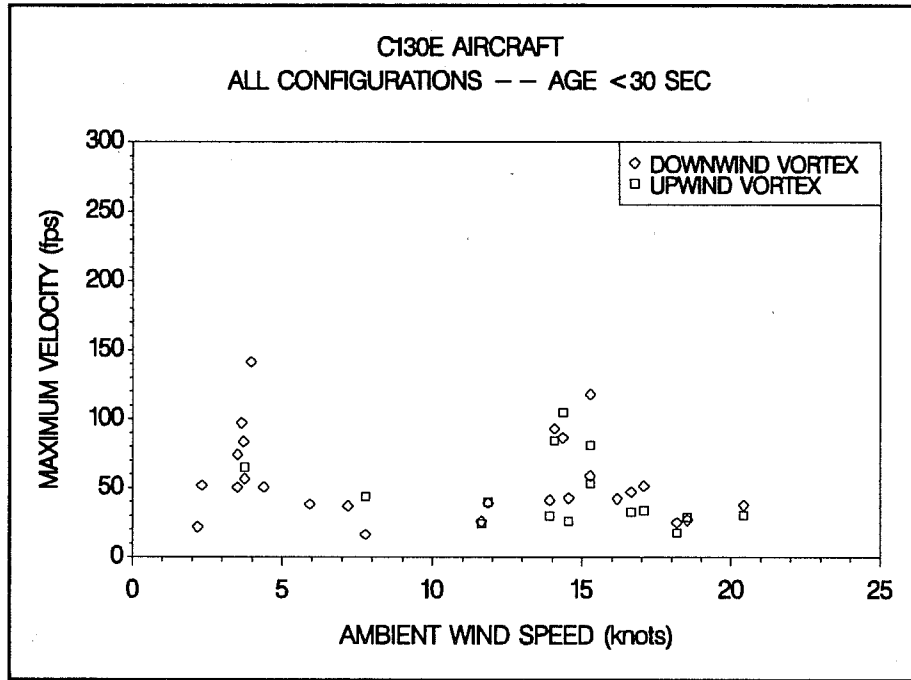


Figure 20. C130E peak recorded vortex tangential velocity ( $V_{\theta}$ ) vs. ambient wind speed, all configurations,  $\delta_F=0$  to 50%, upwind and downwind vortices, 0 to 30 seconds age.

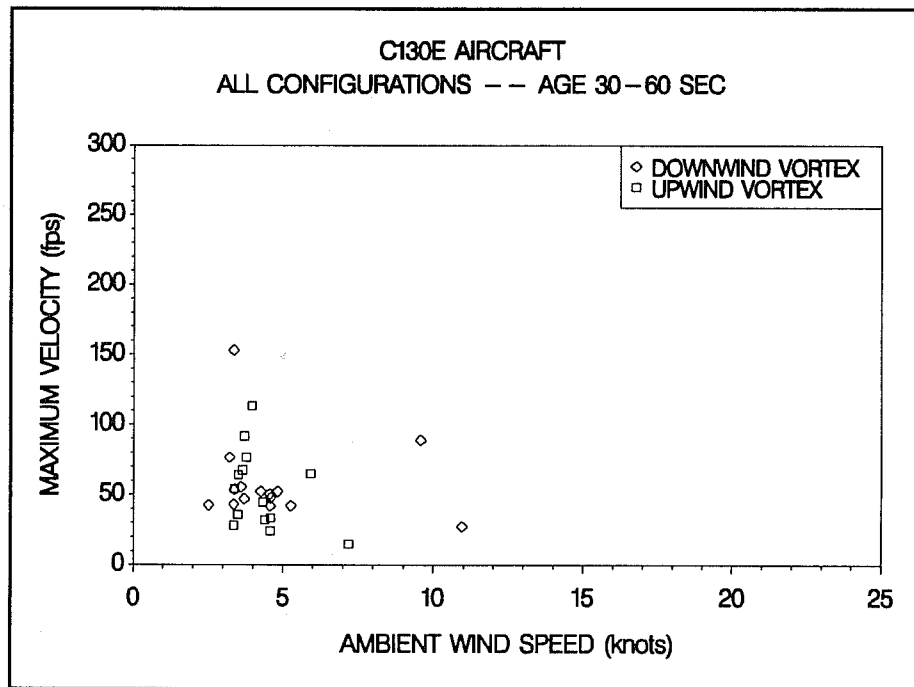


Figure 21. C130E peak recorded vortex tangential velocity ( $V_{\theta}$ ) vs. ambient wind speed, all configurations,  $\delta_F=0$  to 50%, upwind and downwind vortices, 30 to 60 seconds age.

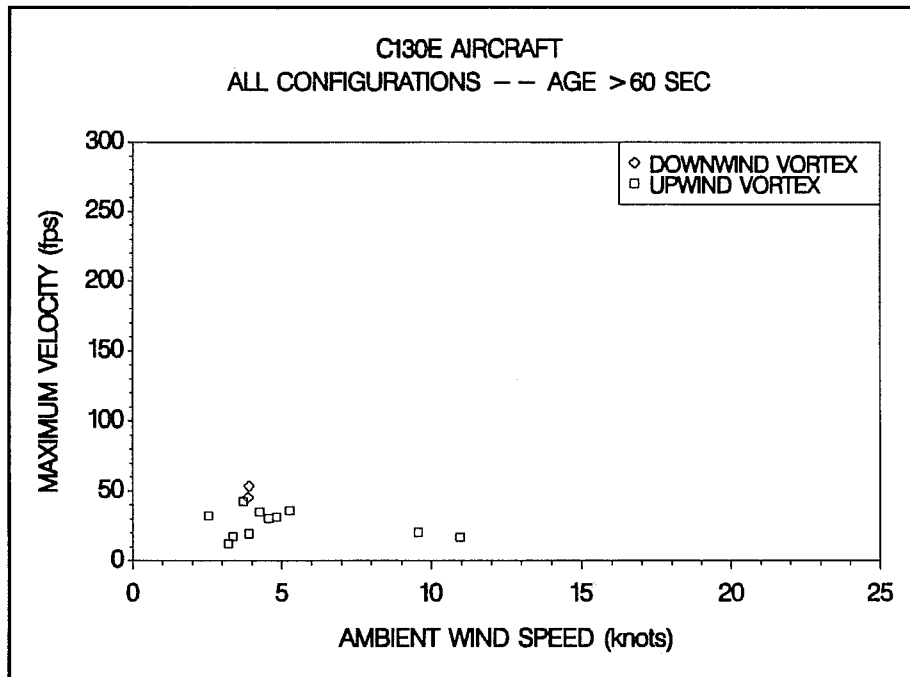


Figure 22. C130E peak recorded vortex tangential velocity ( $V_{\theta}$ ) vs. ambient wind speed, all configurations,  $\delta_F=0$  to 50%, upwind and downwind vortices, > 60 seconds age.

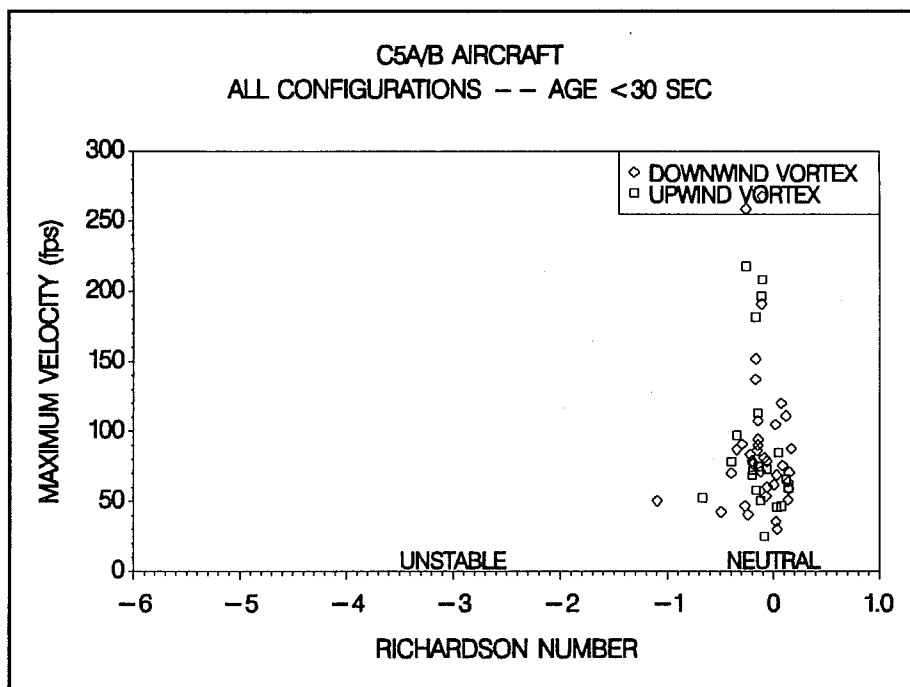
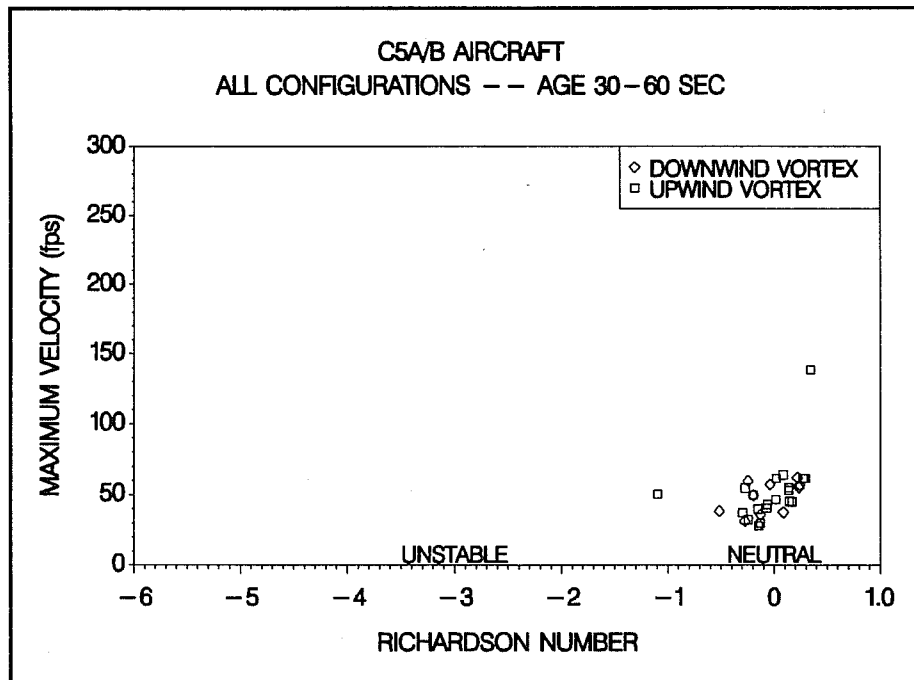
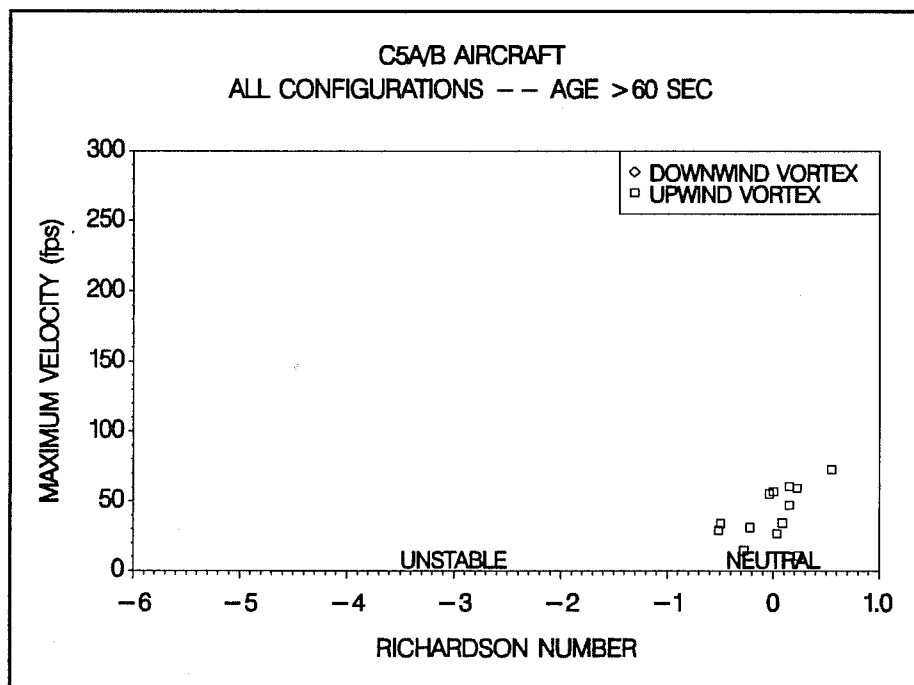


Figure 23. C5A/B peak recorded vortex tangential velocity ( $V_{\theta}$ ) vs. Richardson Number ( $Ri$ ), all configurations,  $\delta_F=15$  to 100%, upwind and downwind vortices, 0 to 30 seconds age.



**Figure 24.** C5A/B peak recorded vortex tangential velocity ( $V_\theta$ ) vs. Richardson Number (Ri), all configurations,  $\delta_F = 15$  to 100%, upwind and downwind vortices, 30 to 60 seconds age.



**Figure 25.** C5A/B peak recorded vortex tangential velocity ( $V_\theta$ ) vs. Richardson Number (Ri), all configurations,  $\delta_F = 15$  to 100%, upwind and downwind vortices, > 60 seconds age.

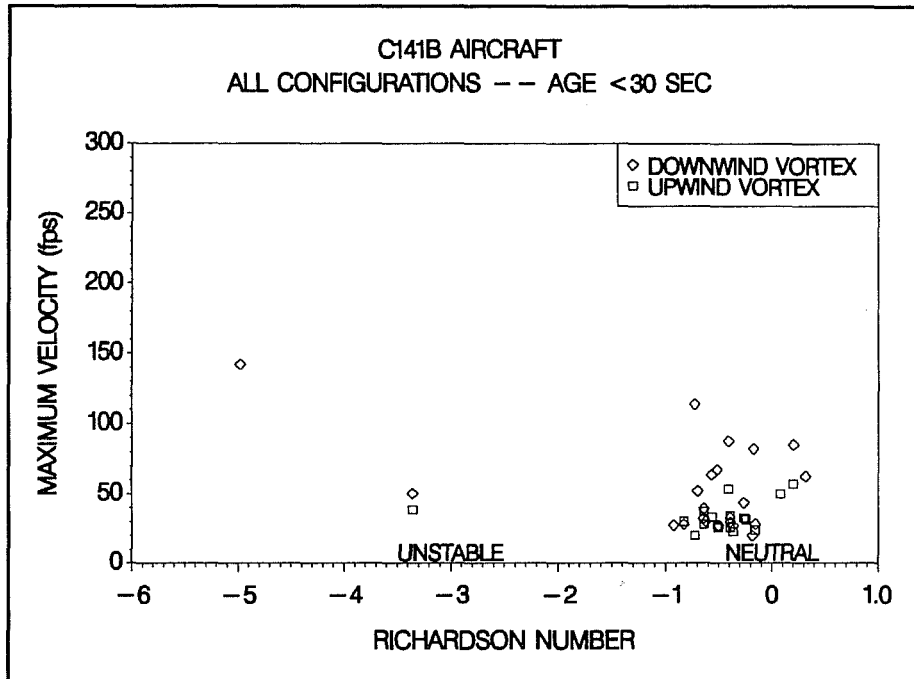


**Figure 26.** C141B peak recorded vortex tangential velocity ( $V_\theta$ ) vs. Richardson Number (Ri), all configurations,  $\delta_F=11$  to 70% (one at 0%), upwind and downwind vortices, 0 to 30 seconds age.

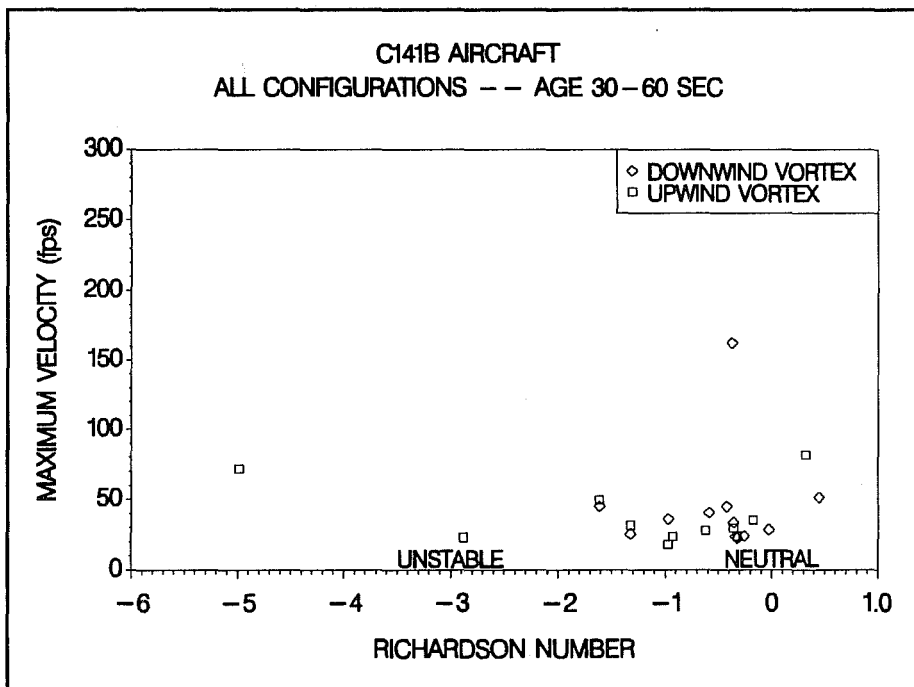


**Figure 27.** C141B peak recorded vortex tangential velocity ( $V_\theta$ ) vs. Richardson Number (Ri), all configurations,  $\delta_F=11$  to 70% (one at 0%), upwind and downwind vortices, 30 to 60 seconds age.

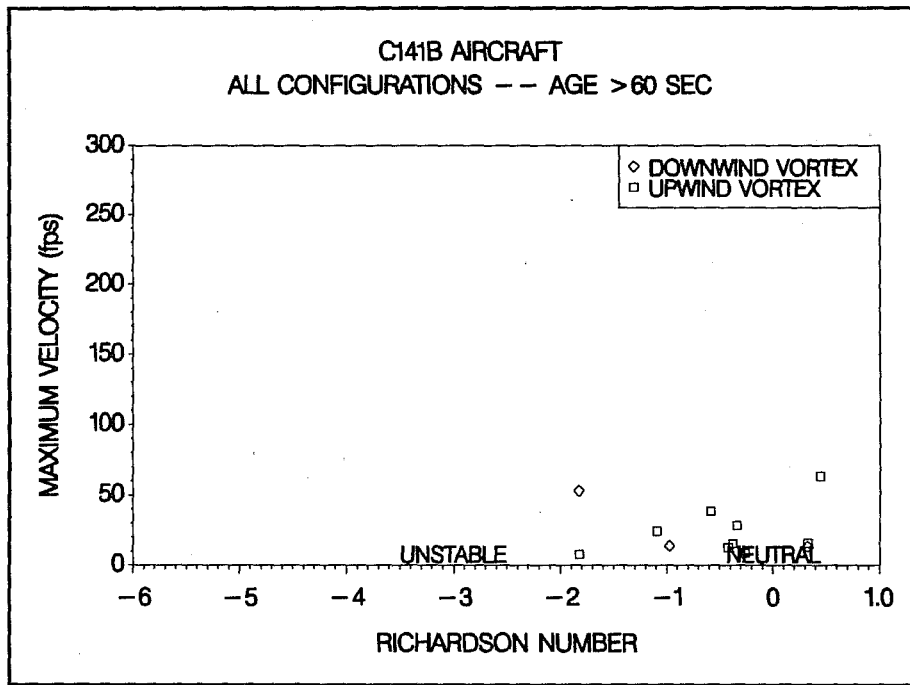


**Figure 28.** C141B peak recorded vortex tangential velocity ( $V_\theta$ ) vs. Richardson Number (Ri), all configurations,  $\delta_F=11$  to 70% (one at 0%), upwind and downwind vortices, > 60 seconds age.

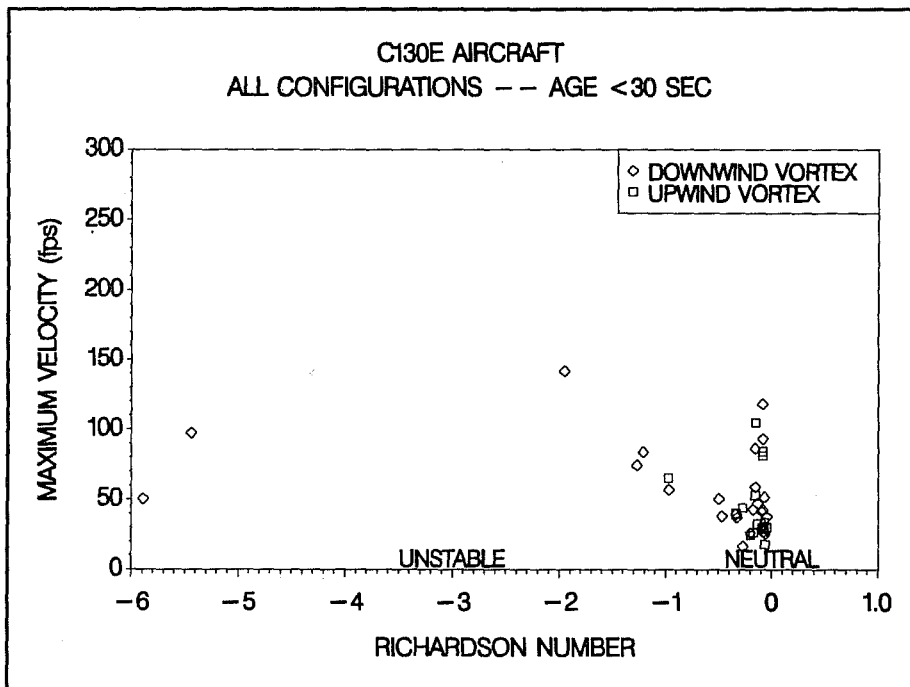


**Figure 29.** C130E peak recorded vortex tangential velocity ( $V_\theta$ ) vs. Richardson Number (Ri), all configurations,  $\delta_F=0$  to 50%, upwind and downwind vortices, 0 to 30 seconds age.

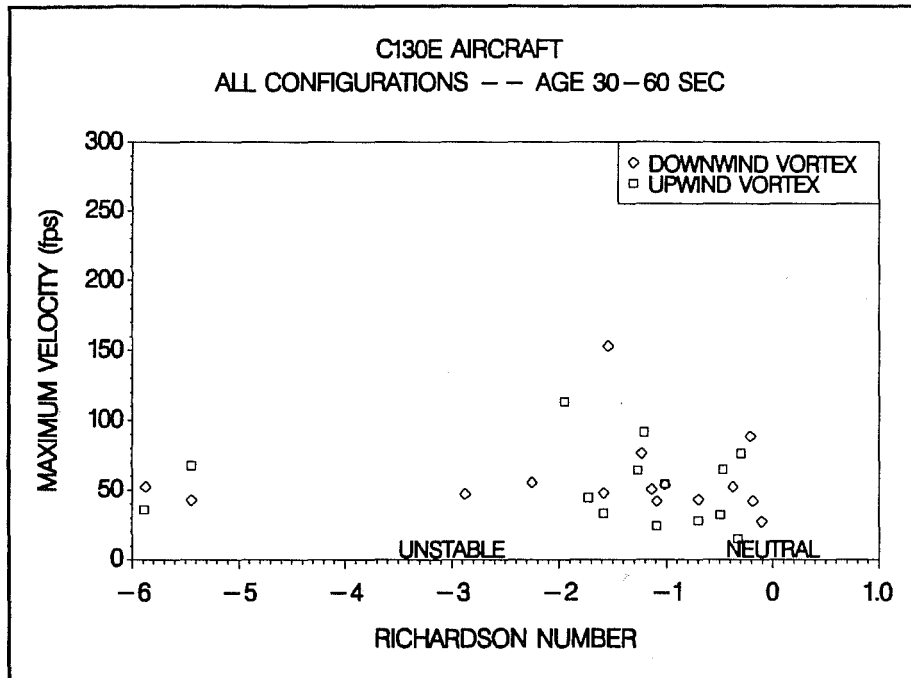


**Figure 30.** C130E peak recorded vortex tangential velocity ( $V_{\theta}$ ) vs. Richardson Number (Ri), all configurations,  $\delta_F=0$  to 50%, upwind and downwind vortices, 30 to 60 seconds age.

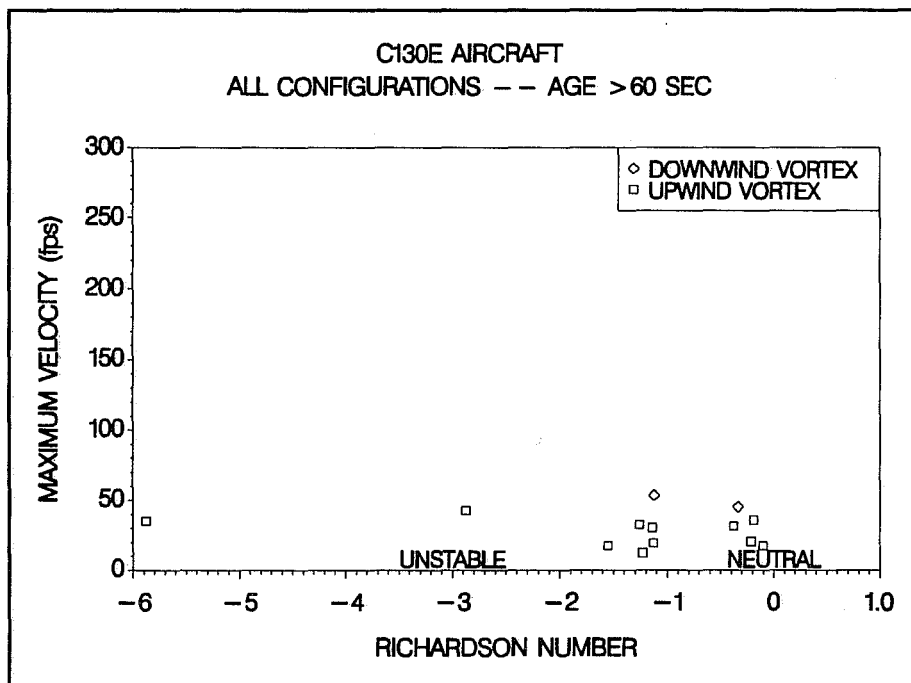


**Figure 31.** C130E peak recorded vortex tangential velocity ( $V_{\theta}$ ) vs. Richardson Number (Ri), all configurations,  $\delta_F=0$  to 50%, upwind and downwind vortices, >60 seconds age.

Correlations were also investigated for  $V_\theta$  with the atmospheric temperature gradient. Plots of  $V_\theta$  versus ambient atmospheric temperature gradient ( $\Delta T/\Delta z$ ) from 6.25 to 200 feet AGL are shown in Figs. 32-40. Atmospheric stability categories were assigned to the vertical air temperature gradients according to Nuclear Regulatory Commission (NRC) regulations (Anon., 1980) as follows:

$$\begin{aligned} \text{stable: } \Delta T/\Delta z &> -0.5 \text{ }^\circ\text{C}/100 \text{ m} \\ \text{neutral: } -0.5 \text{ }^\circ\text{C}/100 \text{ m} &\geq \Delta T/\Delta z \geq -1.5 \text{ }^\circ\text{C}/100 \text{ m} \\ \text{unstable: } \Delta T/\Delta z &< -1.5 \text{ }^\circ\text{C}/100 \text{ m} \end{aligned}$$

Identical vortex age categories were employed as those used in Figs. 23-31. It was surmised that this parameter might provide a simpler, yet more reliable correlation with vortex strength than  $Ri$ .

Correlations of vortex descent velocity with vortex/tower intercept height were also investigated. Figures 41-43 illustrate the graphs generated for the C5A/B, C141B, and C130E, respectively. An initial vortex decent velocity  $\dot{z}_v$  can be calculated using an elliptical lift distribution by:

$$\dot{z}_v = \frac{\Gamma}{2\pi r} \quad (4)$$

where  $r = b' = \frac{\pi b}{4}$ .

For the test aircraft involved,  $\dot{z}_v$  would be:

$$\begin{aligned} &7.0 \text{ feet/second for the C5A/B} \\ &4.9 \text{ feet/second for the C141B} \\ &4.8 \text{ feet/second for the C130E} \end{aligned}$$

As previously discussed, the height of the vortex during lateral movement in ground-effect approximates that calculated using an elliptical lift distribution.

A plot incorporating vortex persistence as a function of ambient wind velocity and aircraft height above the ground was generated using the current flight test data and data from Garodz and Miller (1975). The graph is illustrated in Fig. 44. This figure originated with McGowan (1971) and includes NASA and Boeing data from Condit and Tracey (1970).

Vortex tangential velocity profiles from all fly-bys were also investigated. The profiles (one each for the upwind and downwind vortices of each fly-by) were obtained by taking a "snapshot" of velocities from all hot-film sensors at the precise moment when the maximum vortex tangential velocity was observed. That particular moment in time was when the vortex core was

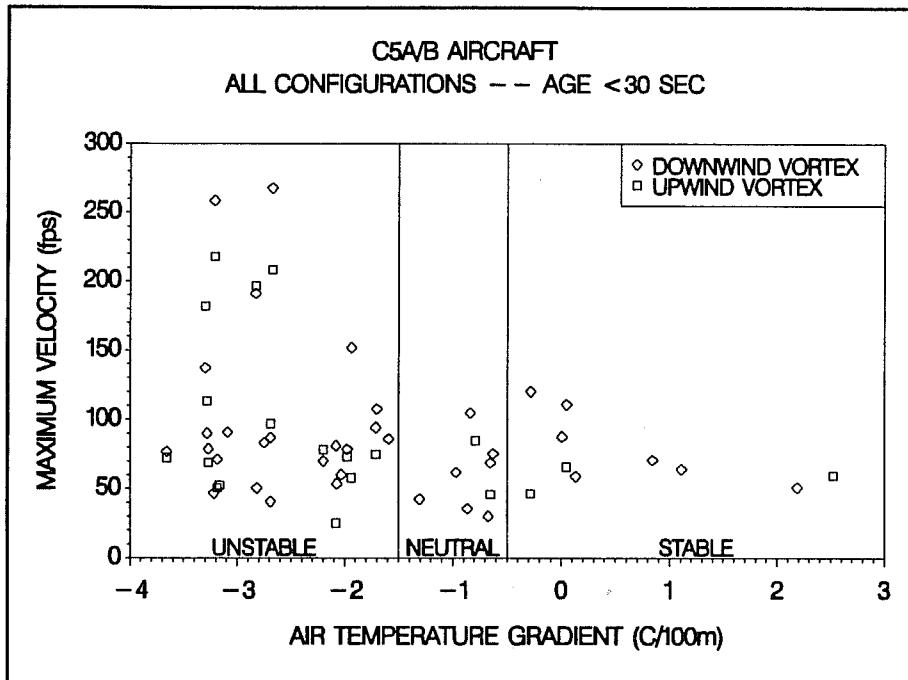


**Figure 32.** C5A/B peak recorded vortex tangential velocity ( $V_{\theta}$ ) vs. vertical air temperature difference, all configurations,  $\delta_F=15$  to 100%, upwind and downwind vortices, 0 to 30 seconds age.

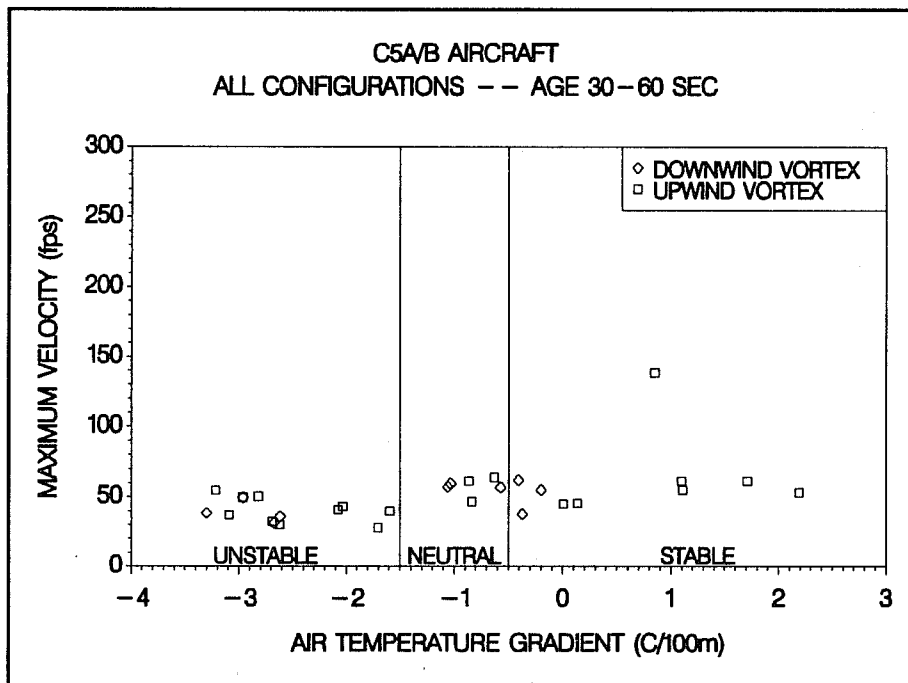


**Figure 33.** C5A/B peak recorded vortex tangential velocity ( $V_{\theta}$ ) vs. vertical air temperature difference, all configurations,  $\delta_F=15$  to 100%, upwind and downwind vortices, 30 to 60 seconds age.

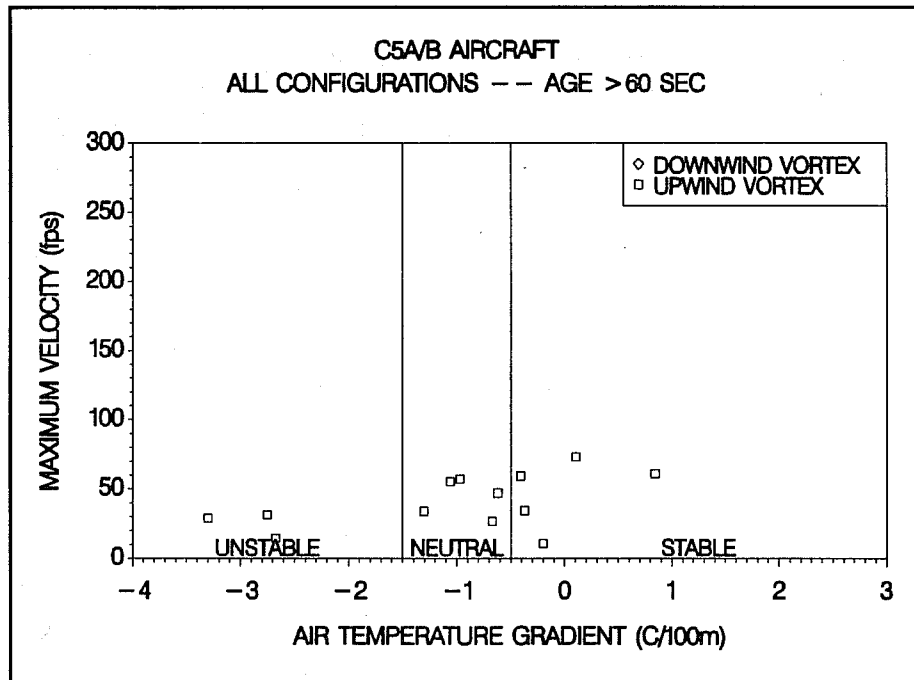


**Figure 34.** C5A/B peak recorded vortex tangential velocity ( $V_{\theta}$ ) vs. vertical air temperature difference, all configurations,  $\delta_F=15$  to 100%, upwind and downwind vortices, > 60 seconds age.

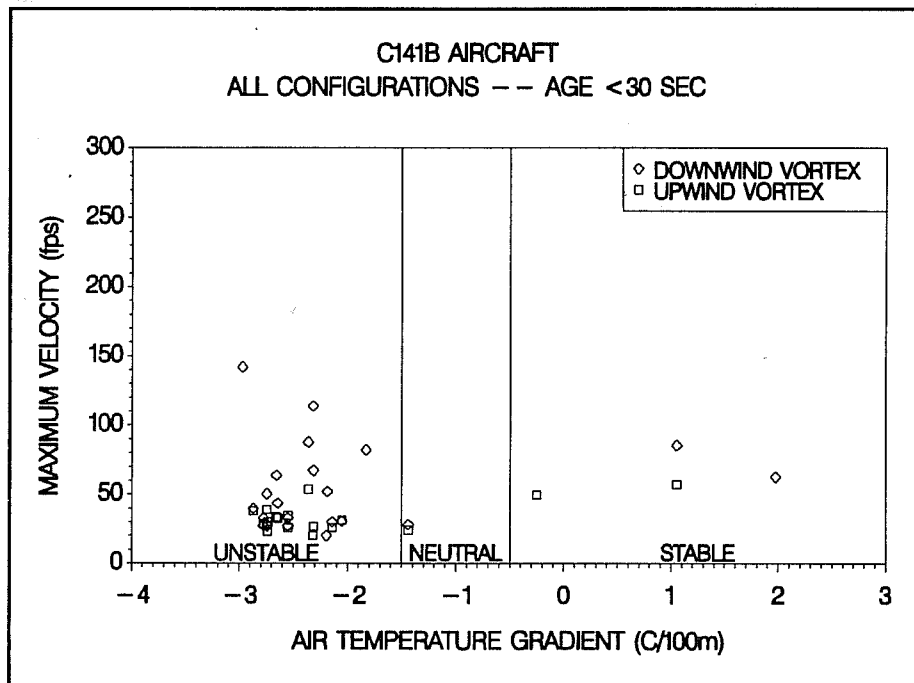


**Figure 35.** C141B peak recorded vortex tangential velocity ( $V_{\theta}$ ) vs. vertical air temperature difference, all configurations,  $\delta_F=11$  to 70% (one at 0%), upwind and downwind vortices, 0 to 30 seconds age.

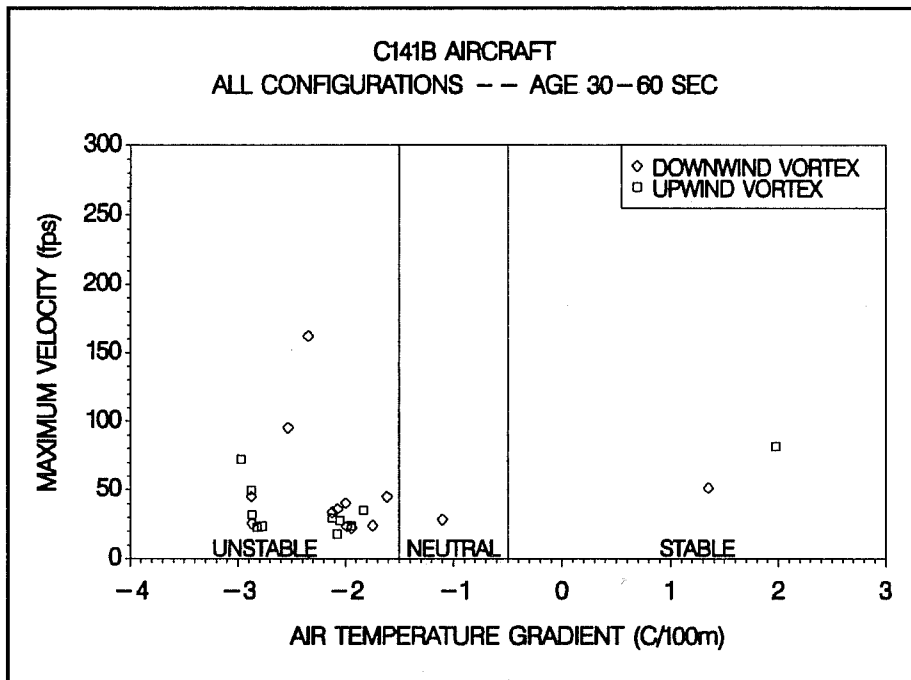


Figure 36. C141B peak recorded vortex tangential velocity ( $V_{\theta}$ ) vs. vertical air temperature difference, all configurations,  $\delta_F = 11$  to 70% (one at 0%), upwind and downwind vortices, 30 to 60 seconds age.

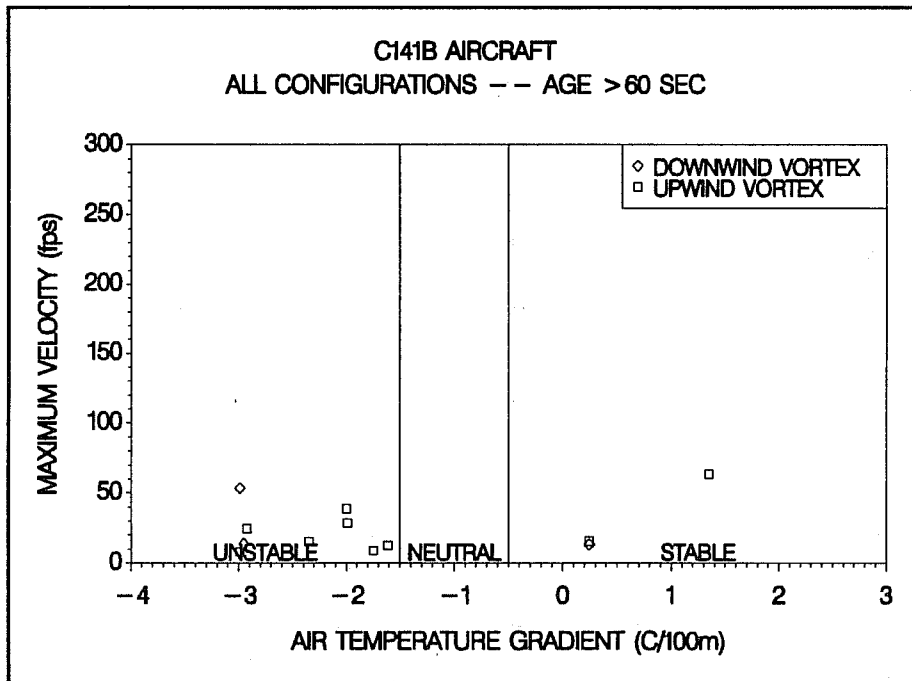
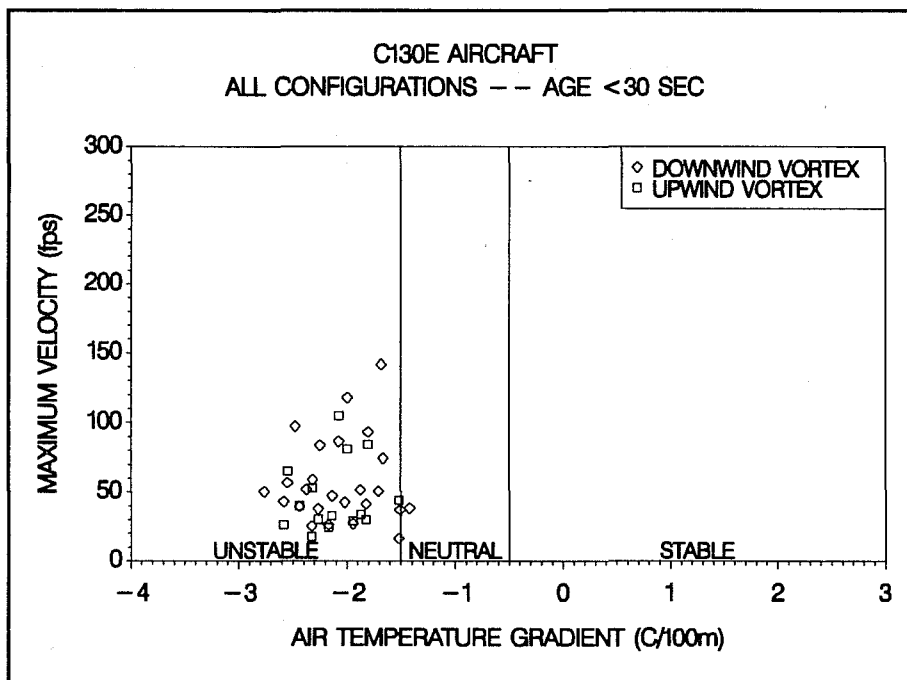
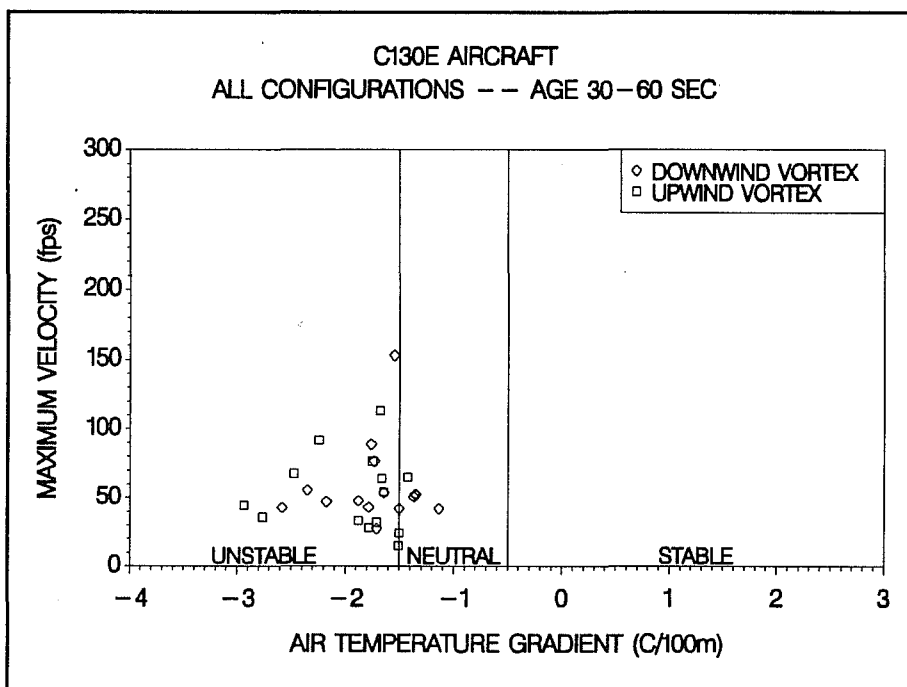


Figure 37. C141B peak recorded vortex tangential velocity ( $V_{\theta}$ ) vs. vertical air temperature difference, all configurations,  $\delta_F = 11$  to 70% (one at 0%), upwind and downwind vortices, > 60 seconds age.



**Figure 38.** C130E peak recorded vortex tangential velocity ( $V_{\theta}$ ) vs. vertical air temperature difference, all configurations,  $\delta_F=0$  to 50%, upwind and downwind vortices, 0 to 30 seconds age.



**Figure 39.** C130E peak recorded vortex tangential velocity ( $V_{\theta}$ ) vs. vertical air temperature difference, all configurations,  $\delta_F=0$  to 50%, upwind and downwind vortices, 30 to 60 seconds age.

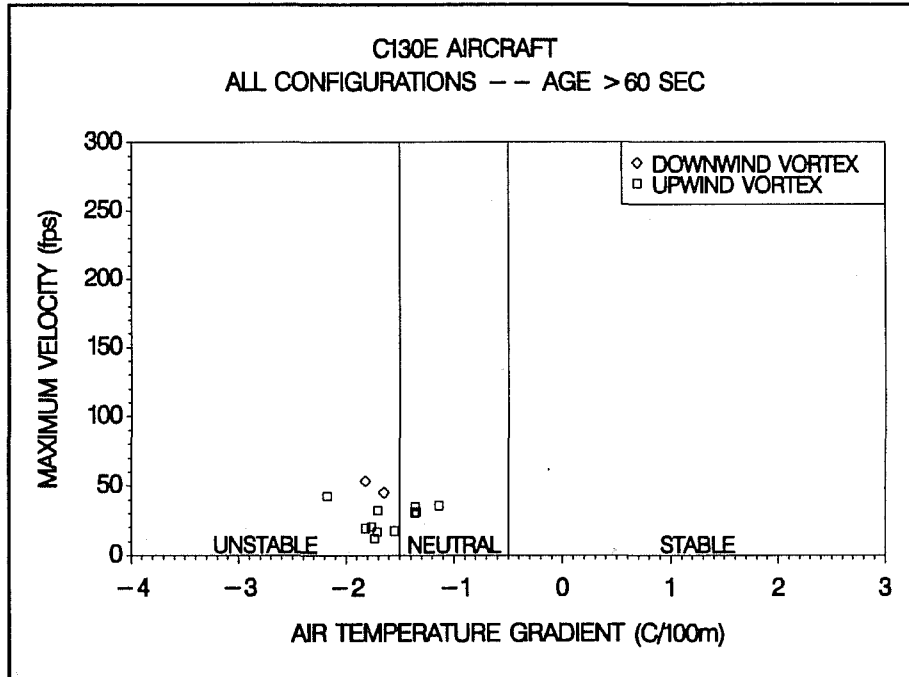


**Figure 40.** C130E peak recorded vortex tangential velocity ( $\dot{V}_\theta$ ) vs. vertical air temperature difference, all configurations,  $\delta_F=0$  to 50%, upwind and downwind vortices, > 60 seconds age.

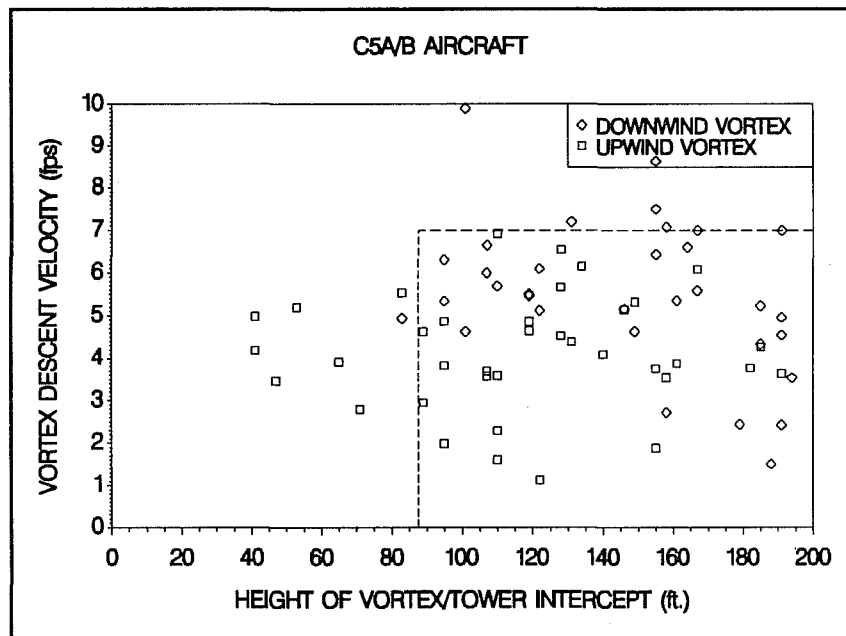


**Figure 41.** C5A/B vortex descent velocity ( $\dot{z}_V$ ) vs. vortex/tower intercept height, all configurations,  $\delta_F=80$  to 100%, upwind and downwind vortices. The vertical dashed line represents a calculated  $h_{Vge}$  of 87.5 ft. while the horizontal dashed line represents an initial calculated  $\dot{z}_V$  of 7.0 fps.

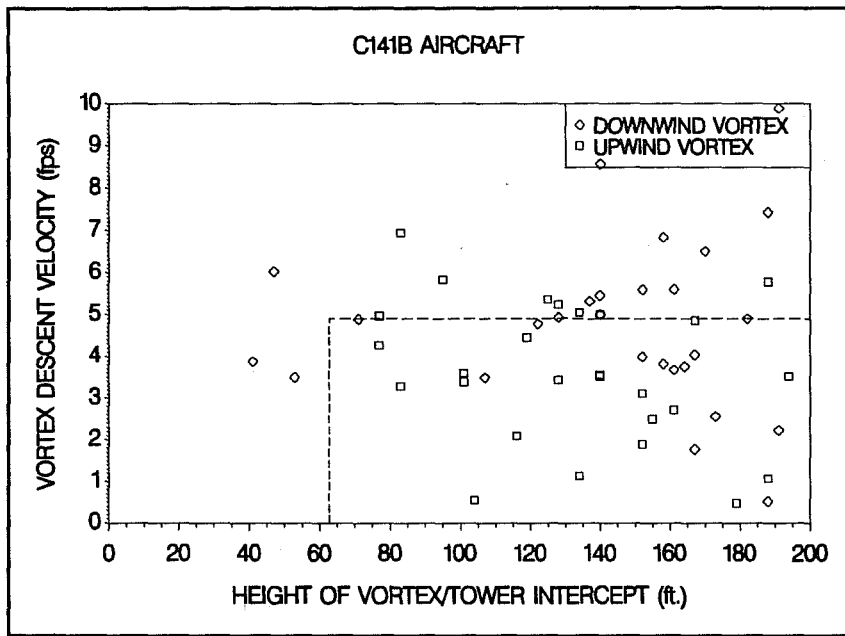


**Figure 42.** C141B vortex descent velocity ( $\dot{z}_v$ ) vs. vortex/tower intercept height, all configurations,  $\delta_F=80$  to 100%, upwind and downwind vortices. The vertical dashed line represents a calculated  $h_{vge}$  of 62.8 ft. while the horizontal dashed line represents an initial calculated  $\dot{z}_v$  of 4.9 fps.

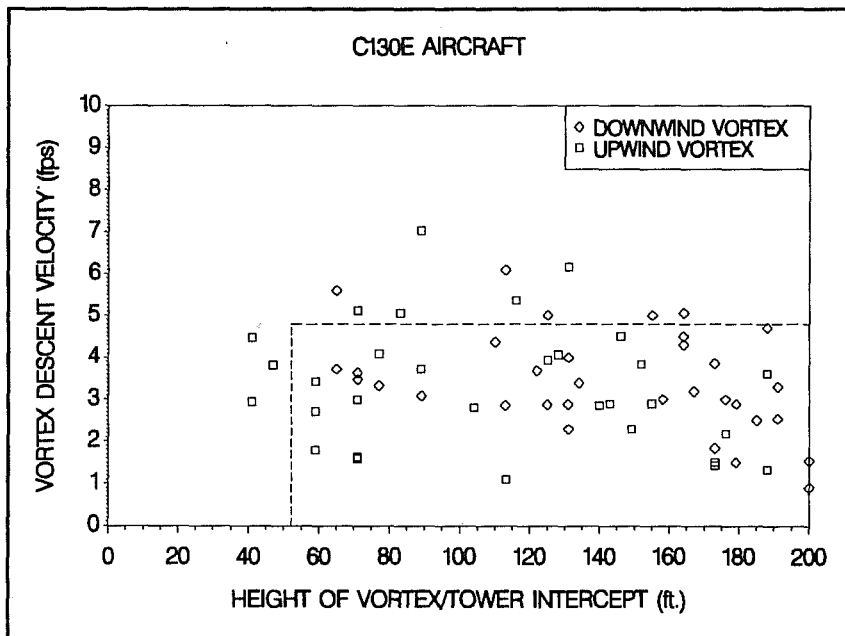


**Figure 43.** C130E vortex descent velocity ( $\dot{z}_v$ ) vs. vortex/tower intercept height, all configurations,  $\delta_F=80$  to 100%, upwind and downwind vortices. The vertical dashed line represents a calculated  $h_{vge}$  of 52.1 ft. while the horizontal dashed line represents an initial calculated  $\dot{z}_v$  of 4.8 fps.

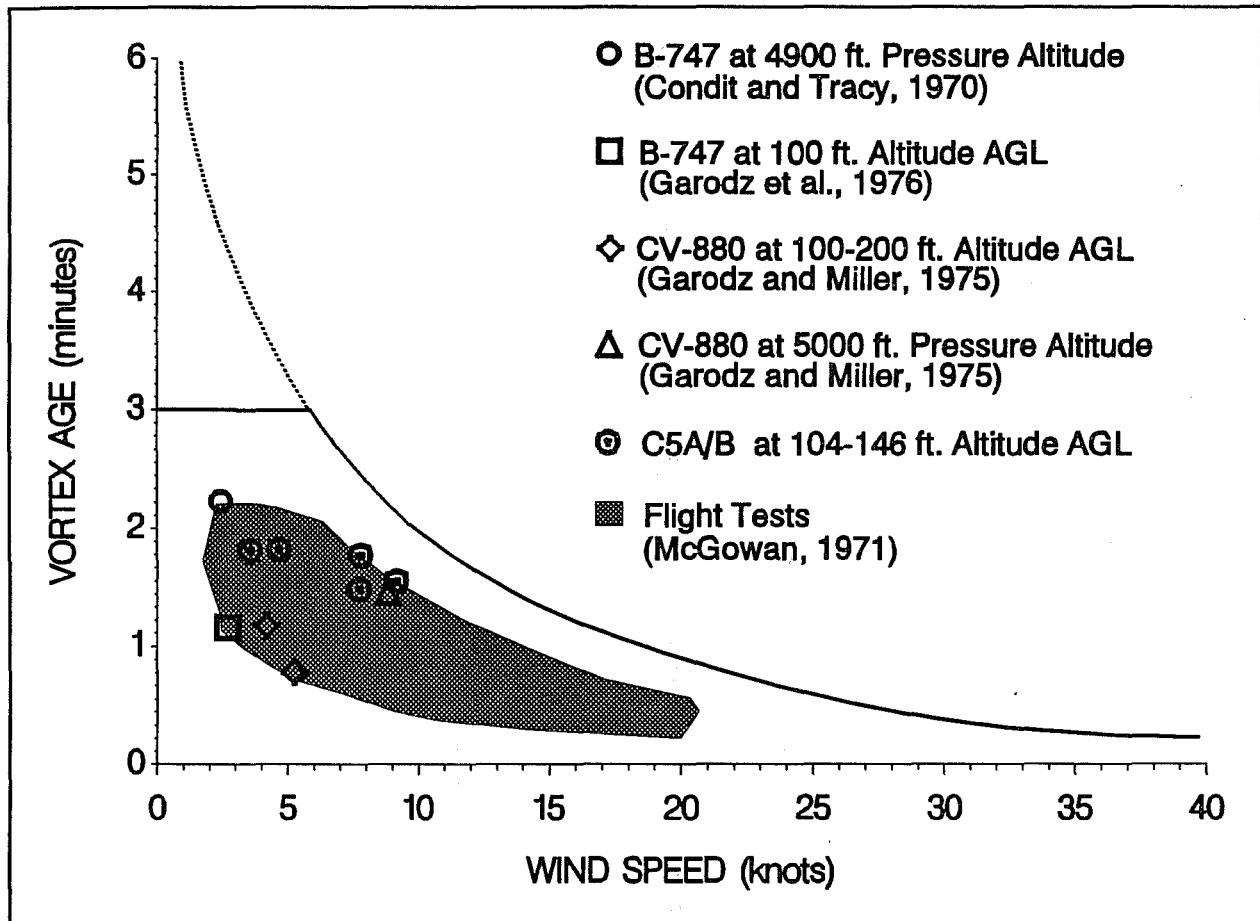


Figure 44. Vortex persistence as a function of ambient wind speed and height above the ground.

penetrated by a hot film anemometer. The profiles were then corrected for horizontal wind as a function of sensor height above the ground. A logarithmic model was subsequently fit to the profile when the size of the vortex core was known. The model is a function of both core size ( $r_c$ ) and velocity ( $V_{\theta_{max}}$ ), and is expressed as follows:

$$V_{\theta} = V_{\theta_{max}} \left[ \frac{1 + \ln(r/r_c)}{(r/r_c)} \right] \quad (5)$$

where  $r$  is the distance from the vortex core. Example graphs are illustrated in Figs. 45A-45C for the C5A/B, Figs. 46A-46C for the C141B, and Figs. 47A-47C for the C130E. The entire body of graphs is given in Appendix C.

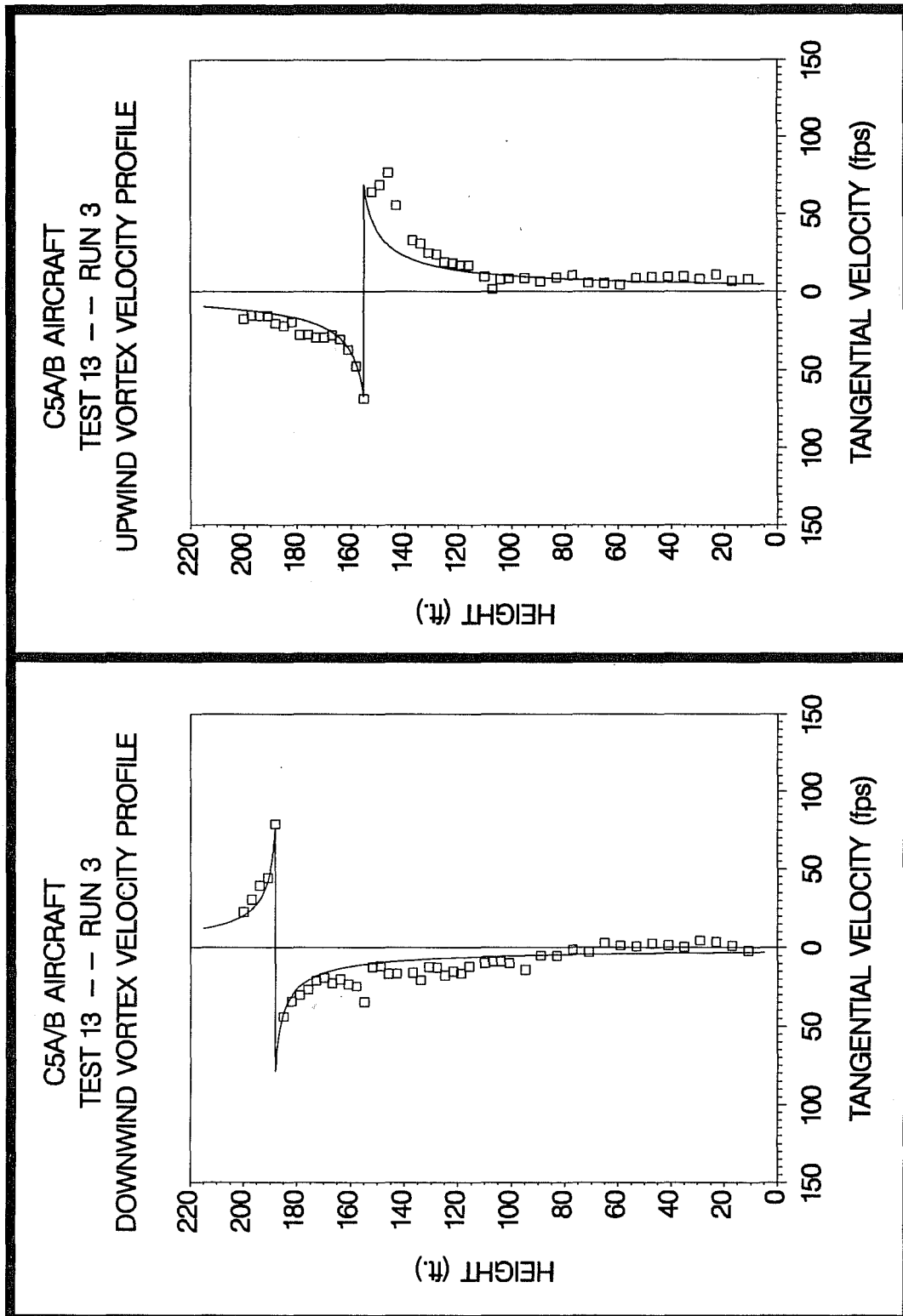


Figure 45A. C5A/B upwind (top) and downwind (bottom) vortex tangential velocity profile at maximum intensity from Test 13, Run 3, ambient wind speed=31.1 fps,  $\delta_F = 100\%$ , IAS=150 knots, GW=689k lb. Ages, radii, and velocities of the vortex cores are 12 and 8 sec., 2.6 and 1.4 ft., and 69 and 79 fps, respectively.

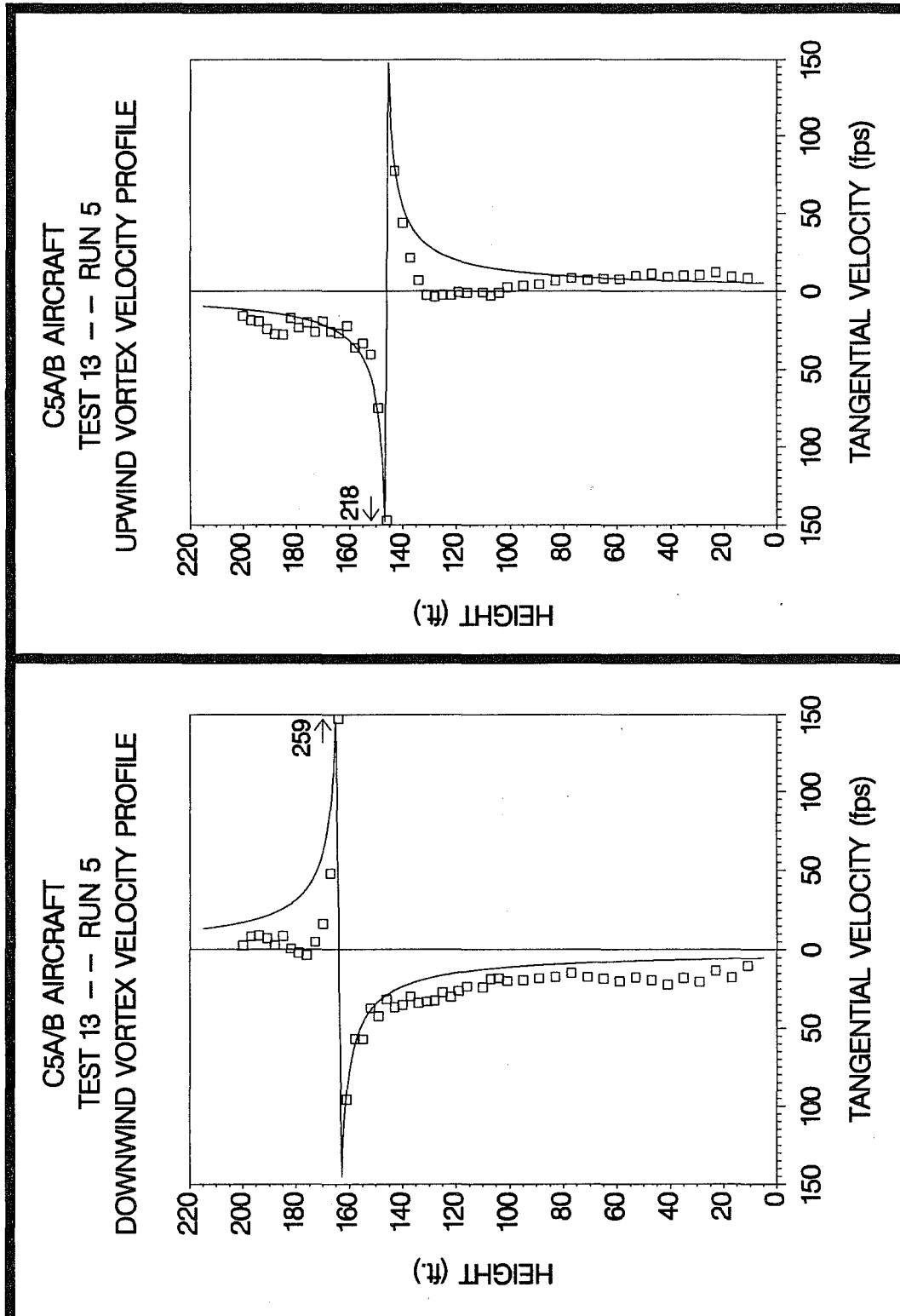


Figure 45B. C5A/B upwind (top) and downwind (bottom) vortex tangential velocity profile at maximum intensity from Test 13, Run 5, ambient wind speed=24.5 fps,  $\delta_F = 15\%$ , IAS=180 knots, GW=682k lb. Ages, radii, and velocities of the vortex cores are 14 and 7 sec., 0.7 and 0.6 ft., and 218 and 259 fps, respectively. Arrows and values above data points indicate an off-scale value.

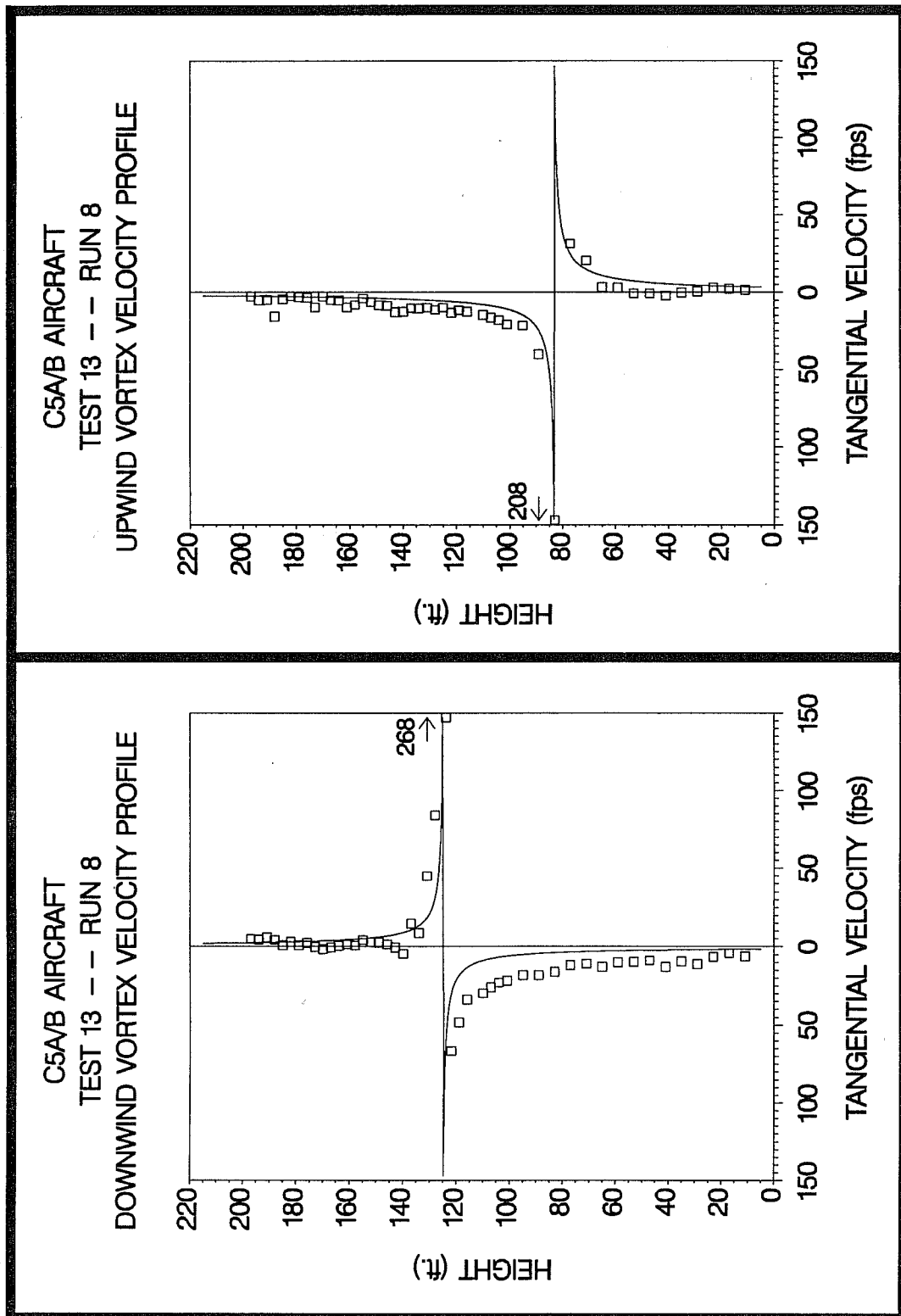


Figure 45C. C5A/B upwind (top) and downwind (bottom) vortex tangential velocity profile at maximum intensity from Test 13, Run 8, ambient wind speed=24.7 fps,  $\delta_F=15\%$ , IAS=175 knots, GW=670k lb. Ages, radii, and velocities of the vortex cores are 23 and 13 sec., 0.2 (measured) and 0.1 ft. (estimated), and 208 and 268 fps, respectively. Arrows and values above data points indicate an off-scale value.

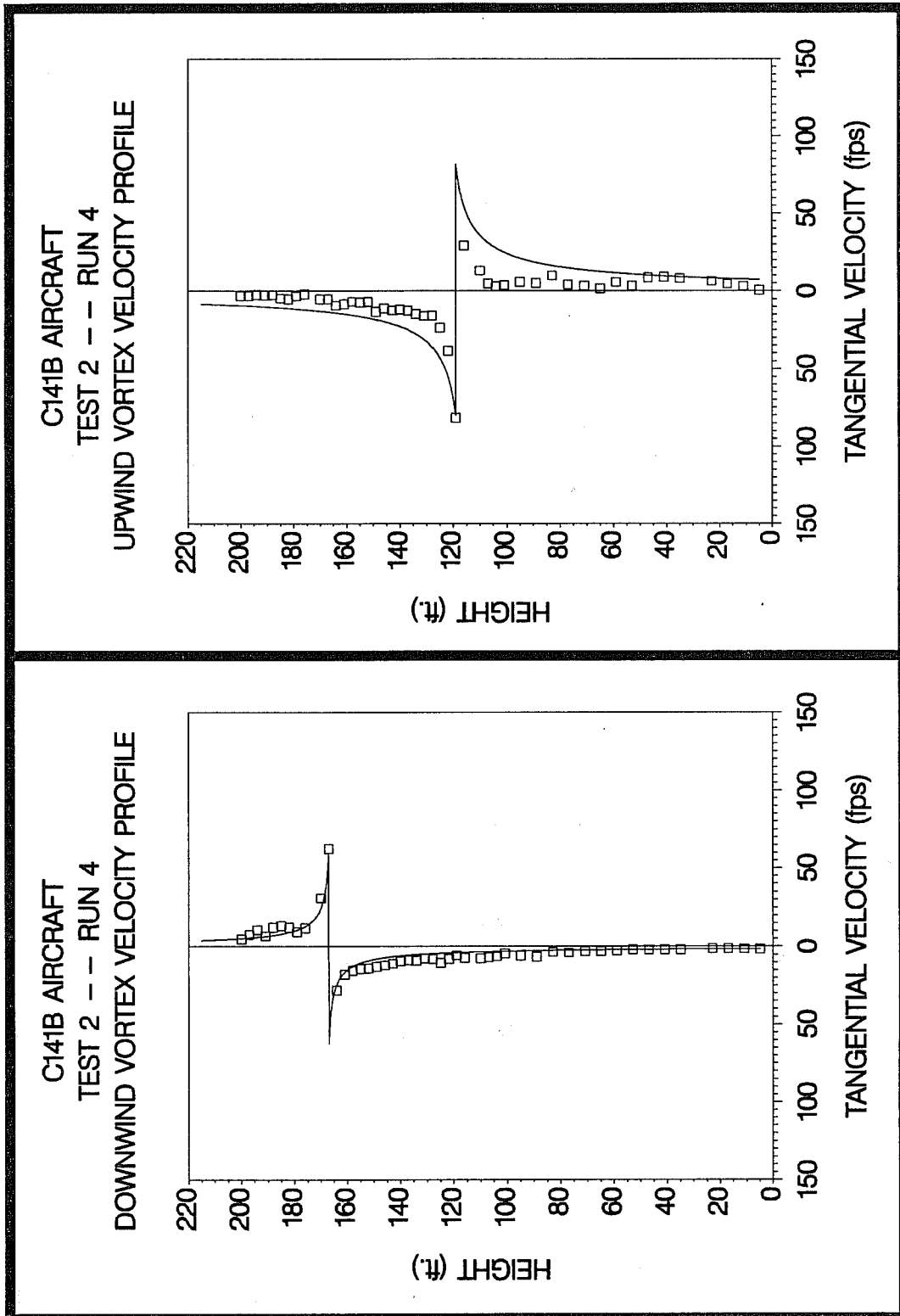


Figure 46A. C141B upwind (top) and downwind (bottom) vortex tangential velocity profile at maximum intensity from Test 2, Run 4, ambient wind speed=11.7 fps,  $\delta_F=39\%$ , IAS=150 knots, GW=225k lb. Ages, radii, and velocities of the vortex cores are 38 and 19 sec., 2.7 and 0.7 ft., and 82 and 63 fps, respectively.

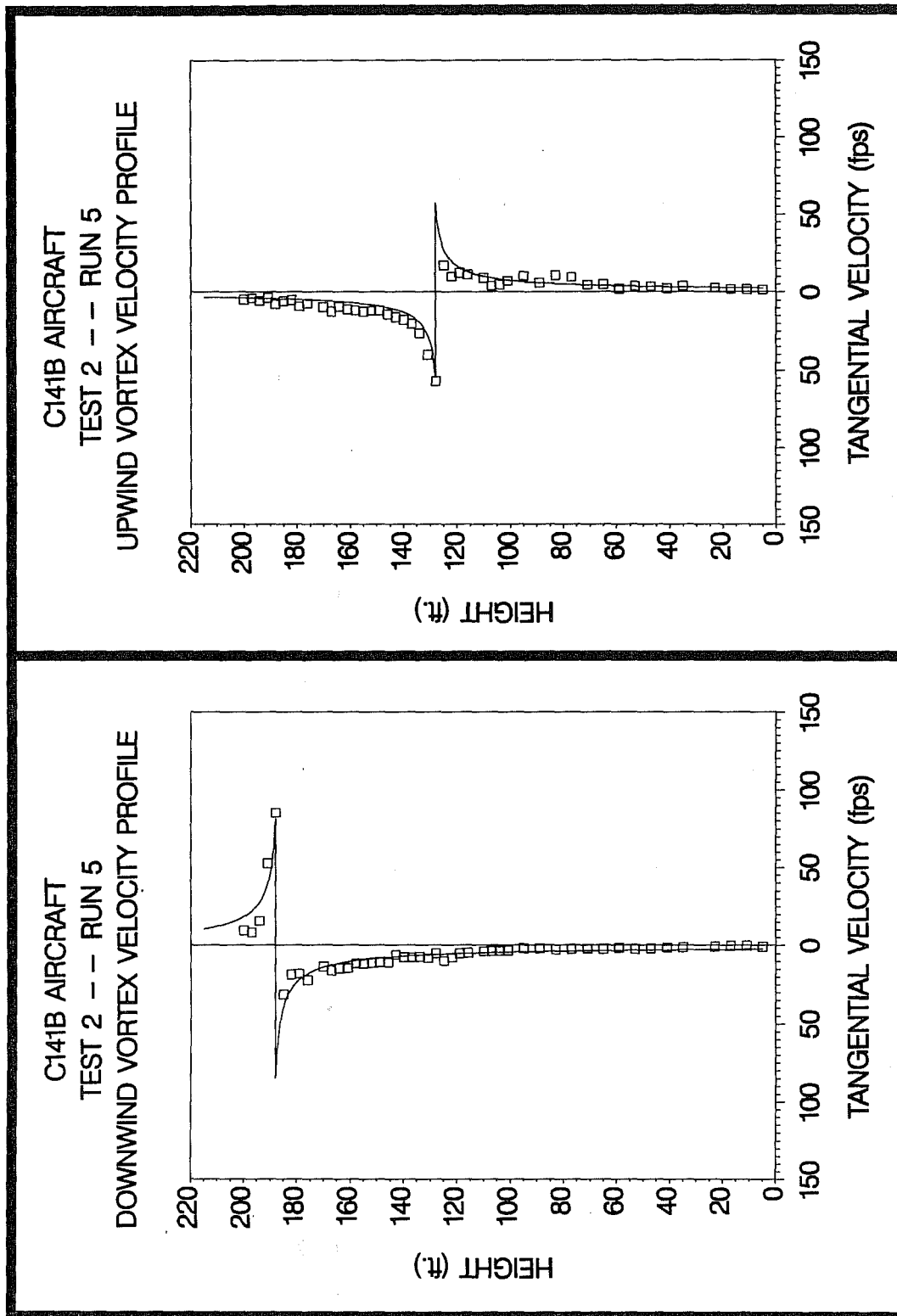


Figure 46B. C141B upwind (top) and downwind (bottom) vortex tangential velocity profile at maximum intensity from Test 2, Run 5, ambient wind speed=12.7 fps,  $\delta_F=39\%$ , IAS=150 knots, GW=223k lb. Ages, radii, and velocities of the vortex cores are 28 and 14 sec., 1.1 (measured) and 0.7 ft. (estimated), and 57 and 85 fps, respectively.

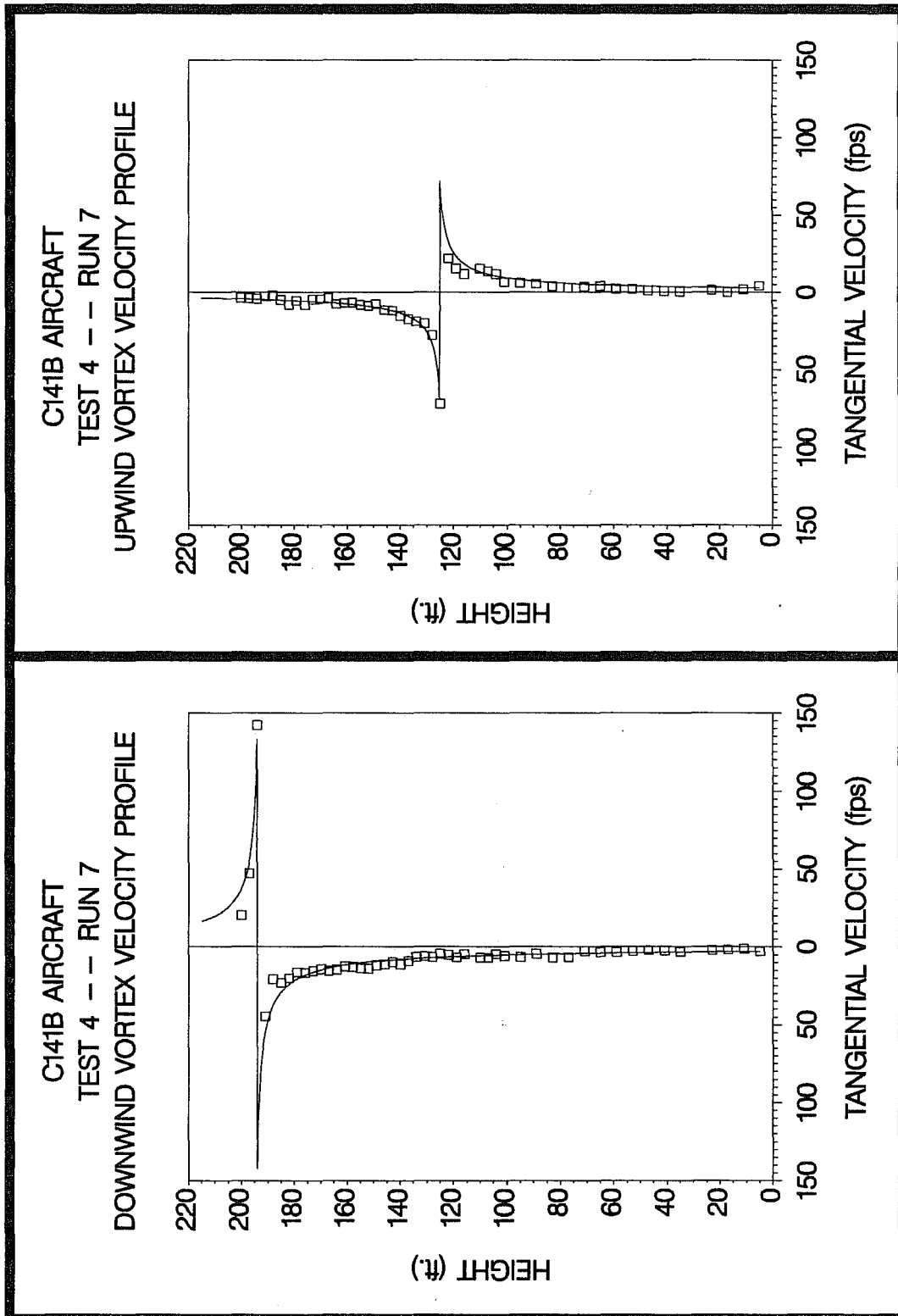


Figure 46C. C141B upwind (top) and downwind (bottom) vortex tangential velocity profile at maximum intensity from Test 4, Run 7, ambient wind speed=5.8 fps,  $\delta_F=11\%$ , IAS=180 knots, GW=257k lb. Ages, radii, and velocities of the vortex cores are 39 and 17 sec., 1.0 (estimated) and 0.7 ft. (measured), and 72 and 142 fps, respectively.

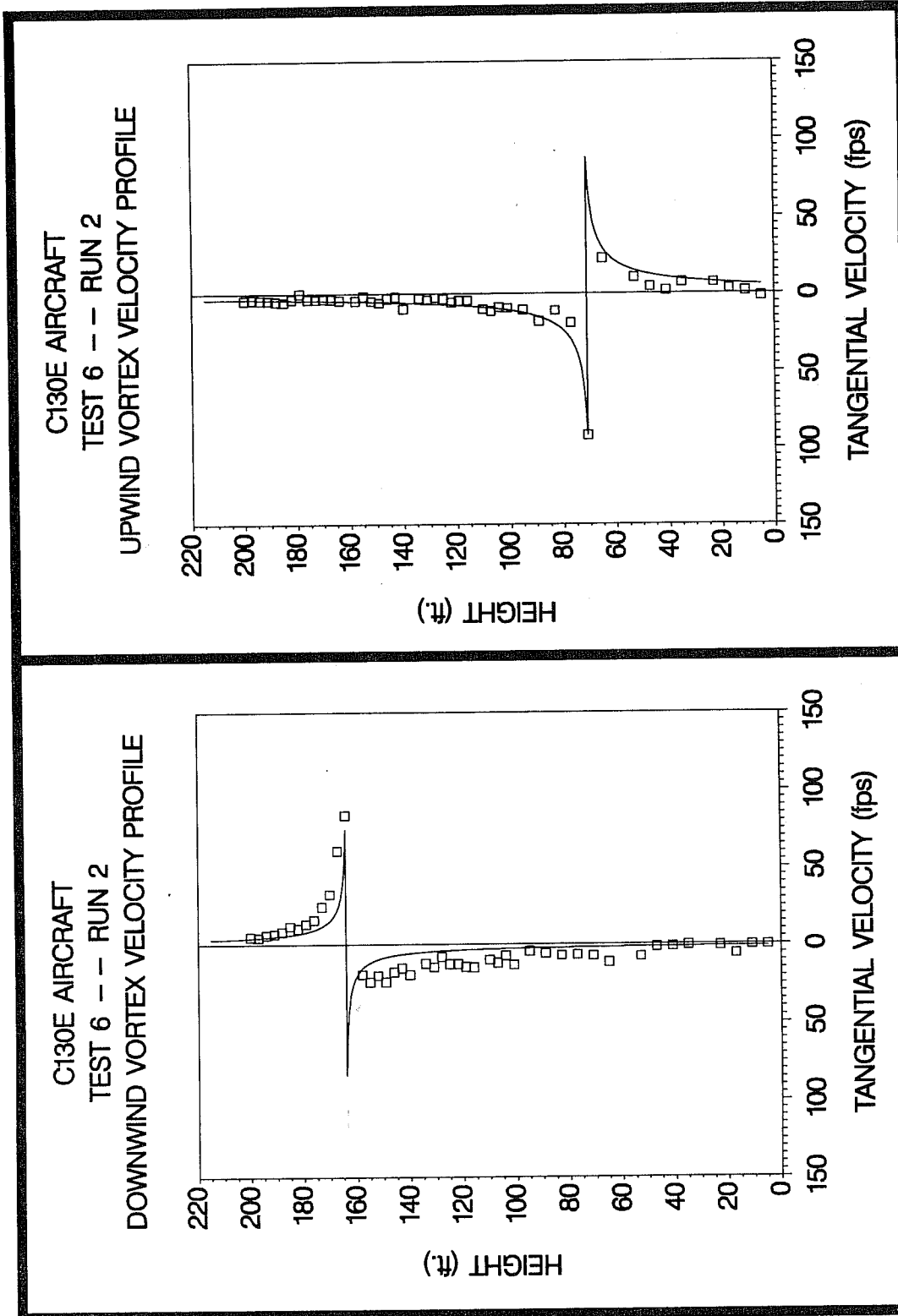


Figure 47A. C130E upwind (top) and downwind (bottom) vortex tangential velocity profile at maximum intensity from Test 6, Run 2, ambient wind speed=6.3 fps,  $\delta_F=27\%$ , IAS=130 knots, GW=145k lb. Ages, radii, and velocities of the vortex cores are 35 and 20 sec., 1.0 and 0.4 ft., and 92 and 84 fps, respectively.

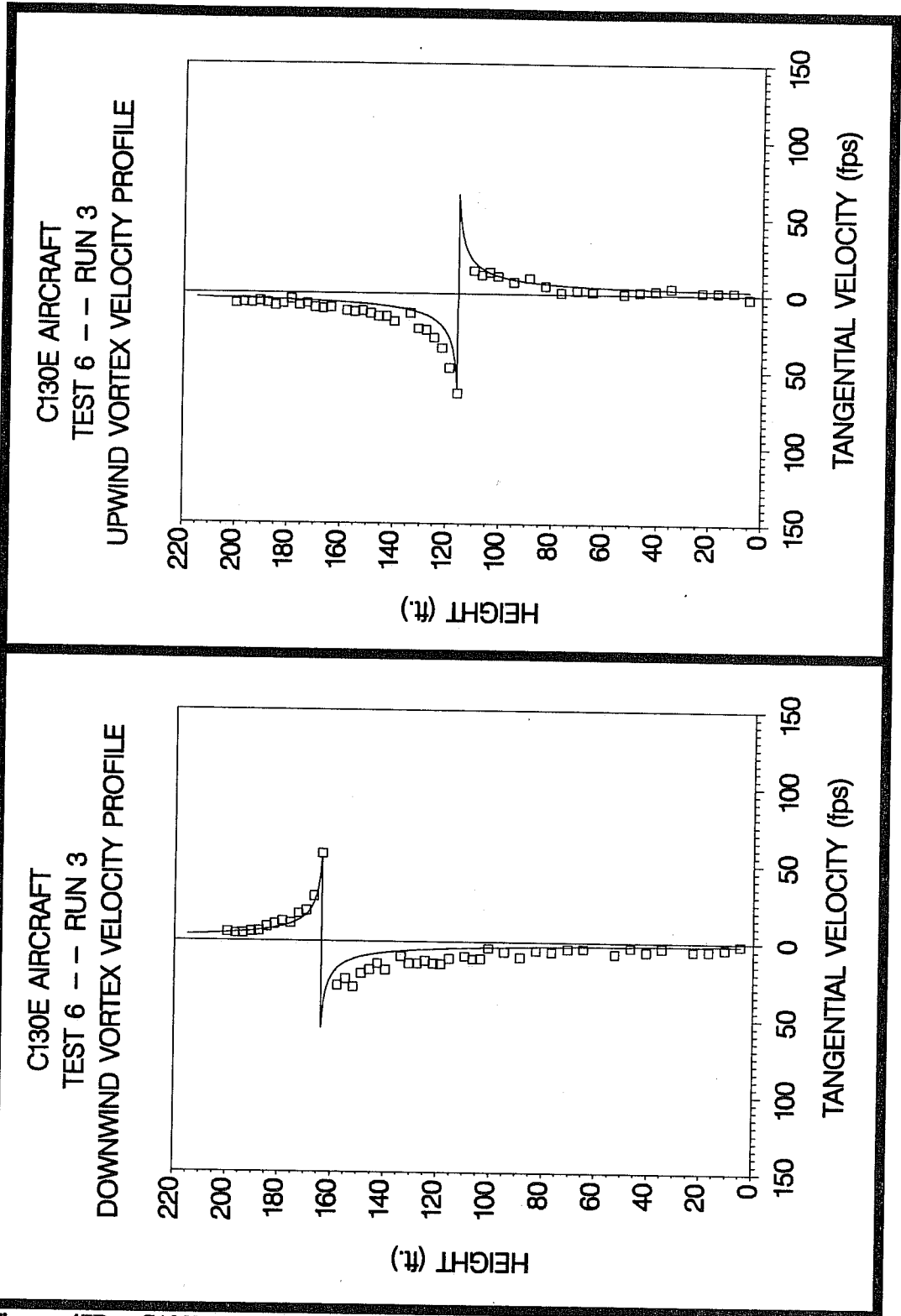


Figure 47B. C130E upwind (top) and downwind (bottom) vortex tangential velocity profile at maximum intensity from Test 6, Run 3, ambient wind speed=6.3 fps,  $\delta_F=27\%$ , IAS=130 knots, GW=144k lb. Ages, radii, and velocities of the vortex cores are 25 and 17 sec., 1.0 (measured) and 0.9 ft. (estimated), and 65 and 57 fps, respectively.

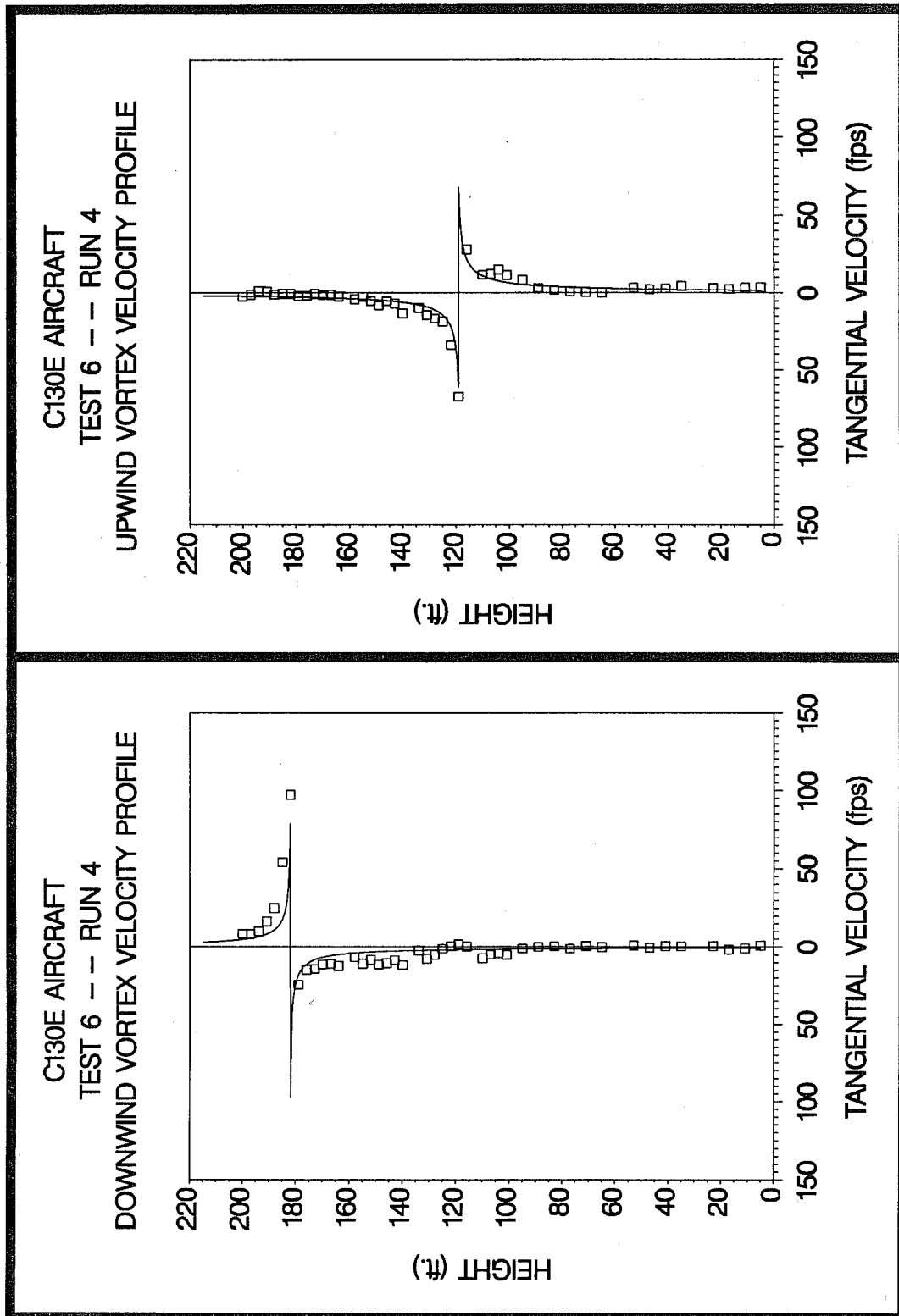


Figure 47C. C130E upwind (top) and downwind (bottom) vortex tangential velocity profile at maximum intensity from Test 6, Run 4, ambient wind speed = 6.2 fps,  $\delta_F = 0\%$ , IAS = 180 knots, GW = 143k lb. Ages, radii, and velocities of the vortex cores are 35 and 19 sec., 0.5 and 0.2 ft., and 68 and 97 fps, respectively.

Although the data were available, no detailed analysis was performed on vortex characteristics as a function of vertical ambient wind velocity gradients (boundary layer profile). Such analyses were considered to be beyond the scope of this task. From an ATC operational application view point, the analysis concentrated on the analyses specified above. However, air temperature and wind velocity profiles at the beginning and the termination of each test period are provided in Appendix B.

## DISCUSSION

The vortices of all three airplanes did not persist for longer than 180 seconds as shown in Figs. 11-13. The data show that longer-lived vortices were generated by the C141B as compared to the C5A/B. The C5A/B vortex tangential velocities were significantly higher than those generated by the C141B with similar ages. The long-lived C141B vortices greater than 120 seconds exhibited very low velocities and were too low to be of any significance. The large spread in observed maximum tangential velocities at relatively young ages are due to various factors, including flap settings.

The visual record of vortex behavior contradicts the vortex ages observed in hot film data. Visual observations of tower-released smoke entrained within the vortex cores indicated that many of the C5A/B vortices did approach a 3 minute life span. This demonstrates that it may be possible to obtain longer-lived vortices than those actually measured during these flight tests. This presumption is most significant inasmuch as the present ATC operation standards for terminal area type flights, including parallel runway operations, are based on a 120 second maximum time to dissipation premise. The standards were derived after considerable full-scale flight test investigations of vortex systems of other airplanes.

The possibility of C5A/B vortex ages older than 3 minutes should be viewed with a certain degree of caution. Attempts to obtain longer time-history data on C5A/B vortex persistence did not result in older vortices. Even though the aircraft flight path distances from the tower were as great as 2500 ft., strong ambient wind speeds which occurred during the C5A/B flight tests rapidly advected the wake vortex to the tower. The greater offset distances made it difficult to maintain passage of the wake vortex system through the tower. Many of the vortices generated under these conditions did not advect through the tower. When the vortices did pass through the tower, the ages were still less than 120 seconds. Since no vortex flow visualization system was installed on the C5A/B airplane, it was not possible to ascertain the movement or the dissipation mode of the vortices which did not pass through the tower and entrain the tower-released smoke. The USAF did not require a large amount of very long vortex time-history data. Hence most of the data collection effort was concentrated on younger vortices.

It is pertinent to point out that most of the recorded data was acquired under ambient atmospheric conditions considered to be quite unstable by both meteorological definition and actual encounter. The atmosphere at the test site is historically stable during the nocturnal hours. About 1-3 hours after sunrise, the atmosphere enters a transition phase, followed by unstable conditions for the remainder of the day. The flight tests were conducted after sunrise,

with a significant portion during the afternoon. That is the period of the day wherein atmospheric turbulence is historically expected.

The plots of vortex persistence as a function of ambient wind speed (Figs. 14-22) indicate that ambient wind velocity is fairly well correlated with vortex persistence. Ambient wind speed is also a good indicator of the distance of vortex lateral movement. The three plots for vortex ages greater than 60 seconds (Figs. 16, 19, and 22) generally indicate that the vortices were most persistent in the 3 to 10 knot ambient wind speed band. Vortex ages greater than 60 seconds are in the time period of most interest regarding ATC operational applications. These trends agree very well with previous work reported by both NASA and the FAA, e.g. Garodz and Miller (1975) and Kurkowski et al. (1976).

In view of these results and the general vortex persistence plots of Figs. 11-13, it may be concluded that the FAA's 2,500 foot parallel runway lateral separation criteria for ATC aircraft spacing based on the vortex hazard is indeed valid. It may be marginal, however, for the C5A/B type airplane. Such a conclusion indicates the need for further flight tests with this type, size, and gross weight airplane under neutrally stable to stable atmospheric conditions. Exploration of the upper area limit of vortex persistence is still desirable. This is not necessarily of concern to the USAF which uses a 4 minute or 10 nautical mile separation criteria for aircraft following C5A/B aircraft in terminal area flight operations. It could very well be that the latter criteria may be somewhat over conservative.

The correlations of vortex persistence versus Richardson Number were somewhat disappointing or perplexing. They revealed a fairly persistent vortex system particularly for the C141B at ages greater than 60 seconds, even for negative values of  $Ri$  (Fig. 28).  $Ri$  is customarily determined using time averages of 15 minutes or longer. This type of averaging technique could not be employed during this study due to the nature of the tower fly-by technique. The very presence of aircraft wake turbulence measured by hot-film anemometers mounted on the tall tower also influences the collocated  $Ri$  meteorological sensors mounted on the same tower. Hence, small blocks of time are used when averaging ambient wind speed and air temperature to insure that the data are not influence by the presence of the vortex wake. The result can be wildly varying Richardson Numbers which are not well correlated with vortex persistence.

Another factor greatly influencing the correlation of  $Ri$  with vortex persistence is related to the method of data collection. The primary purpose of the flight tests was to obtain vortices of various strengths and ages. This obscures the secondary purpose to correlate  $Ri$  with  $V_{\theta}$ . Both parameters are allowed to vary during the course of the study which makes the deconvolution of the two signals difficult, if not impossible. Hence, future flight tests should maintain a category of constant vortex ages while the atmosphere is allowed to vary. Direct correlation would then be possible.

It is also possible that the definition of and numerical limits for the unstable, neutrally stable, and stable segments of the atmosphere in the earth's planetary boundary layer are not

well or properly defined or substantiated. Several references list various limits for these three segments or bands. Rosenberg (1970) states the following: "Ri of zero is neutral stability, negative Ri is instability, and positive Ri is stability" with no further resolution as to the degree of stability or instability. Lumley and Panofsky (1964) and Hansen (1967) also discuss Ri and certain limits regarding the unstable, neutrally stable, and stable regimes. However, the peripheral (atmospheric condition) qualifiers regarding useful or appropriate application of Ri make this parameter too complex to use at this time with any degree of confidence. The Ri parameter may have been oversold by some as being the "magic" parameter to use in predicting vortex life span after generation.

The somewhat greater persistence of the vortices under rather unstable (by definition) ambient atmospheric conditions may be due in part to aircraft design geometry when compared to other large commercial jet transport aircraft. As previously stated, all three aircraft tested are high wing airplanes with relatively high aspect ratios. The high wing design is obviously necessary for operational mission considerations. However, it also affects the induced and parasite (interference) drag characteristics of the airplane differently as compared to a low or mid-wing configured aircraft. The high wing permits an undisturbed air flow over the top of the wing which provides additional lift compared to a mid or low wing design of identical wingspan. A detailed analysis regarding the air flow relative to a high wing type airplane and the subsequent characterization of the vortex flow field would require knowledge of the wing load distribution in each flight configuration. Such was not available for this investigation.

The geometry of the low-slung jet engines found on the C5A/B and the C141B (generally lower than commercial jet transport engines) may also increase vortex longevity. Their position would diminish the interaction of the wing vortex sheet with the jet engine exhaust. In addition, the engines on the C5A/B are placed low enough beneath the wing that flap cut-outs are not needed (see Fig. 6A). This type of wing configuration would preclude the generation of multiple flap vortices which would normally accelerate vortex decay during take-off or landing. An engine position effect would not be observed on the C130E airplane, which has turbo-prop engines in line with the wing chord. Because the engines are in line with the wing chord, the fore-aft airflow over the wing in forward flight is accelerated in the wing areas behind the engine nacelles by the propeller slipstream. As the flaps are deflected, a pseudo-localized jet flap situation is created in 4 areas laterally along the wing. This results in additional circulation and lift on the airplane. With increased flap deflection and accompanying increased drag, additional engine thrust is required. This, in turn, will further increase the circulation on the wing.

No detailed examination of the data was made to determine the effects of propeller rotation direction and slipstream on the trailing vortices. Intuitively, the vortex rotating in the same direction as the propellers (and near-field slipstream) might be more orderly, intense or persistent when compared with the opposite wing vortex/slipstream interaction. This would probably be more pronounced as the landing flaps were lowered. The landing flap vortex would likely become the predominant vortex and would roll-up at a position further inboard of the unflapped or clean-wing vortex. The vortex would be closer to the outboard engine slipstream/jet engine exhaust centerline. Further detailed examination of the data might clarify

this, assuming sufficient out of ground-effect data are available with very short time differences between upwind and downwind tower/vortex interceptions.

The T-tail geometry of the C5A/B and C141B may also contribute to the persistence of the vortices. The T-tail horizontal surface is also a lifting surface (negative lift) which generates its own vortex pair. This pair normally does not become imbedded in the wing vortex sheet or down wash flow field unless the airplane angle of attack is extremely high and approaching stall. Imbedded vortices are usually found on commercial jet transport airplanes like the B747, for example. Thus, there is very little or no interaction between the wing vortex sheet and the horizontal T-tail vortex system which would be one less disturbance imposed upon the wing trailing vortex system.

No detailed analysis was made or attempted regarding the effect of wing configuration changes on trailing vortex wake characteristics. However, a cursory look at the vortex tangential velocity flow fields as a function of wing configuration (flap and leading edge slat deflection or extension, as appropriate) for the C5A/B and C141B revealed that higher peak velocities were recorded when the wing was clean. Conversely, lower peak vortex velocities were recorded with increased flap deflection. This was not unexpected in that similar conclusions were noted for previous full-scale vortex wake flight tests conducted with other large jet transport aircraft.

The vortex tangential velocities of the C130E aircraft appeared to be fairly independent of landing flap deflection. This could be for reasons cited earlier in that increased flap deflection required increased engine thrust. This produced a condition analogous to a jet-flap wing configuration at 4 locations laterally along the wing behind the turbo-prop engines. This, in turn, produced an increase in dynamic pressure aft of the propellers, added momentum to the slipstream, momentum lift from slipstream curvature due to the flap deflection, and circulation to the wing. The summary plots of  $V_{\theta}$  versus age for all aircraft and all configurations indicate the worst case scenario regarding vortex persistence and movement in close proximity to the ground. These are the cases most applicable to ATC separation standards in the terminal area.

A cursory look was made at the nature of the radial distribution of vortex tangential velocity, i.e.,  $V_{\theta}$  versus  $r$ . In most cases, a logarithmic variation of vortex tangential velocity as a function of vortex radius (Eqn. 5) appeared to fit the data fairly well. Figures 45A-47C illustrate this agreement. This same type of tangential velocity distribution has been observed in several previous full-scale vortex wake flight test measurements using the tower fly-by and other flight test techniques (e.g. Eisenhuth et al., 1971 and Garodz, 1976).

**This page intentionally left blank.**

## CONCLUSIONS

- In general, the maximum duration of the vortex systems for all three airplanes was approximately two minutes under all tested configurations and atmospheric conditions. The vortex systems followed the classical intensity and persistence envelopes of  $V_\theta$  vs. time, and duration vs. ambient wind velocity, respectively.
- The C5A/B vortex time-history data obtained from visual observation revealed a relatively high residual vortex tangential velocity for certain data runs at the upper time limit of two minutes.
- Inasmuch as these particular flight tests were conducted to meet USAF tactical operational needs, it was not possible to acquire longer time-history (persistence/intensity) vortex wake data on the C5A/B airplane during the course of these flight tests.
- It is not known, at this time, with any high degree of certainty, if the C5A/B vortex persists longer than two minutes with any significant intensity.
- Lack of an aircraft-mounted vortex flow visualization system on the C5A/B precluded determination of the vortex decay mode. In some cases it also precluded the determination of persistence, i.e., organized rotary flow after tower passage when the tower smoke had dissipated.
- Additional longer time-history data are required on the C5A/B airplane if the airplane is to be operated from non-military type airports with a mix of other commercial type aircraft. This is necessary to insure safe ATC separation (based on the vortex hazard) of departing and arriving aircraft, including operations with parallel runways. Similar type aircraft (size and weight) such as the Boeing 747-400 should also be tested.
- An unstable ambient atmospheric condition existed during approximately 73% of the time during these flight tests. Neutral conditions were observed 14% of the time while stable conditions occurred 13% of the time, as determined by NRC stability categories based on vertical air temperature gradients (Anon., 1980).
- The recorded data indicated that many of the vortices persisted at fairly high tangential velocities for ages greater than 60 seconds, even under relatively highly unstable ambient air mass conditions.
- Insufficient long-term meteorological data was acquired during these flight tests to be able to definitely correlate vortex persistence as a function of Richardson Number (Ri). The test design specified wind speed and air temperature sensors to be mounted on the same tower as the hot film anemometers. Thus, the collection of those data were not continuous, which

is required for calculation of accurate  $Ri$ . In addition, the inability to acquire multiple vortex strengths and ages at constant  $Ri$  confounded the data. Deconvolution of the multitude of effects was not possible.

- The Richardson Number may be oversold as being the magic parameter with which to correlate vortex persistence in the earth's boundary layer.
- There appeared to be fairly good correlation between vortex persistence and certain ambient wind velocity spectra for vortex ages over 60 seconds in duration. These spectra were 2.5 to 5.5, 4.0 to 7.5, and 4 to 10 knots ambient wind velocity for the C130E, C141B, and C5A/B, respectively. The latter exhibited the most scatter wind speed-wise. These results correspond fairly closely with those acquired during previous full-scale flight test investigations of aircraft vortex wake characteristics which simulated terminal area flight operations and which were conducted at various locations over the past 20 years.
- The wind speed bands, composed primarily of a crosswind, also compared favorably with that crosswind component which was developed by the FAA in the mid-1970's as a result of extensive vortex data collection in the field. The latter were used in the Vortex Advisory System (VAS) algorithm.
- There also appeared to be some correlation, although limited, between vortex persistence and temperature gradient recorded along the vertical span of the test tower.
- The C130E trailing vortex system exhibited sinuous type instability or Crow instability on the majority of the fly-bys, as visualized by the vortex flow visualization system mounted on the wings. Whether this was due to vortex/atmospheric interaction, vortex interaction with its ground induced image, or vortex/propeller slipstream interaction is not clearly known. The latter is suspected because Crow instability was rarely, if at all, experienced with the C141B which had identical smoke generators mounted on the wings and was flown under similar atmospheric conditions.
- In general, there appeared to be good correlation between peak recorded vortex tangential velocity and the percent of landing flap deflection.  $V_\theta$  decreased with increased  $\delta_F$  on the C5A/B and C141B. This was expected, based upon previous flight tests with other airplanes. For example, for identical vortex ages generated by the C5A/B,  $V_\theta$  went from 191 to 259 feet/second for 15% flaps, to approximately 77 to 79 feet/second for 100% flaps. However, the C130E did not exhibit this trend to any noticeable degree, which perhaps could be due to propeller-wash/vortex sheet interaction during the vortex roll-up process.
- The C130E did not exhibit a correlation between peak recorded vortex tangential velocity and the percent of landing flap deflection. This could be due to the fact that increased flap setting required higher engine thrust because of the increase in airplane drag. This, in turn, added momentum to the slipstream and circulation to the wing.

## RECOMMENDATIONS

- In view of the findings on the C5A/B vortex wake characteristics, particularly the persistence of the wake with still relatively high residual vortex tangential velocities, the FAA should consider some additional limited, but very precisely controlled C5A/B vortex wake tower fly-by and probe flight tests. These should be conducted at high gross weights to insure that this airplane, when operated from commercial airports, properly fits into the Heavy category regarding separation standards in terminal area-type flight operations. It may well be that a "Super-Heavy", or a similarly named category, should be designated for this high weight aircraft (greater than 700,000 pounds), and appropriate separation standards established.
- It is strongly recommended that flight tests be undertaken as soon as possible to gather quantitative data on the vortex wake characteristics of the Boeing B-747-400 using the tower fly-by technique. If flow visualization can also be installed in this airplane, then some vortex probe tests should also be conducted. The B-747-400 should be operated at the maximum take-off gross weight of 800,000 pounds. If the flight test results are similar to those of the C5A/B, then it too, may belong in a "Super-Heavy" category. It may be that some separation standard between that used by the USAF (4 minutes or 10 nautical miles) and that used by the FAA ATC system might be appropriate for flight operations behind this airplane class.
- Until further full-scale vortex wake flight test data are acquired on Heavy category aircraft, it is recommended that the present parallel runway separation distance criteria of 2,500 feet continue to be adhered to by ATC.
- The FAA should continue to use the ambient wind velocity as a vortex persistence parameter for any projected deployment and use of a vortex advisory system or wake vortex avoidance system. This should continue until such time as a low cost, reliable, easily maintainable, and unobstructive meteorological data acquisition system can be developed, tested, and proven in the field that it provides an improved and reliable index/parameter for correlation with vortex persistence.
- Either NASA or large aircraft manufacturers, e.g., Boeing and McDonald Douglas, should undertake studies to examine and compare the vortex characteristics of high-wing versus low-wing, and T-tail versus conventional-tail characteristics of large jet transport type aircraft. This could be for either proposed or currently operational aircraft, with the objective of determining if one particular aircraft geometry produces trailing vortex systems which are more intense and/or persistent than another.

**This page intentionally left blank.**

## REFERENCES

- Anon. 1980. Meteorological programs in support of nuclear power plants. U.S. NRC Regulatory Guide 1.23 (Rev. 1). U.S. Nuclear Regulatory Commission, Washington, D.C.
- Clawson, K. L. 1988. Measurement of wingtip vortex characteristics from C-130, C-141 and C-5A/B aircraft. U.S. Dept. of Commerce, National Oceanic and Atmospheric Administration, Air Resources Laboratory Field Research Division, Idaho Falls, ID.
- Condit, P. M., and P. W. Tracey. 1970. Results of the Boeing wake turbulence test program. Boeing Document No. D6-3085H. Boeing Aircraft Corp., Seattle, WA.
- Crow, S. D. 1970. Stability theory for a pair of trailing vortices. AIAA J. 8:2172-2179.
- Eisenhuth, J. J., B. W. McCormick, R. C. Nelson, and L. J. Garodz. 1971. Analysis of experimental measurements of trailing vortex systems of large jet transport aircraft. Aero Engineering Associates, State College, PA.
- Garodz, L. J. 1970. Investigation of the relatively long time history vortex characteristics of the Convair CV-880 airplane in terminal area type flight operation: Flight test period July-August, 1970. FAA Data Report Project No. 504-303-03X (Special Task Number Three). U.S. Department of Transportation, Federal Aviation Administration, Washington, D.C.
- Garodz, L. J. 1976. Abbreviated full-scale flight test investigation of the Lockheed L1011 trailing vortex system using tower fly-by technique. Report No. FAA-AFS-1-76-2. U.S. Department of Transportation, Federal Aviation Administration, Washington, D.C.
- Garodz, L. J., D. Lawrence, and N. Miller. 1976. Measurement of the trailing vortex systems of large transport aircraft, using tower fly-by and flow visualization: Summary comparison, and application. Report No. FAA-RD-75-127. U.S. Department of Transportation, Federal Aviation Administration, Washington, D.C.
- Garodz, L. J. and N. Miller. 1975. Investigation of the vortex wake characteristics of jet transports during climbout and turning flights. Report No. FAA-AEQ-75-1. U.S. Department of Transportation, Federal Aviation Administration, Washington, D.C.
- Hansen, F. V. 1967. Spacial and temporal distribution of the gradient Richardson Number in the surface and planetary layers. ECOM-5123 Report, Atmospheric Sciences Laboratory, White Sands Missile Range, NM.

Kurkowski, R. L., M. R. Barber, and L. J. Garodz. 1976. Characteristics of wake vortex generated by a Boeing 727 jet transport during two-segment and normal ILS approach flight paths. NASA Technical Note NASA TN D-8222. Ames Research Center, Moffett Field, CA.

Lumley, J. L., and H. A. Panofsky. 1964. The structure of atmospheric turbulence. Interscience Publishers, John Wiley and Sons, New York, NY.

McGowan, W. A. 1971. Aircraft wake turbulence avoidance. *In* NASA Headquarters 12th Anglo-American Aeronautical Conference, Calgary, July 7-9, 1971. Canadian Aeronautics and Space Institute, Ottawa, Canada.

Rosenberg, N. J. 1970. Microclimate: The biological environment. John Wiley and Sons, New York, NY.

## **APPENDIX A**

### **Test Aircraft Specifications**

## Lockheed C5A/B Galaxy

Wingspan	222 feet, 8 inches
Length	247 feet, 10 inches
Height	65 feet, 1 inch
Wing Area	6,200 square feet
Wing Root Chord	45 feet, 5 inches
Wing Tip Chord	15 feet, 4 inches
Wing Aspect Ratio	7.75 (Span/Average Chord)
Wing Taper Ratio	0.34
Wing Quarter-Chord Sweep Back	25 degrees
Maximum Takeoff Weight	764,500 pounds
Maximum Landing Weight	635,850 pounds
Powerplant	General Electric TF39-GE=1 Turbofan (4)

The C5A lateral control system consists of conventional ailerons outboard and differentially-operated flight spoilers inboard. High-lift devices are full span leading-edge slats and Fowler flaps. There are no cut-outs in either of these two devices. The engines are placed low enough beneath the wing that flap cut-outs are not needed.

## Lockheed C141B Starlifter

Wingspan	160 feet
Length	168 feet
Height	39 feet, 3 inches
Wing Area	3,228 square feet
Wing Root Chord	33 feet, 2 inches
Wing Tip Chord	N/A
Wing Aspect Ratio	7.9 (Span/Average Chord)
Wing Taper Ratio	N/A
Wing Quarter-Chord Sweep Back	25 degrees
Maximum Takeoff Weight	316,600 pounds
Maximum Landing Weight	257,700 pounds
Powerplant	Pratt & Whitney TF33-P-7 (4)

The lateral control system consists of conventional ailerons outboard and differentially-operated flight spoilers inboard. Fowler flaps extend over the complete trailing-edge of the wing inboard of the ailerons.

## Lockheed C130E Hercules

Wingspan	132 feet, 7 inches
Length	97 feet, 9 inches
Height	38 feet, 3 inches
Wing Area	1745 square feet
Wing Root Chord	16 feet, 0 inches
Wing Tip Chord	N/A
Wing Aspect Ratio	10.09 (Span/Average Chord)
Wing Taper Ratio	N/A
Wing Quarter-Chord Sweep Back	0 degrees
Maximum Takeoff Weight (normal)	155,000 pounds
Maximum Landing Weight	130,000 pounds
Powerplant	Allison T56-A-7 Turbo Prop Engines (4)
Propeller Diameter	13 feet, 6 inches

The lateral control system consists of conventional aluminum alloy ailerons which have tandem-piston hydraulic boost, operated by either of two independent hydraulic systems. Aircraft has Lockheed-Fowler aluminum alloy trailing-edge flaps. Trim-tabs are on the ailerons.

## **APPENDIX B**

### **Temperature and Wind Velocity Profiles at Start and Termination of Each Flight Test Period**

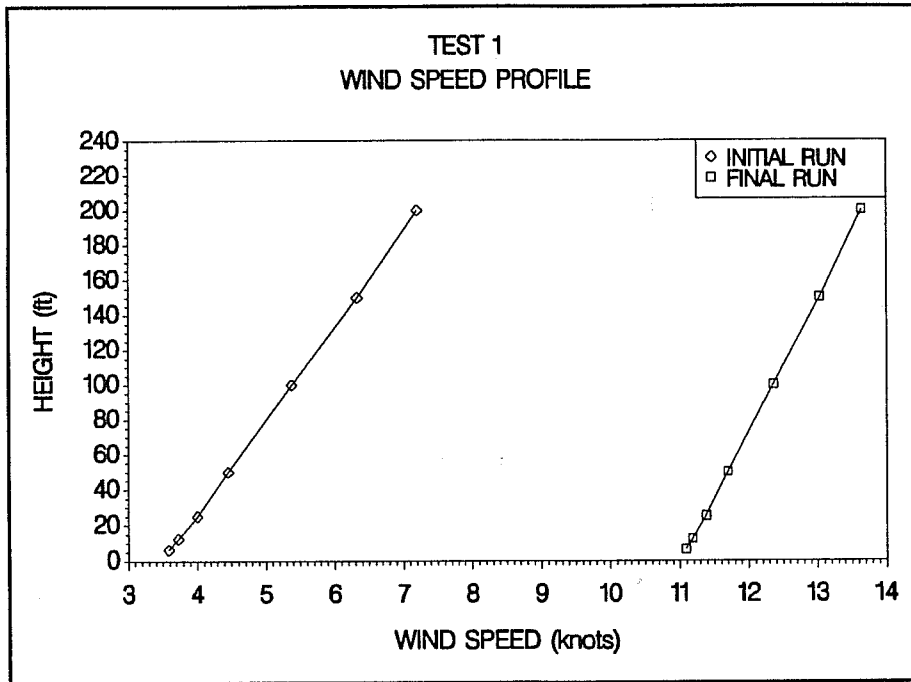


Figure B-1A. Wind speed profiles for the initial and final fly-bys of test 1 (C130E).

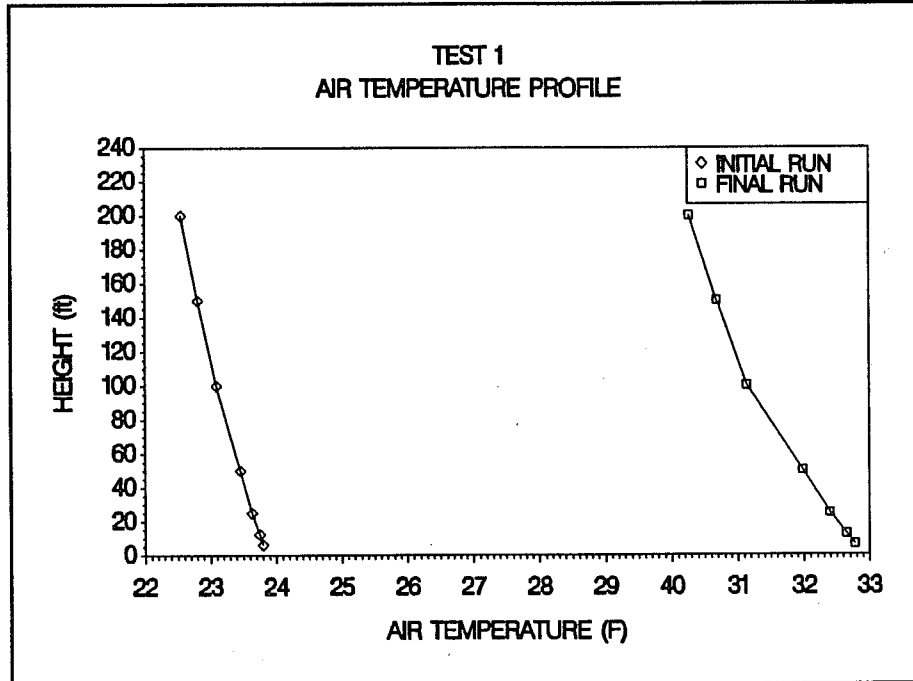


Figure B-1B. Air temperature profiles for the initial and final fly-bys of test 1 (C130E).

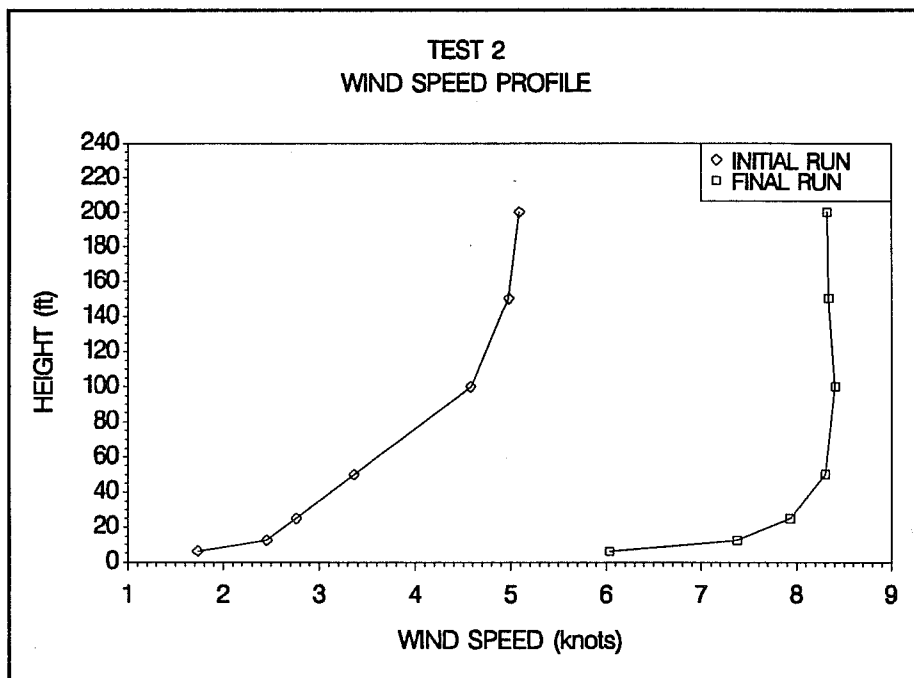


Figure B-2A. Wind speed profiles for the initial and final fly-bys of test 2 (C141B).

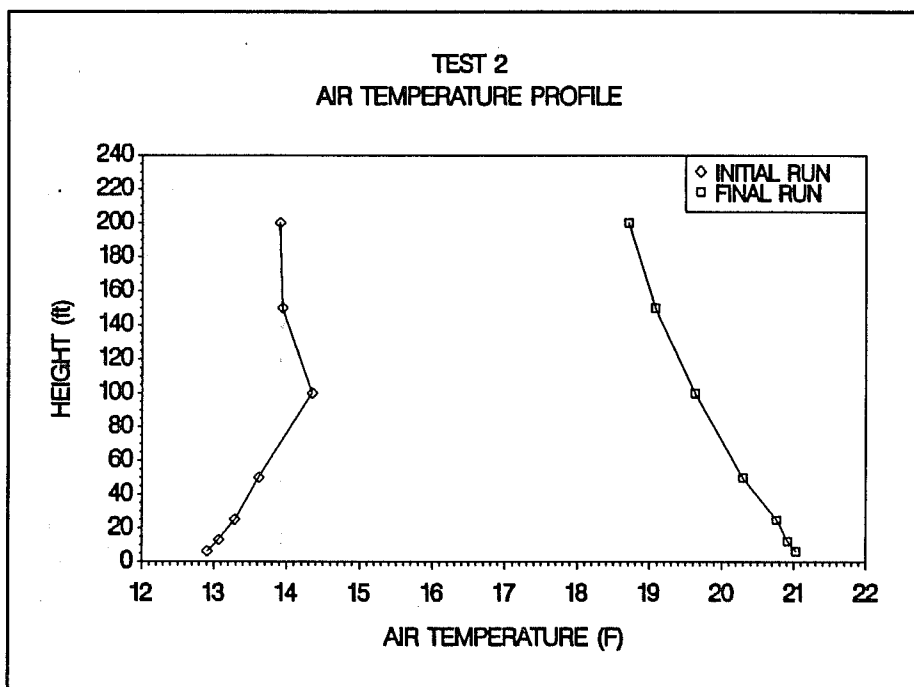
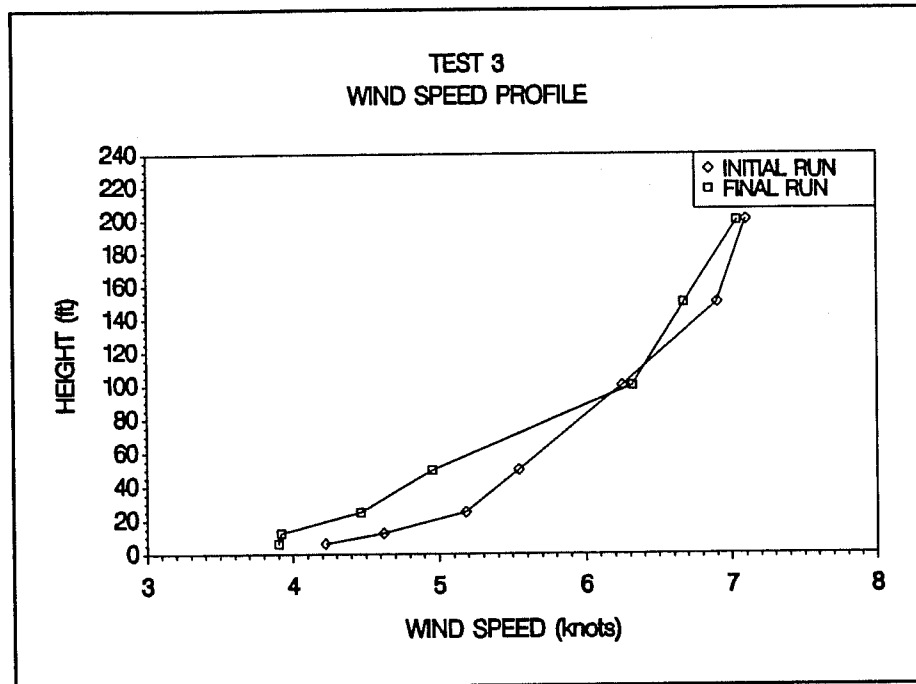
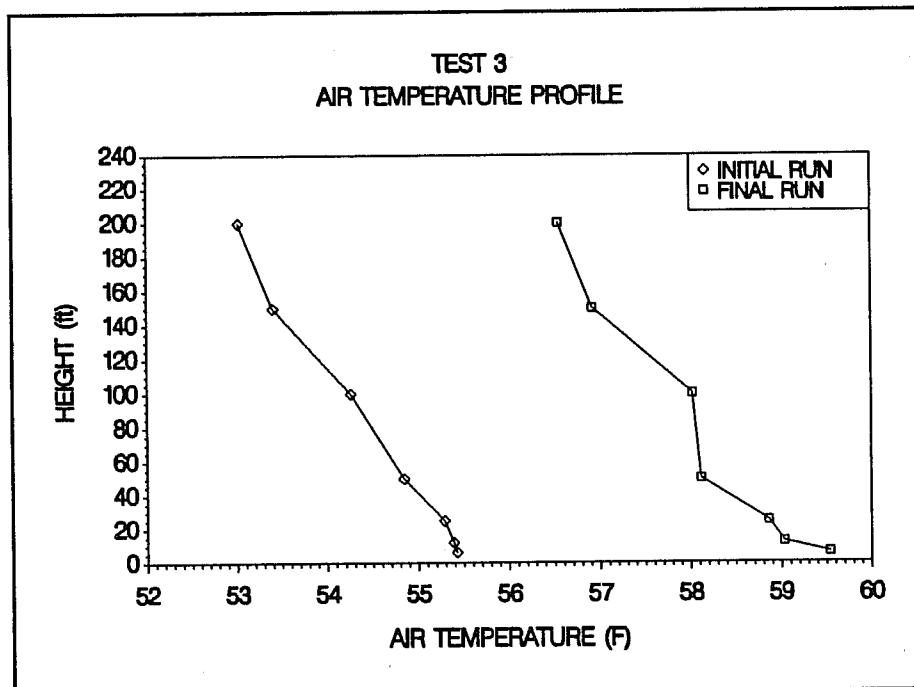


Figure B-2B. Air temperature profiles for the initial and final fly-bys of test 2 (C141B).



**Figure B-3A.** Wind speed profiles for the initial and final fly-bys of test 3 (C141B).



**Figure B-3B.** Air temperature profiles for the initial and final fly-bys of test 3 (C141B).

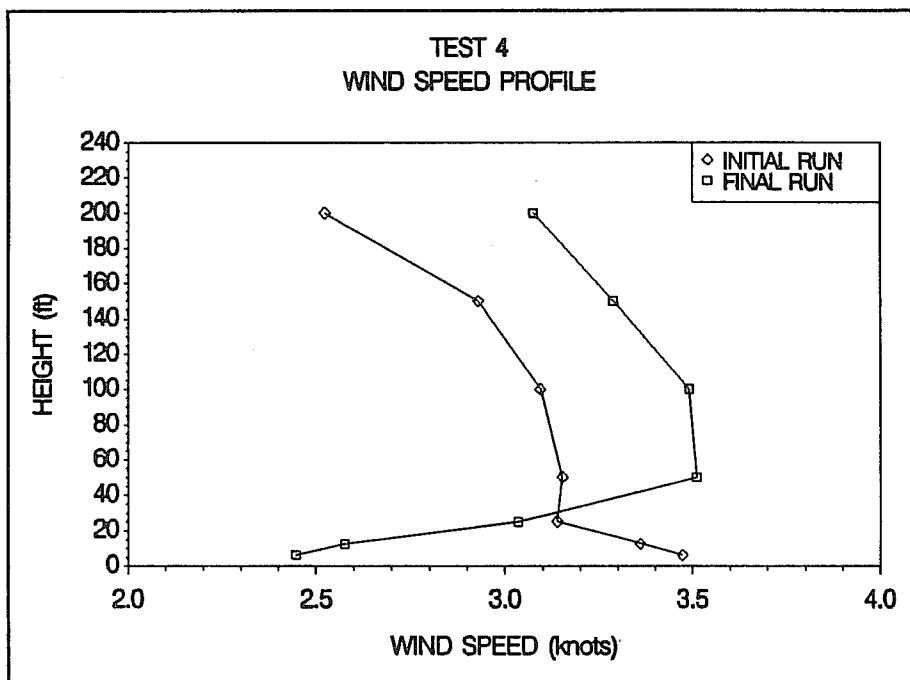


Figure B-4A. Wind speed profiles for the initial and final fly-bys of test 4 (C141B and C130E).

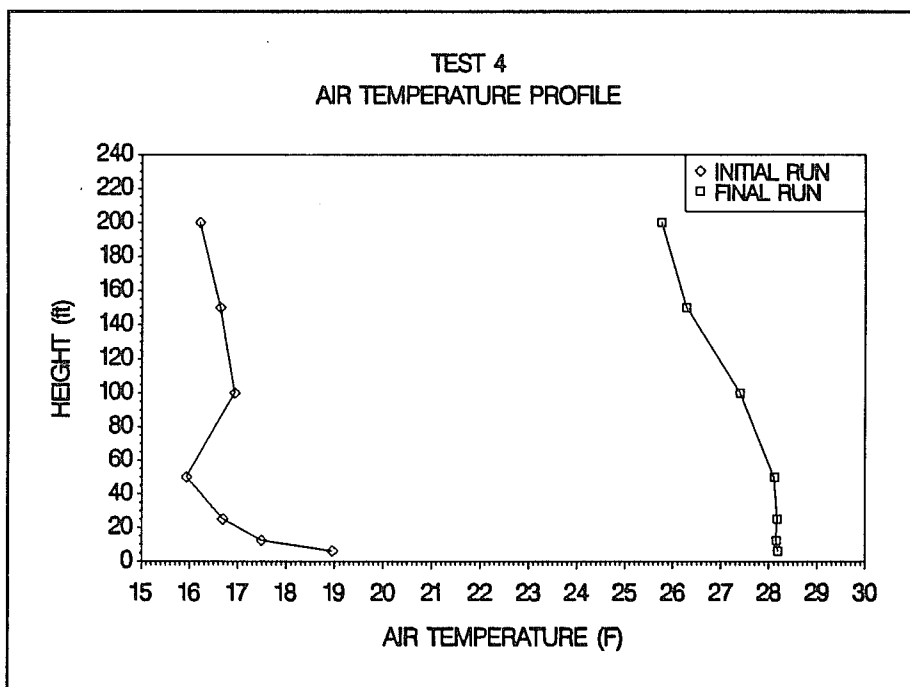
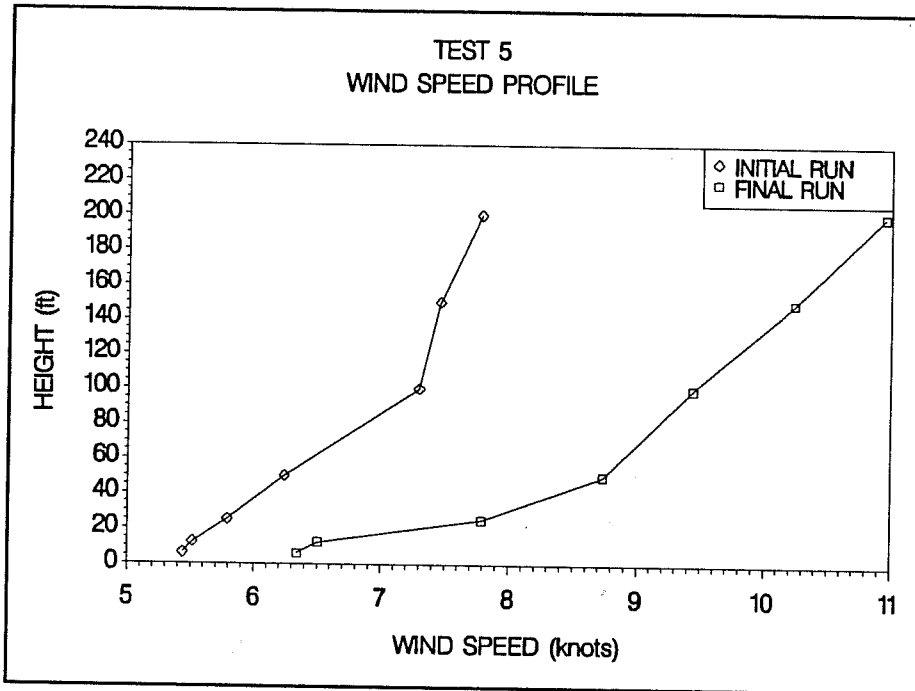
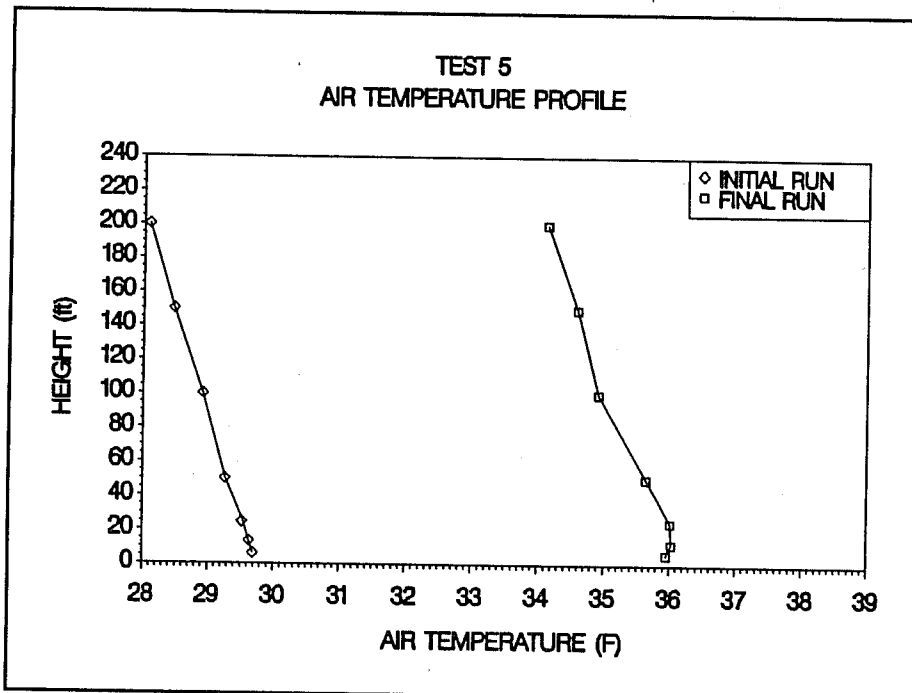


Figure B-4B. Air temperature profiles for the initial and final fly-bys of test 4 (C141B and C130E).



**Figure B-5A.** Wind speed profiles for the initial and final fly-bys of test 5 (C130E).



**Figure B-5B.** Air temperature profiles for the initial and final fly-bys of test 5 (C130E).

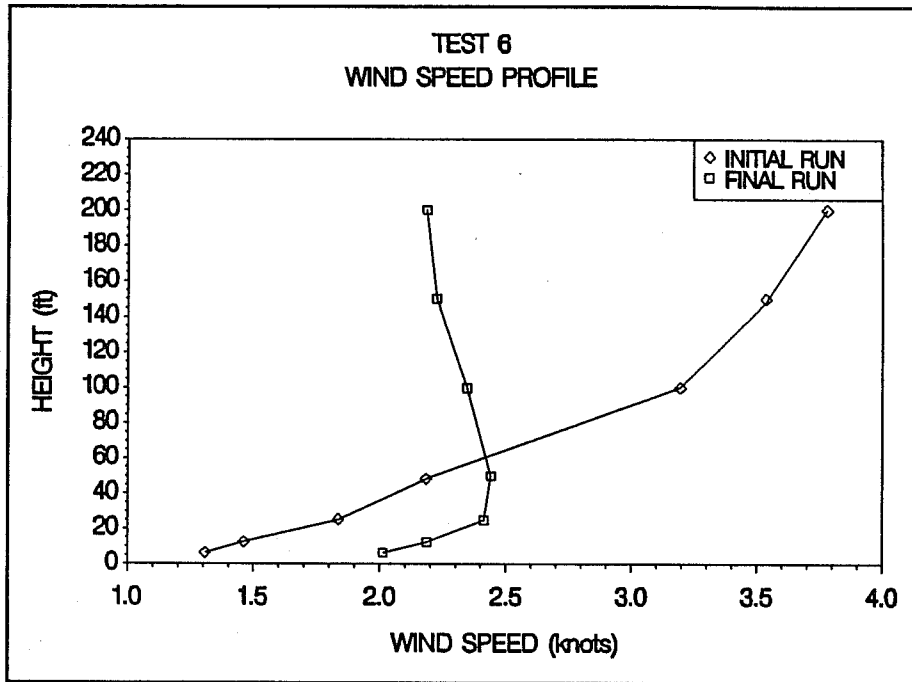


**Figure B-6A.** Wind speed profiles for the initial and final fly-bys of test 6 (C130E).

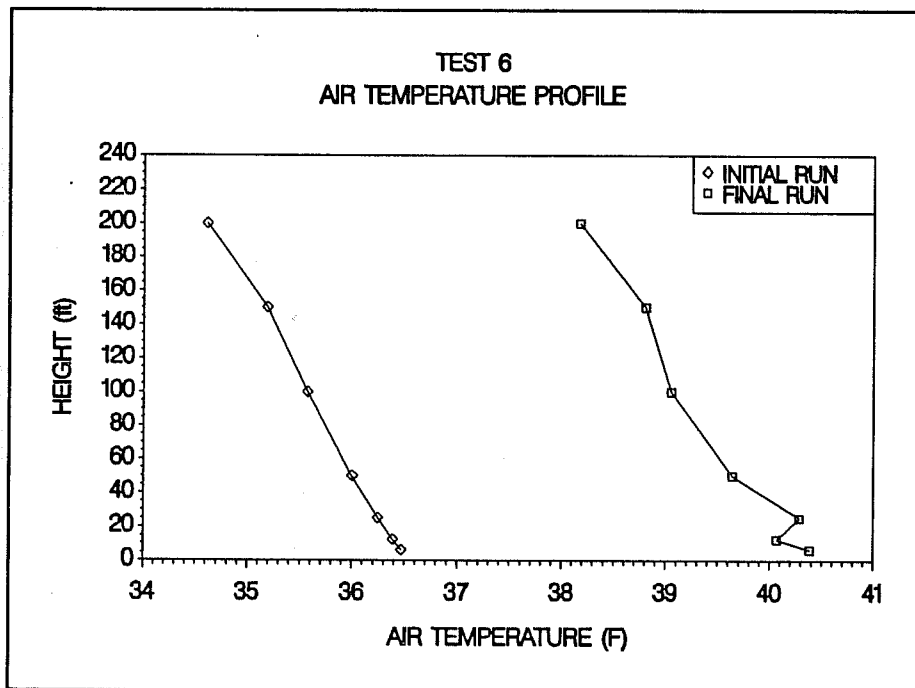


**Figure B-6B.** Air temperature profiles for the initial and final fly-bys of test 6 (C130E).

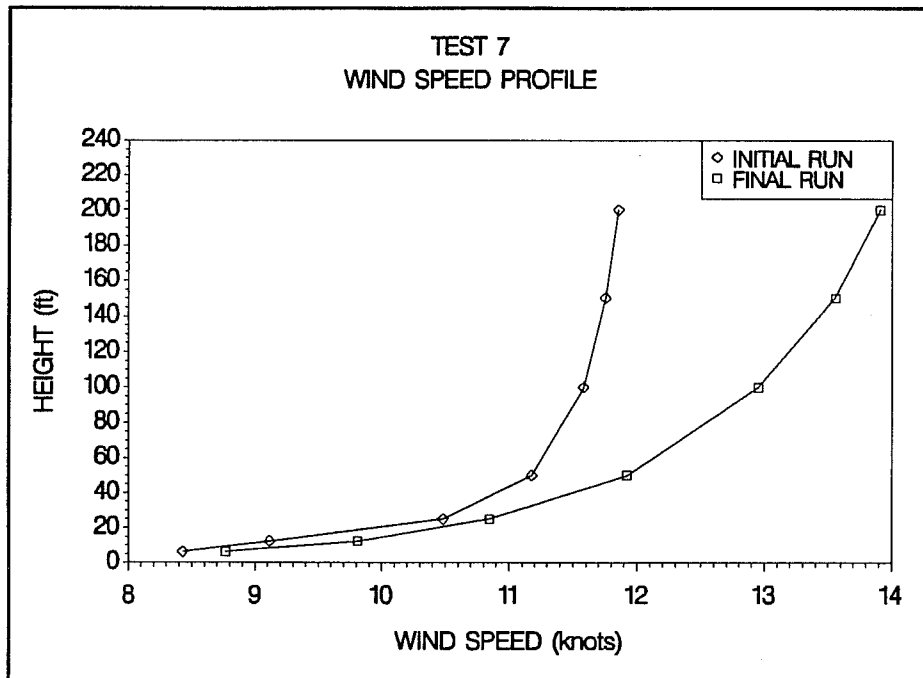


**Figure B-7A.** Wind speed profiles for the initial and final fly-bys of test 7 (C130E).

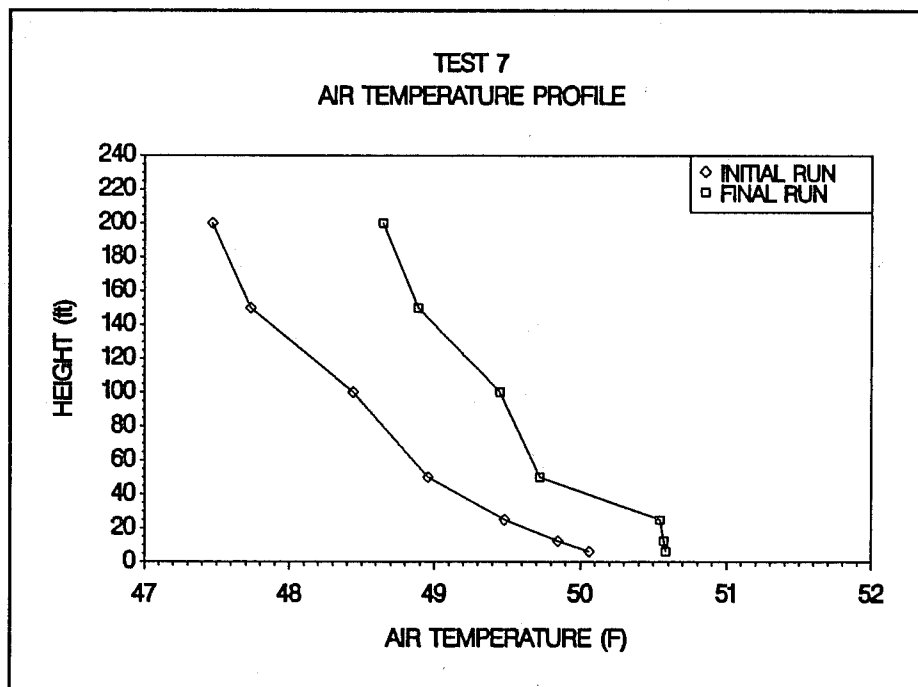


**Figure B-7B.** Air temperature profiles for the initial and final fly-bys of test 7 (C130E).

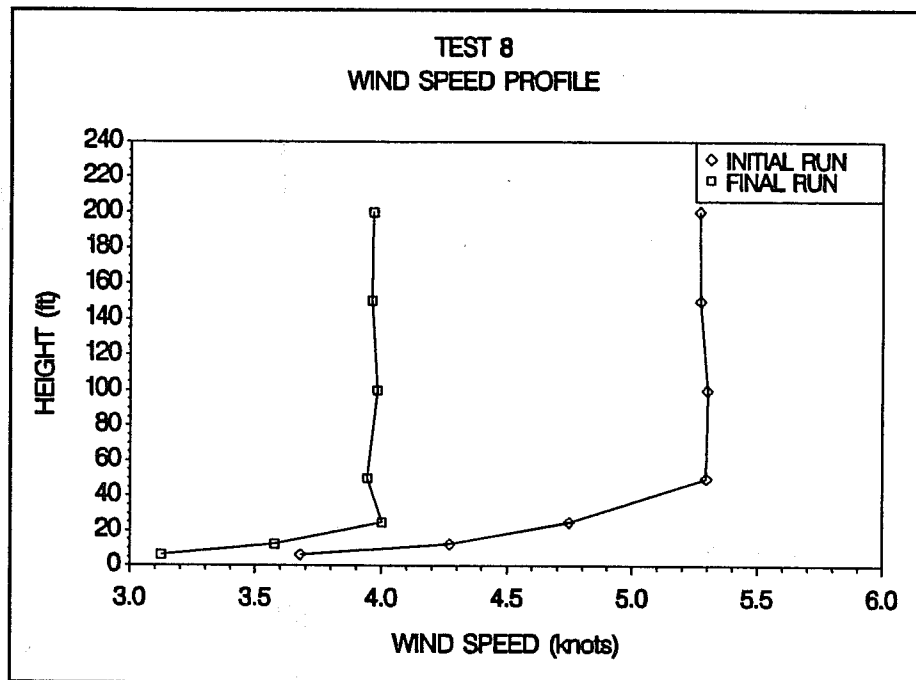


Figure B-8A. Wind speed profiles for the initial and final fly-bys of test 8 (C130E).

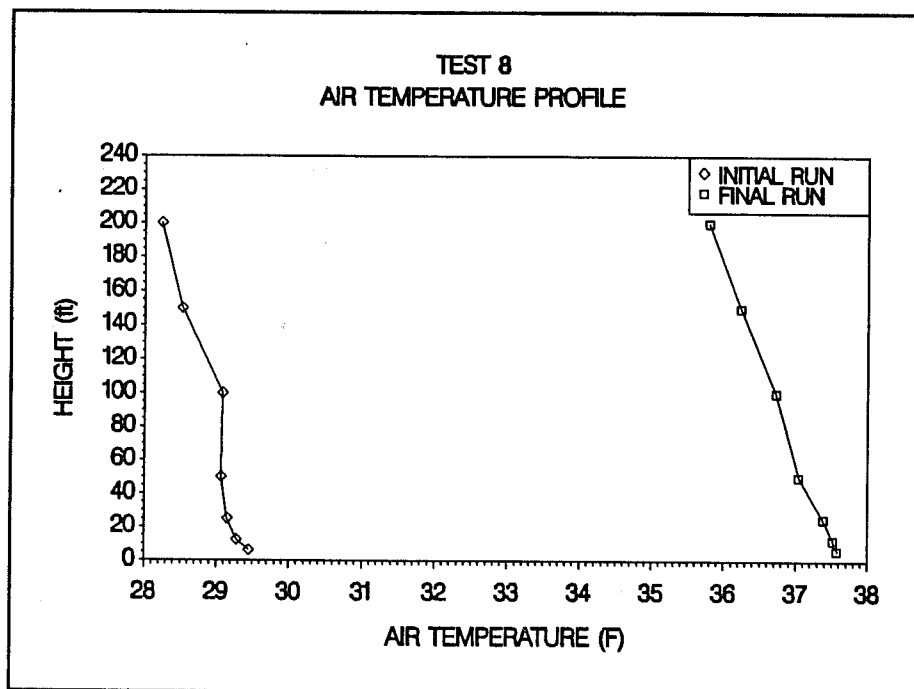


Figure B-8B. Air temperature profiles for the initial and final fly-bys of test 8 (C130E).

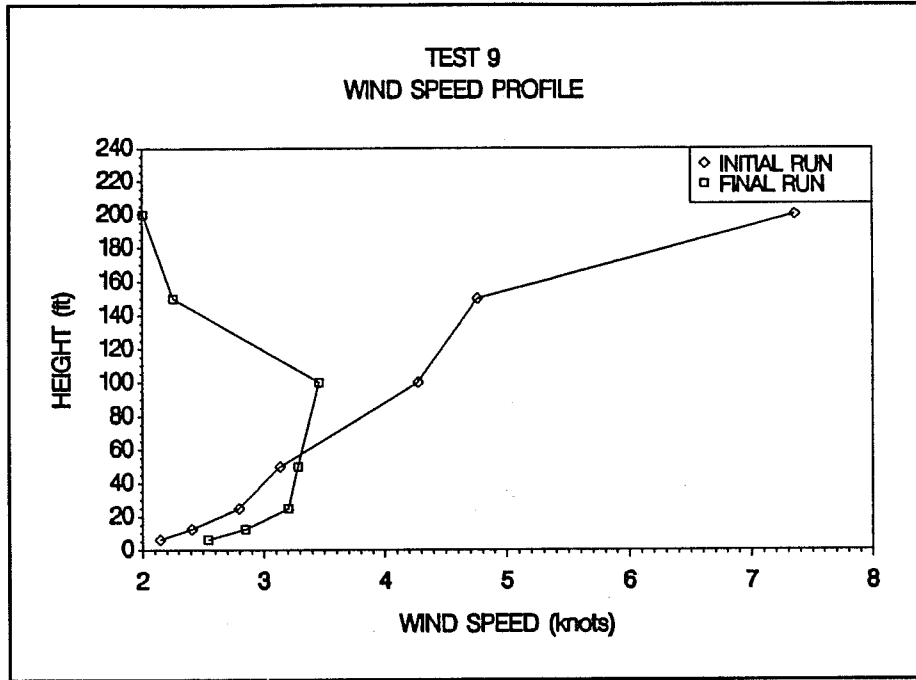


Figure B-9A. Wind speed profiles for the initial and final fly-bys of test 9 (C5A/B).

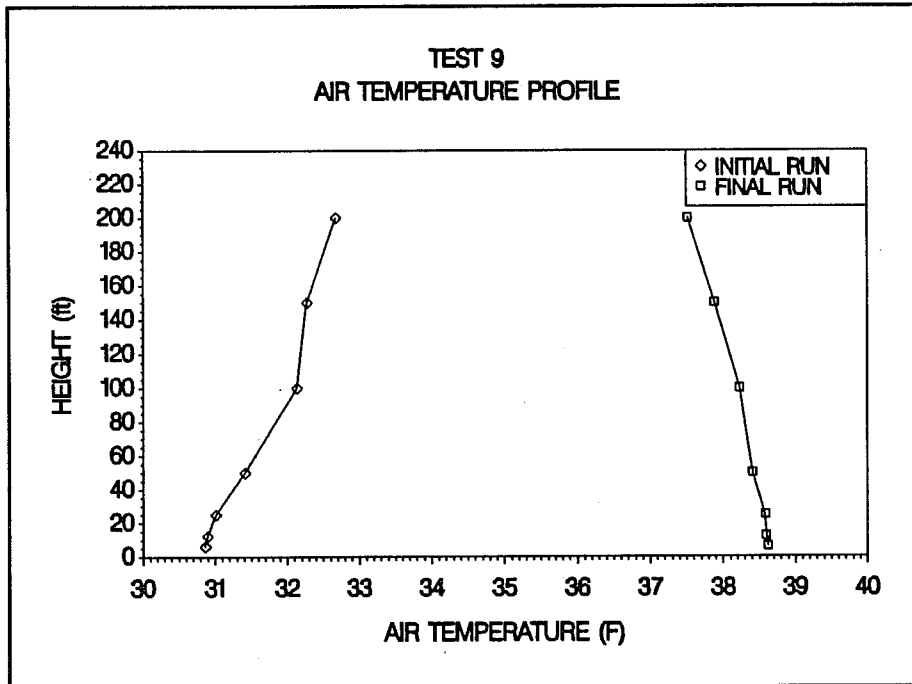
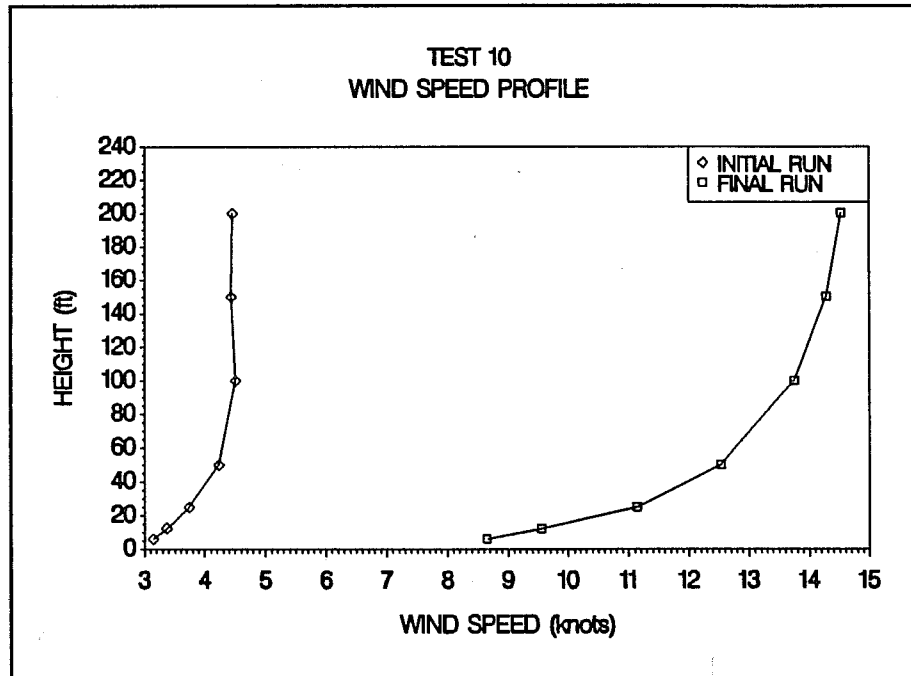
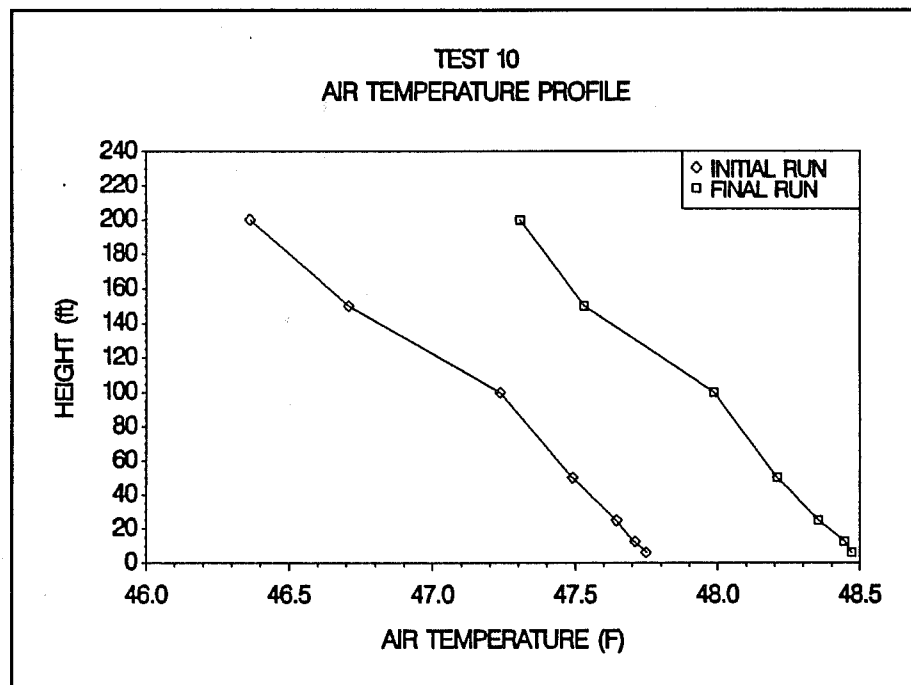


Figure B-9A. Air temperature profiles for the initial and final fly-bys of test 9 (C5A/B).



**Figure B-10A.** Wind speed profiles for the initial and final fly-bys of test 10 (C5A/B).



**Figure B-10B.** Air temperature profiles for the initial and final fly-bys of test 10 (C5A/B).

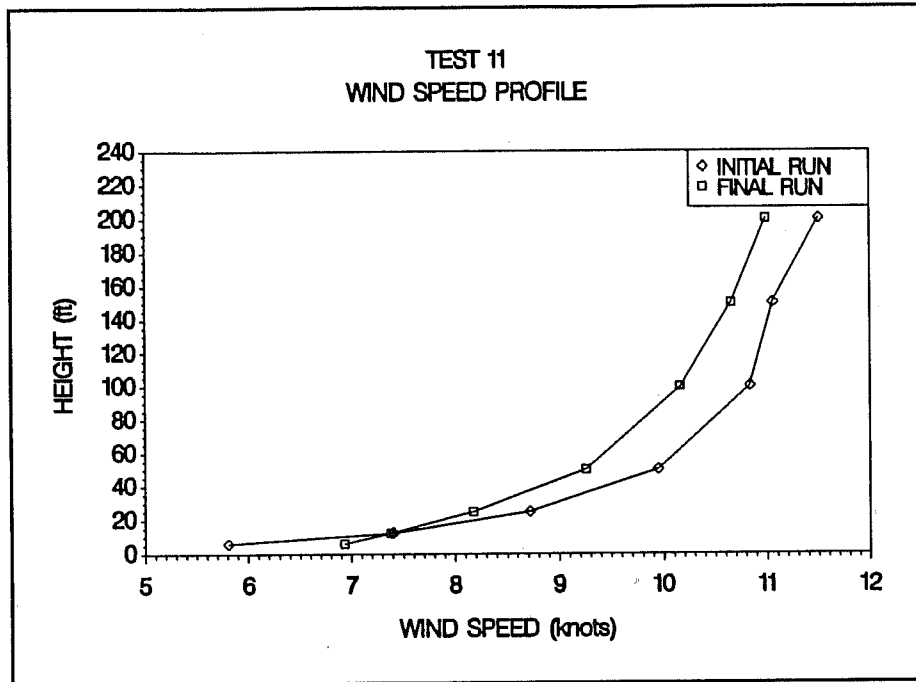


**Figure B-11A.** Wind speed profiles for the initial and final fly-bys of test 11 (C5A/B).

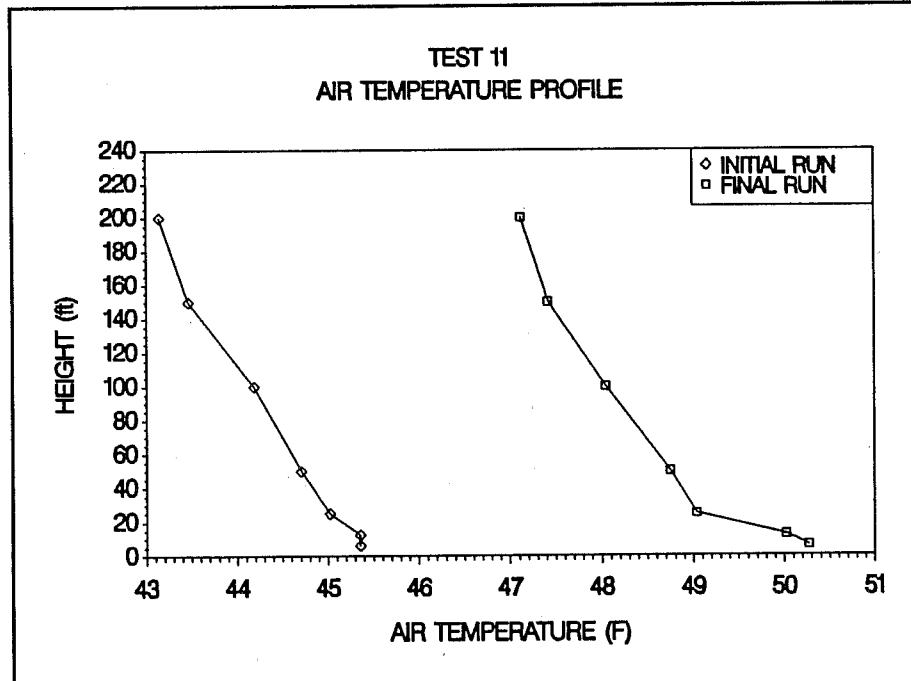


**Figure B-11B.** Air temperature profiles for the initial and final fly-bys of test 11 (C5A/B).

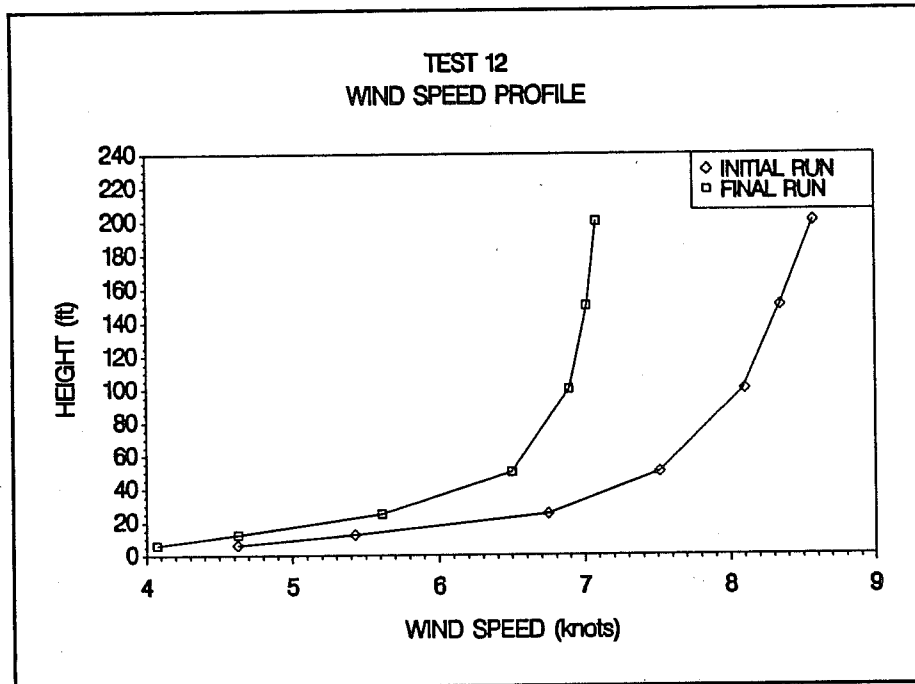


**Figure B-12A.** Wind speed profiles for the initial and final fly-bys of test 12 (C5A/B).

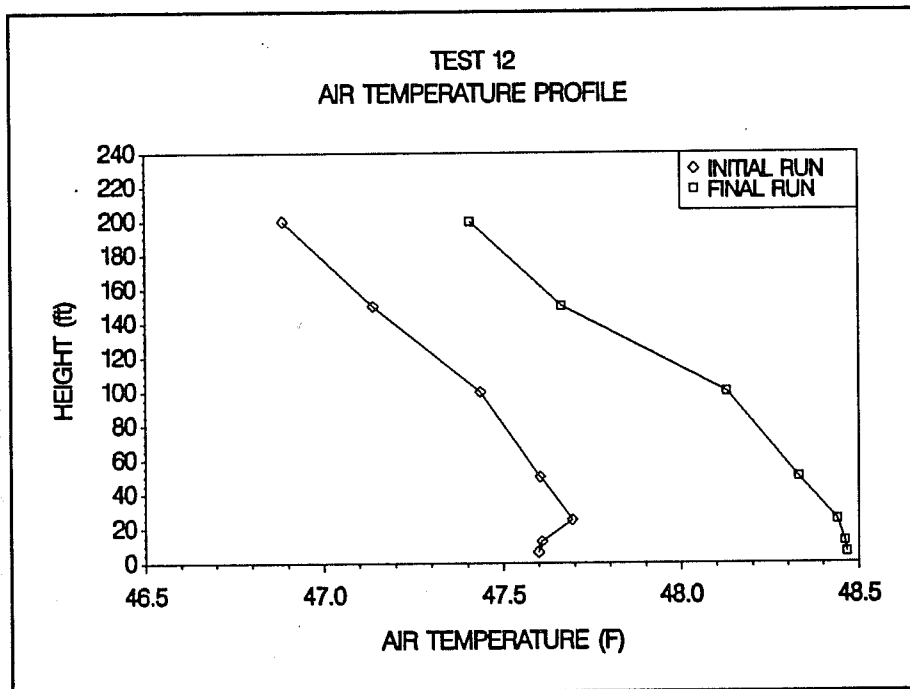


**Figure B-12B.** Air temperature profiles for the initial and final fly-bys of test 12 (C5A/B).

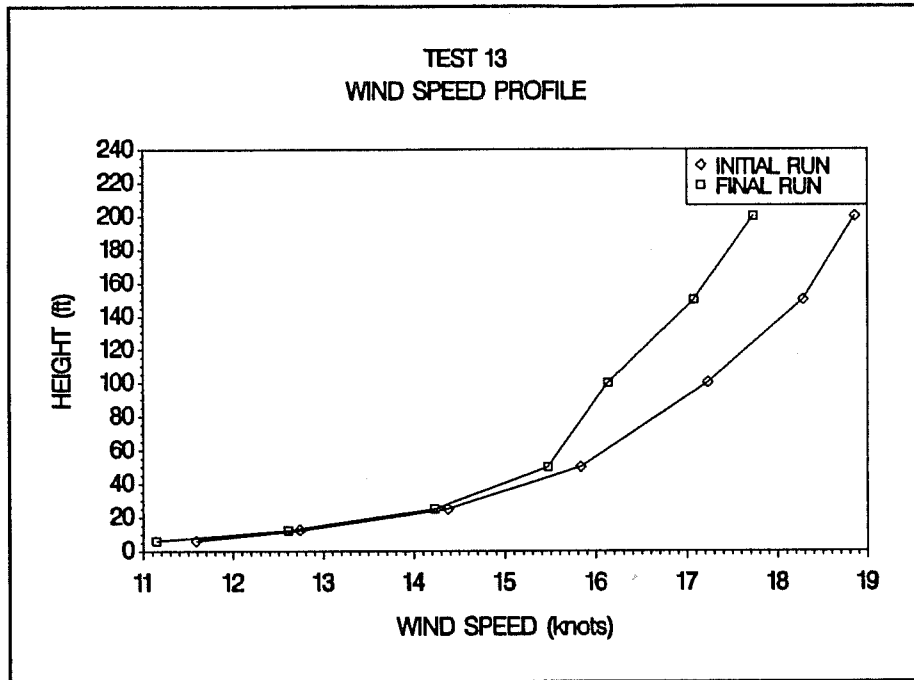


**Figure B-13A.** Wind speed profiles for the initial and final fly-bys of test 13 (C5A/B).

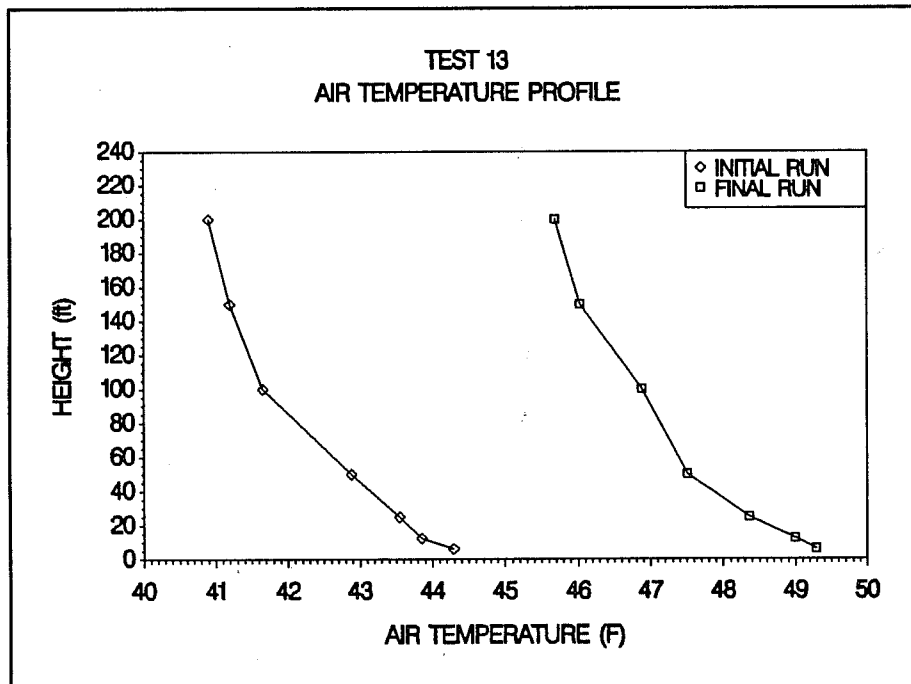


**Figure B-13B.** Air temperature profiles for the initial and final fly-bys of test 13 (C5A/B).

## **APPENDIX C**

### **Vortex Tangential Velocity Distributions**

**LOCKHEED**

**C141B**

**STARLIFTER**

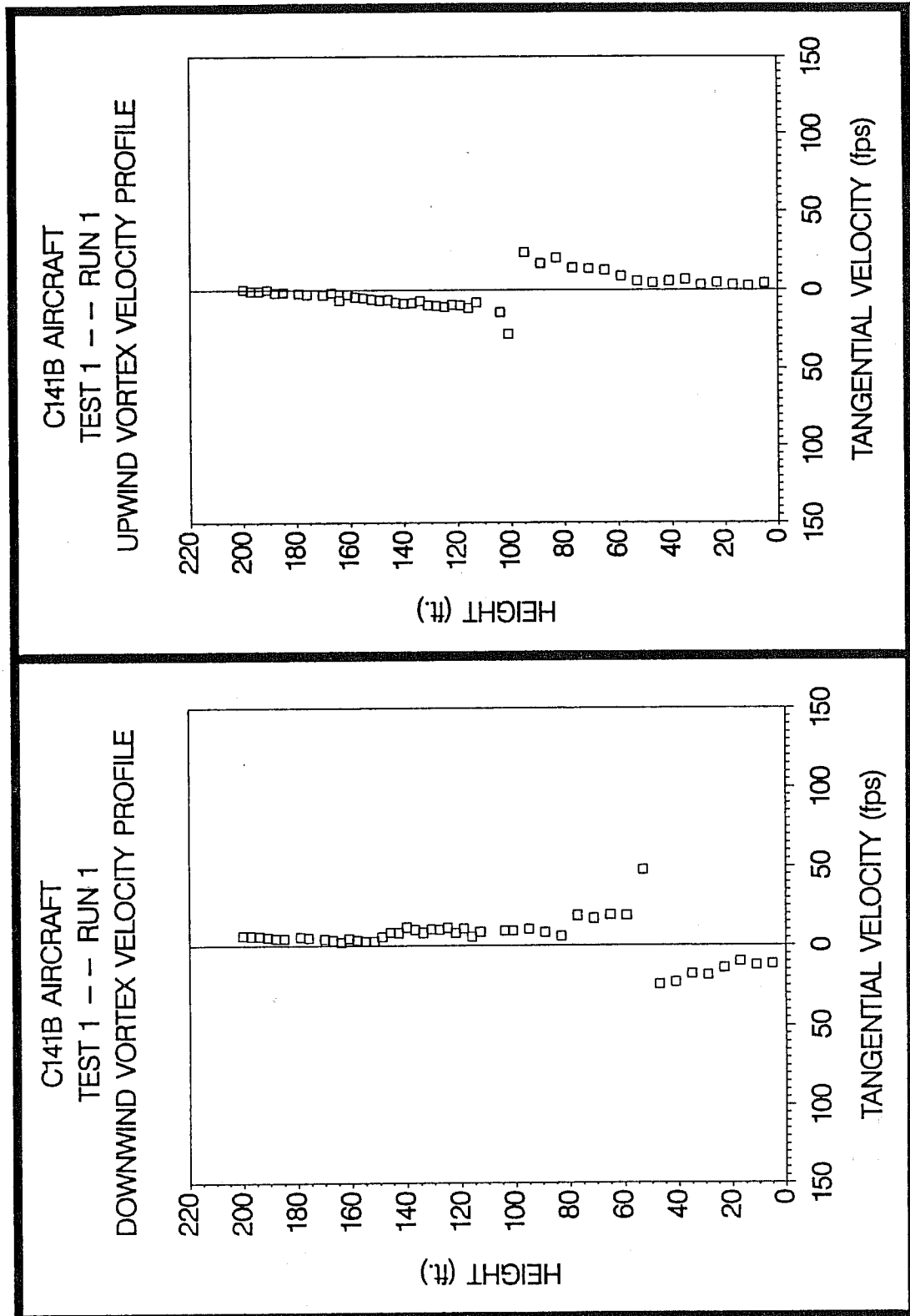


**Figure C-1.** C141B upwind (top) and downwind (bottom) vortex tangential velocity profile at maximum intensity from Test 1, Run 1, ambient wind speed=12.2 fps,  $\delta_F=50\%$ , IAS=150 knots, GW=254.0k lbs. Ages, radii, and velocities of the vortex cores are (N/A) and (N/A) sec., (N/A) and (N/A) ft., and 28.0 and 47.6 fps, respectively.

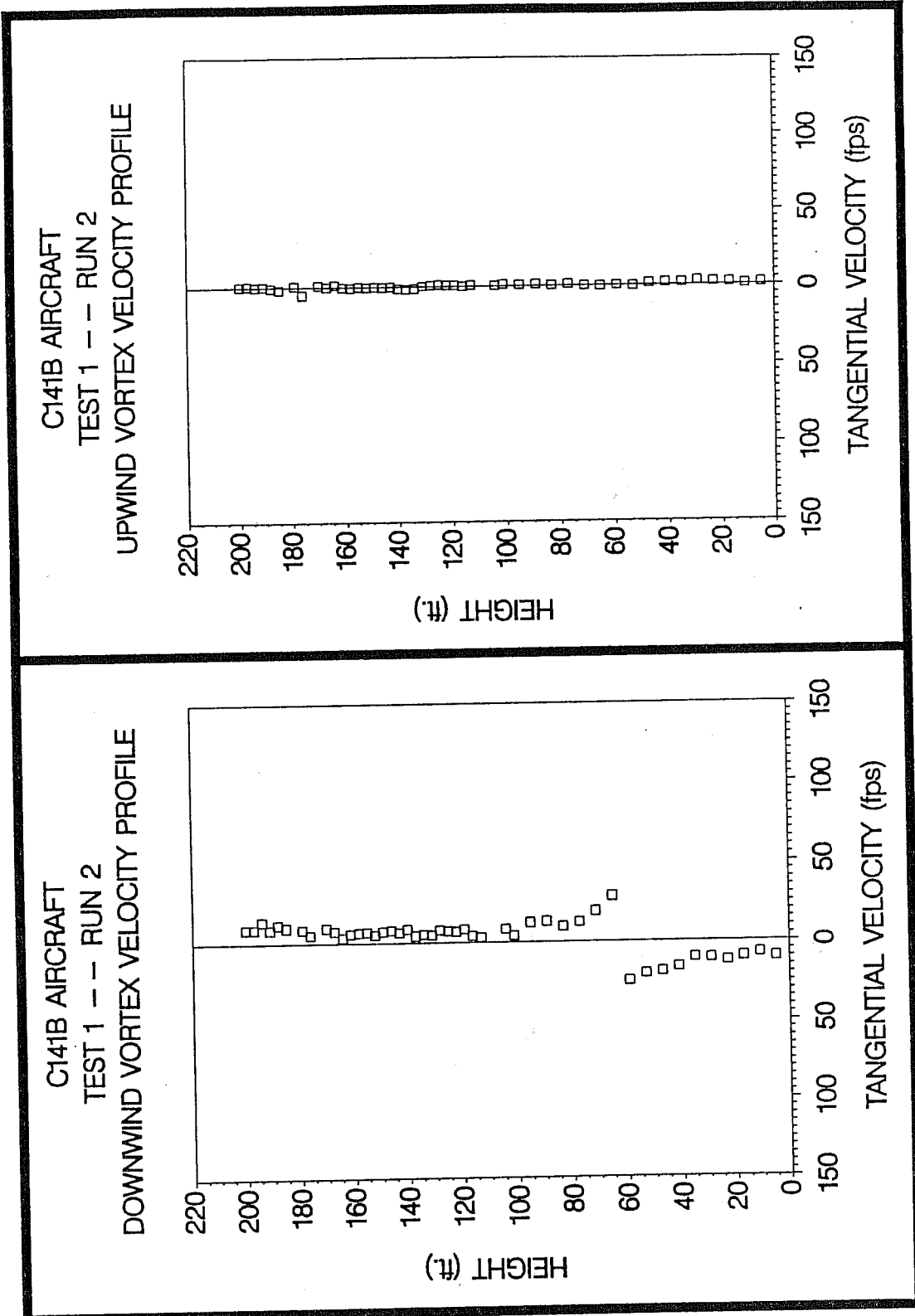


Figure C-2. C141B upwind (top) and downwind (bottom) vortex tangential velocity profile at maximum intensity from Test 1, Run 2, ambient wind speed=10.6 fps,  $\delta_F=77\%$ , IAS=150 knots, GW=251.0k lbs. Ages, radii, and velocities of the vortex cores are (N/A) and 35 sec., (N/A) and (N/A) ft., and (N/A) and 28.4 fps, respectively.

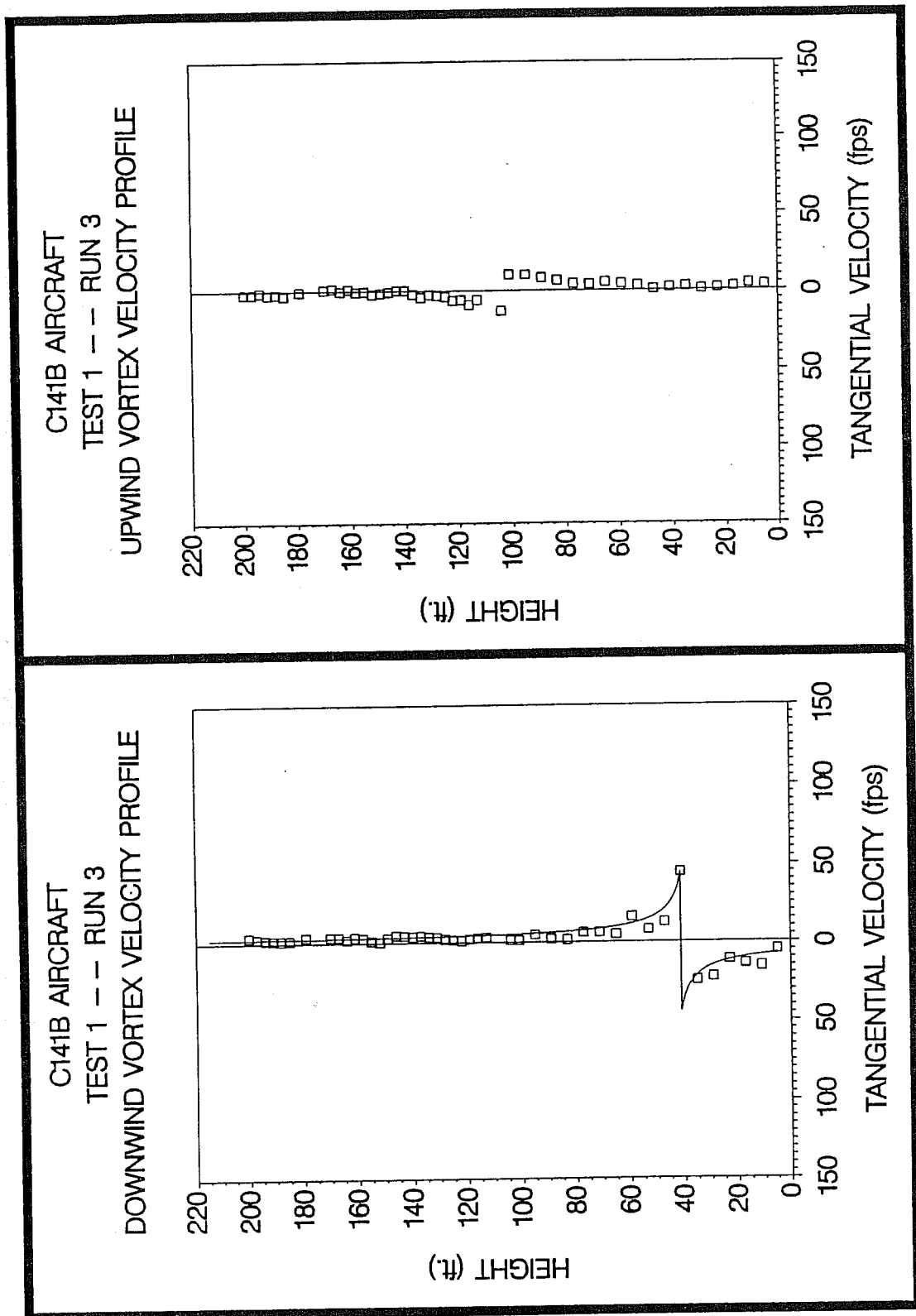
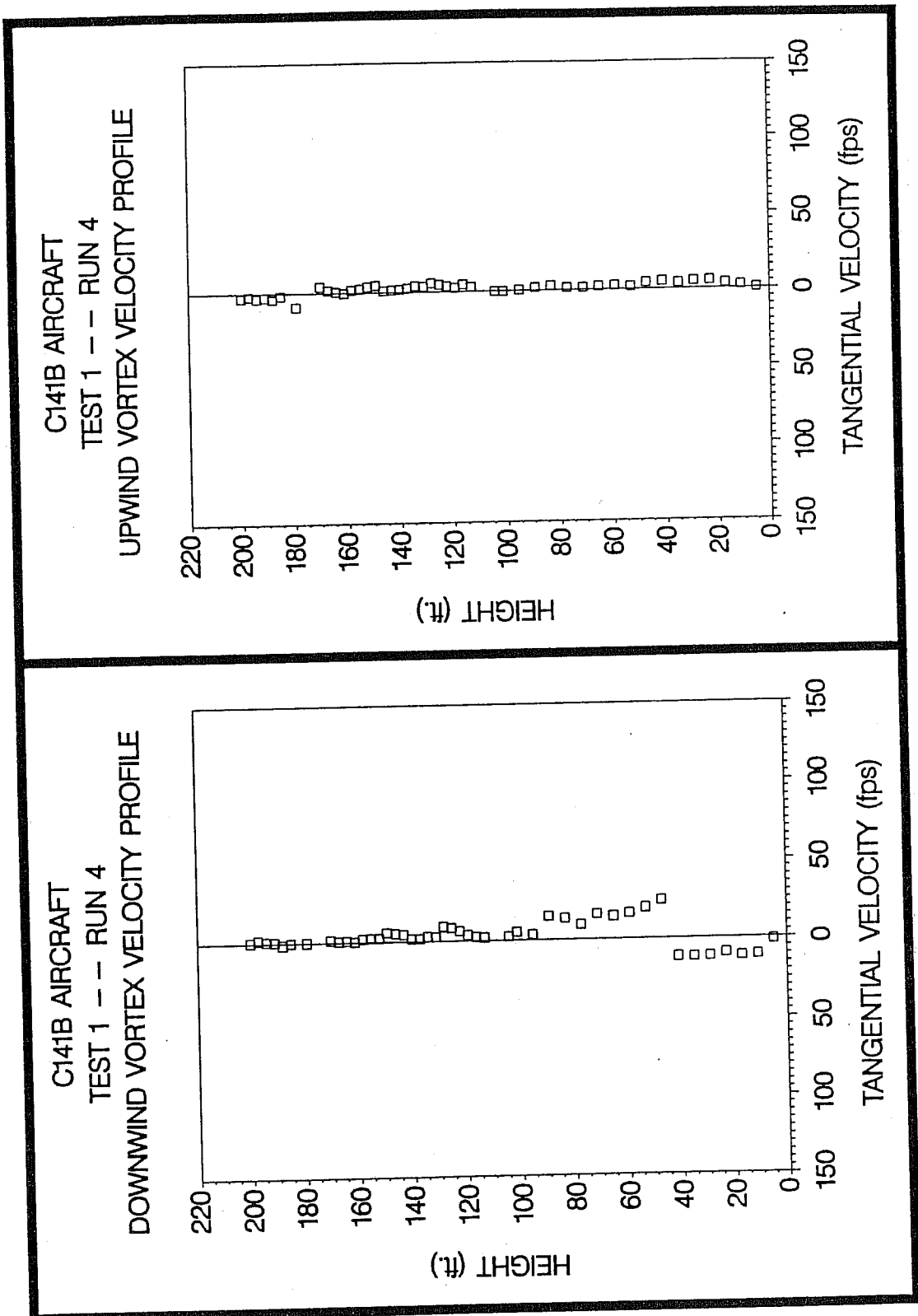


Figure C-3. C141B upwind (top) and downwind (bottom) vortex tangential velocity profile at maximum intensity from Test 1, Run 3, ambient wind speed=8.1 fps,  $\delta_F=50\%$ , IAS=150 knots, GW=249.0k lbs. Ages, radii, and velocities of the vortex cores are 176 and 41 sec., (N/A) and 2.1 ft., and 12.7 and 44.8 fps, respectively.



**Figure C-4.** C141B upwind (top) and downwind (bottom) vortex tangential velocity profile at maximum intensity from Test 1, Run 4, ambient wind speed=7.9 fps,  $\delta_F=49\%$ , IAS=150 knots, GW=246.0k lbs. Ages, radii, and velocities of the vortex cores are 129 and 32 sec., (N/A) and (N/A) ft., and 8.9 and 24.1 fps, respectively.

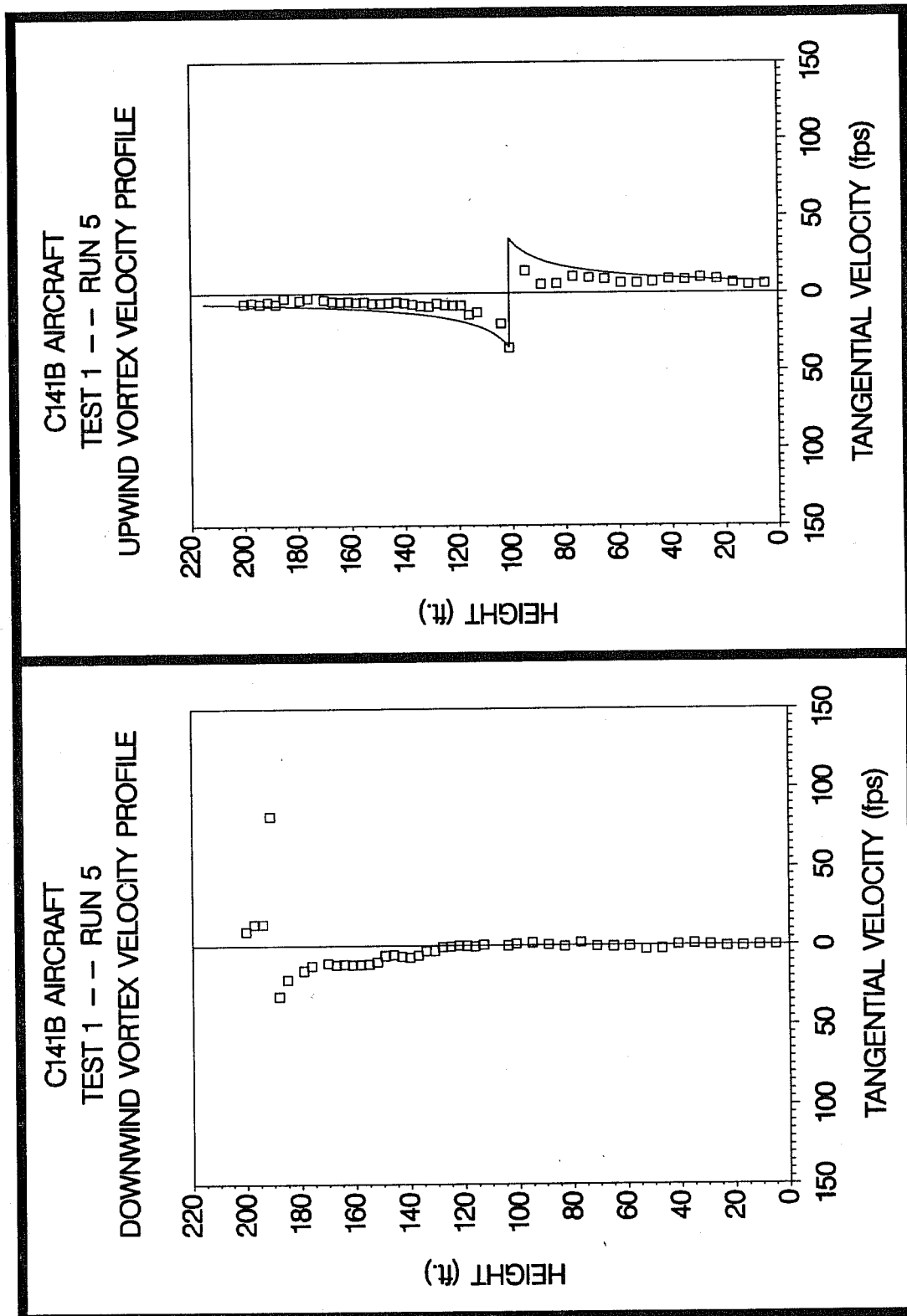


Figure C-5. C141B upwind (top) and downwind (bottom) vortex tangential velocity profile at maximum intensity from Test 1, Run 5, ambient wind speed=8.9 fps,  $\delta_F=49\%$ , IAS=150 knots, GW=244.0k lbs. Ages, radii, and velocities of the vortex cores are 41 and 22 sec., 7.7 and (N/A) ft., and 35.3 and 82.2 fps, respectively.

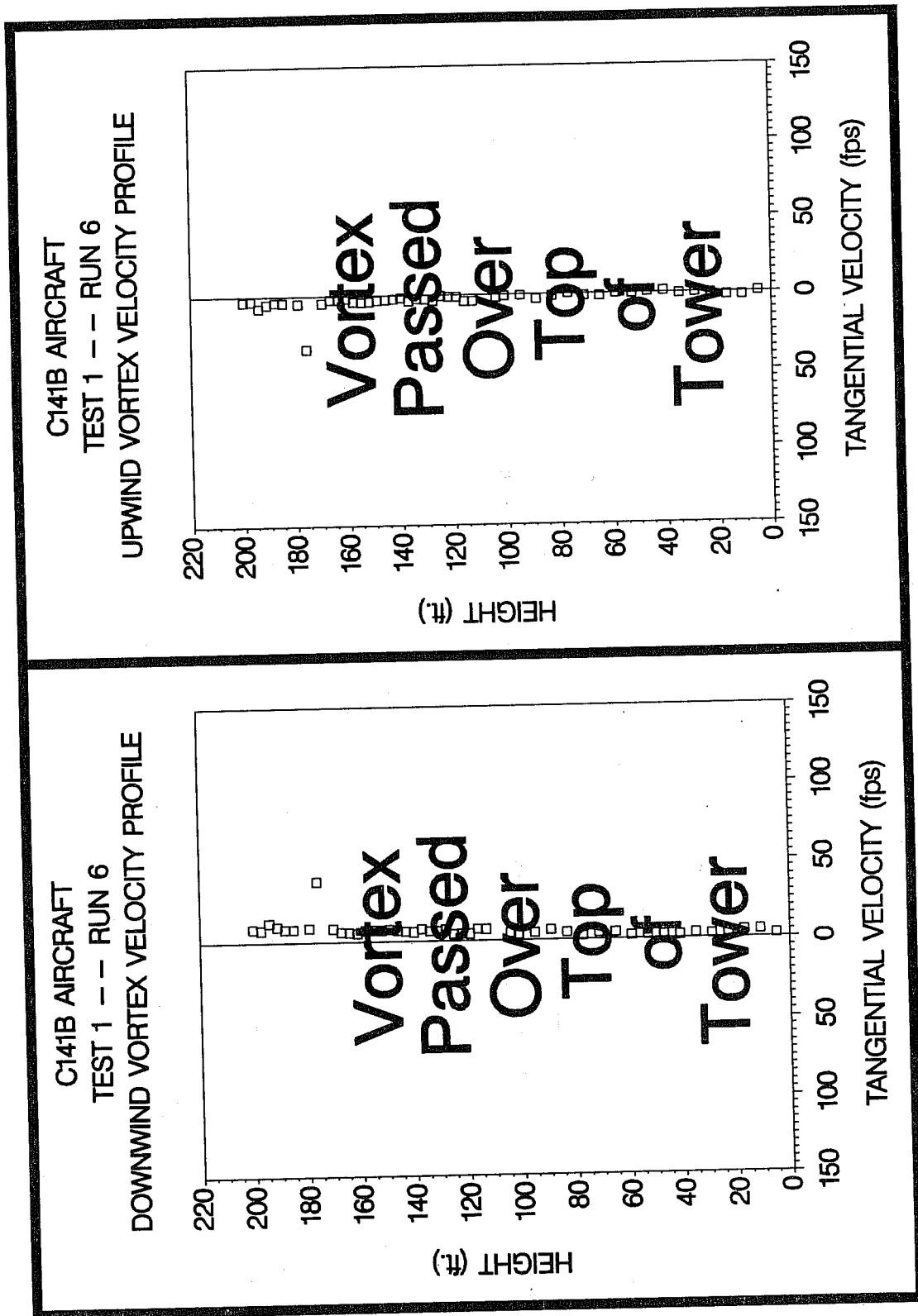
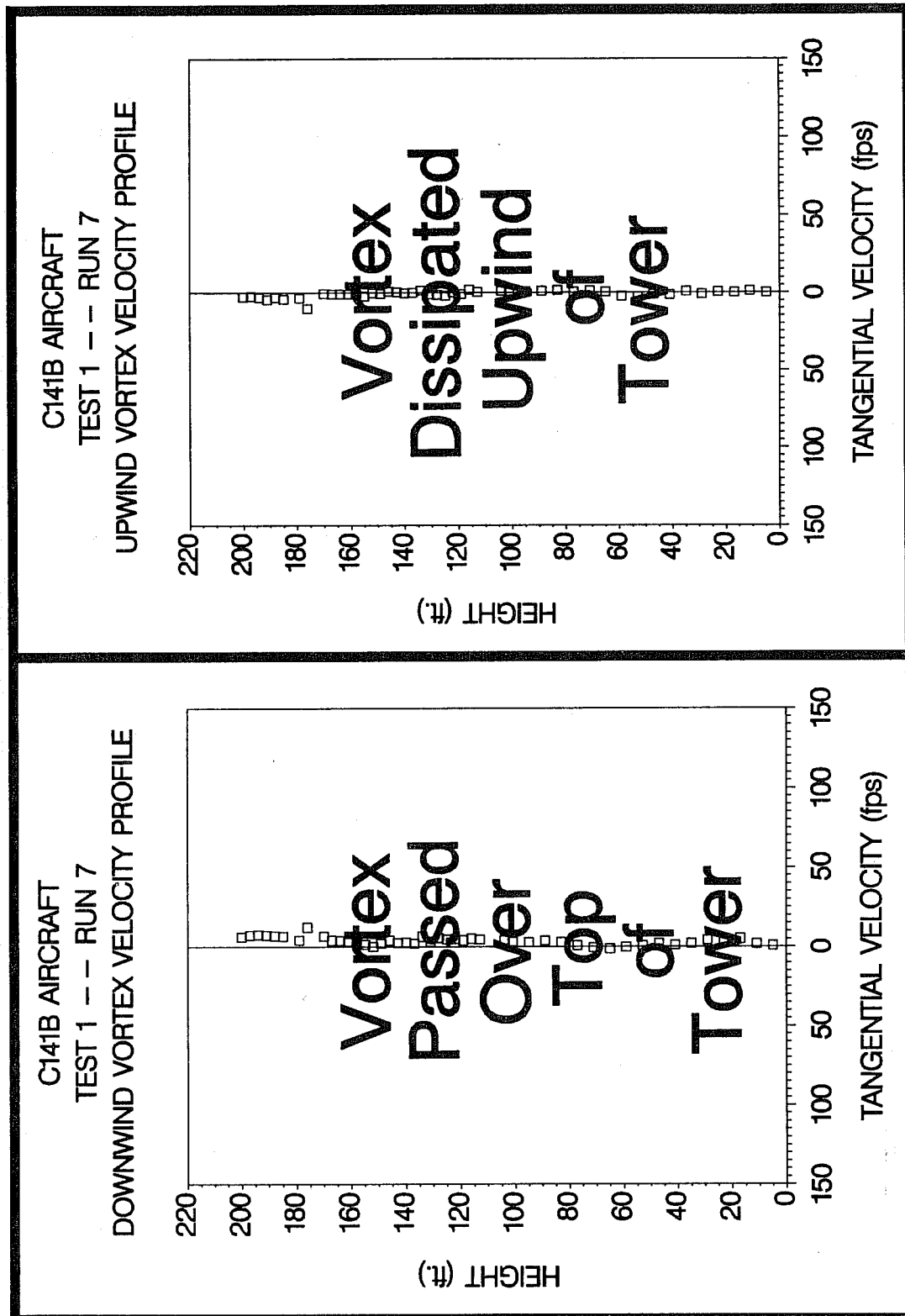
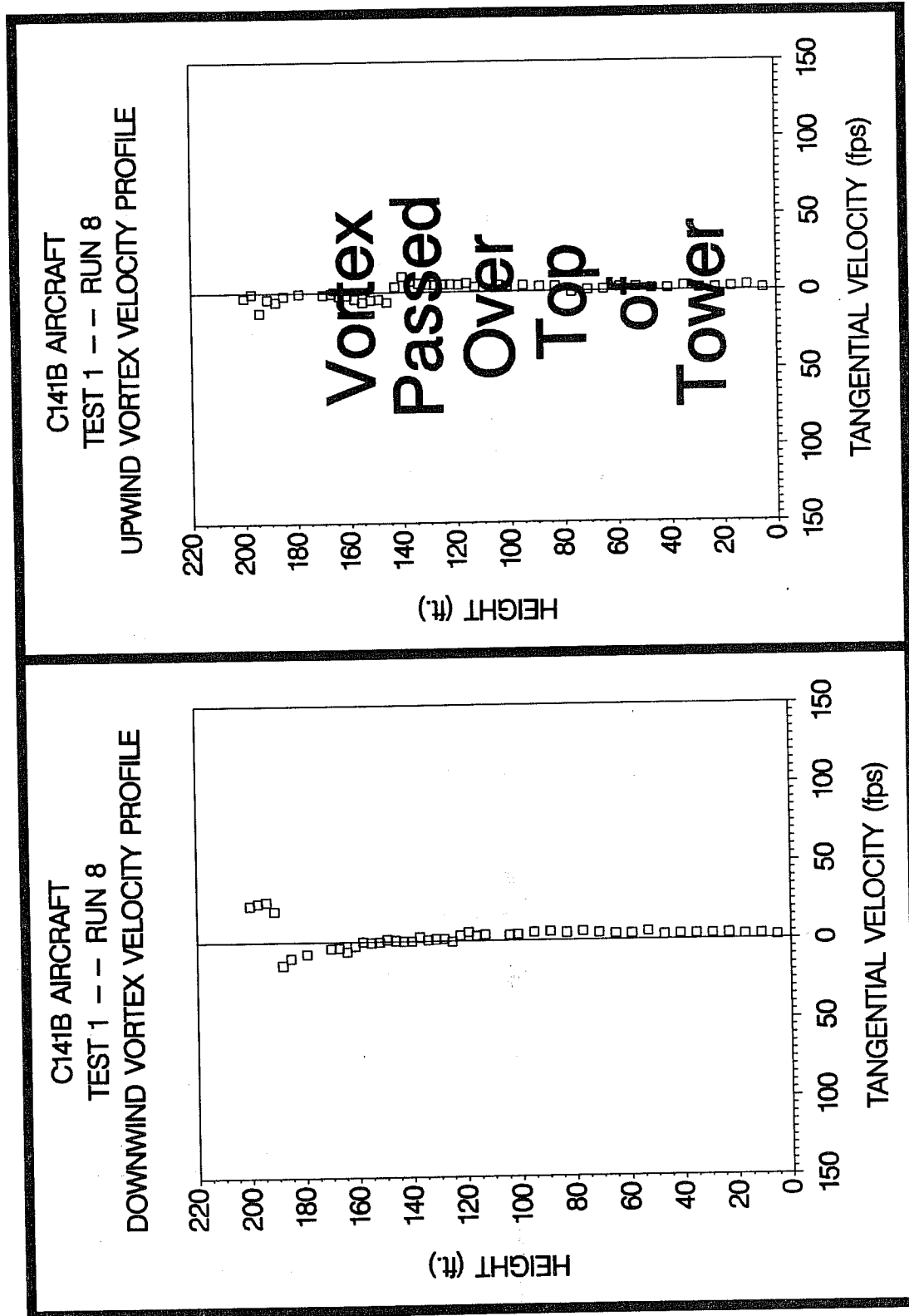


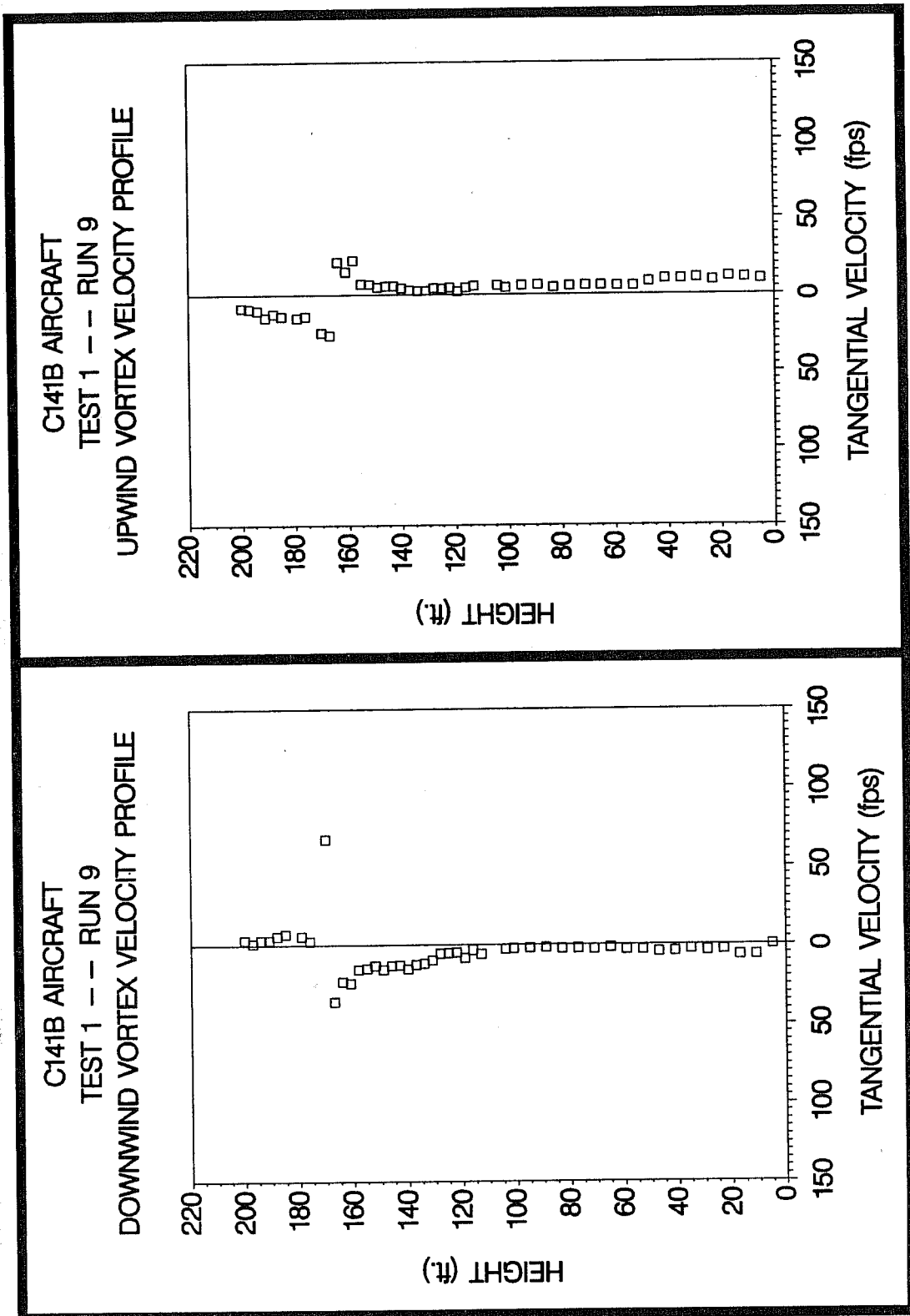
Figure C-6. C141B upwind (top) and downwind (bottom) vortex tangential velocity profile at maximum intensity from Test 1, Run 6, ambient wind speed=8.2 fps,  $\delta_F=(N/A)\%$ , IAS=(N/A) knots, GW=(N/A)k lbs. Ages, radii, and velocities of the vortex cores are (N/A) and (N/A) sec., (N/A) and (N/A) ft., and (N/A) and (N/A) fps, respectively.



**Figure C-7.** C141B upwind (top) and downwind (bottom) vortex tangential velocity profile at maximum intensity from Test 1, Run 7, ambient wind speed=9.7 fps,  $\delta_F=(N/A)\%$ , IAS=(N/A) knots, GW=(N/A)k lbs. Ages, radii, and velocities of the vortex cores are (N/A) and (N/A) sec., (N/A) and (N/A) ft., and (N/A) and (N/A) fps, respectively.



**Figure C-8.** C141B upwind (top) and downwind (bottom) vortex tangential velocity profile at maximum intensity from Test 1, Run 8, ambient wind speed=18.3 fps,  $\delta_F=42\%$ , IAS=150 knots, GW=237.0k lbs. Ages, radii, and velocities of the vortex cores are (N/A) and 9 sec., (N/A) and (N/A) ft., and (N/A) and 19.9 fps, respectively.



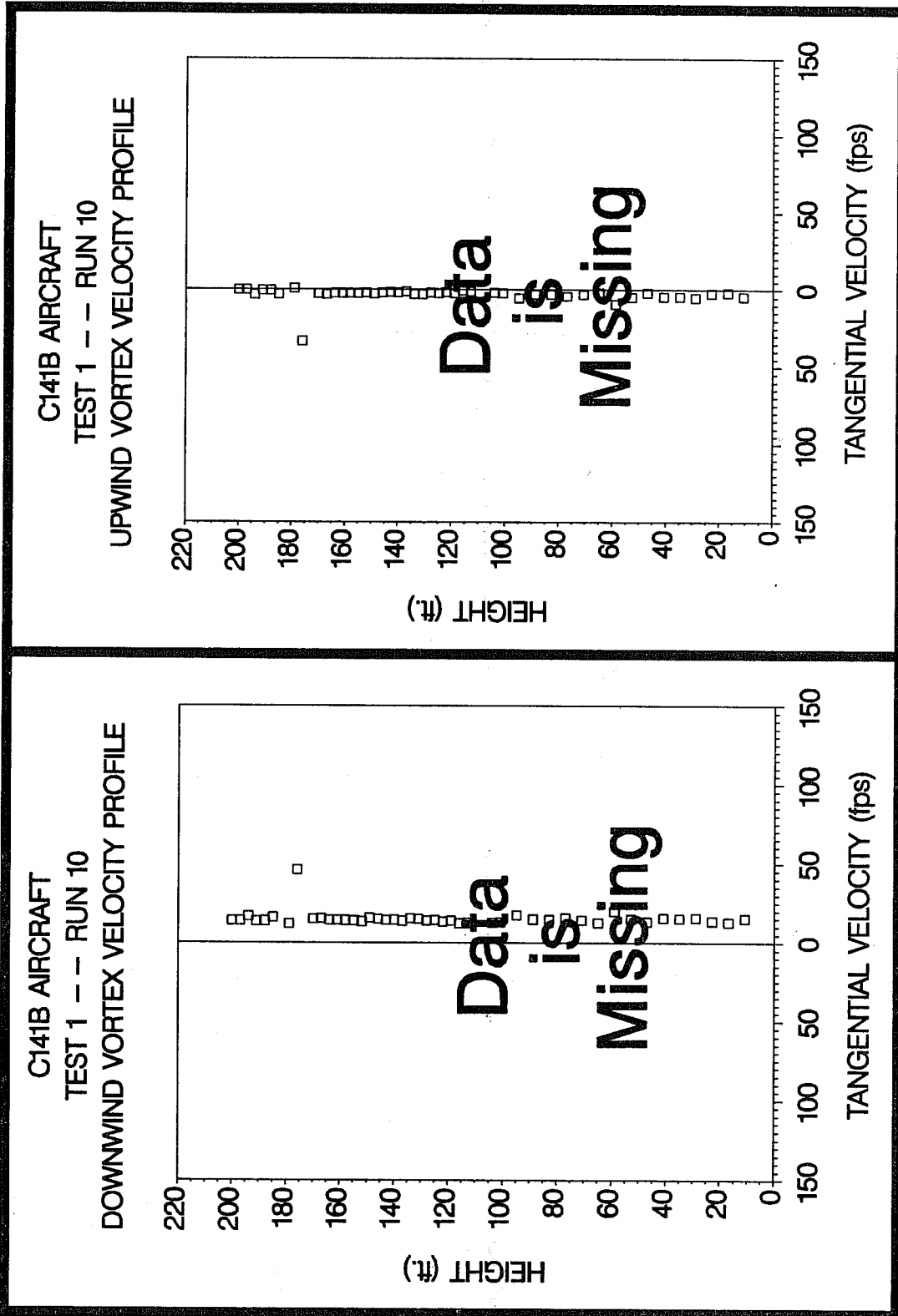


**Figure C-10.** C141B upwind (top) and downwind (bottom) vortex tangential velocity profile at maximum intensity from Test 1, Run 10, ambient wind speed=22.6 fps,  $\delta_F=42\%$ , IAS=150 knots, GW=233.0k lbs. Ages, radii, and velocities of the vortex cores are (N/A) and (N/A) sec., (N/A) and (N/A) ft., and (N/A) and (N/A) fps, respectively.

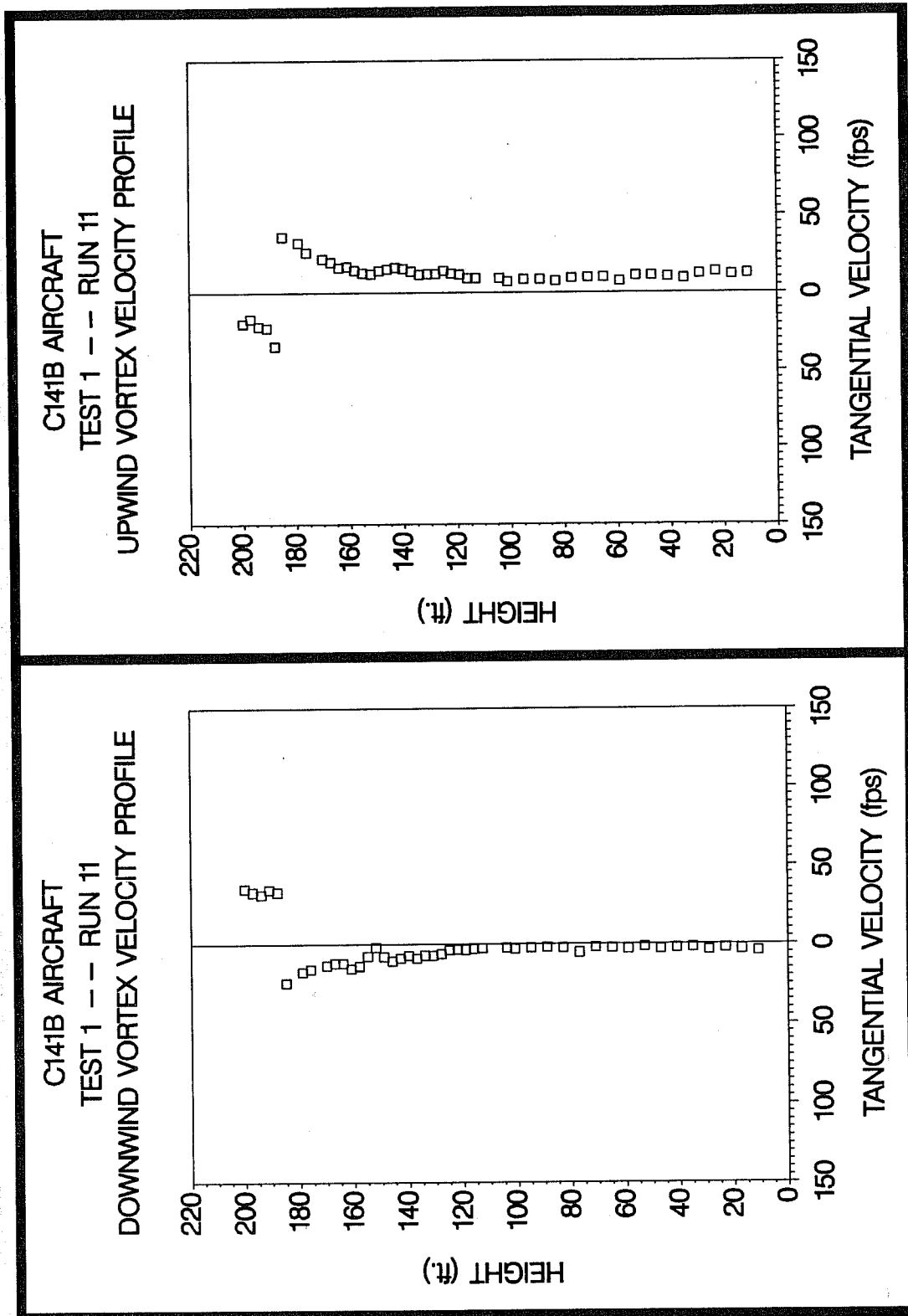
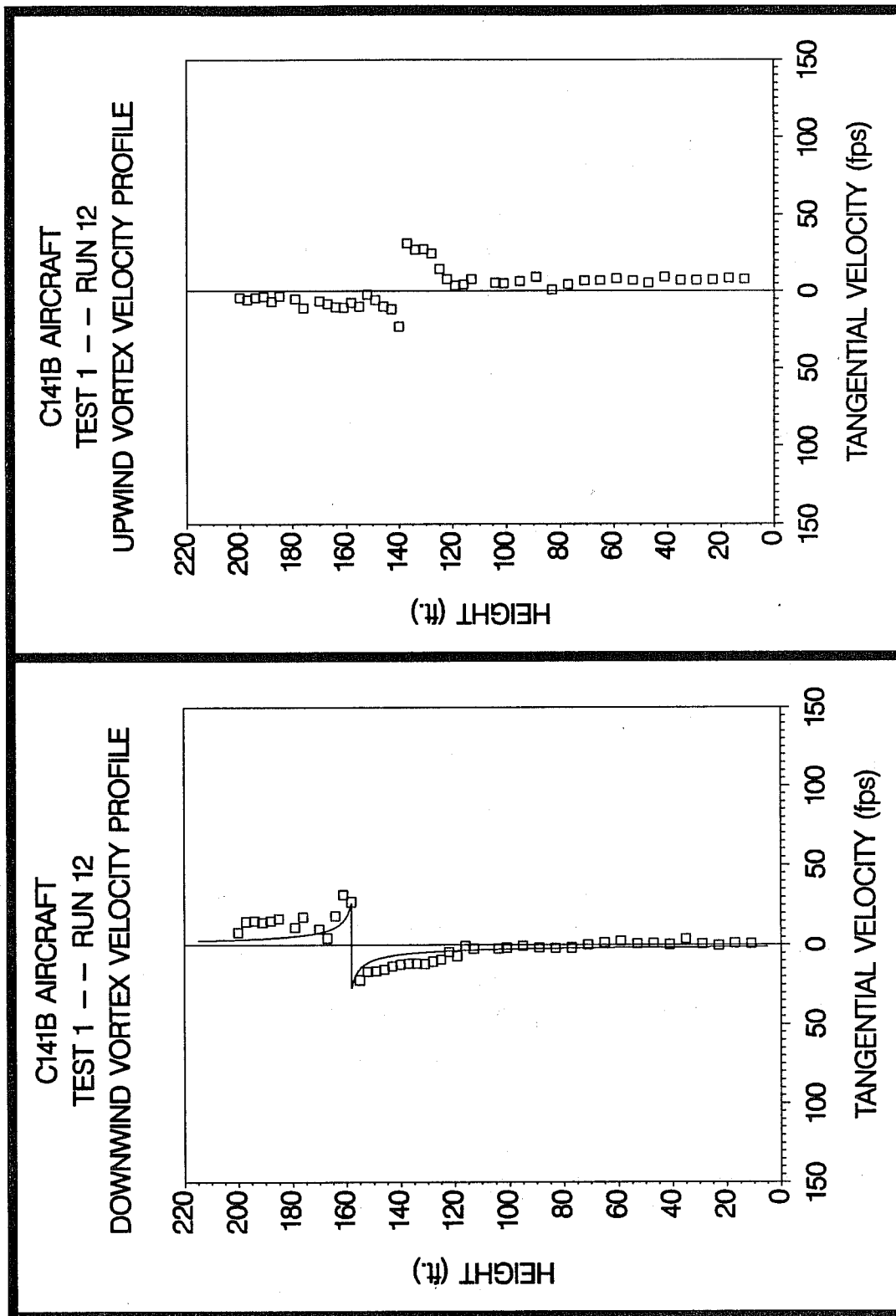
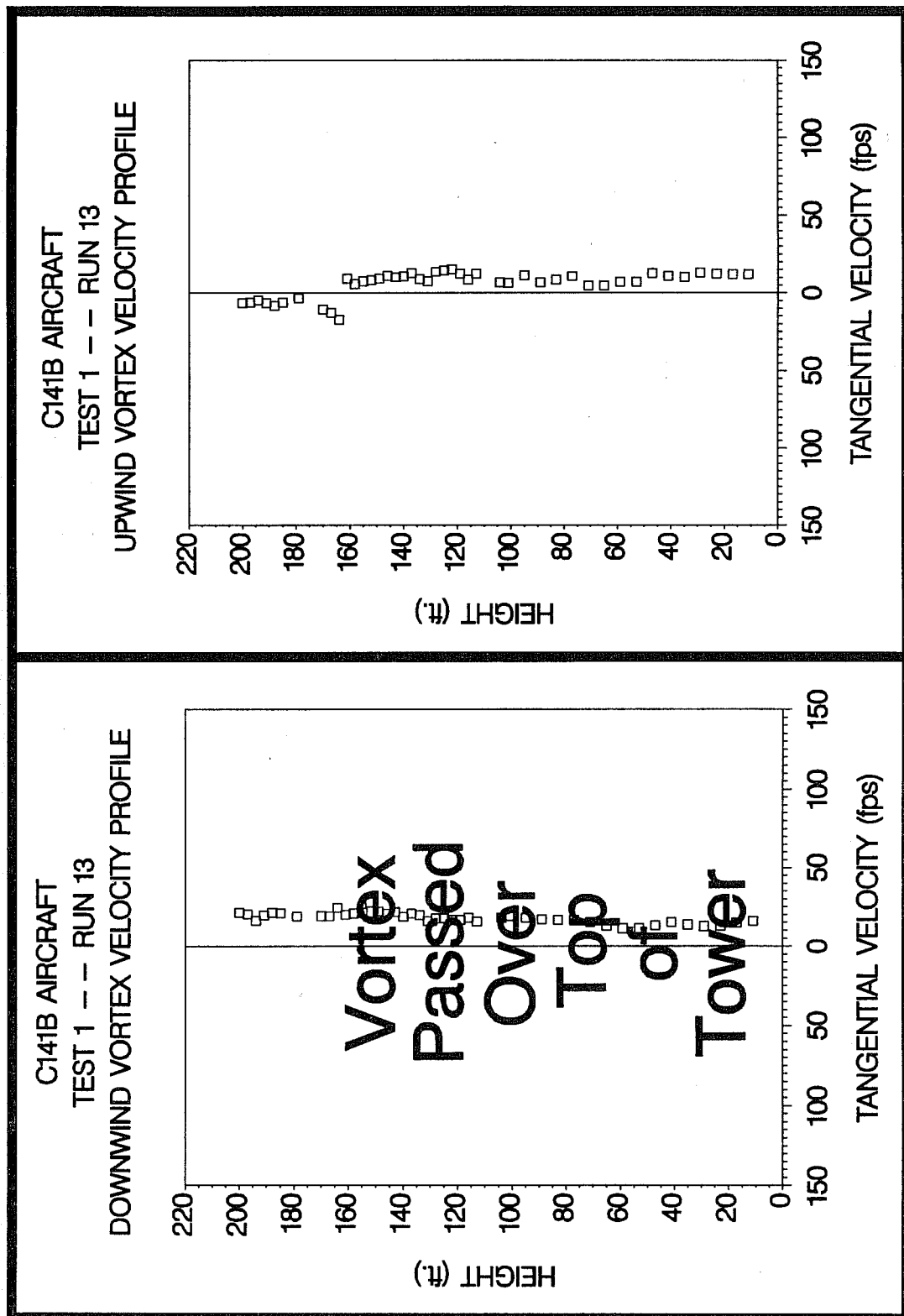


Figure C-11. C141B upwind (top) and downwind (bottom) vortex tangential velocity profile at maximum intensity from Test 1, Run 11, ambient wind speed=24.6 fps,  $\delta_F=61\%$ , IAS=150 knots, GW=231.0k lbs. Ages, radii, and velocities of the vortex cores are 9 and 7 sec., (N/A) and (N/A) ft., and 34.5 and 32.8 fps, respectively.



**Figure C-12.** C141B upwind (top) and downwind (bottom) vortex tangential velocity profile at maximum intensity from Test 1, Run 12, ambient wind speed=25.2 fps,  $\delta_F=61\%$ , IAS=150 knots, GW=229.0k lbs. Ages, radii, and velocities of the vortex cores are 17 and 11 sec., (N/A) and 1.6 ft., and 22.8 and 27.0 fps, respectively.



**Figure C-13.** C141B upwind (top) and downwind (bottom) vortex tangential velocity profile at maximum intensity from Test 1, Run 13, ambient wind speed=23.7 fps,  $\delta_F=(N/A)\%$ , IAS=(N/A) knots, GW=(N/A)k lbs. Ages, radii, and velocities of the vortex cores are (N/A) and (N/A) sec., (N/A) and (N/A) ft., and 17.3 and (N/A) fps, respectively.

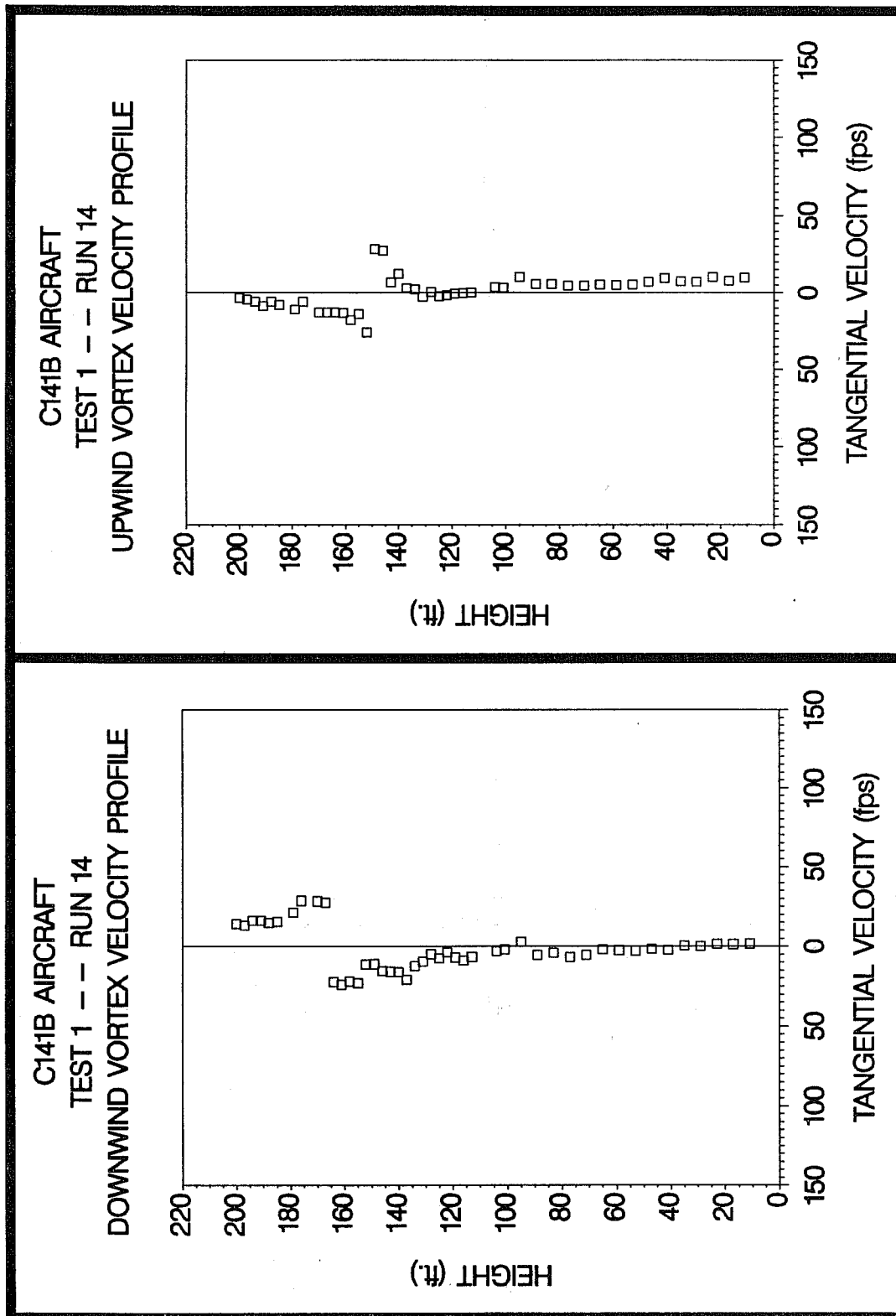


**Figure C-14.** C141B upwind (top) and downwind (bottom) vortex tangential velocity profile at maximum intensity from Test 1, Run 14, ambient wind speed=23.4 fps,  $\delta_F=74\%$ , IAS=135 knots, GW=223.0k lbs. Ages, radii, and velocities of the vortex cores are 19 and 15 sec., (N/A) and (N/A) ft., and 25.7 and 27.4 fps, respectively.

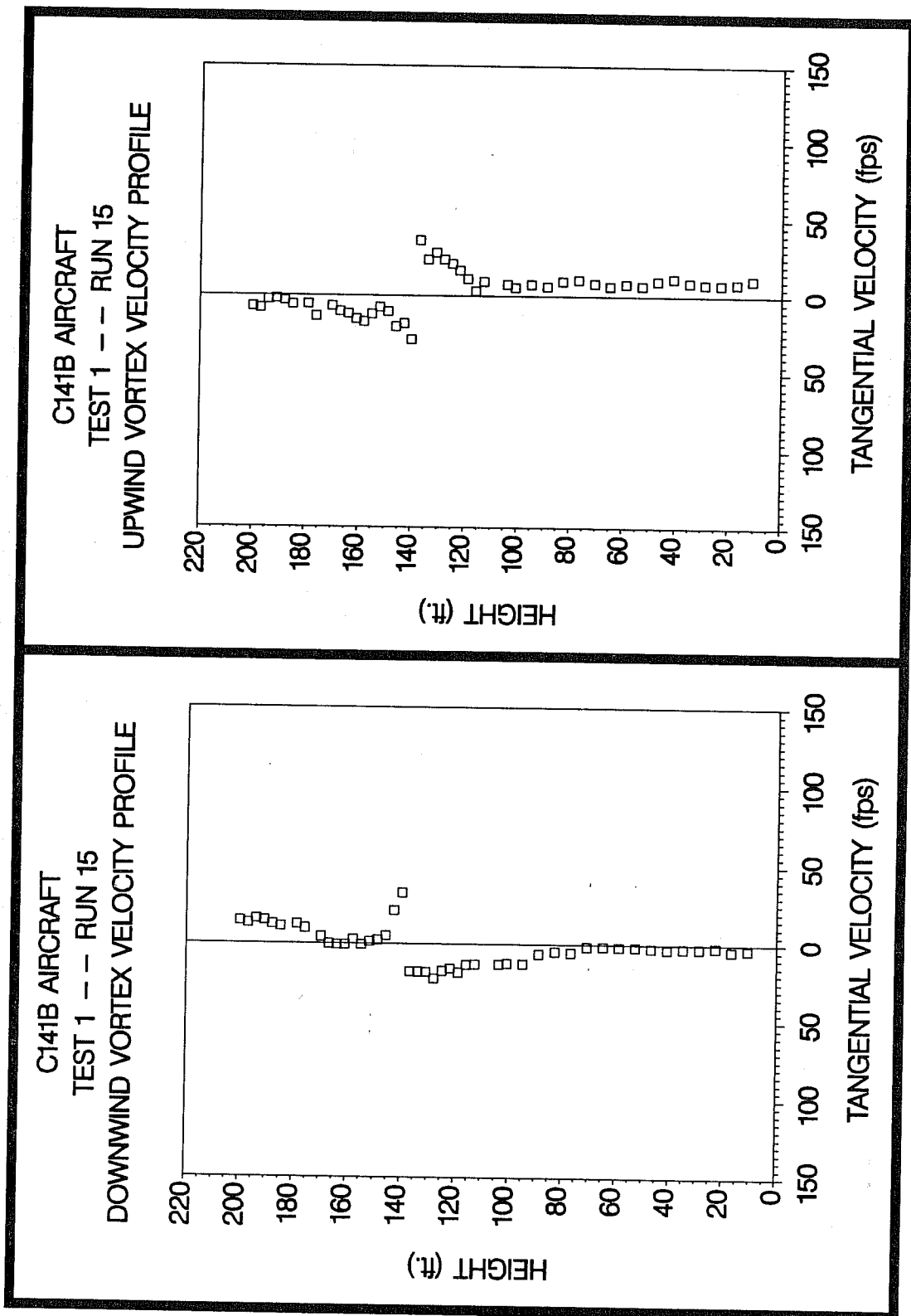
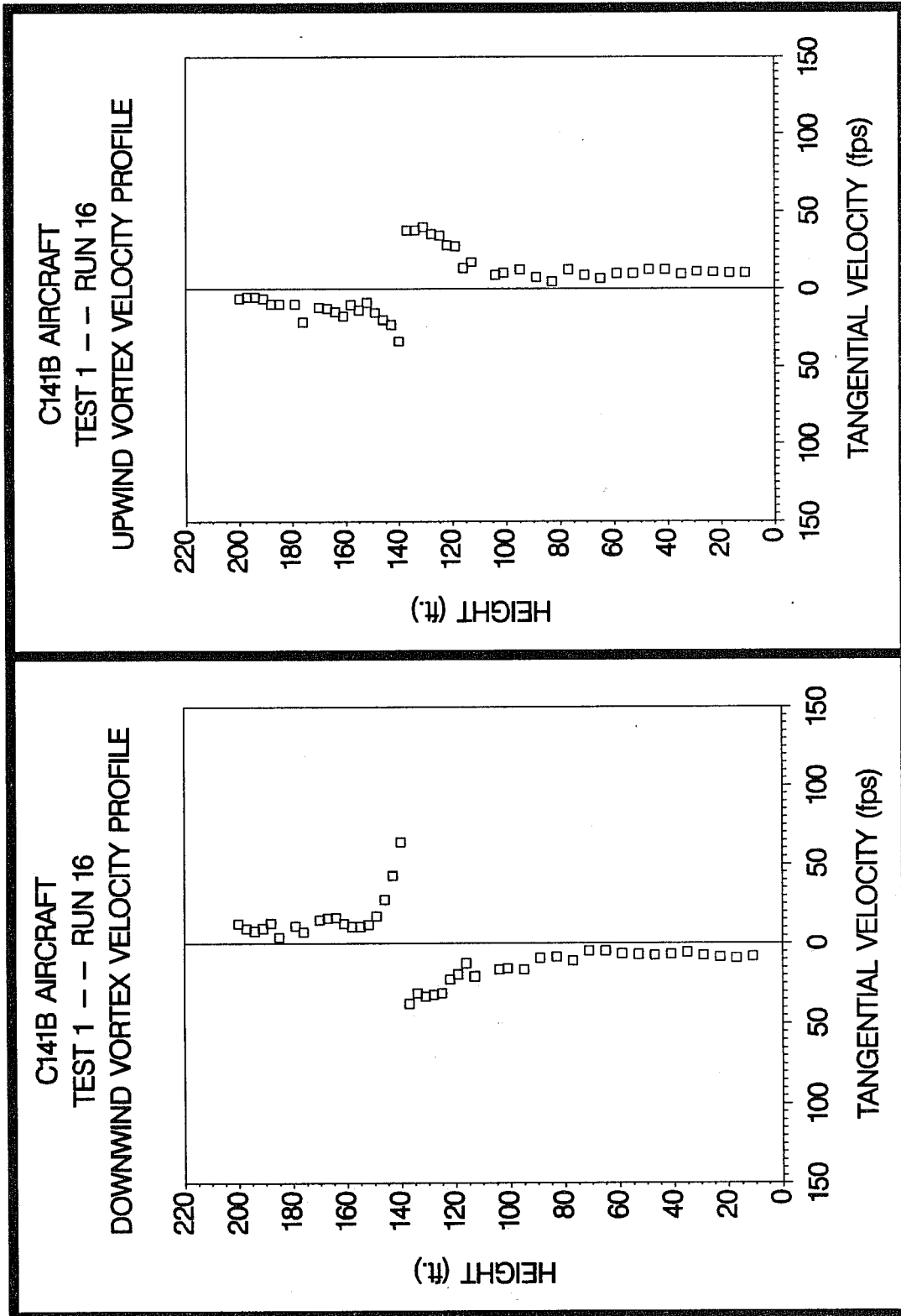


Figure C-15. C141B upwind (top) and downwind (bottom) vortex tangential velocity profile at maximum intensity from Test 1, Run 15, ambient wind speed=24.2 fps,  $\delta_F=73\%$ , IAS=135 knots, GW=221.0k lbs. Ages, radii, and velocities of the vortex cores are 14 and 10 sec., (N/A) and (N/A) ft., and 28.4 and 32.8 fps, respectively.



**Figure C-16.** C141B upwind (top) and downwind (bottom) vortex tangential velocity profile at maximum intensity from Test 1, Run 16, ambient wind speed=22.6 fps,  $\delta_F=70\%$ , IAS=134 knots, GW=218.0k lbs. Ages, radii, and velocities of the vortex cores are 12 and 7 sec., (N/A) and (N/A) ft., and 33.5 and 63.8 fps, respectively.

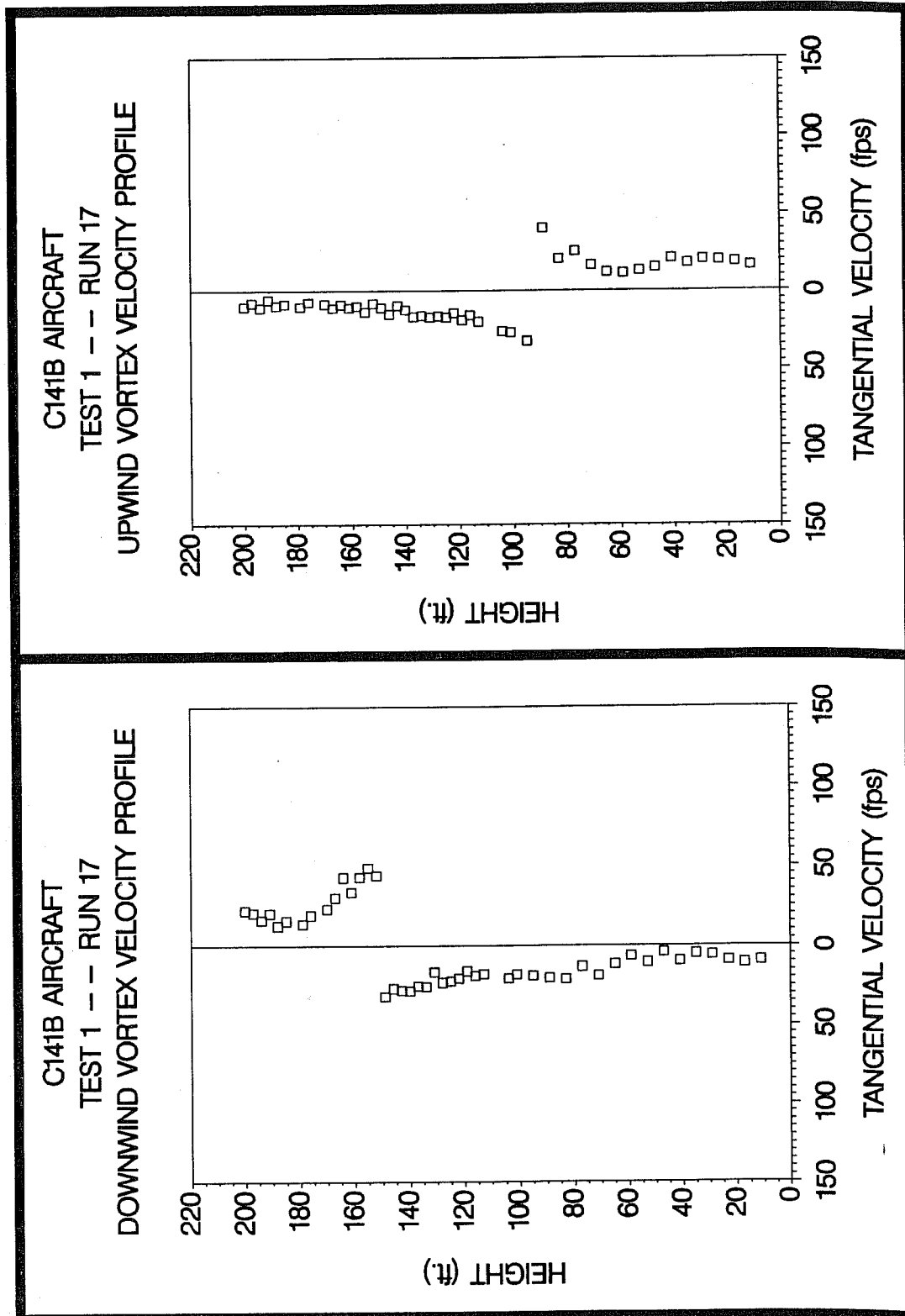
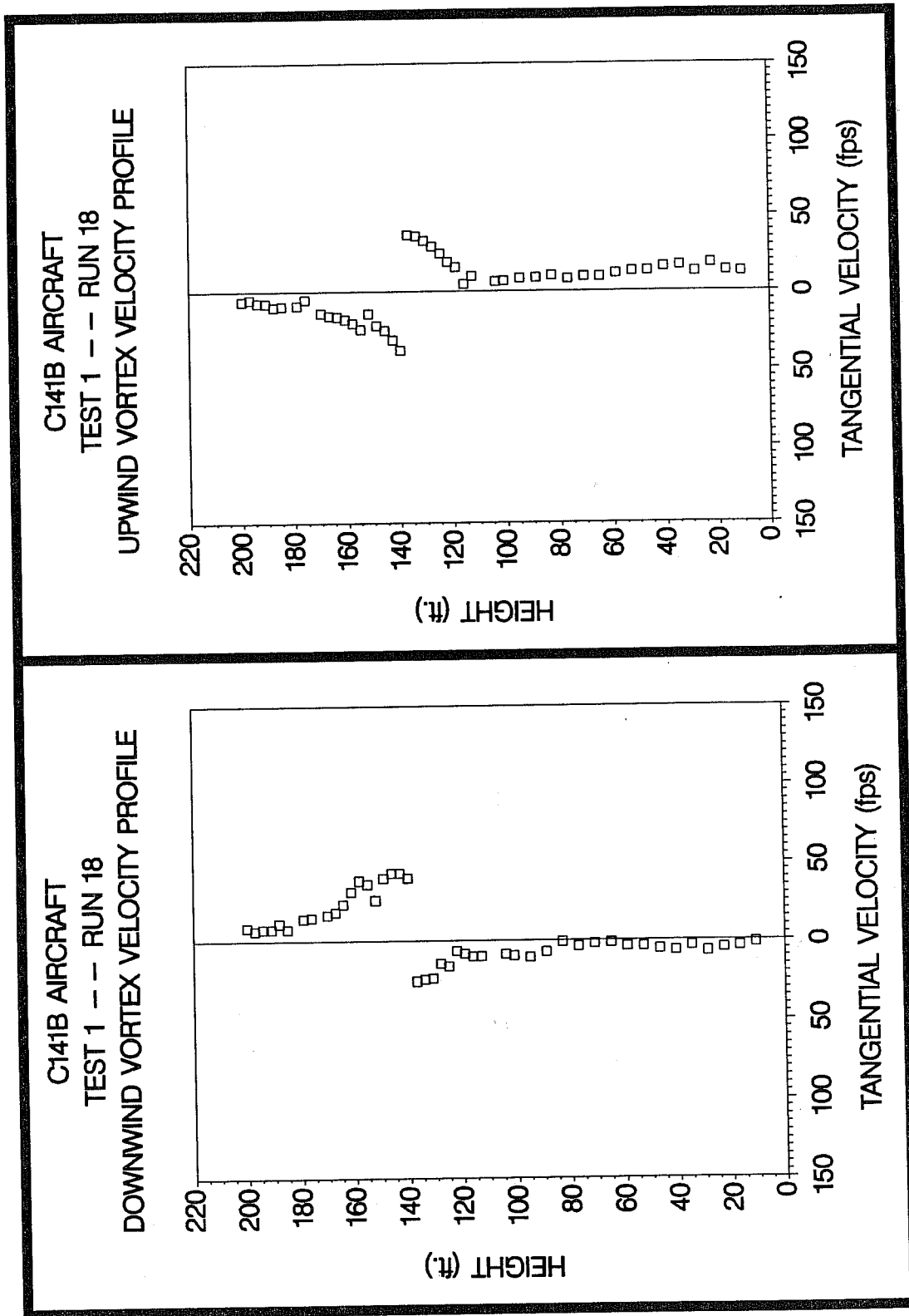
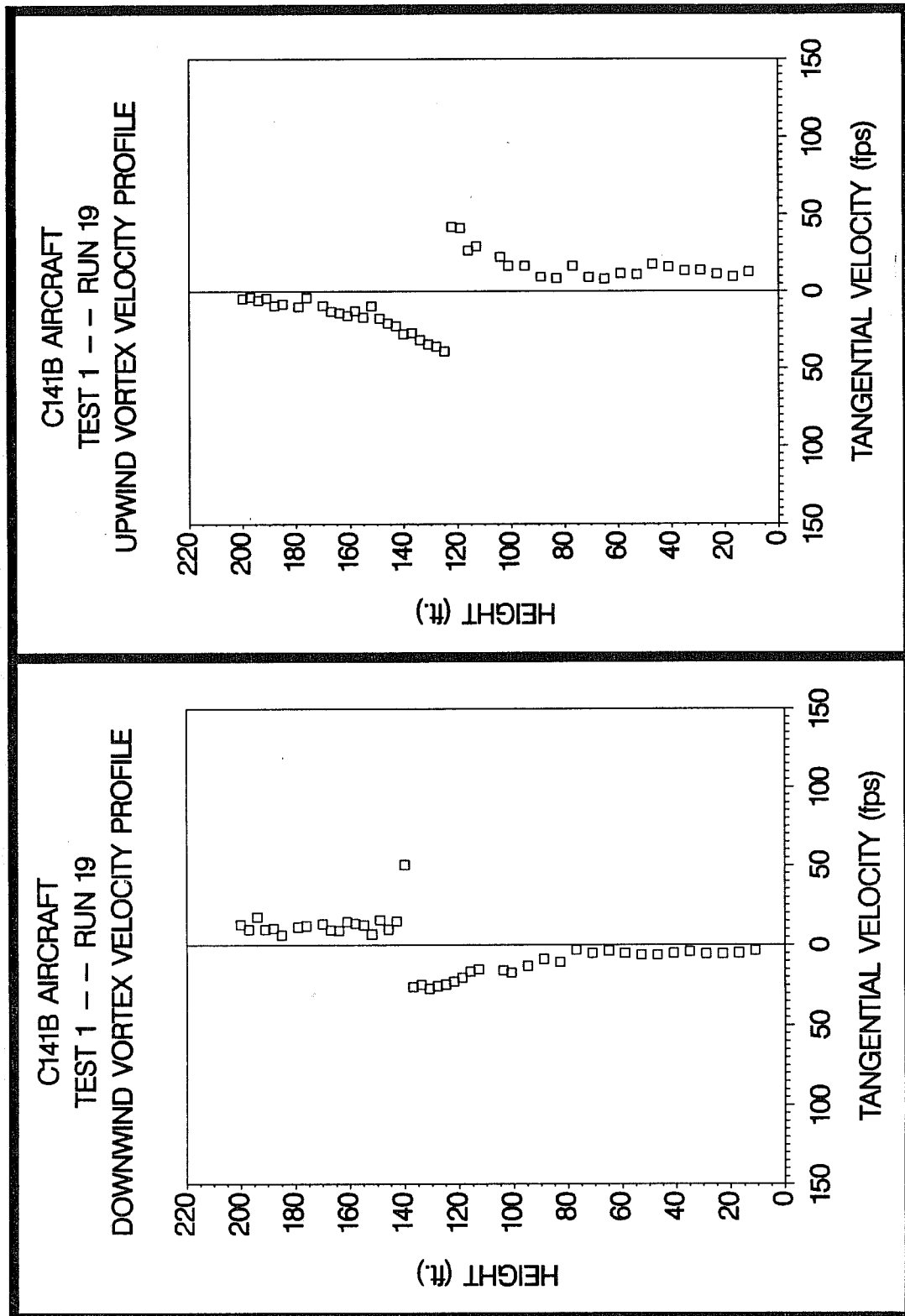


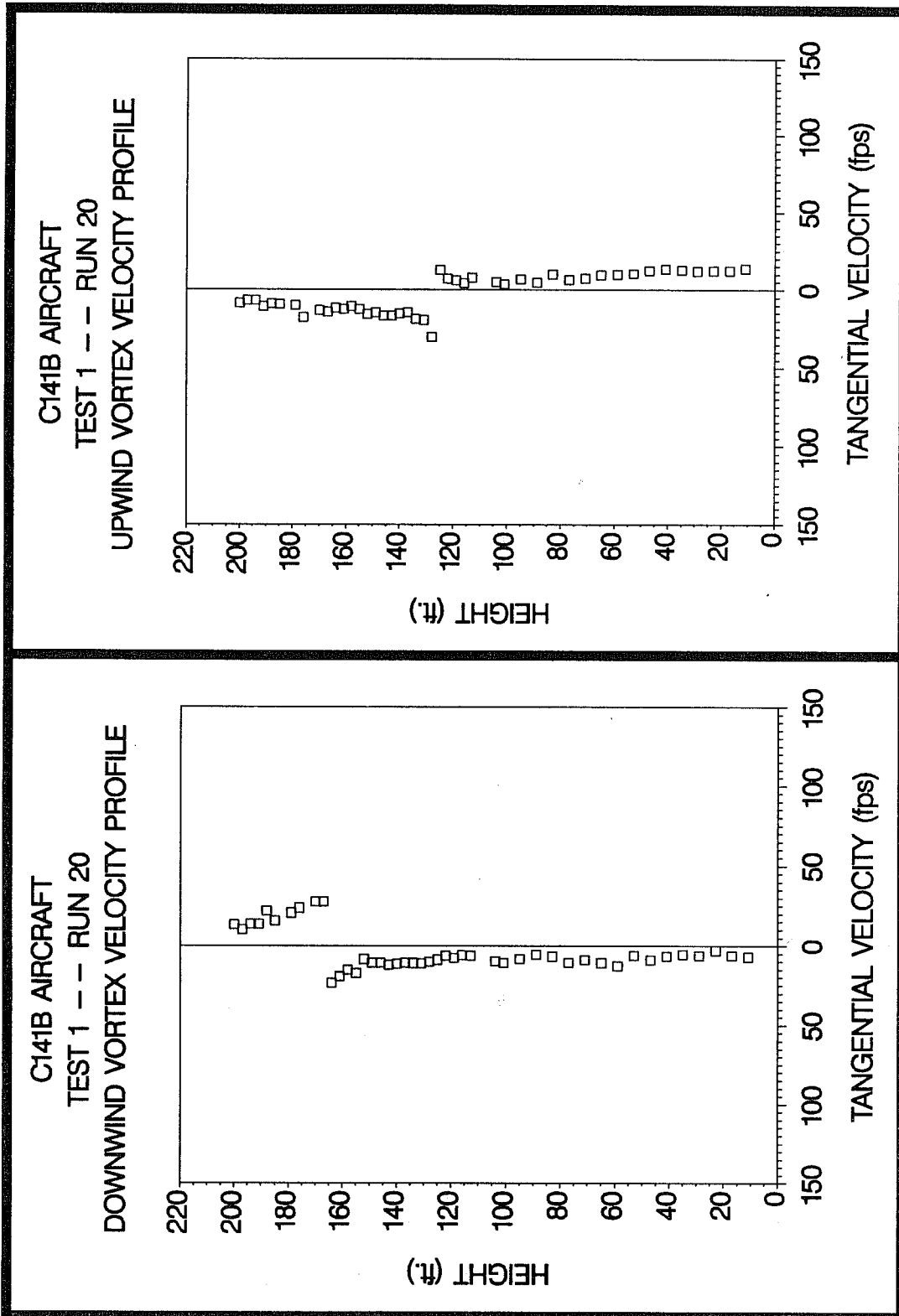
Figure C-17. C141B upwind (top) and downwind (bottom) vortex tangential velocity profile at maximum intensity from Test 1, Run 17, ambient wind speed=31.1 fps,  $\delta_F=70\%$ , IAS=134 knots, GW=217.0k lbs. Ages, radii, and velocities of the vortex cores are 18 and 12 sec., (N/A) and (N/A) ft., and 32.6 and 43.6 fps, respectively.

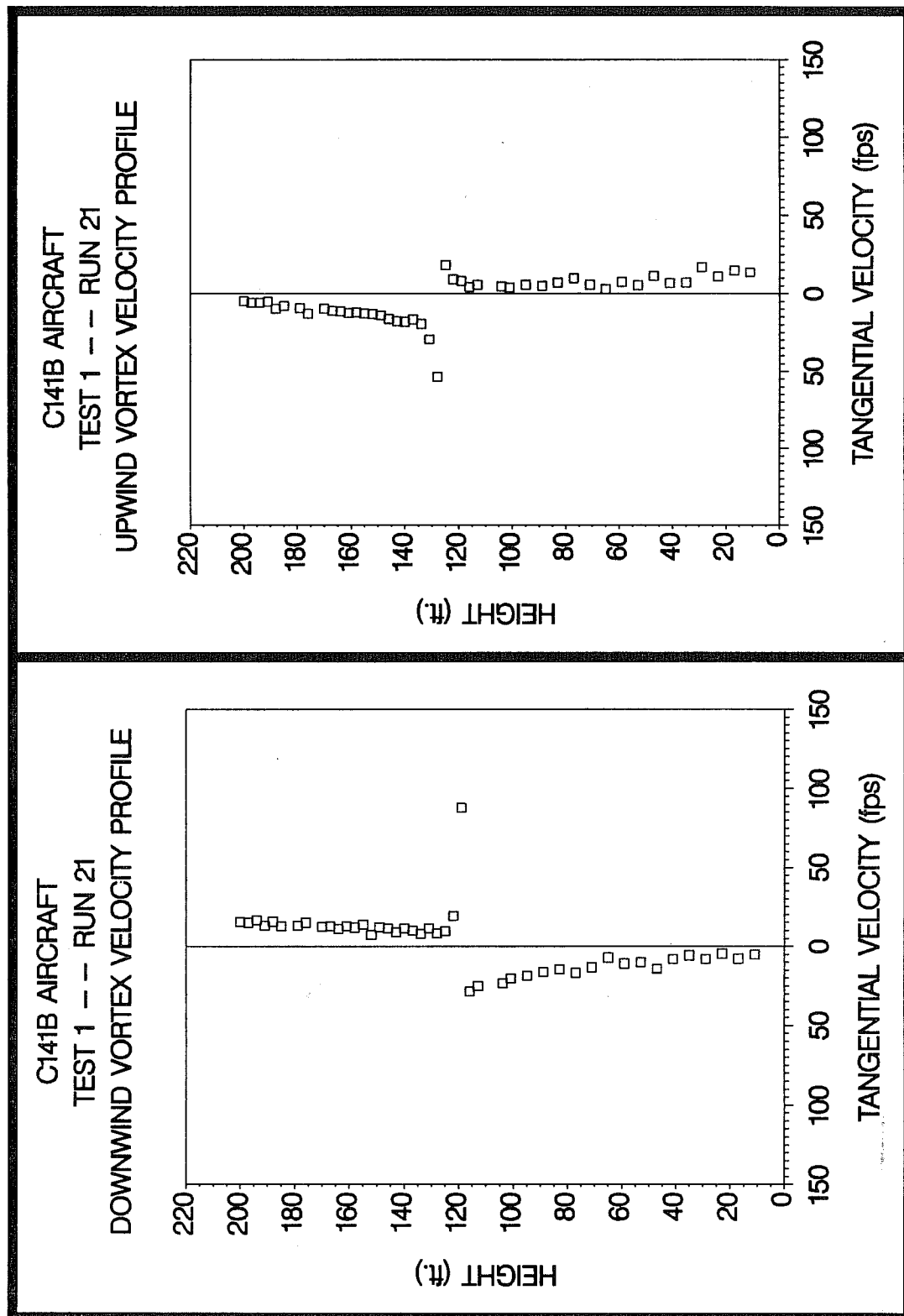


**Figure C-18.** C141B upwind (top) and downwind (bottom) vortex tangential velocity profile at maximum intensity from Test 1, Run 18, ambient wind speed=26.5 fps,  $\delta_F=70\%$ , IAS=134 knots, GW=215.0k lbs. Ages, radii, and velocities of the vortex cores are 14 and 10 sec., (N/A) and (N/A) ft., and 37.8 and 39.8 fps, respectively.

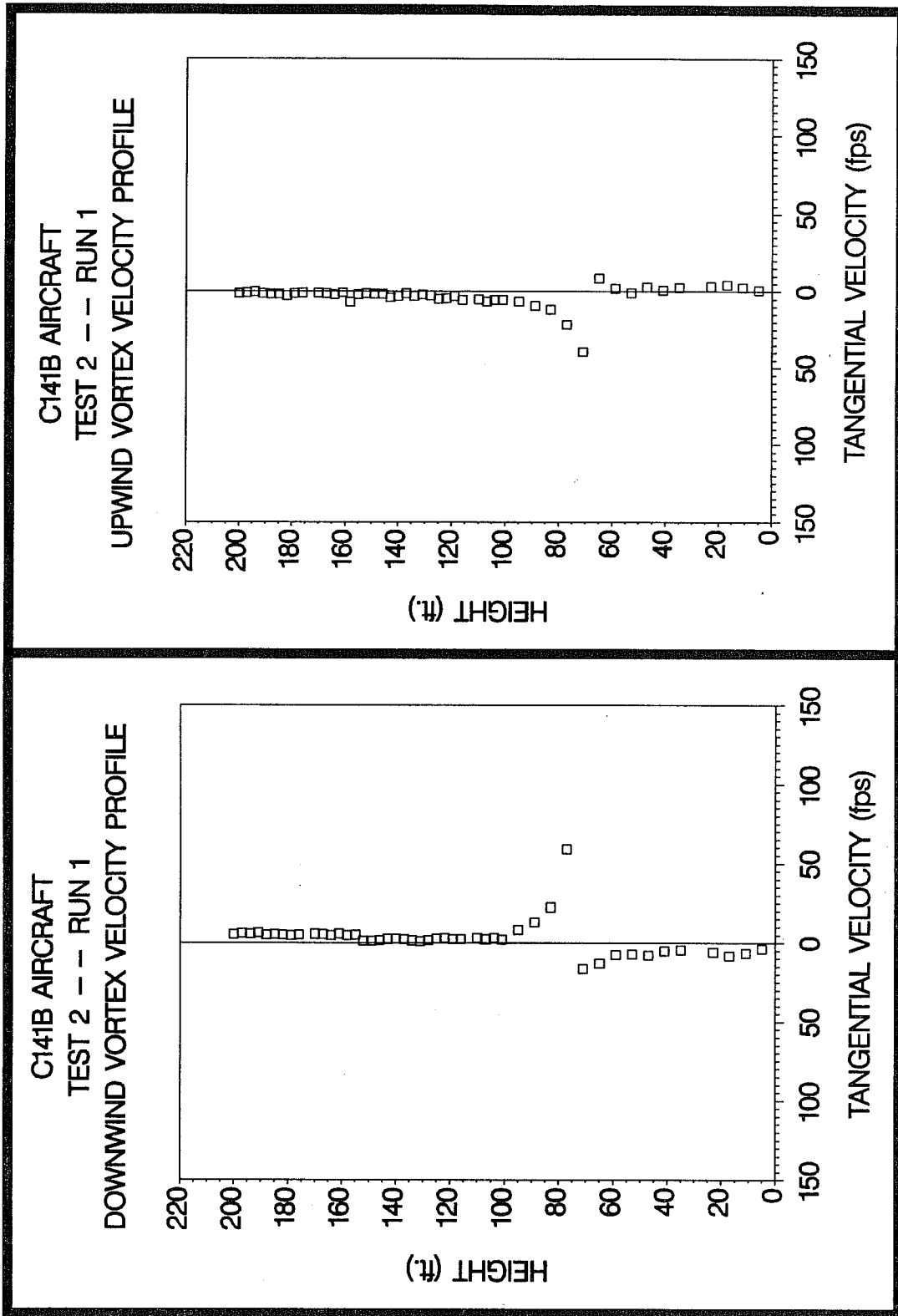


**Figure C-19.** C141B upwind (top) and downwind (bottom) vortex tangential velocity profile at maximum intensity from Test 1, Run 19, ambient wind speed=22.3 fps,  $\delta_F=70\%$ , IAS=134 knots, GW=213.0k lbs. Ages, radii, and velocities of the vortex cores are 14 and 11 sec., (N/A) and (N/A) ft., and 38.8 and 50.3 fps, respectively.

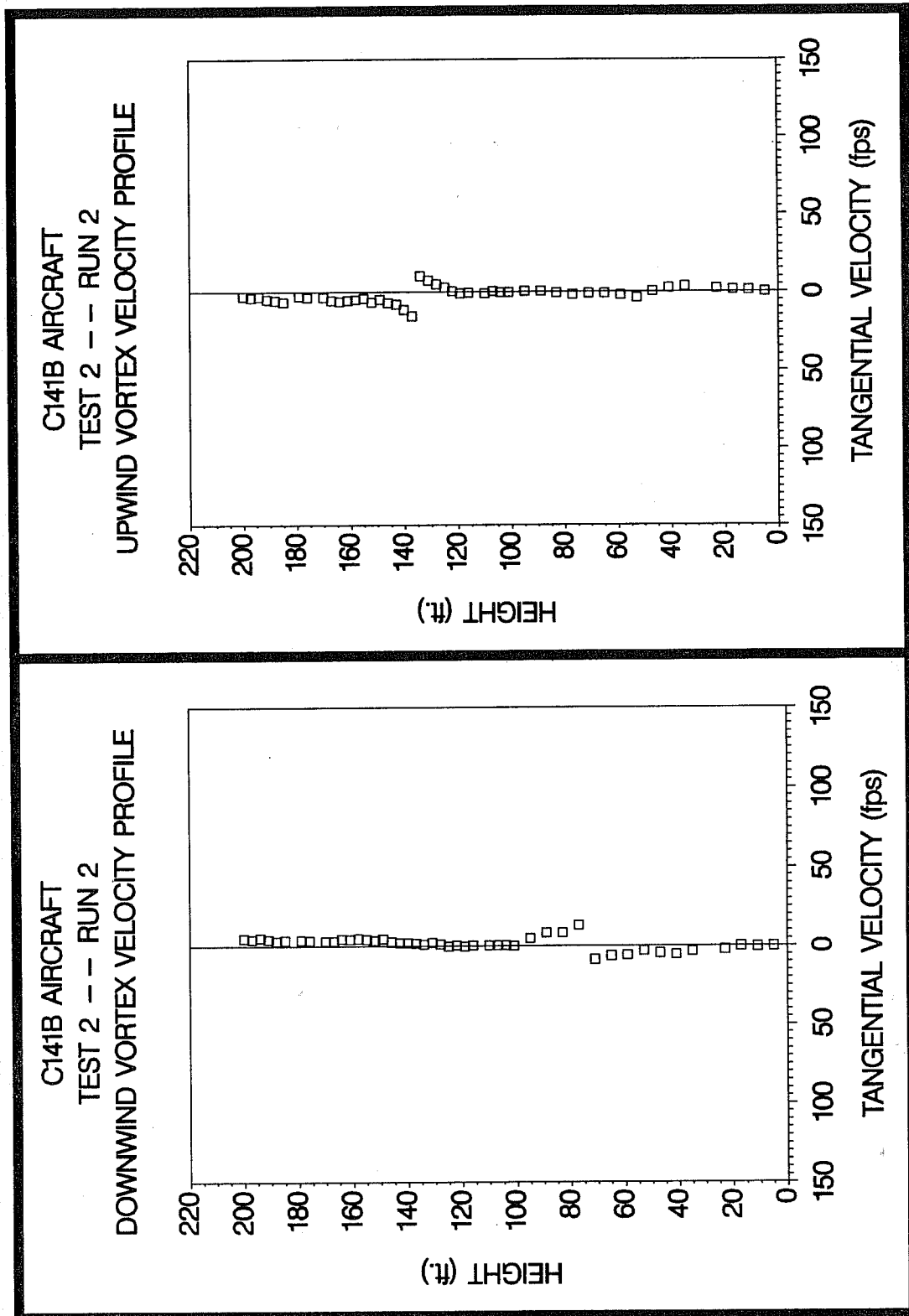




**Figure C-21.** C141B upwind (top) and downwind (bottom) vortex tangential velocity profile at maximum intensity from Test 1, Run 21, ambient wind speed=23.0 fps,  $\delta_F=26\%$ , IAS=150 knots, GW=209.0k lbs. Ages, radii, and velocities of the vortex cores are 12 and 6 sec., (N/A) and (N/A) ft., and 53.7 and 87.8 fps, respectively.



**Figure C-22.** C141B upwind (top) and downwind (bottom) vortex tangential velocity profile at maximum intensity from Test 2, Run 1, ambient wind speed=8.6 fps,  $\delta_F=39\%$ , IAS=150 knots, GW=231.0k lbs. Ages, radii, and velocities of the vortex cores are (N/A) and (N/A) sec., (N/A) and (N/A) ft., and 39.4 and 59.0 fps, respectively.



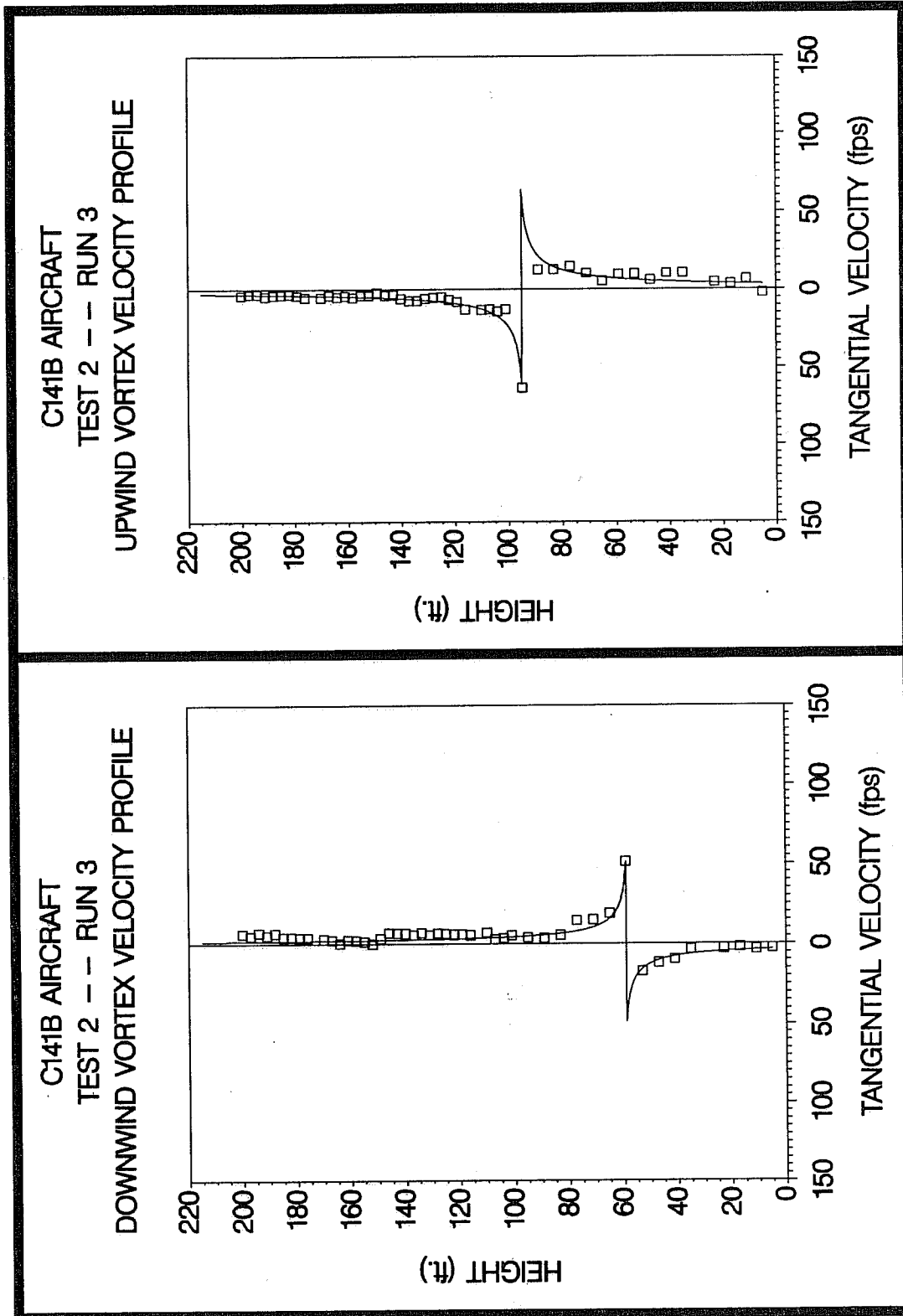


**Figure C-24.** C141B upwind (top) and downwind (bottom) vortex tangential velocity profile at maximum intensity from Test 2, Run 3, ambient wind speed=9.5 fps,  $\delta_F=39\%$ , IAS=150 knots, GW=227.0k lbs. Ages, radii, and velocities of the vortex cores are 98 and 46 sec., 1.1 and 0.9 ft., and 63.5 and 51.3 fps, respectively.

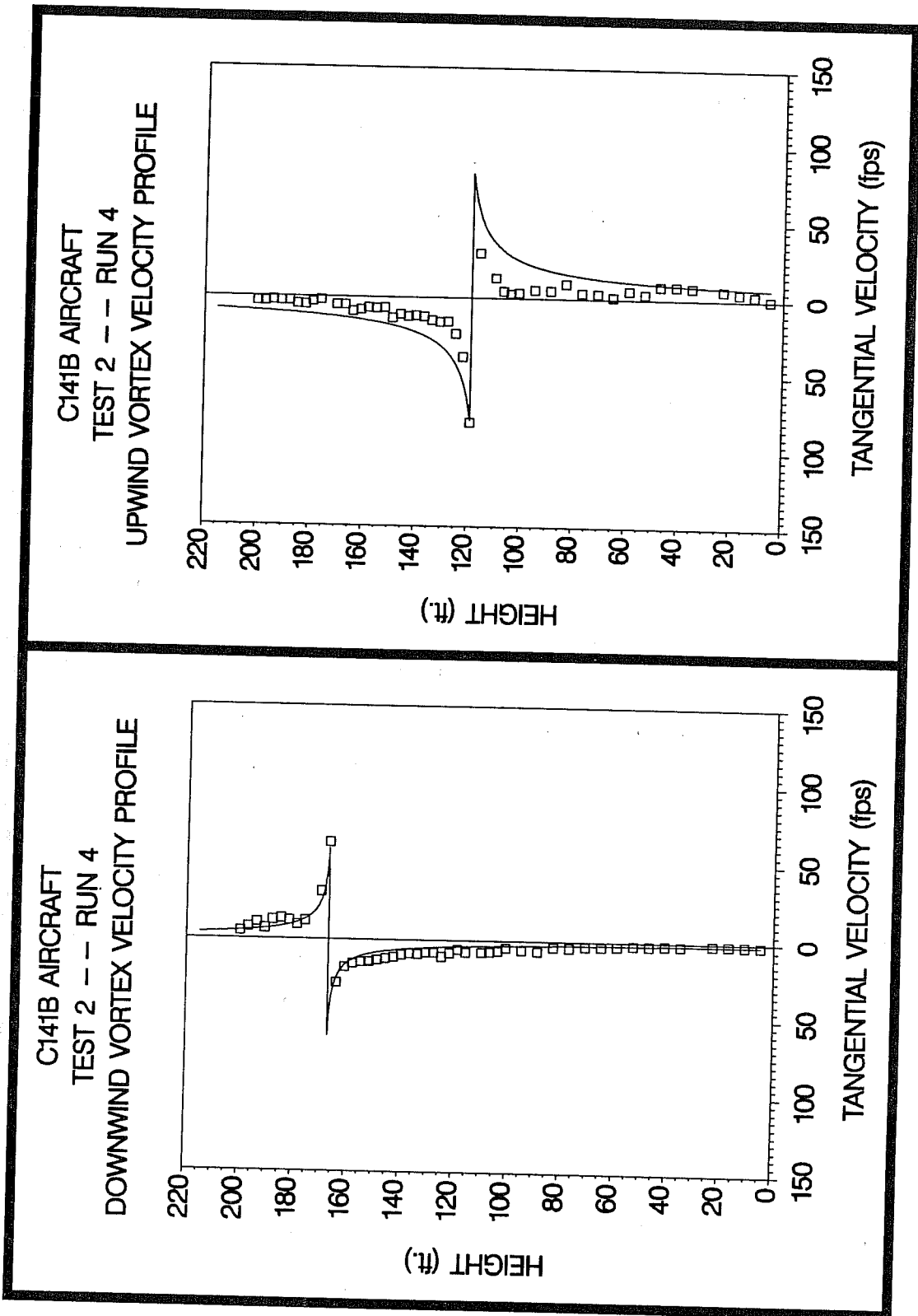


Figure C-25. C141B upwind (top) and downwind (bottom) vortex tangential velocity profile at maximum intensity from Test 2, Run 4, ambient wind speed=11.7 fps,  $\delta_F=39\%$ , IAS=150 knots, GW=225.0k lbs. Ages, radii, and velocities of the vortex cores are 38 and 19 sec., 2.7 and 0.7 ft., and 81.6 and 62.6 fps, respectively.

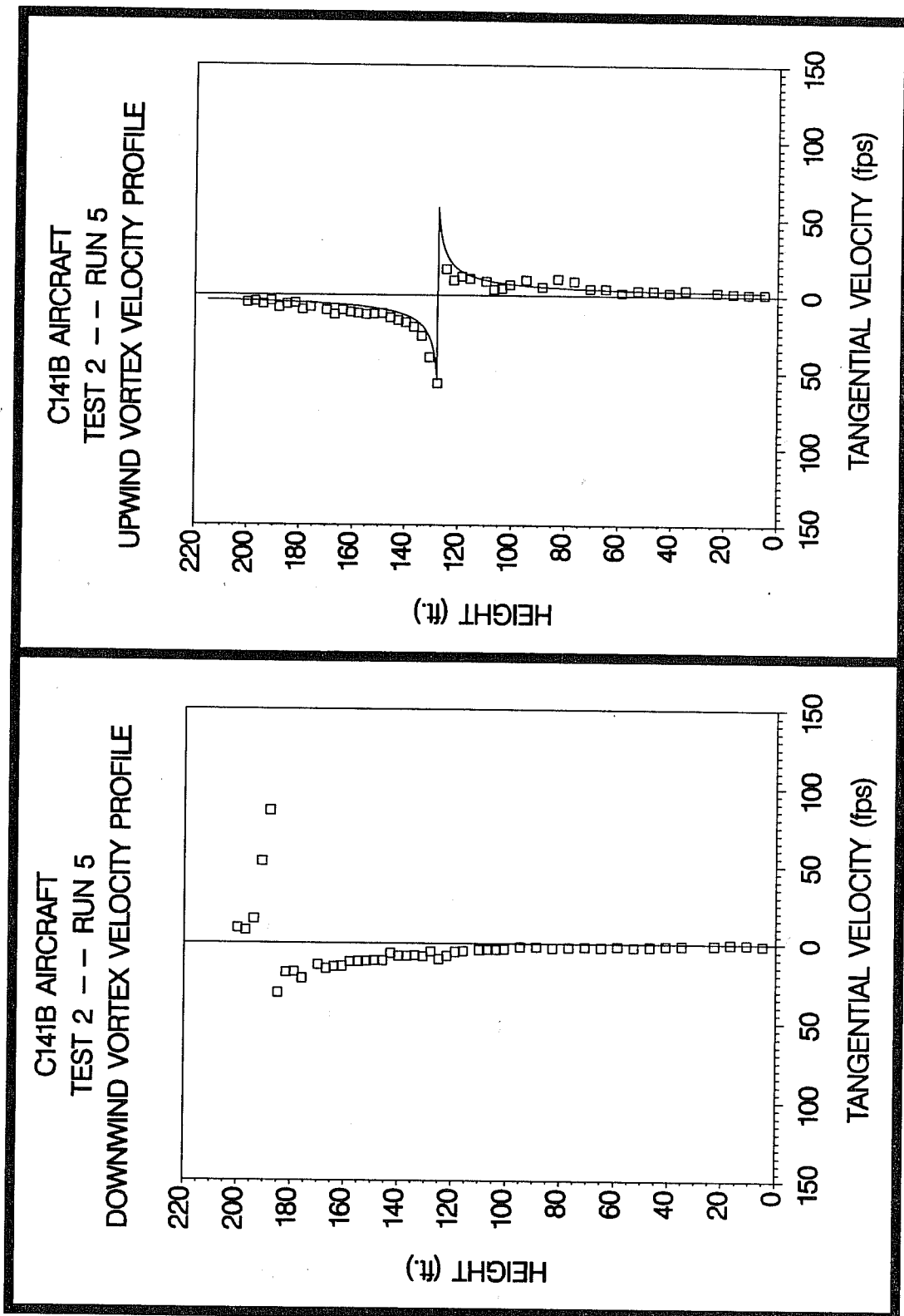
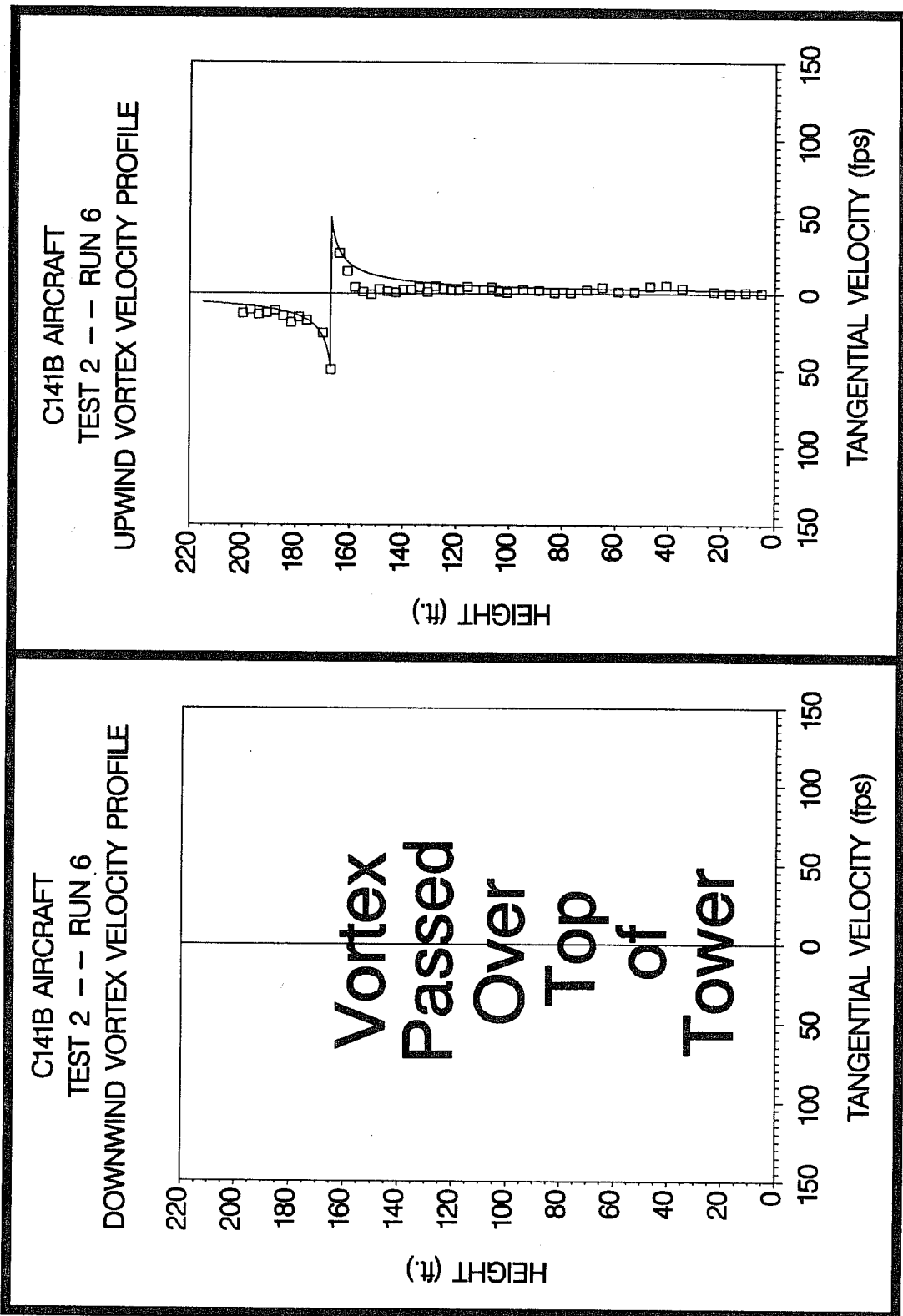


Figure C-26. C141B upwind (top) and downwind (bottom) vortex tangential velocity profile at maximum intensity from Test 2, Run 5, ambient wind speed=12.7 fps,  $\delta_F=39\%$ , IAS=150 knots, GW=223.0k lbs. Ages, radii, and velocities of the vortex cores are 28 and 14 sec., 1.1 and (N/A) ft., and 57.2 and 85.3 fps, respectively.



**Figure C-27.** C141B upwind (top) and downwind (bottom) vortex tangential velocity profile at maximum intensity from Test 2, Run 6, ambient wind speed=11.9 fps,  $\delta_F=35\%$ , IAS=150 knots, GW=221.0k lbs. Ages, radii, and velocities of the vortex cores are 21 and (N/A) sec., 1.7 and (N/A) ft., and 49.7 and (N/A) fps, respectively.

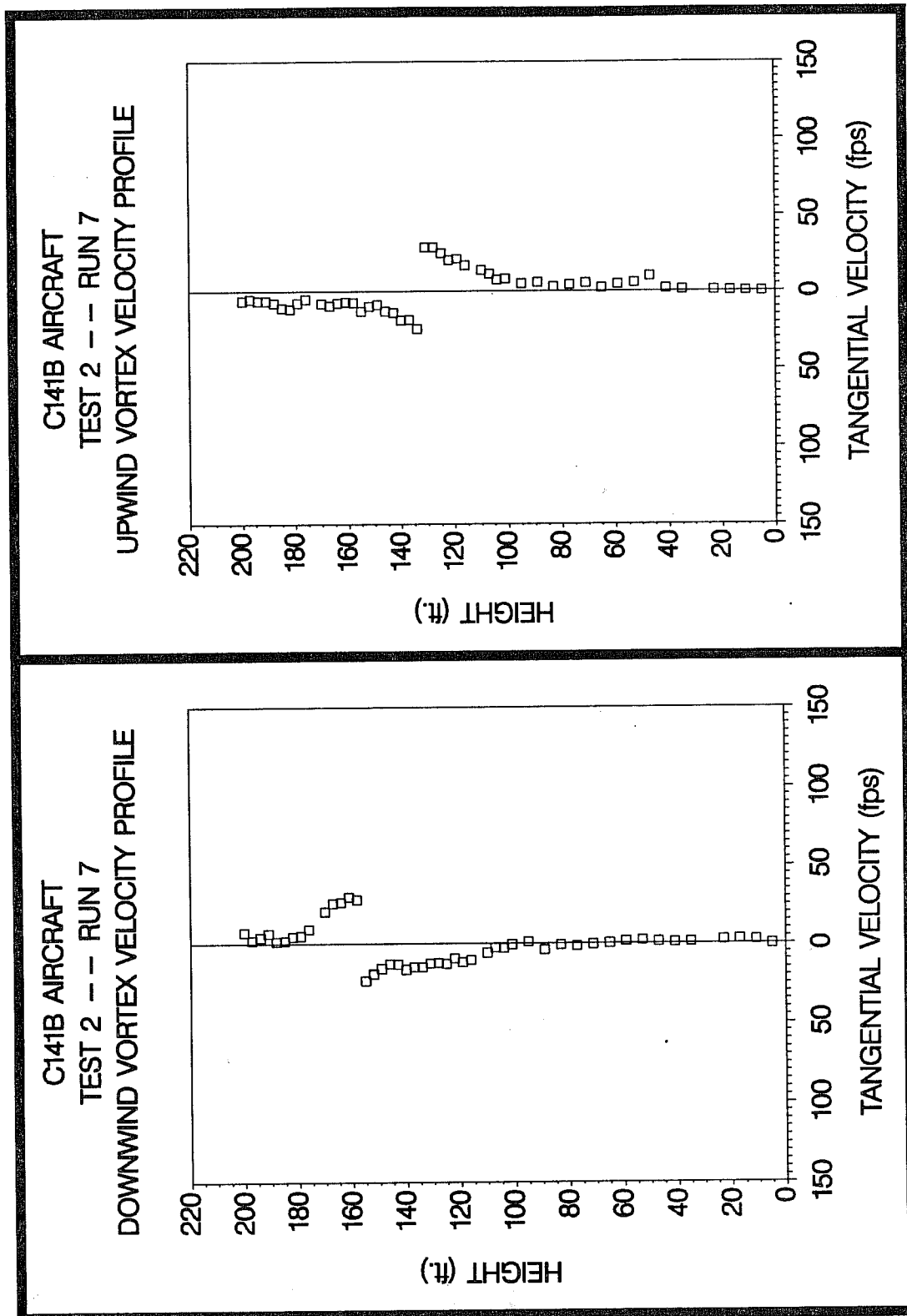
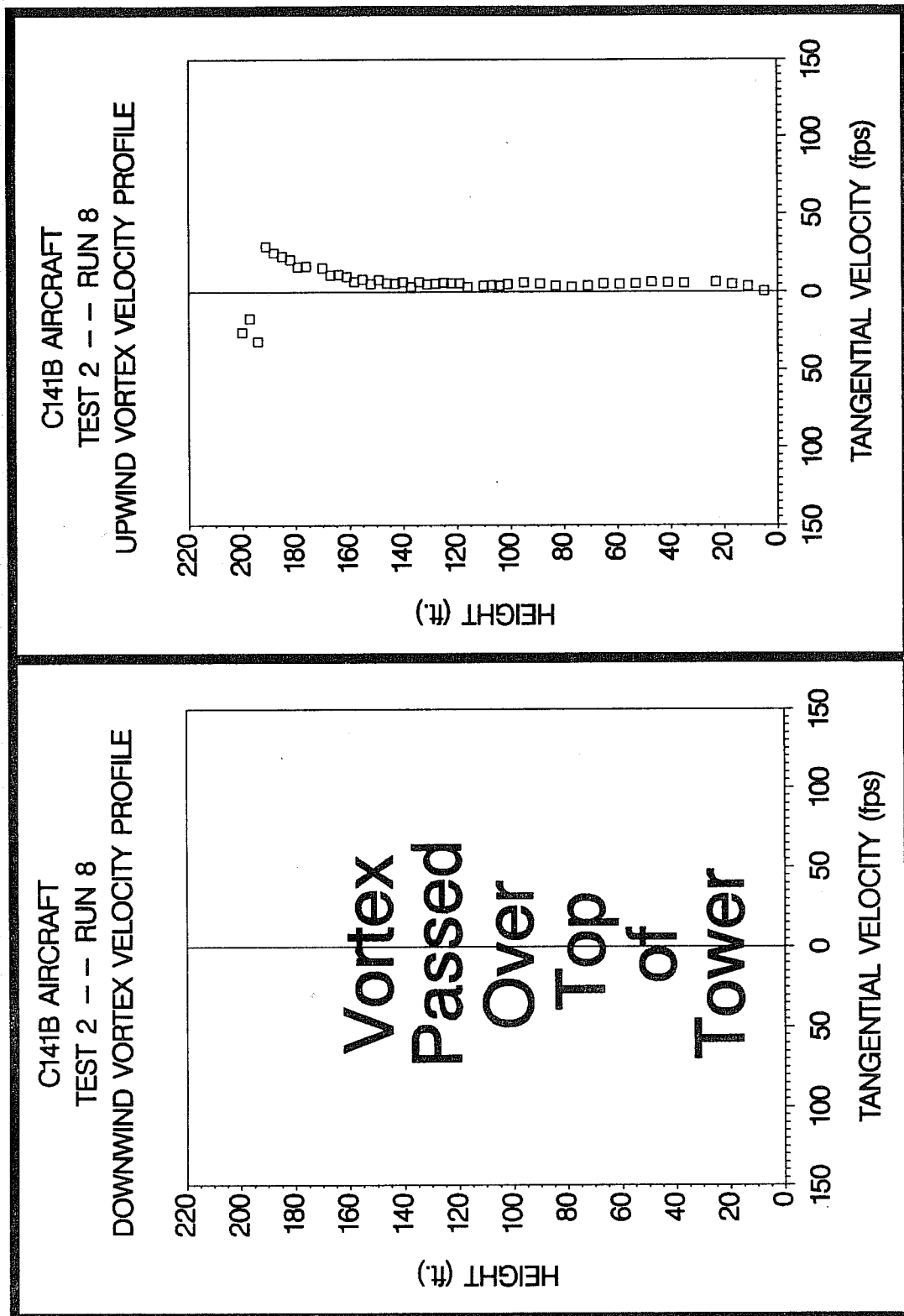


Figure C-28. C141B upwind (top) and downwind (bottom) vortex tangential velocity profile at maximum intensity from Test 2, Run 7, ambient wind speed=15.4 fps,  $\delta_F=57\%$ , IAS=150 knots, GW=219.0k lbs. Ages, radii, and velocities of the vortex cores are 21 and 12 sec., (N/A) and (N/A) ft., and 24.1 and 28.2 fps, respectively.



**Figure C-29.** C141B upwind (top) and downwind (bottom) vortex tangential velocity profile at maximum intensity from Test 2, Run 8, ambient wind speed=15.0 fps,  $\delta_F=57\%$ , IAS=150 knots, GW=215.0k lbs. Ages, radii, and velocities of the vortex cores are 23 and (N/A) sec., (N/A) and (N/A) ft., and 31.5 and (N/A) fps, respectively.

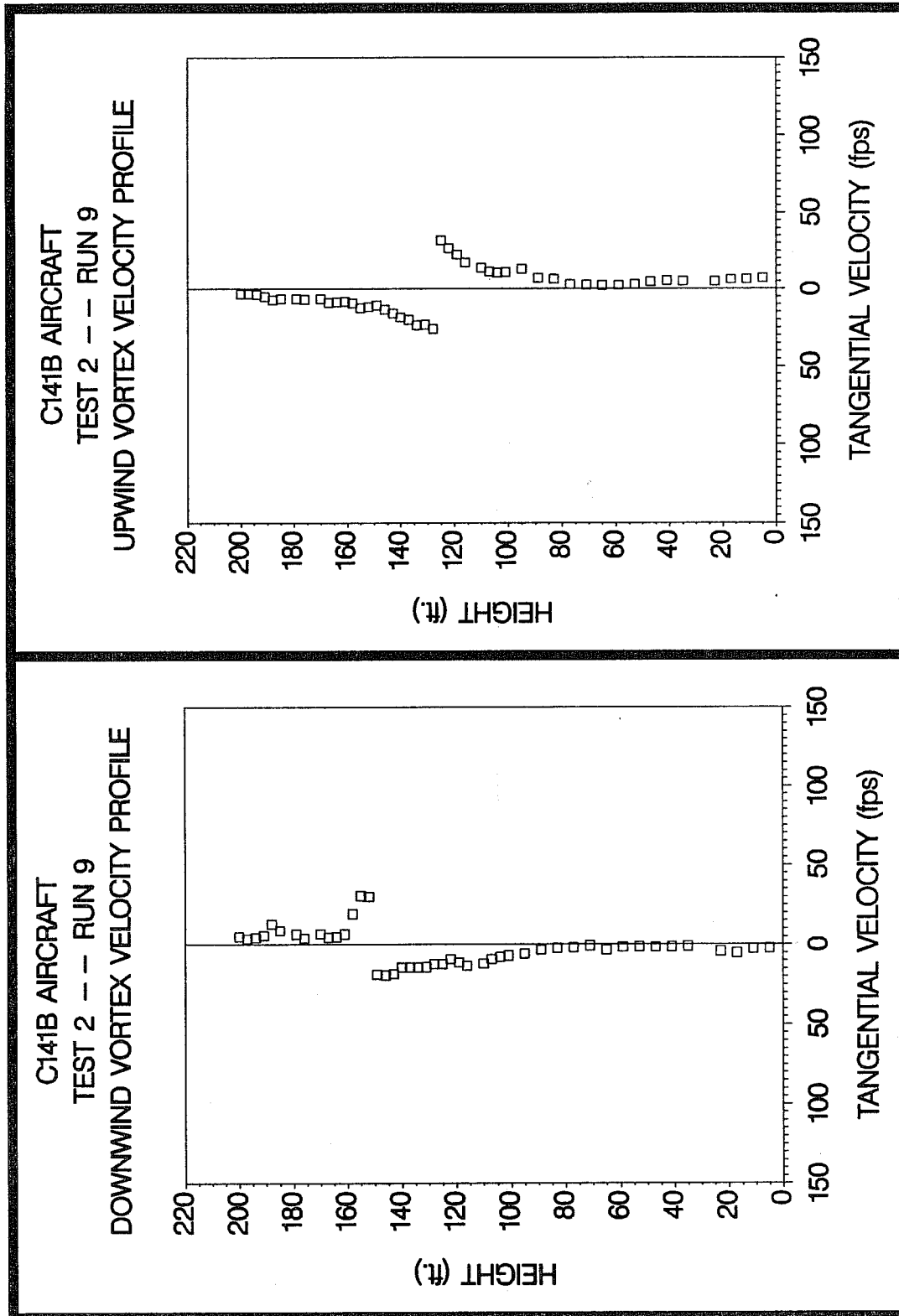


Figure C-30. C141B upwind (top) and downwind (bottom) vortex tangential velocity profile at maximum intensity from Test 2, Run 9, ambient wind speed=13.5 fps,  $\delta_F=57\%$ , IAS=150 knots, GW=214.0k lbs. Ages, radii, and velocities of the vortex cores are 28 and 22 sec., (N/A) and (N/A) ft., and 25.9 and 29.9 fps, respectively.

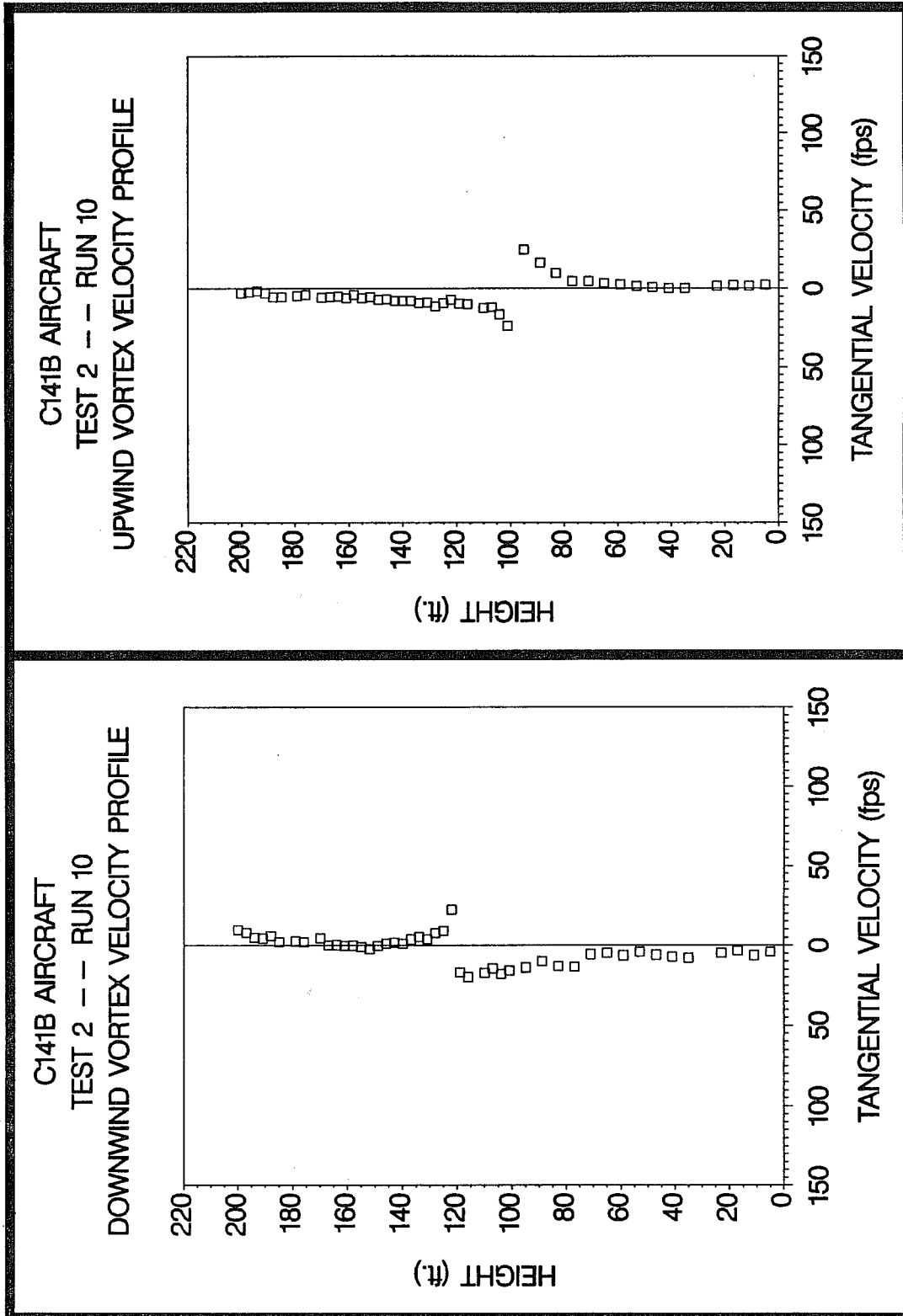


Figure C-31. C141B upwind (top) and downwind (bottom) vortex tangential velocity profile at maximum intensity from Test 2, Run 10, ambient wind speed=11.3 fps,  $\delta_F=53\%$ , IAS=150 knots, GW=211.0k lbs. Ages, radii, and velocities of the vortex cores are 47 and 31 sec., (N/A) and (N/A) ft., and 23.9 and 22.4 fps, respectively.

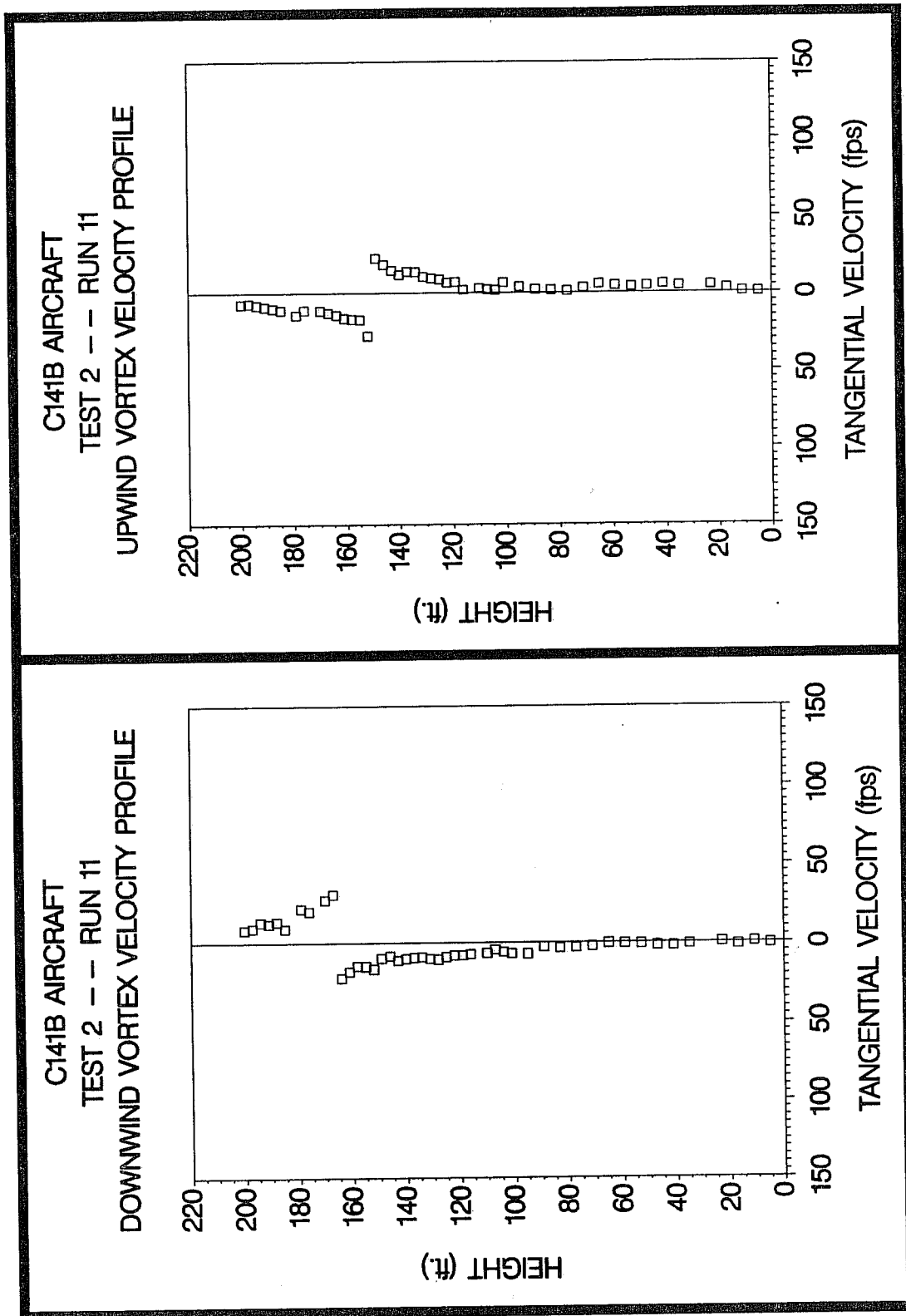
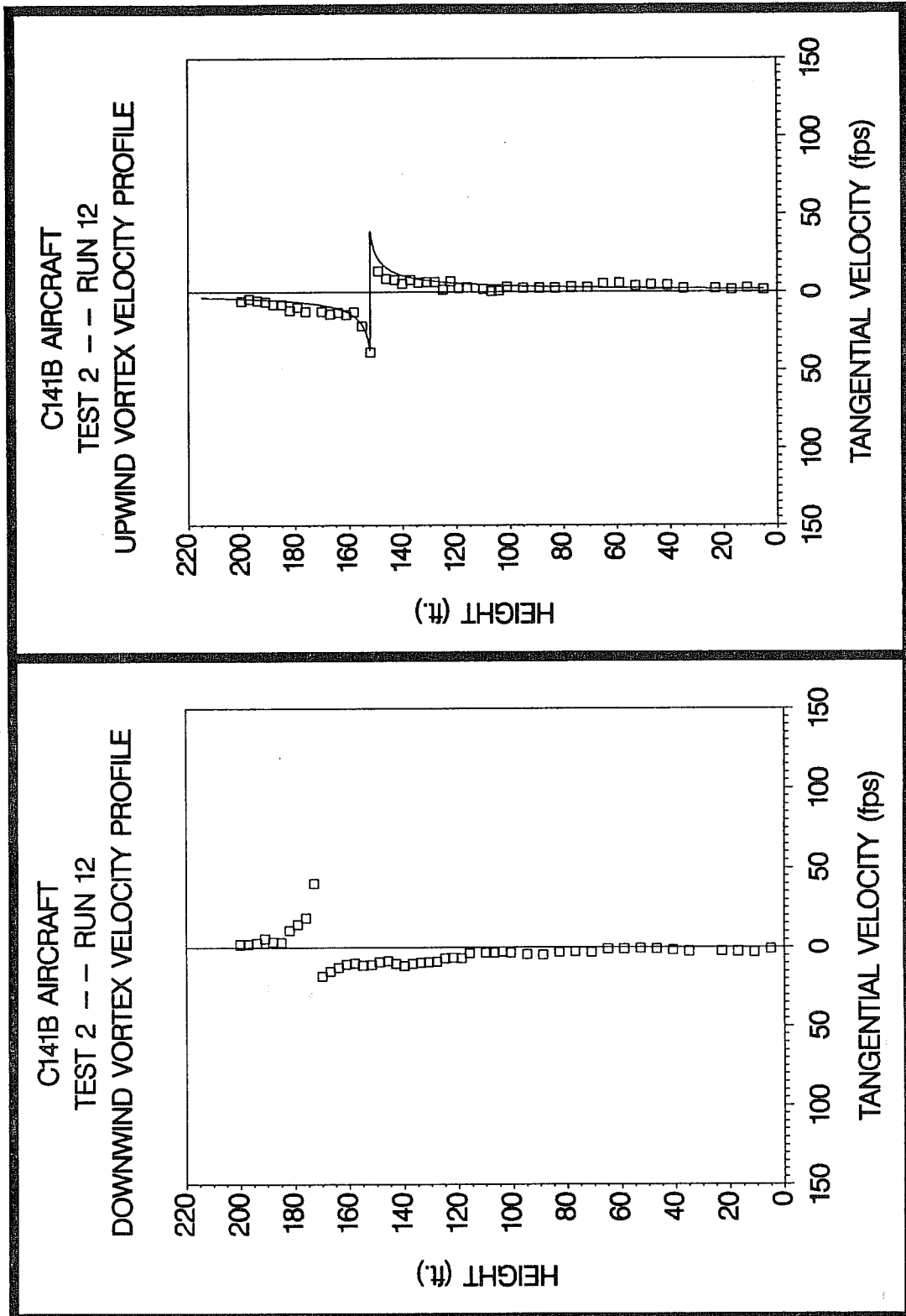
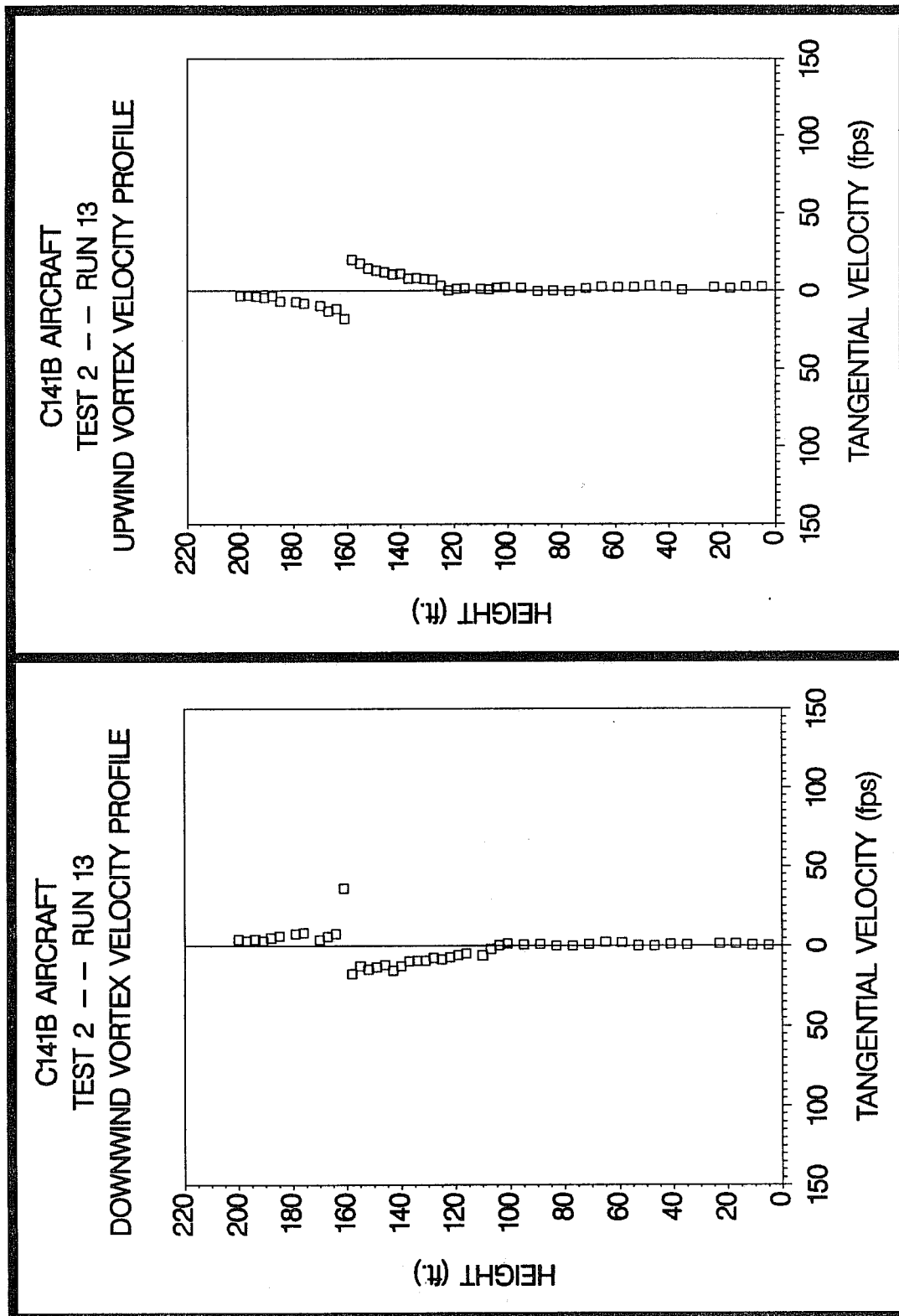


Figure C-32. C141B upwind (top) and downwind (bottom) vortex tangential velocity profile at maximum intensity from Test 2, Run 11, ambient wind speed=10.4 fps,  $\delta_F=53\%$ , IAS=150 knots, GW=209.0k lbs. Ages, radii, and velocities of the vortex cores are 41 and 28 sec., (N/A) and (N/A) ft., and 27.7 and 30.5 fps, respectively.



**Figure C-33.** C141B upwind (top) and downwind (bottom) vortex tangential velocity profile at maximum intensity from Test 2, Run 12, ambient wind speed=8.9 fps,  $\delta_F=53\%$ , IAS=150 knots, GW=206.0k lbs. Ages, radii, and velocities of the vortex cores are 65 and 40 sec., 1.5 and (N/A) ft., and 38.6 and 40.3 fps, respectively.



**Figure C-34.** C141B upwind (top) and downwind (bottom) vortex tangential velocity profile at maximum intensity from Test 2, Run 13, ambient wind speed=11.4 fps,  $\delta_F=49\%$ , IAS=150 knots, GW=205.0k lbs. Ages, radii, and velocities of the vortex cores are 42 and 31 sec., (N/A) and (N/A) ft., and 18.1 and 36.0 fps, respectively.

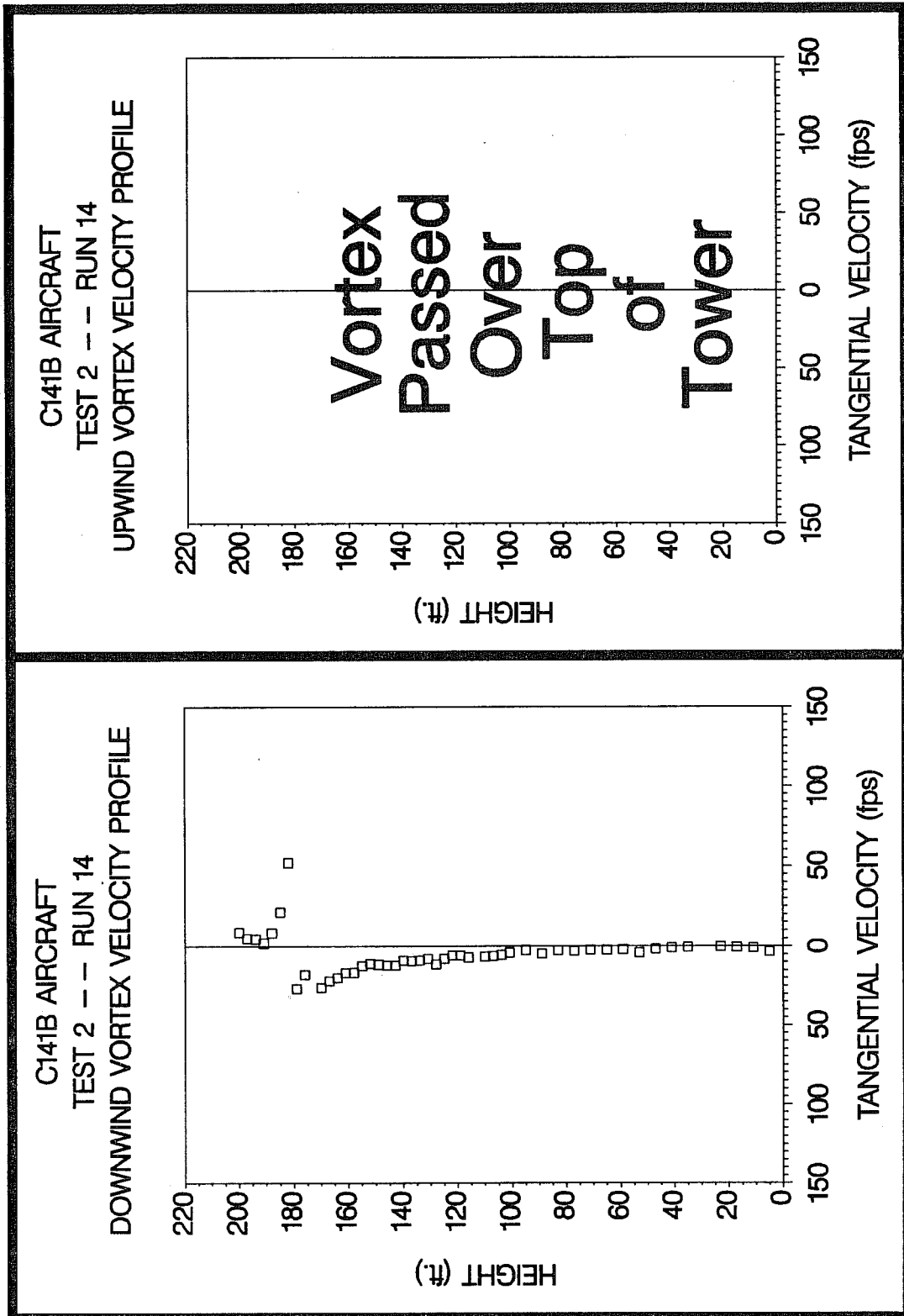


**Figure C-35.** C141B upwind (top) and downwind (bottom) vortex tangential velocity profile at maximum intensity from Test 2, Run 14, ambient wind speed=14.0 fps,  $\delta_F=70\%$ , IAS=130 knots, GW=203.0k lbs. Ages, radii, and velocities of the vortex cores are (N/A) and 19 sec., (N/A) and (N/A) ft., and (N/A) and 52.0 fps, respectively.

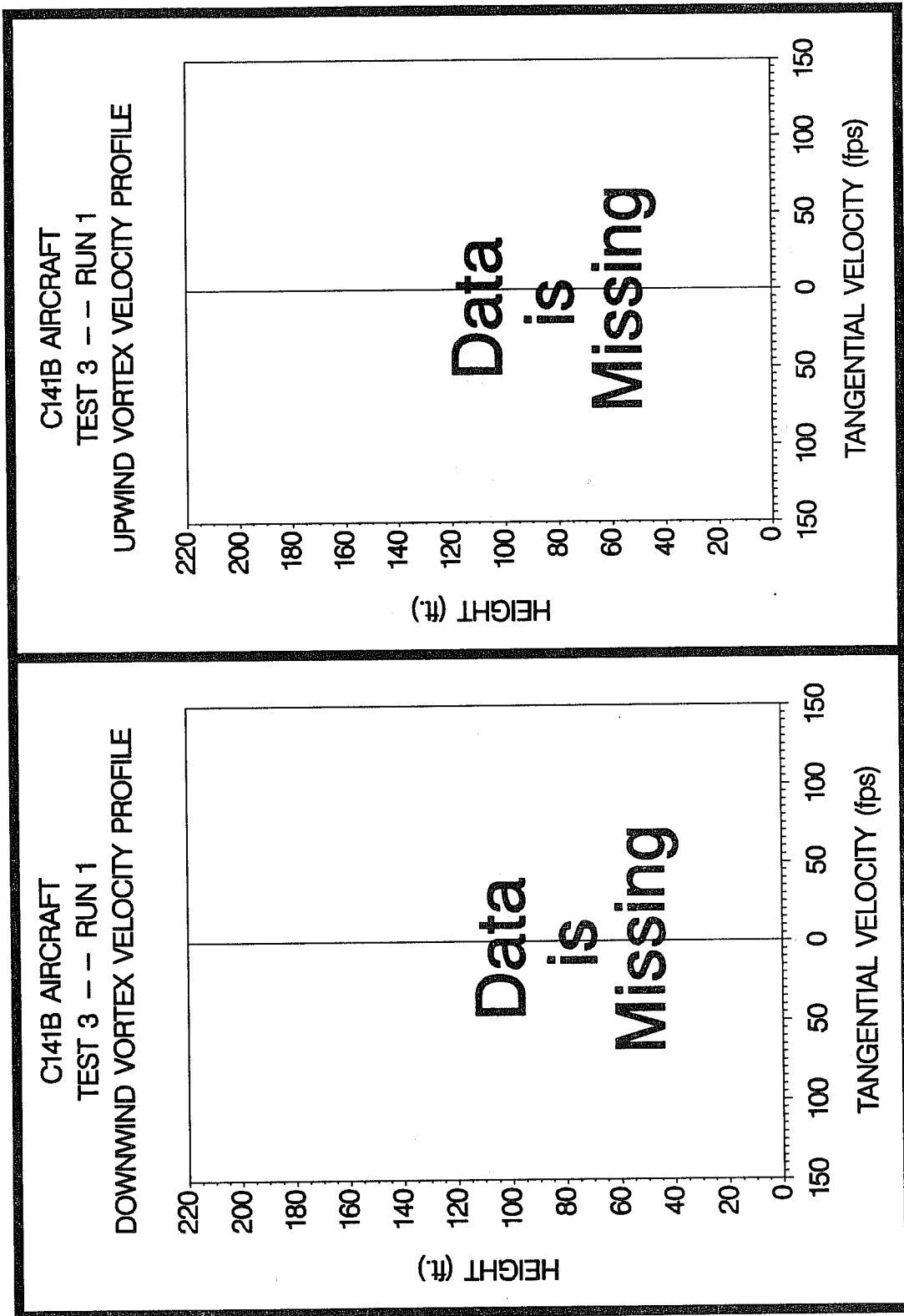


Figure C-36. C141B upwind (top) and downwind (bottom) vortex tangential velocity profile at maximum intensity from Test 3, Run 1, ambient wind speed=12.0 fps,  $\delta_F=55\%$ , IAS=150 knots, GW=214.0k lbs. Ages, radii, and velocities of the vortex cores are (N/A) and (N/A) sec., (N/A) and (N/A) ft., and (N/A) and (N/A) fps, respectively.

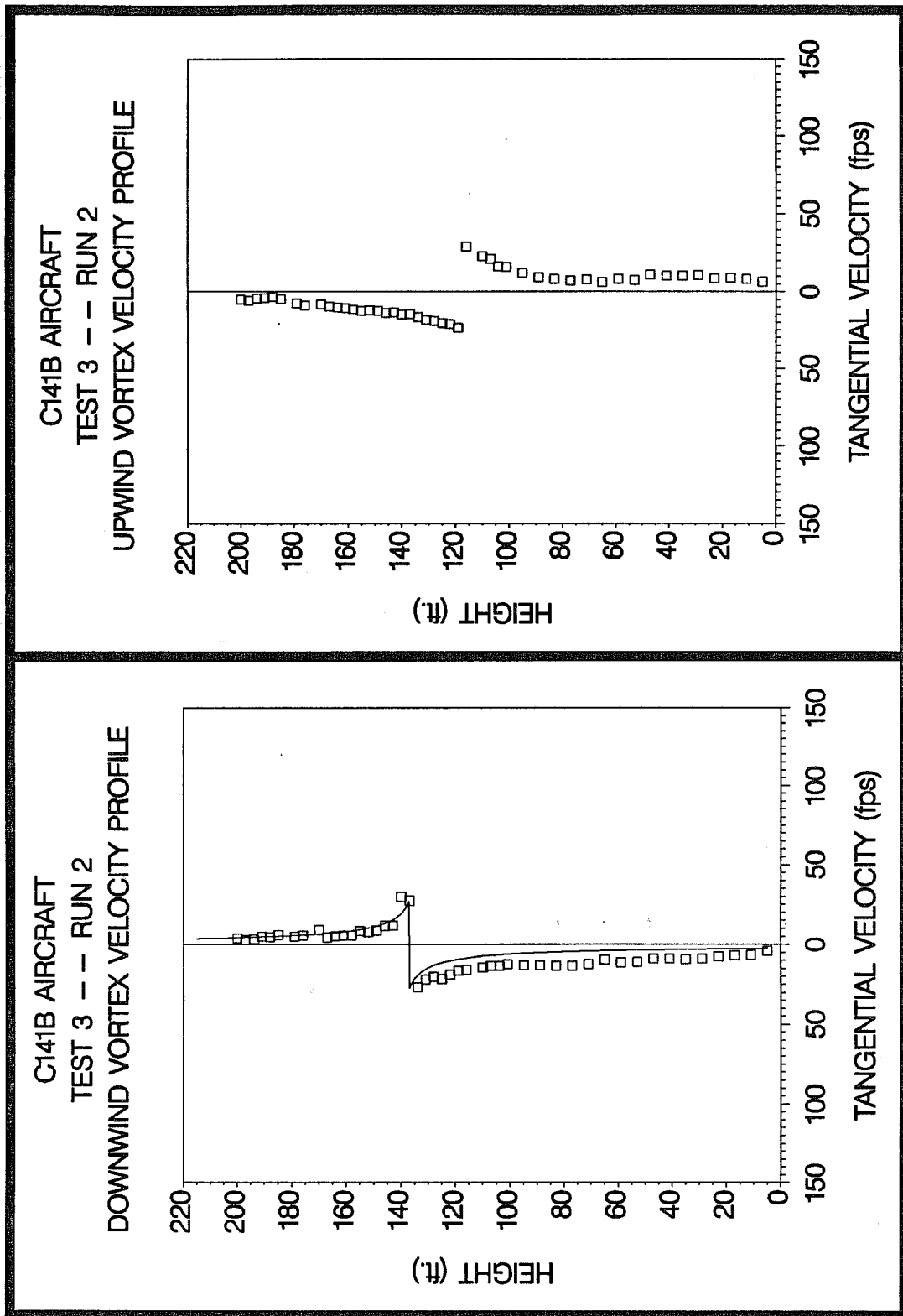


Figure C-37. C141B upwind (top) and downwind (bottom) vortex tangential velocity profile at maximum intensity from Test 3, Run 2, ambient wind speed=13.8 fps,  $\delta_F=55\%$ , IAS=150 knots, GW=212.0k lbs. Ages, radii, and velocities of the vortex cores are 35 and 26 sec., (N/A) and 3.2 ft., and 23.7 and 27.4 fps, respectively.

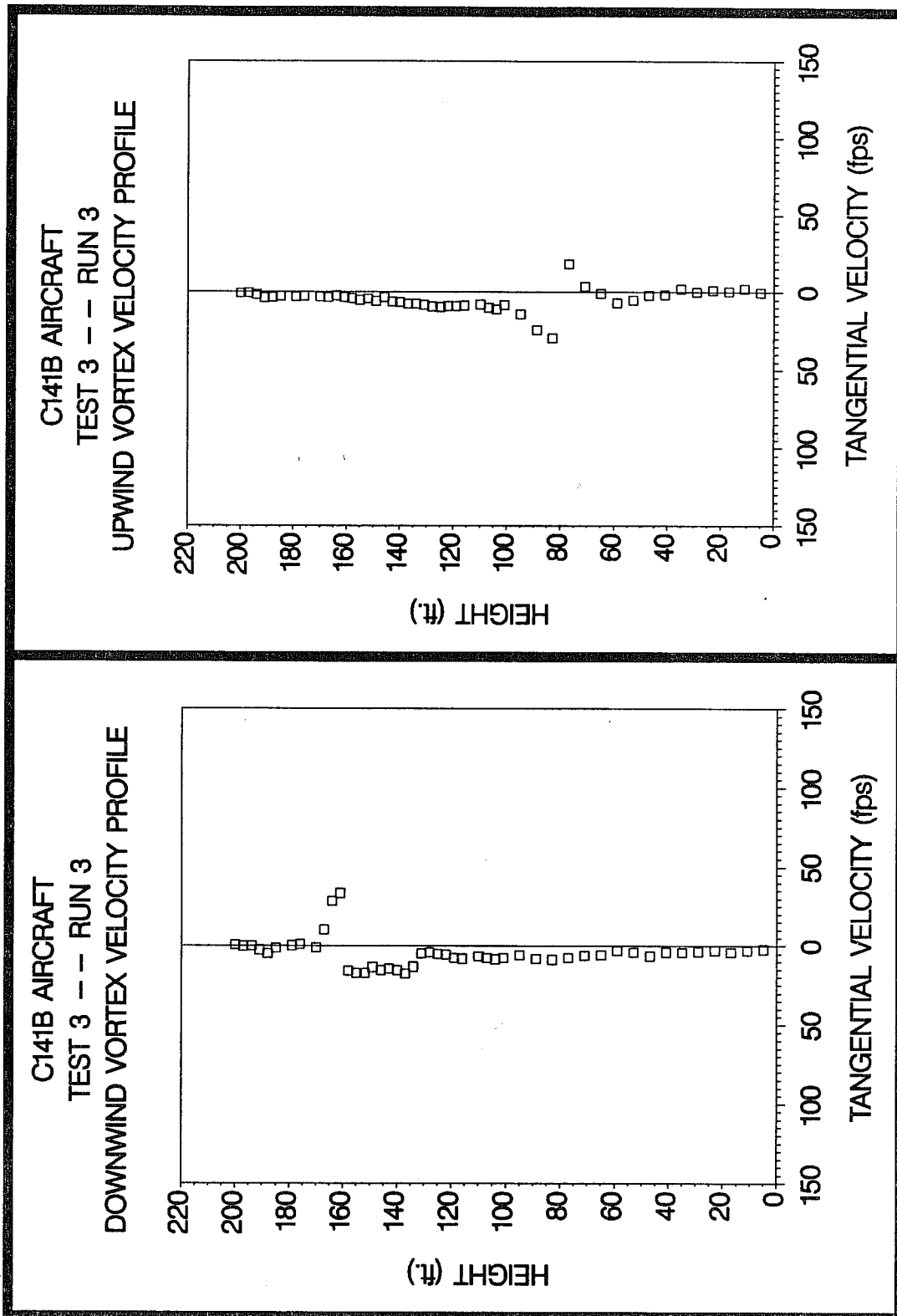
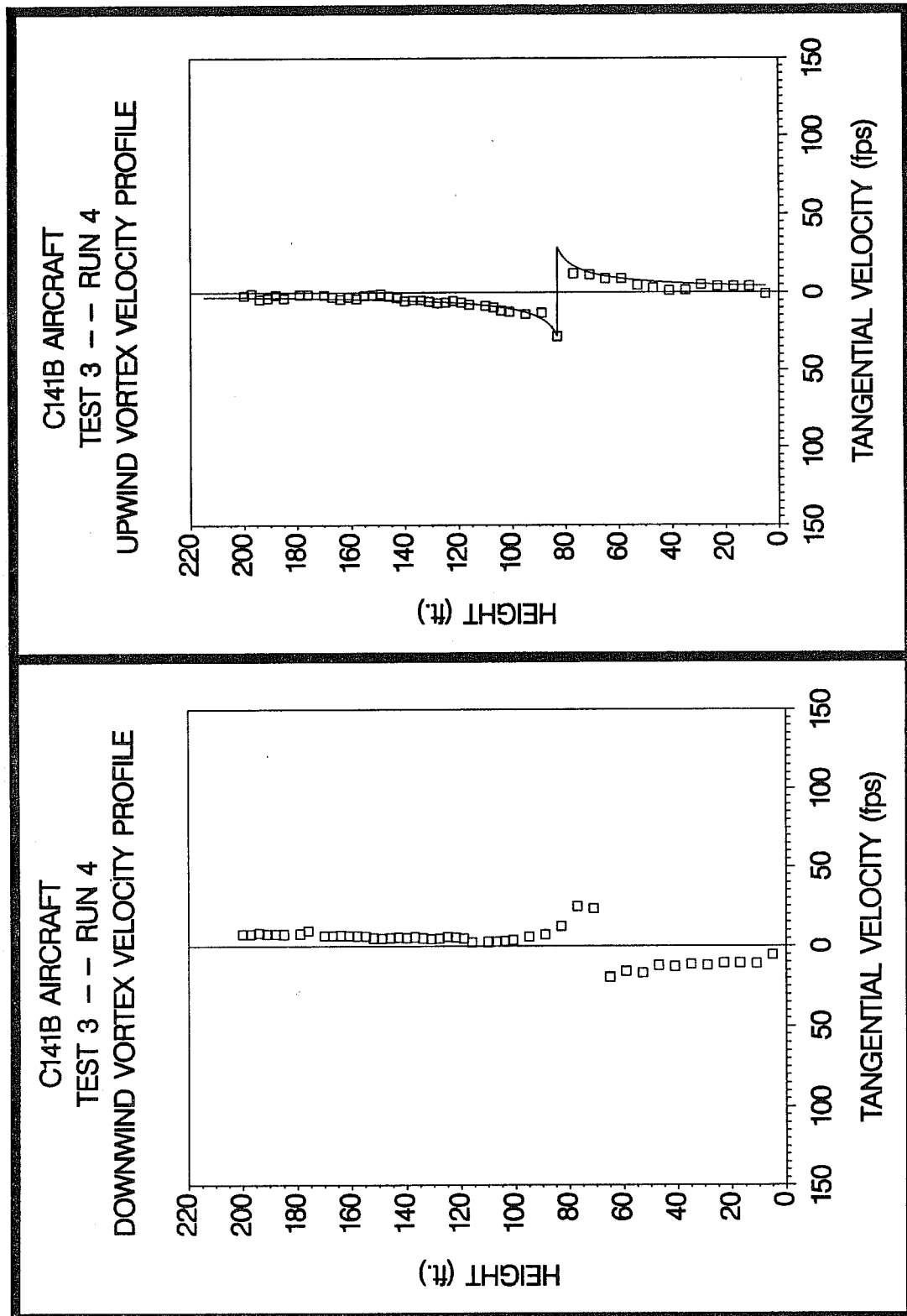


Figure C-38. C141B upwind (top) and downwind (bottom) vortex tangential velocity profile at maximum intensity from Test 3, Run 3, ambient wind speed=11.3 fps,  $\delta_F=55\%$ , IAS=150 knots, GW=211.0k lbs. Ages, radii, and velocities of the vortex cores are 37 and 32 sec., (N/A) and (N/A) ft., and 29.7 and 33.5 fps, respectively.



**Figure C-39.** C141B upwind (top) and downwind (bottom) vortex tangential velocity profile at maximum intensity from Test 3, Run 4, ambient wind speed=12.1 fps,  $\delta_F=55\%$ , IAS=150 knots, GW=208.0k lbs. Ages, radii, and velocities of the vortex cores are 72 and 51 sec., 3.7 and (N/A) ft., and 28.5 and 23.5 fps, respectively.

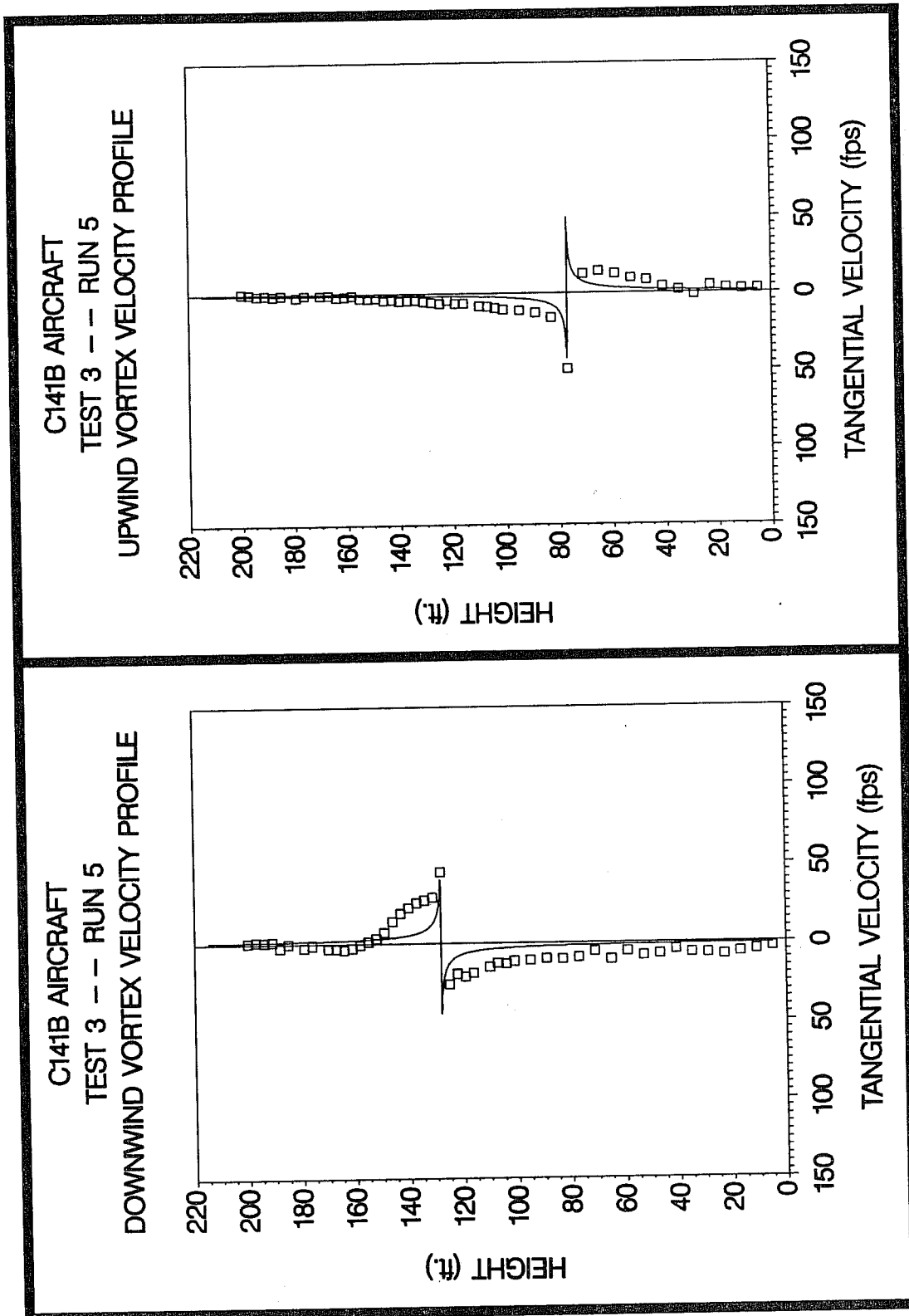


Figure C-40. C141B upwind (top) and downwind (bottom) vortex tangential velocity profile at maximum intensity from Test 3, Run 5, ambient wind speed=11.1 fps,  $\delta_F=70\%$ , IAS=130 knots, GW=206.0k lbs. Ages, radii, and velocities of the vortex cores are 57 and 39 sec., 0.3 and 0.4 ft., and 49.5 and 45.0 fps, respectively.

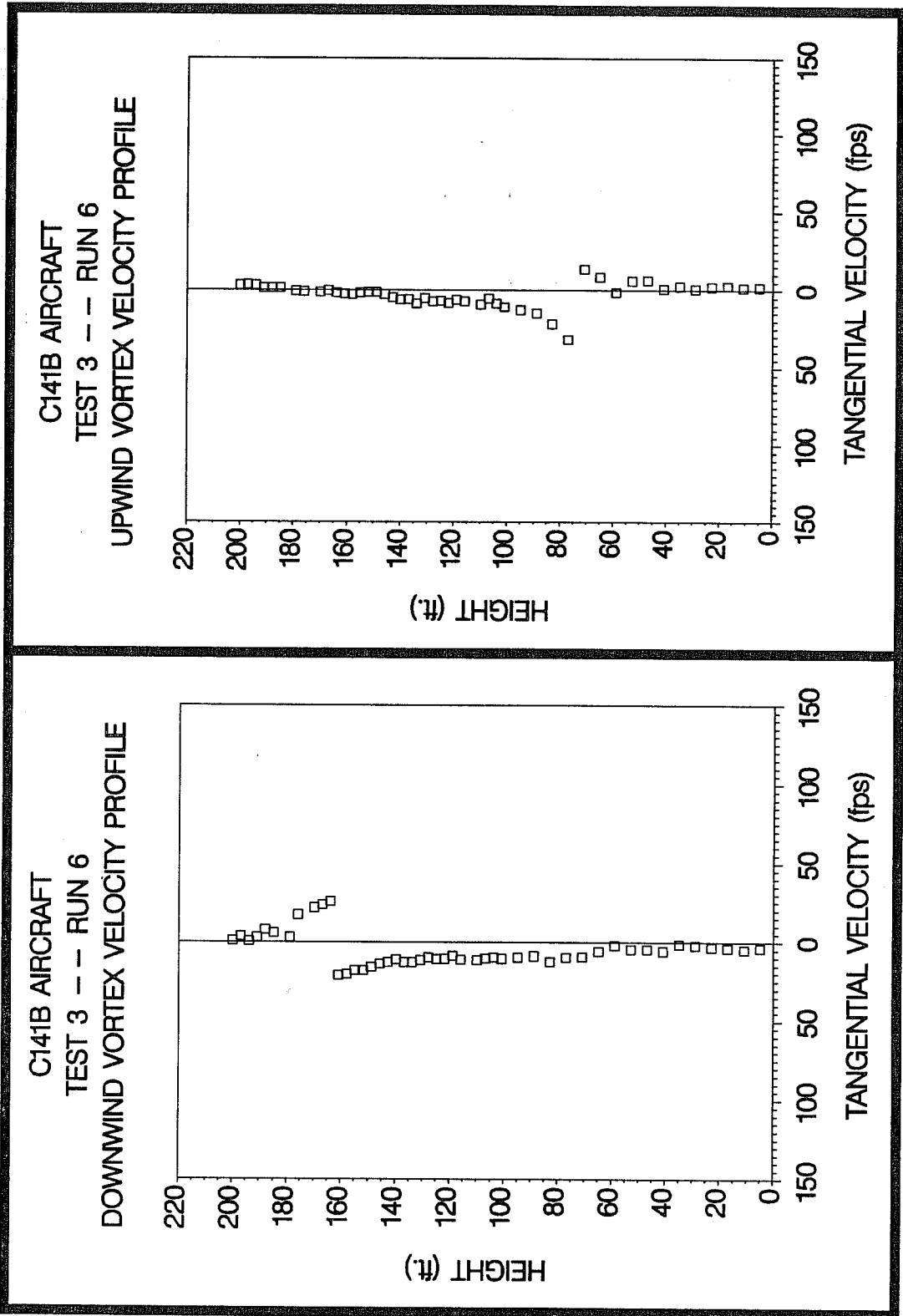


Figure C-41. C141B upwind (top) and downwind (bottom) vortex tangential velocity profile at maximum intensity from Test 3, Run 6, ambient wind speed=8.6 fps,  $\delta_F=70\%$ , IAS=130 knots, GW=204.0k lbs. Ages, radii, and velocities of the vortex cores are 53 and 47 sec., (N/A) and (N/A) ft., and 31.7 and 25.7 fps, respectively.

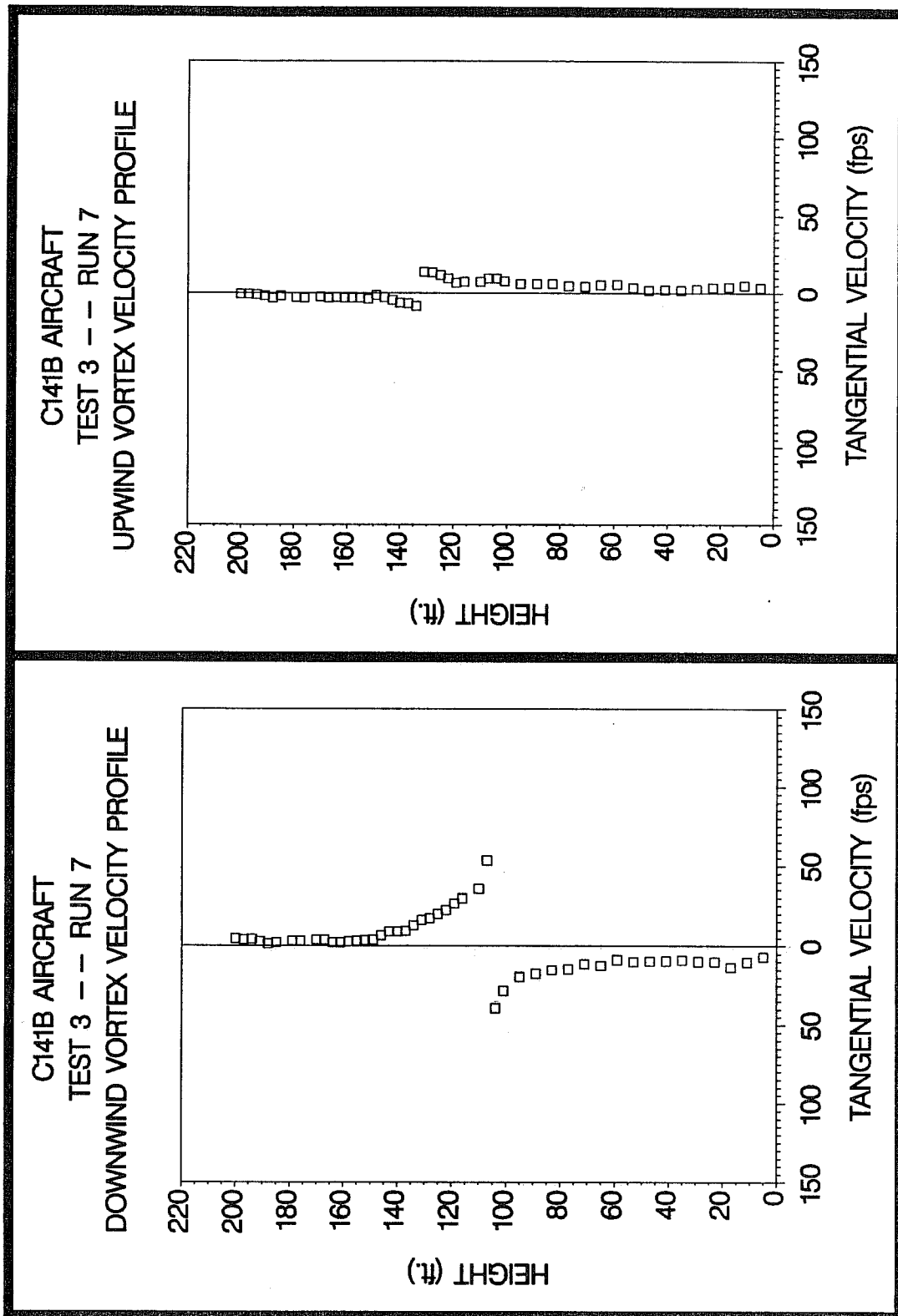
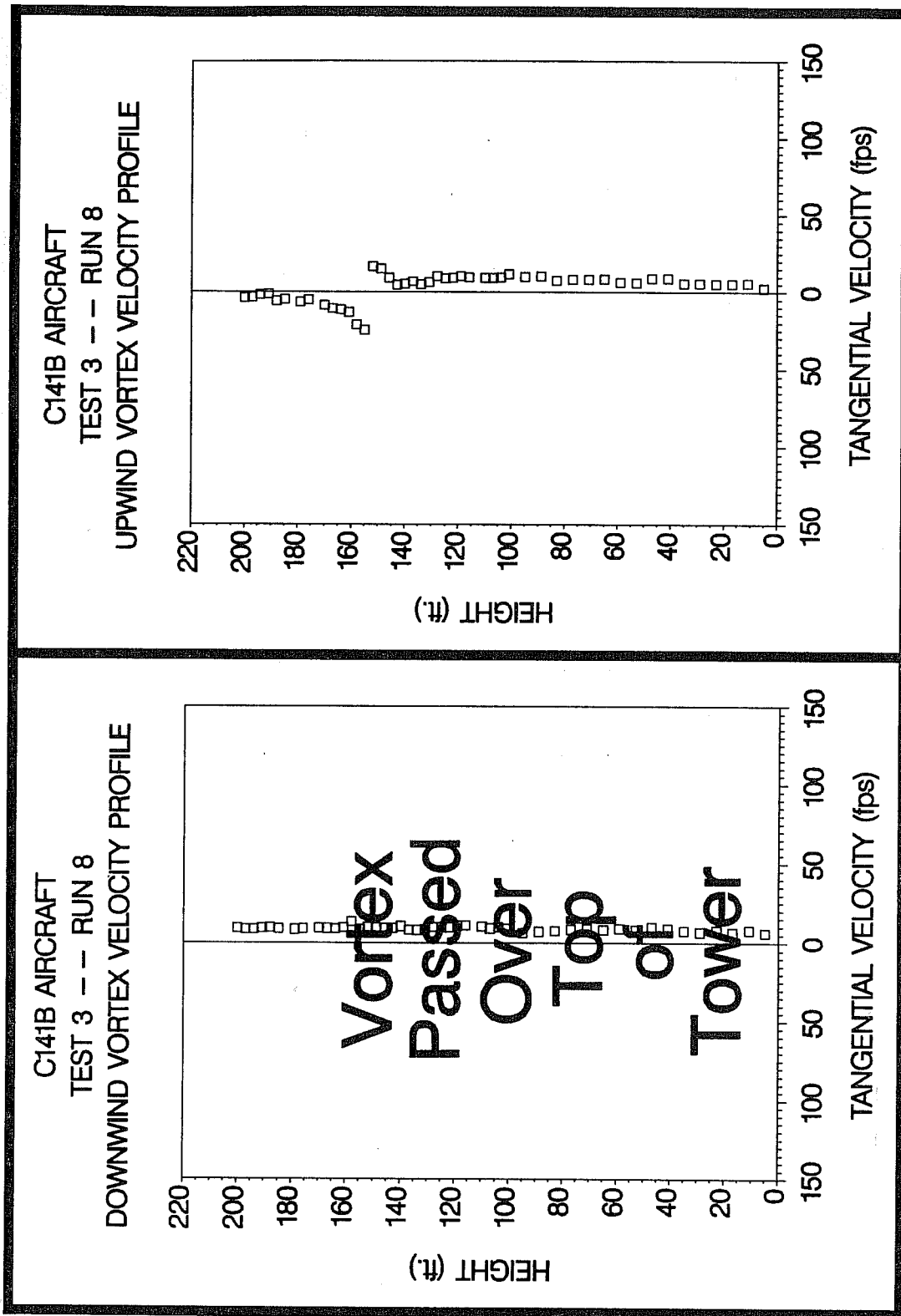
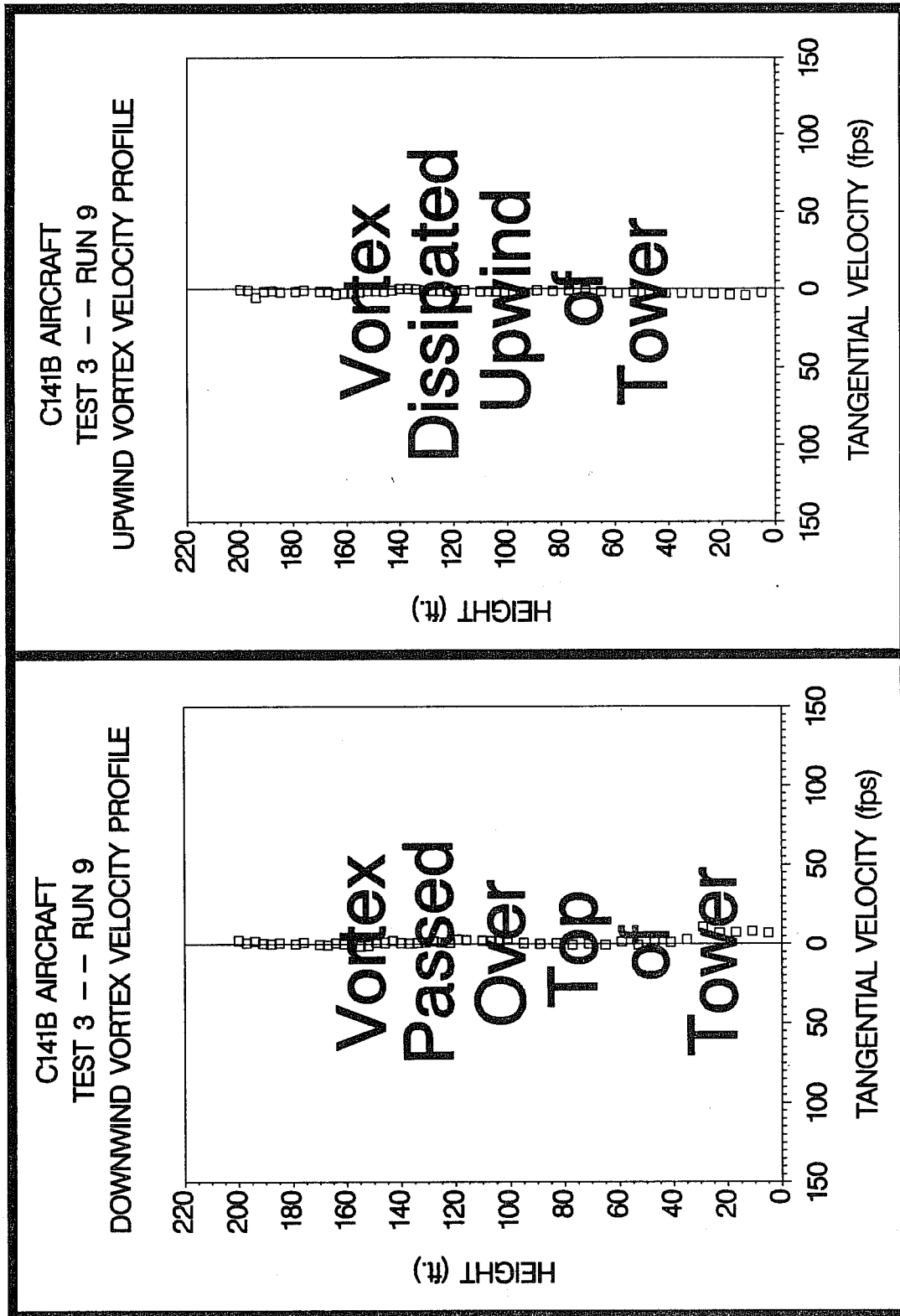


Figure C-42. C141B upwind (top) and downwind (bottom) vortex tangential velocity profile at maximum intensity from Test 3, Run 7, ambient wind speed=10.4 fps,  $\delta_F=70\%$ , IAS=130 knots, GW=202.0k lbs. Ages, radii, and velocities of the vortex cores are 164 and 61 sec., (N/A) and (N/A) ft., and 8.2 and 53.4 fps, respectively.



**Figure C-43.** C141B upwind (top) and downwind (bottom) vortex tangential velocity profile at maximum intensity from Test 3, Run 8, ambient wind speed=11.0 fps,  $\delta_F=70\%$ , IAS=130 knots, GW=200.0k lbs. Ages, radii, and velocities of the vortex cores are 74 and (N/A) sec., (N/A) and (N/A) ft., and 24.6 and (N/A) fps, respectively.



**Figure C-44.** C141B upwind (top) and downwind (bottom) vortex tangential velocity profile at maximum intensity from Test 3, Run 9, ambient wind speed=7.5 fps,  $\delta_F=70\%$ , IAS=130 knots, GW=198.0k lbs. Ages, radii, and velocities of the vortex cores are (N/A) and (N/A) sec., (N/A) and (N/A) ft., and (N/A) and (N/A) fps, respectively.

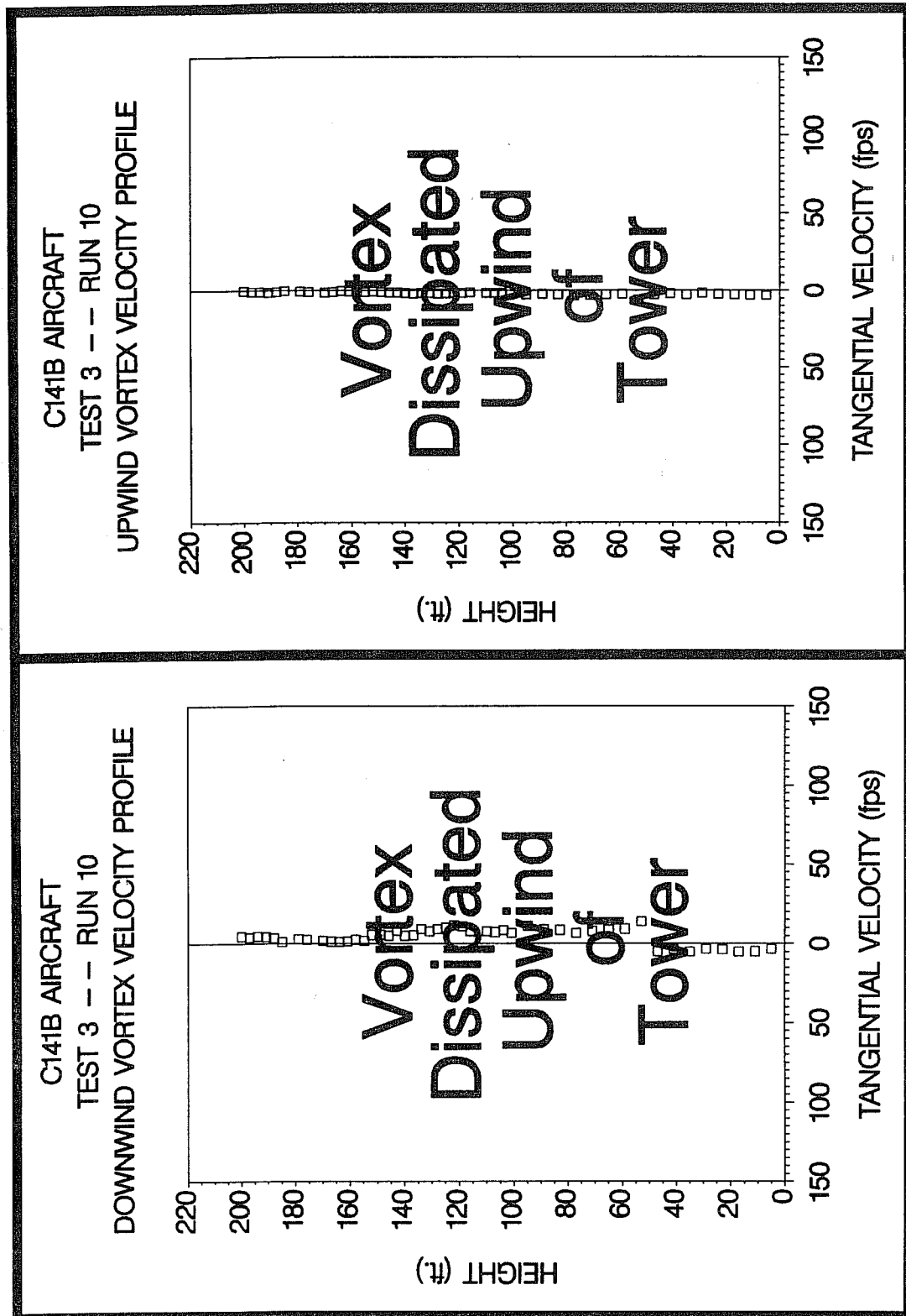
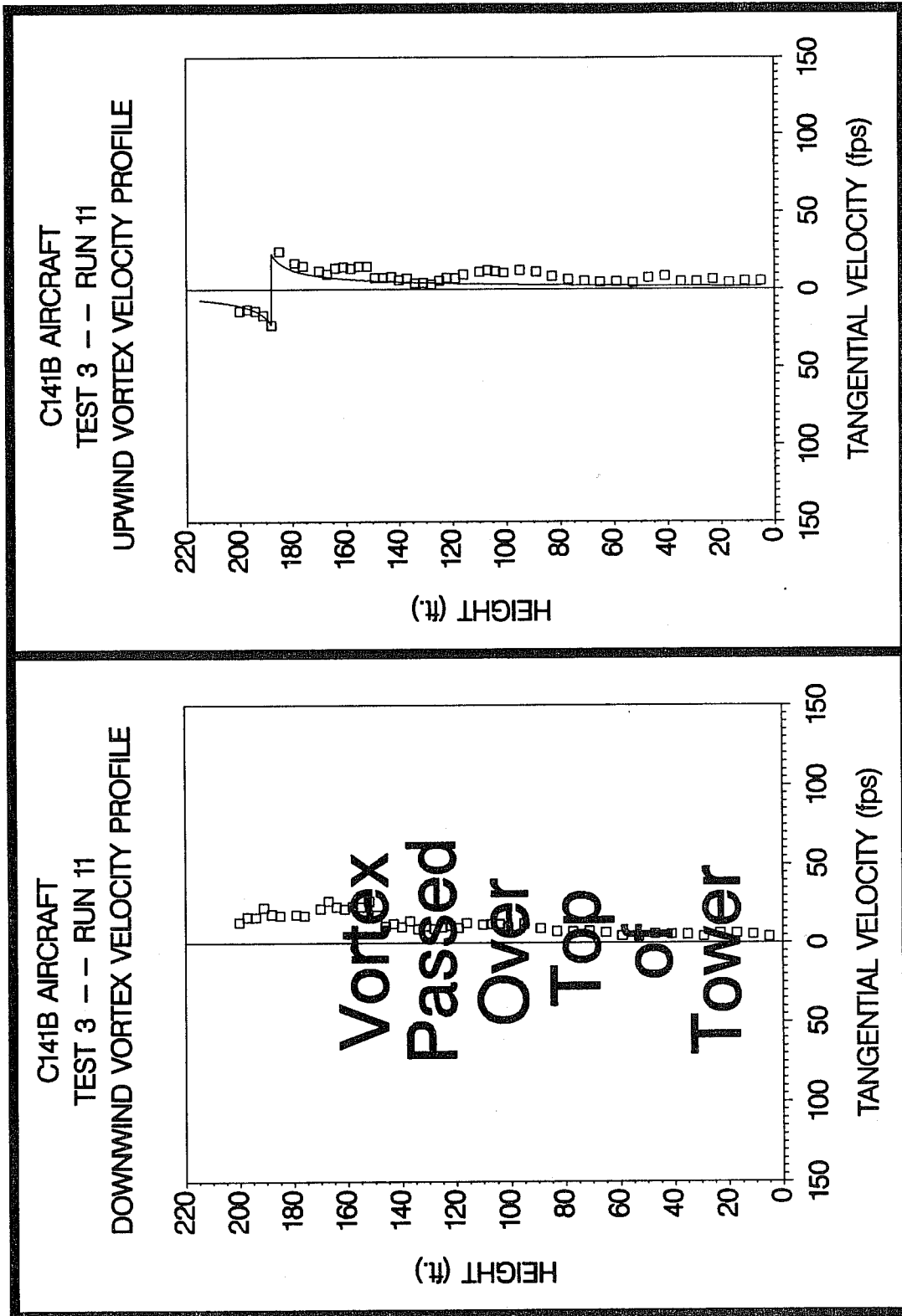


Figure C-45. C141B upwind (top) and downwind (bottom) vortex tangential velocity profile at maximum intensity from Test 3, Run 10, ambient wind speed=8.6 fps,  $\delta_F=70\%$ , IAS=130 knots, GW=196.0k lbs. Ages, radii, and velocities of the vortex cores are (N/A) and 82 sec., (N/A) and (N/A) ft., and (N/A) and 13.8 fps, respectively.



**Figure C-46.** C141B upwind (top) and downwind (bottom) vortex tangential velocity profile at maximum intensity from Test 3, Run 11, ambient wind speed=4.7 fps,  $\delta_F=70\%$ , IAS=130 knots, GW=193.0k lbs. Ages, radii, and velocities of the vortex cores are 58 and (N/A) sec., 3.9 and (N/A) ft., and 22.9 and (N/A) fps, respectively.

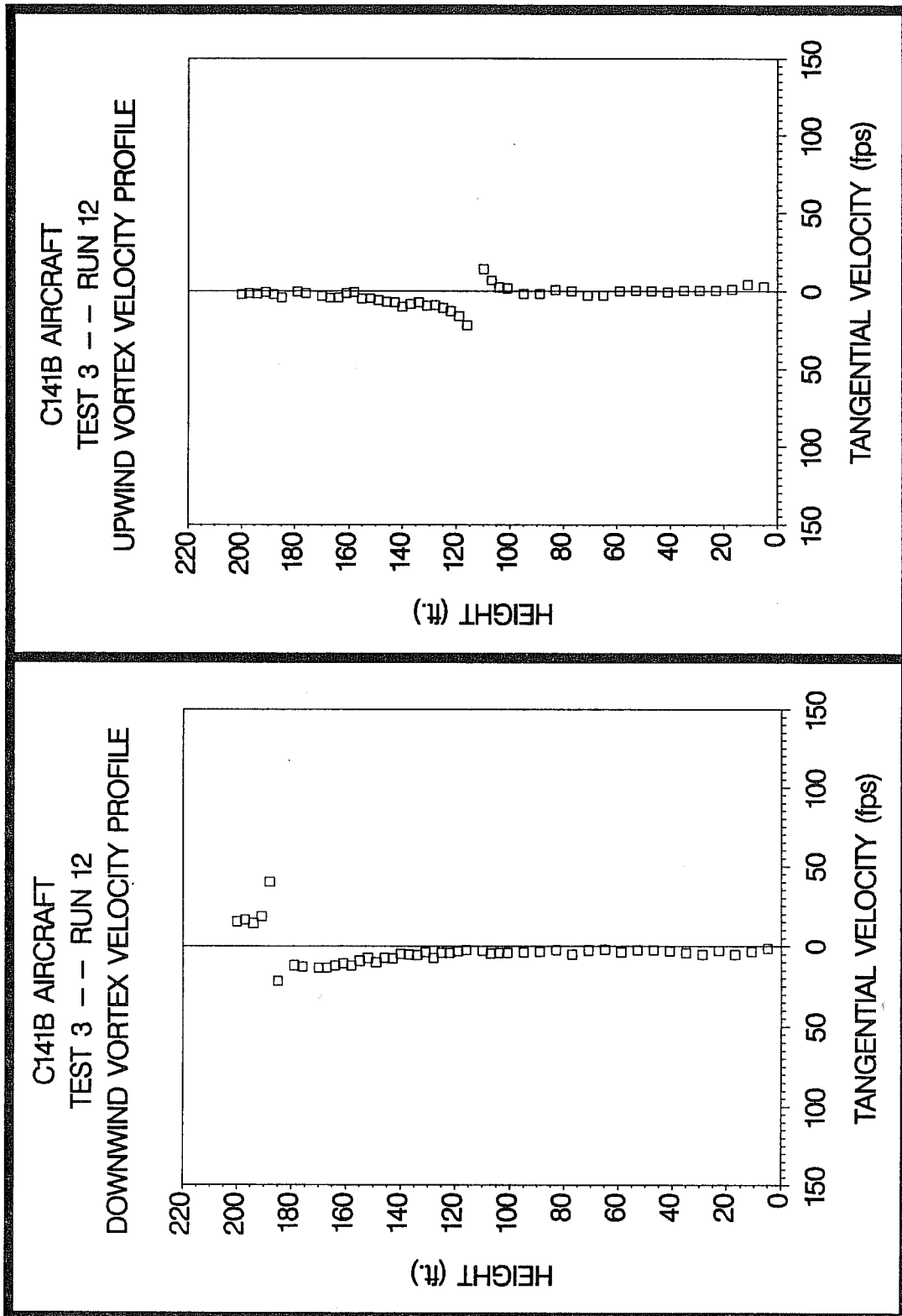


Figure C-47. C141B upwind (top) and downwind (bottom) vortex tangential velocity profile at maximum intensity from Test 3, Run 12, ambient wind speed=4.7 fps,  $\delta_F=70\%$ , IAS=130 knots, GW=192.0k lbs. Ages, radii, and velocities of the vortex cores are 40 and 23 sec., (N/A) and (N/A) ft., and 21.8 and 40.1 fps, respectively.

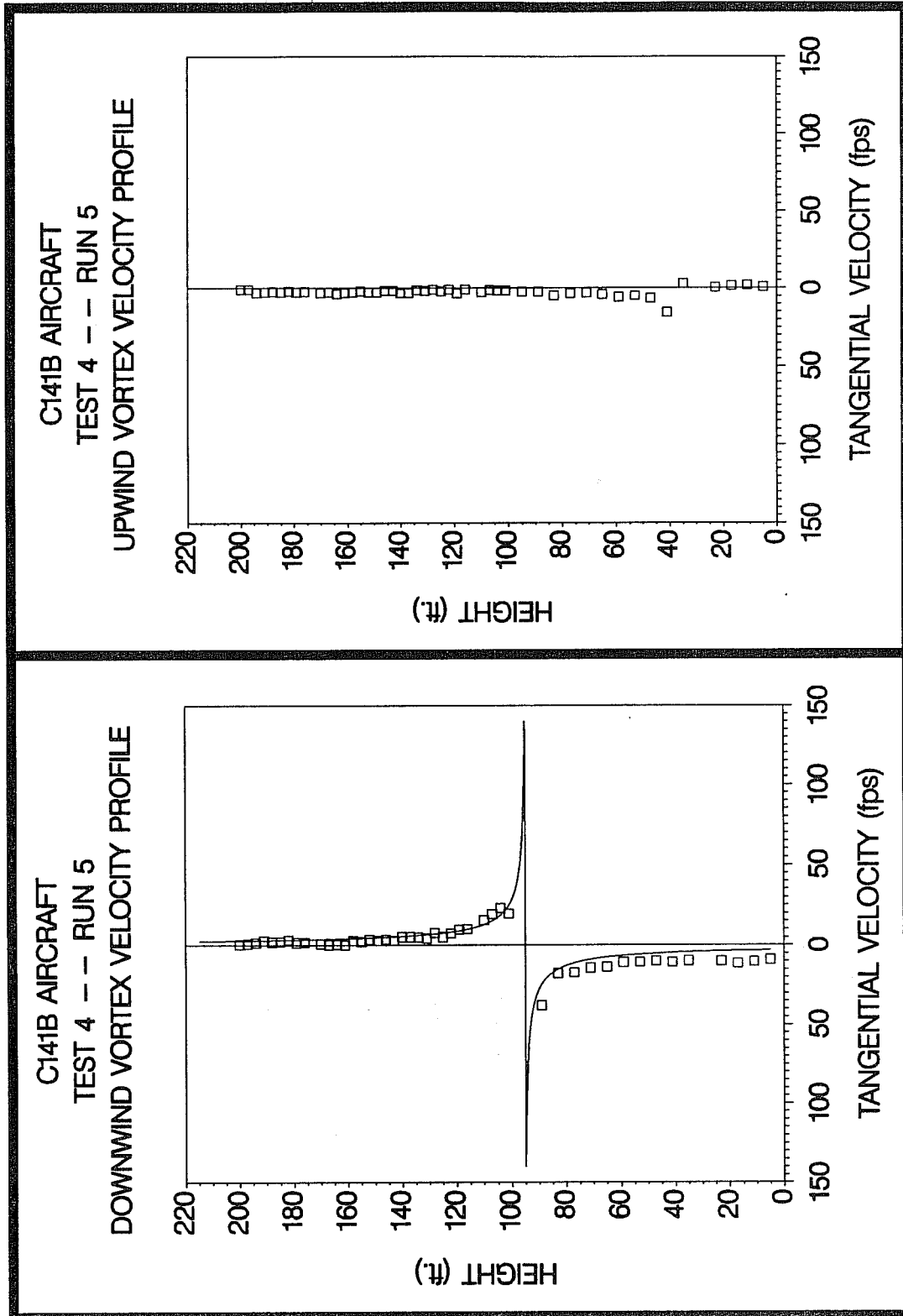


Figure C-48. C141B upwind (top) and downwind (bottom) vortex tangential velocity profile at maximum intensity from Test 4, Run 5, ambient wind speed=5.1 fps,  $\delta_F=11\%$ , IAS=180 knots, GW=261.0k lbs. Ages, radii, and velocities of the vortex cores are 84 and 31 sec., (N/A) and 0.3 ft., and 15.5 and 162.3 fps, respectively.

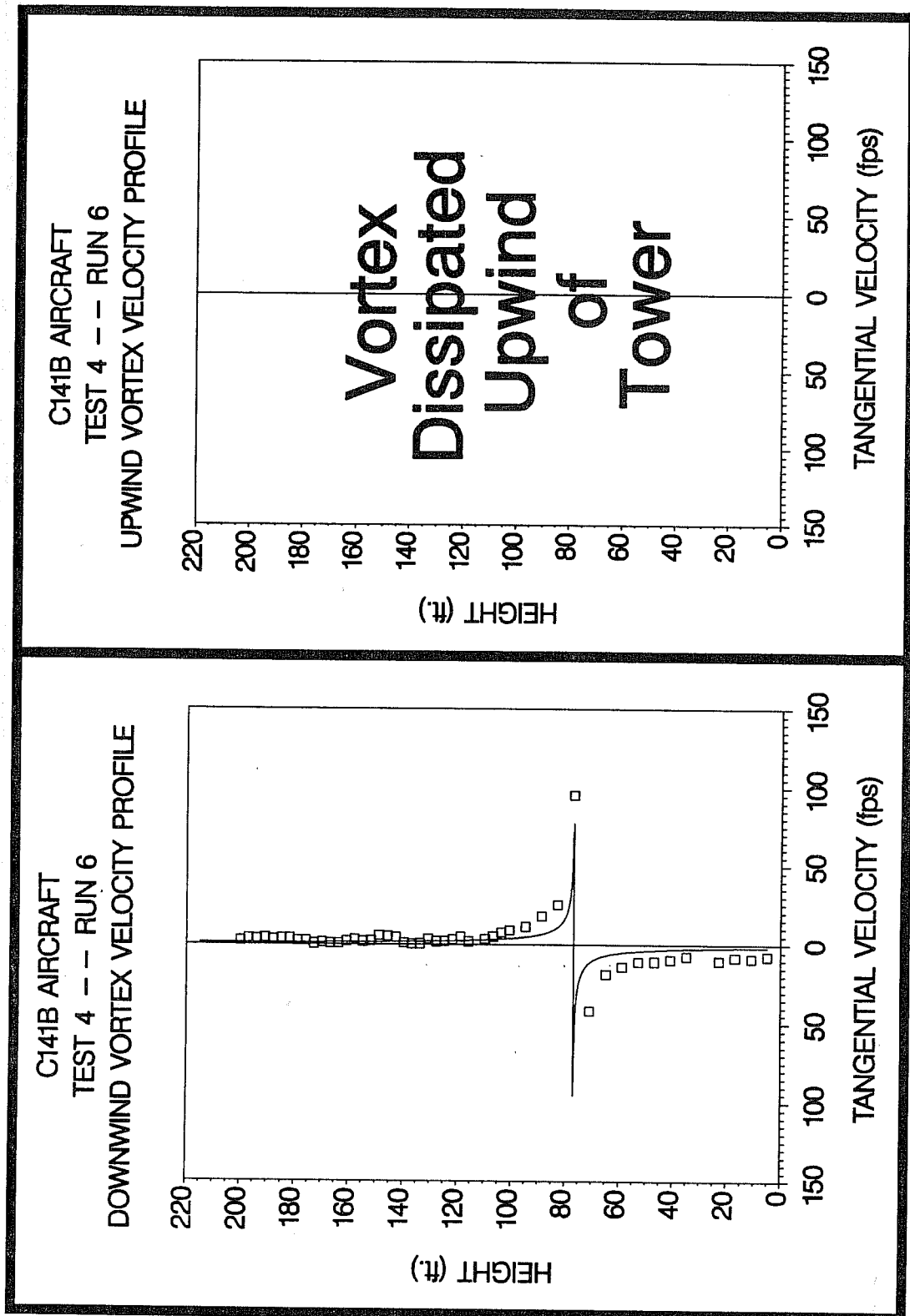


Figure C-49. C141B upwind (top) and downwind (bottom) vortex tangential velocity profile at maximum intensity from Test 4, Run 6, ambient wind speed=6.7 fps,  $\delta_F=11\%$ , IAS=180 knots, GW=259.0k lbs. Ages, radii, and velocities of the vortex cores are (N/A) and 42 sec., (N/A) and 0.2 ft., and (N/A) and 95.4 fps, respectively.

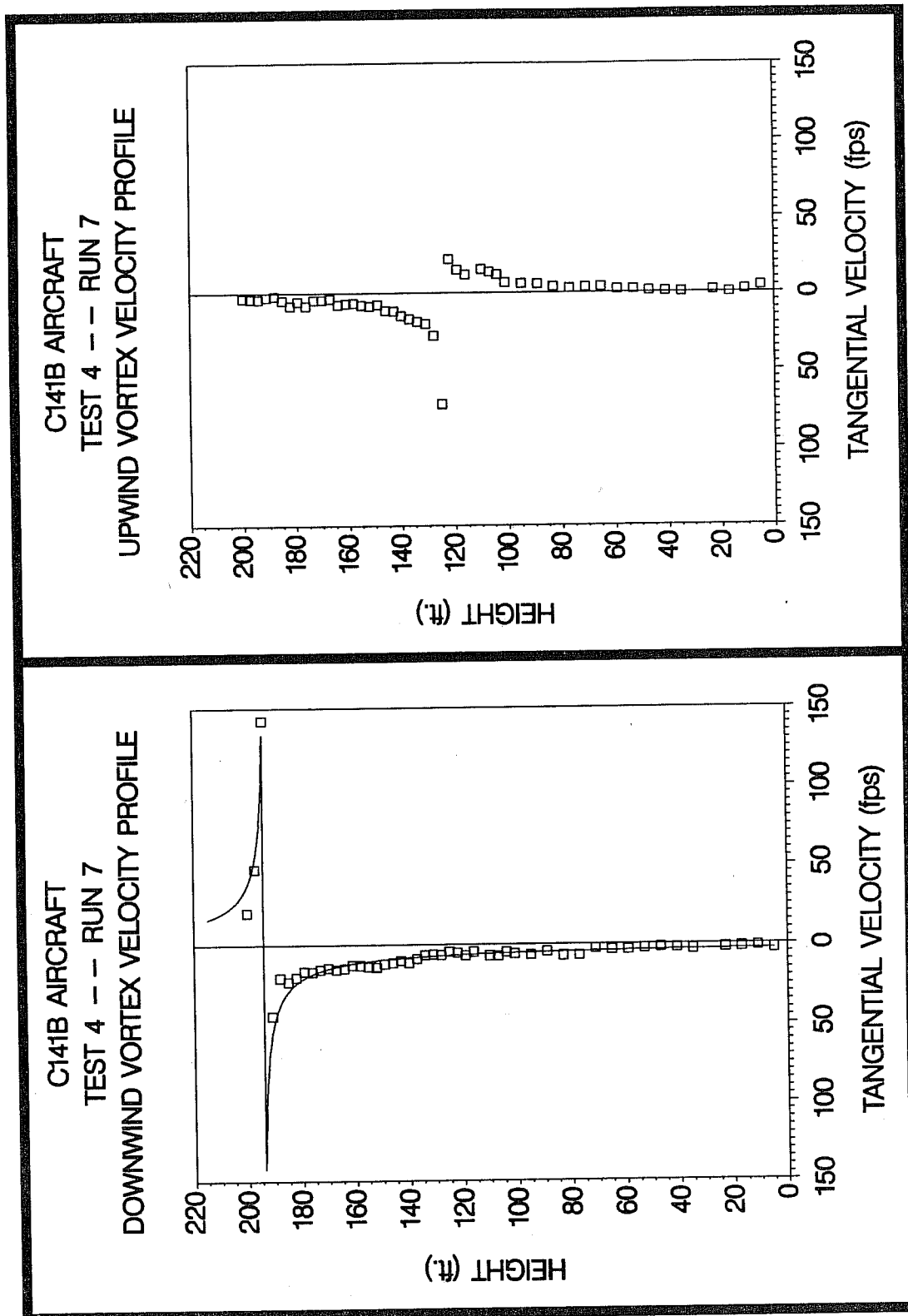
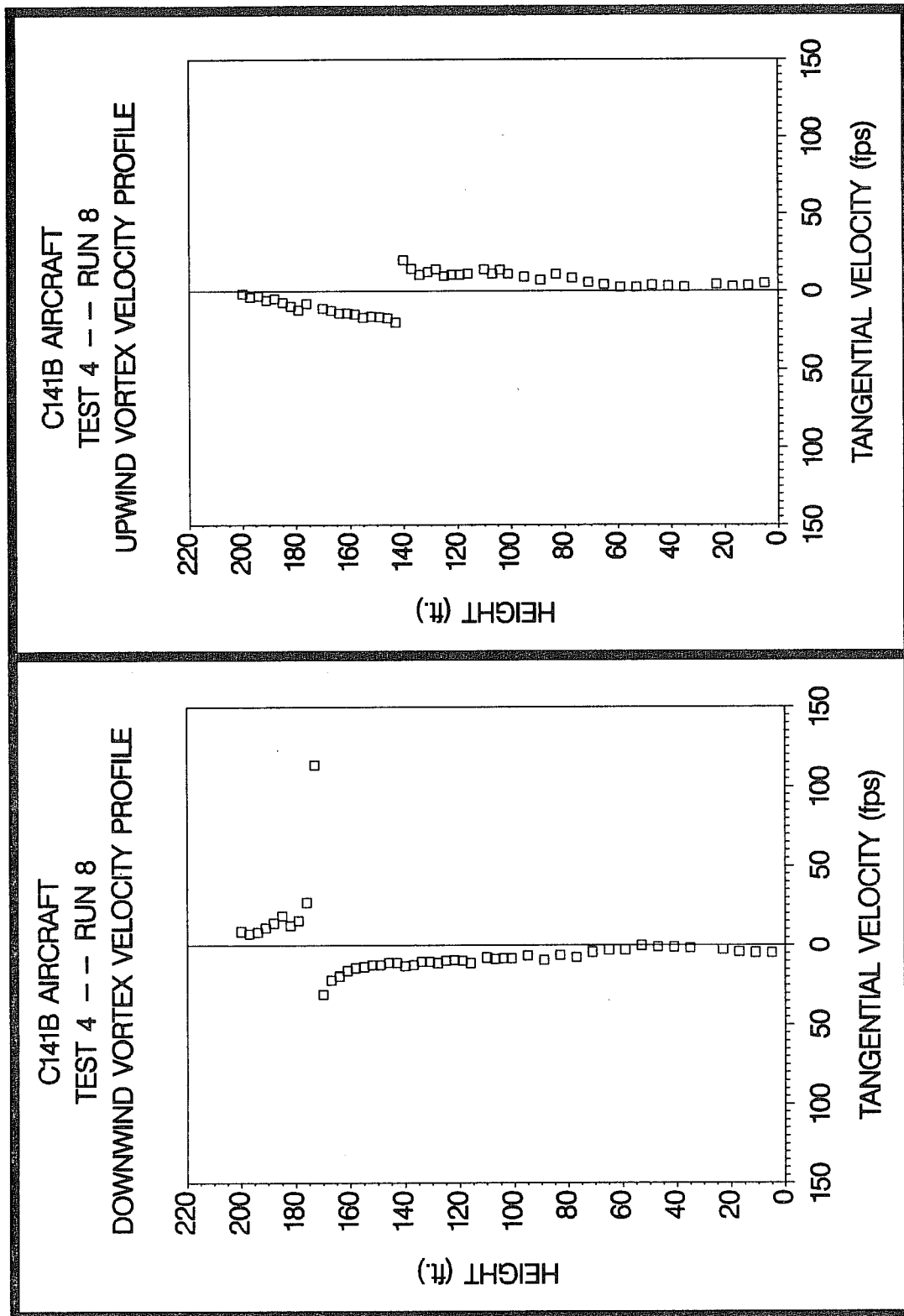
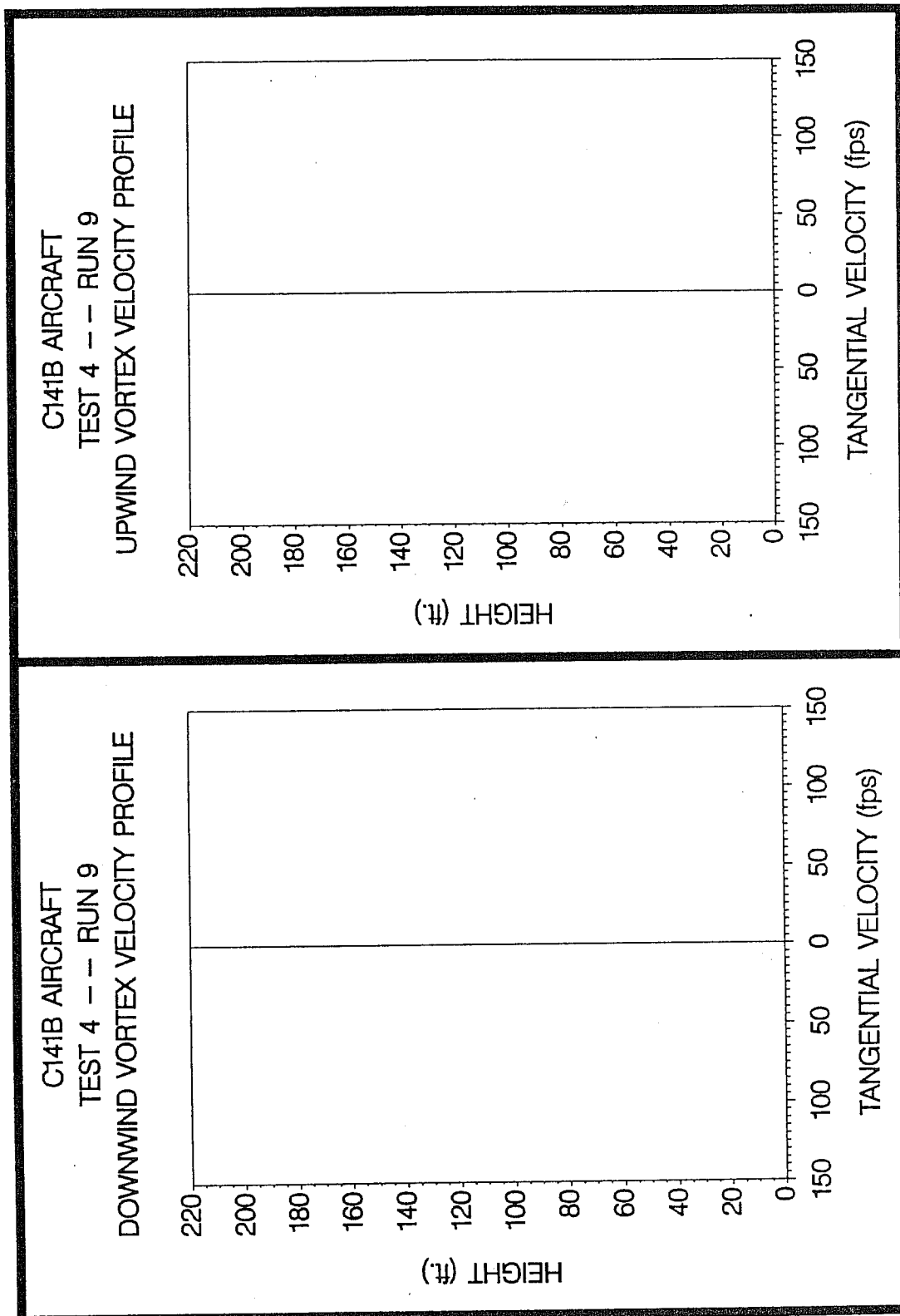


Figure C-50. C141B upwind (top) and downwind (bottom) vortex tangential velocity profile at maximum intensity from Test 4, Run 7, ambient wind speed=5.8 fps,  $\delta_F=11\%$ , IAS=180 knots, GW=257.0k lbs. Ages, radii, and velocities of the vortex cores are 39 and 17 sec., (N/A) and 0.7 ft., and 72.0 and 142.1 fps, respectively.



**Figure C-51.** C141B upwind (top) and downwind (bottom) vortex tangential velocity profile at maximum intensity from Test 4, Run 8, ambient wind speed=6.3 fps,  $\delta_F=36\%$ , IAS=180 knots, GW=254.0k lbs. Ages, radii, and velocities of the vortex cores are 27 and 22 sec., (N/A) and (N/A) ft., and 20.0 and 113.8 fps, respectively.



**Figure C-52.** C141B upwind (top) and downwind (bottom) vortex tangential velocity profile at maximum intensity from Test 4, Run 9, ambient wind speed=6.3 fps,  $\delta_F=0\%$ , IAS=193 knots, GW=250.0k lbs. Ages, radii, and velocities of the vortex cores are (N/A) and (N/A) sec., (N/A) and (N/A) ft., and (N/A) and (N/A) fps, respectively.

**LOCKHEED**

**C130E**

**HERCULES**

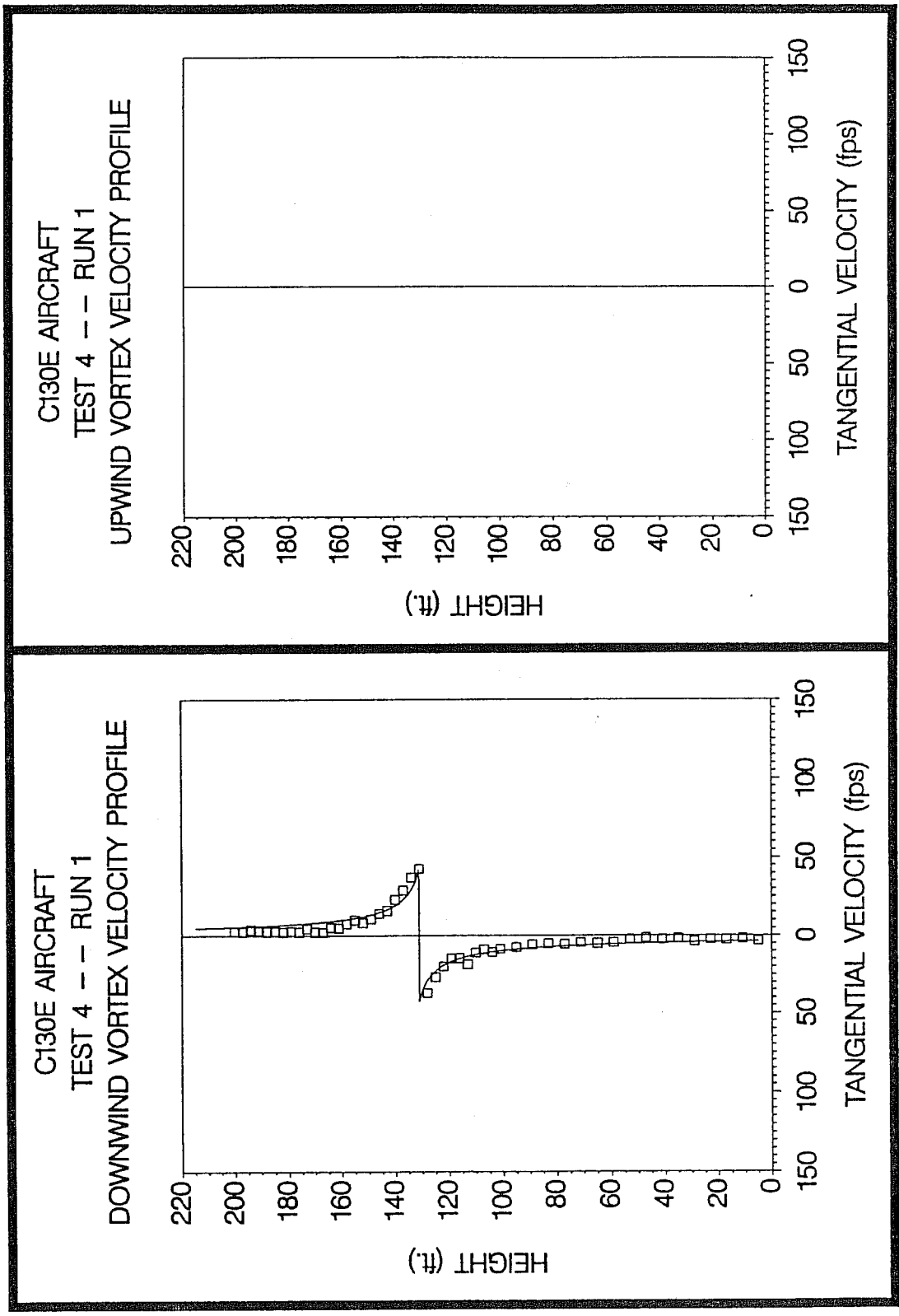


Figure C-53. C130E upwind (top) and downwind (bottom) vortex tangential velocity profile at maximum intensity from Test 4, Run 1, ambient wind speed=4.3 fps,  $\delta_F=50\%$ , IAS=130 knots, GW=148.0k lbs. Ages, radii, and velocities of the vortex cores are (N/A) and 52 sec., (N/A) and 2.8 ft., and (N/A) and 42.7 fps, respectively.

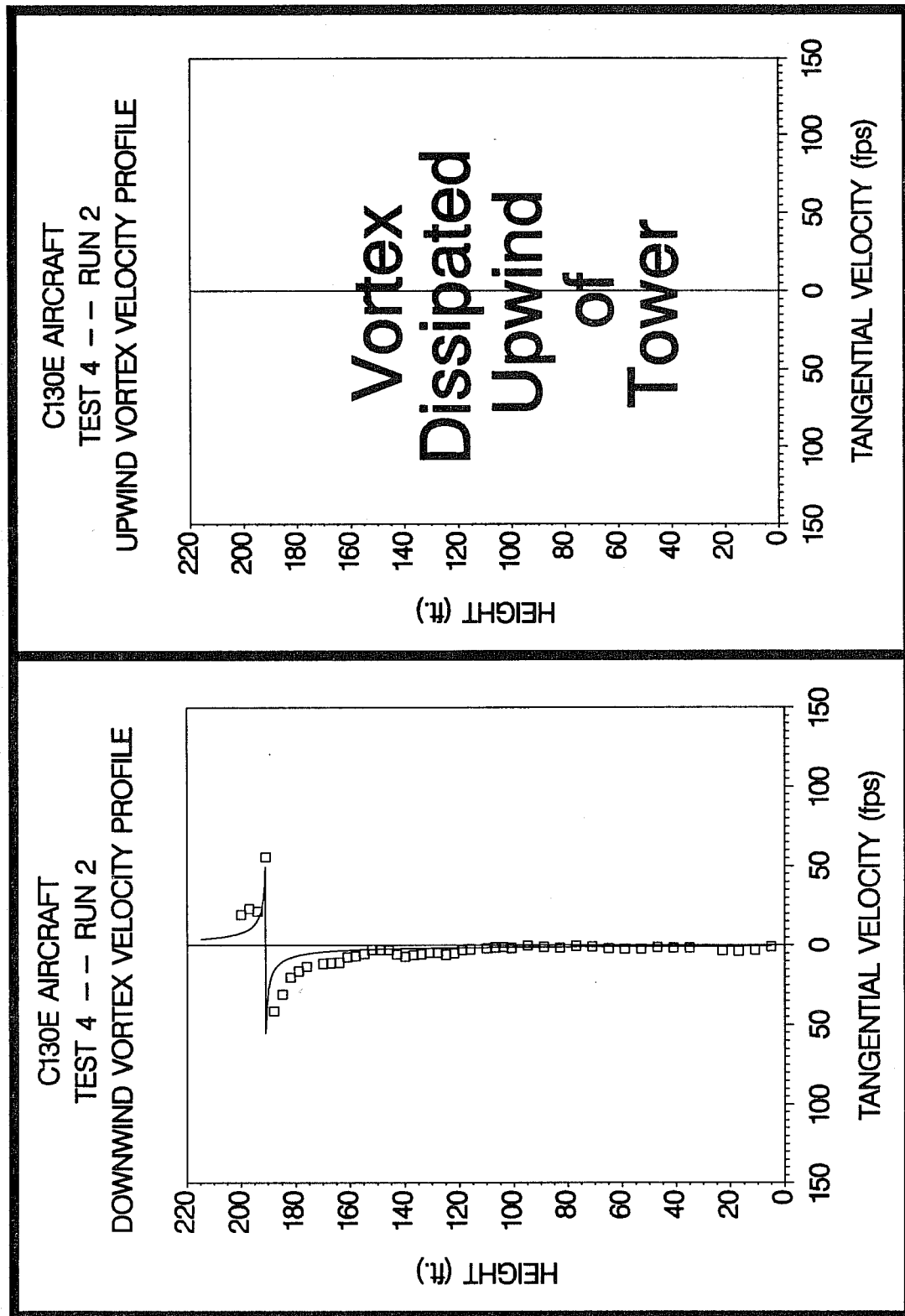


Figure C-54. C130E upwind (top) and downwind (bottom) vortex tangential velocity profile at maximum intensity from Test 4, Run 2, ambient wind speed=6.1 fps,  $\delta_F=50\%$ , IAS=130 knots, GW=147.5k lbs. Ages, radii, and velocities of the vortex cores are (N/A) and 43 sec., (N/A) and 0.4 ft., and (N/A) and 55.6 fps, respectively.

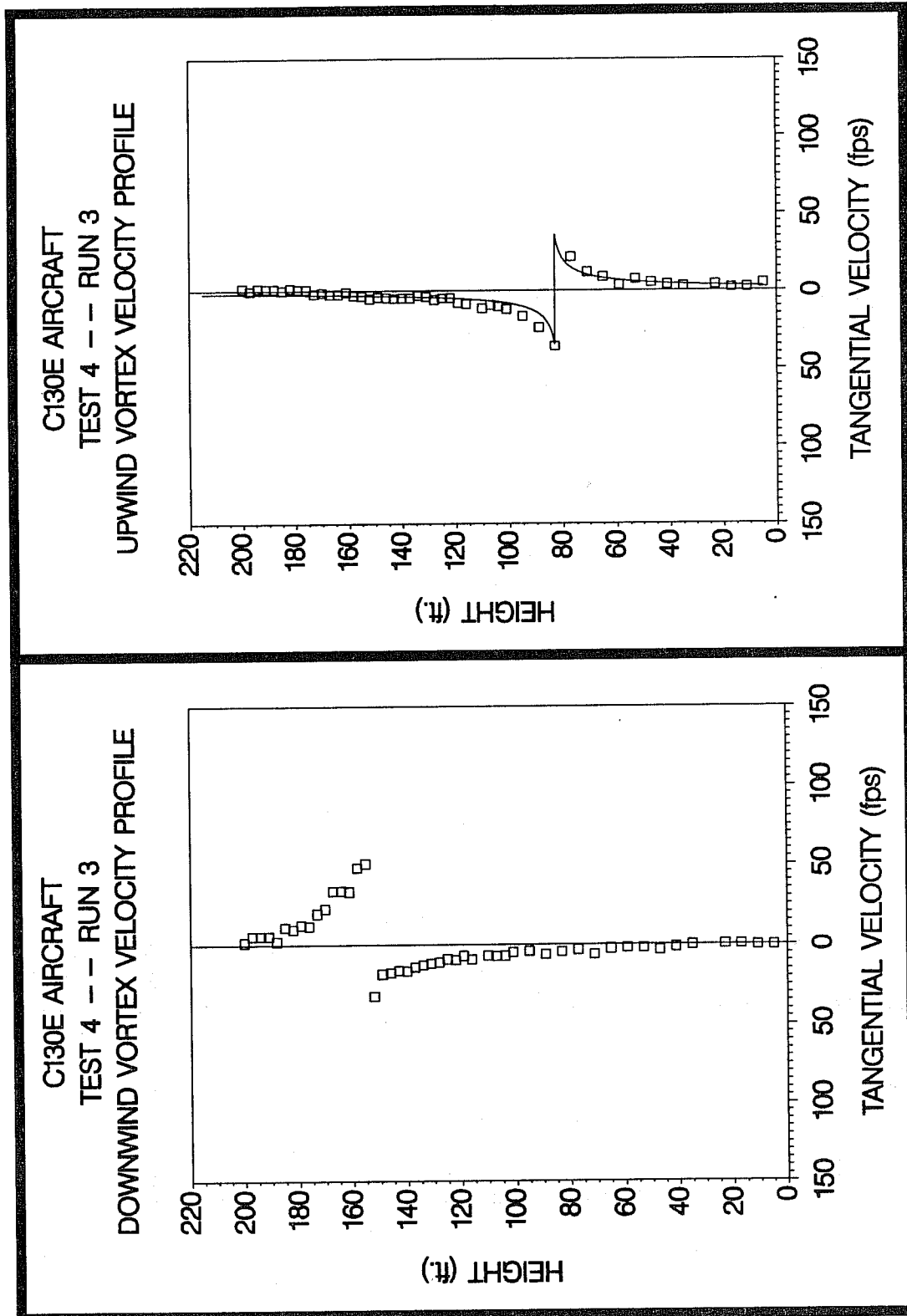
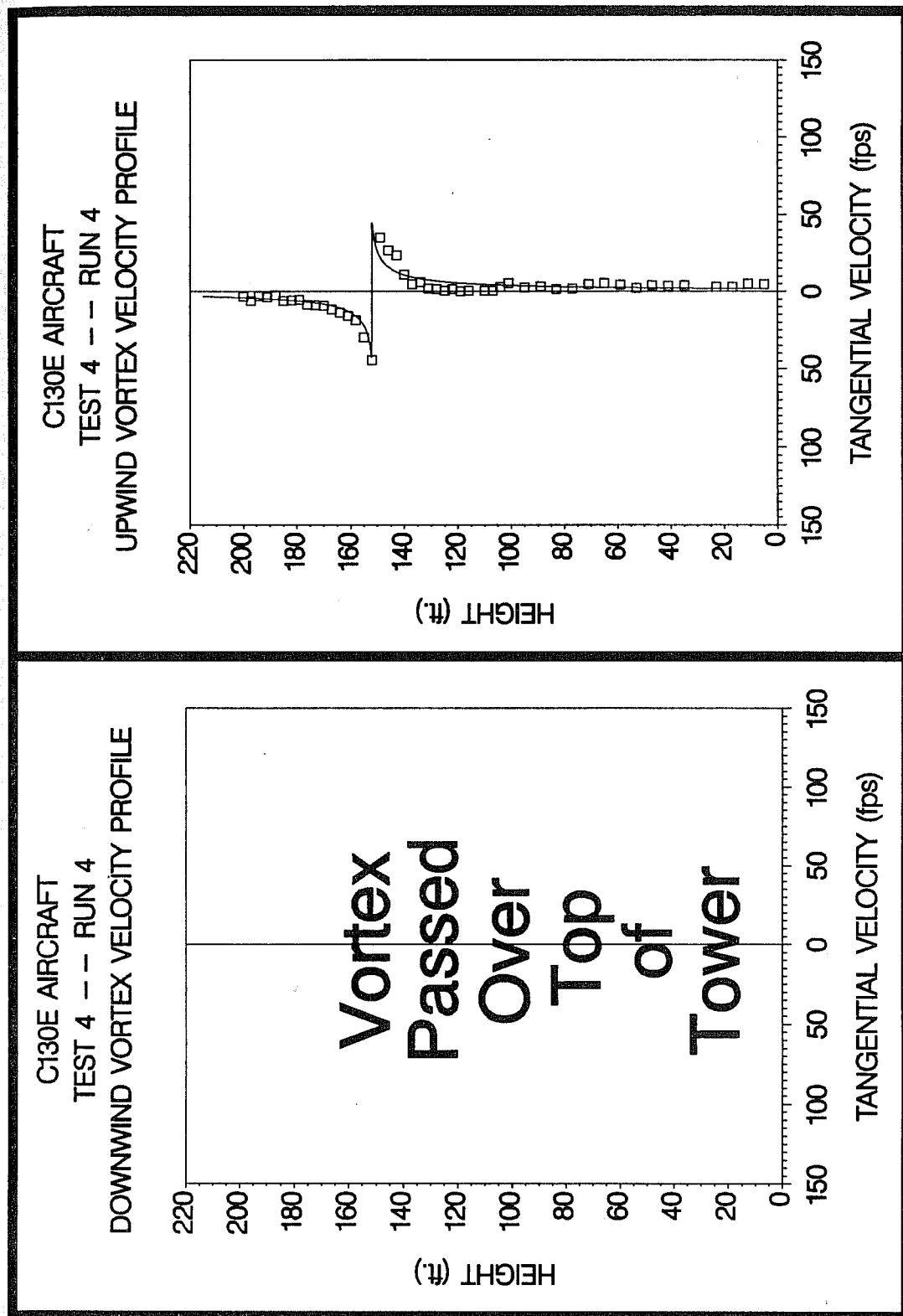


Figure C-55. C130E upwind (top) and downwind (bottom) vortex tangential velocity profile at maximum intensity from Test 4, Run 3, ambient wind speed=5.9 fps,  $\delta_F=50\%$ , IAS=130 knots, GW=147.0k lbs. Ages, radii, and velocities of the vortex cores are 38 and 24 sec., 1.6 and (N/A) ft., and 35.9 and 50.4 fps, respectively.



**Figure C-56.** C130E upwind (top) and downwind (bottom) vortex tangential velocity profile at maximum intensity from Test 4, Run 4, ambient wind speed=7.3 fps,  $\delta_F=50\%$ , IAS=130 knots, GW=146.5k lbs. Ages, radii, and velocities of the vortex cores are 32 and (N/A) sec., 1.2 and (N/A) ft., and 44.5 and (N/A) fps, respectively.

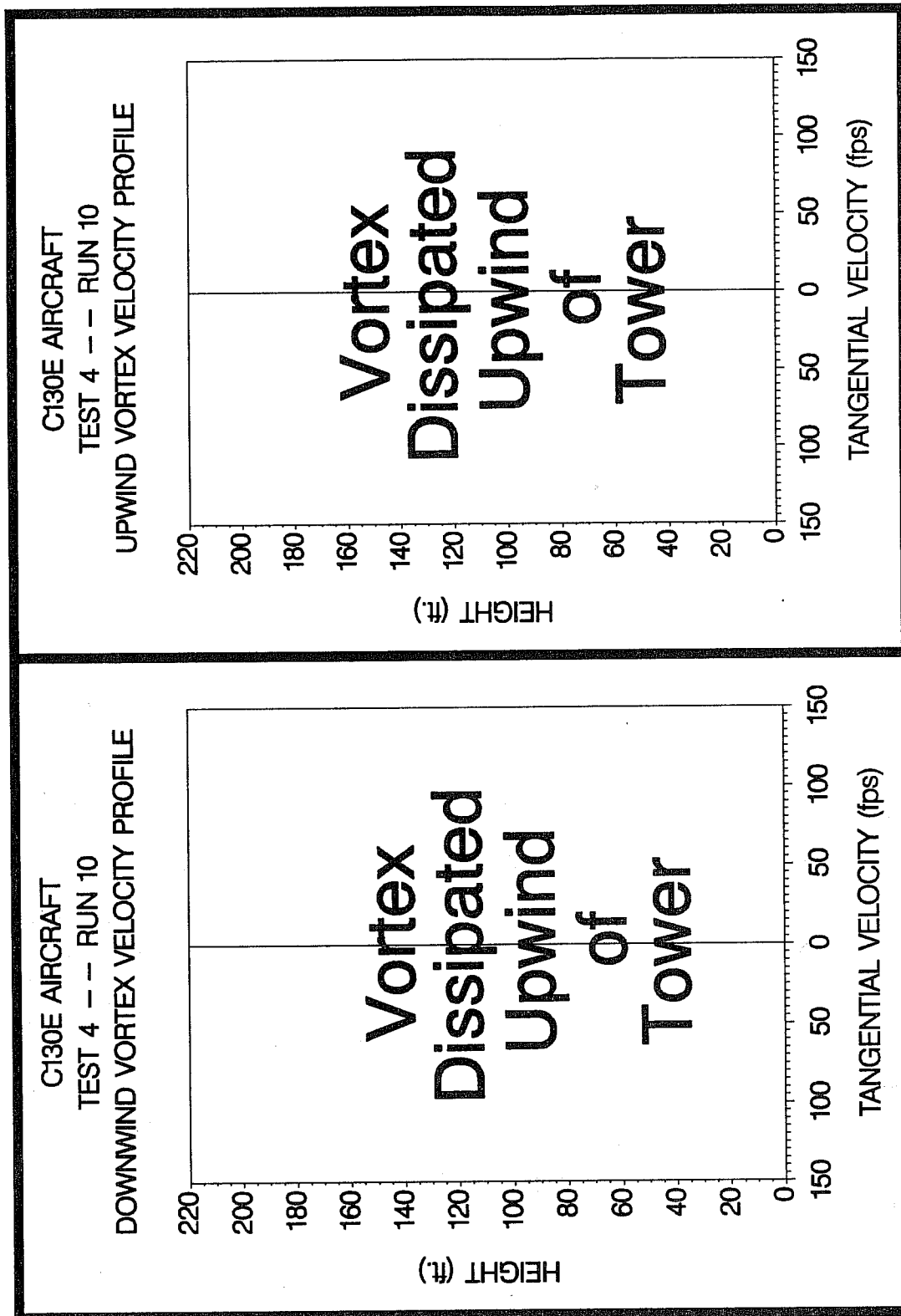


Figure C-57. C130E upwind (top) and downwind (bottom) vortex tangential velocity profile at maximum intensity from Test 4, Run 10, ambient wind speed=4.8 fps,  $\delta_F=50\%$ , IAS=130 knots, GW=142.5k lbs. Ages, radii, and velocities of the vortex cores are (N/A) and (N/A) sec., (N/A) and (N/A) ft., and (N/A) and (N/A) fps, respectively.

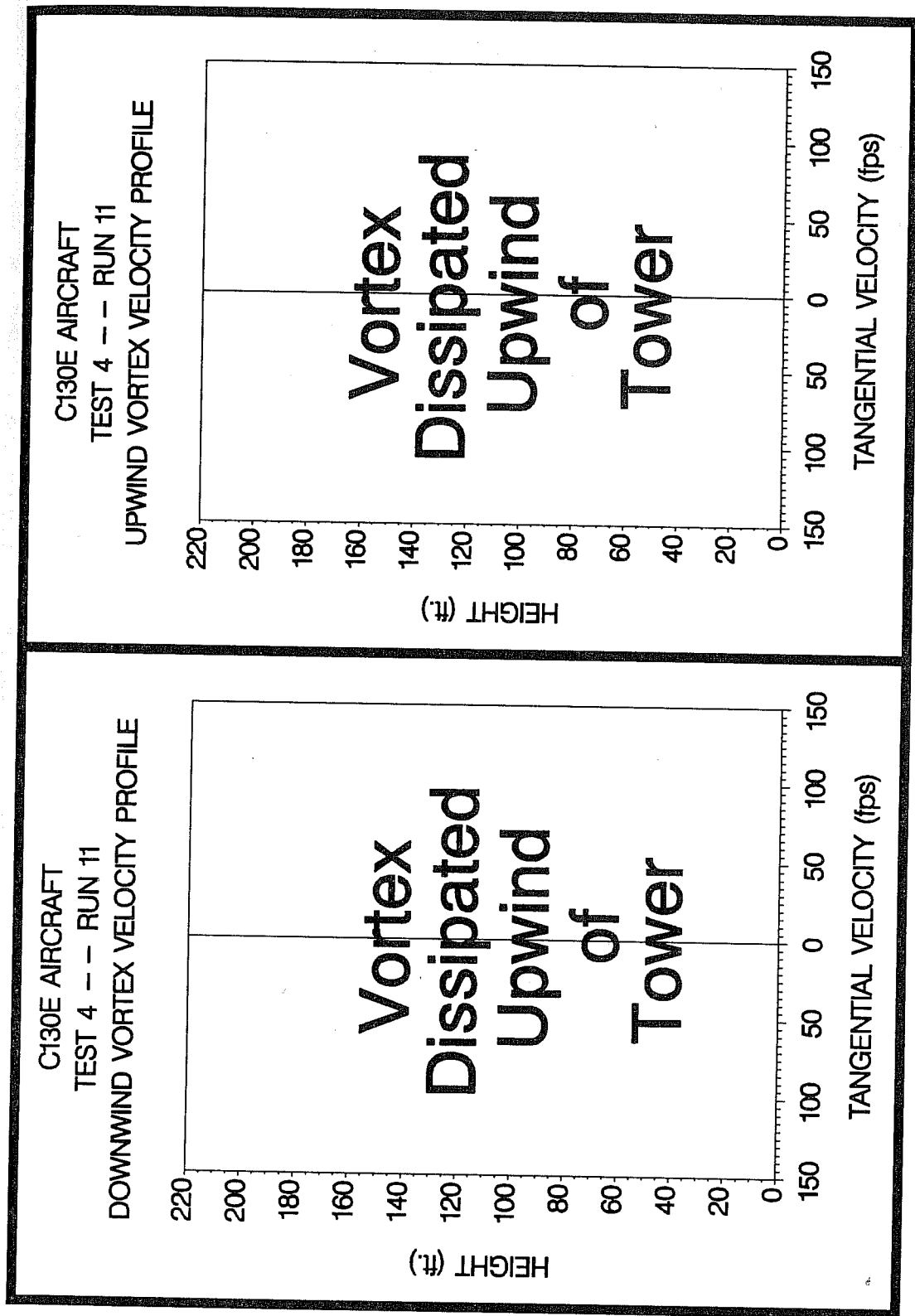
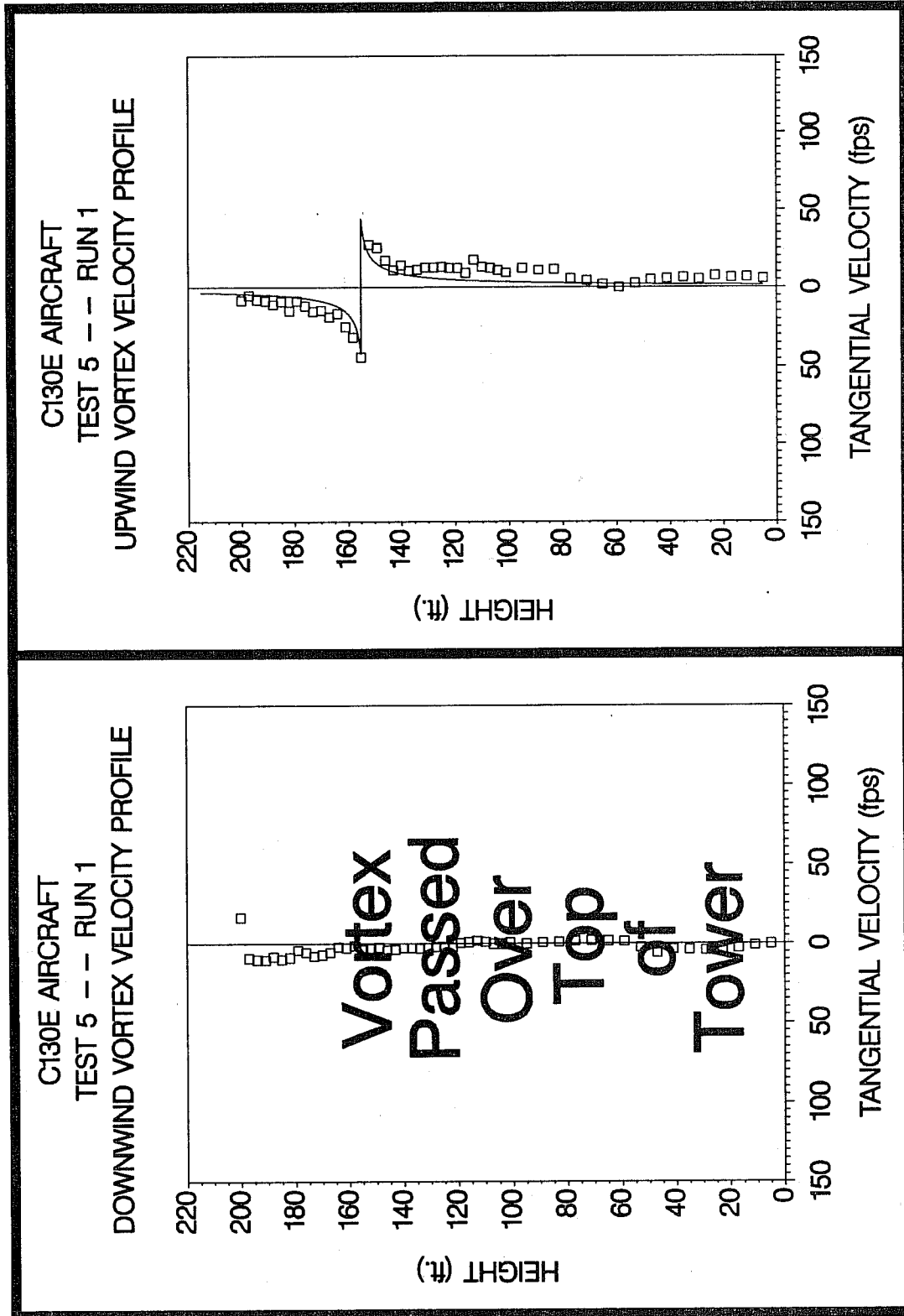


Figure C-58. C130E upwind (top) and downwind (bottom) vortex tangential velocity profile at maximum intensity from Test 4, Run 11, ambient wind speed=5.2 fps,  $\delta_F=50\%$ , IAS=130 knots, GW=142.0k lbs. Ages, radii, and velocities of the vortex cores are (N/A) and (N/A) sec., (N/A) and (N/A) ft., and (N/A) and (N/A) fps, respectively.



**Figure C-59.** C130E upwind (top) and downwind (bottom) vortex tangential velocity profile at maximum intensity from Test 5, Run 1, ambient wind speed=13.1 fps,  $\delta_F=50\%$ , IAS=130 knots, GW=147.0k lbs. Ages, radii, and velocities of the vortex cores are 19 and 11 sec., 1.1 and (N/A) ft., and 44.0 and 16.5 fps, respectively.

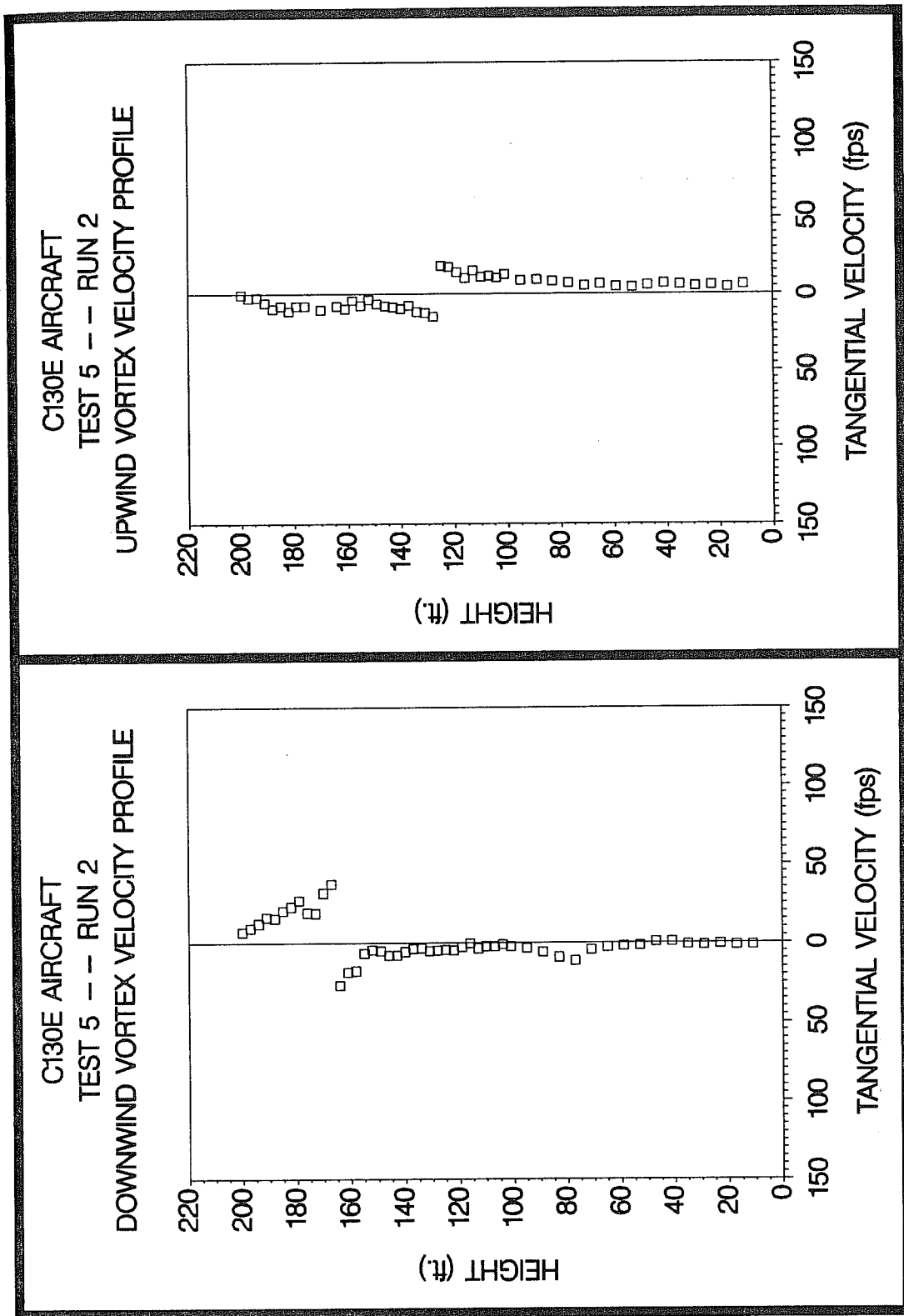


Figure C-60. C130E upwind (top) and downwind (bottom) vortex tangential velocity profile at maximum intensity from Test 5, Run 2, ambient wind speed=12.1 fps,  $\delta_F=50\%$ , IAS=130 knots, GW=146.3k lbs. Ages, radii, and velocities of the vortex cores are 30 and 26 sec., (N/A) and (N/A) ft., and 14.9 and 37.1 fps, respectively.

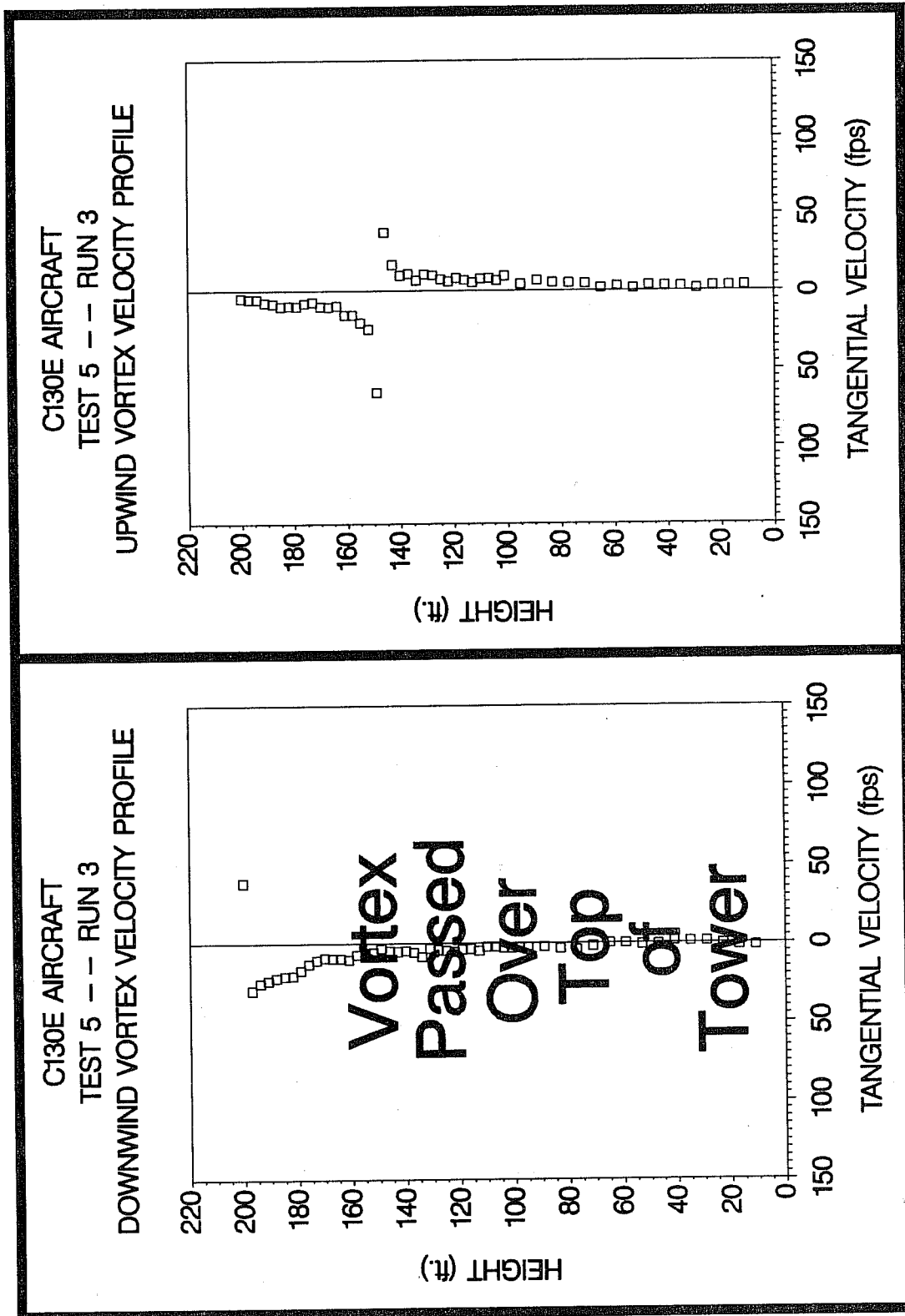
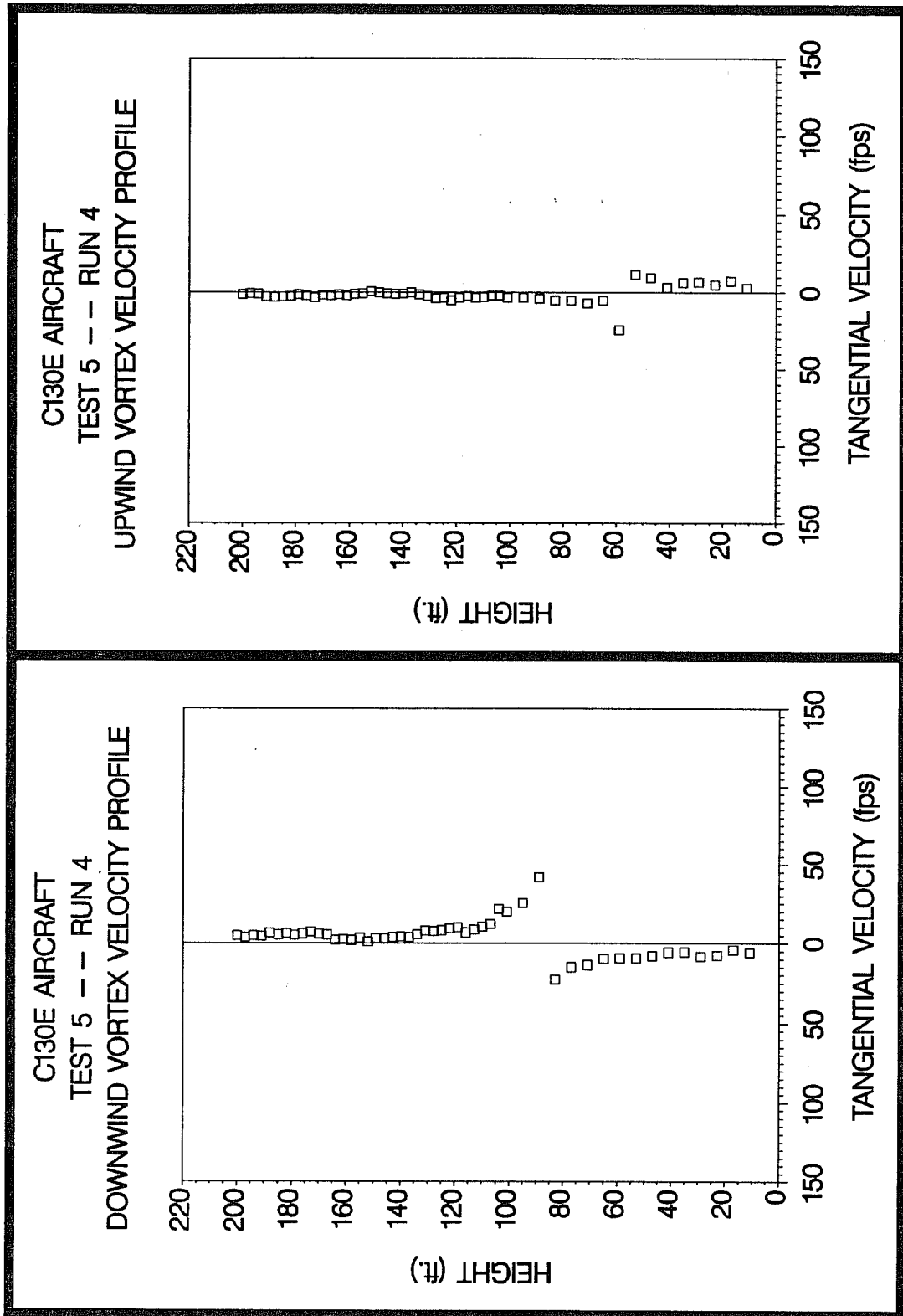
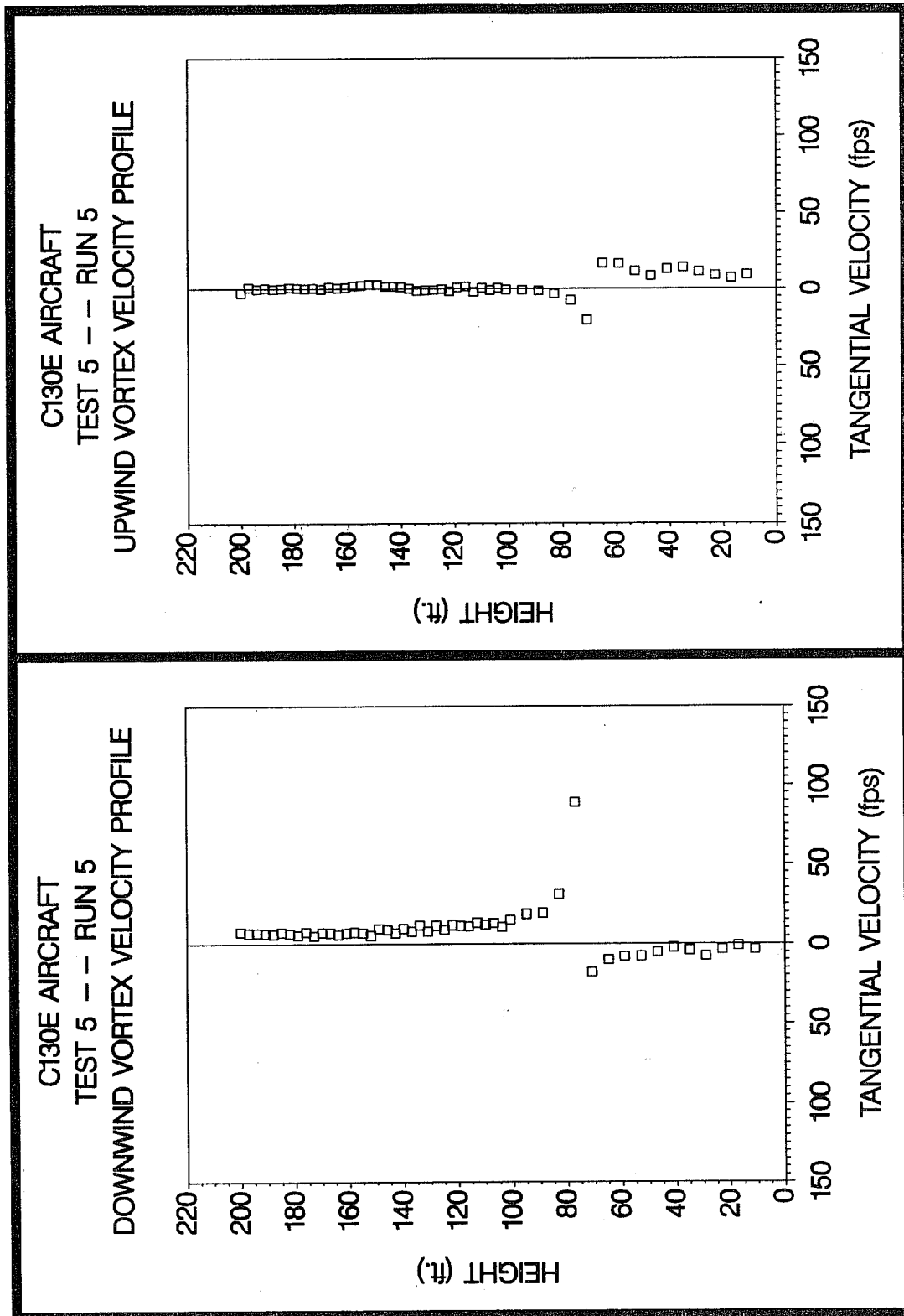


Figure C-61. C130E upwind (top) and downwind (bottom) vortex tangential velocity profile at maximum intensity from Test 5, Run 3, ambient wind speed=10.0 fps,  $\delta_F=27\%$ , IAS=130 knots, GW=145.6k lbs. Ages, radii, and velocities of the vortex cores are 31 and 13 sec., (N/A) and (N/A) ft., and 64.9 and 38.3 fps, respectively.



**Figure C-62.** C130E upwind (top) and downwind (bottom) vortex tangential velocity profile at maximum intensity from Test 5, Run 4, ambient wind speed=7.7 fps,  $\delta_F=27\%$ , IAS=132 knots, GW=144.9k lbs. Ages, radii, and velocities of the vortex cores are 52 and 36 sec., (N/A) and (N/A) ft., and 24.2 and 42.0 fps, respectively.



**Figure C-63.** C130E upwind (top) and downwind (bottom) vortex tangential velocity profile at maximum intensity from Test 5, Run 5, ambient wind speed=16.2 fps,  $\delta_F=27\%$ , IAS=132 knots, GW=144.2k lbs. Ages, radii, and velocities of the vortex cores are 79 and 37 sec., (N/A) and (N/A) ft., and 20.5 and 88.9 fps, respectively.

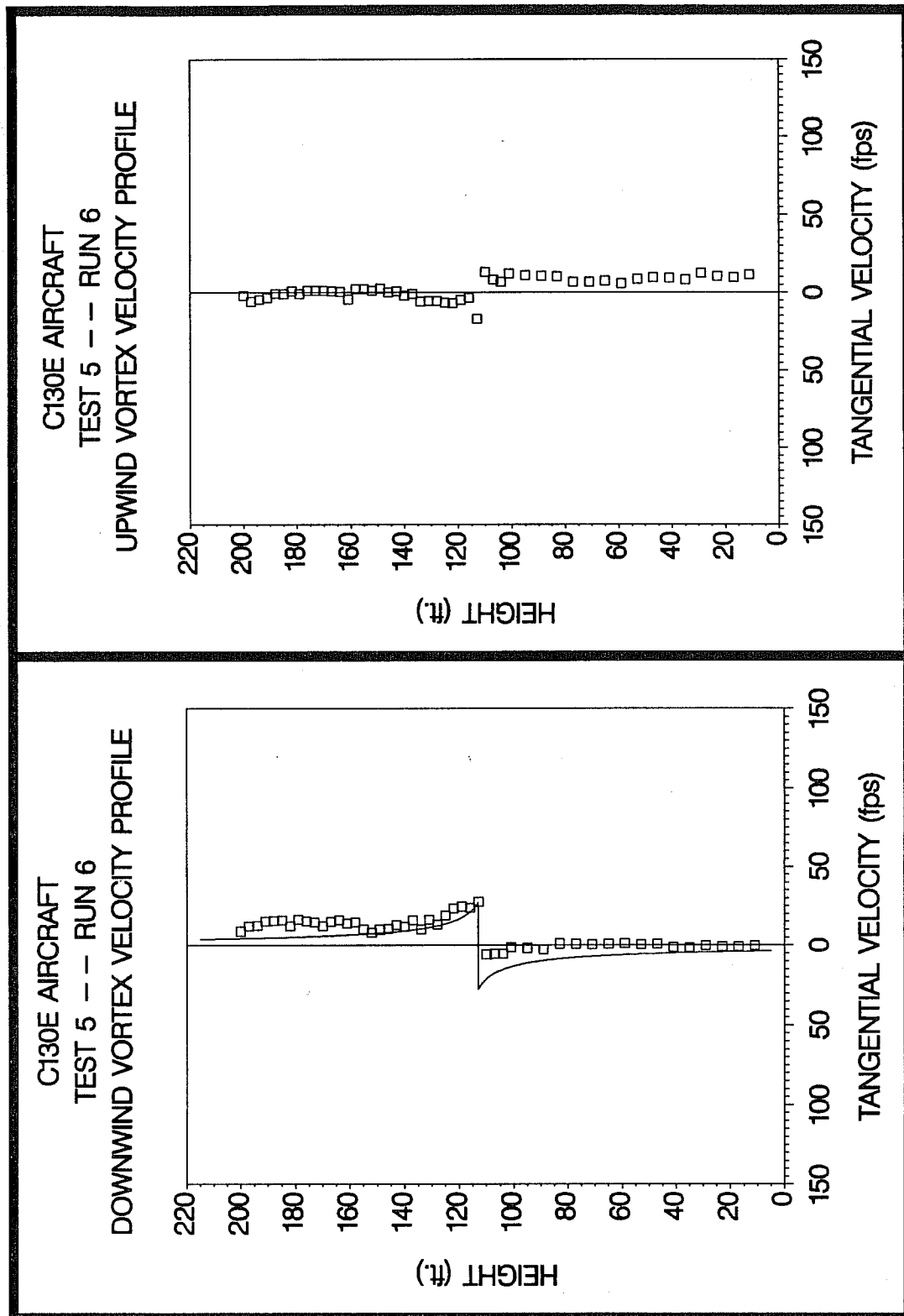


Figure C-64. C130E upwind (top) and downwind (bottom) vortex tangential velocity profile at maximum intensity from Test 5, Run 6, ambient wind speed=18.5 fps,  $\delta_P=27\%$ , IAS=131 knots, GW=143.5k lbs. Ages, radii, and velocities of the vortex cores are 88 and 34 sec., (N/A) and 4.6 ft., and 17.0 and 27.4 fps, respectively.

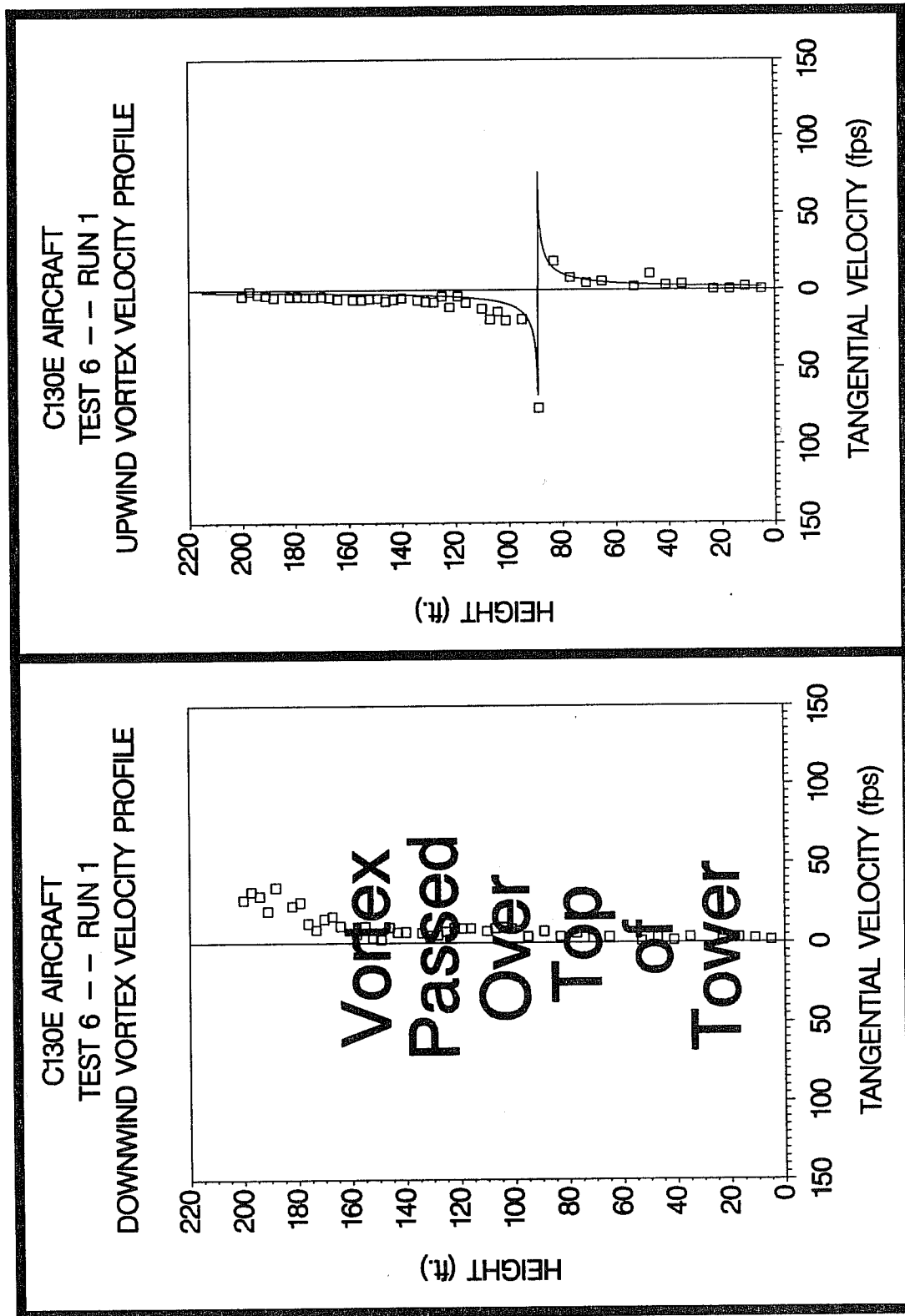


Figure C-65. C130E upwind (top) and downwind (bottom) vortex tangential velocity profile at maximum intensity from Test 6, Run 1, ambient wind speed=6.4 fps,  $\delta_F=27\%$ , IAS=130 knots, GW=146.0k lbs. Ages, radii, and velocities of the vortex cores are 30 and 14 sec., 0.4 and (N/A) ft., and 76.6 and (N/A) fps, respectively.

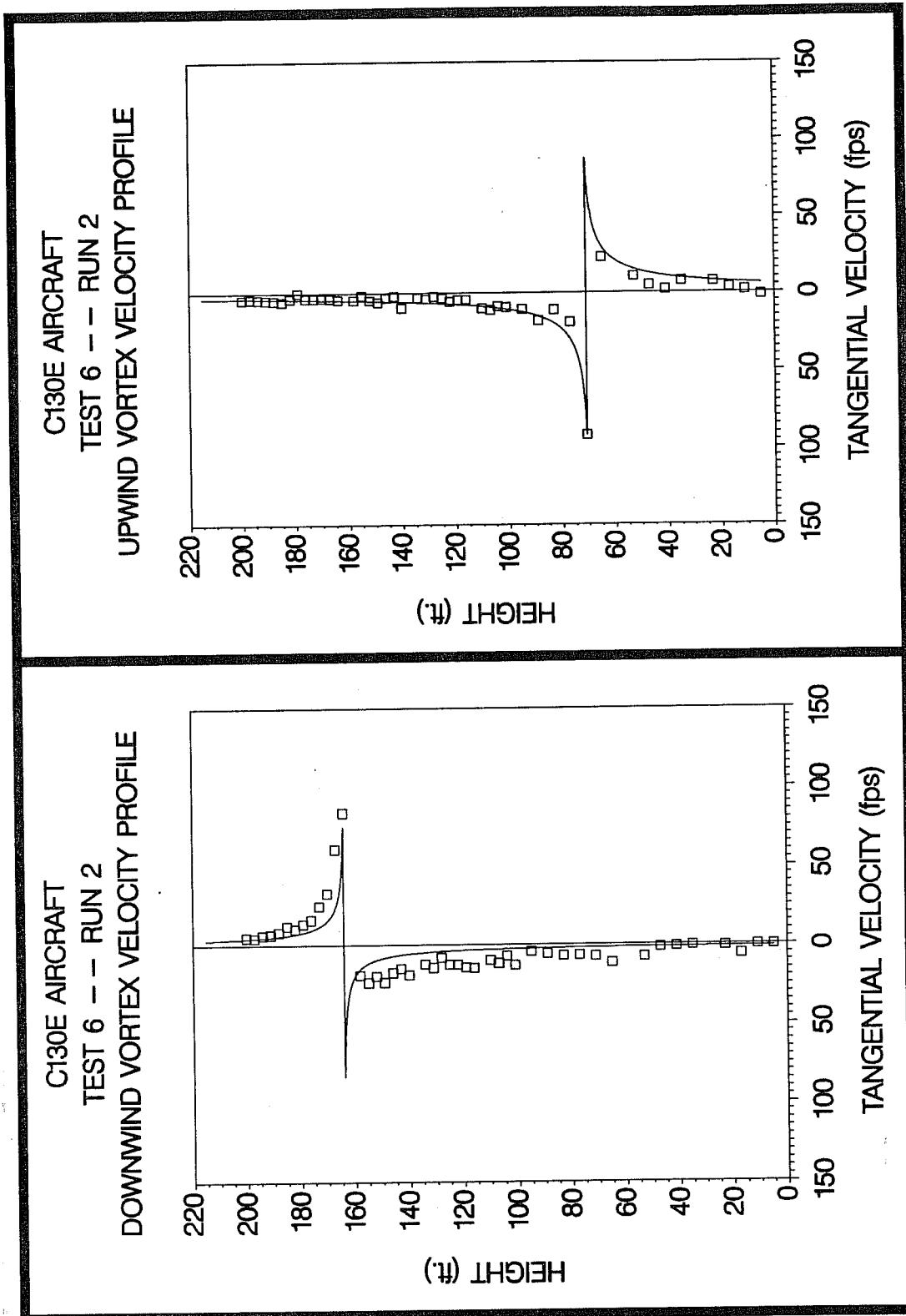
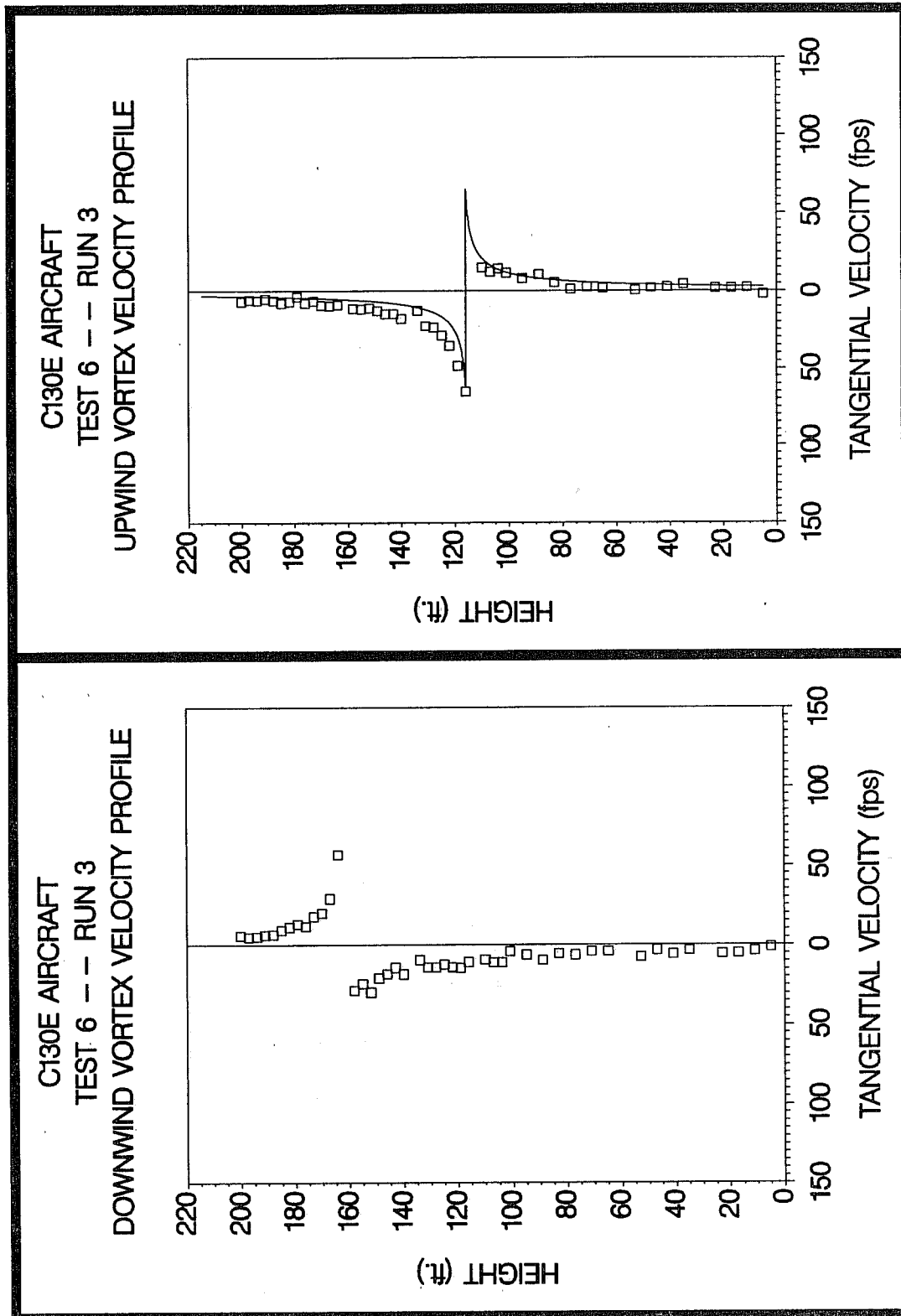


Figure C-66. C130E upwind (top) and downwind (bottom) vortex tangential velocity profile at maximum intensity from Test 6, Run 2, ambient wind speed=6.3 fps,  $\delta_F=27\%$ , IAS=130 knots, GW=145.2k lbs. Ages, radii, and velocities of the vortex cores are 35 and 20 sec., 1.0 and 0.4 ft., and 91.9 and 83.6 fps, respectively.



**Figure C-67.** C130E upwind (top) and downwind (bottom) vortex tangential velocity profile at maximum intensity from Test 6, Run 3, ambient wind speed=6.3 fps,  $\delta_F=27\%$ , IAS=130 knots, GW=144.3k lbs. Ages, radii, and velocities of the vortex cores are 25 and 17 sec., 1.0 and (N/A) ft., and 65.1 and 56.6 fps, respectively.

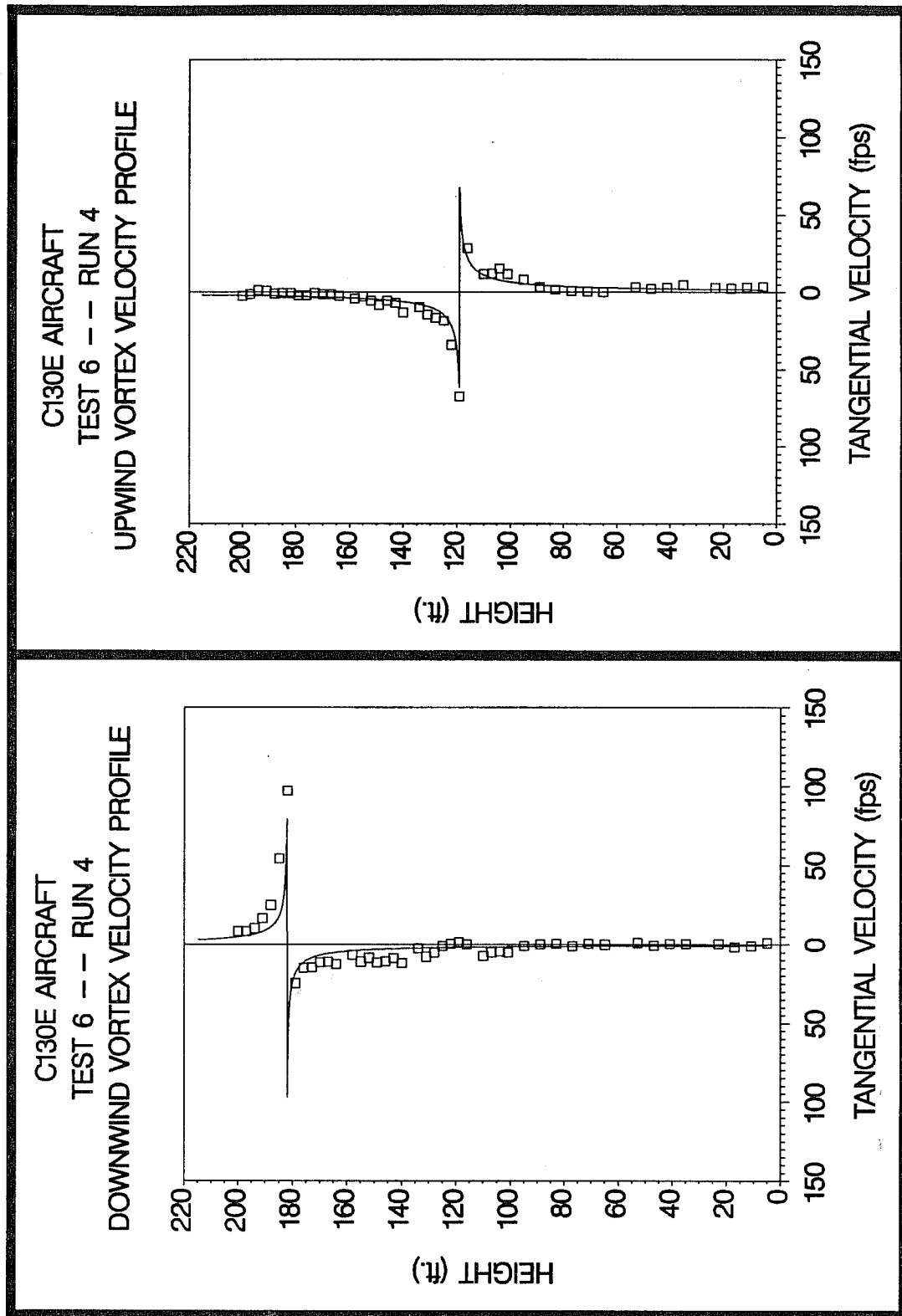


Figure C-68. C130E upwind (top) and downwind (bottom) vortex tangential velocity profile at maximum intensity from Test 6, Run 4, ambient wind speed=6.2 fps,  $\delta_F=0\%$ , IAS=180 knots, GW=143.4k lbs. Ages, radii, and velocities of the vortex cores are 35 and 19 sec., 0.5 and 0.2 ft., and 67.6 and 97.3 fps, respectively.

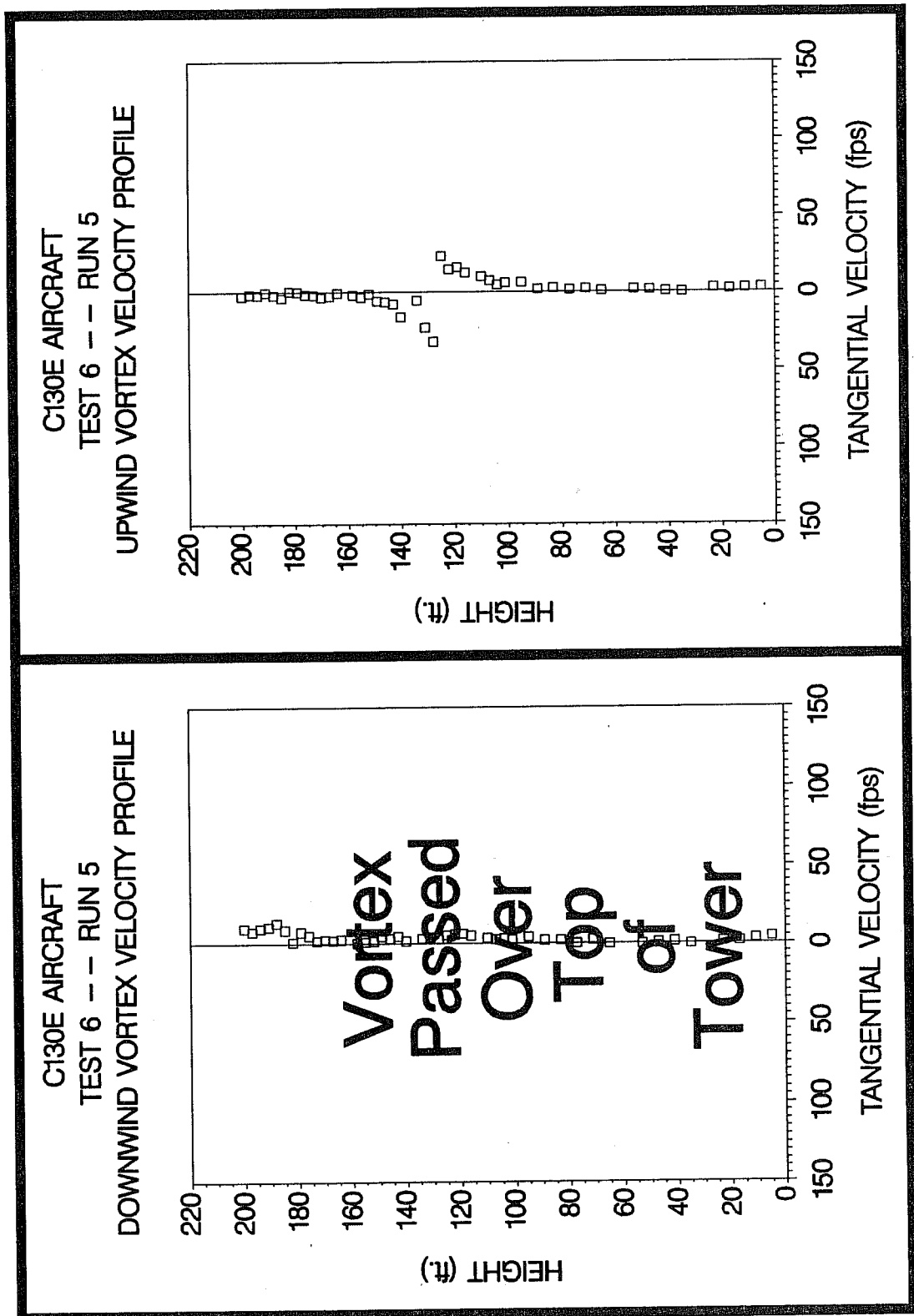
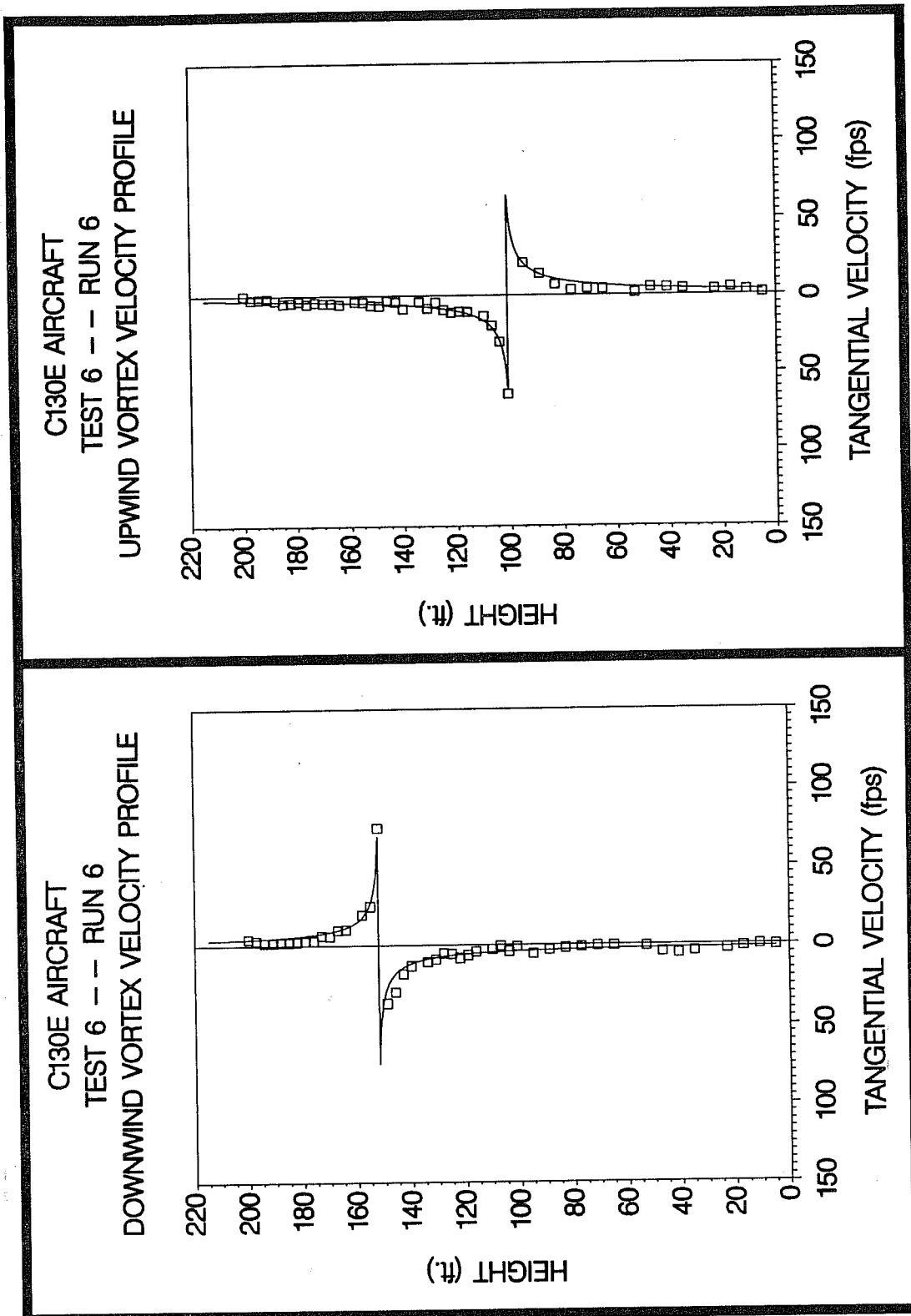


Figure C-69. C130E upwind (top) and downwind (bottom) vortex tangential velocity profile at maximum intensity from Test 6, Run 5, ambient wind speed=4.3 fps,  $\delta_F=0\%$ , IAS=180 knots, GW=142.5k lbs. Ages, radii, and velocities of the vortex cores are 66 and (N/A) sec., (N/A) and (N/A) ft., and 32.3 and (N/A) fps, respectively.



**Figure C-70.** C130E upwind (top) and downwind (bottom) vortex tangential velocity profile at maximum intensity from Test 6, Run 6, ambient wind speed=5.9 fps,  $\delta_F=0\%$ , IAS=180 knots, GW=141.7k lbs. Ages, radii, and velocities of the vortex cores are 45 and 22 sec., 1.0 and 0.6 ft., and 64.1 and 74.3 fps, respectively.

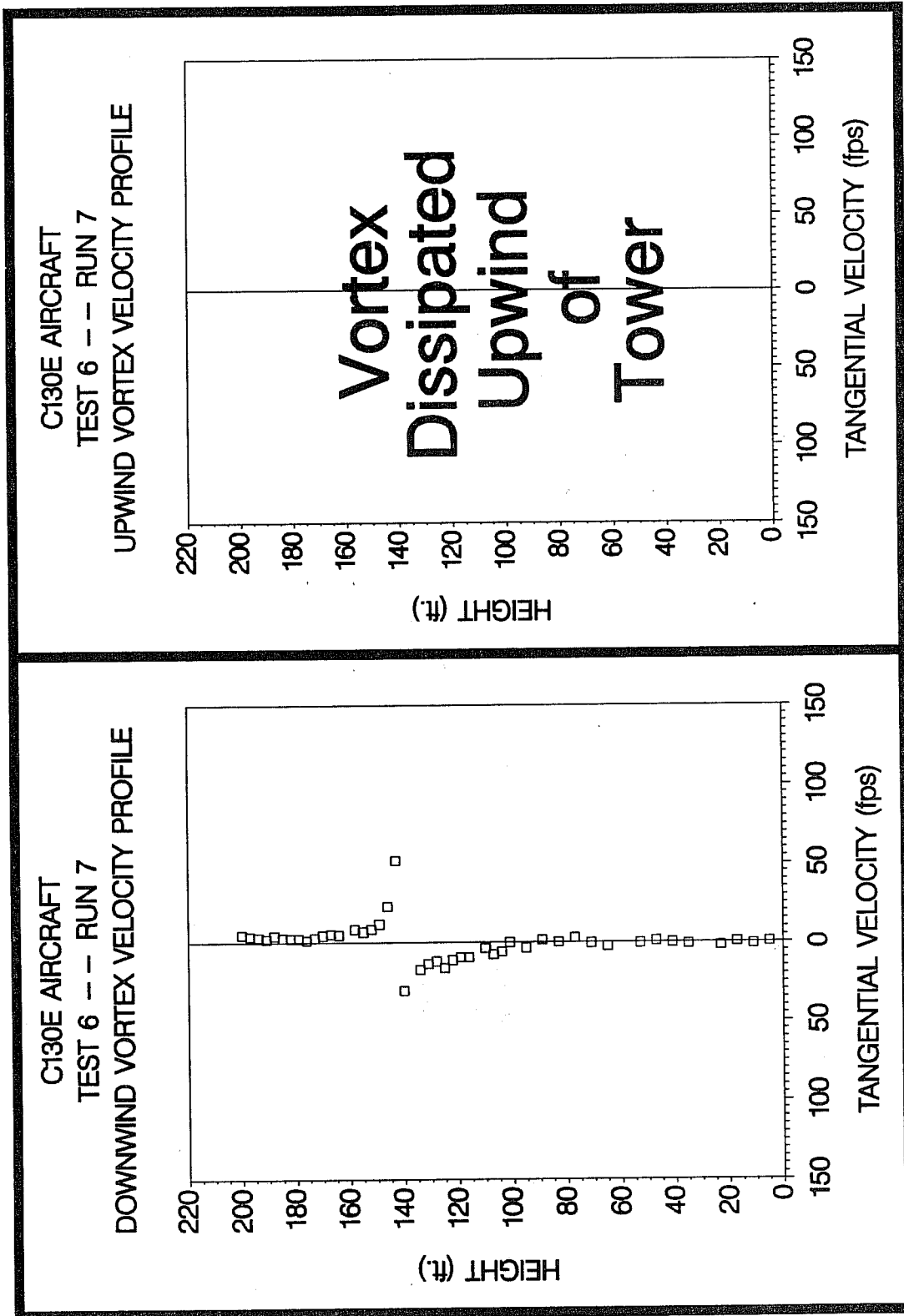


Figure C-71. C130E upwind (top) and downwind (bottom) vortex tangential velocity profile at maximum intensity from Test 6, Run 7, ambient wind speed=3.9 fps,  $\delta_F=0\%$ , IAS=230 knots, GW=141.0k lbs. Ages, radii, and velocities of the vortex cores are (N/A) and 24 sec., (N/A) and (N/A) ft., and (N/A) and 51.8 fps, respectively.

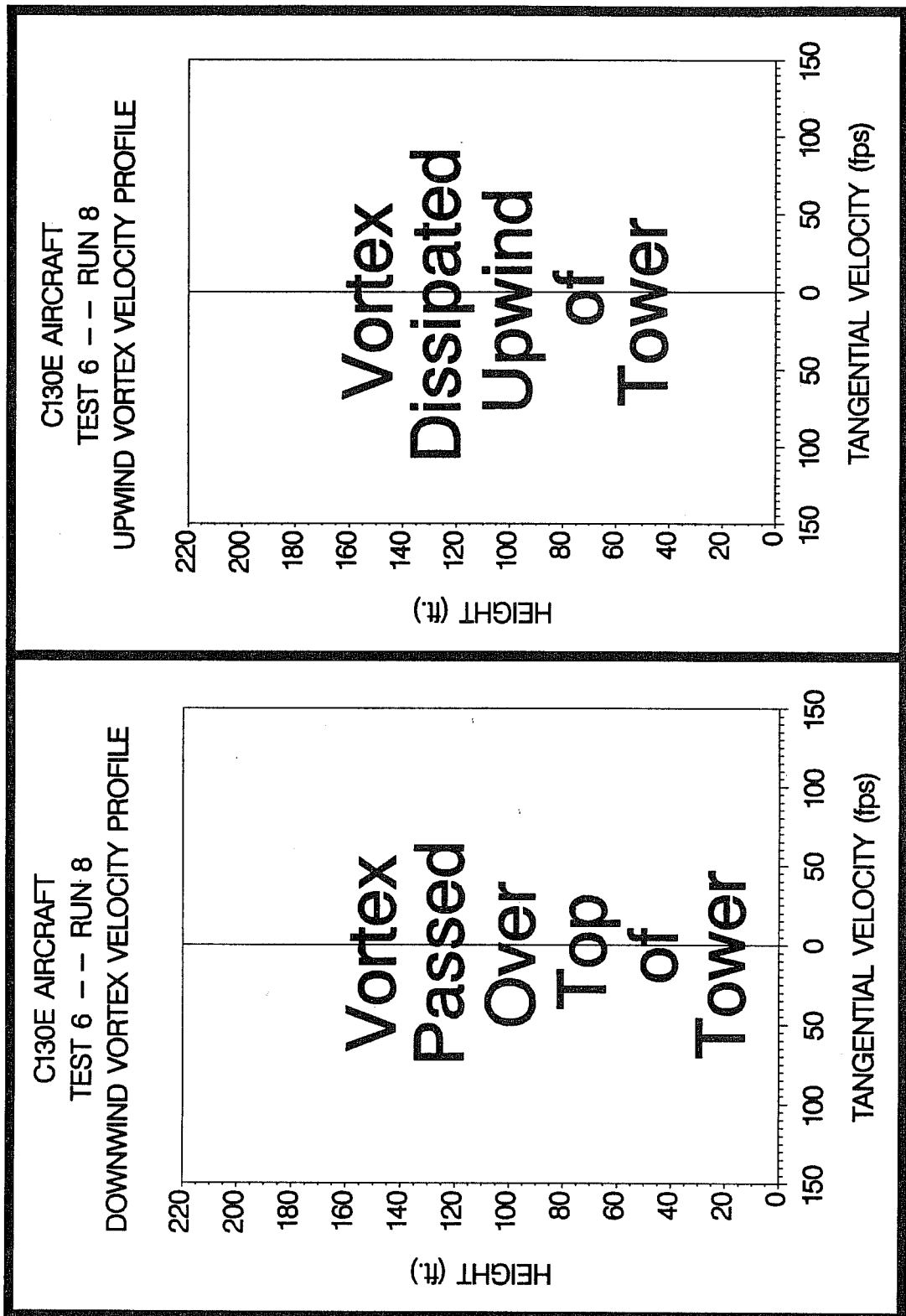


Figure C-72. C130E upwind (top) and downwind (bottom) vortex tangential velocity profile at maximum intensity from Test 6, Run 8, ambient wind speed=5.2 fps,  $\delta_F=0\%$ , IAS=245 knots, GW=140.5k lbs. Ages, radii, and velocities of the vortex cores are (N/A) and (N/A) sec., (N/A) and (N/A) ft., and (N/A) and (N/A) fps, respectively.

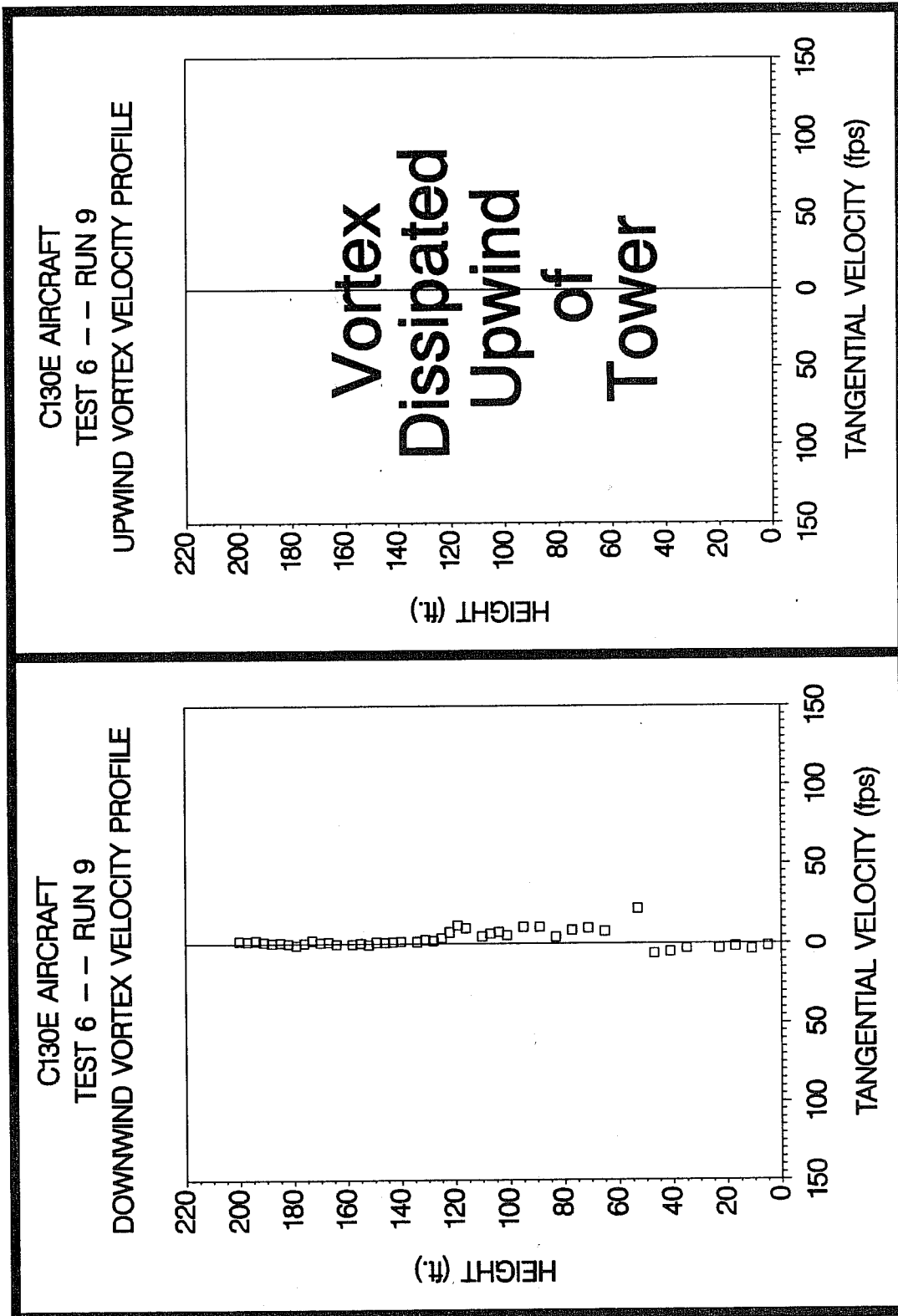
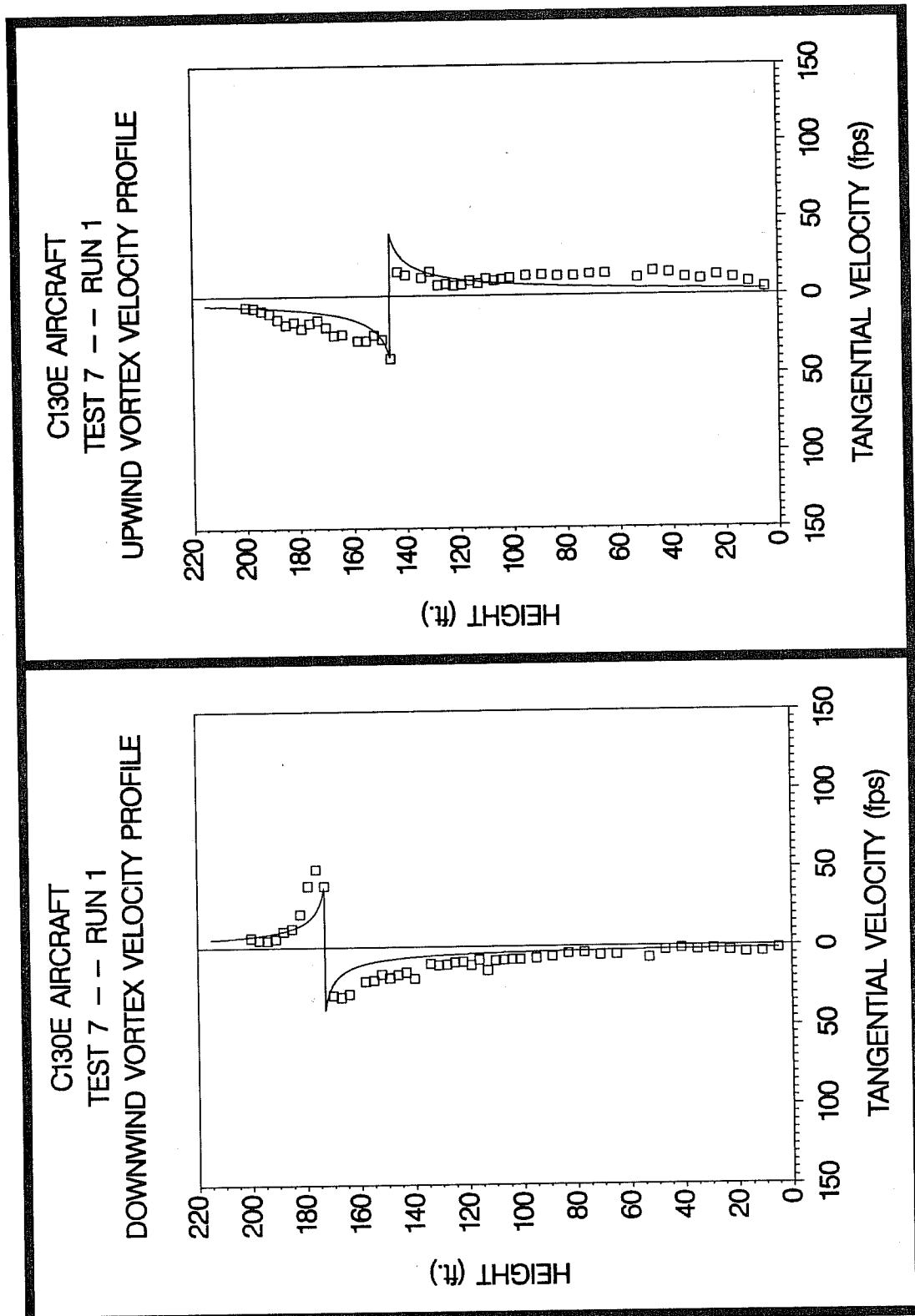


Figure C-73. C130E upwind (top) and downwind (bottom) vortex tangential velocity profile at maximum intensity from Test 6, Run 9, ambient wind speed=3.7 fps,  $\delta_F=50\%$ , IAS=125 knots, GW=140.0k lbs. Ages, radii, and velocities of the vortex cores are (N/A) and (N/A) sec., (N/A) and (N/A) ft., and (N/A) and 21.8 fps, respectively.



**Figure C-74.** C130E upwind (top) and downwind (bottom) vortex tangential velocity profile at maximum intensity from Test 7, Run 1, ambient wind speed=20.0 fps,  $\delta_F=50\%$ , IAS=125 knots, GW=136.0k lbs. Ages, radii, and velocities of the vortex cores are 12 and 7 sec., 3.0 and 1.8 ft., and 40.0 and 39.3 fps, respectively.

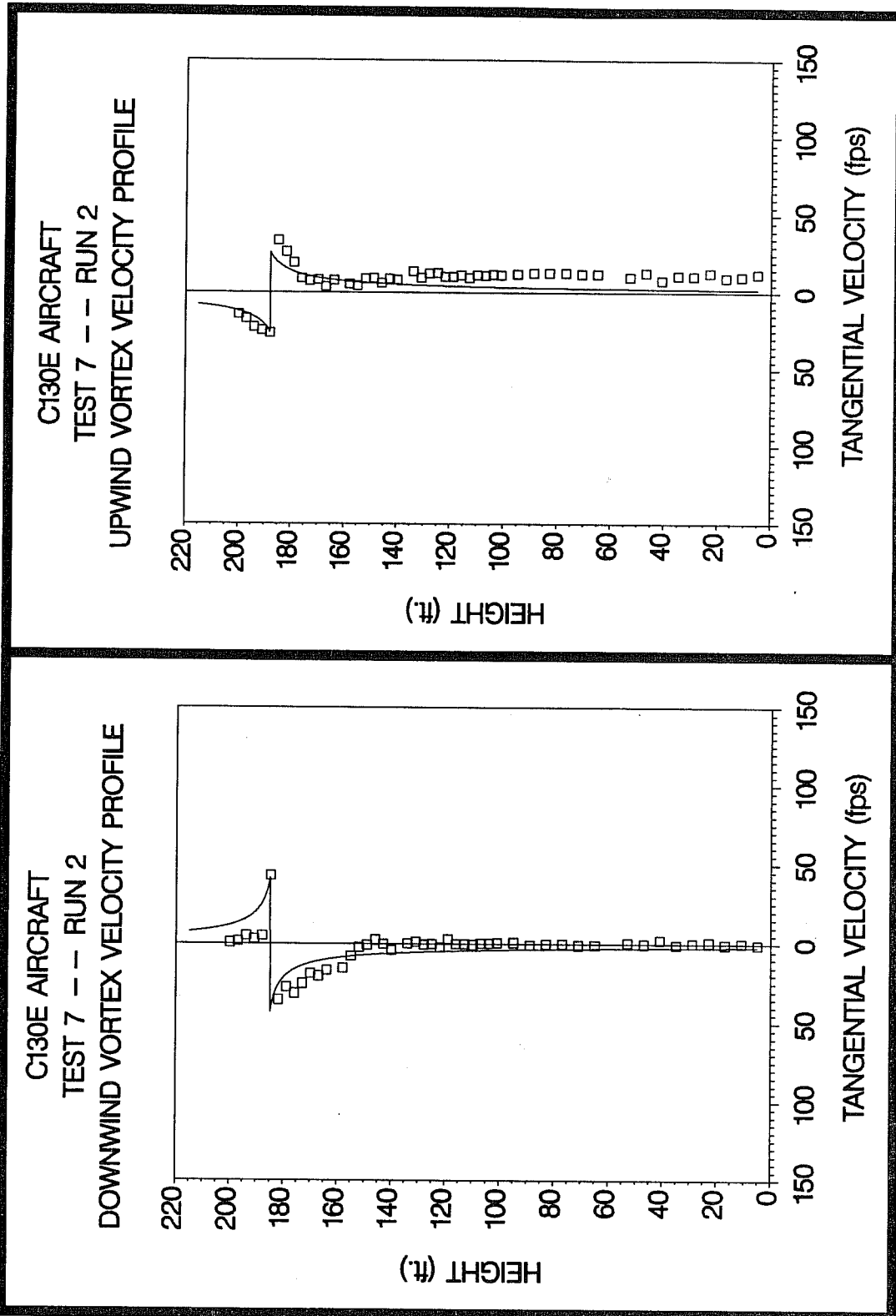
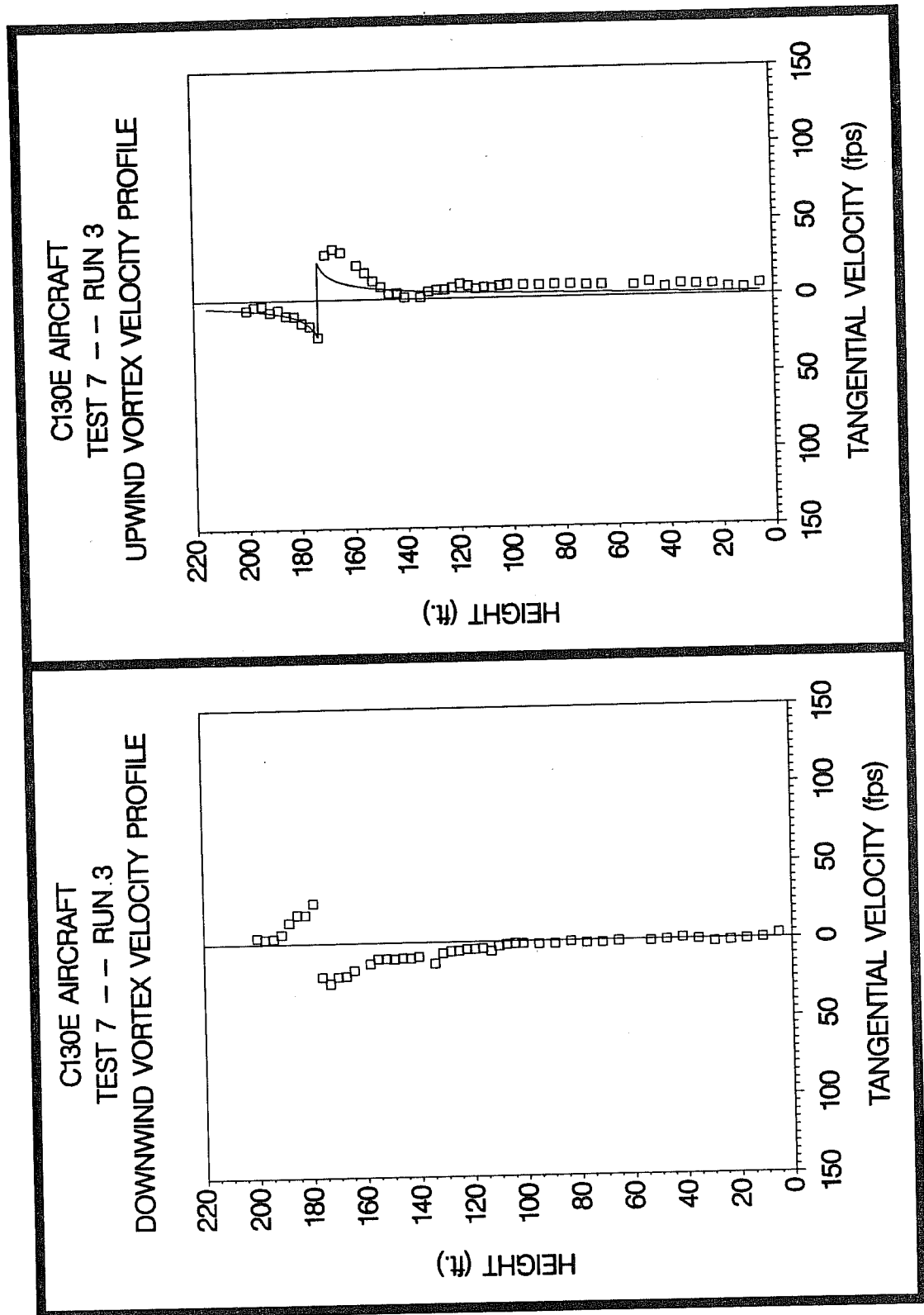
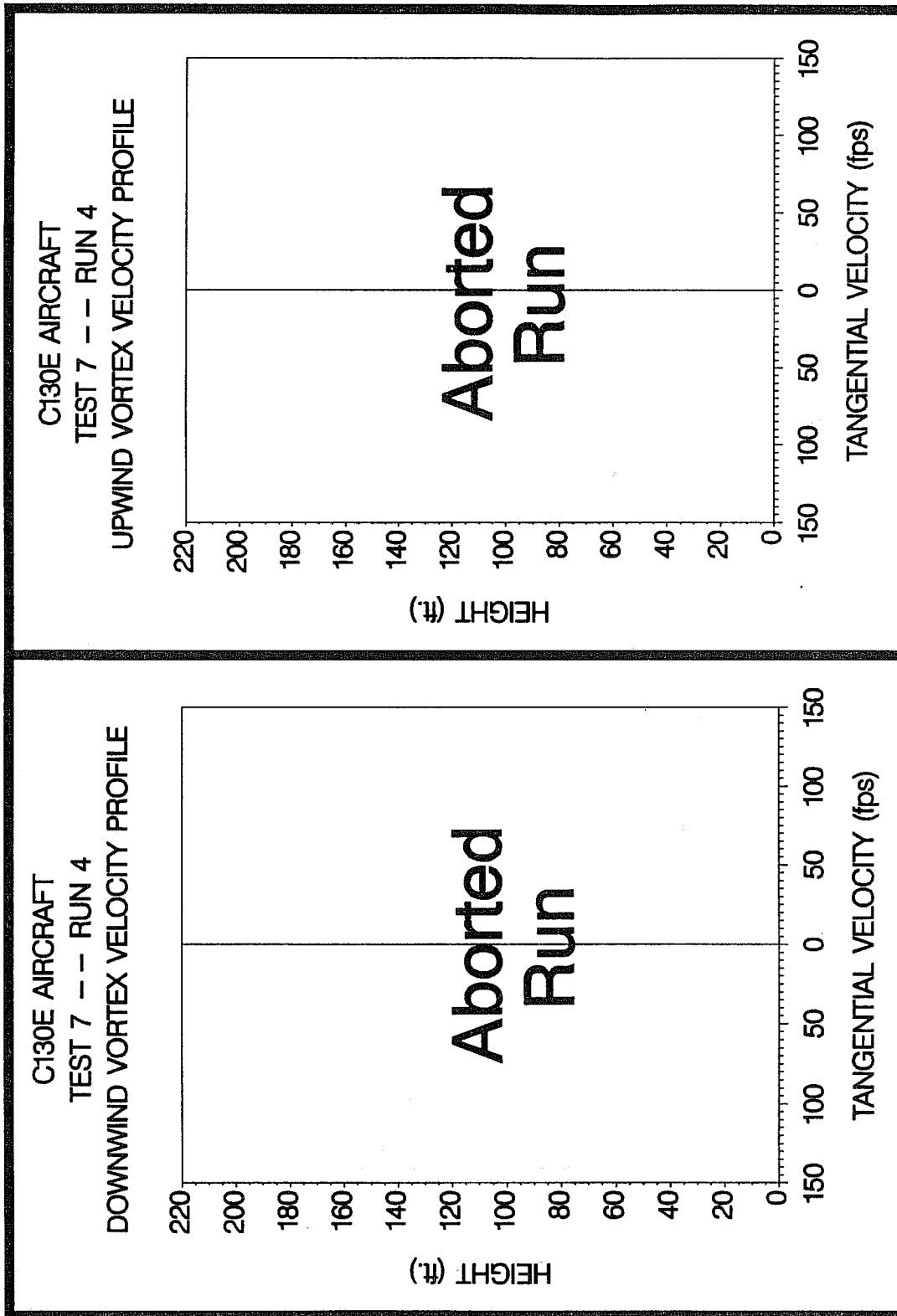


Figure C-75. C130E upwind (top) and downwind (bottom) vortex tangential velocity profile at maximum intensity from Test 7, Run 2, ambient wind speed=24.5 fps,  $\delta_F=50\%$ , IAS=130 knots, GW=135.3k lbs. Ages, radii, and velocities of the vortex cores are 9 and 6 sec., 3.9 and 1.9 ft., and 26.3 and 42.9 fps, respectively.



**Figure C-76.** C130E upwind (top) and downwind (bottom) vortex tangential velocity profile at maximum intensity from Test 7, Run 3, ambient wind speed=19.6 fps,  $\delta_F=50\%$ , IAS=125 knots, GW=134.6k lbs. Ages, radii, and velocities of the vortex cores are 19 and 14 sec., 3.0 and (N/A) ft., and 24.4 and 26.2 fps, respectively.



**Figure C-77.** C130E upwind (top) and downwind (bottom) vortex tangential velocity profile at maximum intensity from Test 7, Run 4, ambient wind speed=31.5 fps,  $\delta_F=(N/A)\%$ , IAS=(N/A) knots, GW=(N/A)k lbs. Ages, radii, and velocities of the vortex cores are (N/A) and (N/A) sec., (N/A) and (N/A) ft., and (N/A) and (N/A) fps, respectively.

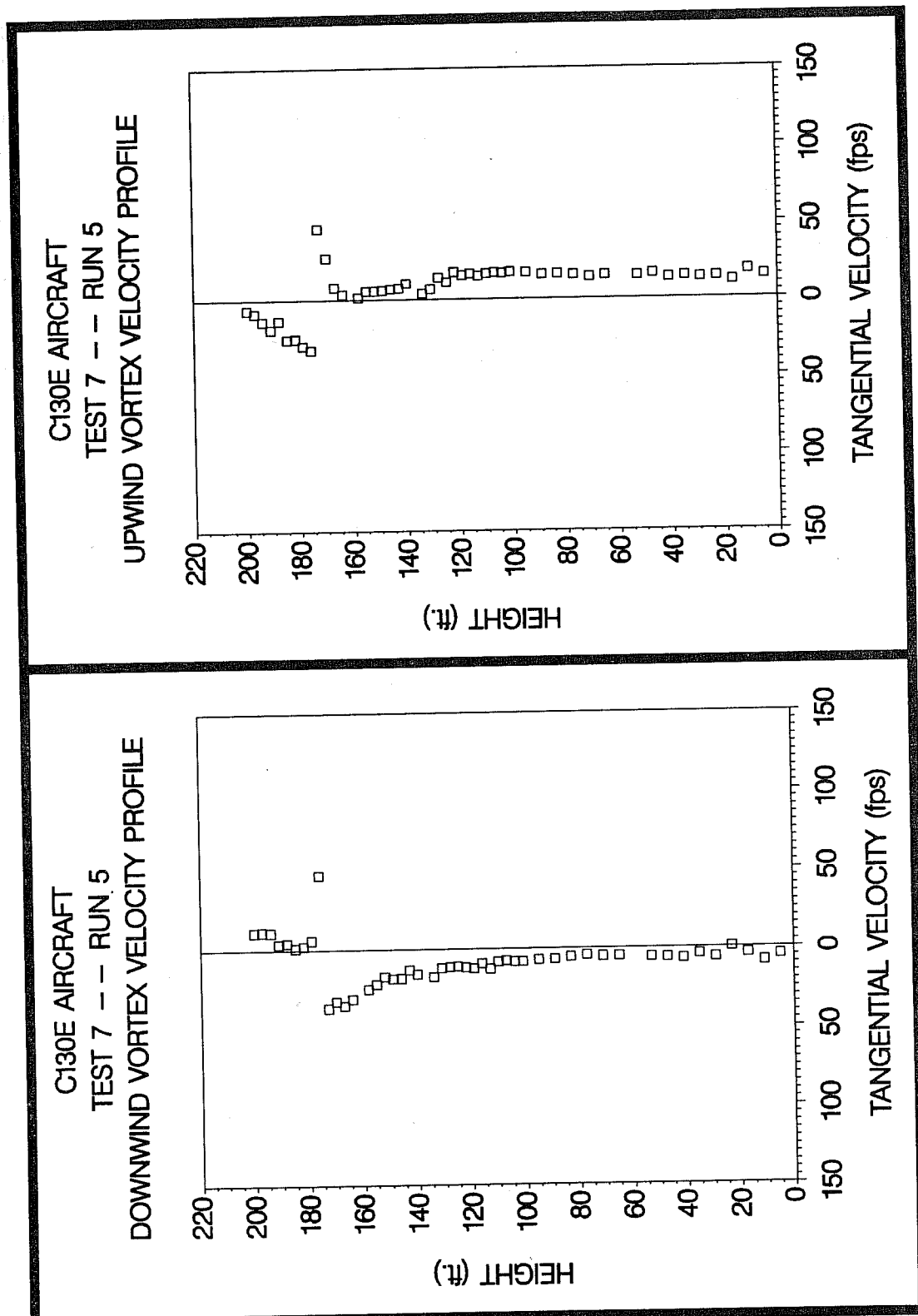


Figure C-78. C130E upwind (top) and downwind (bottom) vortex tangential velocity profile at maximum intensity from Test 7, Run 5, ambient wind speed=28.1 fps,  $\delta_F=50\%$ , IAS=126 knots, GW=132.2k lbs. Ages, radii, and velocities of the vortex cores are 11 and 8 sec., (N/A) and (N/A) ft., and 32.7 and 47.1 fps, respectively.

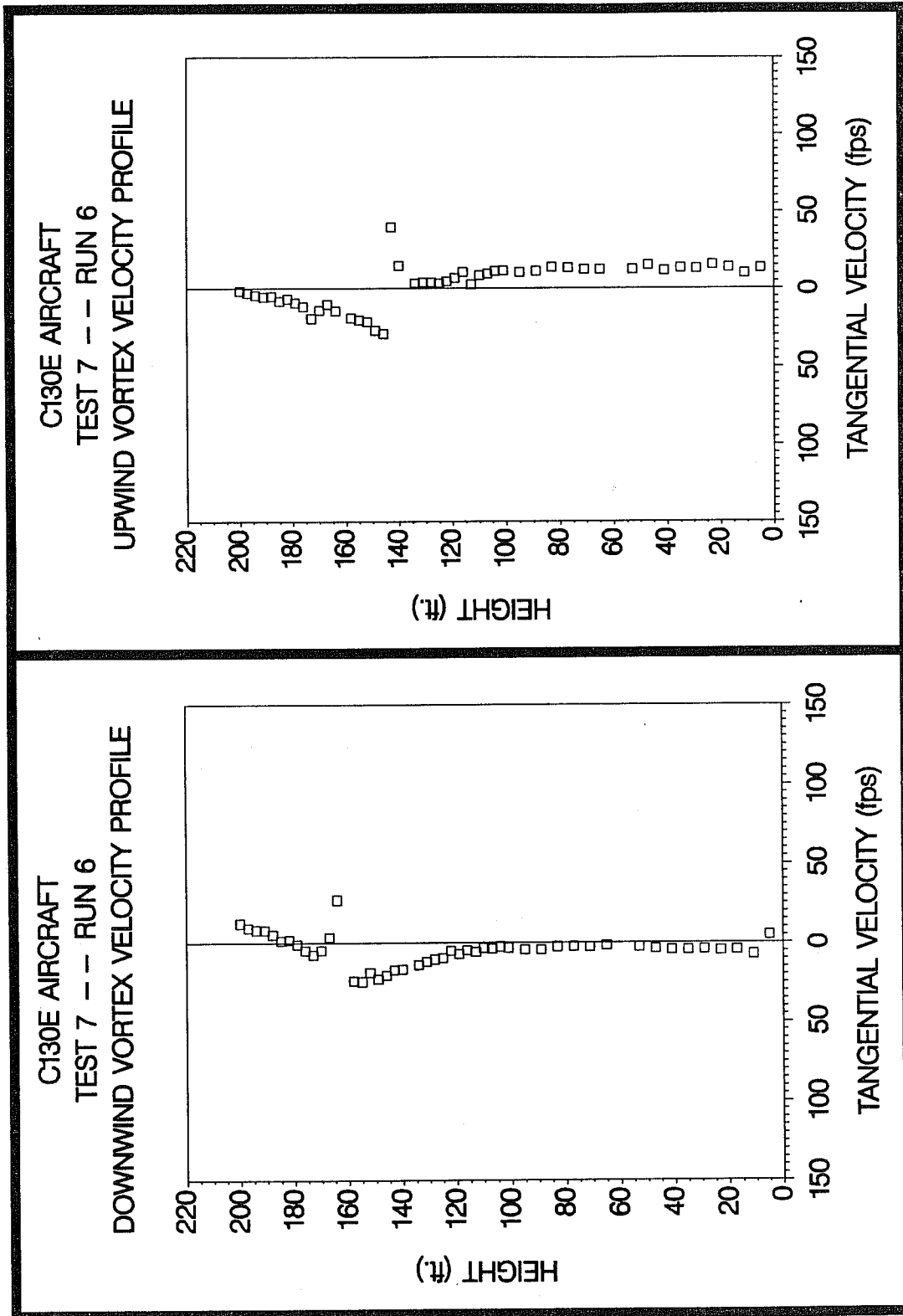


Figure C-79. C130E upwind (top) and downwind (bottom) vortex tangential velocity profile at maximum intensity from Test 7, Run 6, ambient wind speed=31.3 fps,  $\delta_F=50\%$ , IAS=125 knots, GW=131.5k lbs. Ages, radii, and velocities of the vortex cores are 12 and 8 sec., (N/A) and (N/A) ft., and 29.0 and 27.0 fps, respectively.

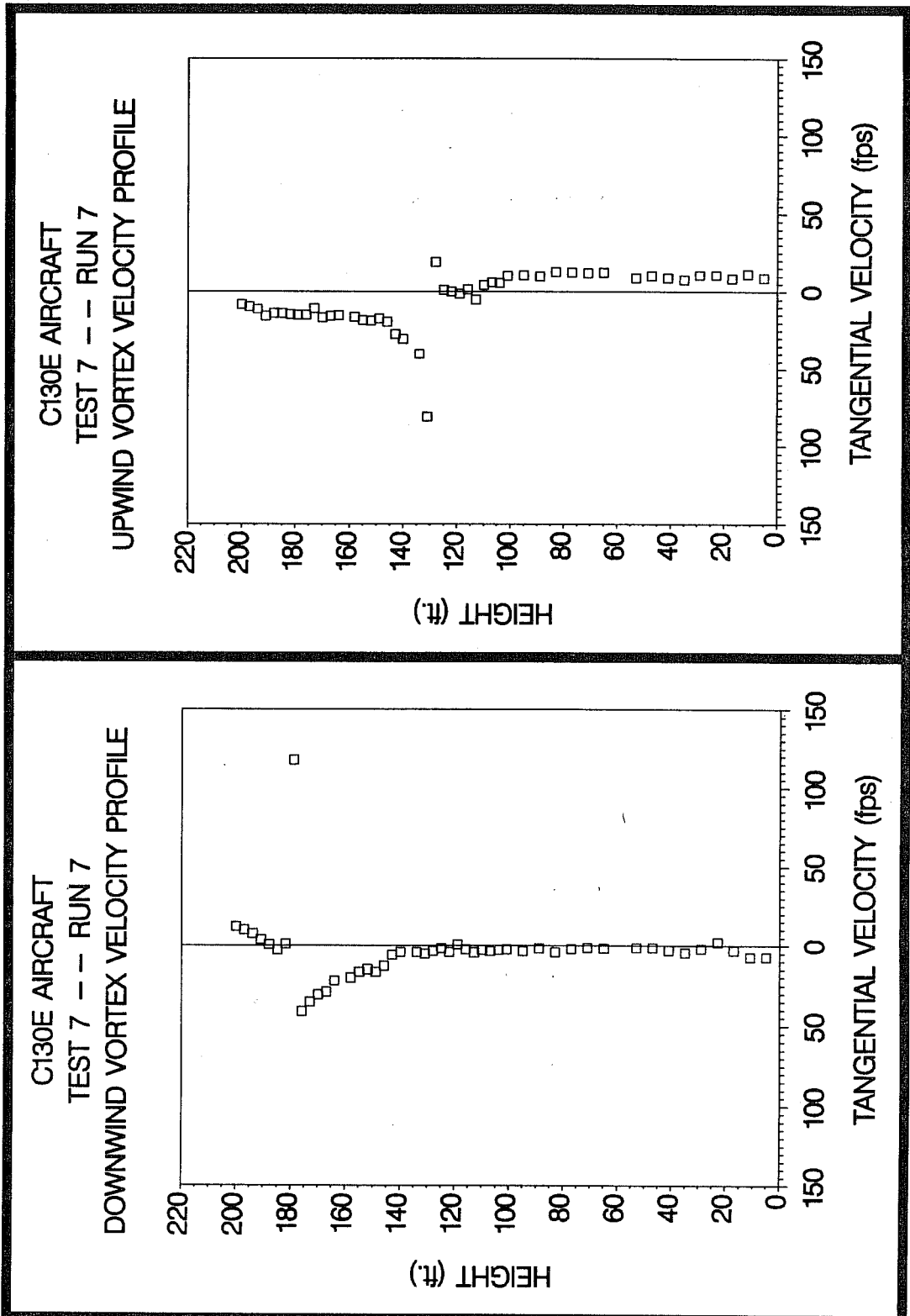
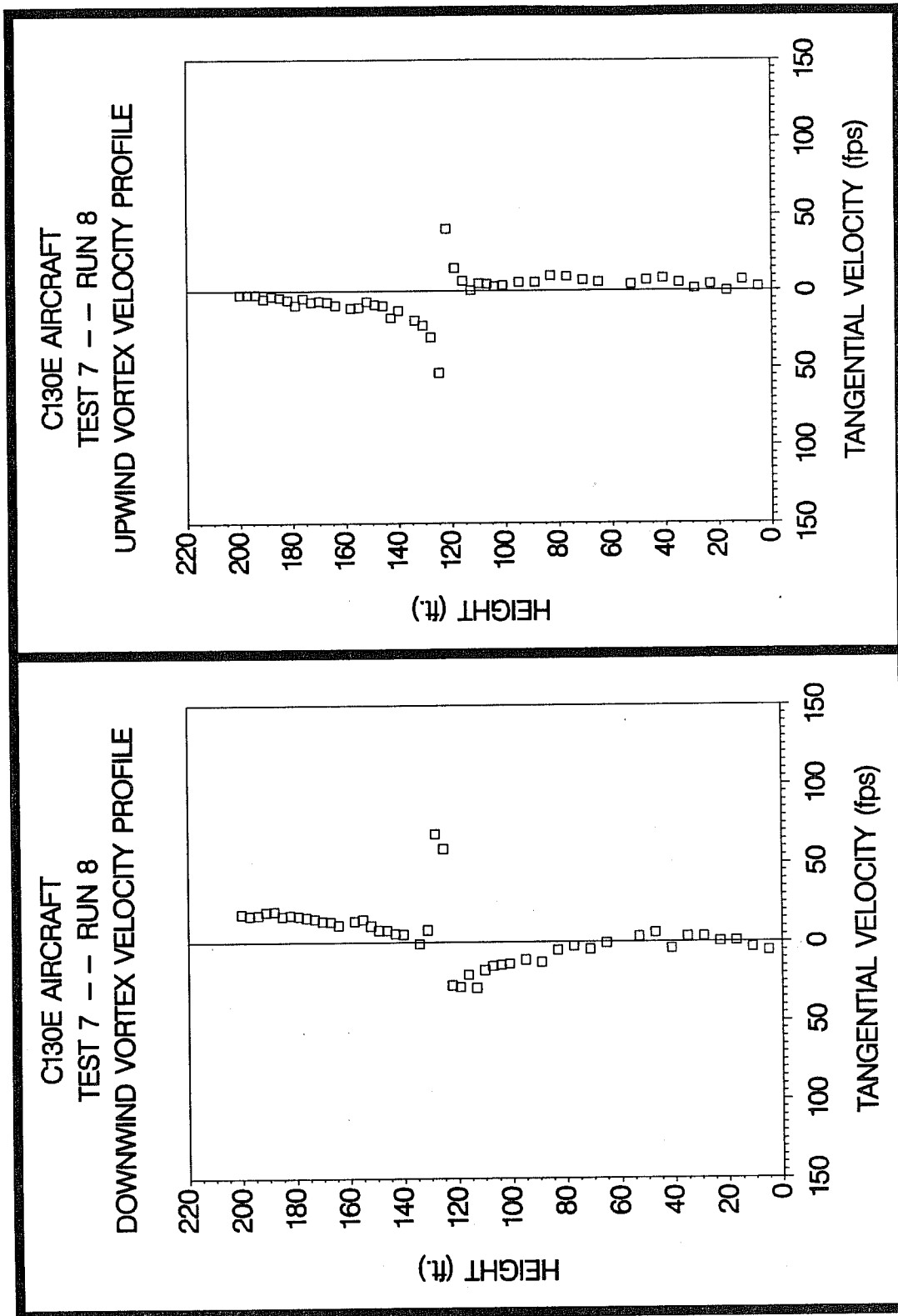


Figure C-80. C130E upwind (top) and downwind (bottom) vortex tangential velocity profile at maximum intensity from Test 7, Run 7, ambient wind speed=25.8 fps,  $\delta_F=20\%$ , IAS=131 knots, GW=129.8k lbs. Ages, radii, and velocities of the vortex cores are 12 and 9 sec., (N/A) and (N/A) ft., and 81.2 and 117.9 fps, respectively.



**Figure C-81.** C130E upwind (top) and downwind (bottom) vortex tangential velocity profile at maximum intensity from Test 7, Run 8, ambient wind speed=25.8 fps,  $\delta_F=20\%$ , IAS=132 knots, GW=129.2k lbs. Ages, radii, and velocities of the vortex cores are 14 and 11 sec., (N/A) and (N/A) ft., and 53.1 and 58.9 fps, respectively.

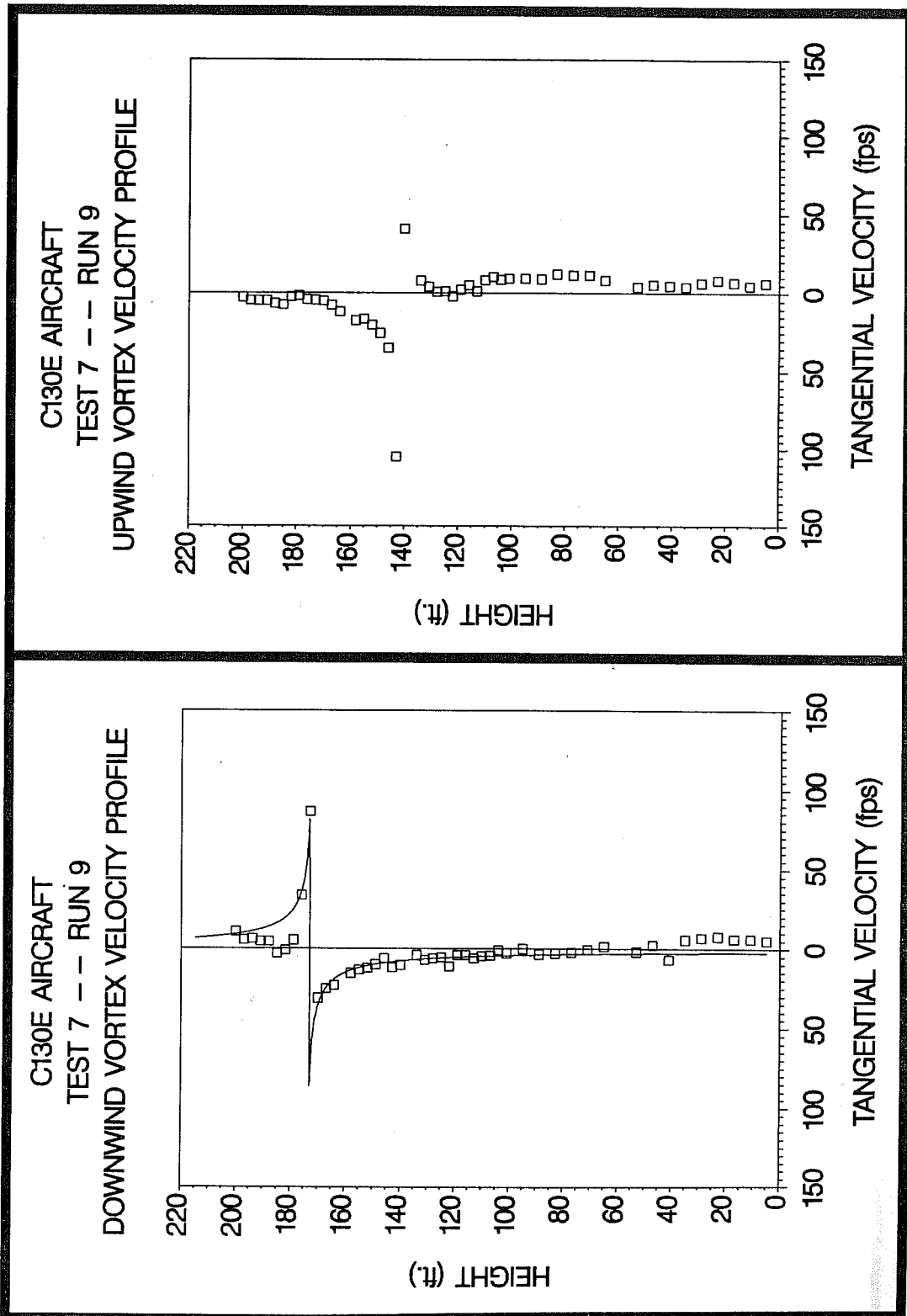


Figure C-82. C130E upwind (top) and downwind (bottom) vortex tangential velocity profile at maximum intensity from Test 7, Run 9, ambient wind speed=24.2 fps,  $\delta_F=20\%$ , IAS=132 knots, GW=128.6k lbs. Ages, radii, and velocities of the vortex cores are 18 and 12 sec., (N/A) and 0.8 ft., and 104.8 and 86.5 fps, respectively.

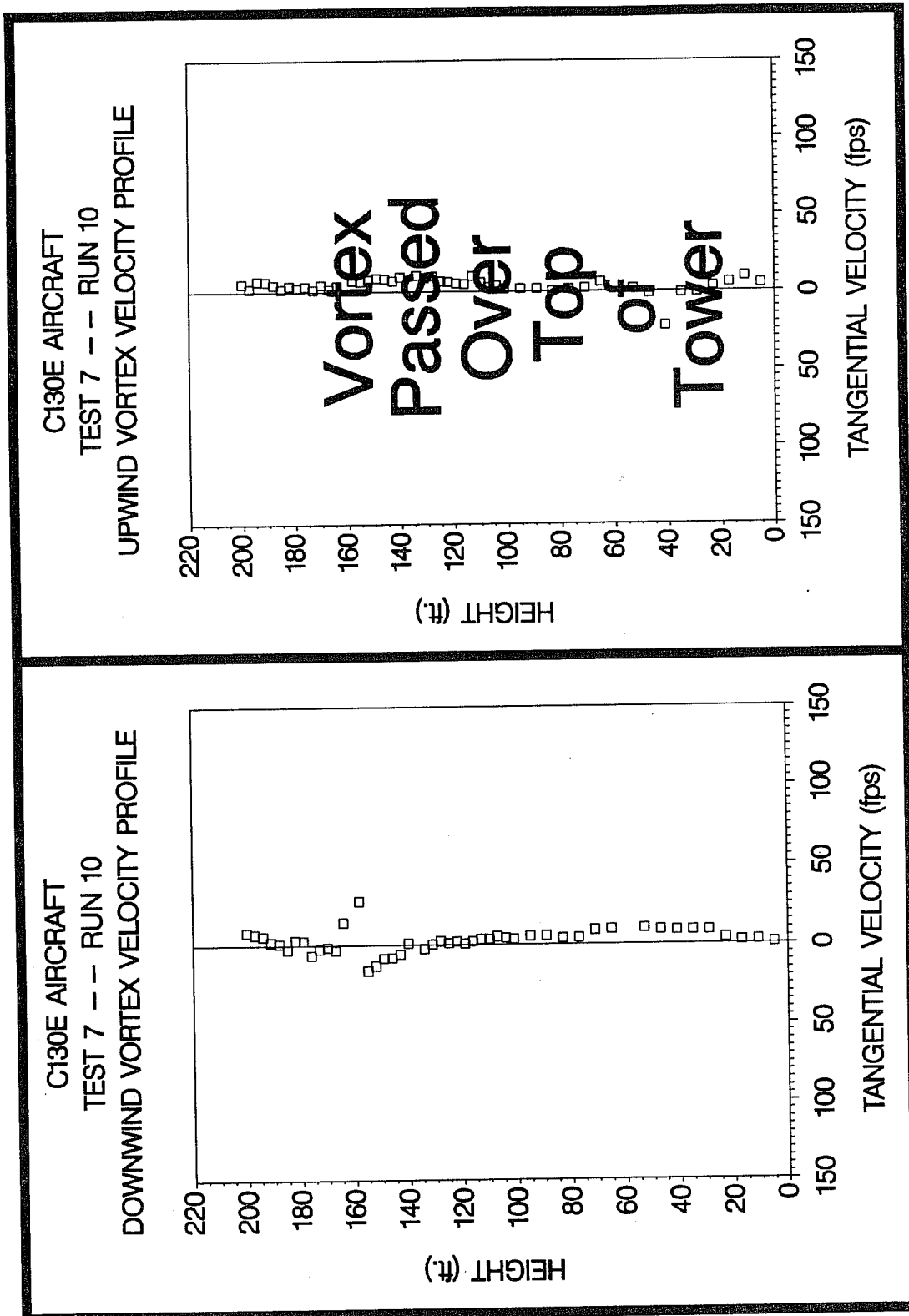
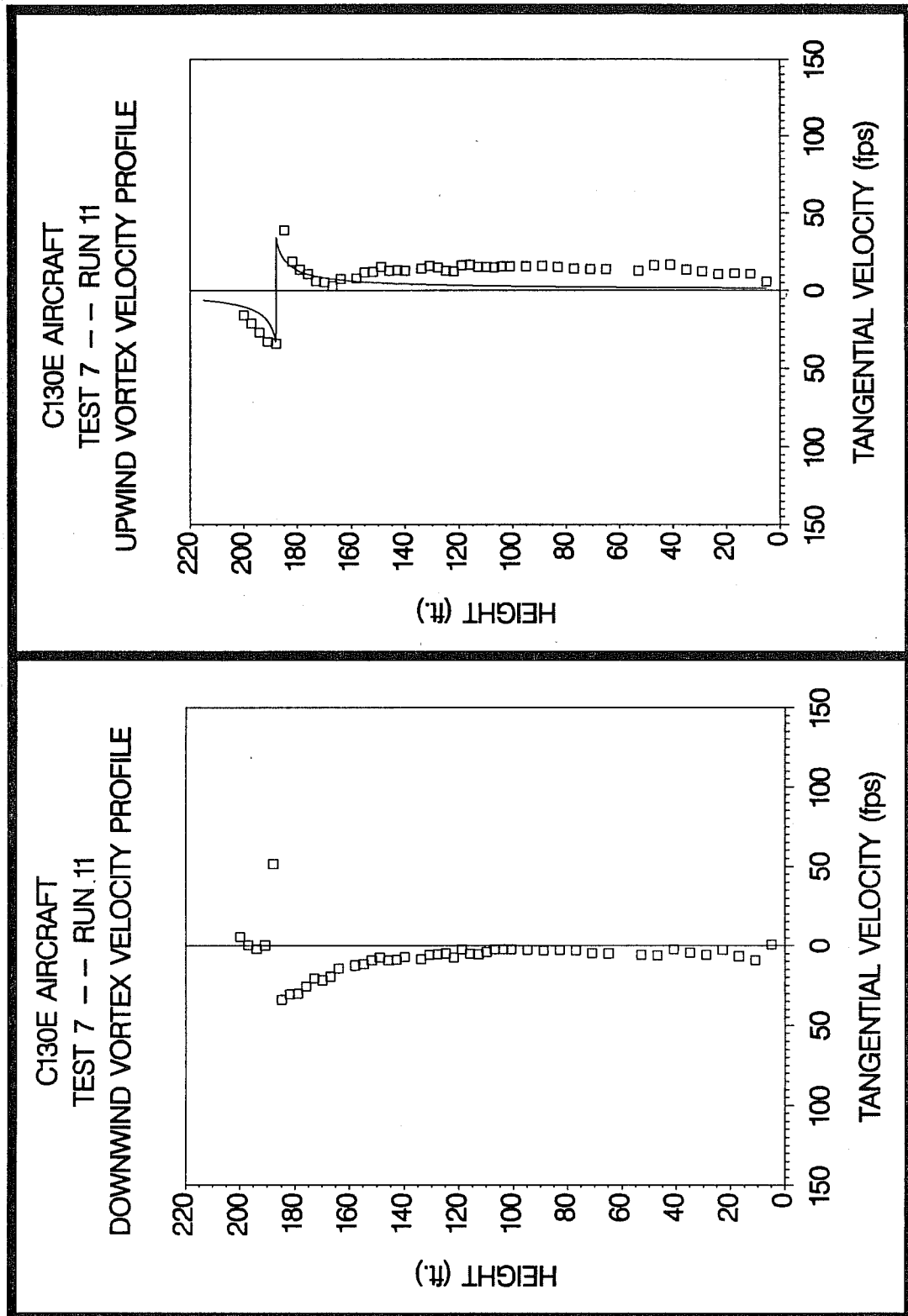


Figure C-83. C130E upwind (top) and downwind (bottom) vortex tangential velocity profile at maximum intensity from Test 7, Run 10, ambient wind speed=32.2 fps,  $\delta_F=20\%$ , IAS=131 knots, GW=128.0k lbs. Ages, radii, and velocities of the vortex cores are (N/A) and (N/A) sec., (N/A) and (N/A) ft., and (N/A) and 27.1 fps, respectively.



**Figure C-84.** C130E upwind (top) and downwind (bottom) vortex tangential velocity profile at maximum intensity from Test 7, Run 11, ambient wind speed=28.8 fps,  $\delta_F=50\%$ , IAS=125 knots, GW=127.4k lbs. Ages, radii, and velocities of the vortex cores are 13 and 10 sec., 1.8 and (N/A) ft., and 33.9 and 51.6 fps, respectively.

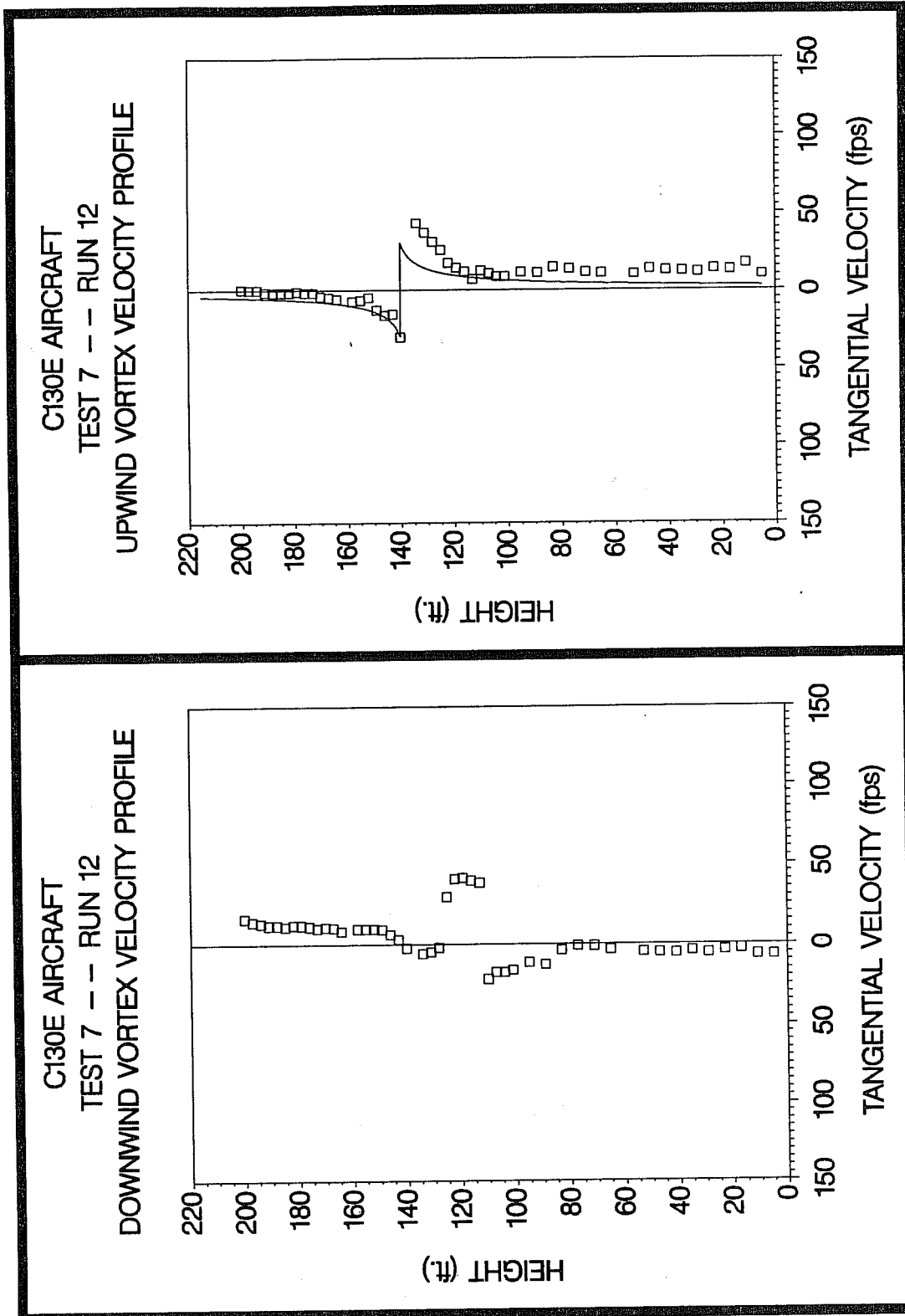
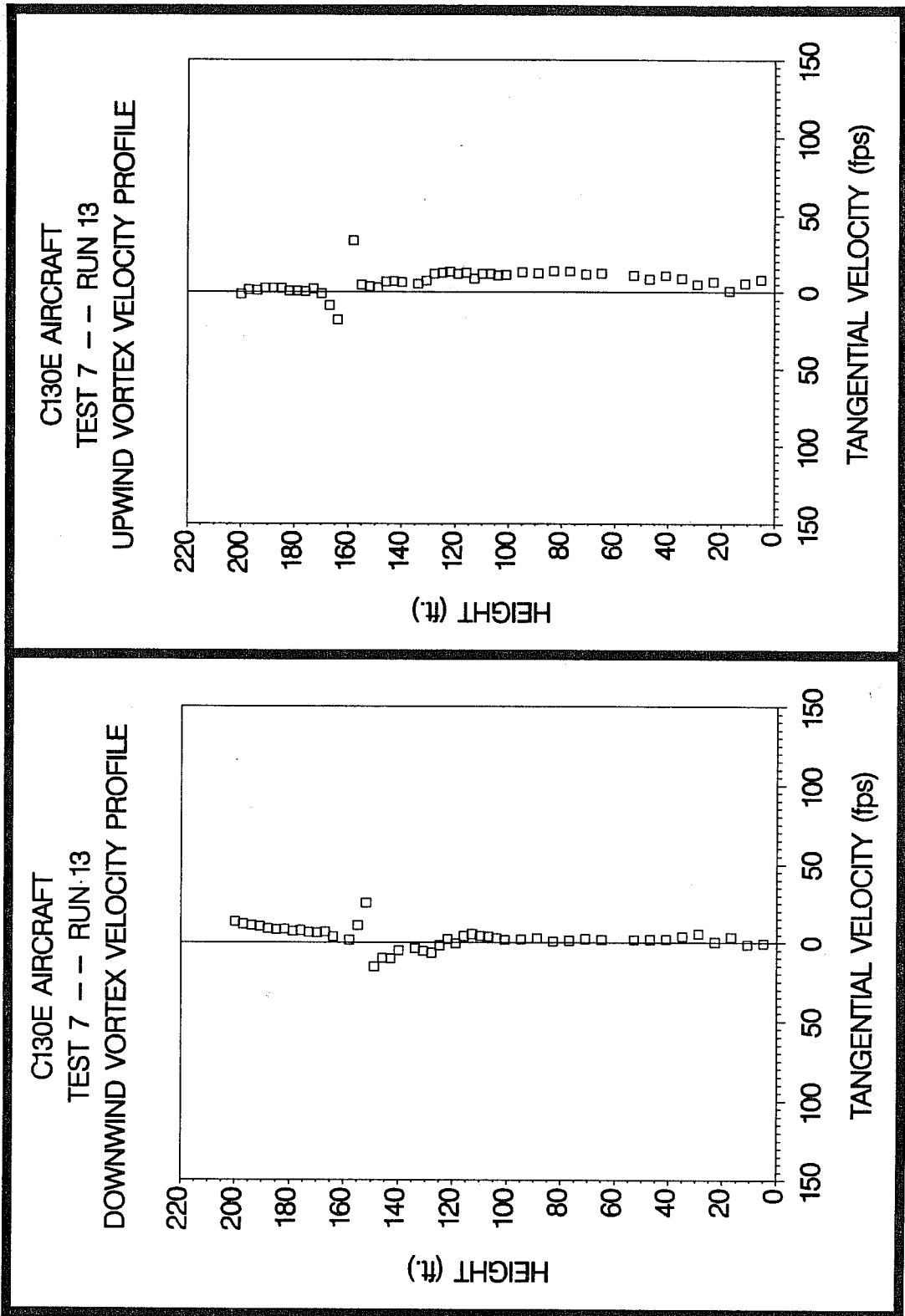


Figure C-85. C130E upwind (top) and downwind (bottom) vortex tangential velocity profile at maximum intensity from Test 7, Run 12, ambient wind speed=34.5 fps,  $\delta_F=50\%$ , IAS=129 knots, GW=126.8k lbs. Ages, radii, and velocities of the vortex cores are 14 and 11 sec., 3.2 and (N/A) ft., and 30.3 and 37.8 fps, respectively.



**Figure C-86.** C130E upwind (top) and downwind (bottom) vortex tangential velocity profile at maximum intensity from Test 7, Run 13, ambient wind speed=30.7 fps,  $\delta_F=0\%$ , IAS=240 knots, GW=126.2k lbs. Ages, radii, and velocities of the vortex cores are 17 and 13 sec., (N/A) and (N/A) ft., and 17.9 and 25.4 fps, respectively.



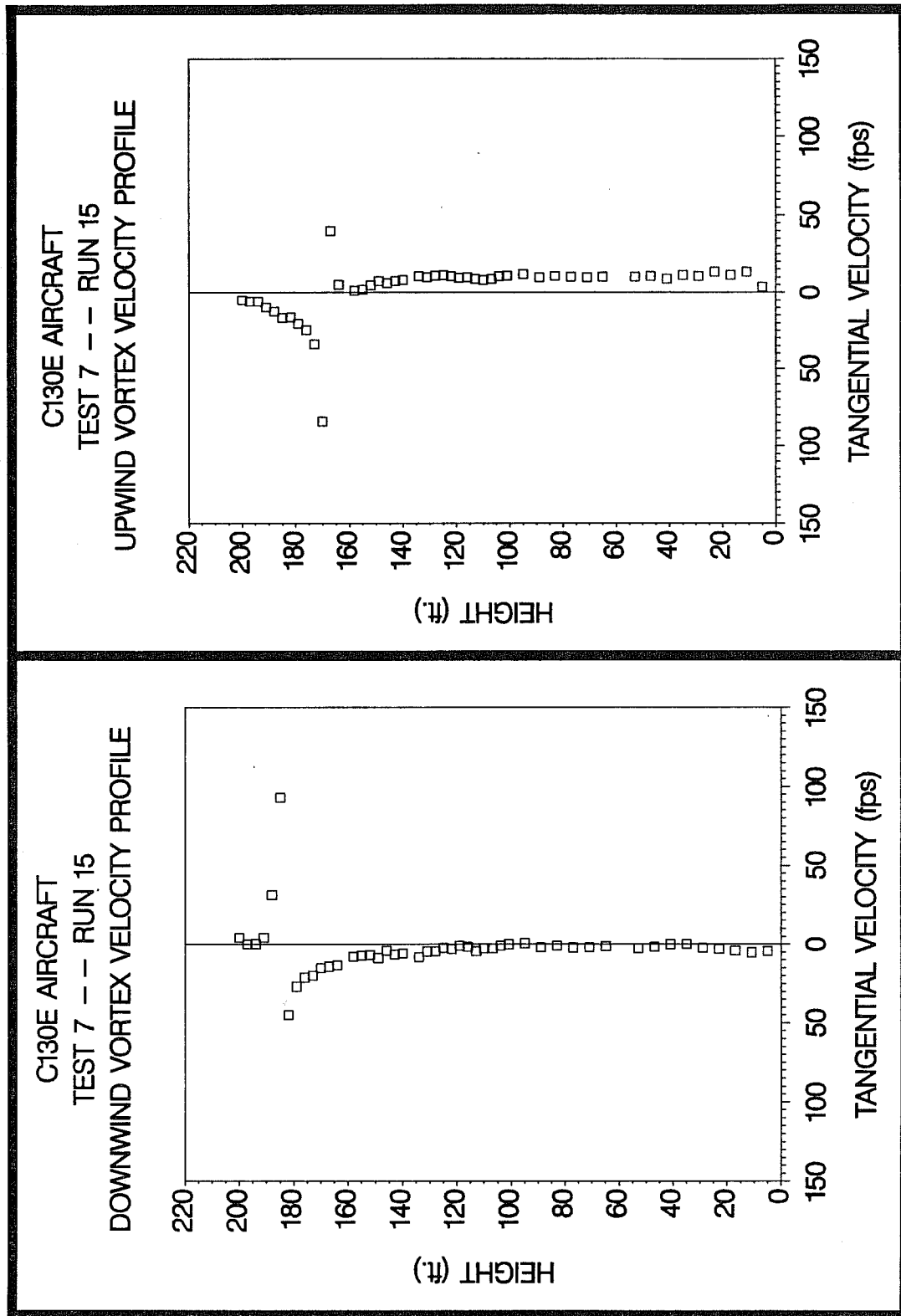


Figure C-88. C130E upwind (top) and downwind (bottom) vortex tangential velocity profile at maximum intensity from Test 7, Run 15, ambient wind speed=23.7 fps,  $\delta_F=0\%$ , IAS=150 knots, GW=125.0k lbs. Ages, radii, and velocities of the vortex cores are 12 and 8 sec., (N/A) and (N/A) ft., and 84.2 and 93.1 fps, respectively.

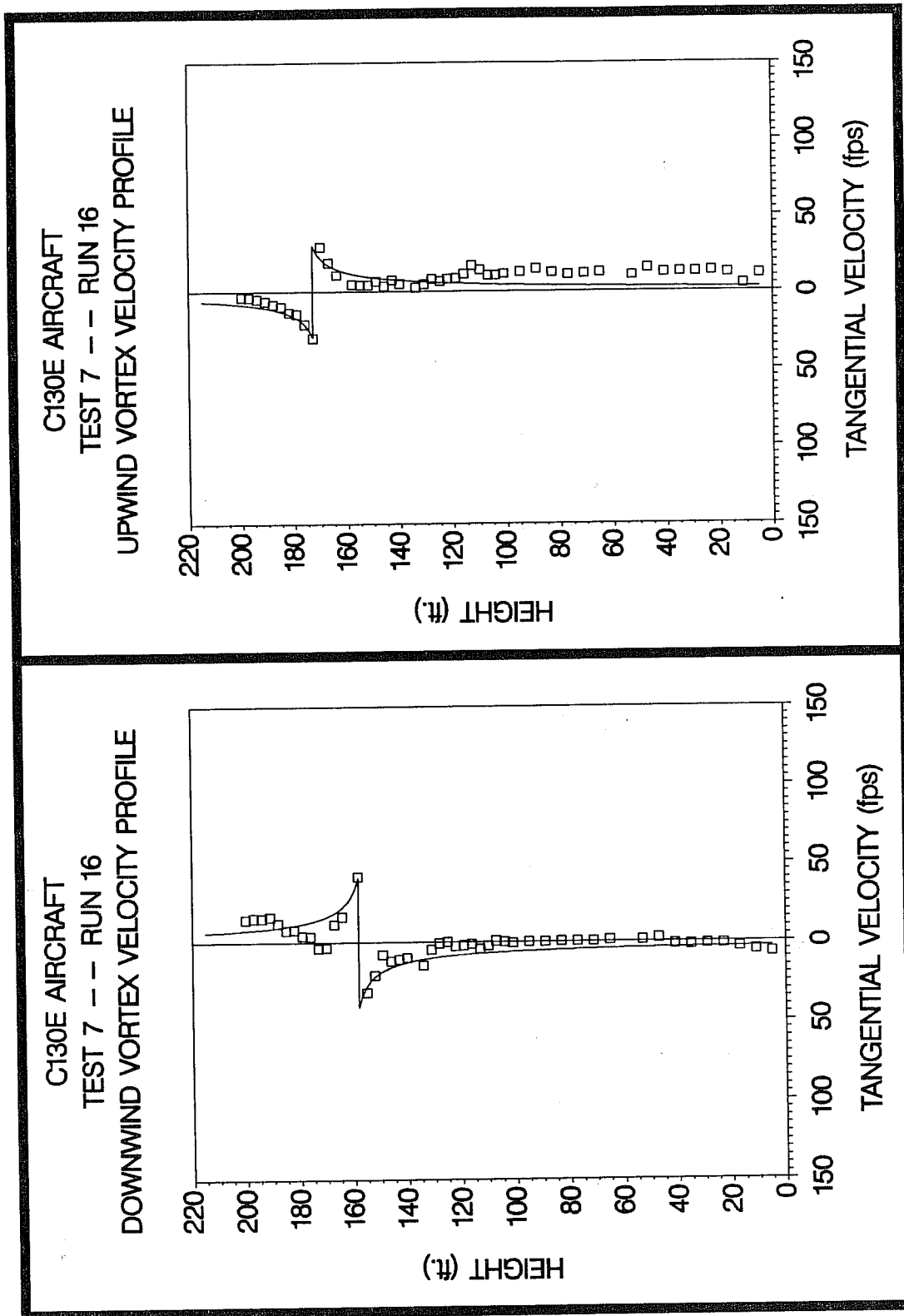


Figure C-89. C130E upwind (top) and downwind (bottom) vortex tangential velocity profile at maximum intensity from Test 7, Run 16, ambient wind speed=23.5 fps,  $\delta_F=50\%$ , IAS=125 knots, GW=124.6k lbs. Ages, radii, and velocities of the vortex cores are 18 and 14 sec., 3.4 and 2.8 ft., and 30.1 and 41.3 fps, respectively.

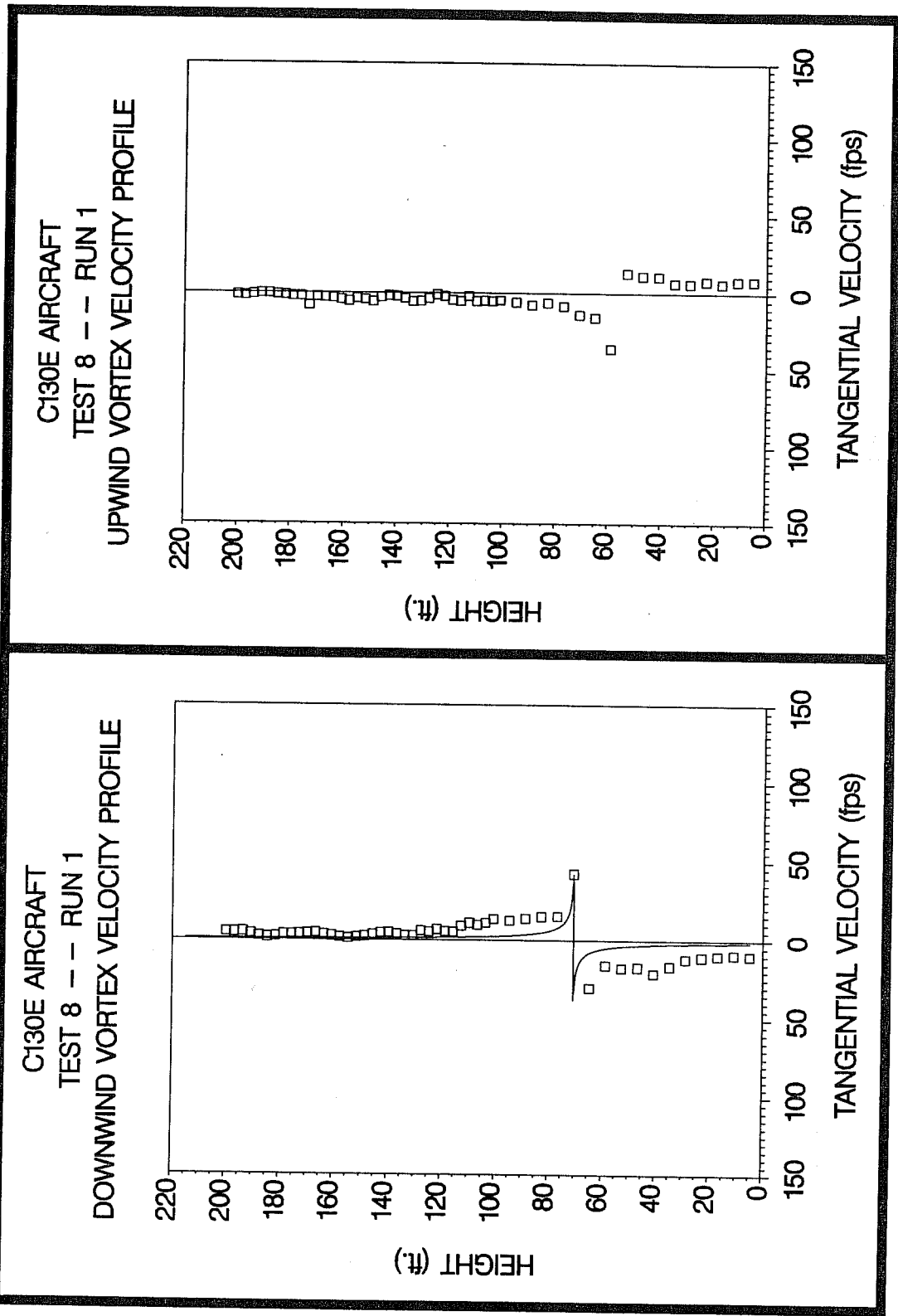


Figure C-90. C130E upwind (top) and downwind (bottom) vortex tangential velocity profile at maximum intensity from Test 8, Run 1, ambient wind speed=8.9 fps,  $\delta_F=50\%$ , IAS=125 knots, GW=147.0k lbs. Ages, radii, and velocities of the vortex cores are 84 and 40 sec., (N/A) and 0.4 ft., and 35.9 and 42.1 fps, respectively.

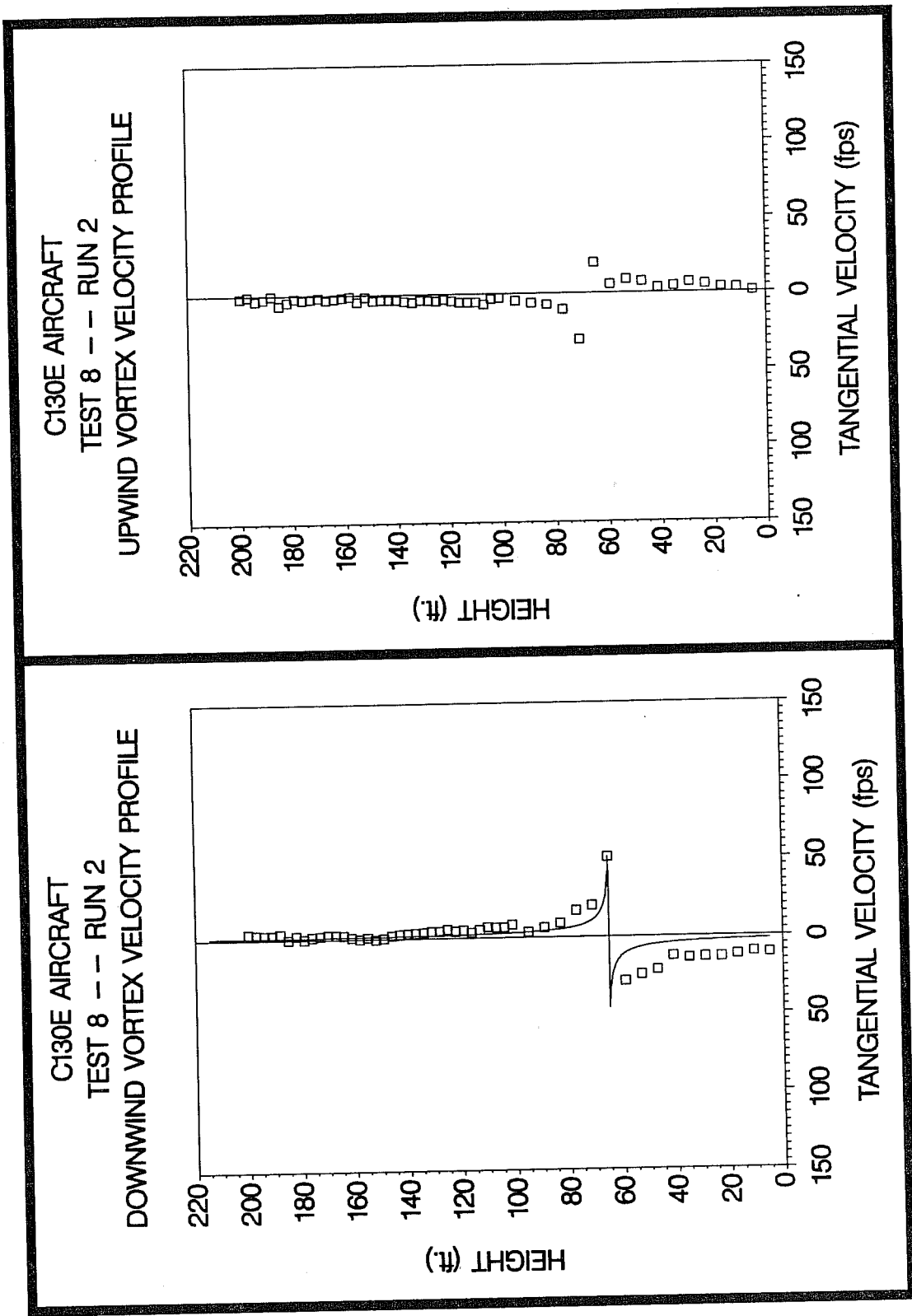
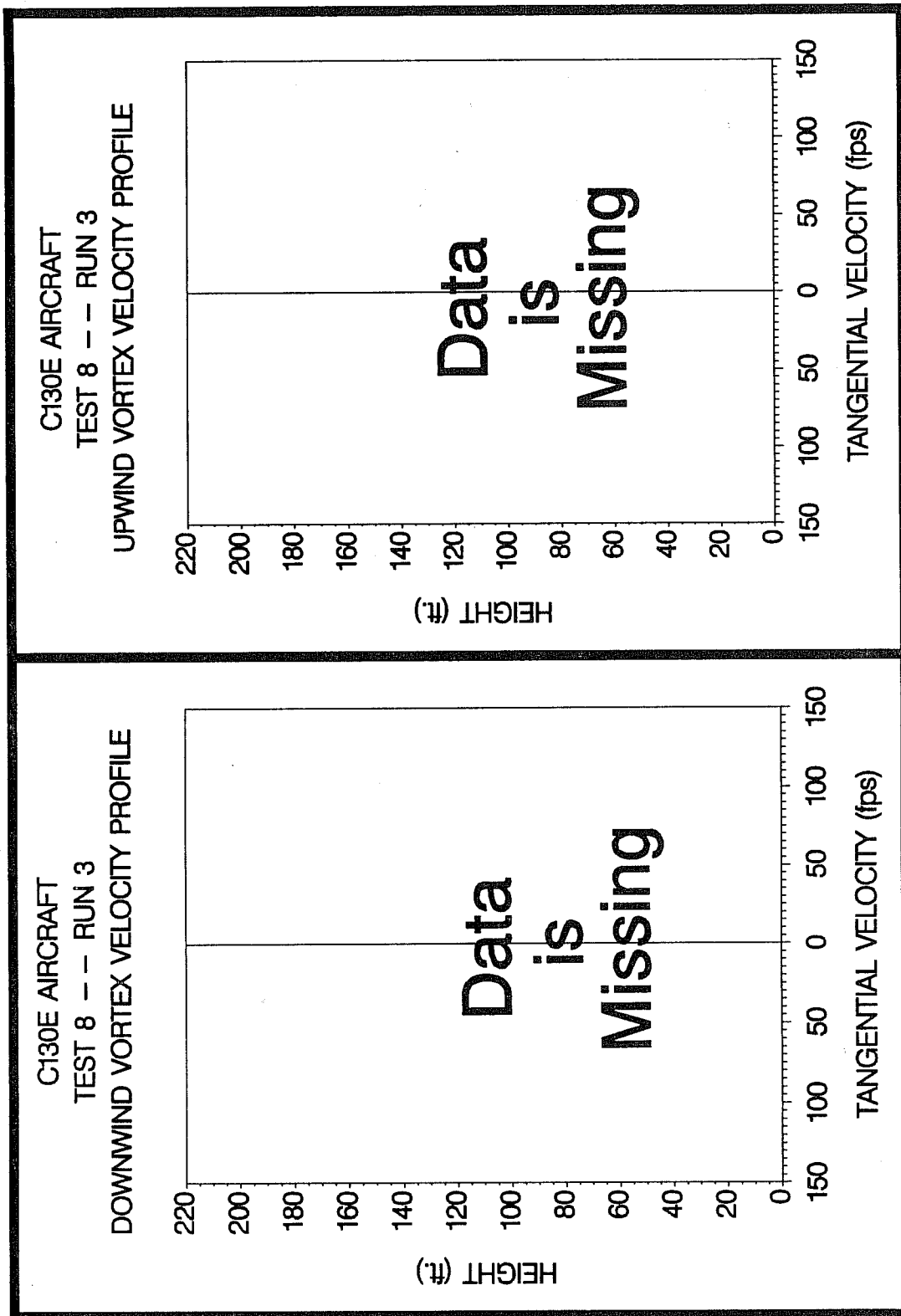


Figure C-91. C130E upwind (top) and downwind (bottom) vortex tangential velocity profile at maximum intensity from Test 8, Run 2, ambient wind speed=7.7 fps,  $\delta_F=50\%$ , IAS=125 knots, GW=146.6k lbs. Ages, radii, and velocities of the vortex cores are 97 and 43 sec., (N/A) and 0.5 ft., and 30.4 and 50.5 fps, respectively.



**Figure C-92.** C130E upwind (top) and downwind (bottom) vortex tangential velocity profile at maximum intensity from Test 8, Run 3, ambient wind speed=5.8 fps,  $\delta_F=50\%$ , IAS=125 knots, GW=146.2k lbs. Ages, radii, and velocities of the vortex cores are (N/A) and (N/A) sec., (N/A) and (N/A) ft., and (N/A) and (N/A) fps, respectively.

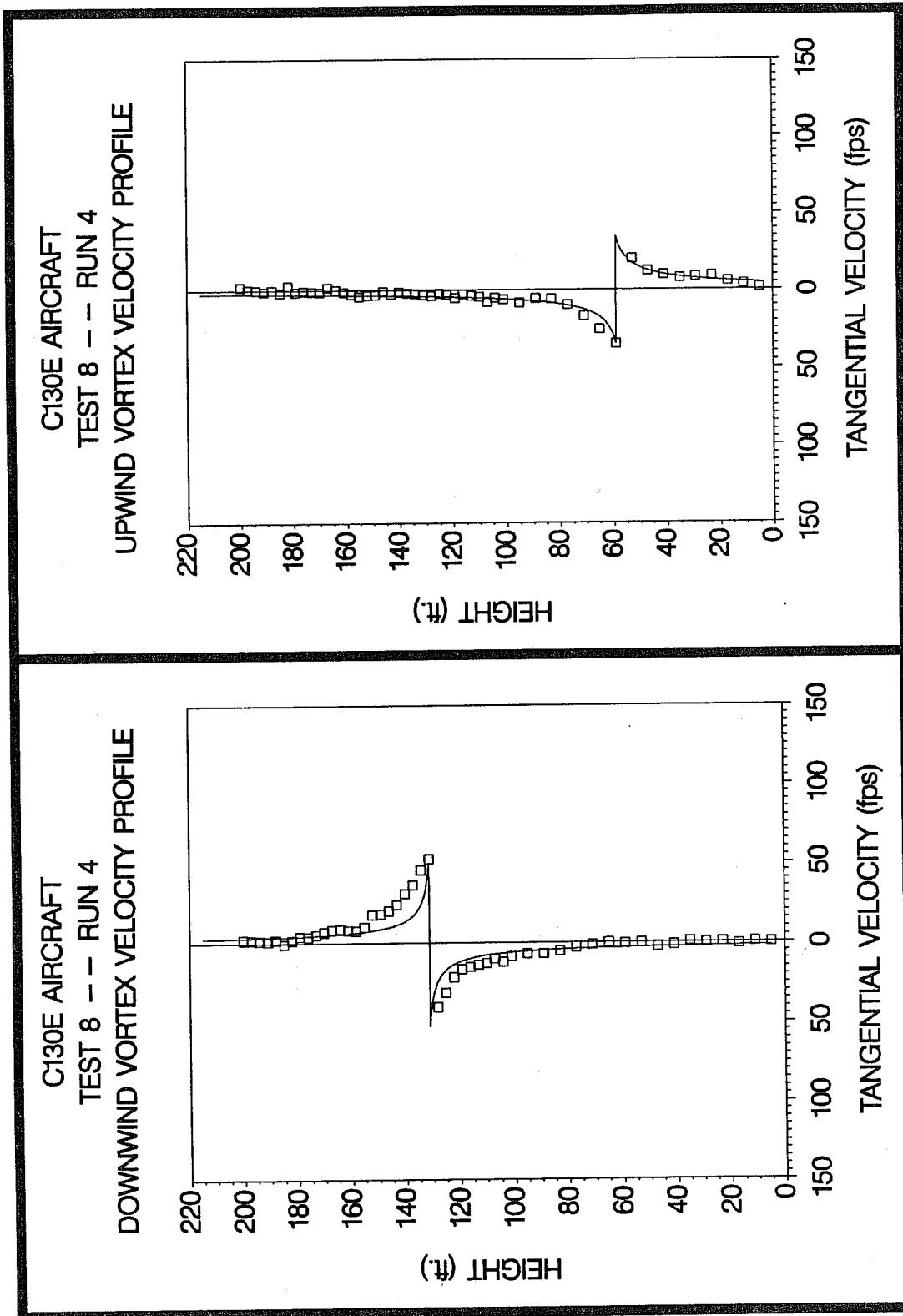
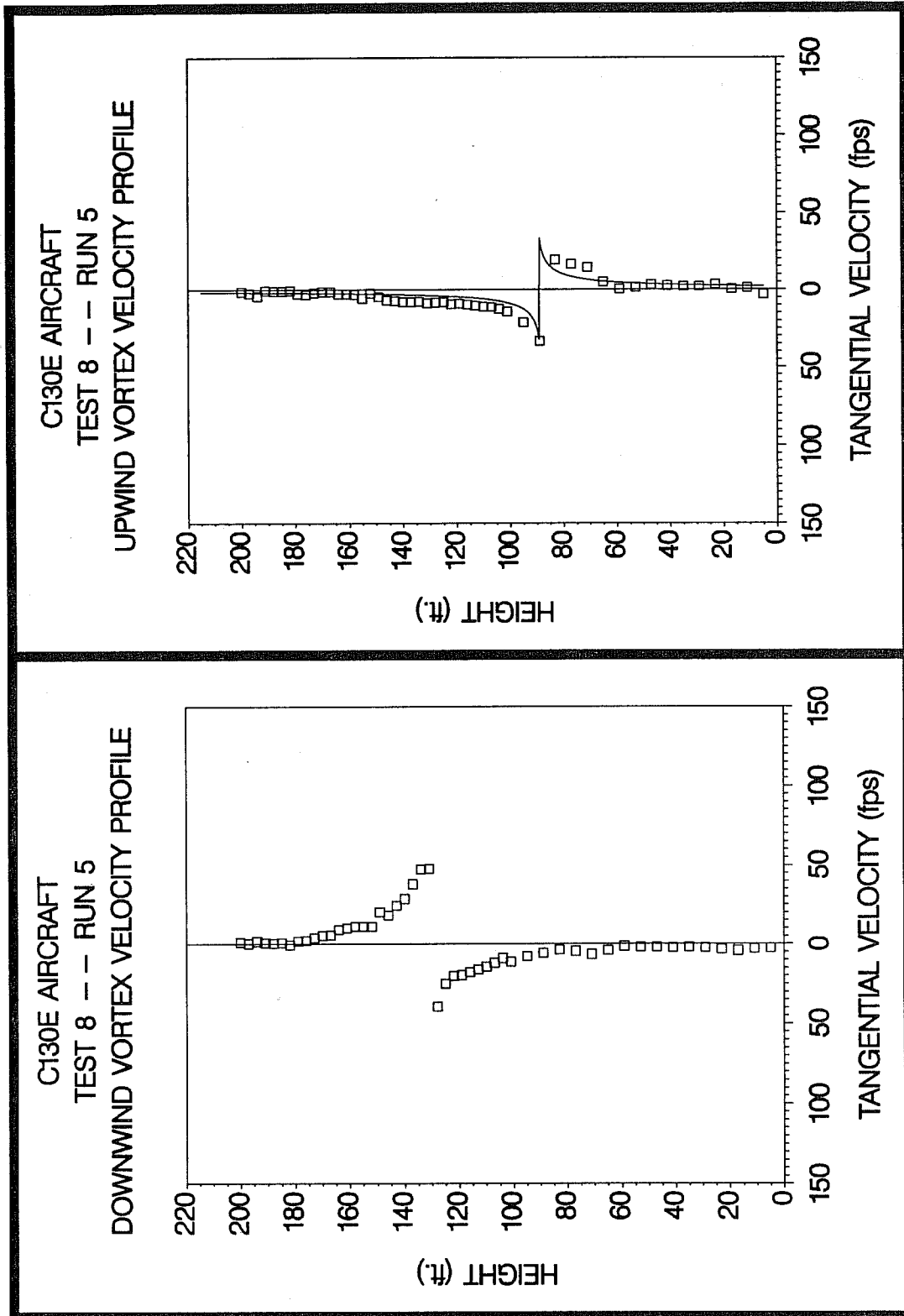


Figure C-93. C130E upwind (top) and downwind (bottom) vortex tangential velocity profile at maximum intensity from Test 8, Run 4, ambient wind speed=7.2 fps,  $\delta_F=50\%$ , IAS=125 knots, GW=145.8k lbs. Ages, radii, and velocities of the vortex cores are 63 and 50 sec., 2.4 and 1.0 ft., and 35.2 and 52.4 fps, respectively.



**Figure C-94.** C130E upwind (top) and downwind (bottom) vortex tangential velocity profile at maximum intensity from Test 8, Run 5, ambient wind speed=7.7 fps,  $\delta_F=50\%$ , IAS=125 knots, GW=145.4k lbs. Ages, radii, and velocities of the vortex cores are 50 and 36 sec., 1.3 and (N/A) ft., and 33.4 and 47.8 fps, respectively.

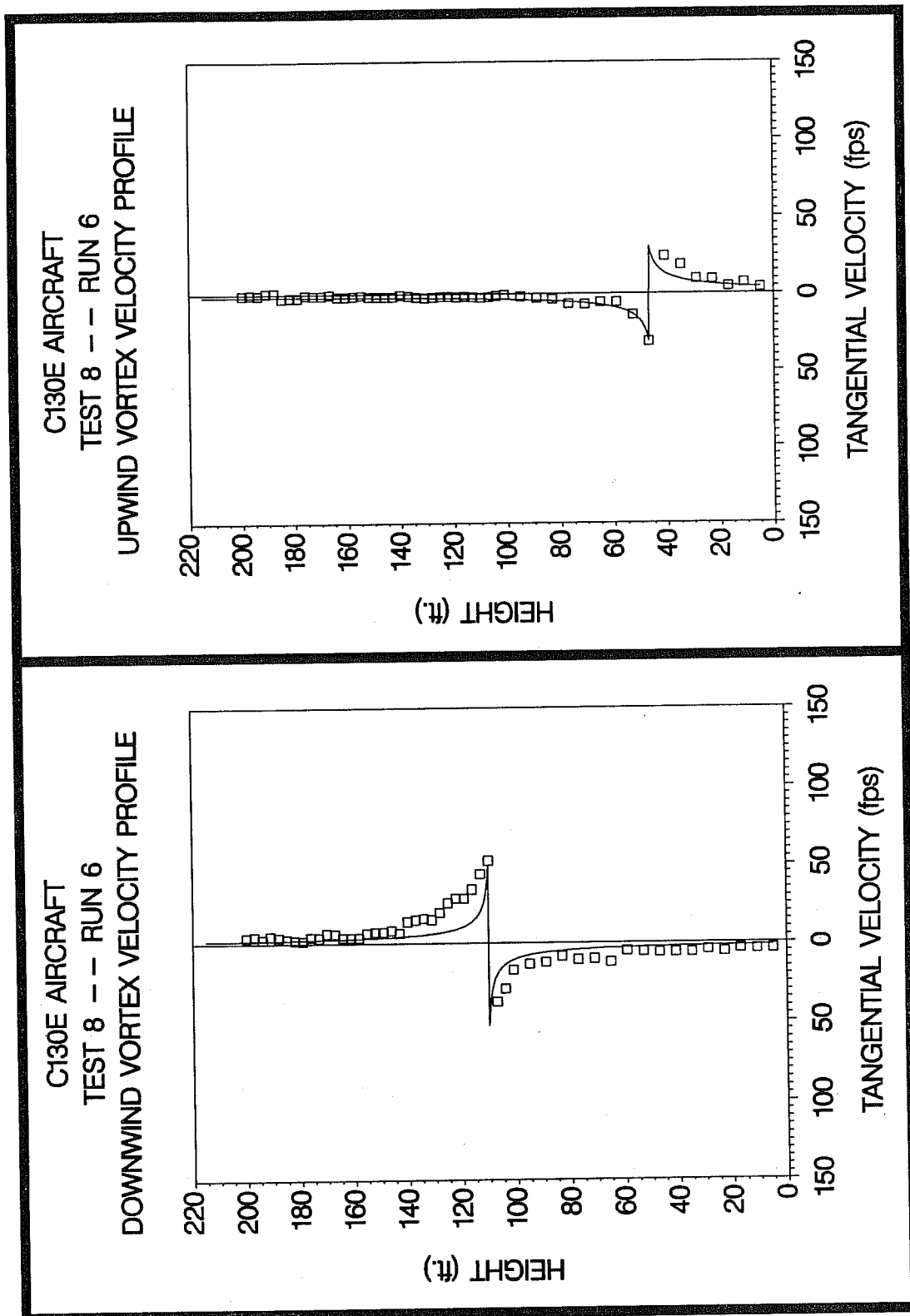


Figure C-95. C130E upwind (top) and downwind (bottom) vortex tangential velocity profile at maximum intensity from Test 8, Run 6, ambient wind speed=8.1 fps,  $\delta_F=50\%$ , IAS=125 knots, GW=145.0k lbs. Ages, radii, and velocities of the vortex cores are 61 and 39 sec., 1.7 and 0.7 ft., and 31.4 and 52.4 fps, respectively.

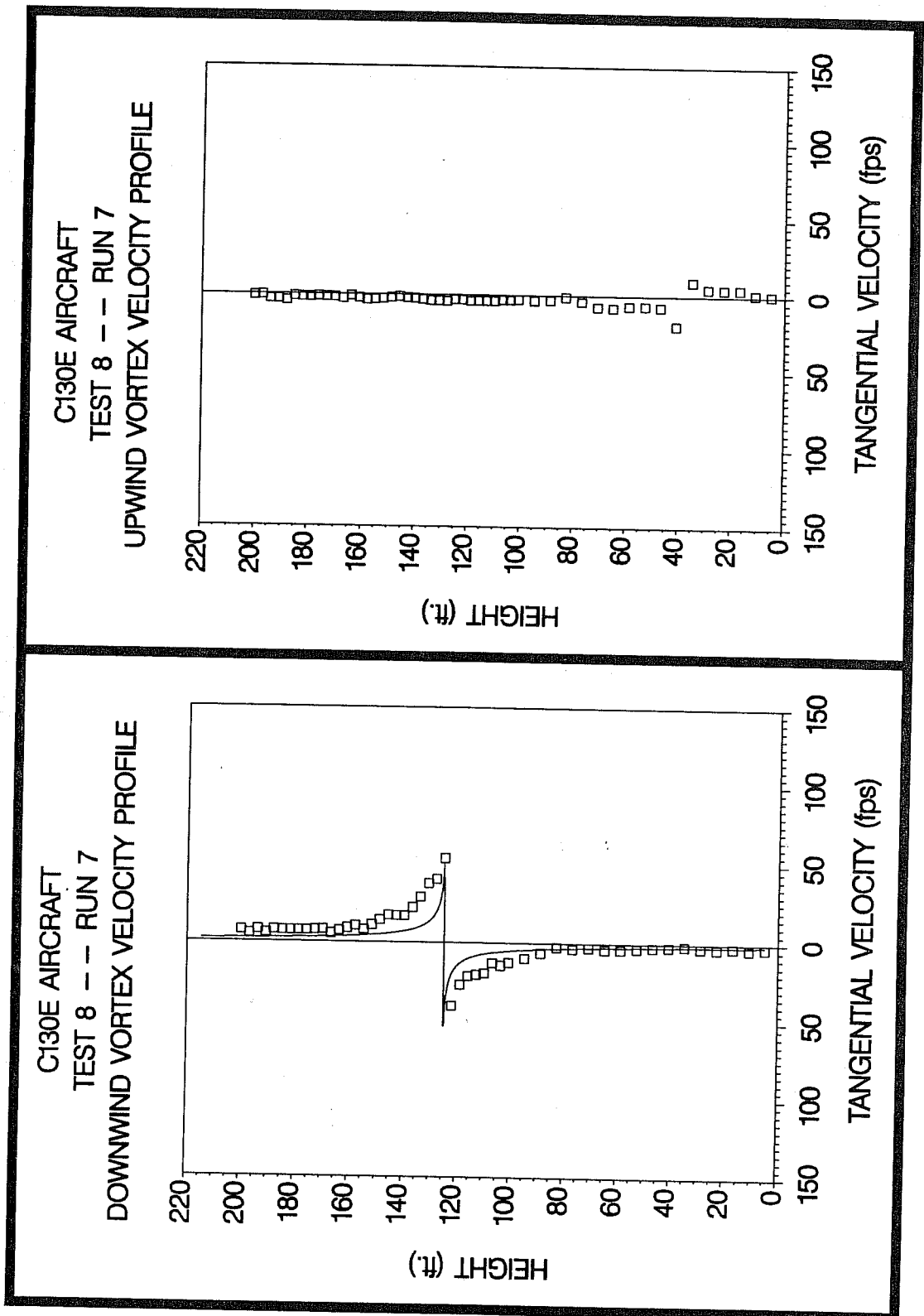


Figure C-96. C130E upwind (top) and downwind (bottom) vortex tangential velocity profile at maximum intensity from Test 8, Run 7, ambient wind speed=6.6 fps,  $\delta_F=50\%$ , IAS=125 knots, GW=144.6k lbs. Ages, radii, and velocities of the vortex cores are 88 and 61 sec., (N/A) and 0.6 ft., and 19.5 and 53.4 fps, respectively.

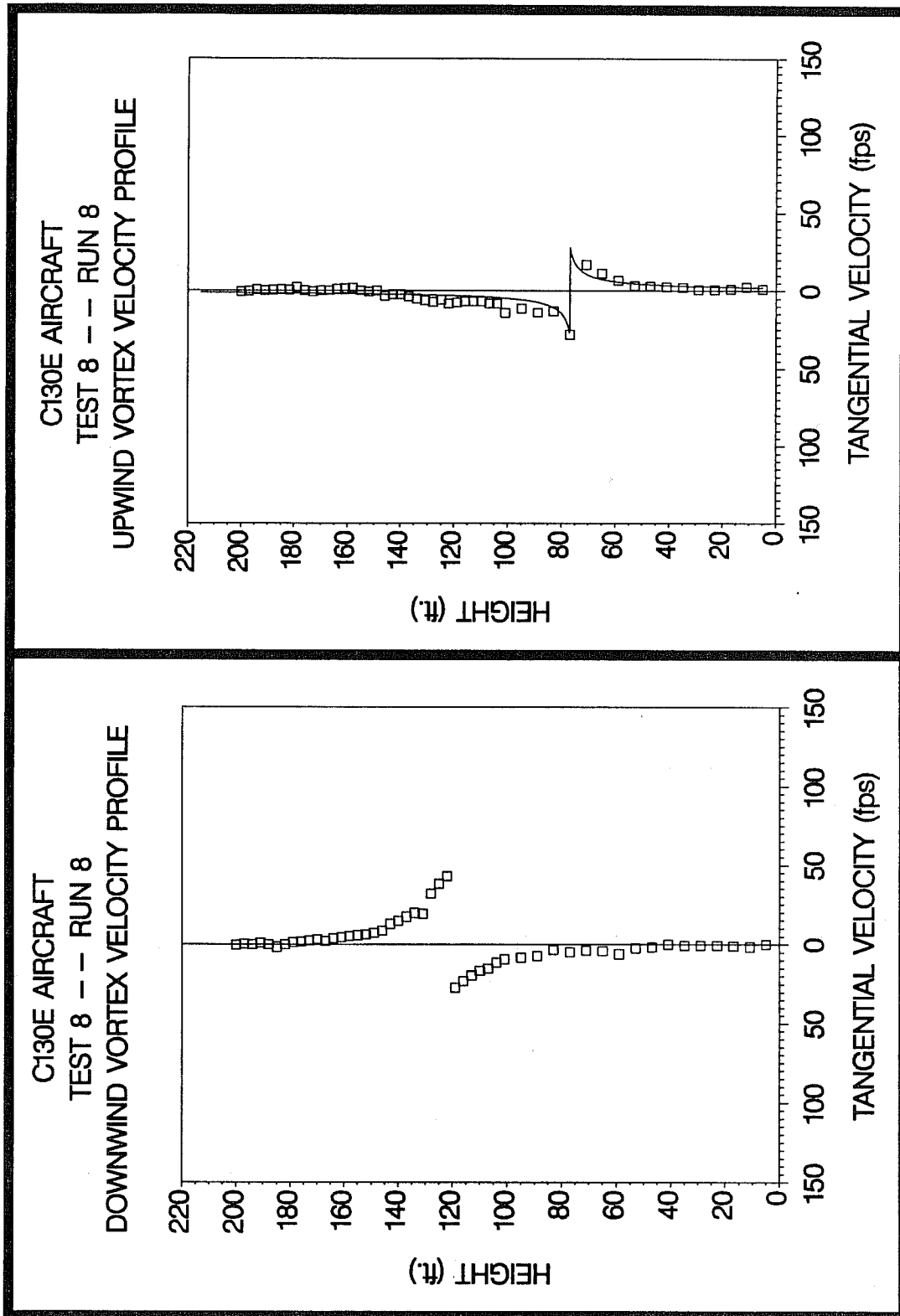


Figure C-97. C130E upwind (top) and downwind (bottom) vortex tangential velocity profile at maximum intensity from Test 8, Run 8, ambient wind speed=5.7 fps,  $\delta_F=50\%$ , IAS=125 knots, GW=144.2k lbs. Ages, radii, and velocities of the vortex cores are 57 and 51 sec., 1.4 and (N/A) ft., and 28.1 and 43.1 fps, respectively.

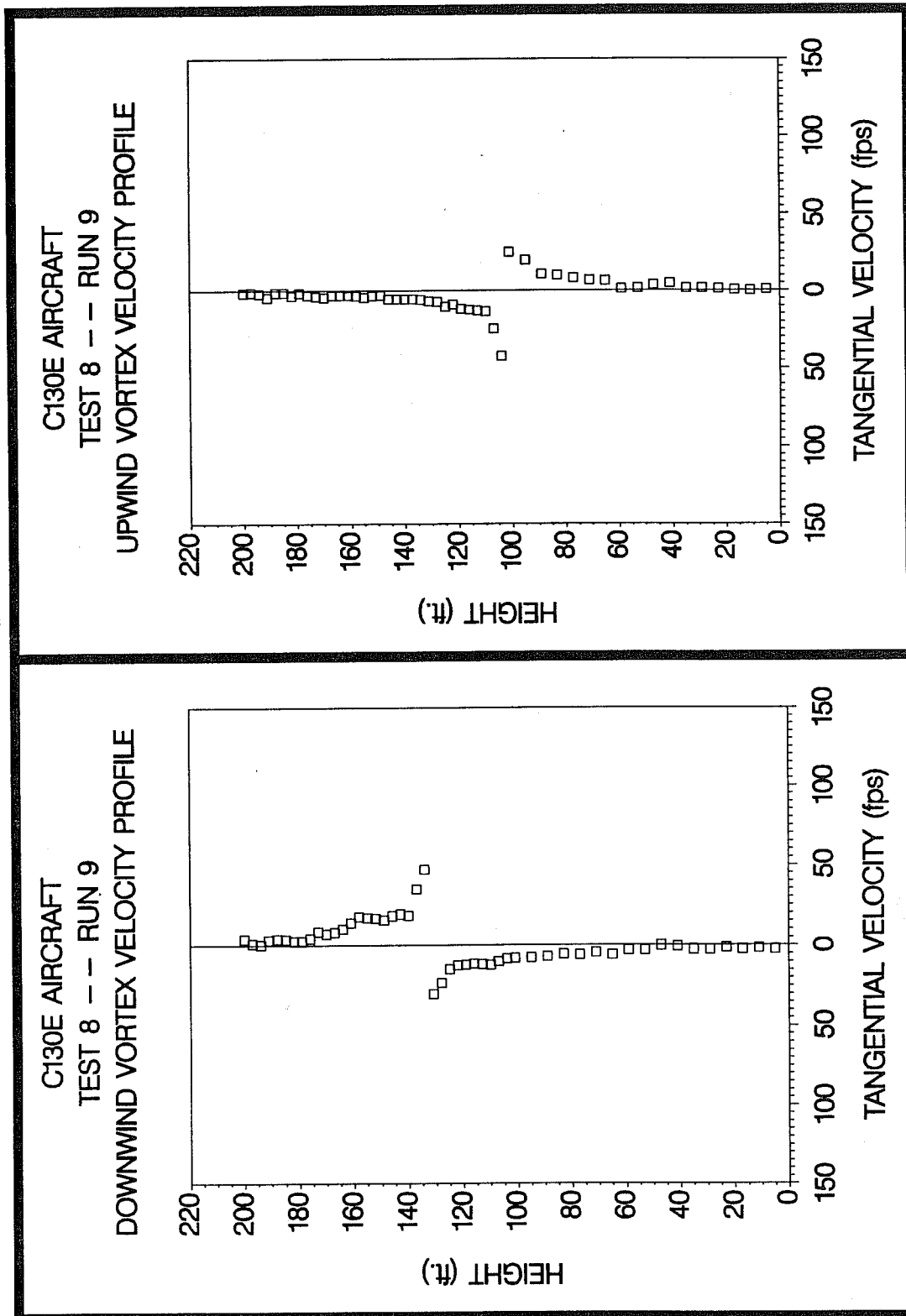
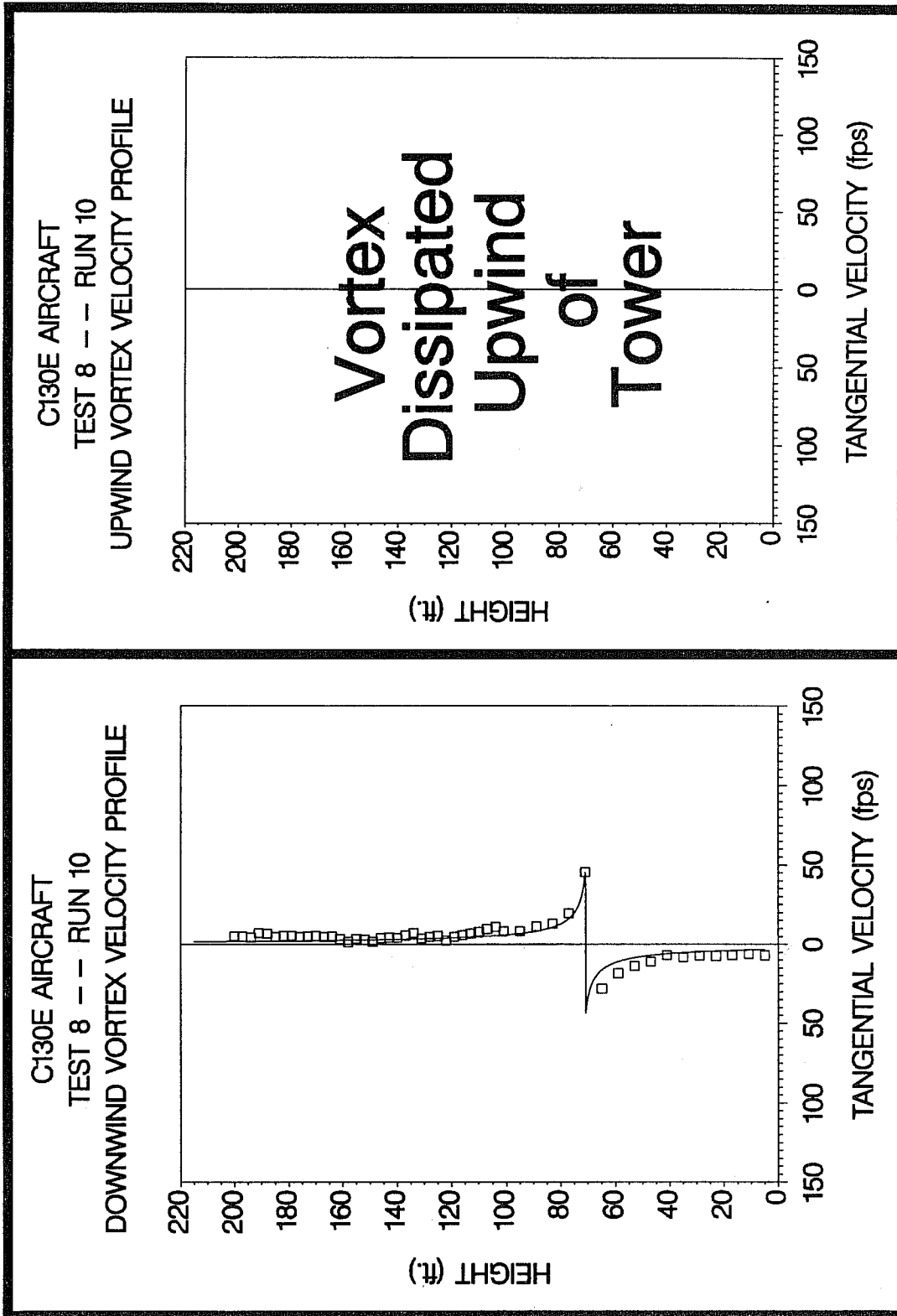
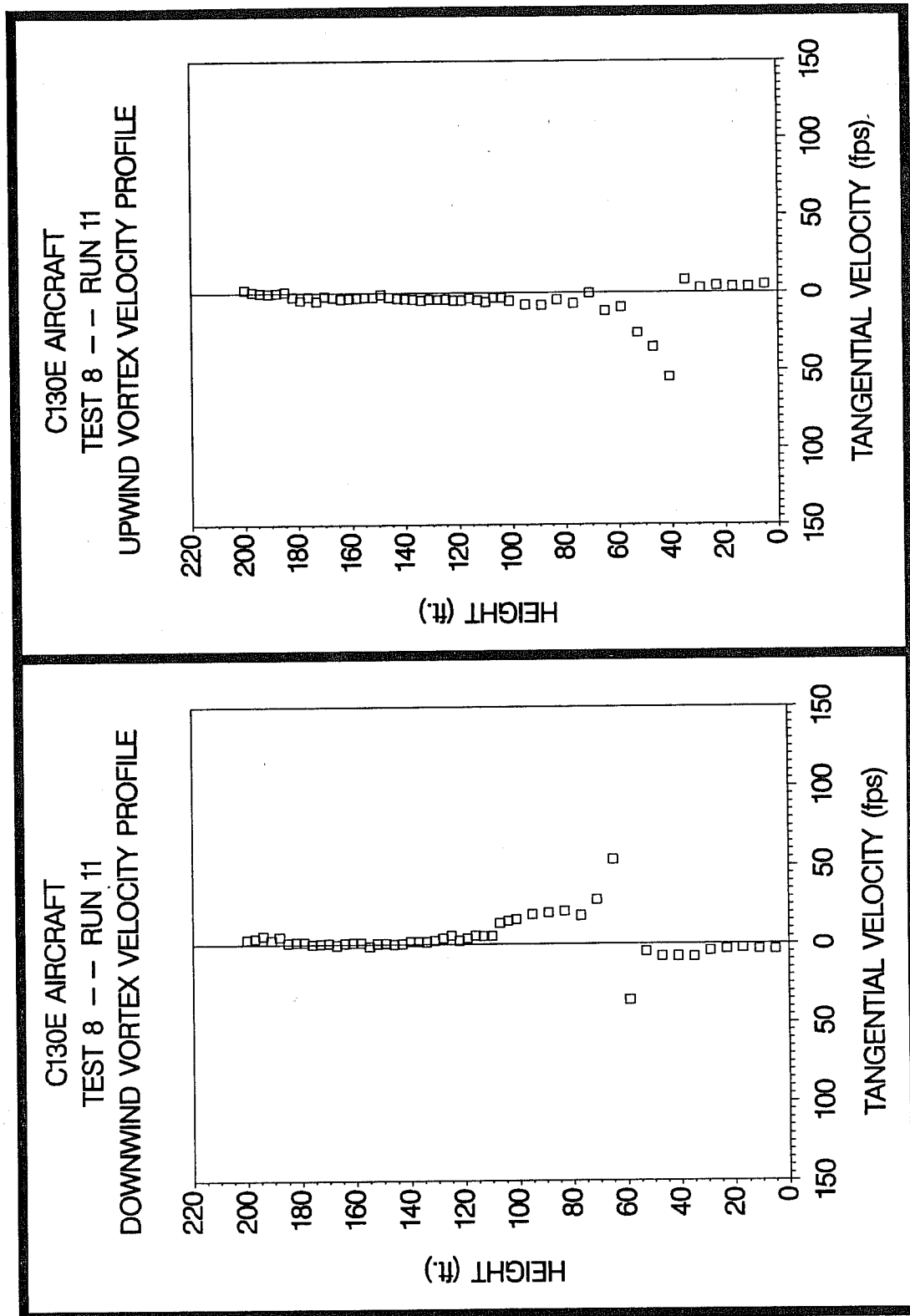


Figure C-98. C130E upwind (top) and downwind (bottom) vortex tangential velocity profile at maximum intensity from Test 8, Run 9, ambient wind speed=6.3 fps,  $\delta_F=50\%$ , IAS=125 knots, GW=143.8k lbs. Ages, radii, and velocities of the vortex cores are 70 and 49 sec., (N/A) and (N/A) ft., and 42.5 and 47.1 fps, respectively.



**Figure C-99.** C130E upwind (top) and downwind (bottom) vortex tangential velocity profile at maximum intensity from Test 8, Run 10, ambient wind speed=6.5 fps,  $\delta_F=50\%$ , IAS=125 knots, GW=143.4k lbs. Ages, radii, and velocities of the vortex cores are (N/A) and 63 sec., (N/A) and 1.2 ft., and (N/A) and 45.3 fps, respectively.



**Figure C-100.** C130E upwind (top) and downwind (bottom) vortex tangential velocity profile at maximum intensity from Test 8, Run 11, ambient wind speed=5.7 fps,  $\delta_F=30\%$ , IAS=130 knots, GW=143.0k lbs. Ages, radii, and velocities of the vortex cores are 58 and 42 sec., (N/A) and (N/A) ft., and 54.4 and 53.7 fps, respectively.

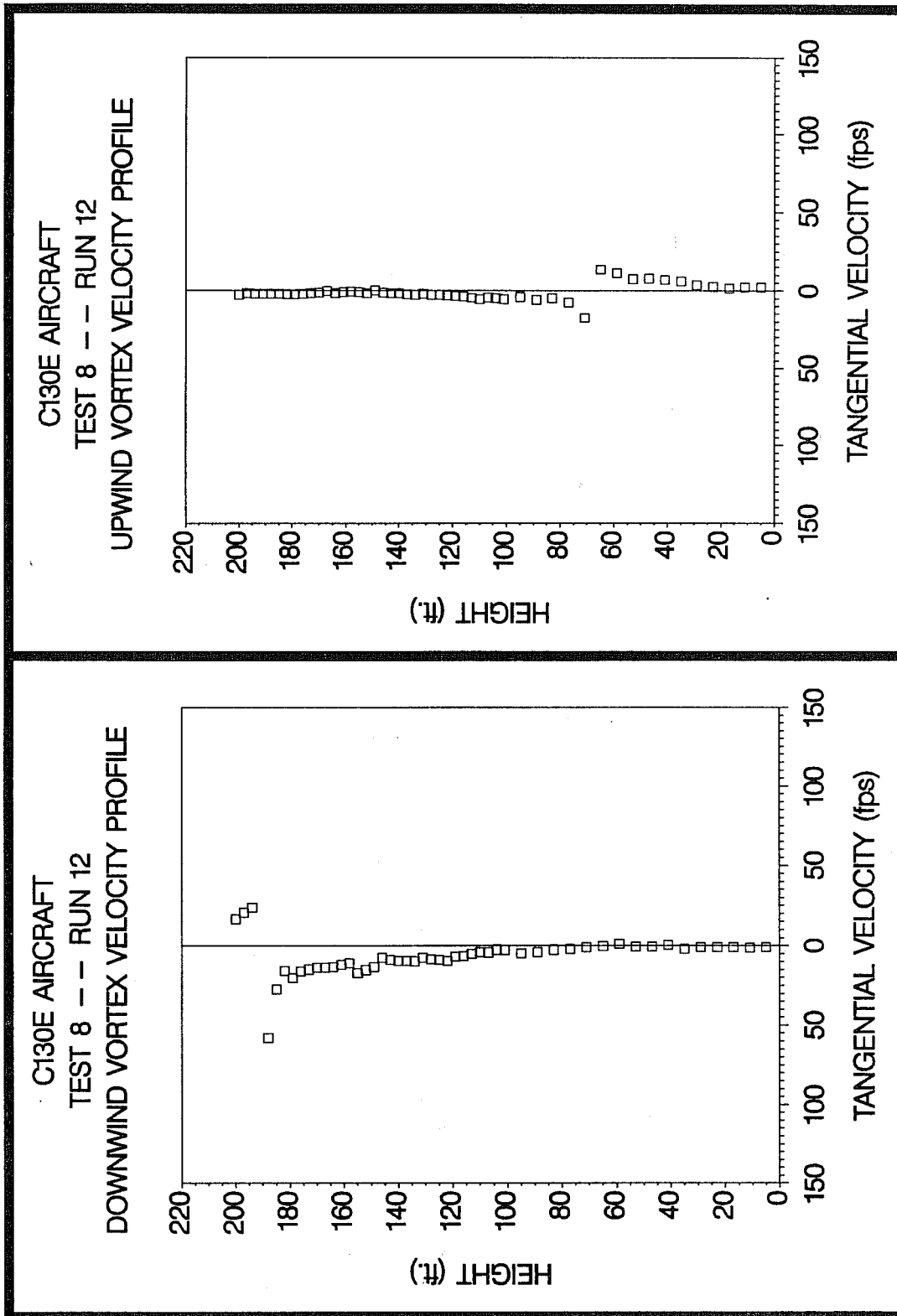


Figure C-101. C130E upwind (top) and downwind (bottom) vortex tangential velocity profile at maximum intensity from Test 8, Run 12, ambient wind speed=5.7 fps,  $\delta_F=30\%$ , IAS=130 knots, GW=142.6k lbs. Ages, radii, and velocities of the vortex cores are 84 and 41 sec., (N/A) and (N/A) ft., and 17.5 and 153.0 fps, respectively.

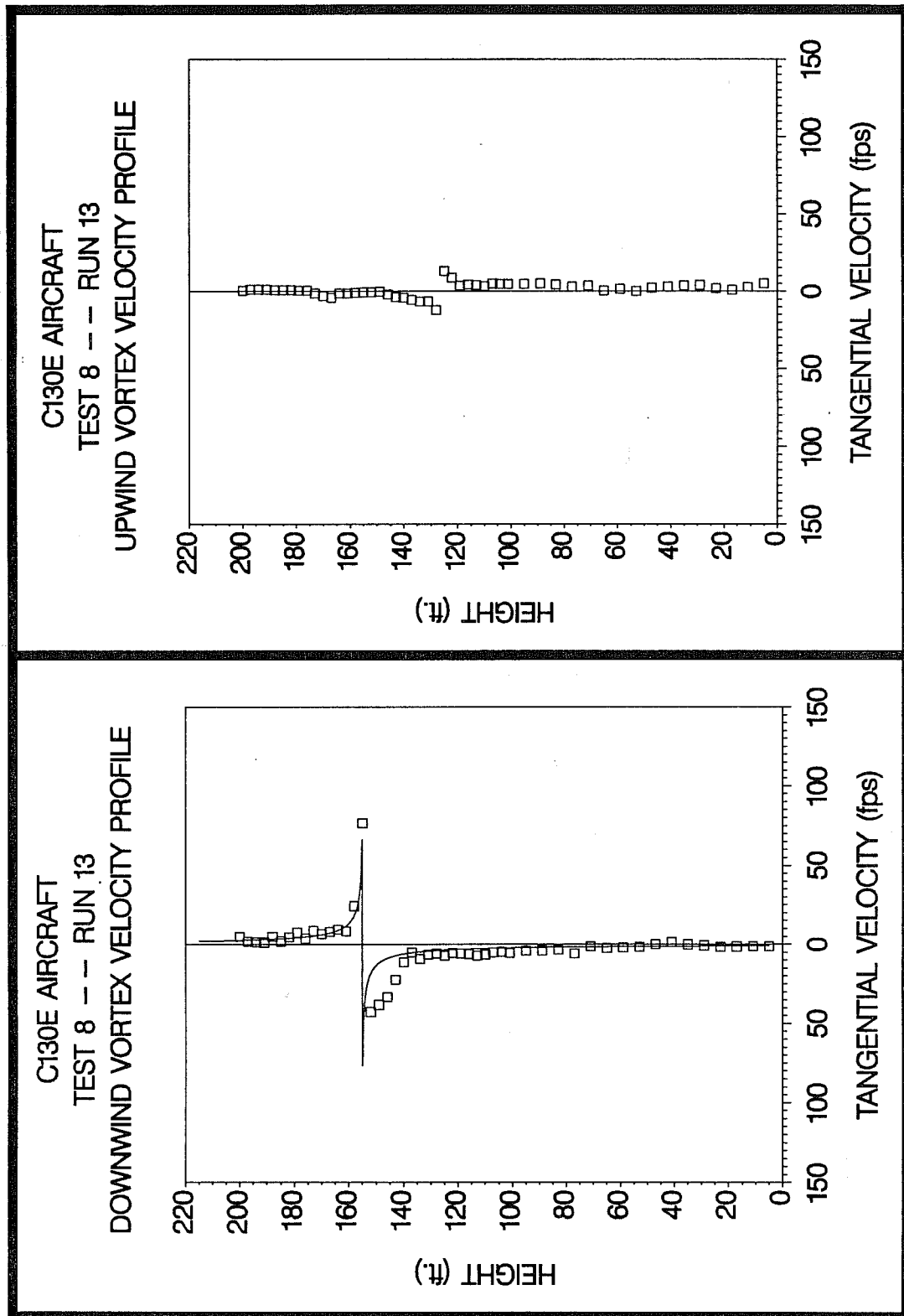
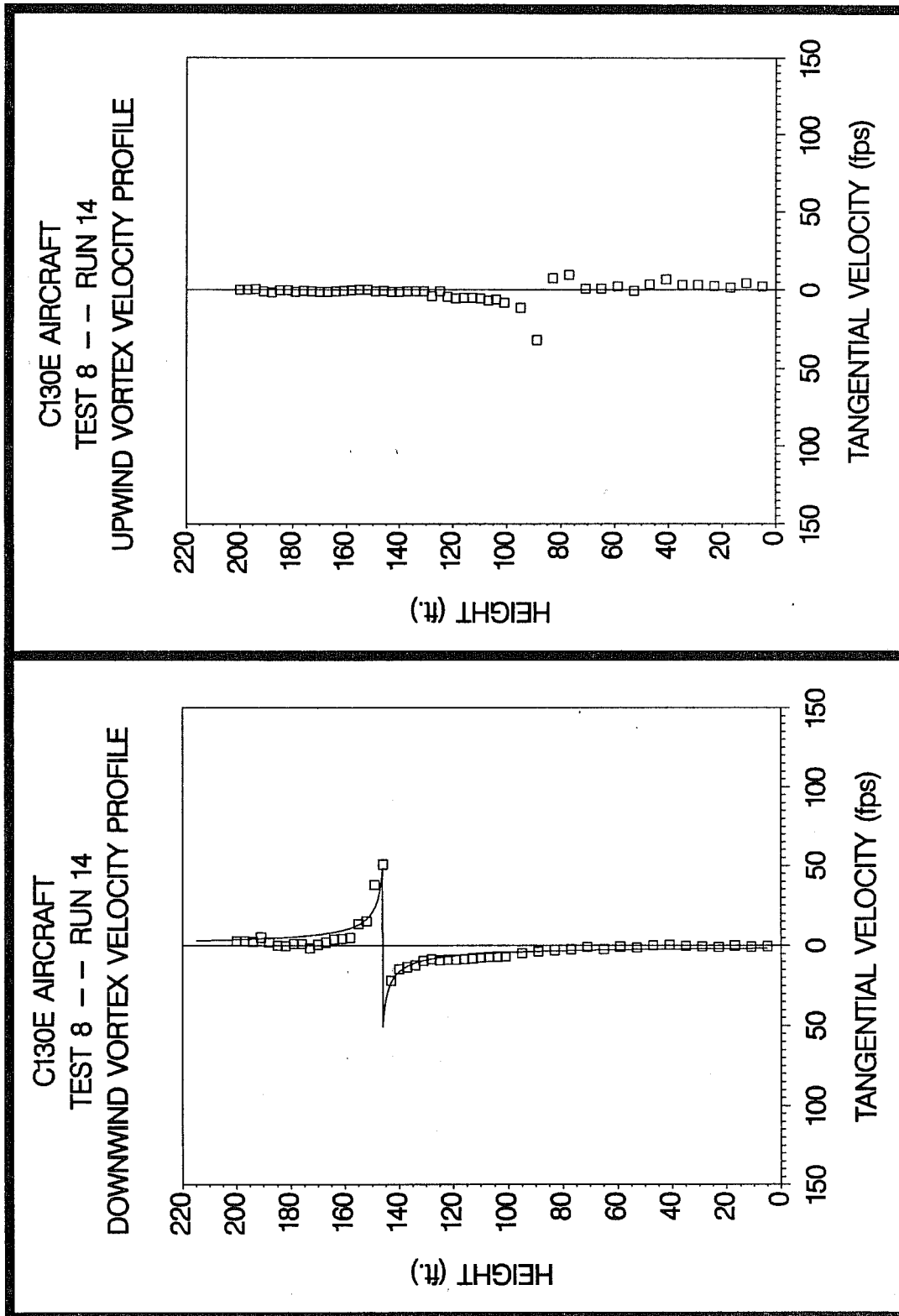


Figure C-102. C130E upwind (top) and downwind (bottom) vortex tangential velocity profile at maximum intensity from Test 8, Run 13, ambient wind speed=5.4 fps,  $\delta_F=0\%$ , IAS=150 knots, GW=142.0k lbs. Ages, radii, and velocities of the vortex cores are 76 and 36 sec., (N/A) and 0.3 ft., and 12.2 and 76.7 fps, respectively.



**Figure C-103.** C130E upwind (top) and downwind (bottom) vortex tangential velocity profile at maximum intensity from Test 8, Run 14, ambient wind speed=7.4 fps,  $\delta_{T1} = 0\%$ , IAS=240 knots, GW=141.2k lbs. Ages, radii, and velocities of the vortex cores are 53 and 24 sec., (N/A) and 1.0 ft., and 32.1 and 50.6 fps, respectively.

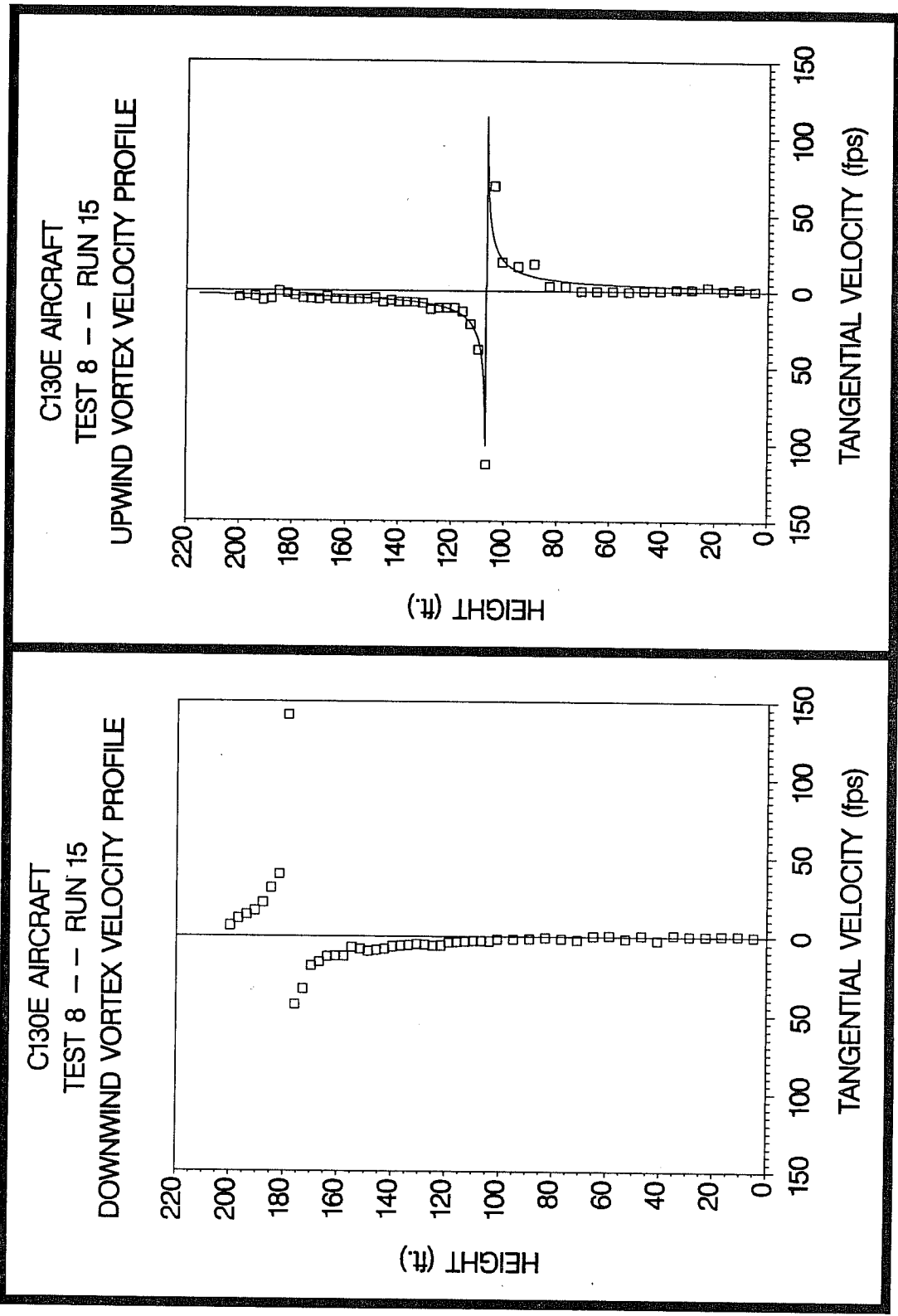


Figure C-104. C130E upwind (top) and downwind (bottom) vortex tangential velocity profile at maximum intensity from Test 8, Run 15, ambient wind speed=6.7 fps,  $\delta_F=0\%$ , IAS=150 knots, GW=140.8k lbs. Ages, radii, and velocities of the vortex cores are 38 and 25 sec., 0.4 and (N/A) ft., and 113.3 and 141.6 fps, respectively.

**LOCKHEED**

**C5A/B**

**GALAXY**

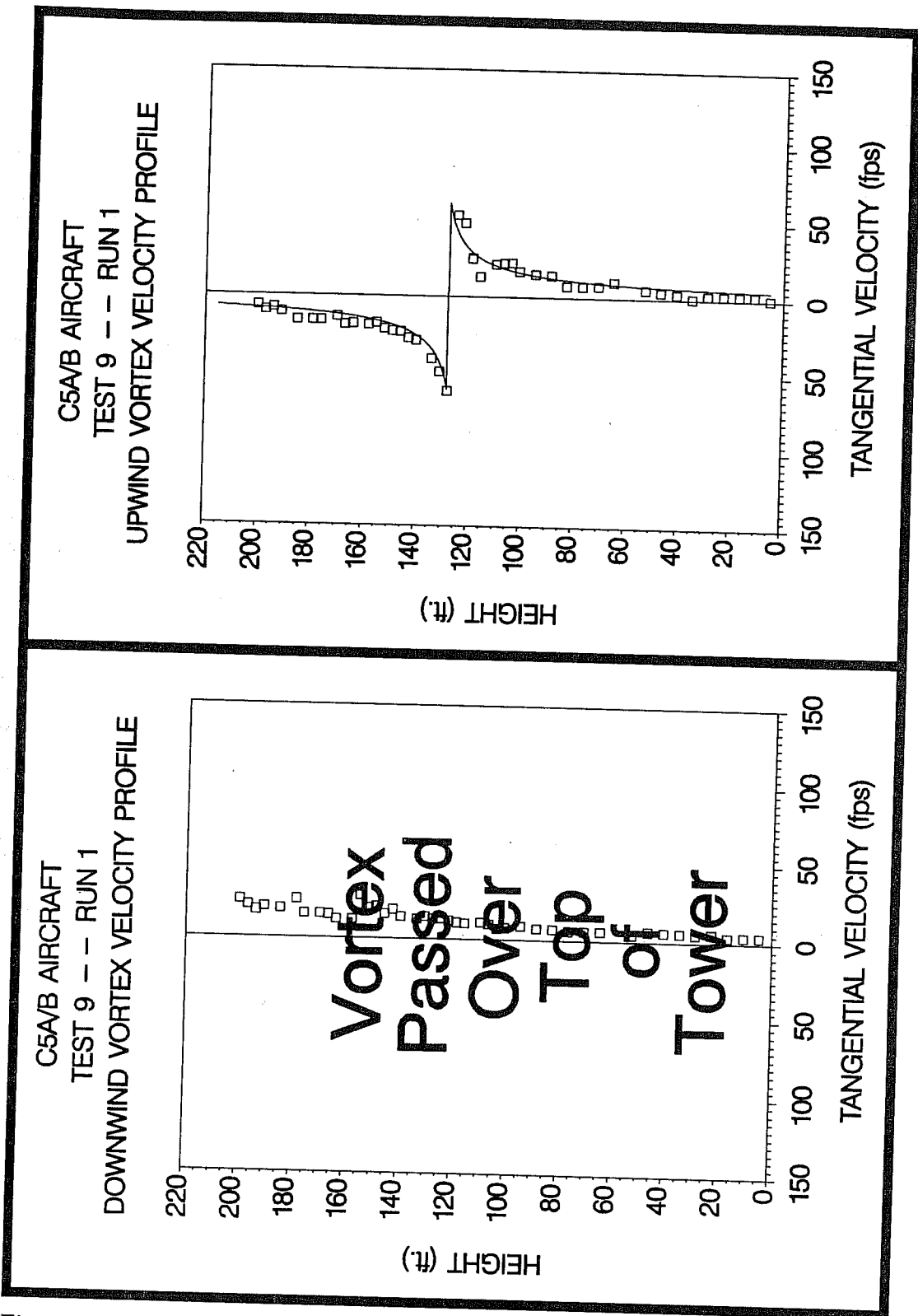


Figure C-105. C5A/B upwind (top) and downwind (bottom) vortex tangential velocity profile at maximum intensity from Test 9, Run 1, ambient wind speed=12.4 fps,  $\delta_F=80\%$ , IAS=150 knots, GW=680.0k lbs. Ages, radii, and velocities of the vortex cores are 38 and (N/A) sec., 3.2 and (N/A) ft., and 61.4 and (N/A) fps, respectively.

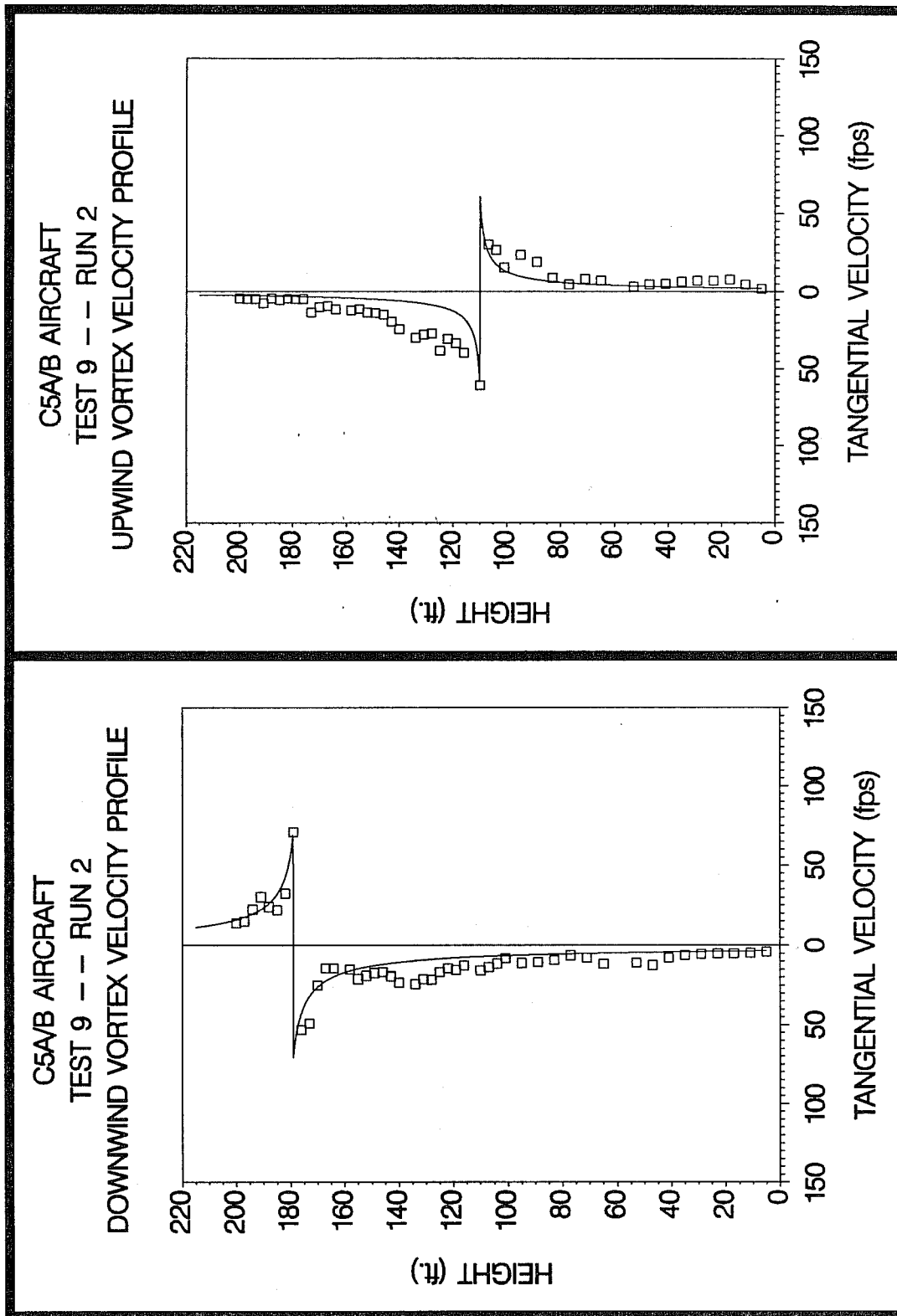


Figure C-106. C5A/B upwind (top) and downwind (bottom) vortex tangential velocity profile at maximum intensity from Test 9, Run 2, ambient wind speed=12.9 fps,  $\delta_F=80\%$ , IAS=150 knots, GW=670.0k lbs. Ages, radii, and velocities of the vortex cores are 81 and 25 sec., 0.8 and 1.9 ft., and 60.8 and 70.7 fps, respectively.

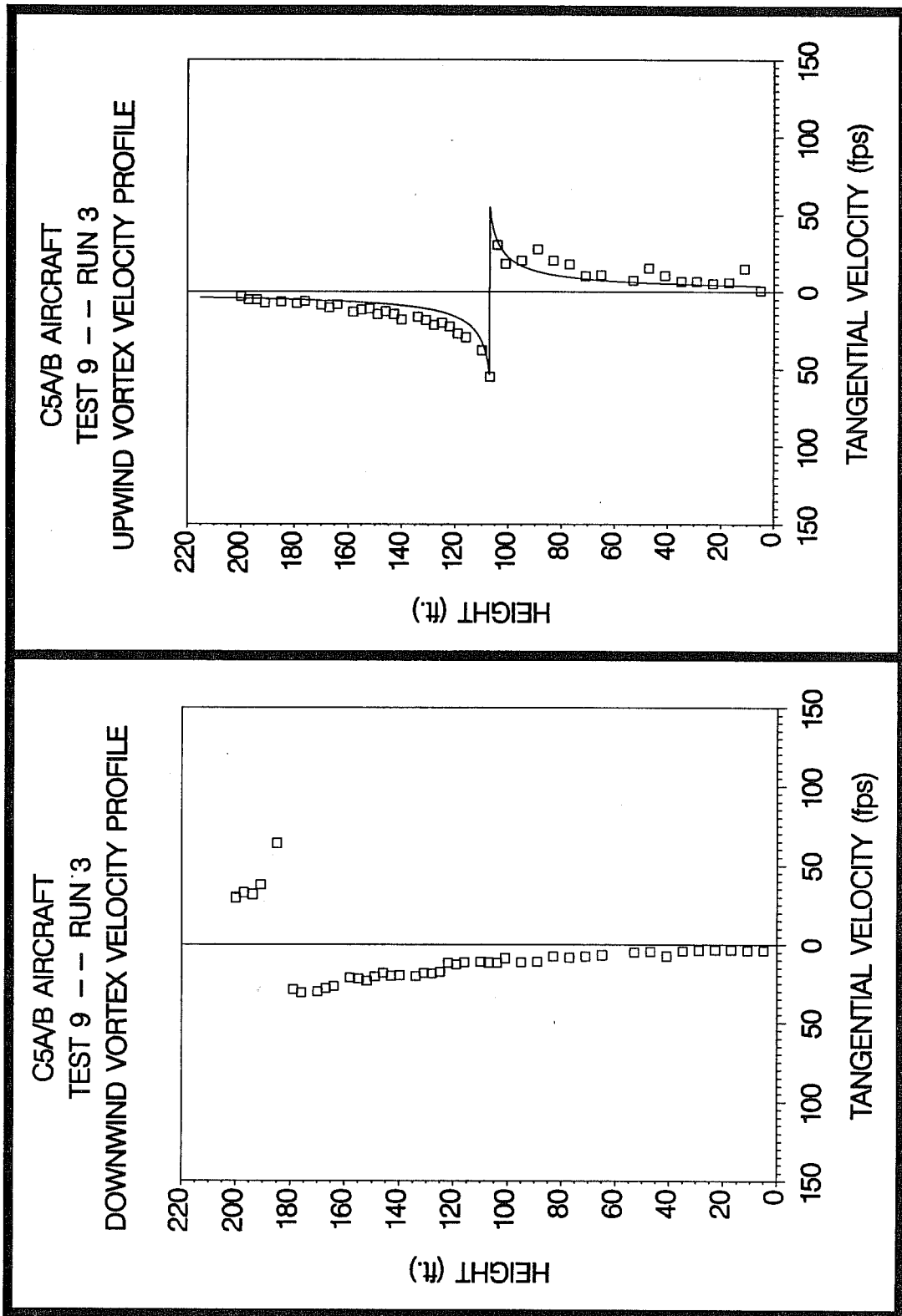


Figure C-107. C5A/B upwind (top) and downwind (bottom) vortex tangential velocity profile at maximum intensity from Test 9, Run 3, ambient wind speed=14.9 fps,  $\delta_F=80\%$ , IAS=150 knots, GW=664.0k lbs. Ages, radii, and velocities of the vortex cores are 40 and 15 sec., 1.8 and (N/A) ft., and 55.0 and 64.0 fps, respectively.

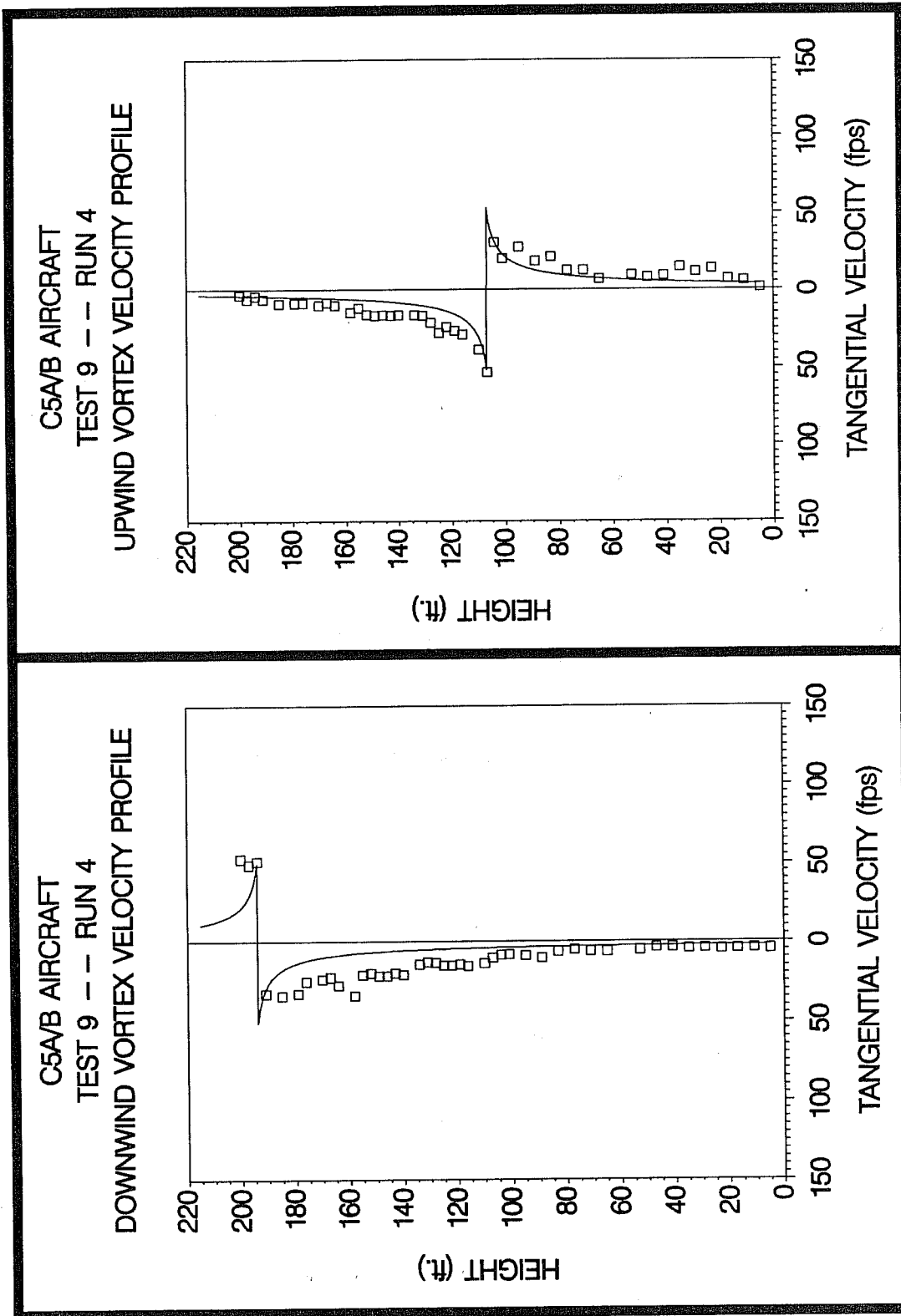
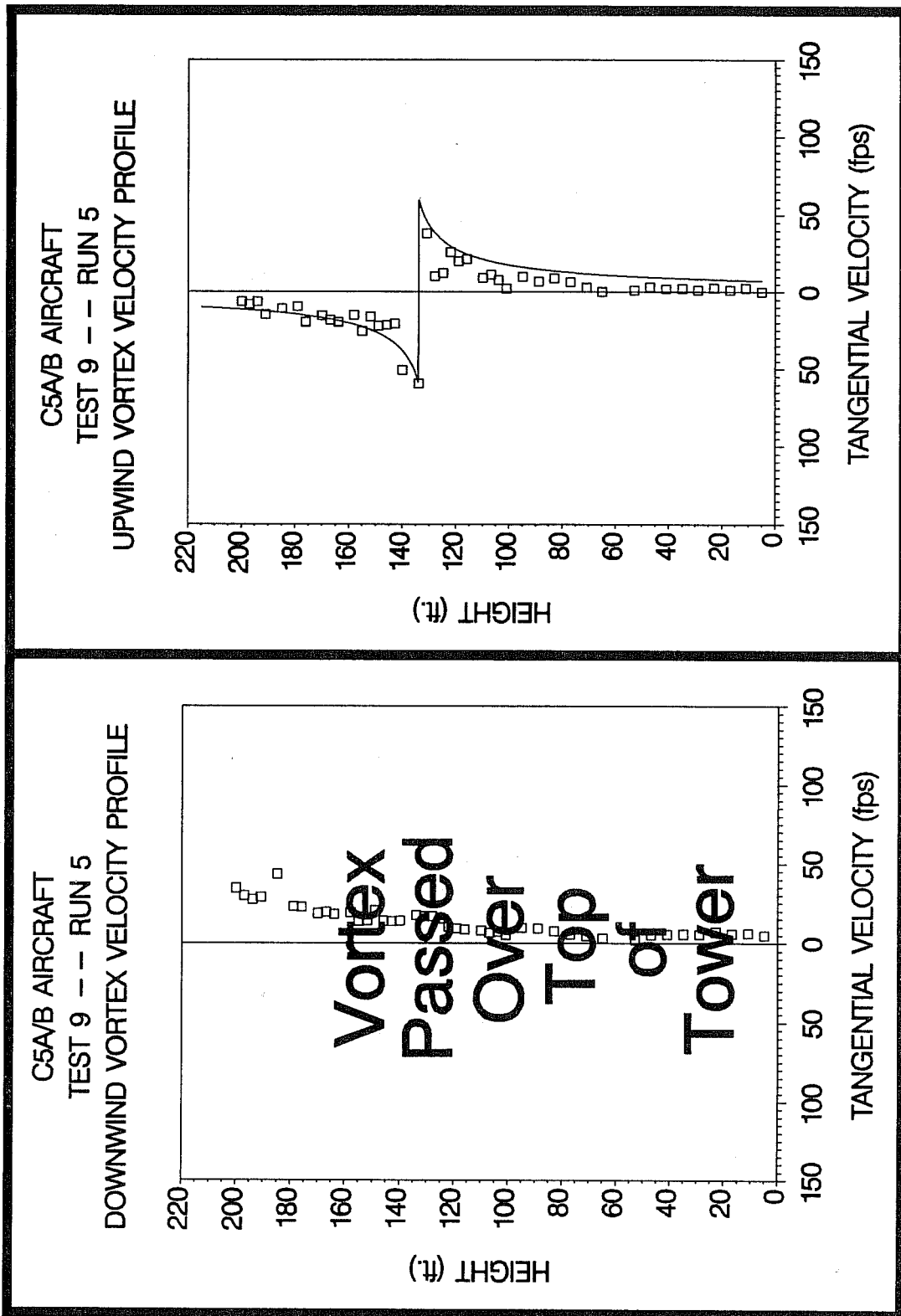
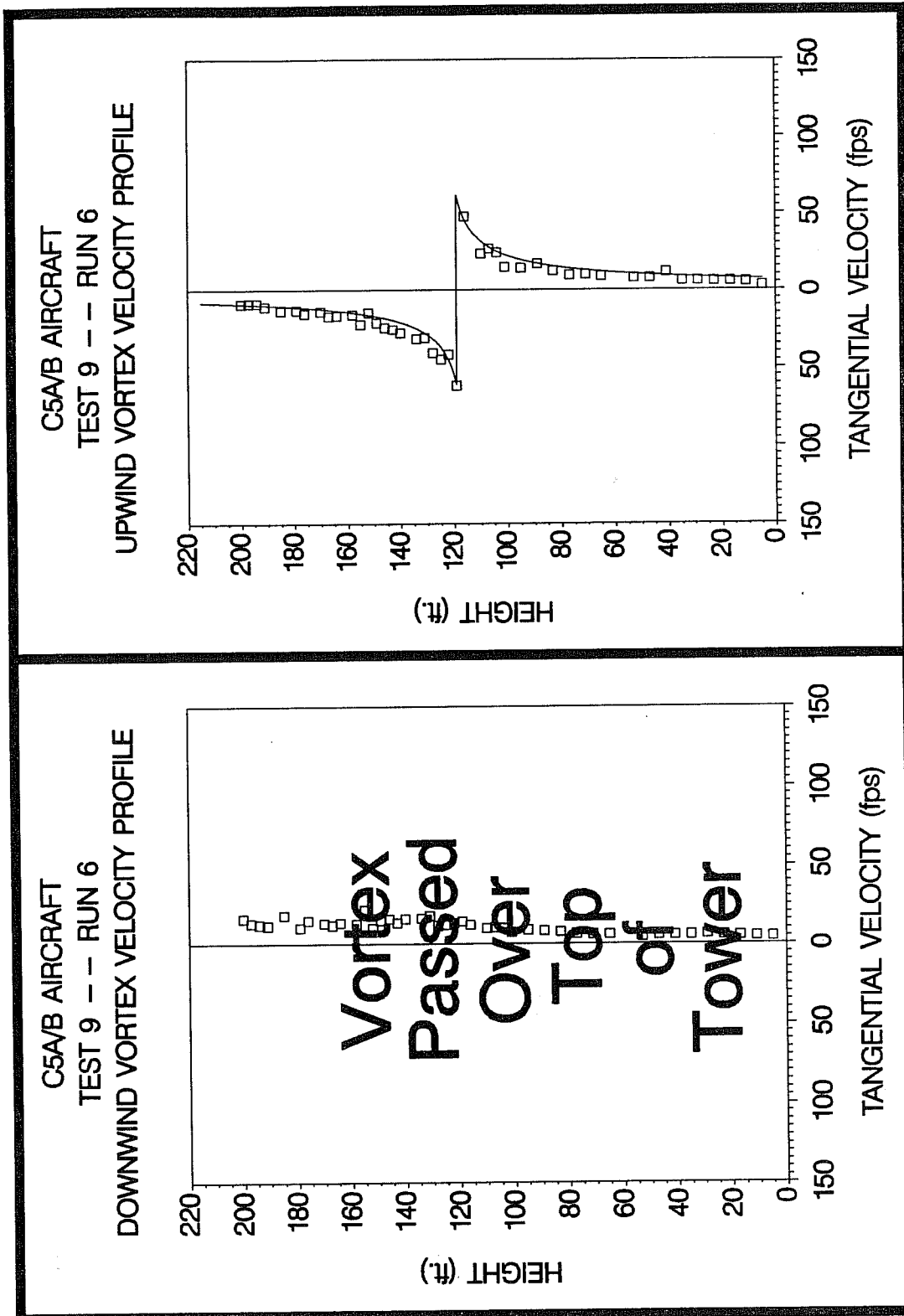


Figure C-108. C5A/B upwind (top) and downwind (bottom) vortex tangential velocity profile at maximum intensity from Test 9, Run 4, ambient wind speed=17.1 fps,  $\delta_F=80\%$ , IAS=150 knots, GW=658.0k lbs. Ages, radii, and velocities of the vortex cores are 36 and 13 sec., 1.7 and 1.7 ft., and 53.2 and 50.9 fps, respectively.



**Figure C-109.** C5A/B upwind (top) and downwind (bottom) vortex tangential velocity profile at maximum intensity from Test 9, Run 5, ambient wind speed=17.6 fps,  $\delta_F=80\%$ , IAS=155 knots, GW=650.0k lbs. Ages, radii, and velocities of the vortex cores are 27 and (N/A) sec., 4.8 and (N/A) ft., and 59.3 and (N/A) fps, respectively.



**Figure C-110.** C5A/B upwind (top) and downwind (bottom) vortex tangential velocity profile at maximum intensity from Test 9, Run 6, ambient wind speed=10.3 fps,  $\delta_F=62\%$ , IAS=155 knots, GW=646.0k lbs. Ages, radii, and velocities of the vortex cores are 40 and (N/A) sec., 3.8 and (N/A) ft., and 61.5 and (N/A) fps, respectively.

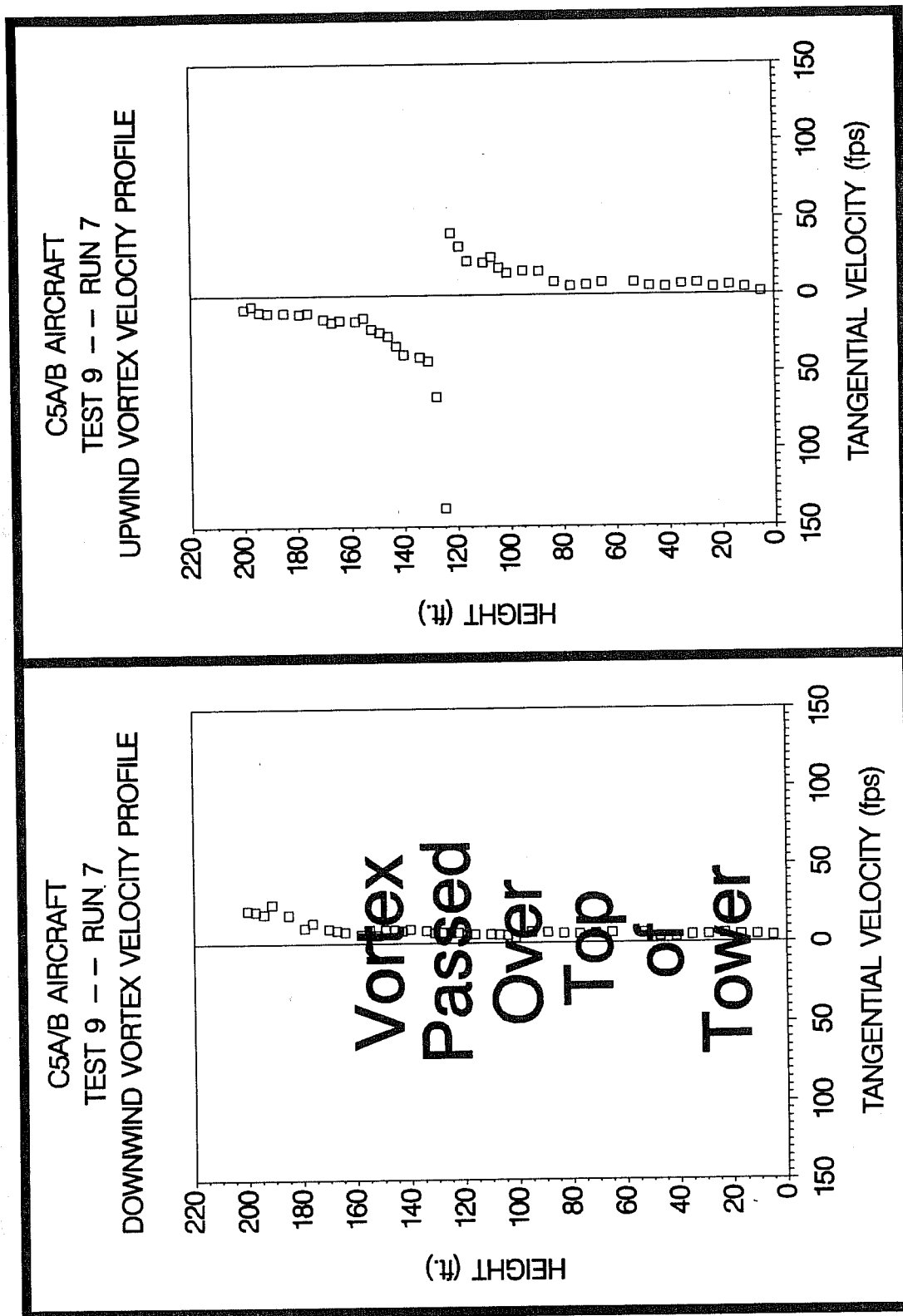
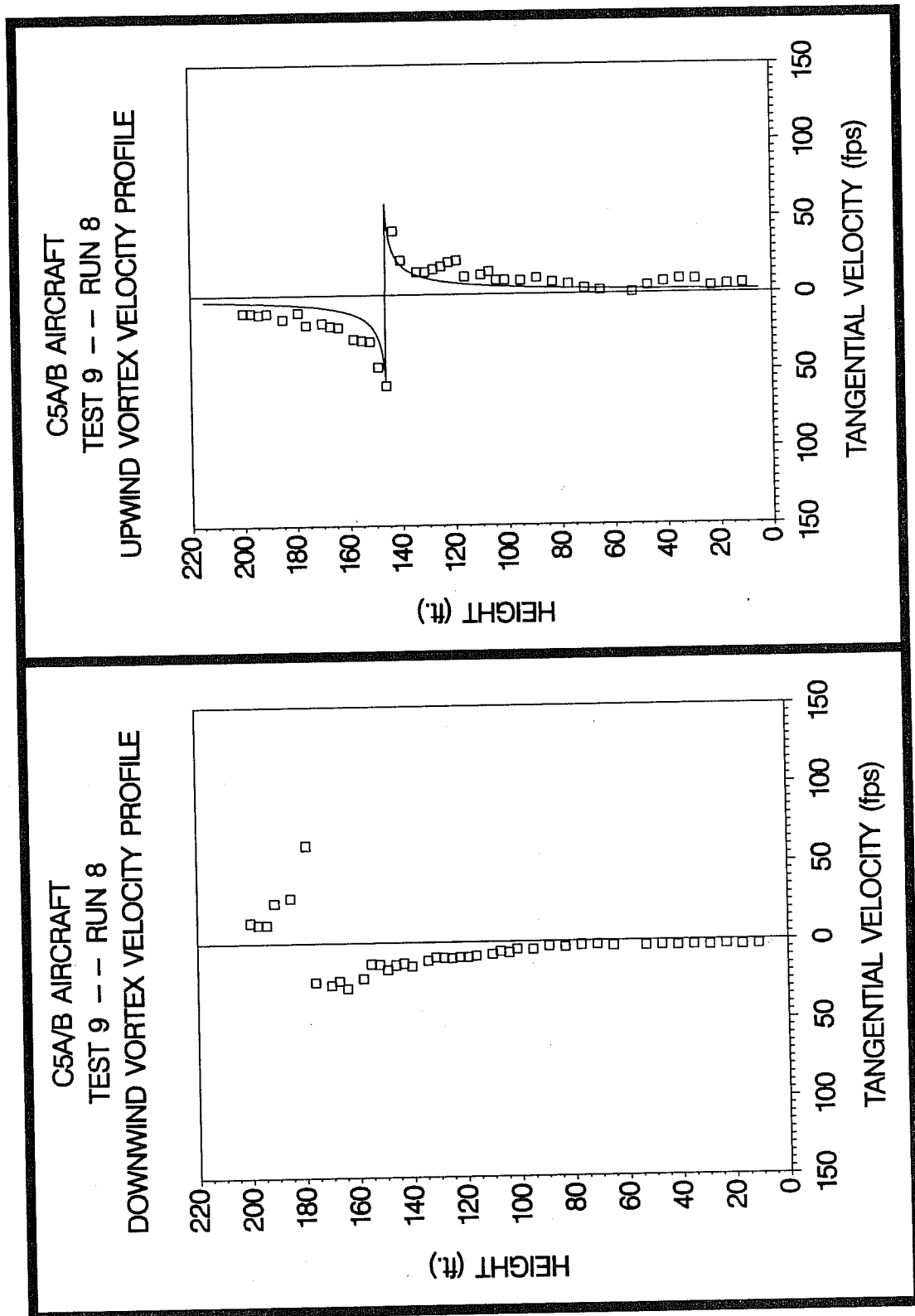
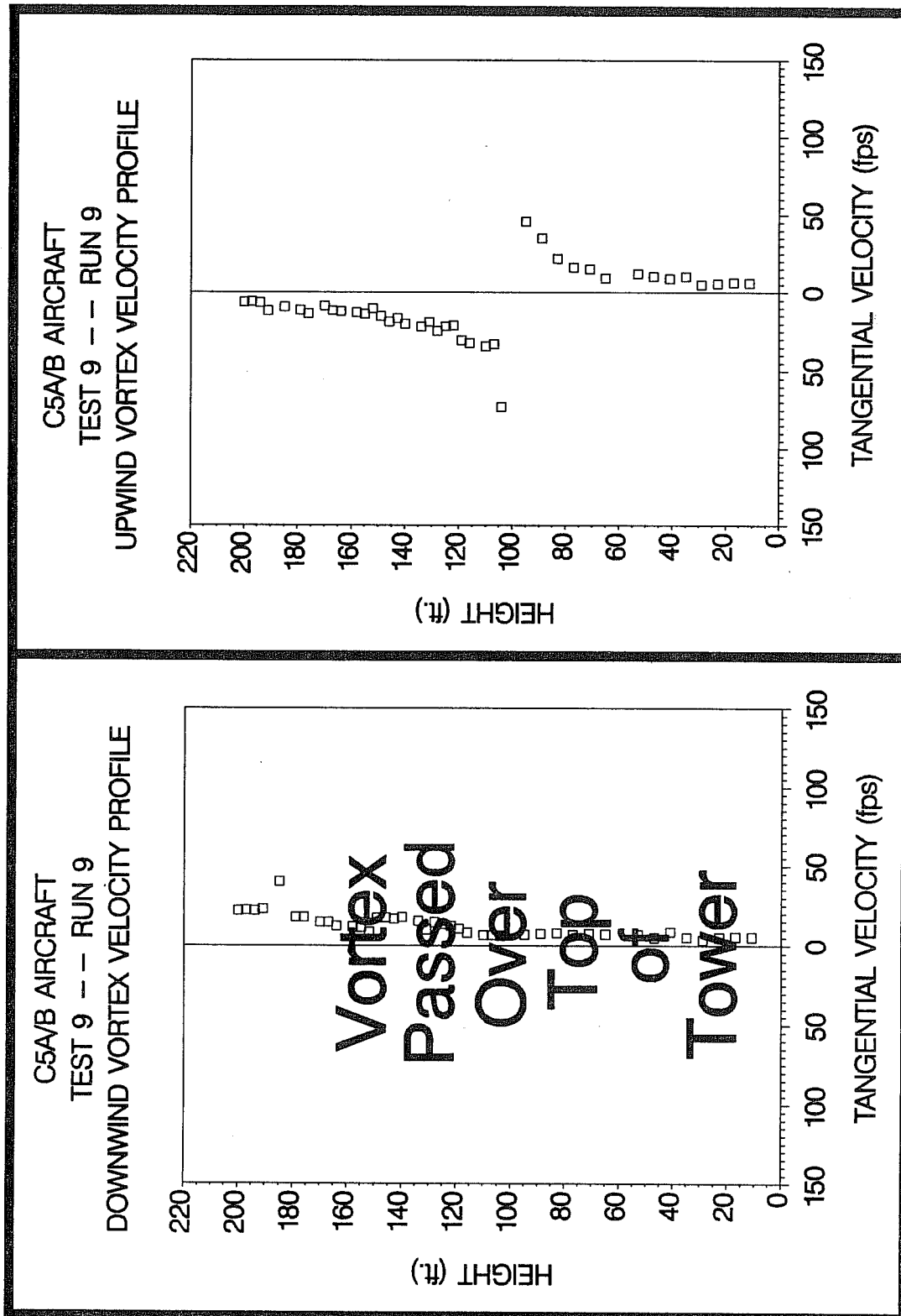


Figure C-111. C5A/B upwind (top) and downwind (bottom) vortex tangential velocity profile at maximum intensity from Test 9, Run 7, ambient wind speed=9.3 fps,  $\delta_F=62\%$ , IAS=155 knots, GW=644.0k lbs. Ages, radii, and velocities of the vortex cores are 48 and (N/A) sec., (N/A) and (N/A) ft., and 138.4 and (N/A) fps, respectively.



**Figure C-112.** C5A/B upwind (top) and downwind (bottom) vortex tangential velocity profile at maximum intensity from Test 9, Run 8, ambient wind speed=6.9 fps,  $\delta_F=62\%$ , IAS=155 knots, GW=640.0k lbs. Ages, radii, and velocities of the vortex cores are 105 and 35 sec., 1.0 and (N/A) ft., and 59.2 and 62.0 fps, respectively.



**Figure C-113.** C5A/B upwind (top) and downwind (bottom) vortex tangential velocity profile at maximum intensity from Test 9, Run 9, ambient wind speed=8.2 fps,  $\delta_F=62\%$ , IAS=155 knots, GW=635.0k lbs. Ages, radii, and velocities of the vortex cores are 85 and (N/A) sec., (N/A) and (N/A) ft., and 72.9 and (N/A) fps, respectively.

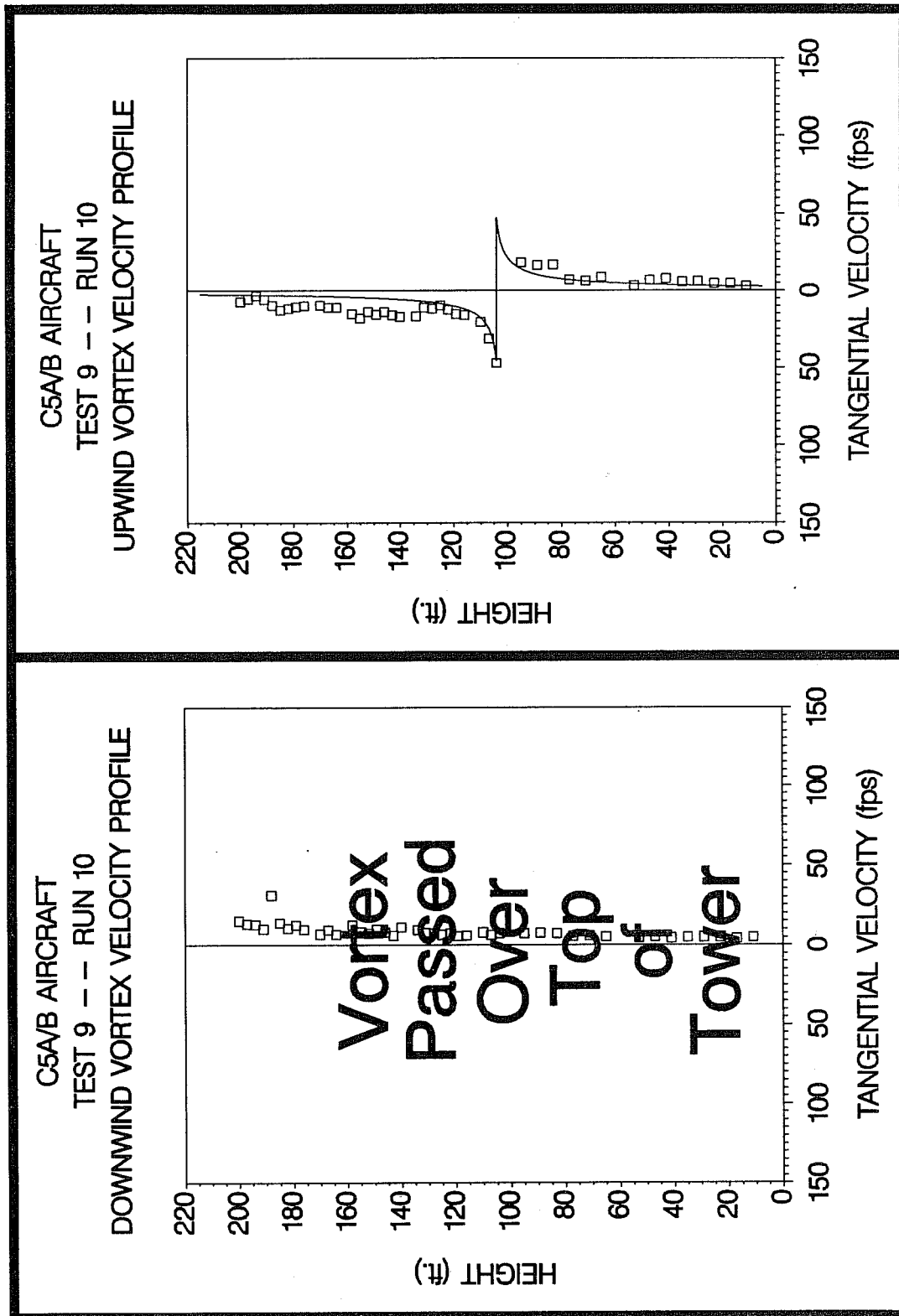


**Figure C-114.** C5A/B upwind (top) and downwind (bottom) vortex tangential velocity profile at maximum intensity from Test 9, Run 10, ambient wind speed=7.8 fps,  $\delta_F=62\%$ , IAS=155 knots, GW=632.0k lbs. Ages, radii, and velocities of the vortex cores are 109 and (N/A) sec., 1.3 and (N/A) ft., and 47.1 and (N/A) fps, respectively.

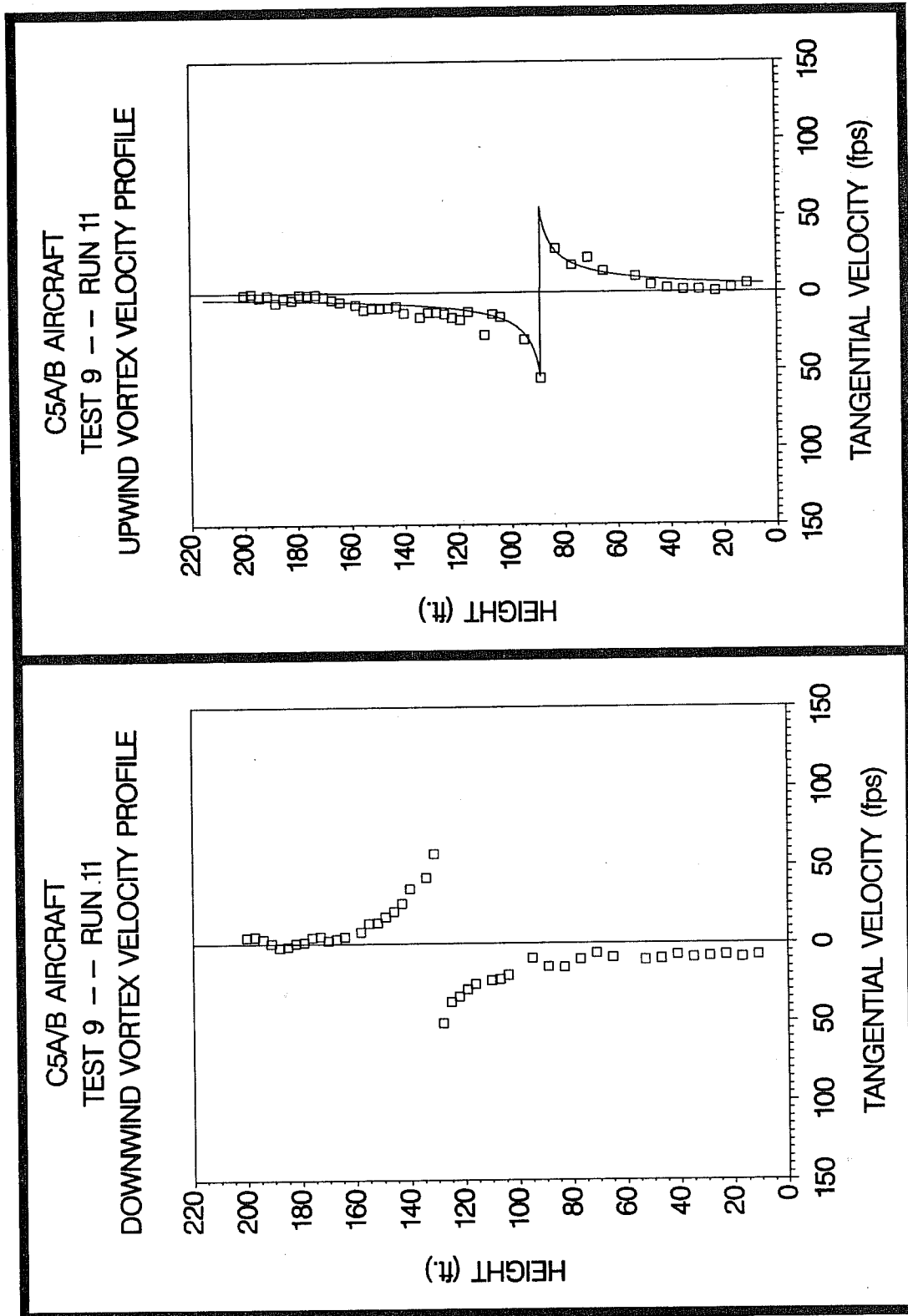


Figure C-115. C5A/B upwind (top) and downwind (bottom) vortex tangential velocity profile at maximum intensity from Test 9, Run 11, ambient wind speed=9.8 fps,  $\delta_F=62\%$ , IAS=155 knots, GW=628.0k lbs. Ages, radii, and velocities of the vortex cores are 90 and 38 sec., 2.2 and (N/A) ft., and 55.4 and 57.3 fps, respectively.

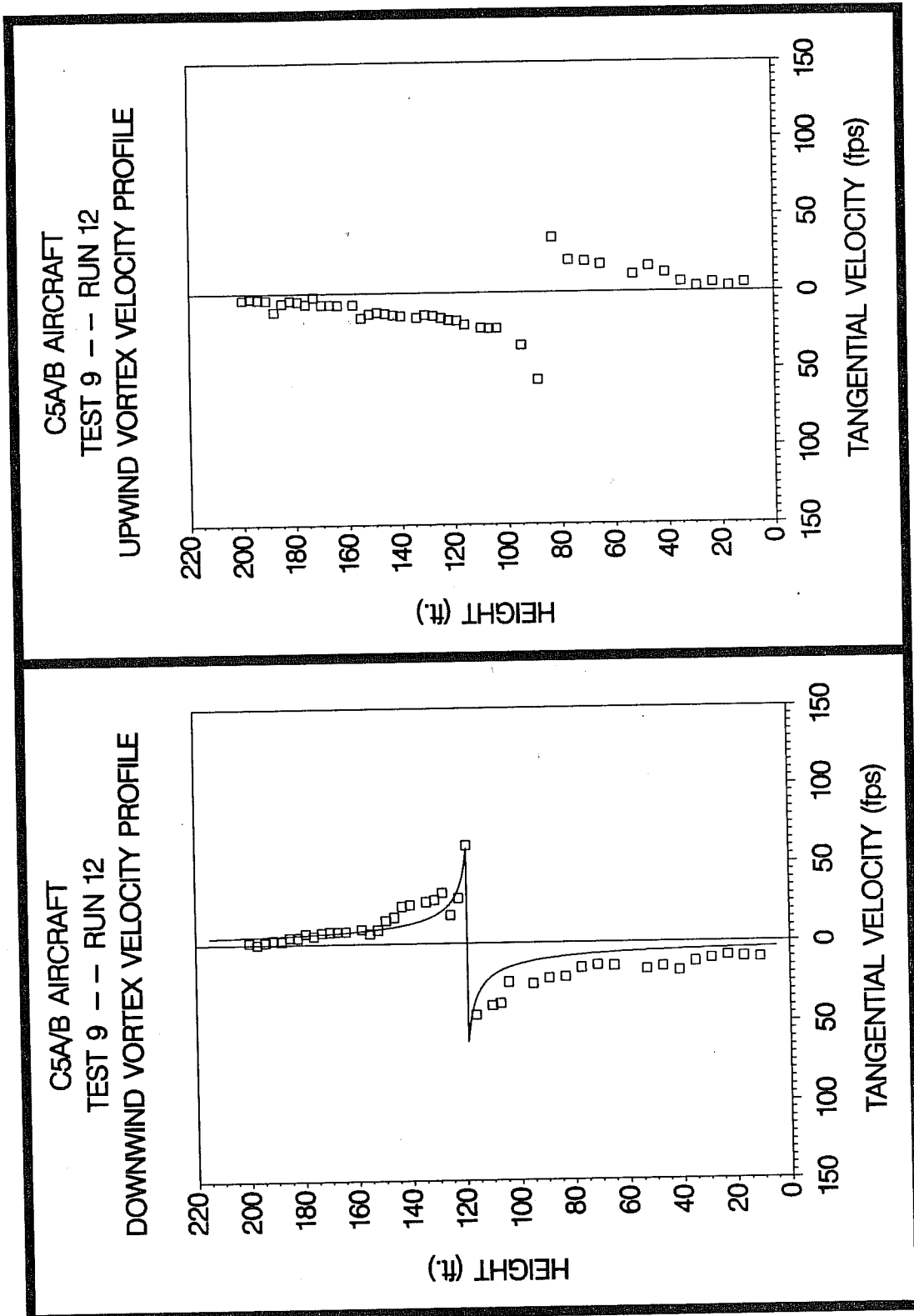


Figure C-116. C5A/B upwind (top) and downwind (bottom) vortex tangential velocity profile at maximum intensity from Test 9, Run 12, ambient wind speed=9.3 fps,  $\delta_F=62\%$ , IAS=155 knots, GW=626.0k lbs. Ages, radii, and velocities of the vortex cores are 68 and 16 sec., (N/A) and 1.6 ft., and 57.0 and 61.8 fps, respectively.

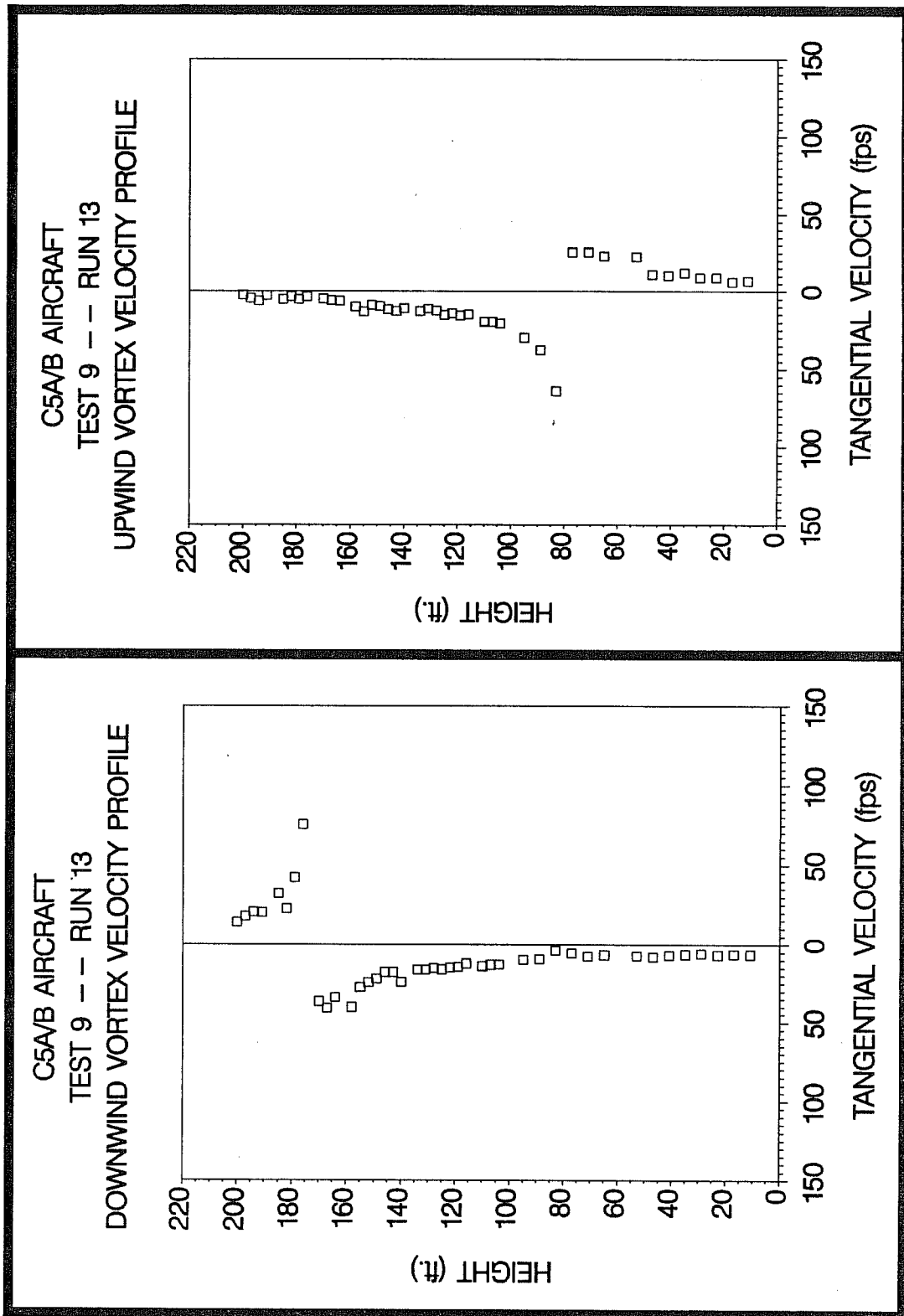
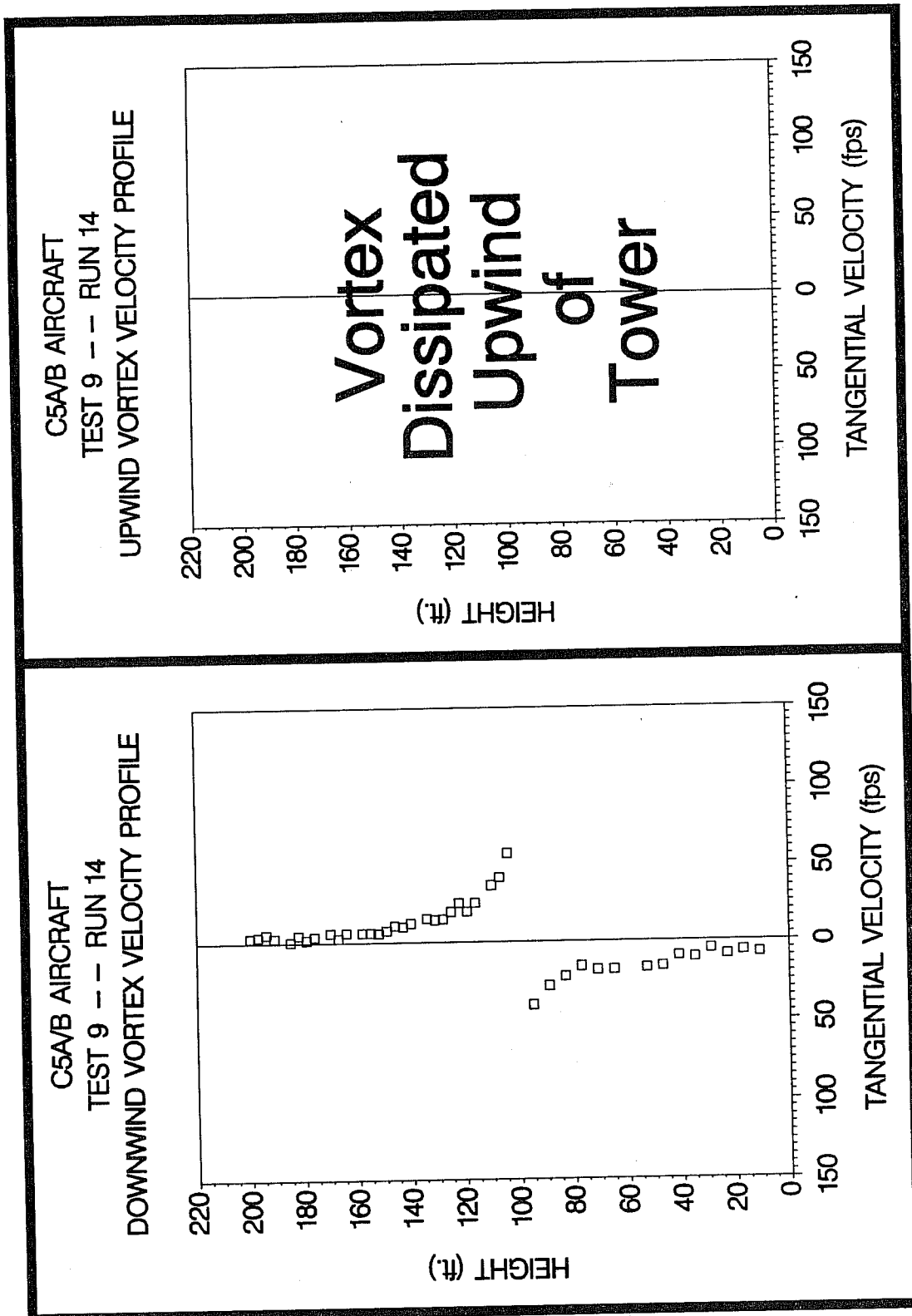


Figure C-117. C5A/B upwind (top) and downwind (bottom) vortex tangential velocity profile at maximum intensity from Test 9, Run 13, ambient wind speed=9.8 fps,  $\delta_F=62\%$ , IAS=150 knots, GW=622.0k lbs. Ages, radii, and velocities of the vortex cores are 60 and 19 sec., (N/A) and (N/A) ft., and 63.9 and 75.5 fps, respectively.



**Figure C-118.** C5A/B upwind (top) and downwind (bottom) vortex tangential velocity profile at maximum intensity from Test 9, Run 14, ambient wind speed=3.3 fps,  $\delta_F=62\%$ , IAS=150 knots, GW=614.0k lbs. Ages, radii, and velocities of the vortex cores are (N/A) and 43 sec., (N/A) and (N/A) ft., and (N/A) and 56.9 fps, respectively.

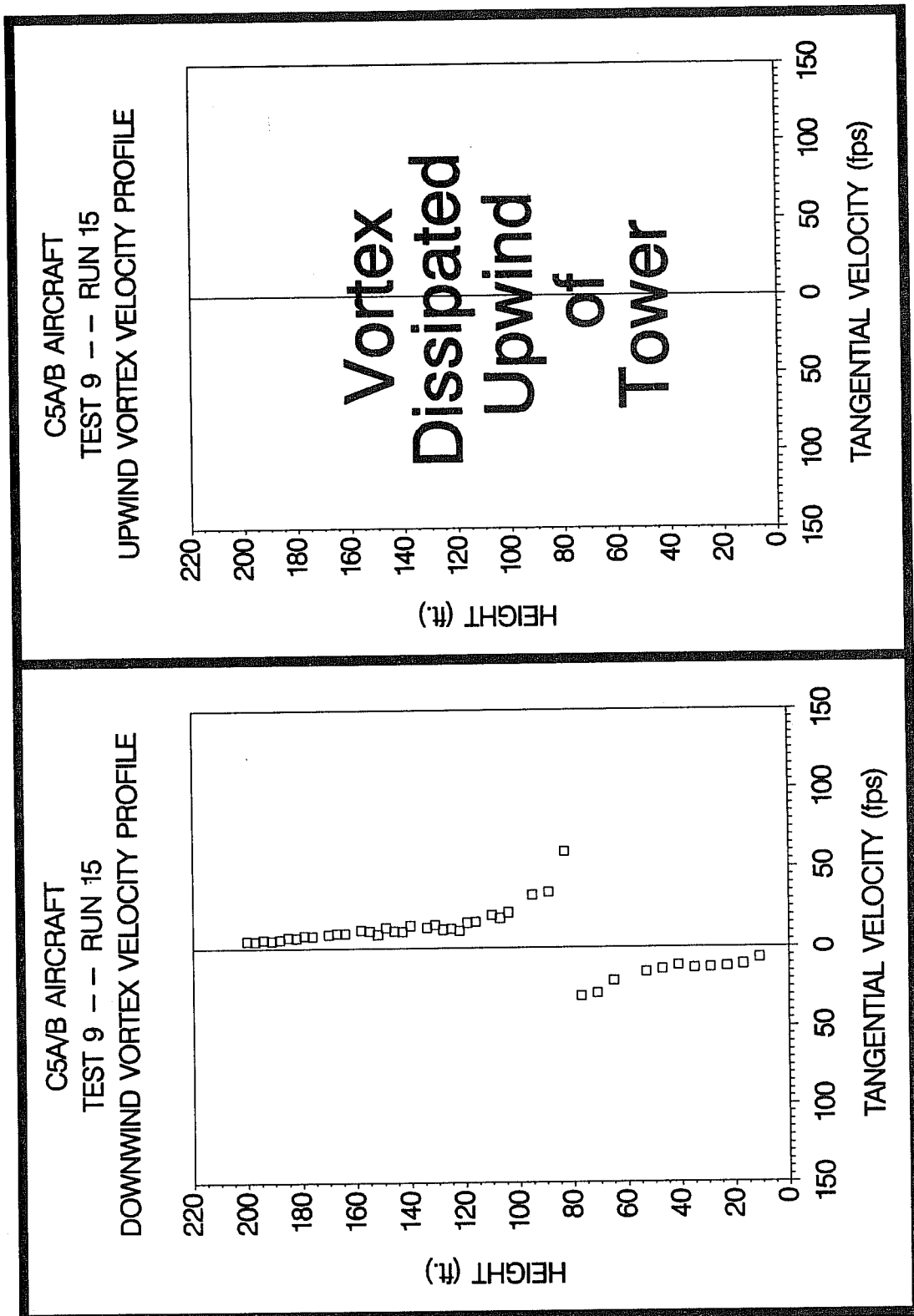


Figure C-119. C5A/B upwind (top) and downwind (bottom) vortex tangential velocity profile at maximum intensity from Test 9, Run 15, ambient wind speed=3.4 fps,  $\delta_F=62\%$ , IAS=150 knots, GW=612.0k lbs. Ages, radii, and velocities of the vortex cores are (N/A) and 59 sec., (N/A) and (N/A) ft., and (N/A) and 59.7 fps, respectively.

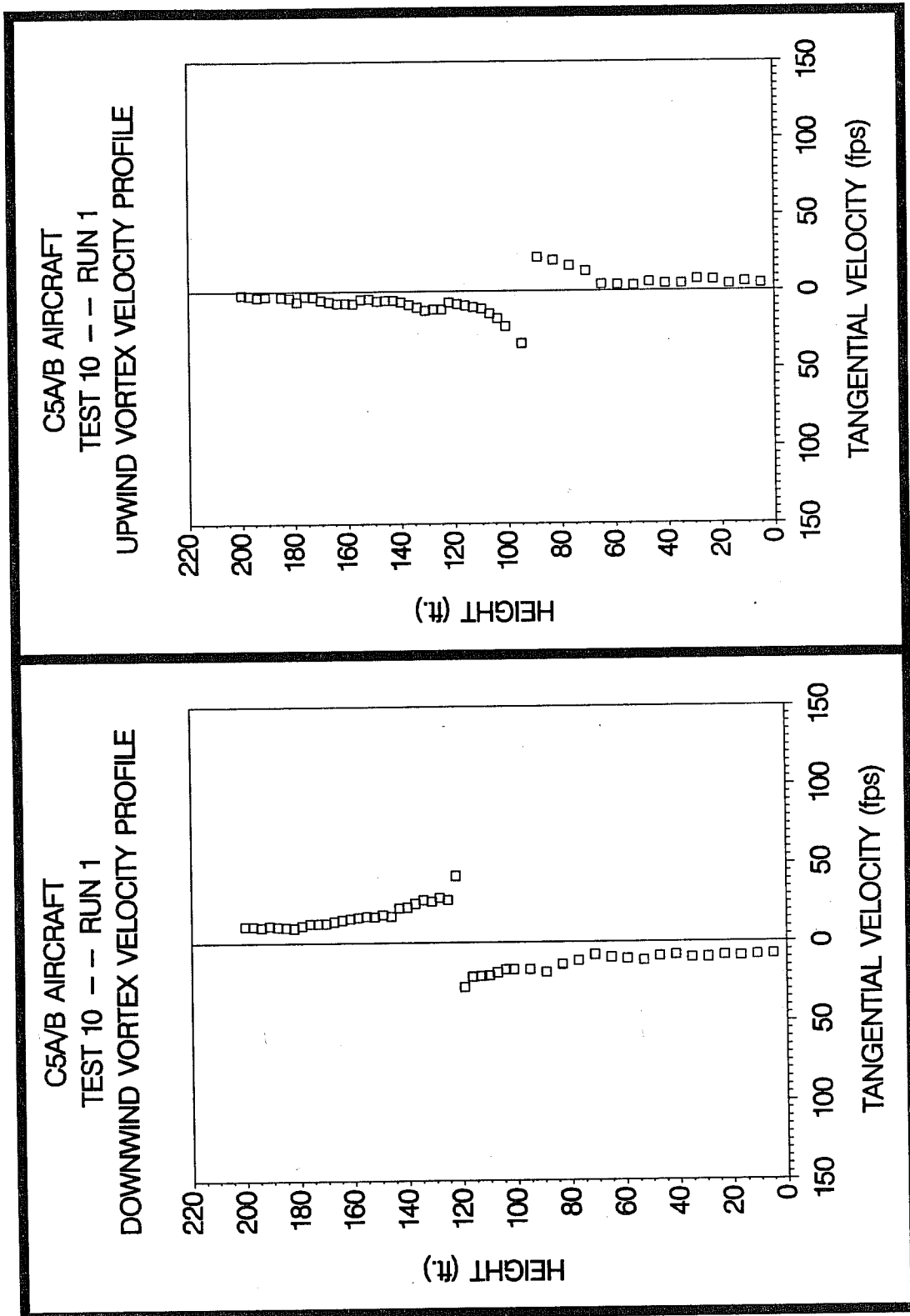


Figure C-120. C5A/B upwind (top) and downwind (bottom) vortex tangential velocity profile at maximum intensity from Test 10, Run 1, ambient wind speed=7.5 fps,  $\delta_F=80\%$ , IAS=150 knots, GW=545.0k lbs. Ages, radii, and velocities of the vortex cores are 78 and 25 sec., (N/A) and (N/A) ft., and 34.0 and 42.4 fps, respectively.

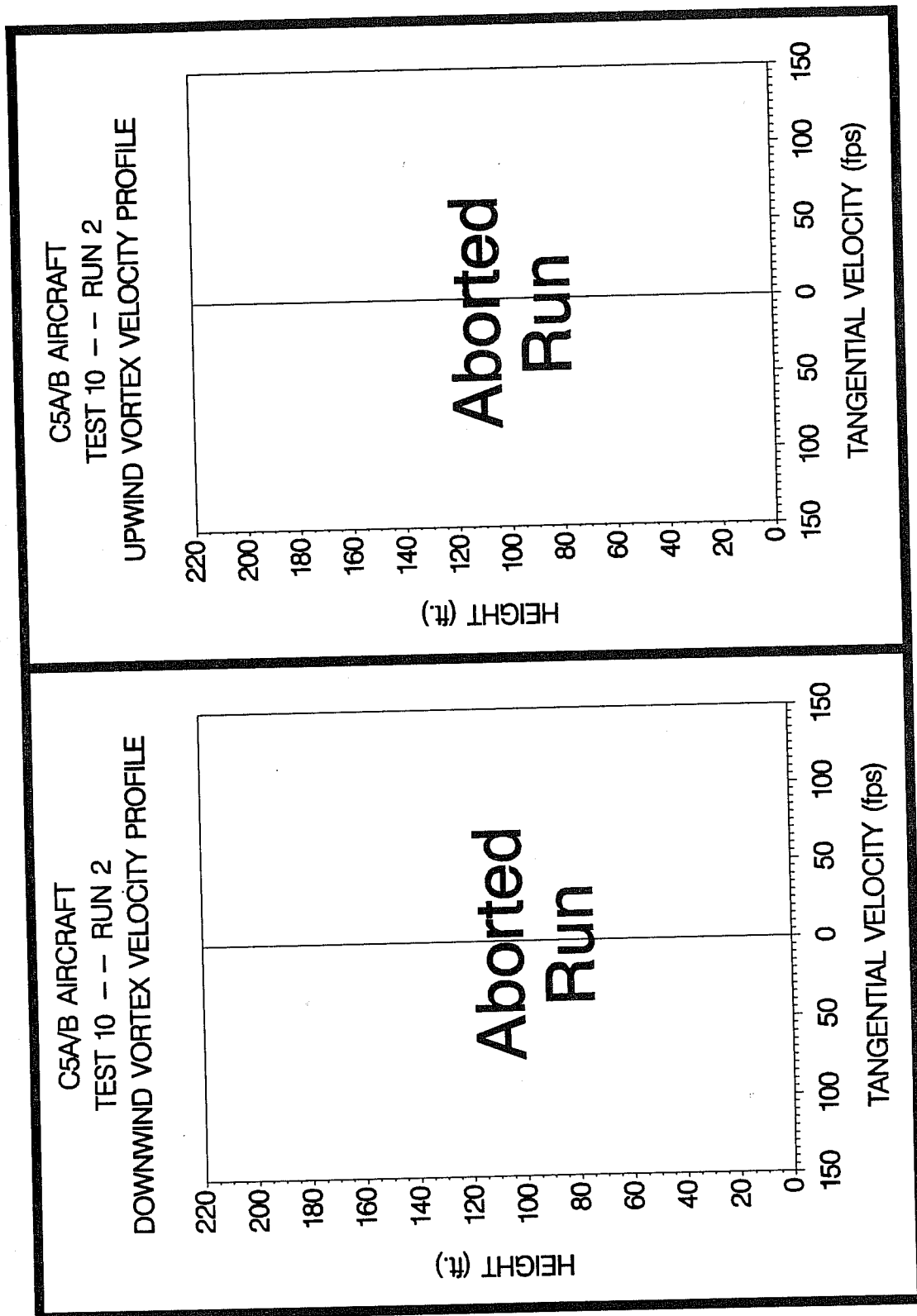
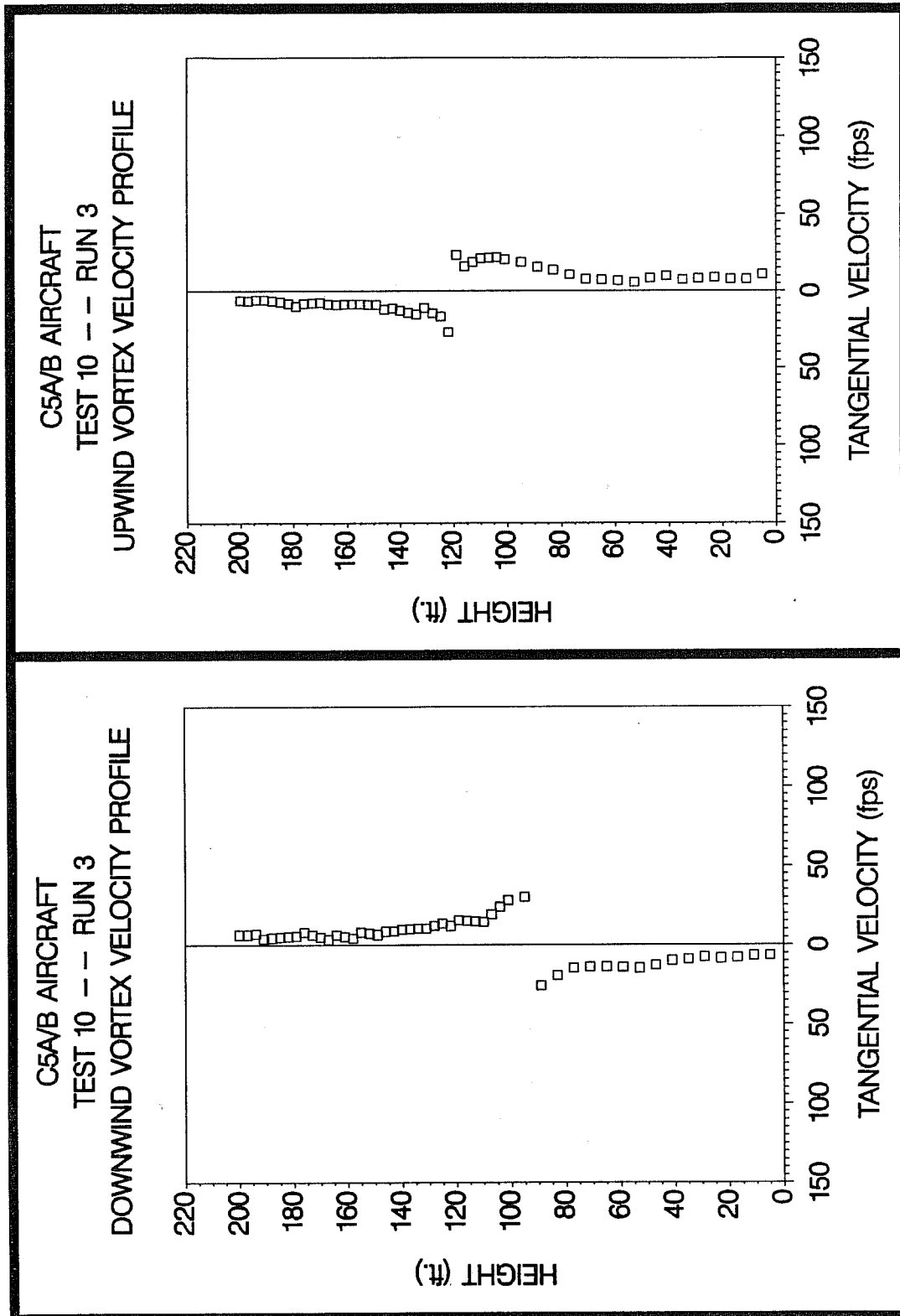


Figure C-121. C5A/B upwind (top) and downwind (bottom) vortex tangential velocity profile at maximum intensity from Test 10, Run 2, ambient wind speed=10.2 fps,  $\delta_F=80\%$ , IAS=(N/A) knots, GW=537.0k lbs. Ages, radii, and velocities of the vortex cores are (N/A) and (N/A) sec., (N/A) and (N/A) ft., and (N/A) and (N/A) fps, respectively.



**Figure C-122.** C5A/B upwind (top) and downwind (bottom) vortex tangential velocity profile at maximum intensity from Test 10, Run 3, ambient wind speed=12.8 fps,  $\delta_F=80\%$ , IAS=150 knots, GW=533.0k lbs. Ages, radii, and velocities of the vortex cores are 105 and 23 sec., (N/A) and (N/A) ft., and 26.9 and 30.2 fps, respectively.

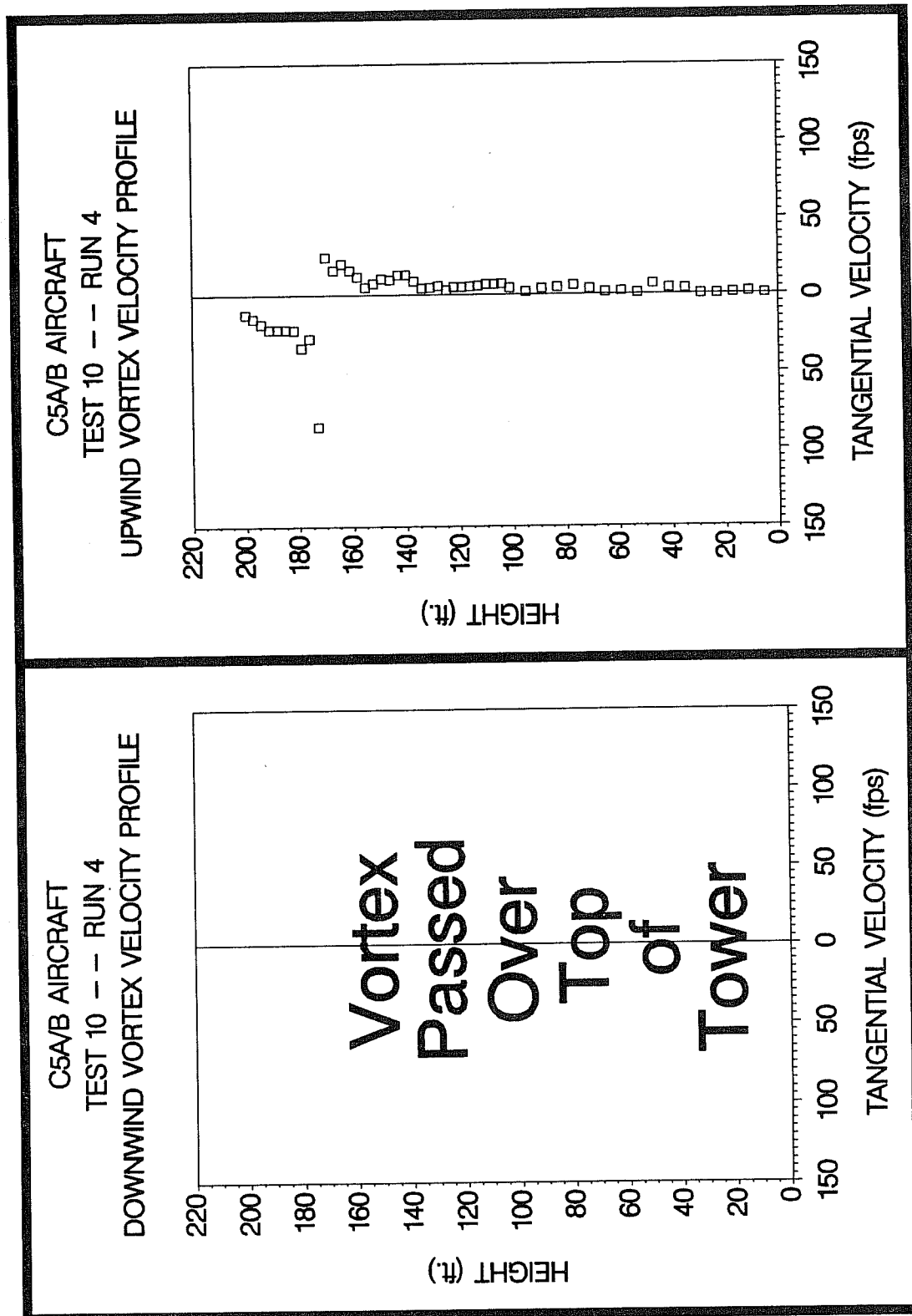
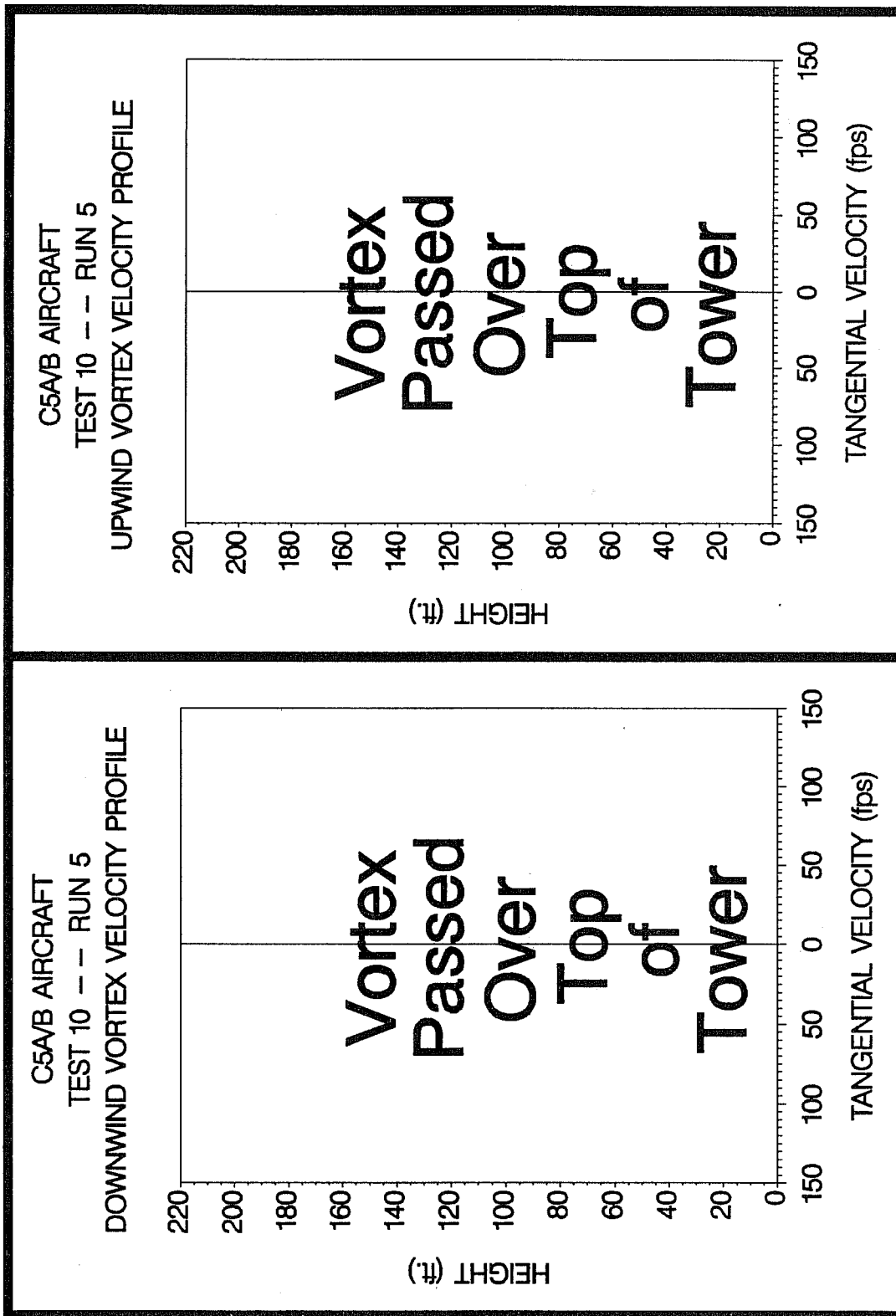
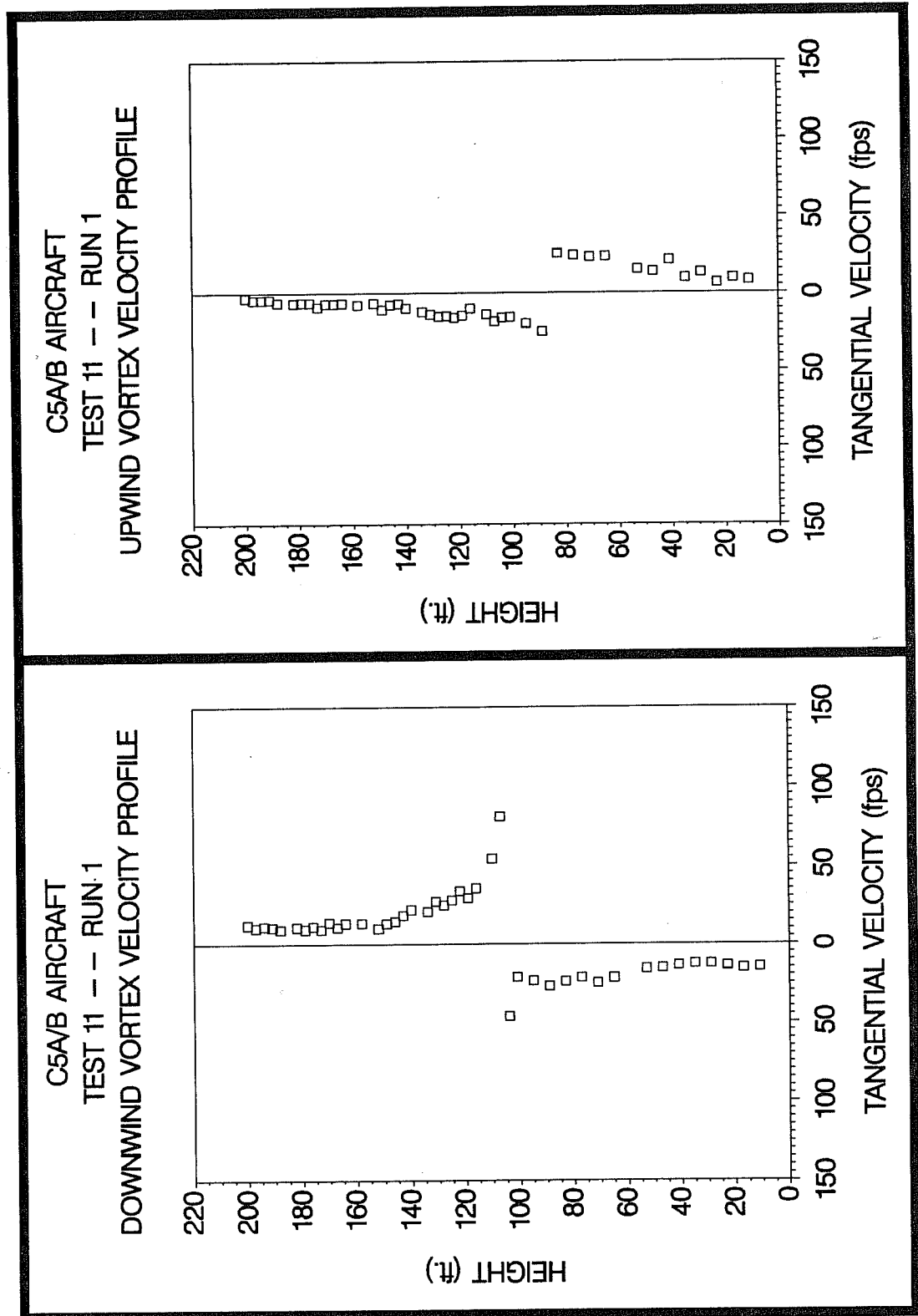


Figure C-123. C5A/B upwind (top) and downwind (bottom) vortex tangential velocity profile at maximum intensity from Test 10, Run 4, ambient wind speed=12.1 fps,  $\delta_F=40\%$ , IAS=150 knots, GW=529.0k lbs. Ages, radii, and velocities of the vortex cores are 29 and (N/A) sec., (N/A) and (N/A) ft., and 85.0 and (N/A) fps, respectively.



**Figure C-124.** C5A/B upwind (top) and downwind (bottom) vortex tangential velocity profile at maximum intensity from Test 10, Run 5, ambient wind speed=24.5 fps,  $\delta_F=80\%$ , IAS=134 knots, GW=526.0k lbs. Ages, radii, and velocities of the vortex cores are (N/A) and (N/A) sec., (N/A) and (N/A) ft., and (N/A) and (N/A) fps, respectively.



**Figure C-125.** C5A/B upwind (top) and downwind (bottom) vortex tangential velocity profile at maximum intensity from Test 11, Run 1, ambient wind speed=19.4 fps,  $\delta_F=100\%$ , IAS=130 knots, GW=546.0k lbs. Ages, radii, and velocities of the vortex cores are 24 and 14 sec., (N/A) and (N/A) ft., and 25.1 and 81.2 fps, respectively.

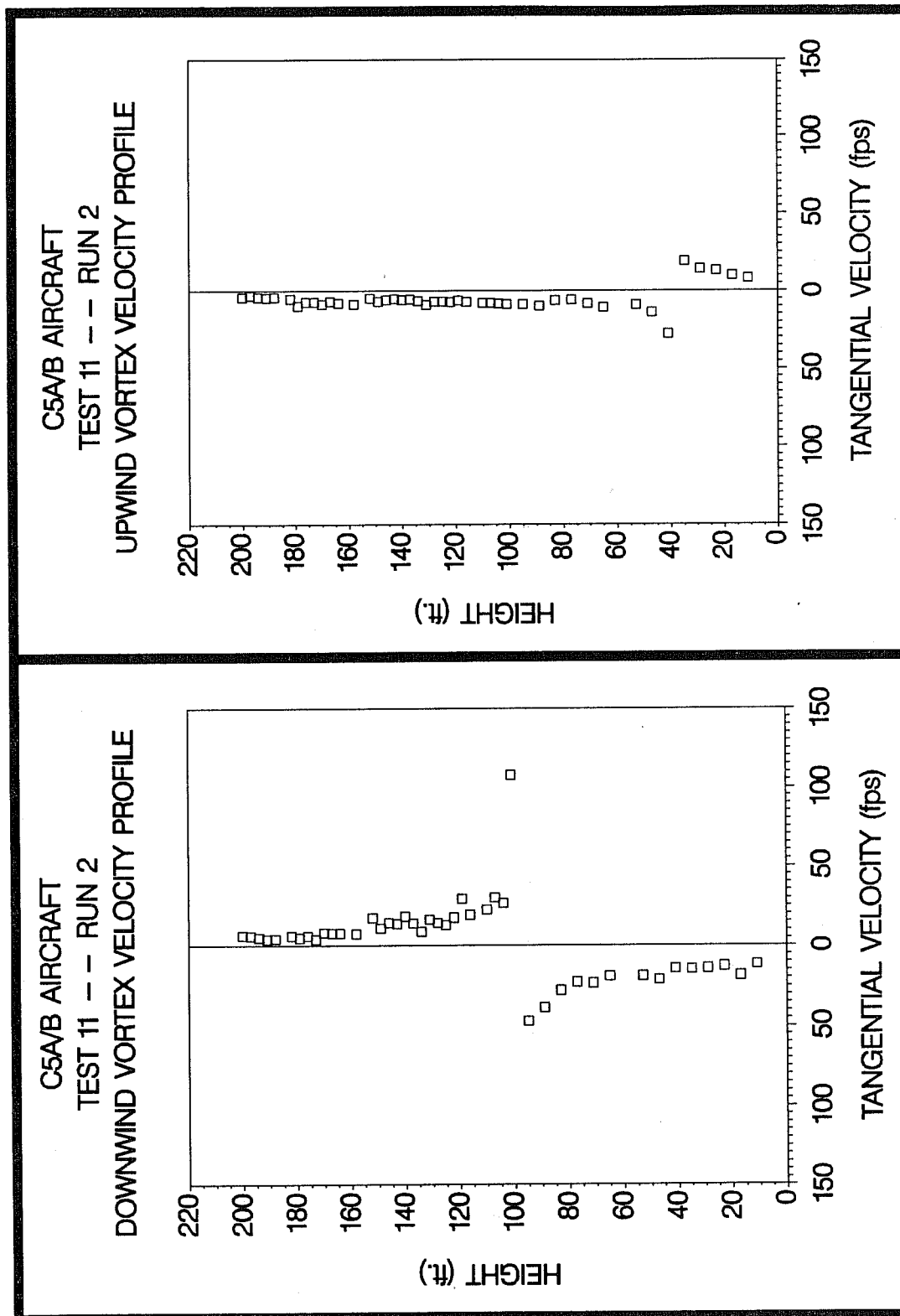


Figure C-126. C5A/B upwind (top) and downwind (bottom) vortex tangential velocity profile at maximum intensity from Test 11, Run 2, ambient wind speed=10.3 fps,  $\delta_F=100\%$ , IAS=130 knots, GW=542.0k lbs. Ages, radii, and velocities of the vortex cores are 38 and 10 sec., (N/A) and (N/A) ft., and 27.9 and 107.6 fps, respectively.

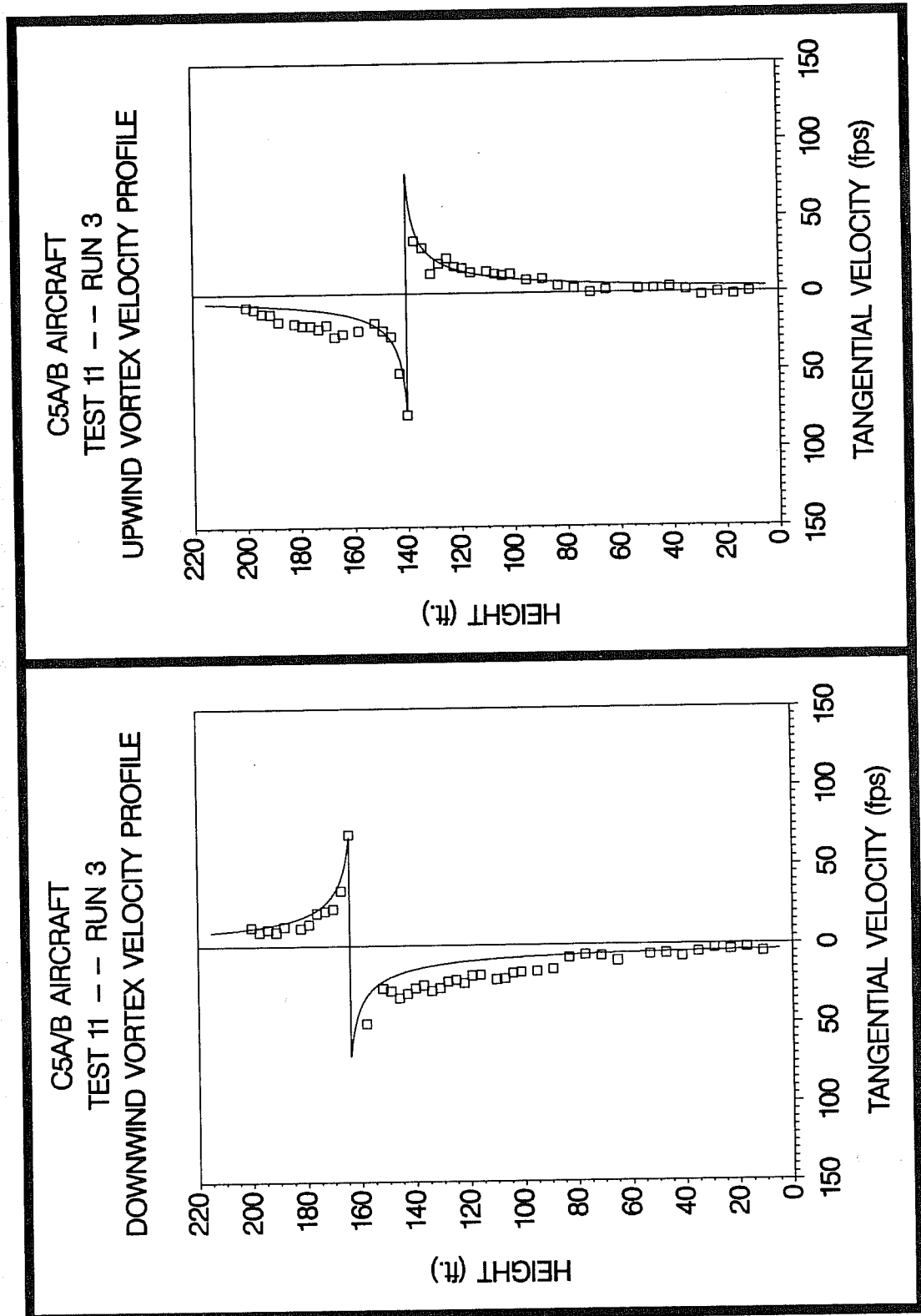


Figure C-127. C5A/B upwind (top) and downwind (bottom) vortex tangential velocity profile at maximum intensity from Test 11, Run 3, ambient wind speed=14.5 fps,  $\delta_F=100\%$ , IAS=130 knots, GW=538.0k lbs. Ages, radii, and velocities of the vortex cores are 22 and 10 sec., 1.4 and 2.0 ft., and 78.4 and 70.1 fps, respectively.

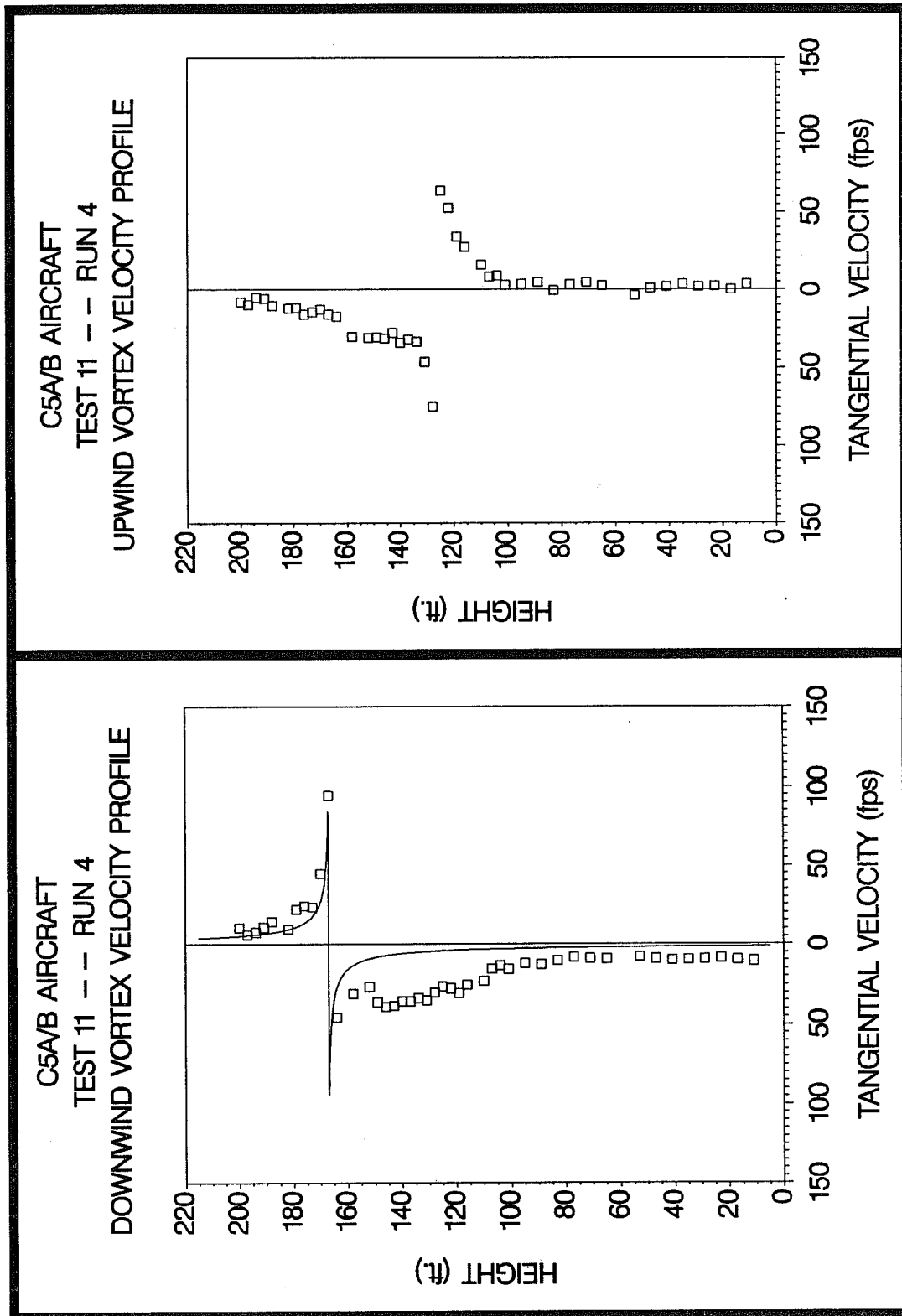


Figure C-128. C5A/B upwind (top) and downwind (bottom) vortex tangential velocity profile at maximum intensity from Test 11, Run 4, ambient wind speed=17.0 fps,  $\delta_F=80\%$ , IAS=130 knots, GW=534.0k lbs. Ages, radii, and velocities of the vortex cores are 18 and 9 sec., (N/A) and 0.4 ft., and 74.9 and 94.3 fps, respectively.

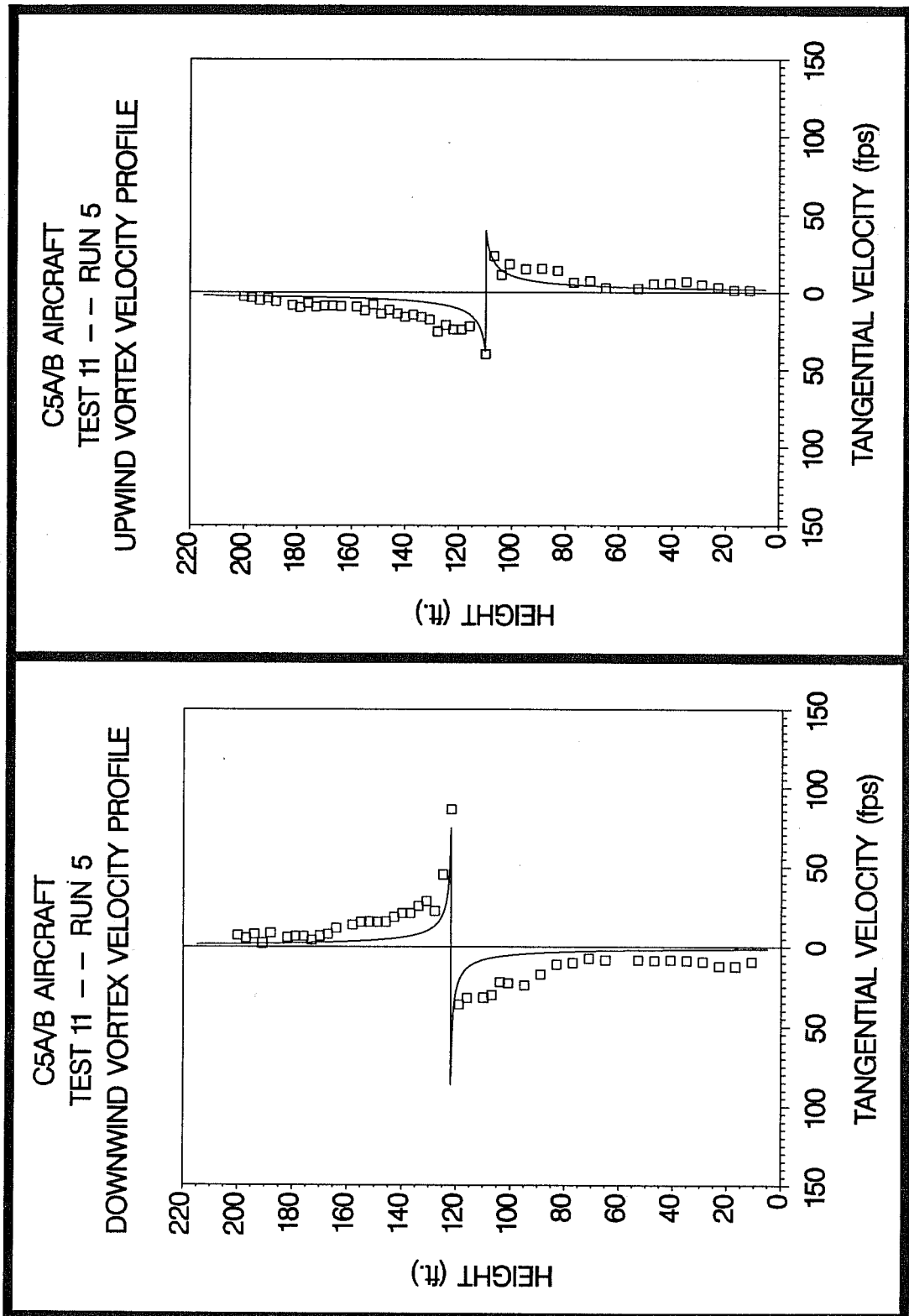


Figure C-129. C5A/B upwind (top) and downwind (bottom) vortex tangential velocity profile at maximum intensity from Test 11, Run 5, ambient wind speed=13.4 fps,  $\delta_F=80\%$ , IAS=130 knots, GW=530.0k lbs. Ages, radii, and velocities of the vortex cores are 39 and 21 sec., 1.2 and 0.3 ft., and 39.9 and 86.2 fps, respectively.

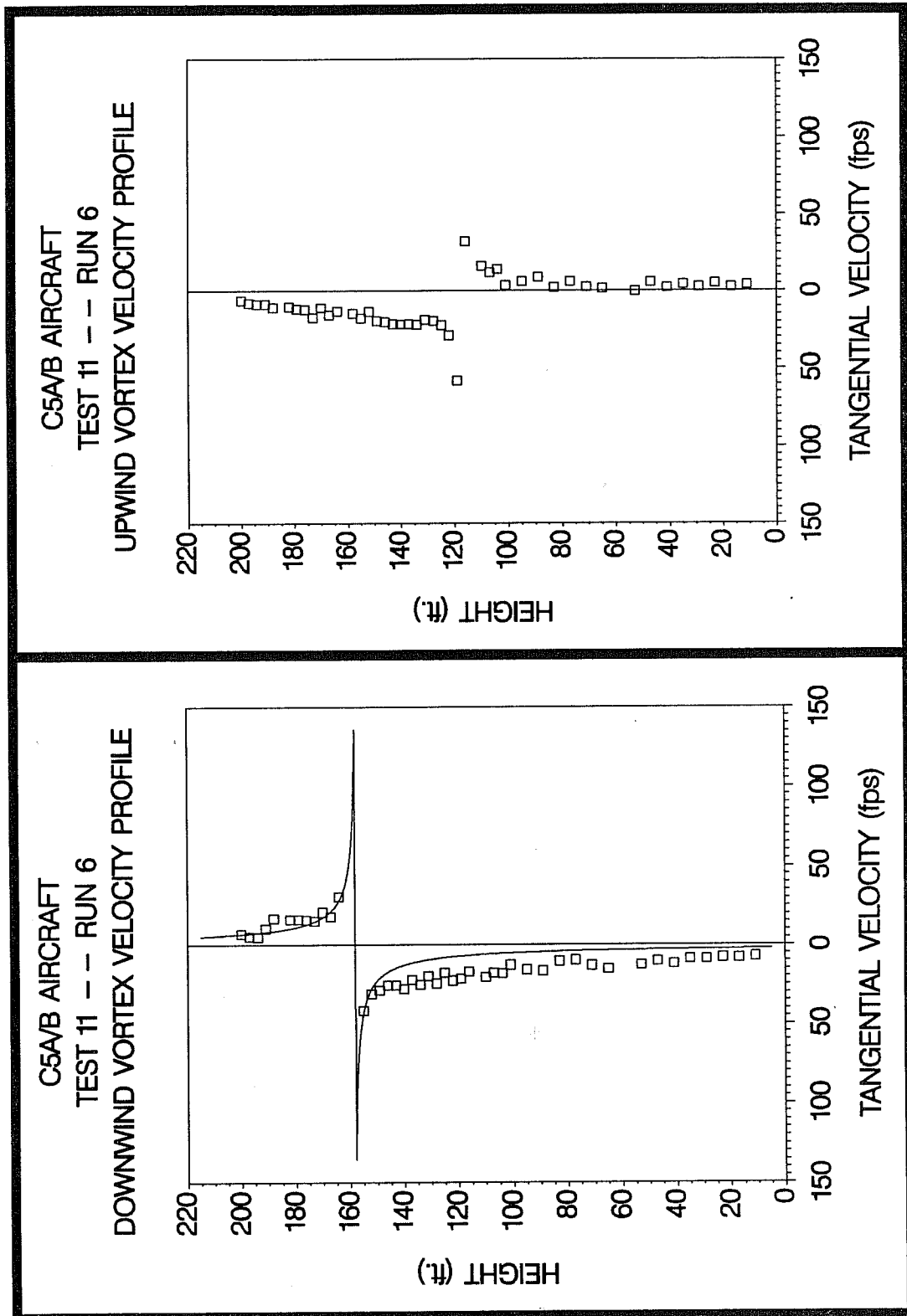


Figure C-130. C5A/B upwind (top) and downwind (bottom) vortex tangential velocity profile at maximum intensity from Test 11, Run 6, ambient wind speed=15.8 fps,  $\delta_F=80\%$ , IAS=130 knots, GW=527.0k lbs. Ages, radii, and velocities of the vortex cores are 27 and 13 sec., (N/A) and 0.4 ft., and 57.9 and 151.9 fps, respectively.

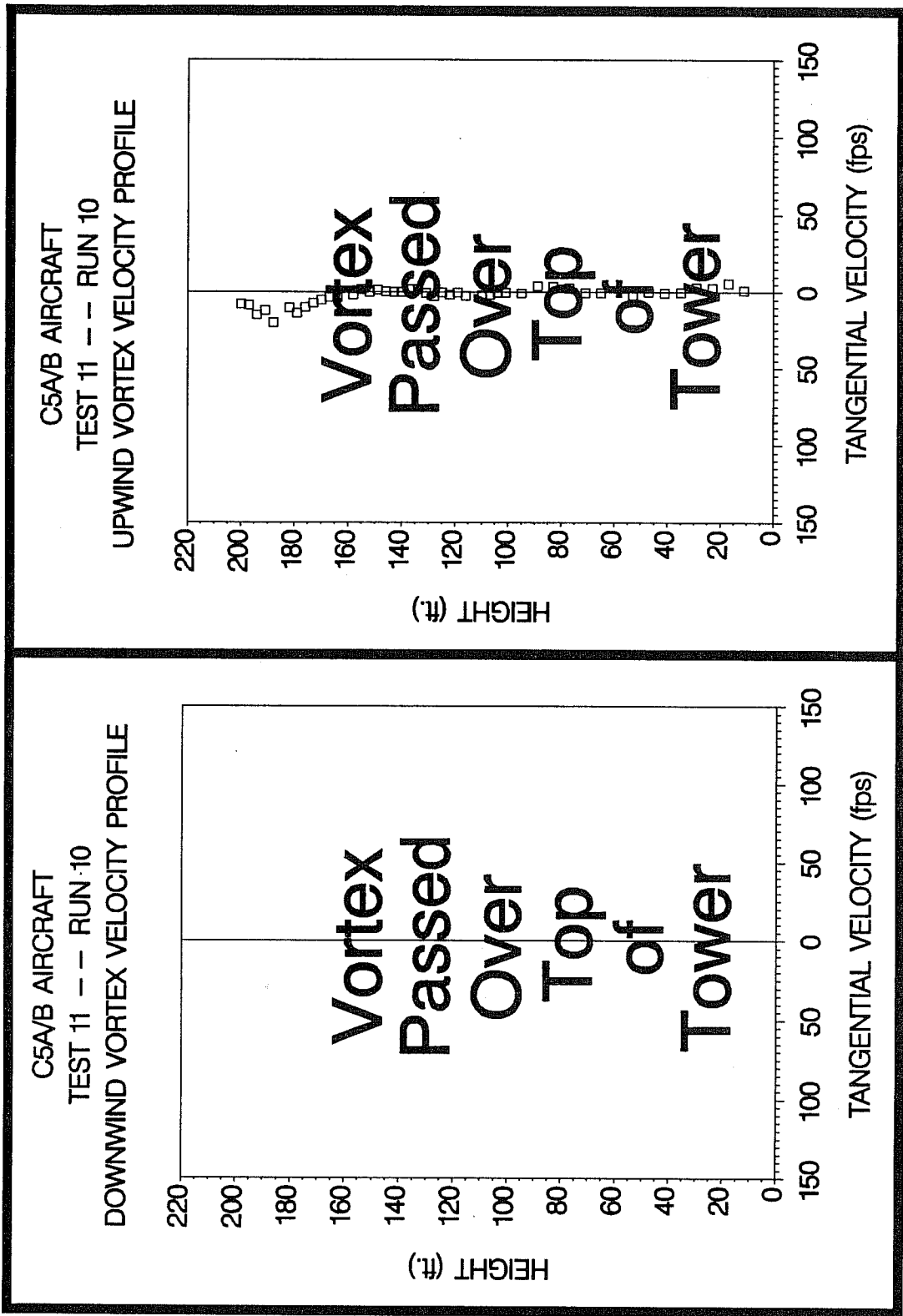


Figure C-134. C5A/B upwind (top) and downwind (bottom) vortex tangential velocity profile at maximum intensity from Test 11, Run 10, ambient wind speed=17.7 fps,  $\delta_F=80\%$ , IAS=130 knots, GW=514.0k lbs. Ages, radii, and velocities of the vortex cores are 29 and (N/A) sec., (N/A) and (N/A) ft., and (N/A) and (N/A) fps, respectively.

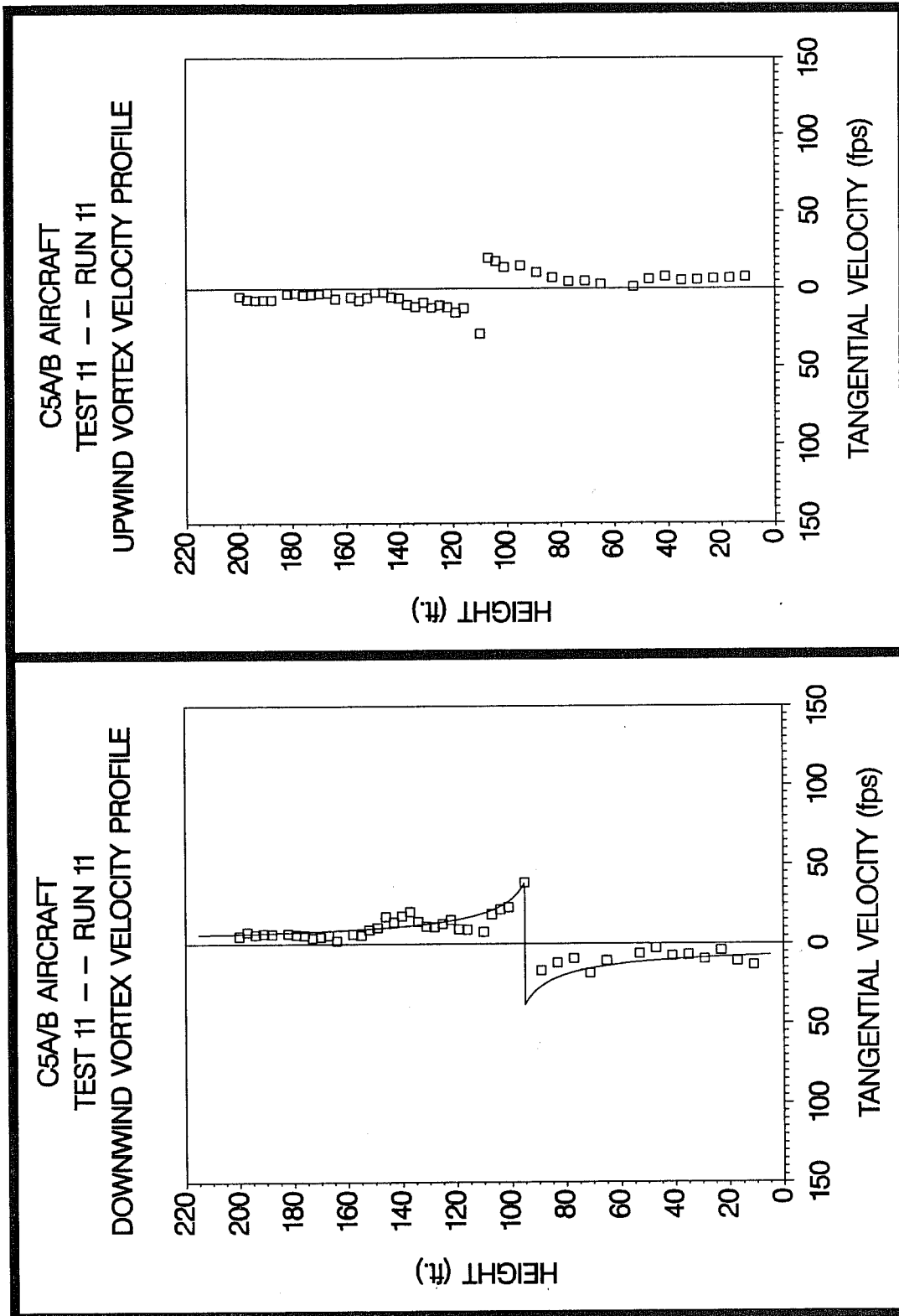


Figure C-135. C5A/B upwind (top) and downwind (bottom) vortex tangential velocity profile at maximum intensity from Test 11, Run 11, ambient wind speed=14.5 fps,  $\delta_F=80\%$ , IAS=130 knots, GW=511.0k lbs. Ages, radii, and velocities of the vortex cores are 96 and 44 sec., (N/A) and 6.1 ft., and 29.2 and 38.4 fps, respectively.

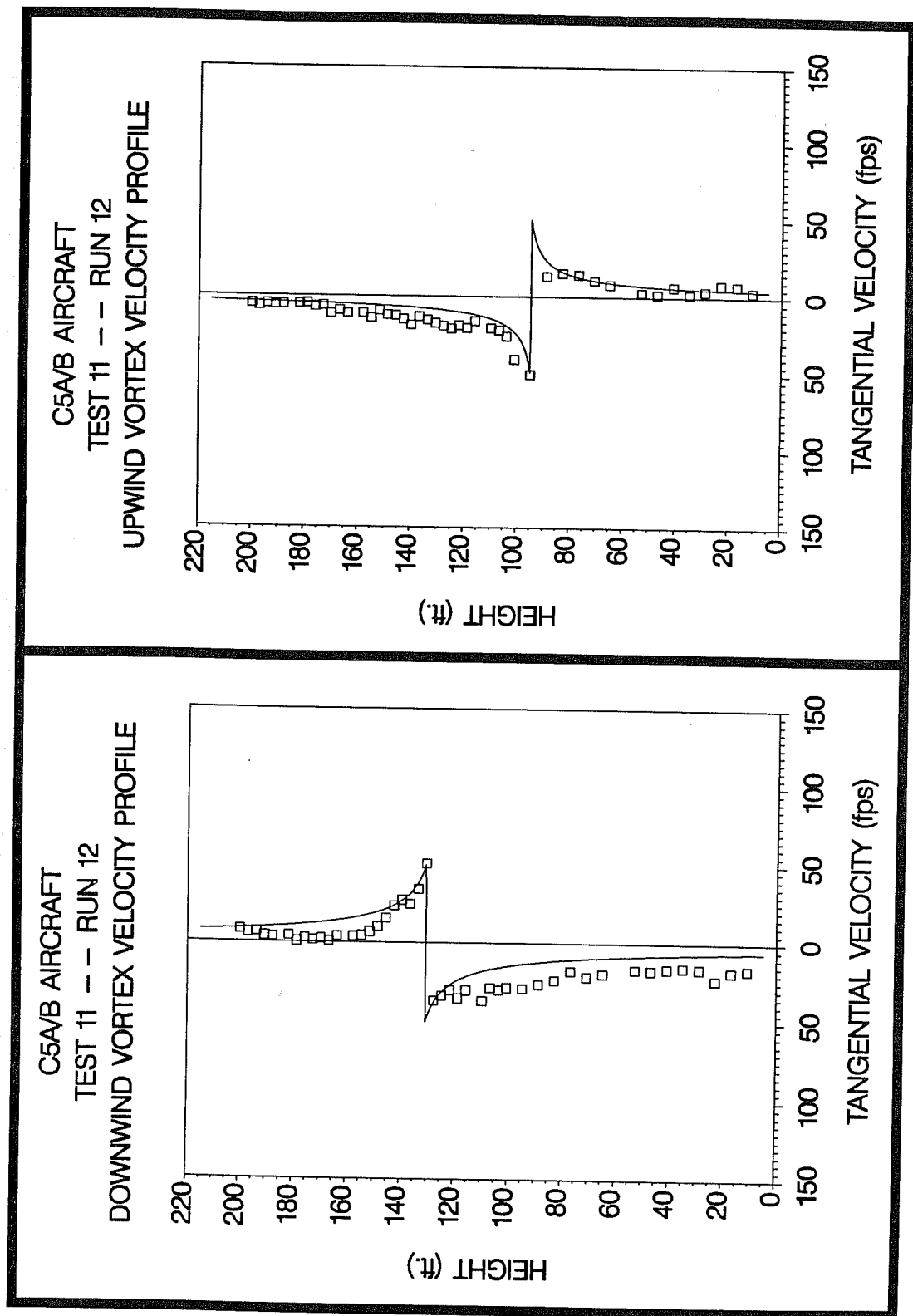


Figure C-136. C5A/B upwind (top) and downwind (bottom) vortex tangential velocity profile at maximum intensity from Test 11, Run 12, ambient wind speed=14.2 fps,  $\delta_F=80\%$ , IAS=130 knots, GW=508.0k lbs. Ages, radii, and velocities of the vortex cores are 37 and 20 sec., 2.0 and 4.1 ft., and 50.3 and 50.4 fps, respectively.

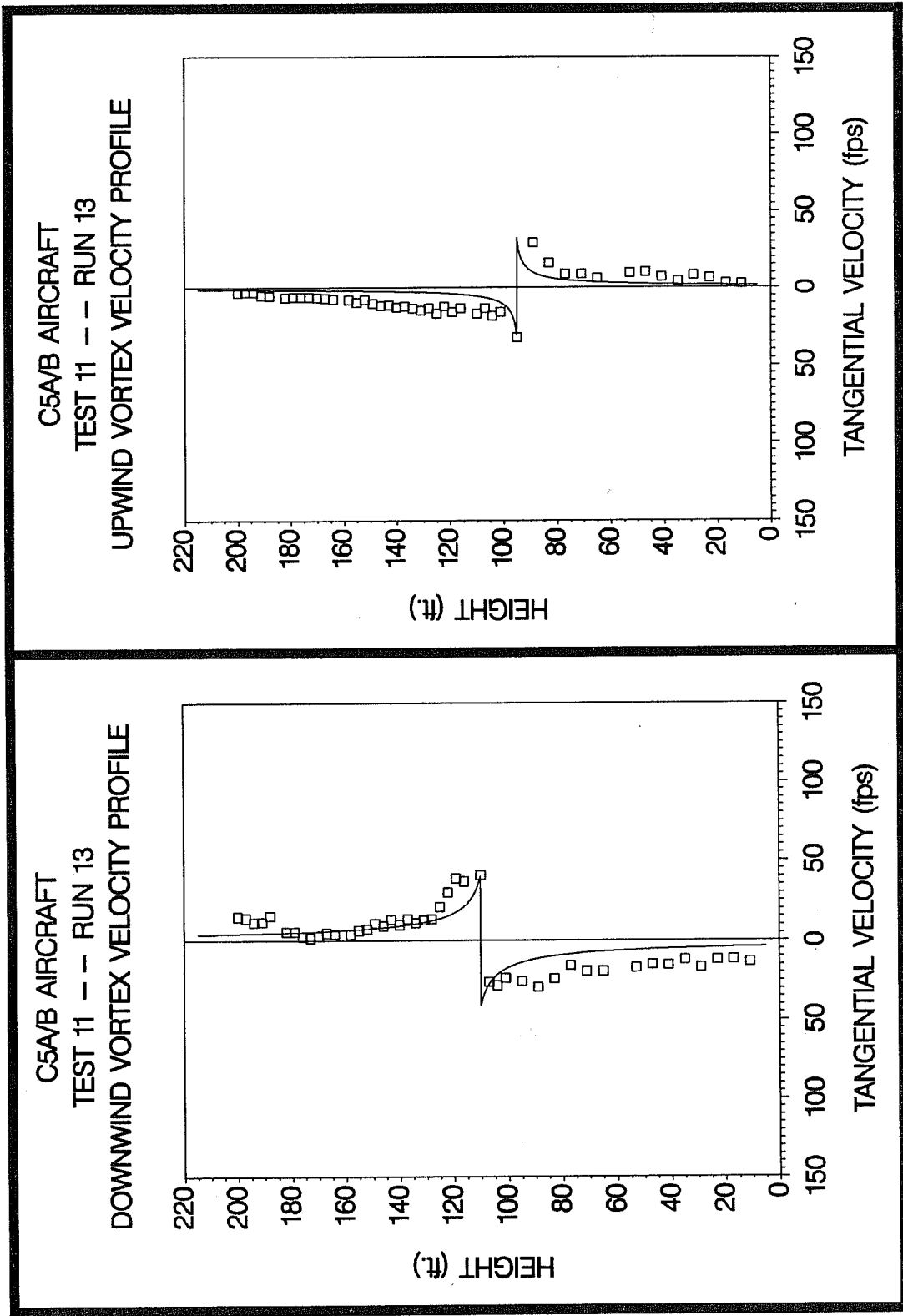
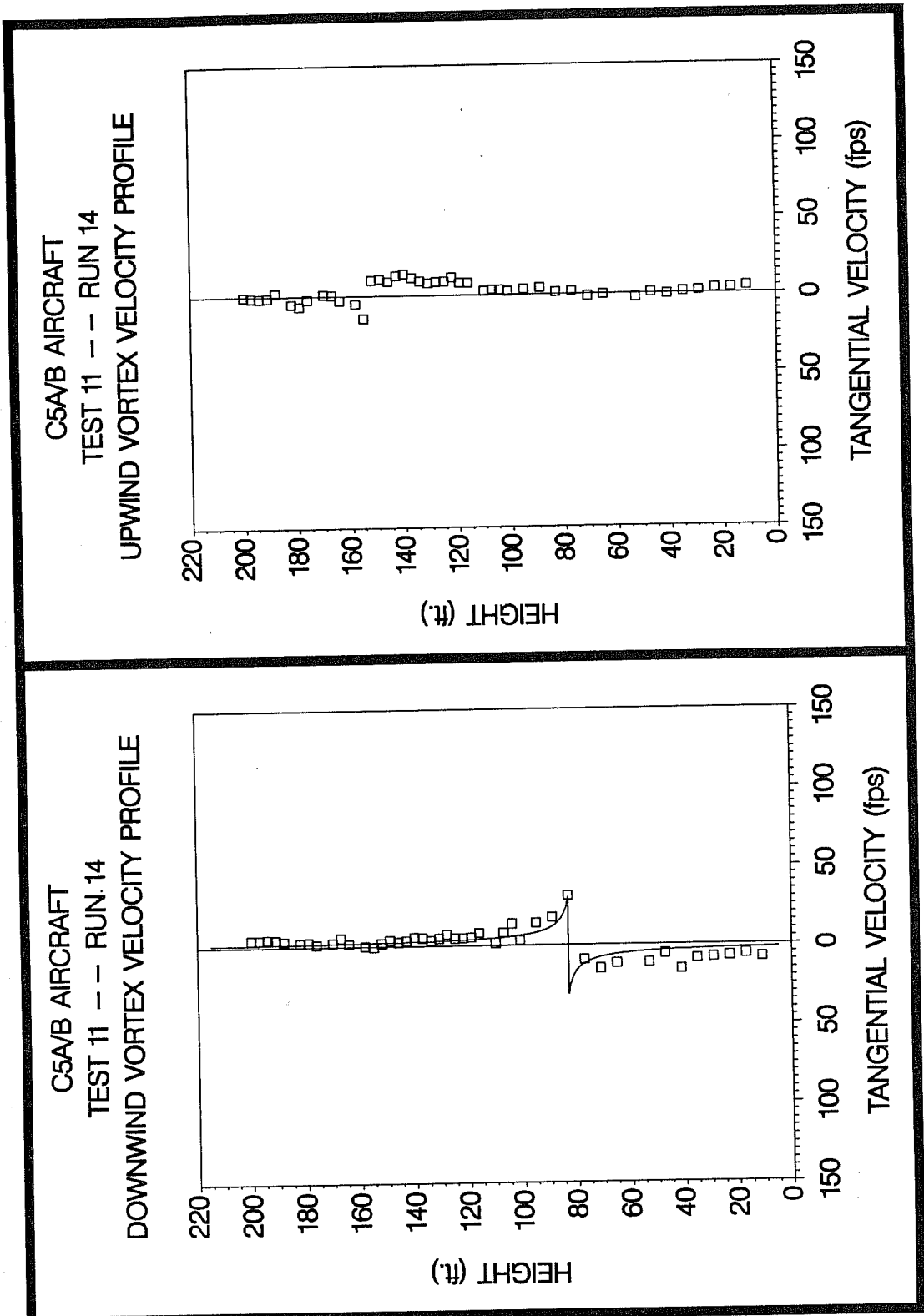
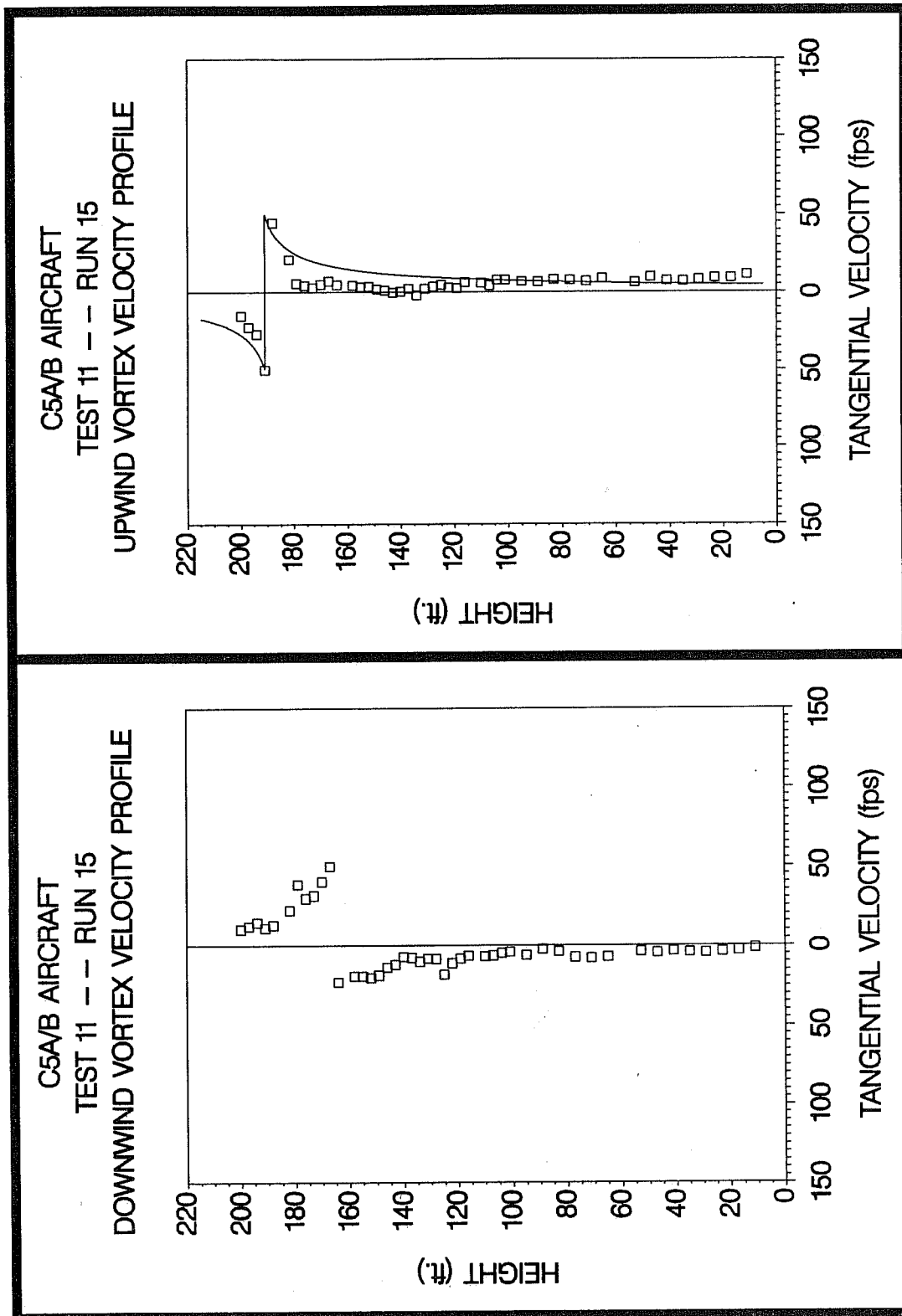


Figure C-137. C5A/B upwind (top) and downwind (bottom) vortex tangential velocity profile at maximum intensity from Test 11, Run 13, ambient wind speed=17.2 fps,  $\delta_F=80\%$ , IAS=130 knots, GW=505.0k lbs. Ages, radii, and velocities of the vortex cores are 47 and 29 sec., 0.9 and 2.7 ft., and 32.4 and 40.6 fps, respectively.



**Figure C-138.** C5A/B upwind (top) and downwind (bottom) vortex tangential velocity profile at maximum intensity from Test 11, Run 14, ambient wind speed=16.3 fps,  $\delta_F=80\%$ , IAS=130 knots, GW=503.0k lbs. Ages, radii, and velocities of the vortex cores are 77 and 44 sec., (N/A) and 1.3 ft., and 14.5 and 31.3 fps, respectively.



**Figure C-139.** C5A/B upwind (top) and downwind (bottom) vortex tangential velocity profile at maximum intensity from Test 11, Run 15, ambient wind speed=18.5 fps,  $\delta_F=80\%$ , IAS=130 knots, GW=500.0k lbs. Ages, radii, and velocities of the vortex cores are 41 and 31 sec., 4.5 and (N/A) ft., and 49.9 and 49.5 fps, respectively.

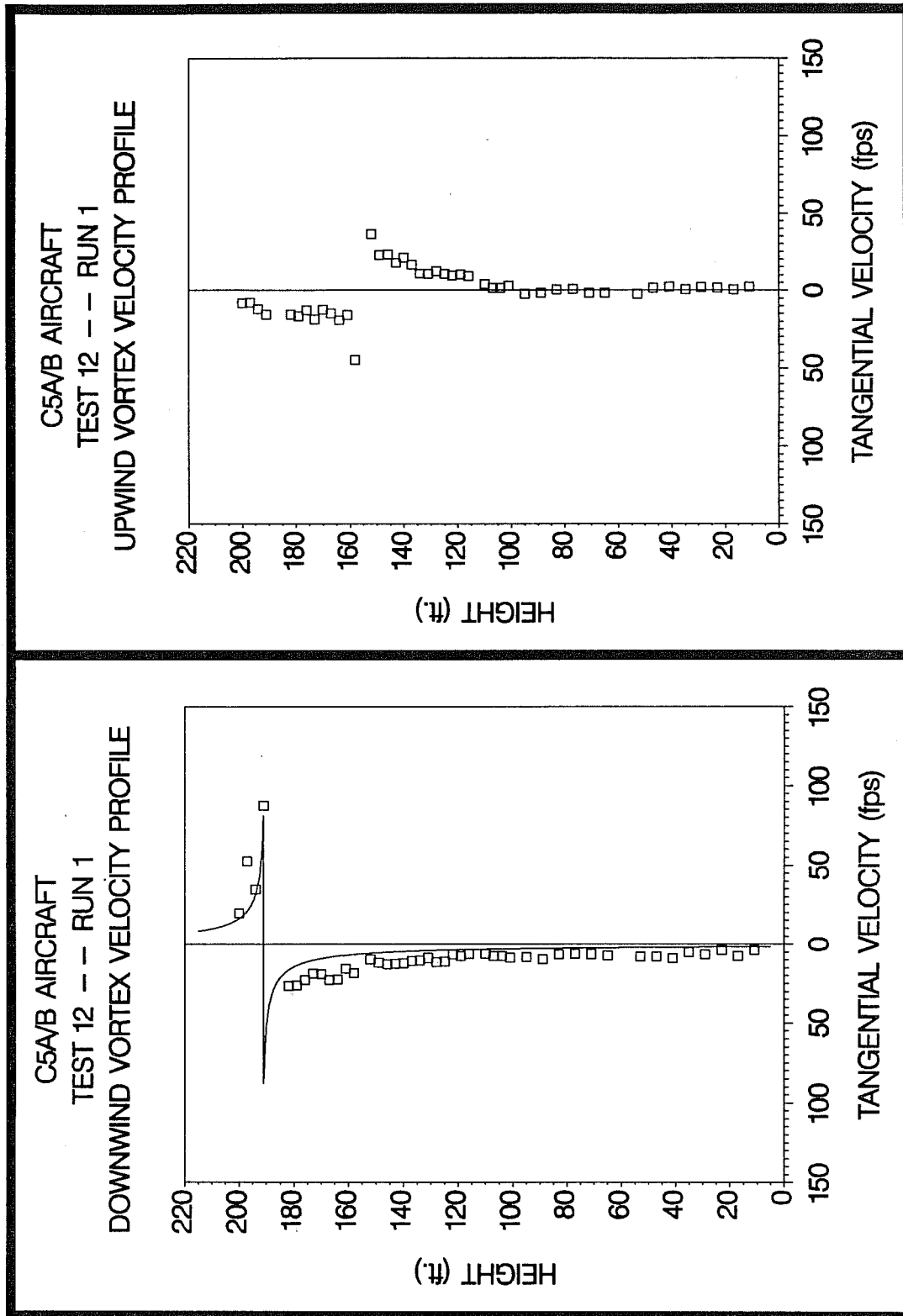


**Figure C-140.** C5A/B upwind (top) and downwind (bottom) vortex tangential velocity profile at maximum intensity from Test 12, Run 1, ambient wind speed=14.5 fps,  $\delta_F=80\%$ , IAS=130 knots, GW=520.0k lbs. Ages, radii, and velocities of the vortex cores are 40 and 24 sec., (N/A) and 0.6 ft., and 44.9 and 87.7 fps, respectively.

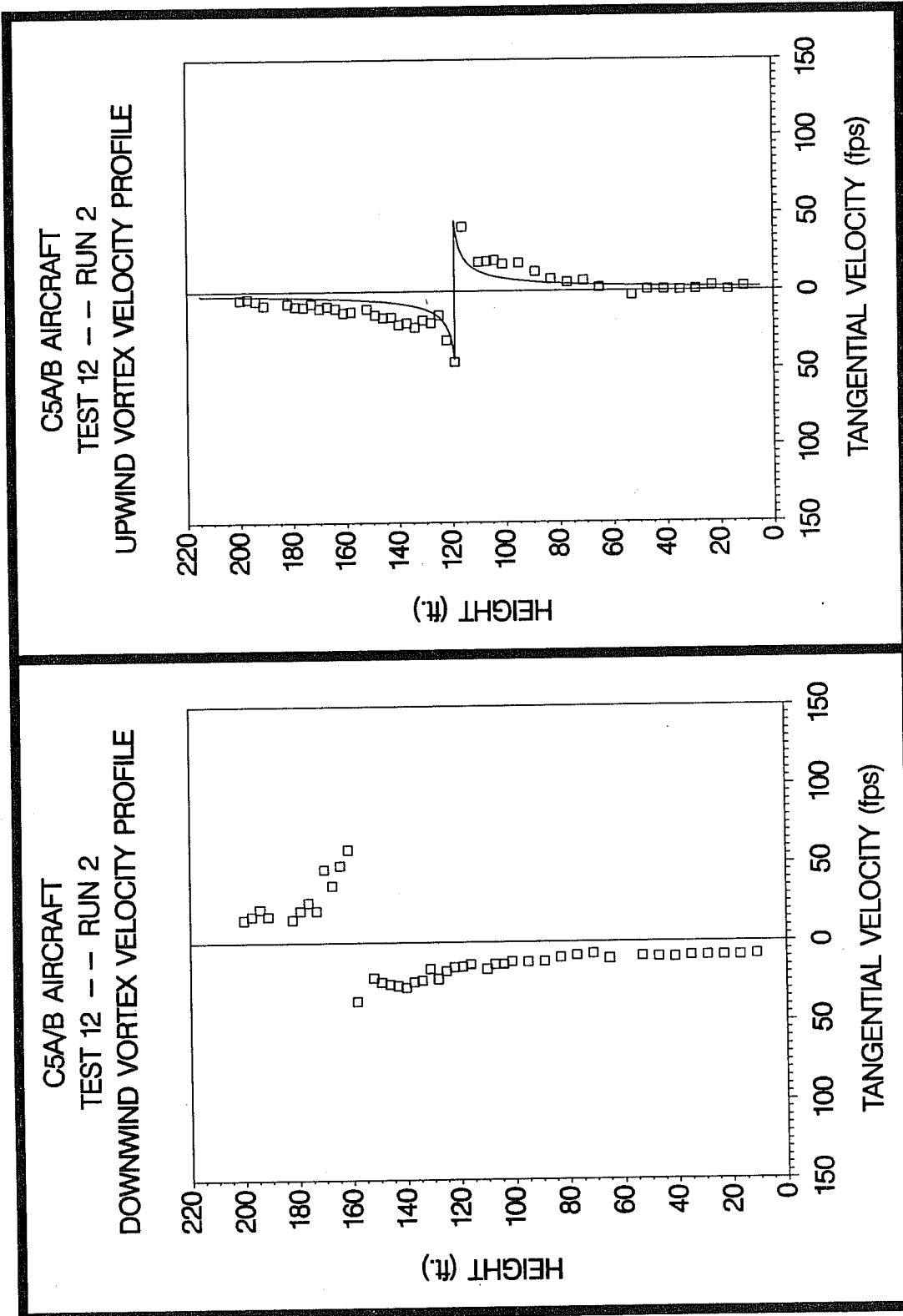


Figure C-141. C5A/B upwind (top) and downwind (bottom) vortex tangential velocity profile at maximum intensity from Test 12, Run 2, ambient wind speed=13.3 fps,  $\delta_F=80\%$ , IAS=130 knots, GW=517.0k lbs. Ages, radii, and velocities of the vortex cores are 39 and 26 sec., 1.2 and (N/A) ft., and 45.5 and 58.9 fps, respectively.

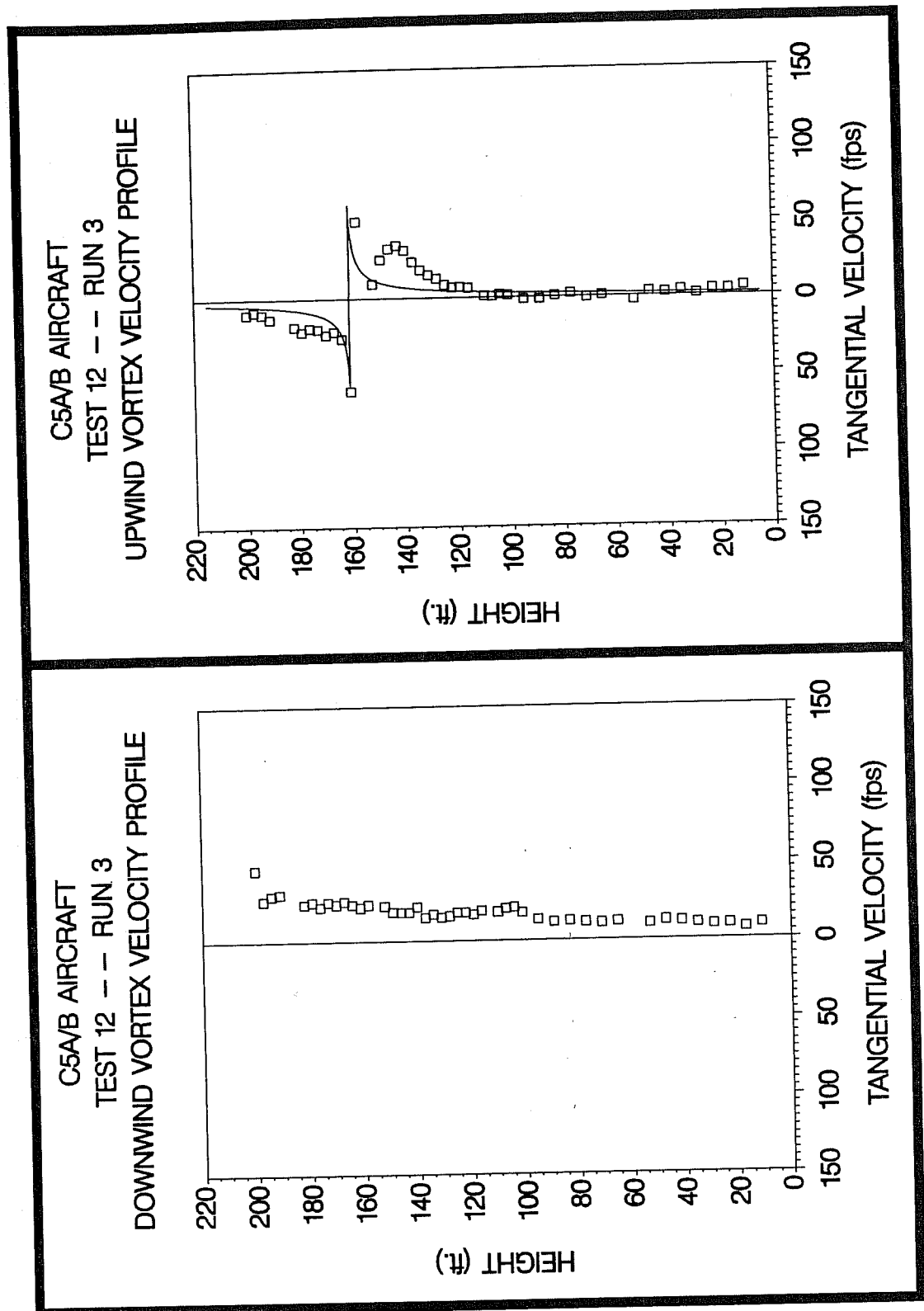


Figure C-142. C5A/B upwind (top) and downwind (bottom) vortex tangential velocity profile at maximum intensity from Test 12, Run 3, ambient wind speed=16.8 fps,  $\delta_F=80\%$ , IAS=130 knots, GW=515.0k lbs. Ages, radii, and velocities of the vortex cores are 41 and 28 sec., 0.7 and (N/A) ft., and 61.3 and 35.6 fps, respectively.

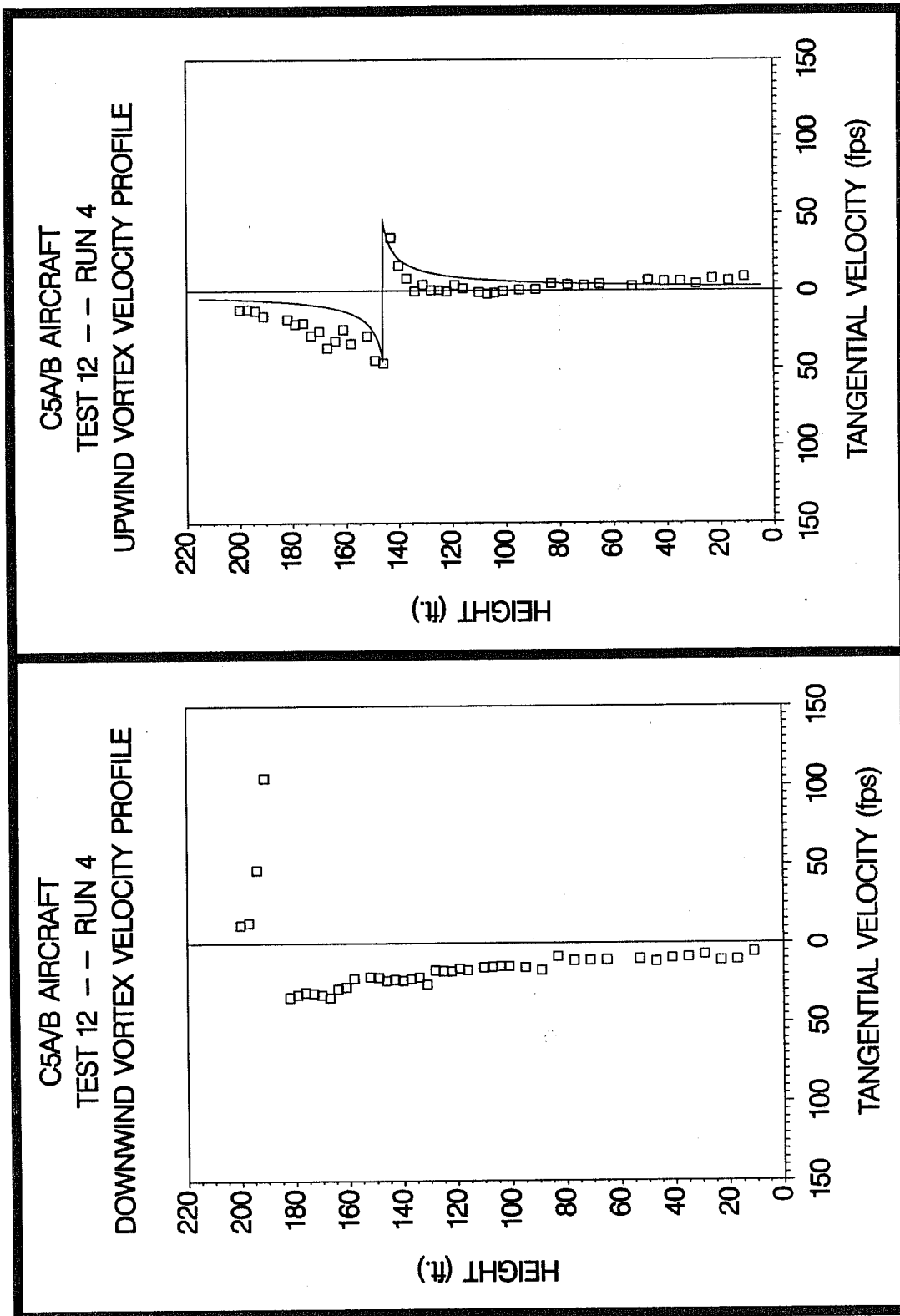
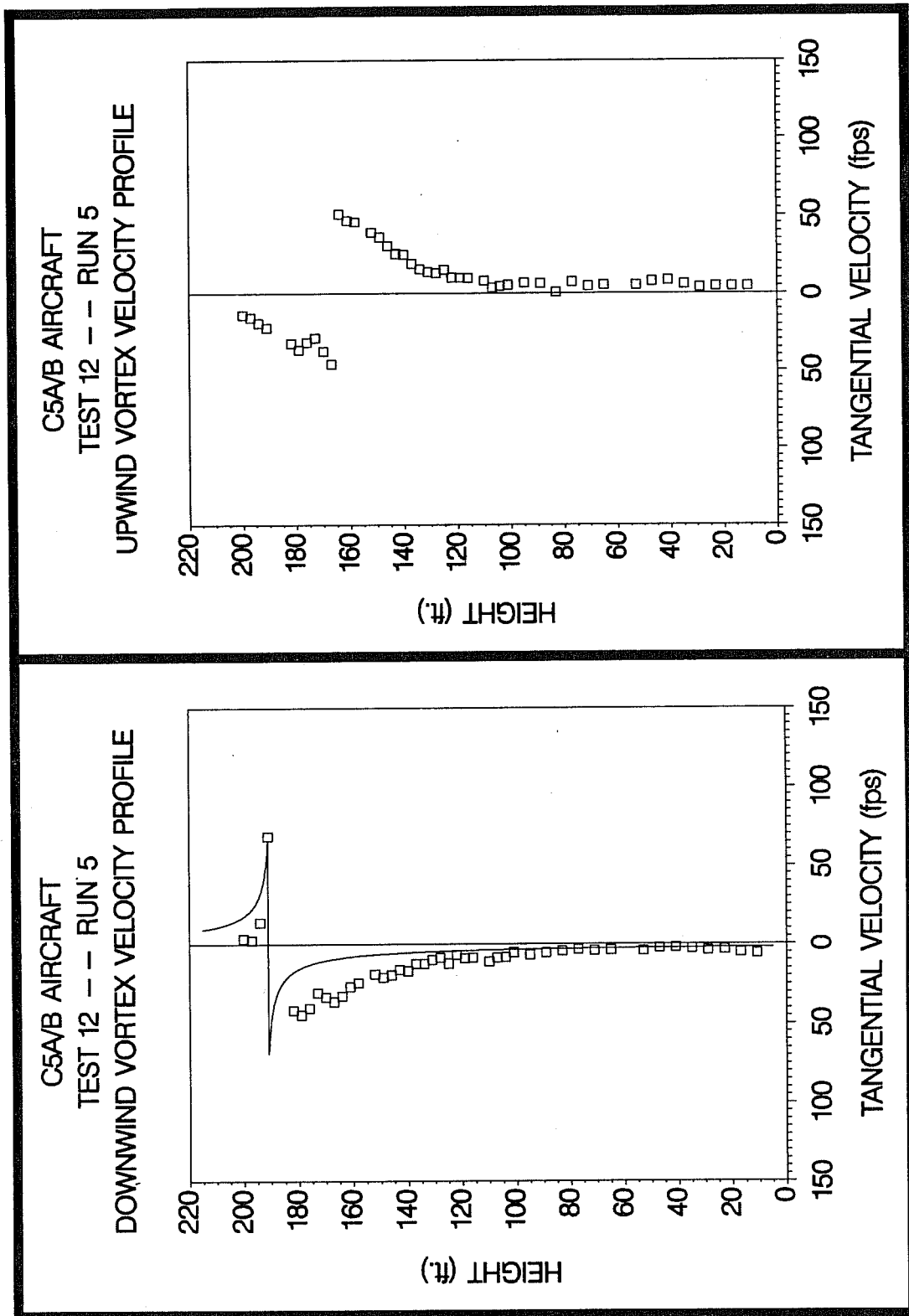


Figure C-143. C5A/B upwind (top) and downwind (bottom) vortex tangential velocity profile at maximum intensity from Test 12, Run 4, ambient wind speed=20.2 fps,  $\delta_F=80\%$ , IAS=130 knots, GW=512.0k lbs. Ages, radii, and velocities of the vortex cores are 30 and 22 sec., 1.9 and (N/A) ft., and 46.7 and 104.9 fps, respectively.



**Figure C-144.** C5A/B upwind (top) and downwind (bottom) vortex tangential velocity profile at maximum intensity from Test 12, Run 5, ambient wind speed=24.4 fps,  $\delta_F=100\%$ , IAS=130 knots, GW=510.0k lbs. Ages, radii, and velocities of the vortex cores are 12 and 7 sec., (N/A) and 1.0 ft., and 45.9 and 68.8 fps, respectively.

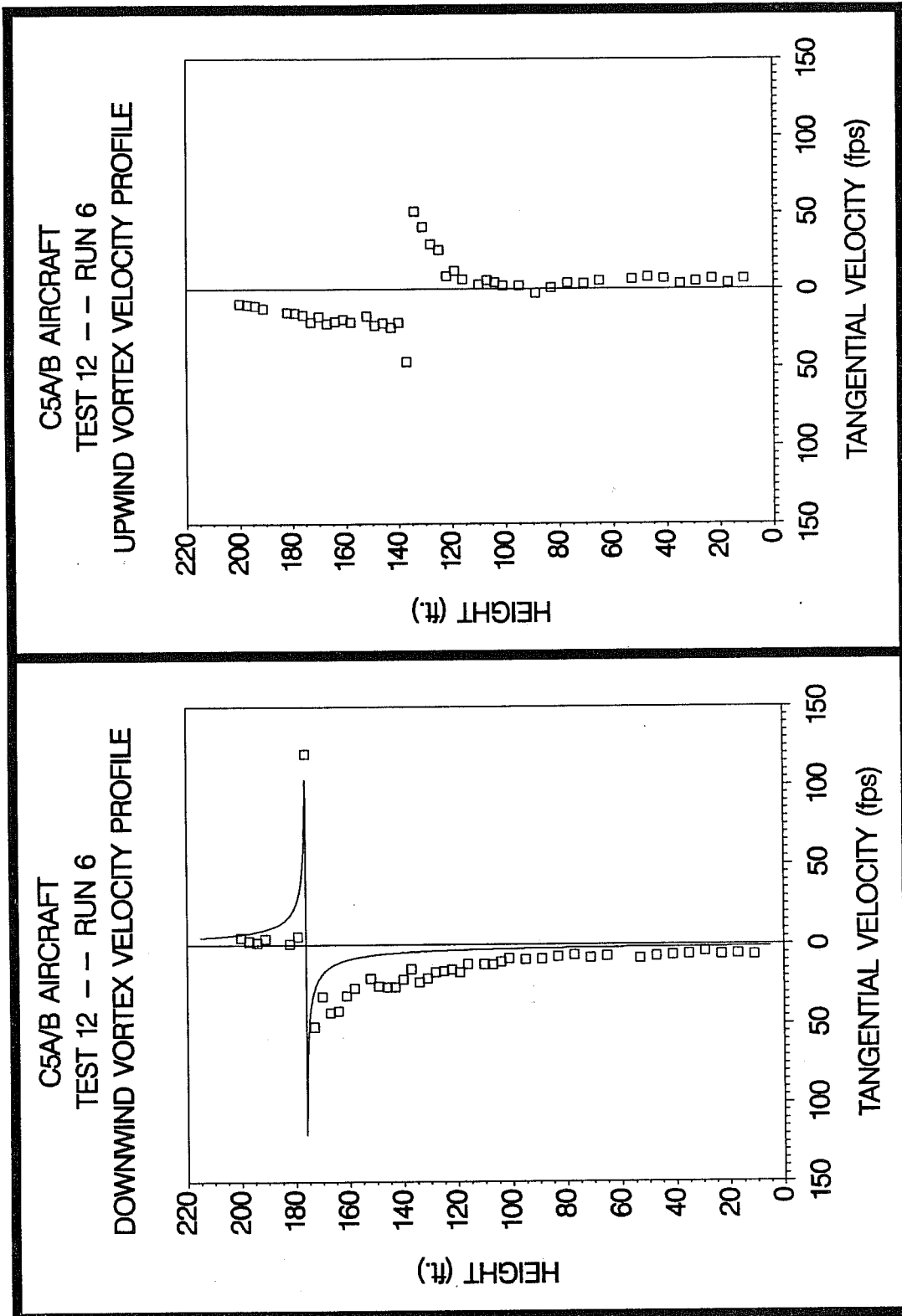


Figure C-145. C5A/B upwind (top) and downwind (bottom) vortex tangential velocity profile at maximum intensity from Test 12, Run 6, ambient wind speed=21.9 fps,  $\delta_F=40\%$ , IAS=150 knots, GW=507.0k lbs. Ages, radii, and velocities of the vortex cores are 15 and 7 sec., (N/A) and 0.3 ft., and 46.6 and 120.2 fps, respectively.

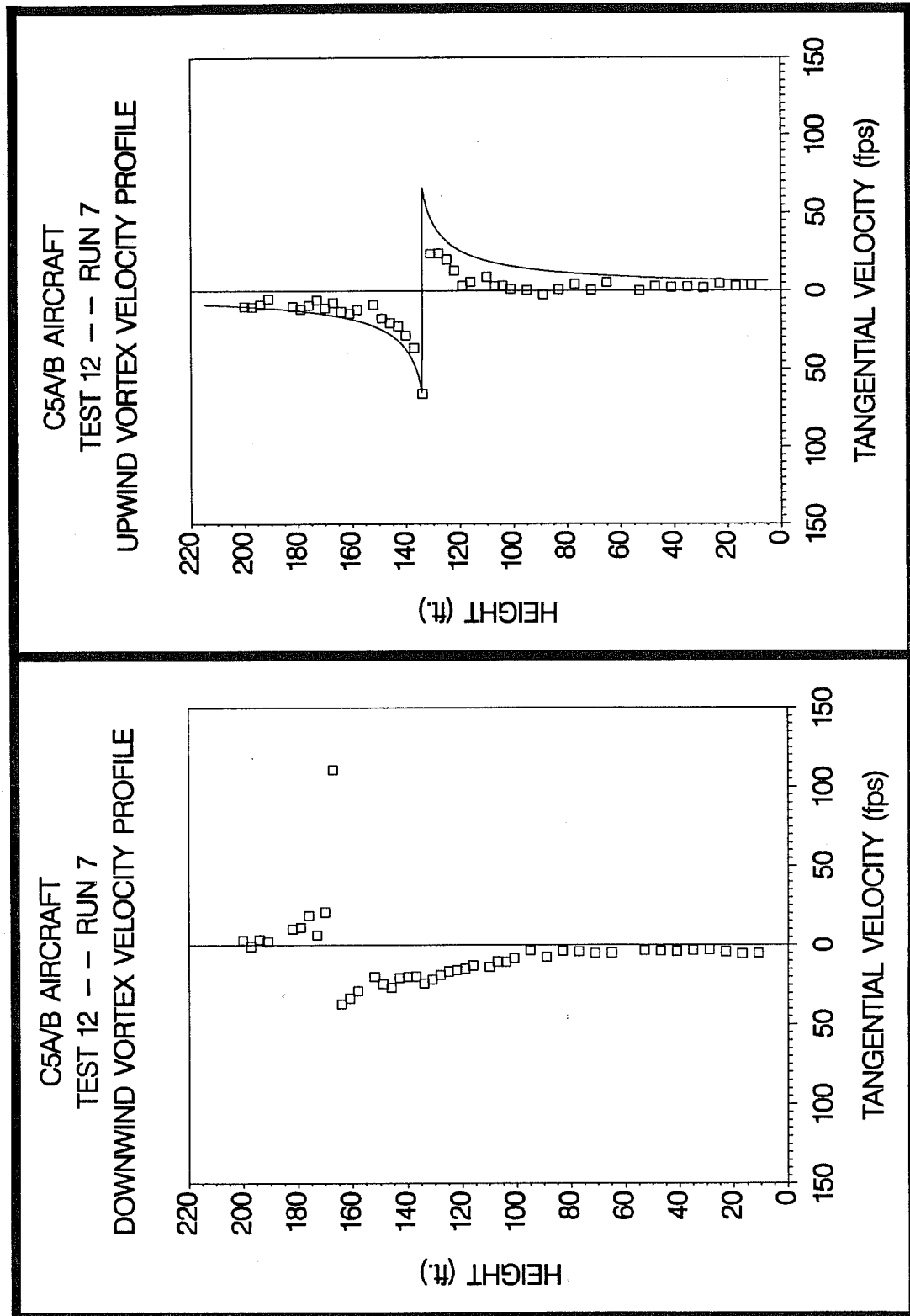


Figure C-146. C5A/B upwind (top) and downwind (bottom) vortex tangential velocity profile at maximum intensity from Test 12, Run 7, ambient wind speed=19.3 fps,  $\delta_F=40\%$ , IAS=155 knots, GW=504.0k lbs. Ages, radii, and velocities of the vortex cores are 19 and 10 sec., 3.3 and (N/A) ft., and 65.9 and 110.9 fps, respectively.

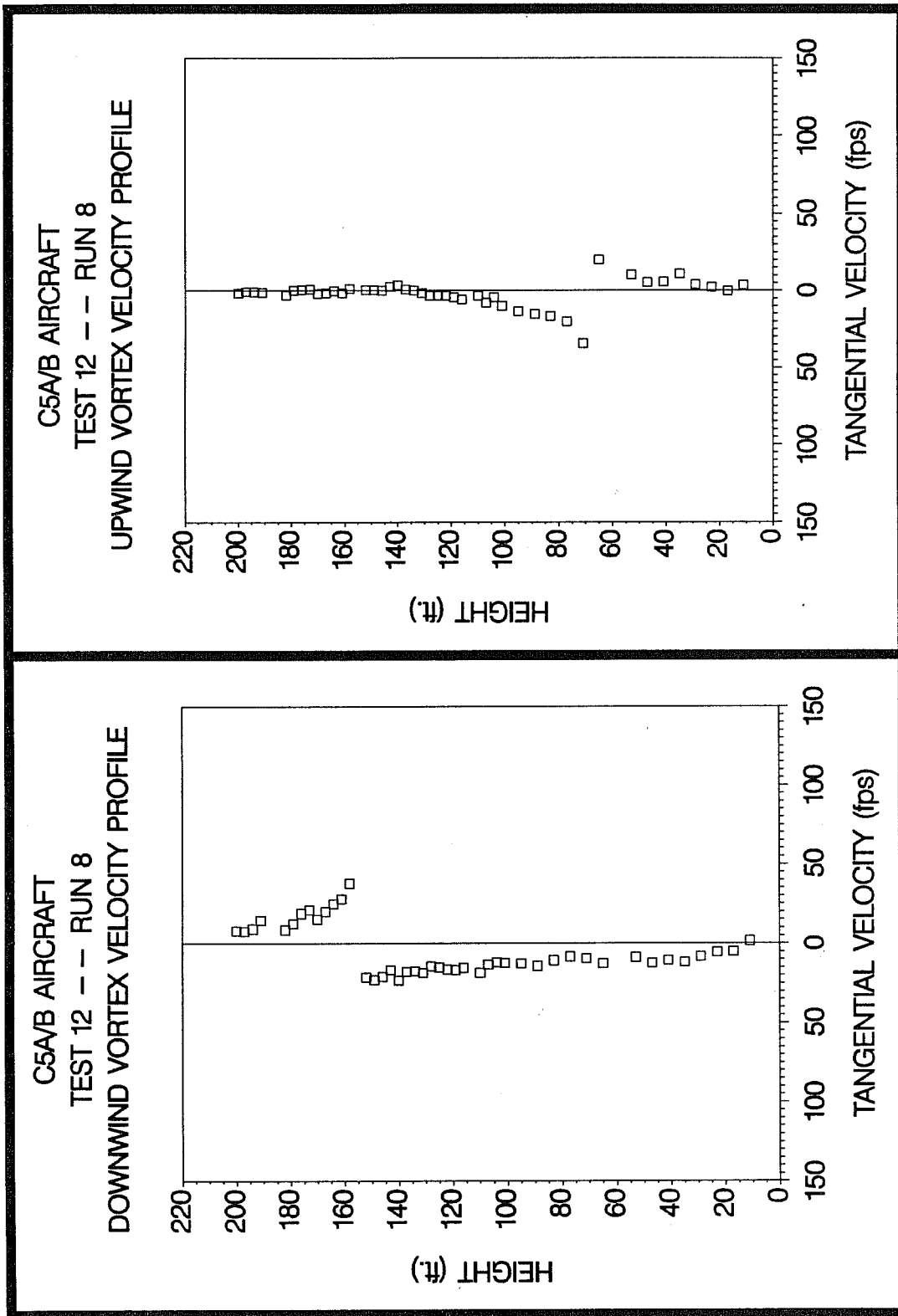


Figure C-147. C5A/B upwind (top) and downwind (bottom) vortex tangential velocity profile at maximum intensity from Test 12, Run 8, ambient wind speed=13.7 fps,  $\delta_F=80\%$ , IAS=130 knots, GW=501.0k lbs. Ages, radii, and velocities of the vortex cores are 75 and 45 sec., (N/A) and (N/A) ft., and 34.5 and 37.7 fps, respectively.

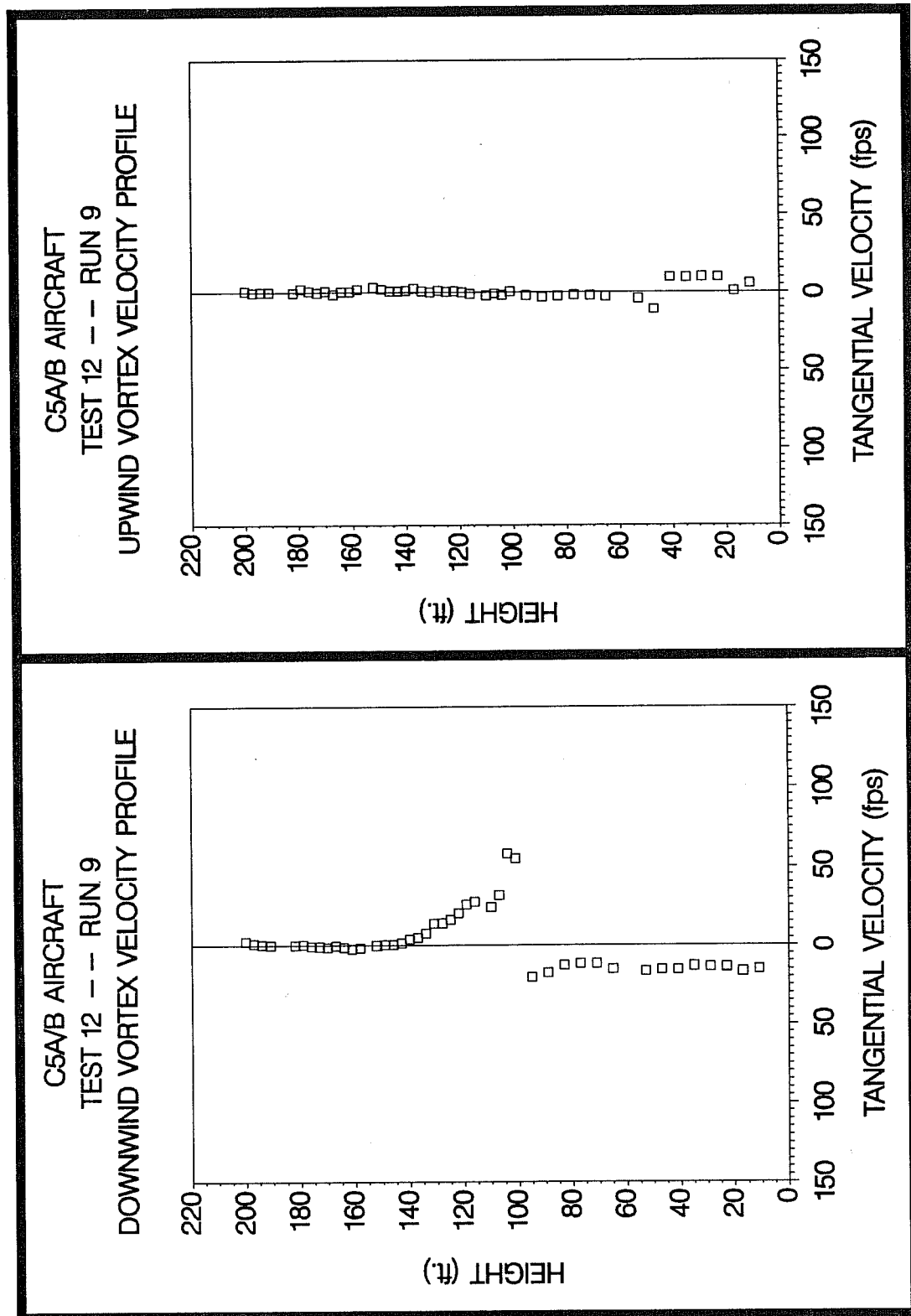


Figure C-148. C5A/B upwind (top) and downwind (bottom) vortex tangential velocity profile at maximum intensity from Test 12, Run 9, ambient wind speed=12.0 fps,  $\delta_F=80\%$ , IAS=130 knots, GW=498.0k lbs. Ages, radii, and velocities of the vortex cores are 73 and 43 sec., (N/A) and (N/A) ft., and 10.9 and 55.1 fps, respectively.

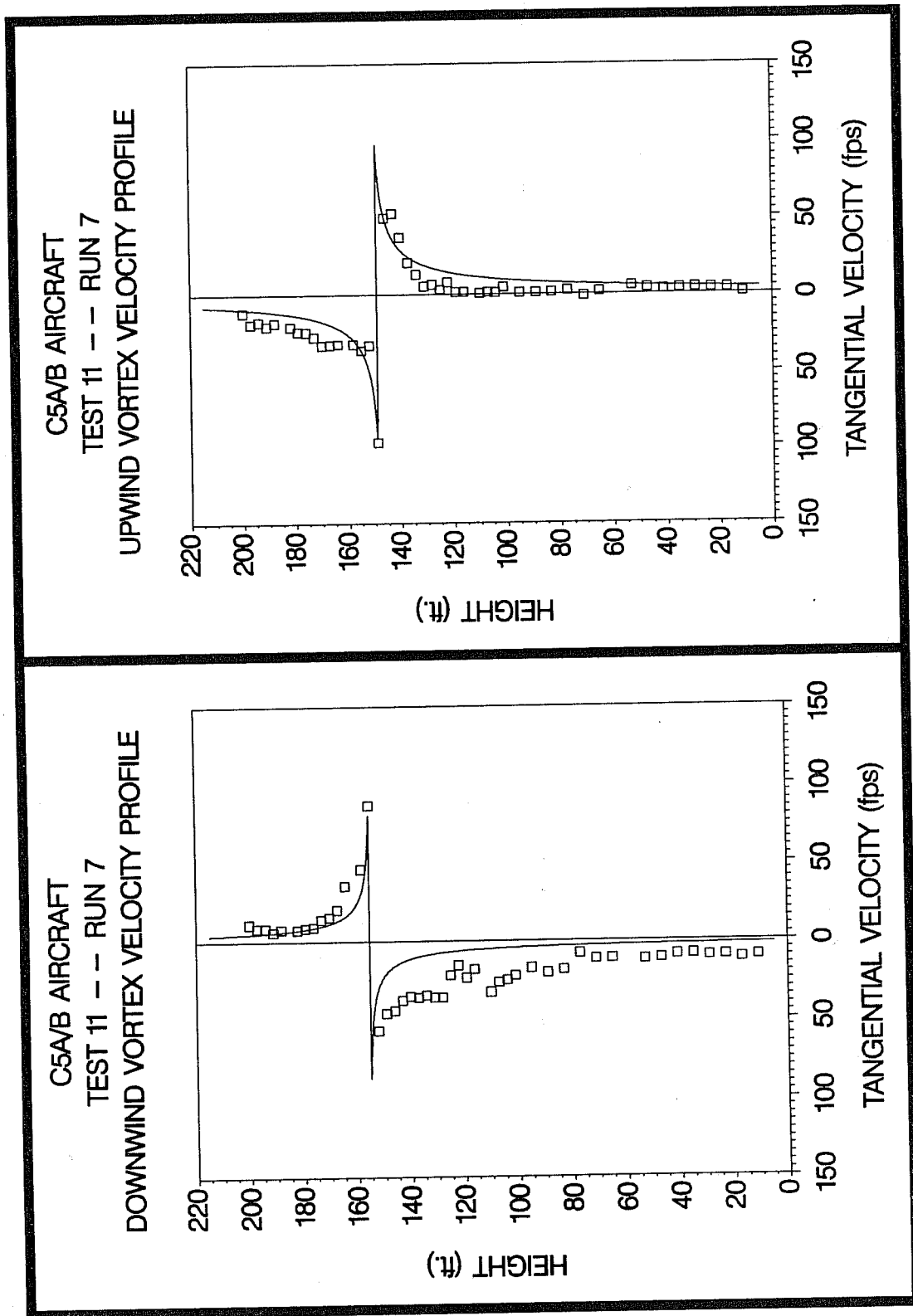


Figure C-131. C5A/B upwind (top) and downwind (bottom) vortex tangential velocity profile at maximum intensity from Test 11, Run 7, ambient wind speed=18.7 fps,  $\delta_F=80\%$ , IAS=130 knots, GW=524.0k lbs. Ages, radii, and velocities of the vortex cores are 19 and 11 sec., 1.3 and 0.6 ft., and 97.1 and 87.0 fps, respectively.

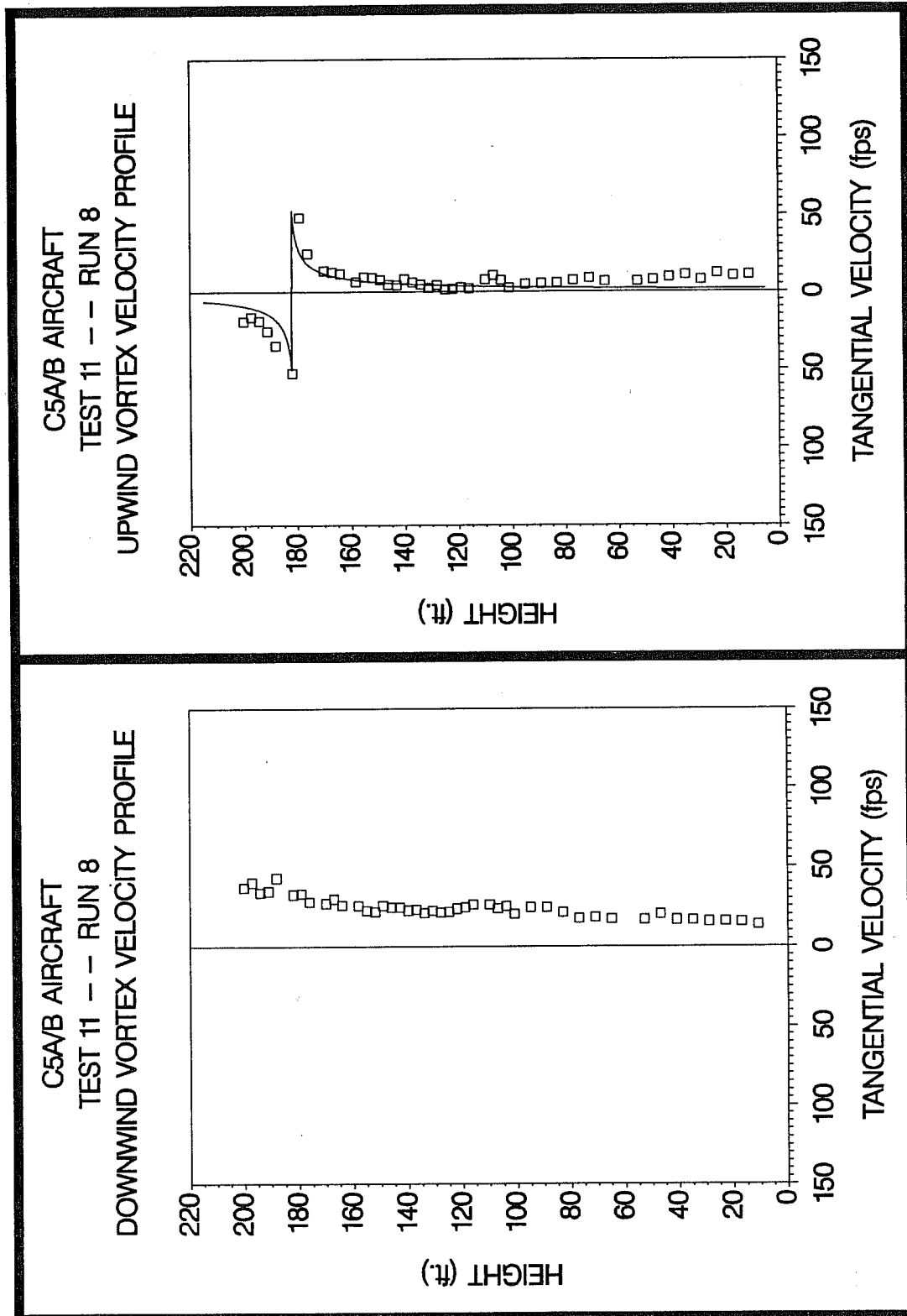


Figure C-132. C5A/B upwind (top) and downwind (bottom) vortex tangential velocity profile at maximum intensity from Test 11, Run 8, ambient wind speed=16.8 fps,  $\delta_P=80\%$ , IAS=130 knots, GW=520.0k lbs. Ages, radii, and velocities of the vortex cores are 26 and 17 sec., 1.1 and (N/A) ft., and 52.6 and (N/A) fps, respectively.

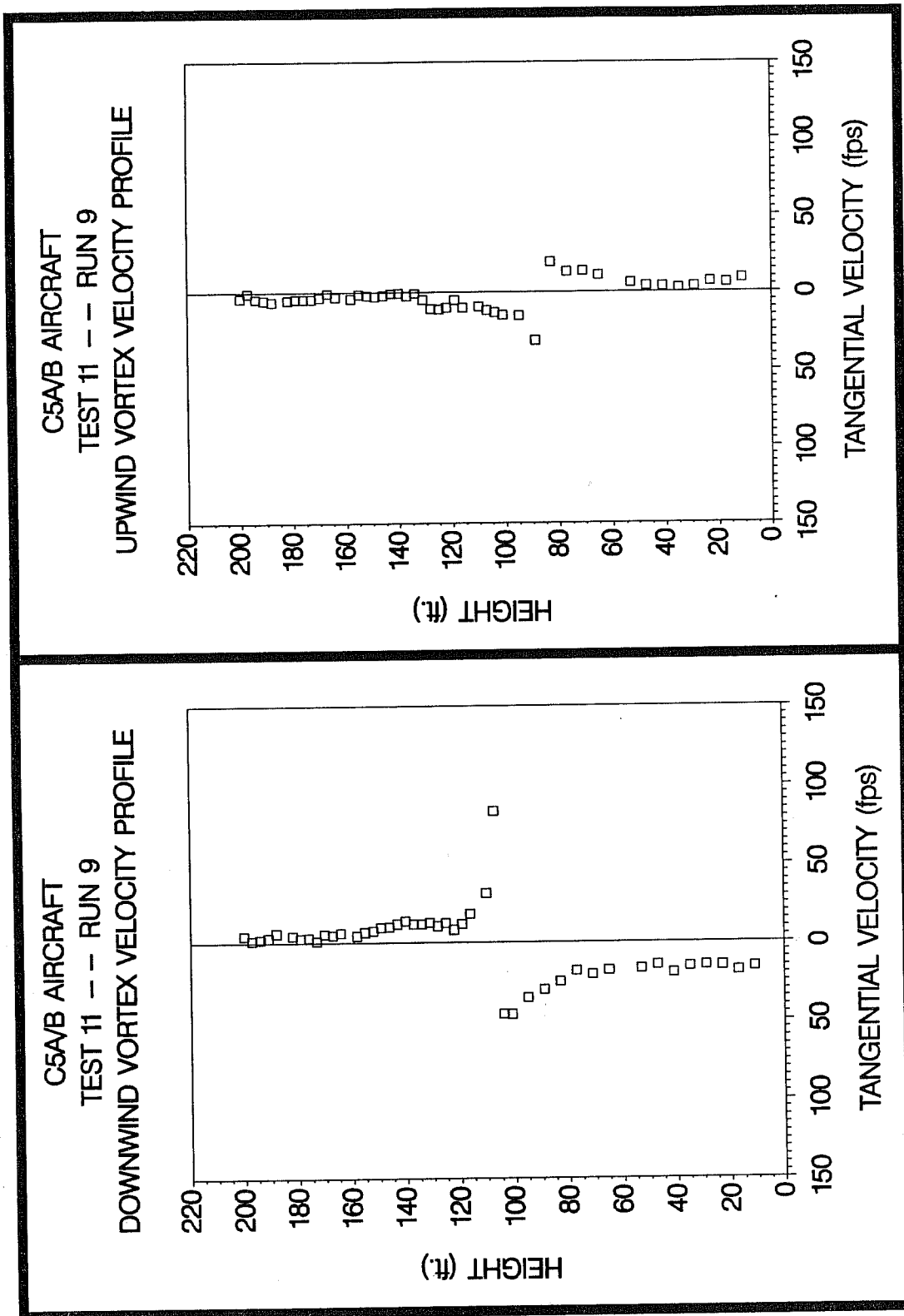


Figure C-133. C5A/B upwind (top) and downwind (bottom) vortex tangential velocity profile at maximum intensity from Test 11, Run 9, ambient wind speed=12.4 fps,  $\delta_F=80\%$ , IAS=130 knots, GW=517.0k lbs. Ages, radii, and velocities of the vortex cores are 63 and 28 sec., (N/A) and (N/A) ft., and 31.2 and 83.4 fps, respectively.

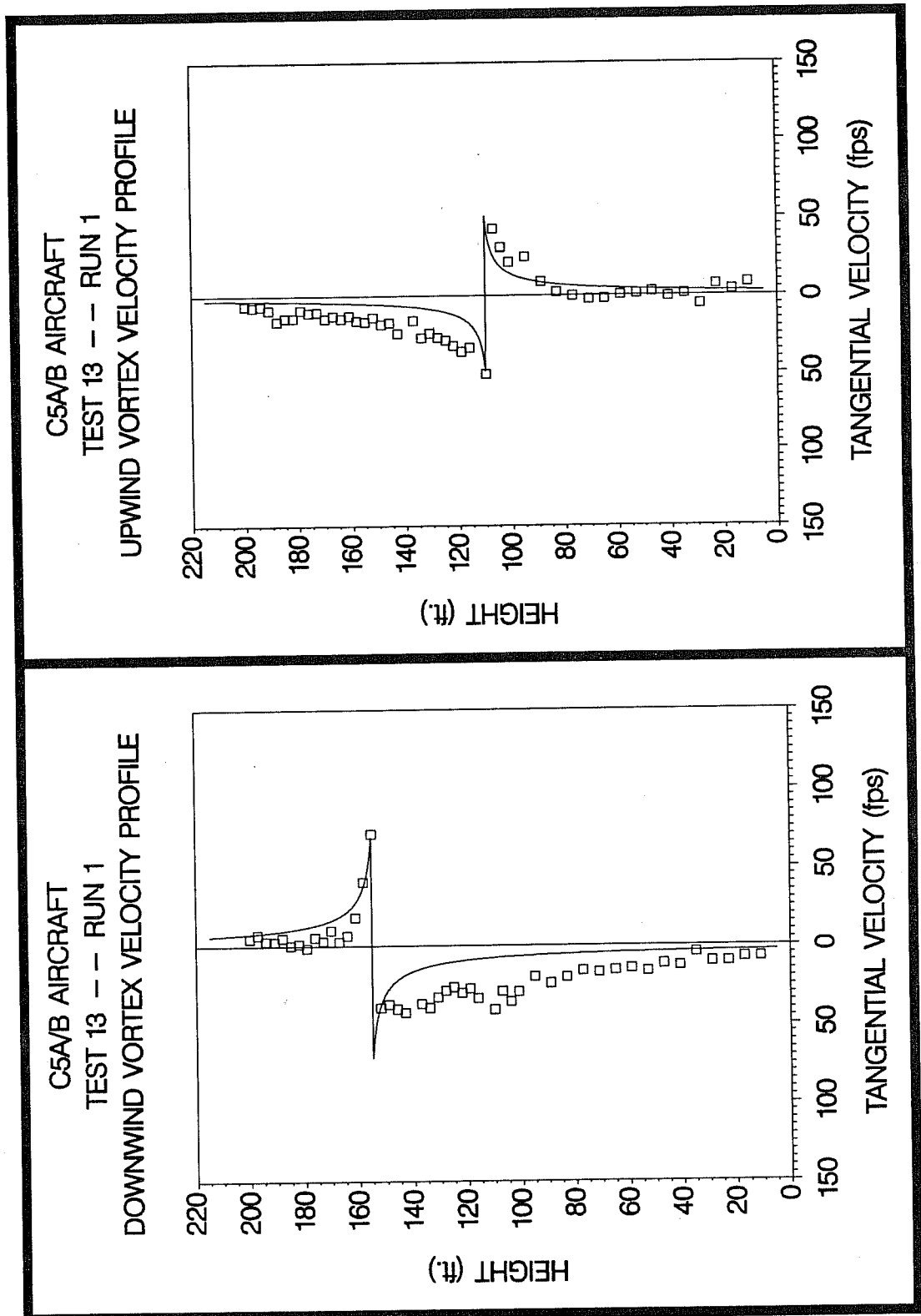
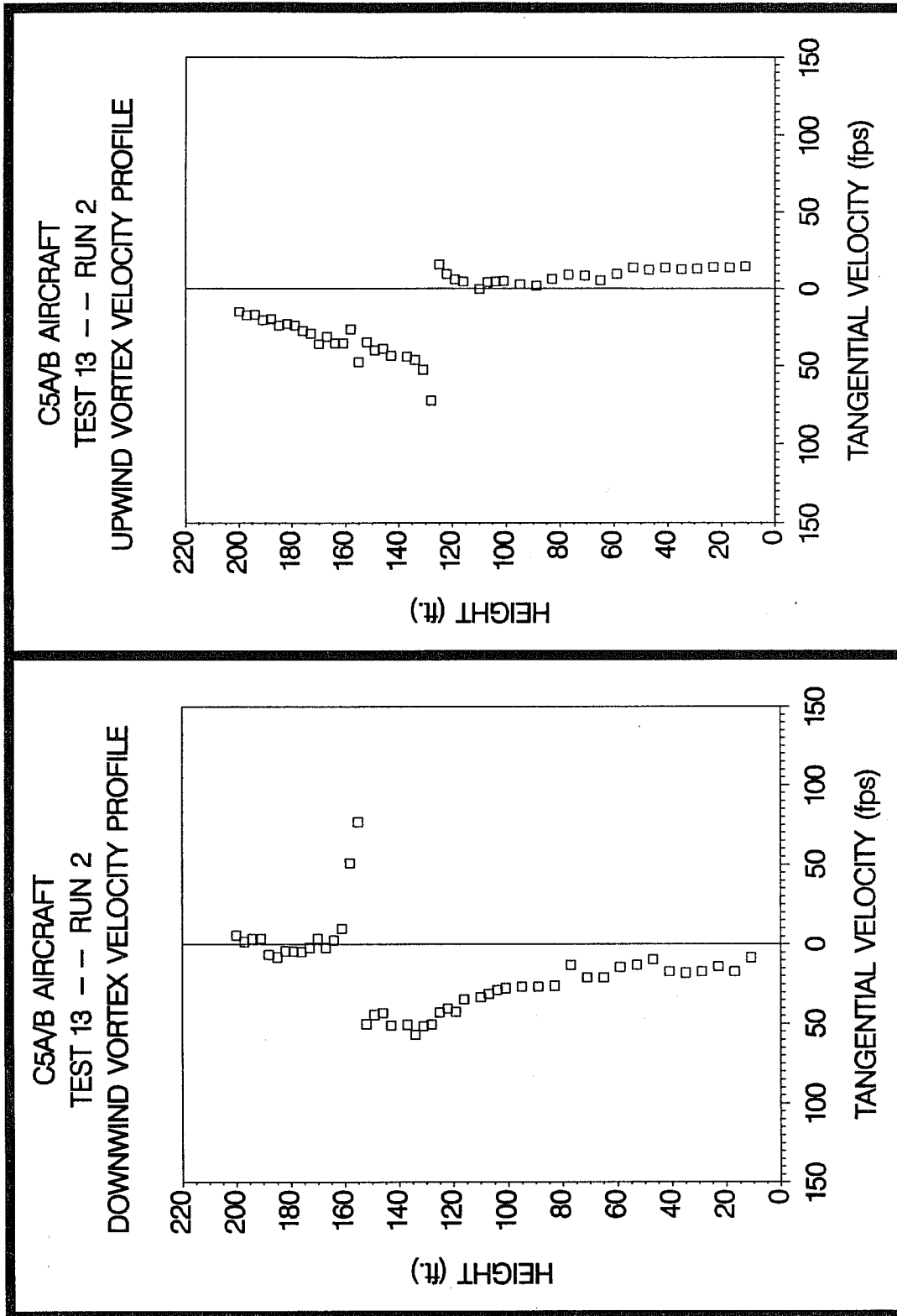


Figure C-149. C5A/B upwind (top) and downwind (bottom) vortex tangential velocity profile at maximum intensity from Test 13, Run 1, ambient wind speed=31.8 fps,  $\delta_F=100\%$ , IAS=150 knots, GW=696.0k lbs. Ages, radii, and velocities of the vortex cores are 13 and 7 sec., 1.2 and 1.4 ft., and 50.6 and 71.2 fps, respectively.



**Figure C-150.** C5A/B upwind (top) and downwind (bottom) vortex tangential velocity profile at maximum intensity from Test 13, Run 2, ambient wind speed=28.6 fps,  $\delta_F=100\%$ , IAS=150 knots, GW=693.0k lbs. Ages, radii, and velocities of the vortex cores are 11 and 6 sec., (N/A) and (N/A) ft., and 72.4 and 76.7 fps, respectively.

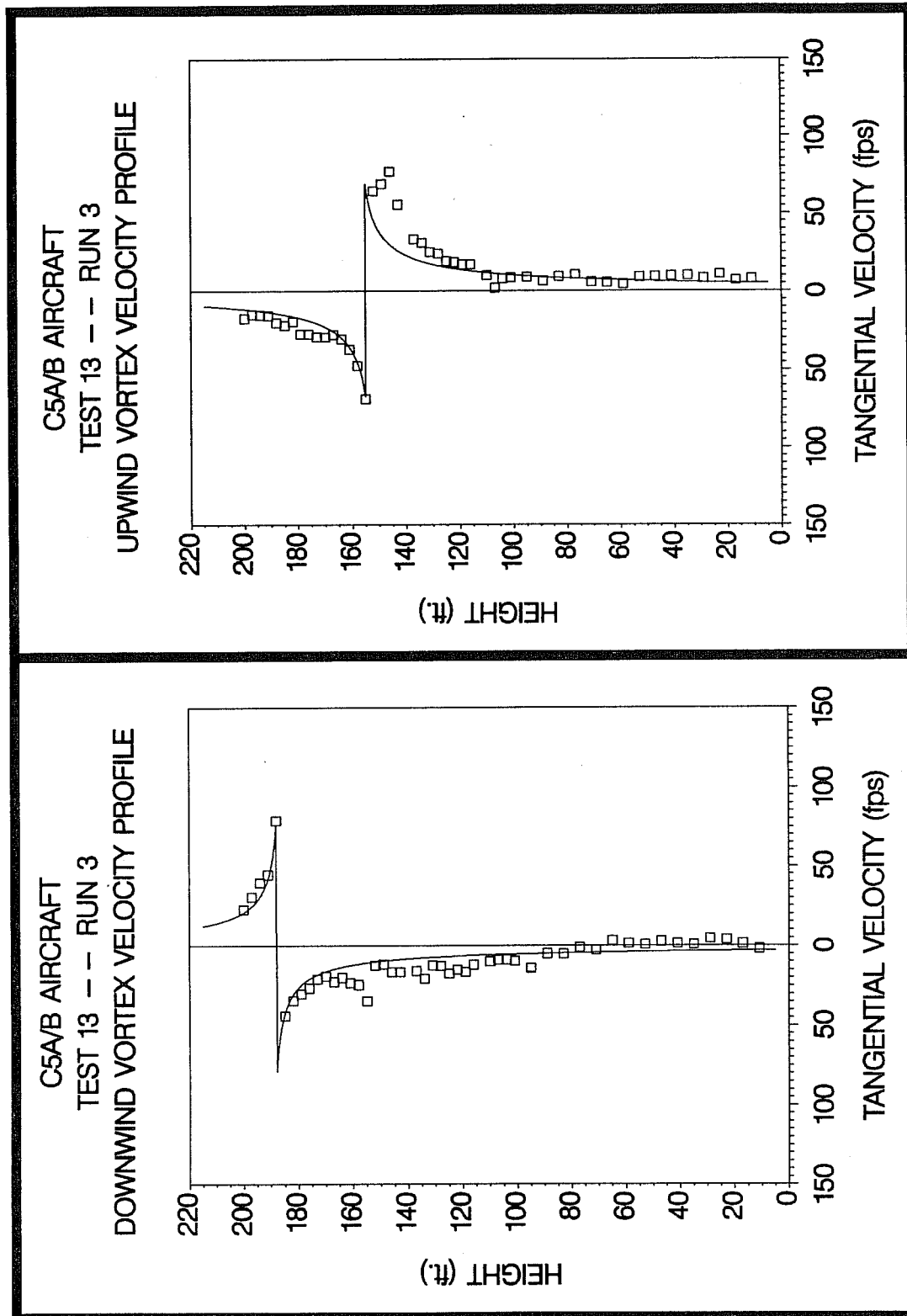


Figure C-151. C5A/B upwind (top) and downwind (bottom) vortex tangential velocity profile at maximum intensity from Test 13, Run 3, ambient wind speed=31.1 fps,  $\delta_F=100\%$ , IAS=150 knots, GW=689.0k lbs. Ages, radii, and velocities of the vortex cores are 12 and 8 sec., 2.6 and 1.4 ft., and 68.7 and 78.9 fps, respectively.

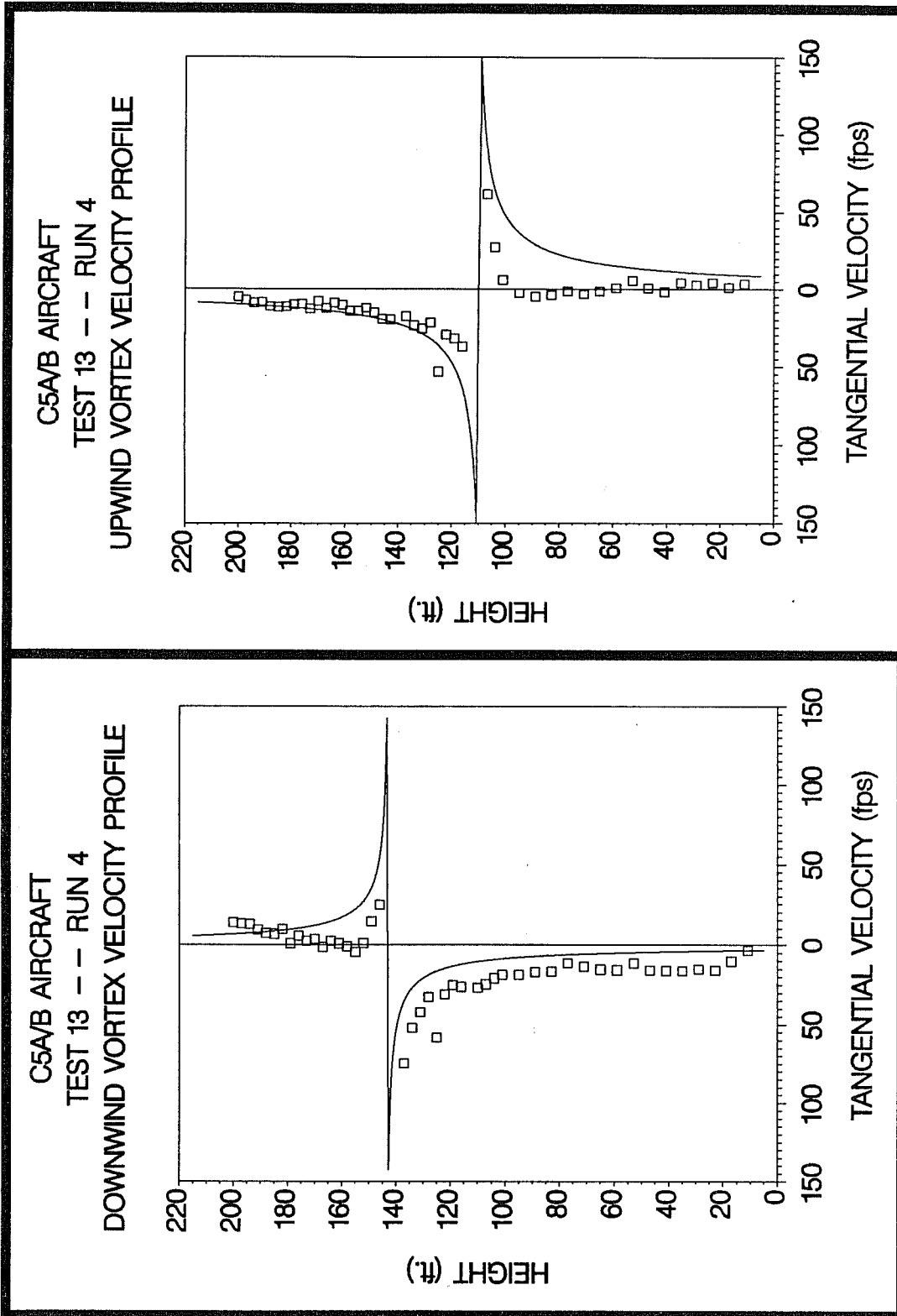


Figure C-152. C5A/B upwind (top) and downwind (bottom) vortex tangential velocity profile at maximum intensity from Test 13, Run 4, ambient wind speed=30.8 fps,  $\delta_F=15\%$ , IAS=180 knots, GW=686.0k lbs. Ages, radii, and velocities of the vortex cores are 15 and 8 sec., 1.0 and 0.4 ft., and 196.7 and 191.0 fps, respectively.

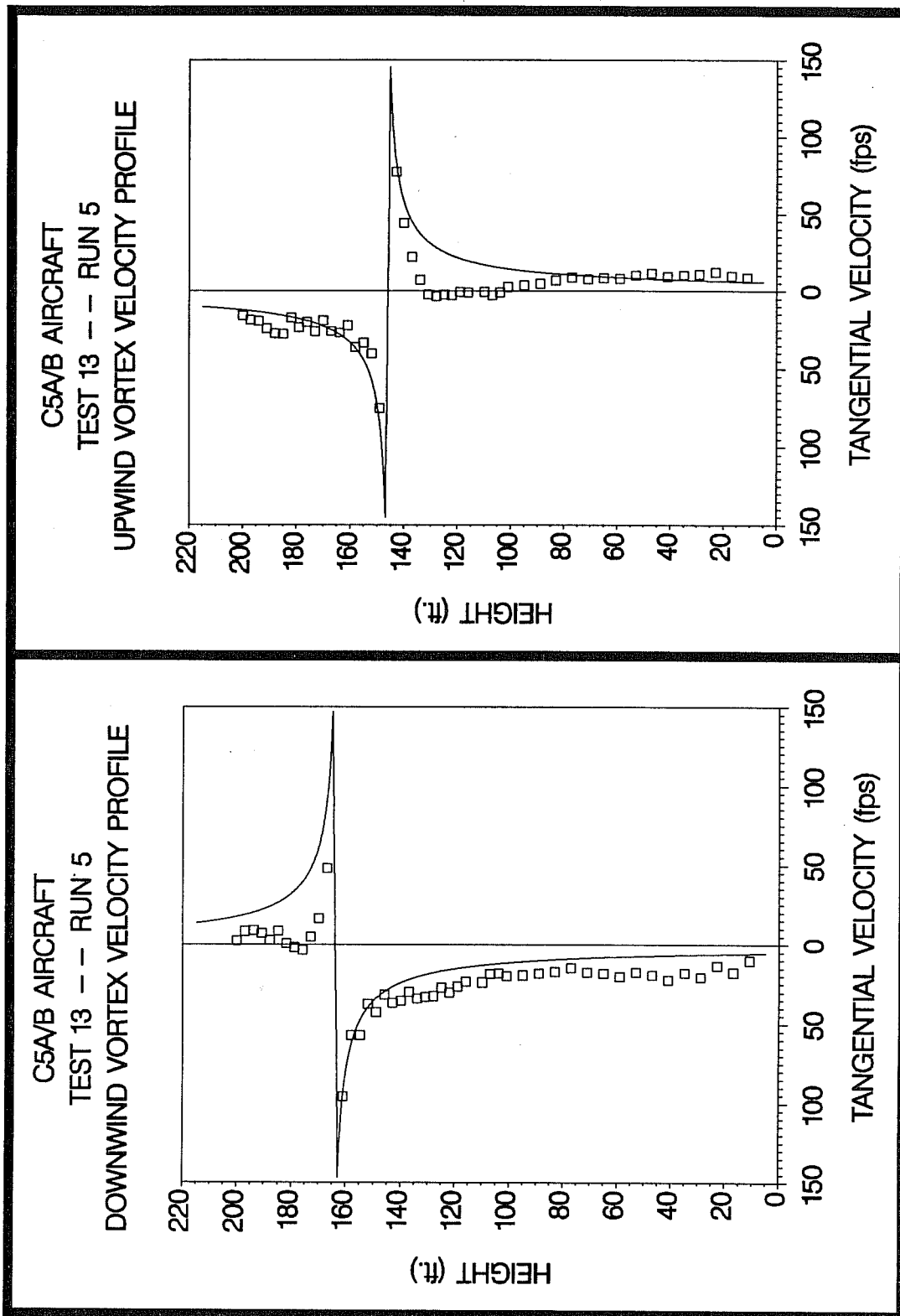
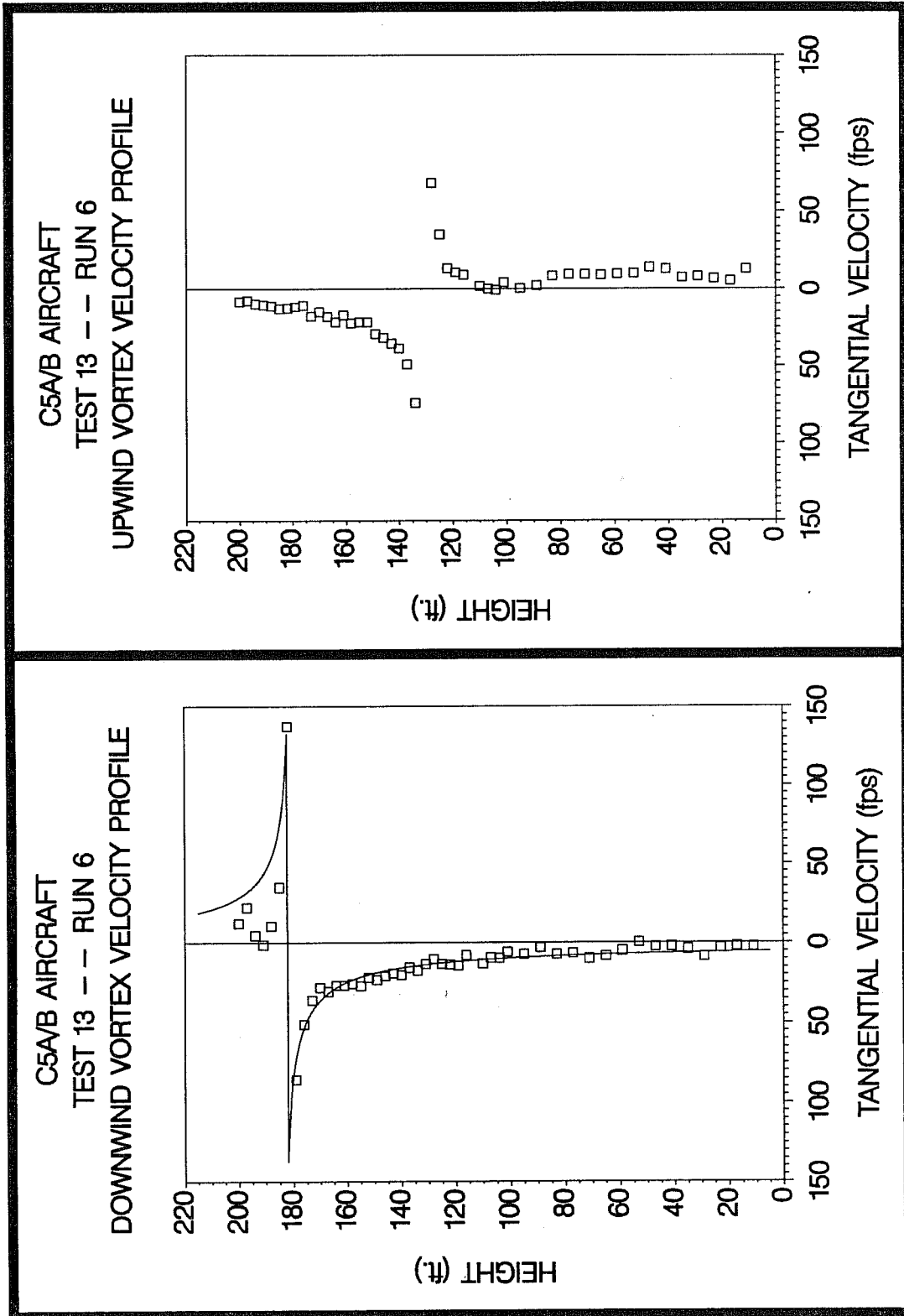


Figure C-153. C5A/B upwind (top) and downwind (bottom) vortex tangential velocity profile at maximum intensity from Test 13, Run 5, ambient wind speed=24.5 fps,  $\delta_F=15\%$ , IAS=180 knots, GW=682.0k lbs. Ages, radii, and velocities of the vortex cores are 14 and 7 sec., 0.7 and 0.6 ft., and 217.9 and 258.6 fps, respectively.



**Figure C-154.** C5A/B upwind (top) and downwind (bottom) vortex tangential velocity profile at maximum intensity from Test 13, Run 6, ambient wind speed=29.3 fps,  $\delta_F=15\%$ , IAS=180 knots, GW=678.0k lbs. Ages, radii, and velocities of the vortex cores are 14 and 10 sec., (N/A) and 1.4 ft., and 181.8 and 137.3 fps, respectively.

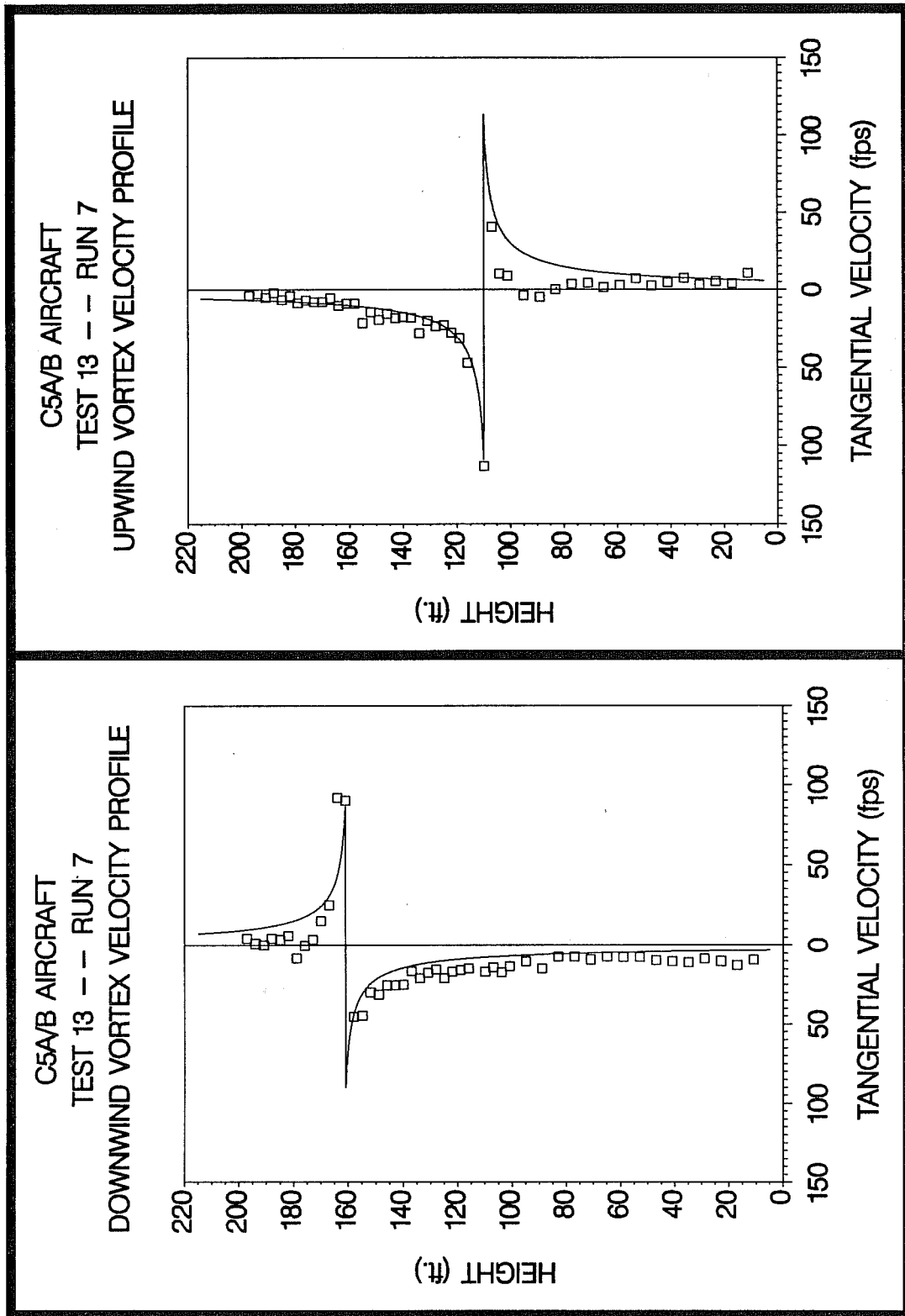


Figure C-155. C5A/B upwind (top) and downwind (bottom) vortex tangential velocity profile at maximum intensity from Test 13, Run 7, ambient wind speed=31.0 fps,  $\delta_F=15\%$ , IAS=185 knots, GW=674.0k lbs. Ages, radii, and velocities of the vortex cores are 15 and 9 sec., 1.2 and 1.1 ft., and 113.3 and 90.1 fps, respectively.

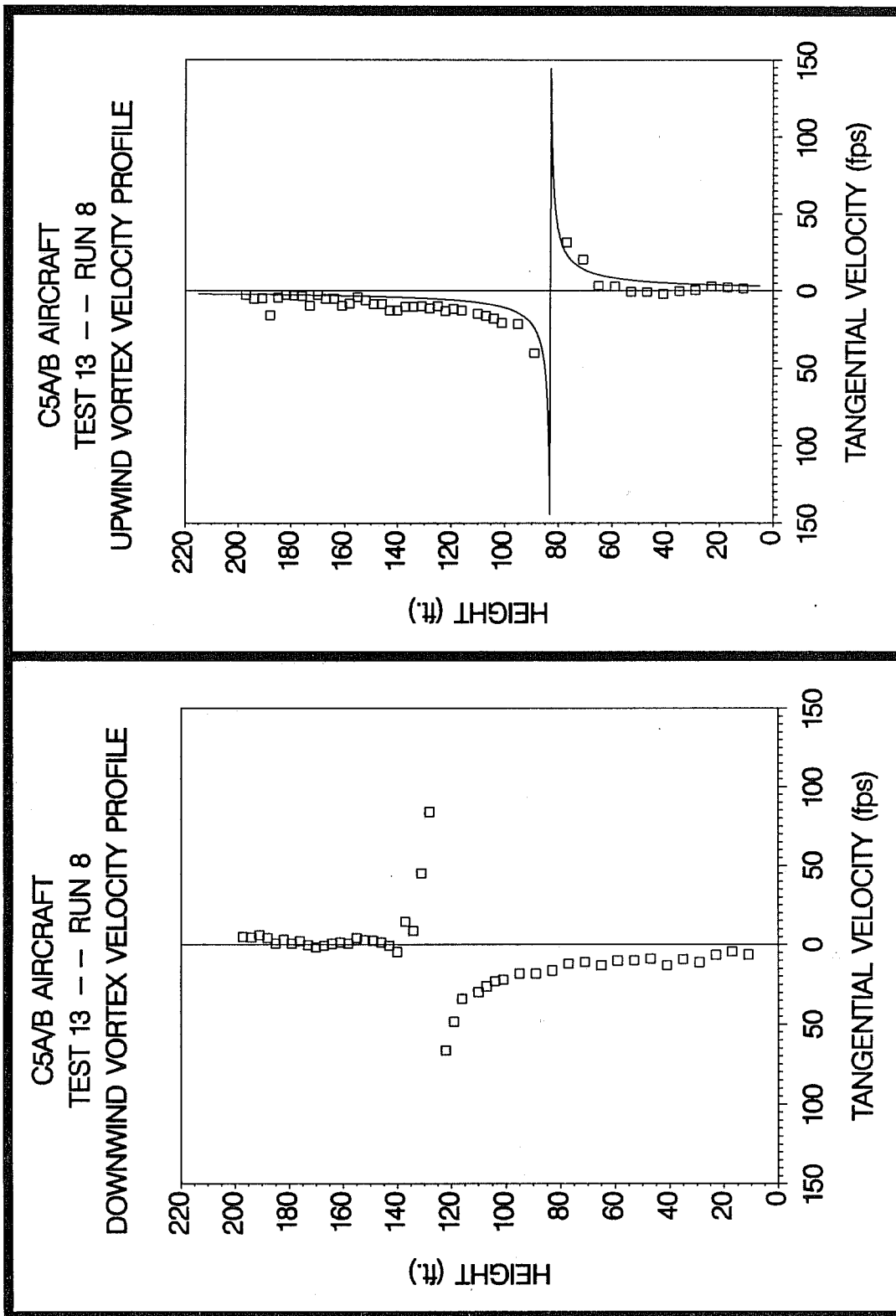
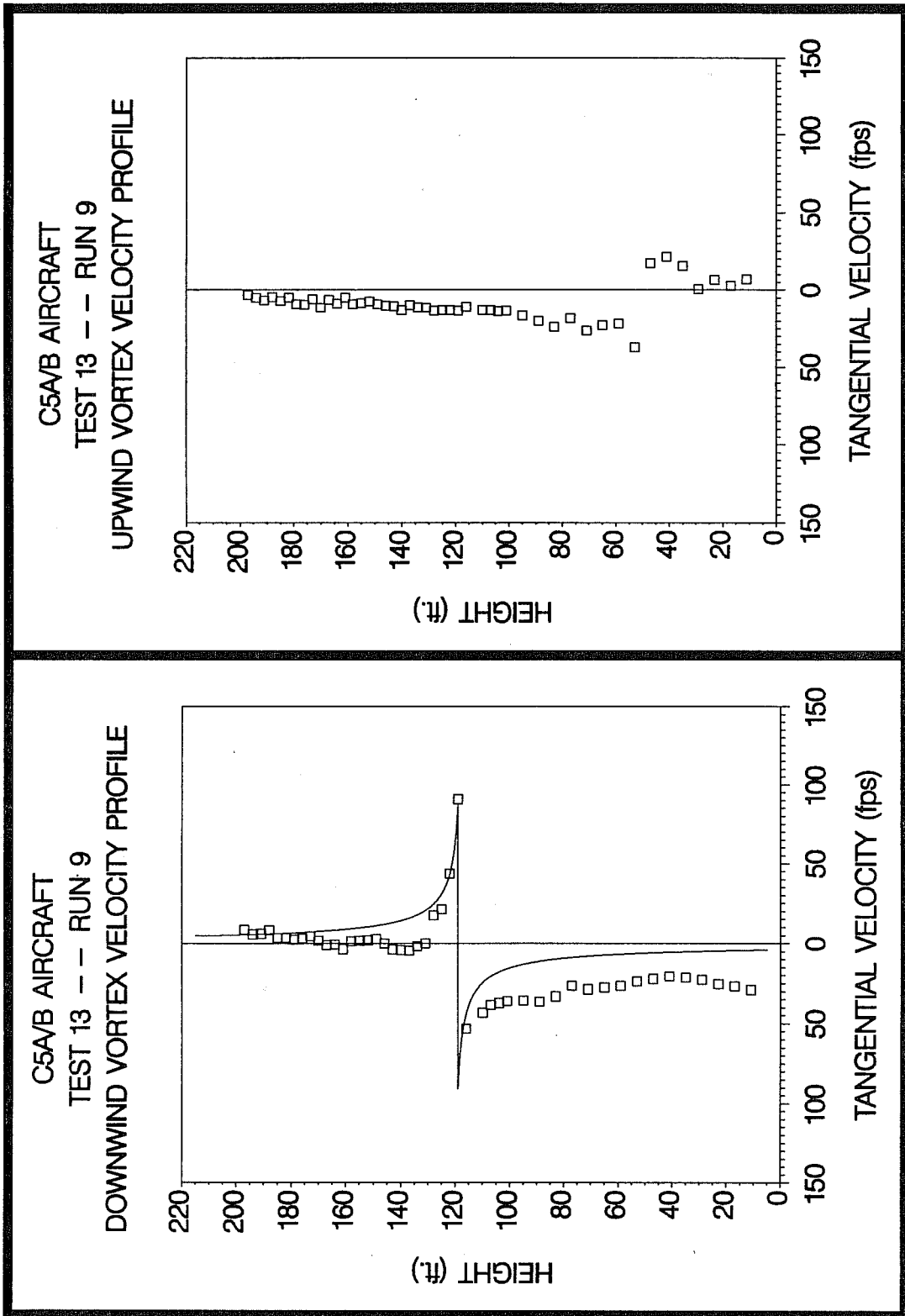


Figure C-156. C5A/B upwind (top) and downwind (bottom) vortex tangential velocity profile at maximum intensity from Test 13, Run 8, ambient wind speed=24.7 fps,  $\delta_F=15\%$ , IAS=175 knots, GW=670.0k lbs. Ages, radii, and velocities of the vortex cores are 23 and 13 sec., 0.2 and (N/A) ft., and 208.3 and 267.7 fps, respectively.



**Figure C-157.** C5A/B upwind (top) and downwind (bottom) vortex tangential velocity profile at maximum intensity from Test 13, Run 9, ambient wind speed=24.5 fps,  $\delta_F=80\%$ , IAS=150 knots, GW=666.0k lbs. Ages, radii, and velocities of the vortex cores are 36 and 22 sec., (N/A) and 1.1 ft., and 37.2 and 90.8 fps, respectively.

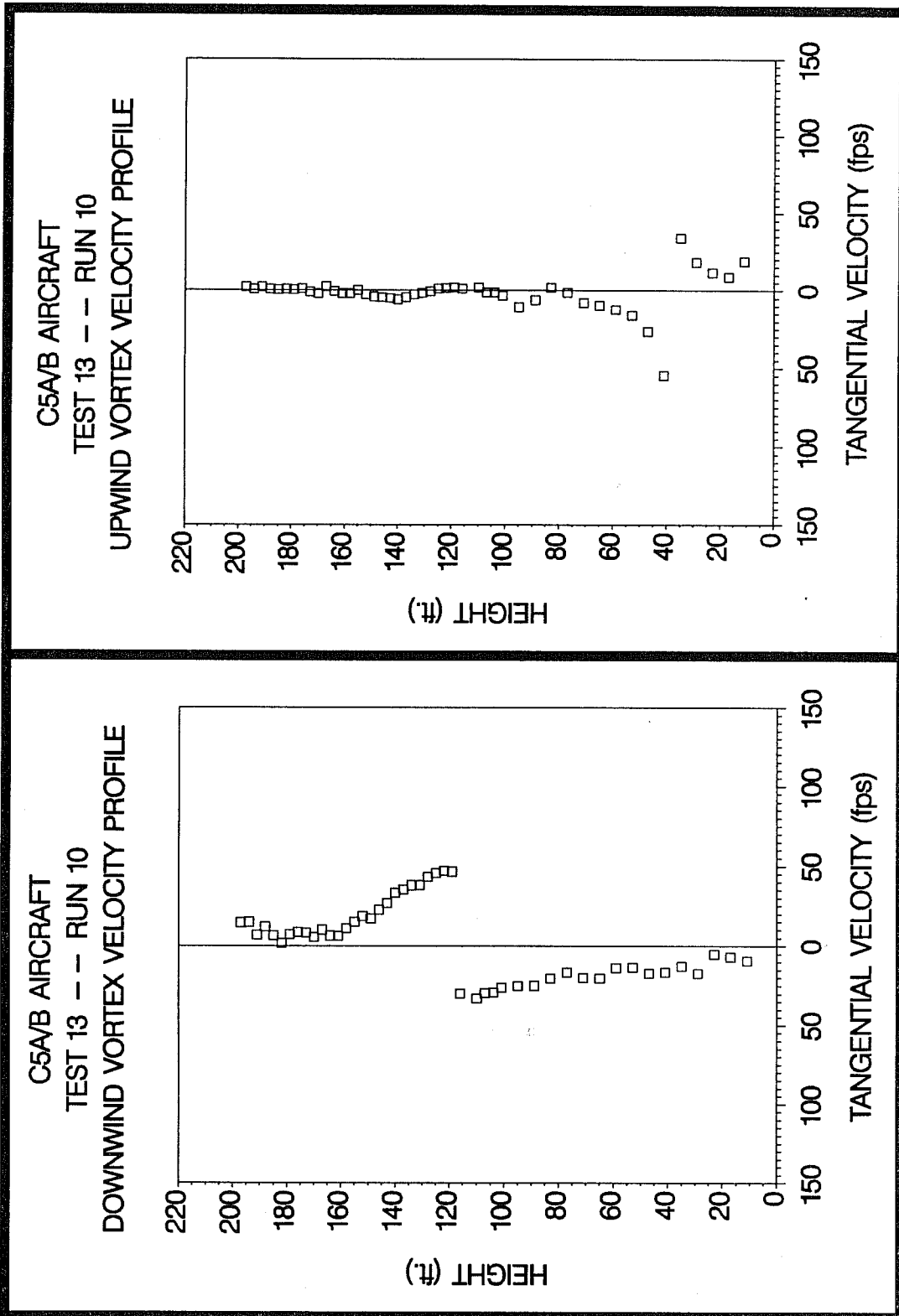
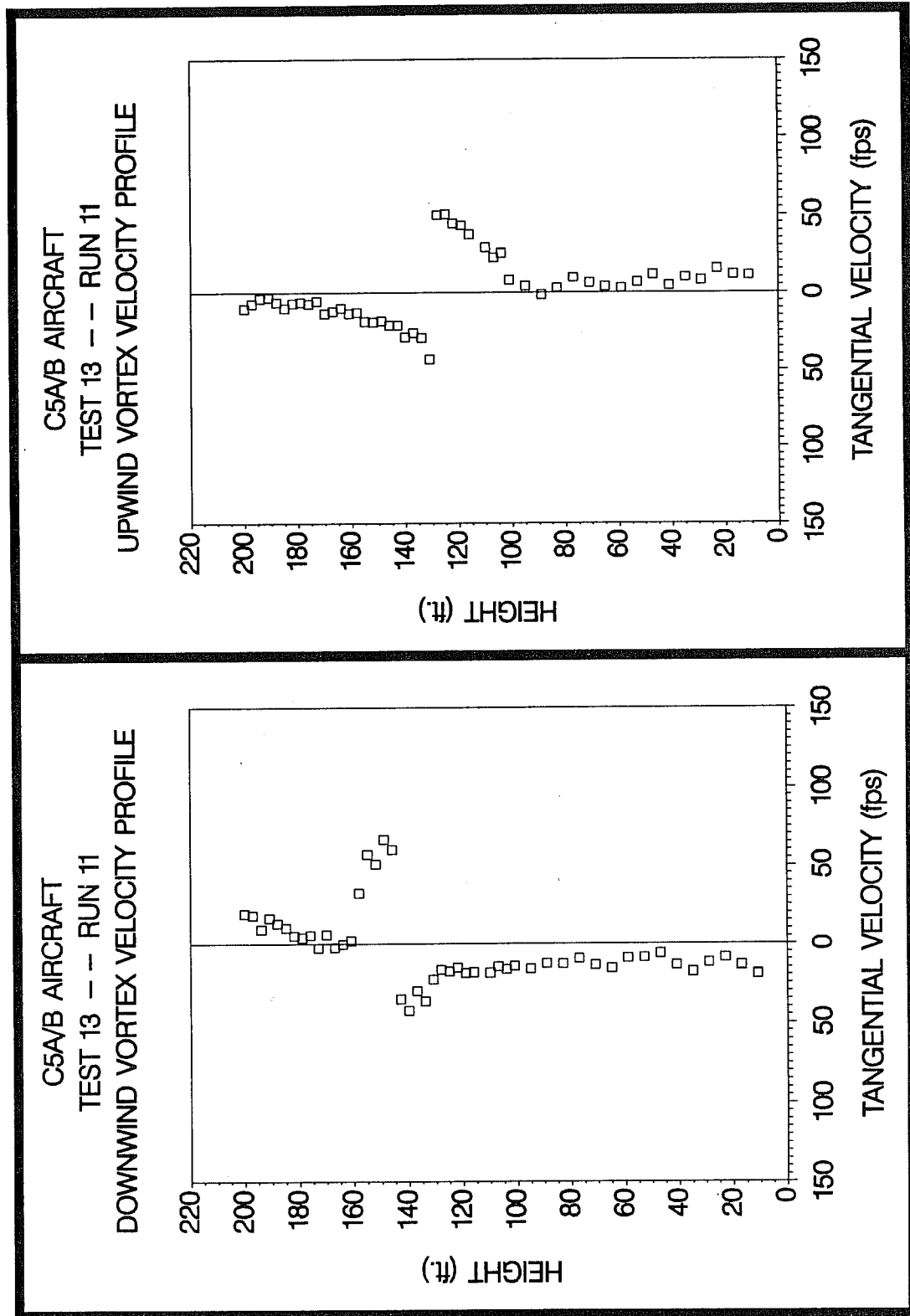
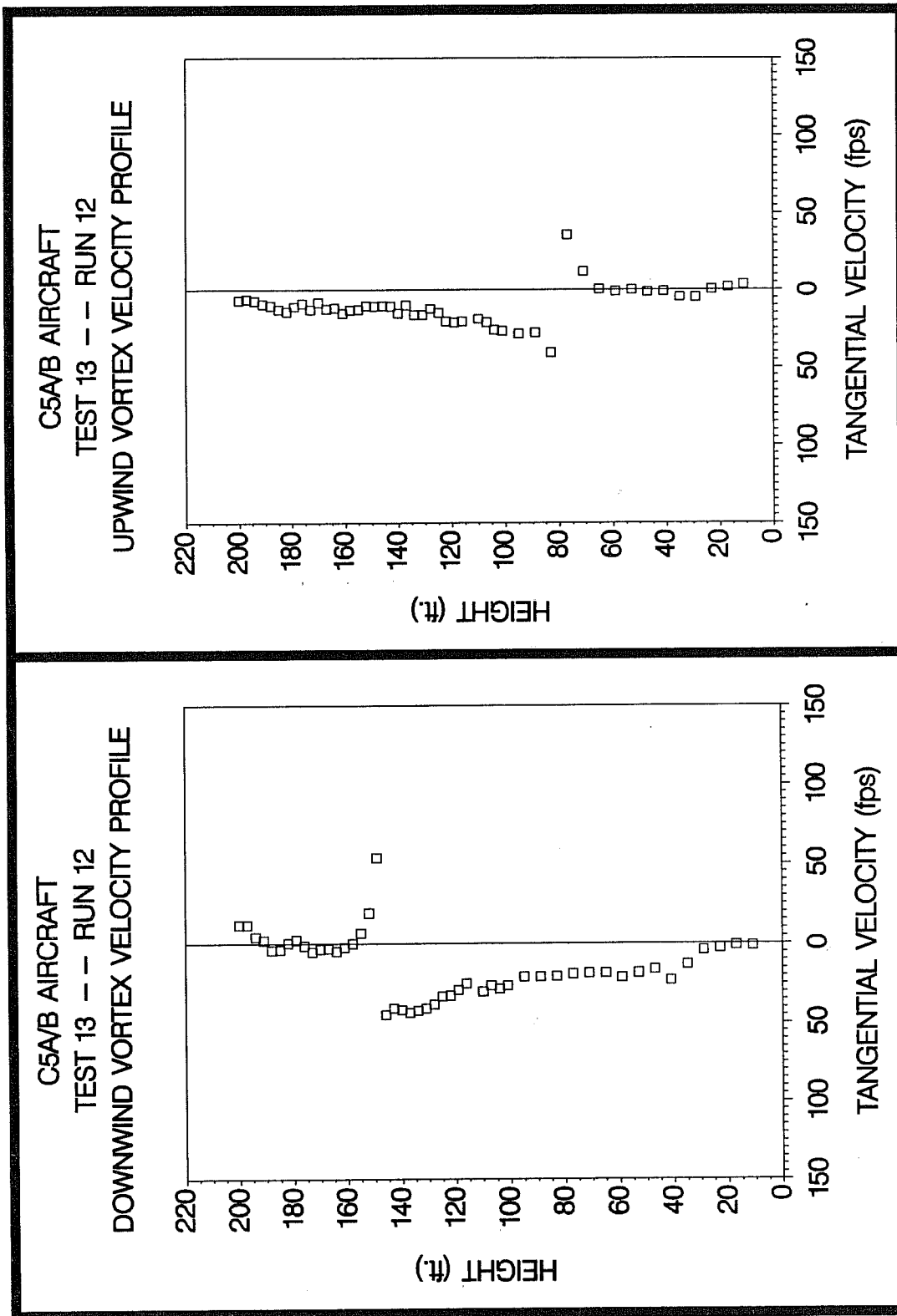


Figure C-158. C5A/B upwind (top) and downwind (bottom) vortex tangential velocity profile at maximum intensity from Test 13, Run 10, ambient wind speed=28.7 fps,  $\delta_F=80\%$ , IAS=150 knots, GW=662.0k lbs. Ages, radii, and velocities of the vortex cores are 42 and 24 sec., (N/A) and (N/A) ft., and 54.6 and 46.6 fps, respectively.



**Figure C-159.** C5A/B upwind (top) and downwind (bottom) vortex tangential velocity profile at maximum intensity from Test 13, Run 11, ambient wind speed=29.2 fps,  $\delta_F=80\%$ , IAS=150 knots, GW=658.0k lbs. Ages, radii, and velocities of the vortex cores are 34 and 26 sec., (N/A) and (N/A) ft., and 43.1 and 60.1 fps, respectively.



**Figure C-160.** C5A/B upwind (top) and downwind (bottom) vortex tangential velocity profile at maximum intensity from Test 13, Run 12, ambient wind speed=30.5 fps,  $\delta_F=80\%$ , IAS=145 knots, GW=654.0k lbs. Ages, radii, and velocities of the vortex cores are 32 and 24 sec., (N/A) and (N/A) ft., and 40.7 and 53.6 fps, respectively.

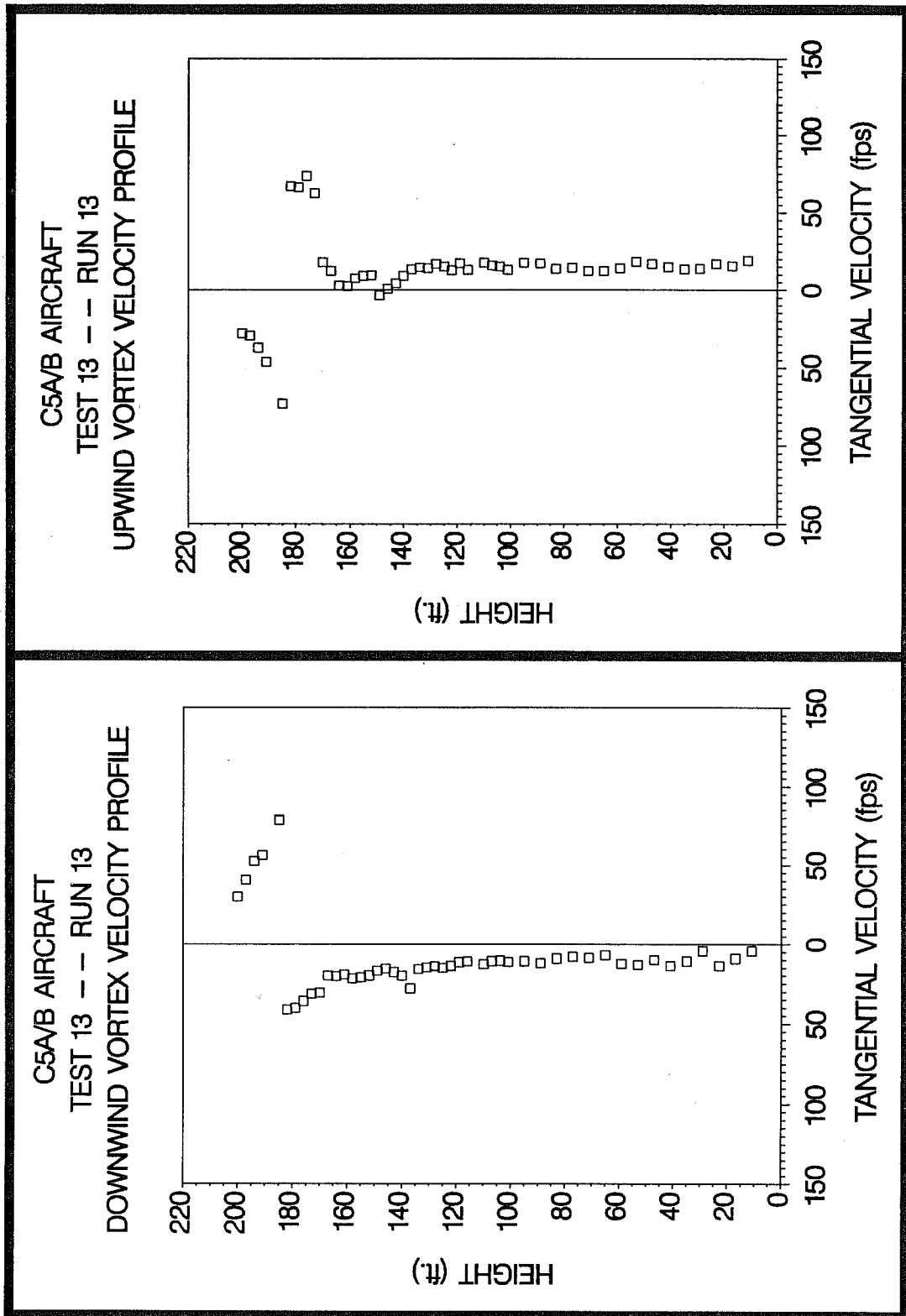


**Figure C-161.** C5A/B upwind (top) and downwind (bottom) vortex tangential velocity profile at maximum intensity from Test 13, Run 13, ambient wind speed=31.3 fps,  $\delta_F=80\%$ , IAS=150 knots, GW=648.0k lbs. Ages, radii, and velocities of the vortex cores are 27 and 22 sec., (N/A) and (N/A) ft., and 73.1 and 78.7 fps, respectively.

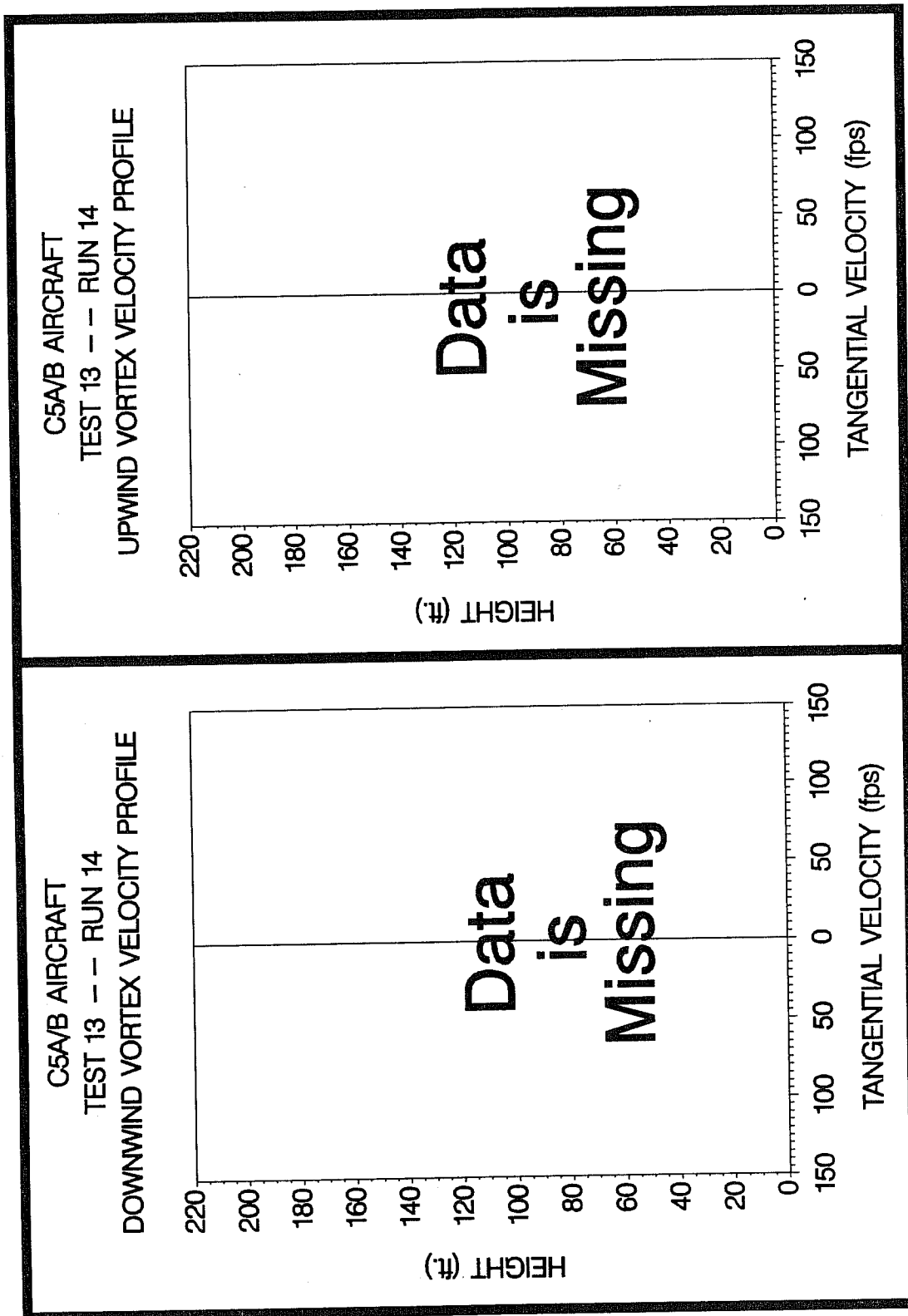


Figure C-162. C5A/B upwind (top) and downwind (bottom) vortex tangential velocity profile at maximum intensity from Test 13, Run 14, ambient wind speed=(N/A) fps,  $\delta_F=80\%$ , IAS=150 knots, GW=644.0k lbs. Ages, radii, and velocities of the vortex cores are (N/A) and (N/A) sec., (N/A) and (N/A) ft., and (N/A) and (N/A) fps, respectively.

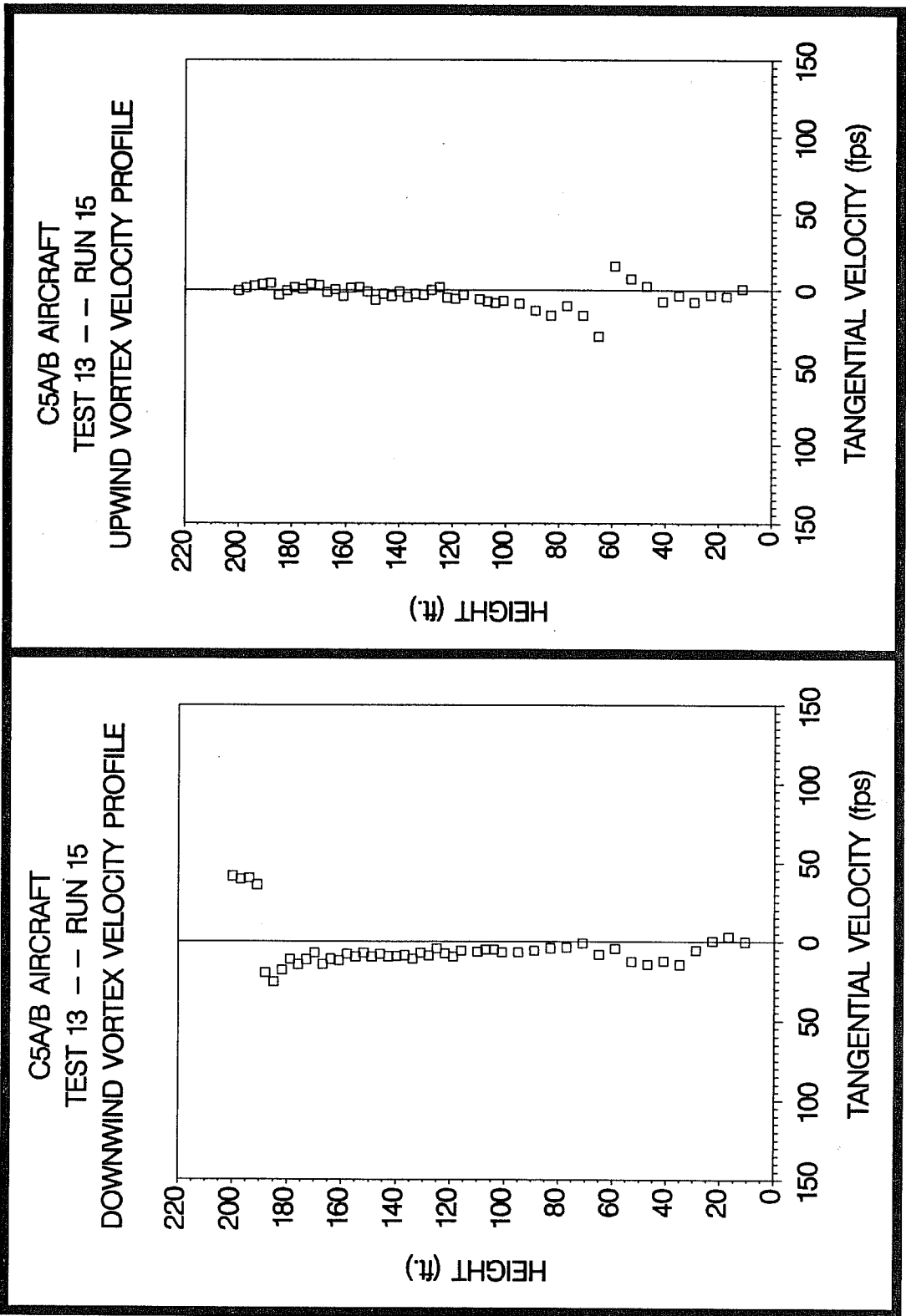


Figure C-163. C5A/B upwind (top) and downwind (bottom) vortex tangential velocity profile at maximum intensity from Test 13, Run 15, ambient wind speed=30.2 fps,  $\delta_F=80\%$ , IAS=160 knots, GW=640.0k lbs. Ages, radii, and velocities of the vortex cores are 60 and 45 sec., (N/A) and (N/A) ft., and 29.8 and 35.9 fps, respectively.

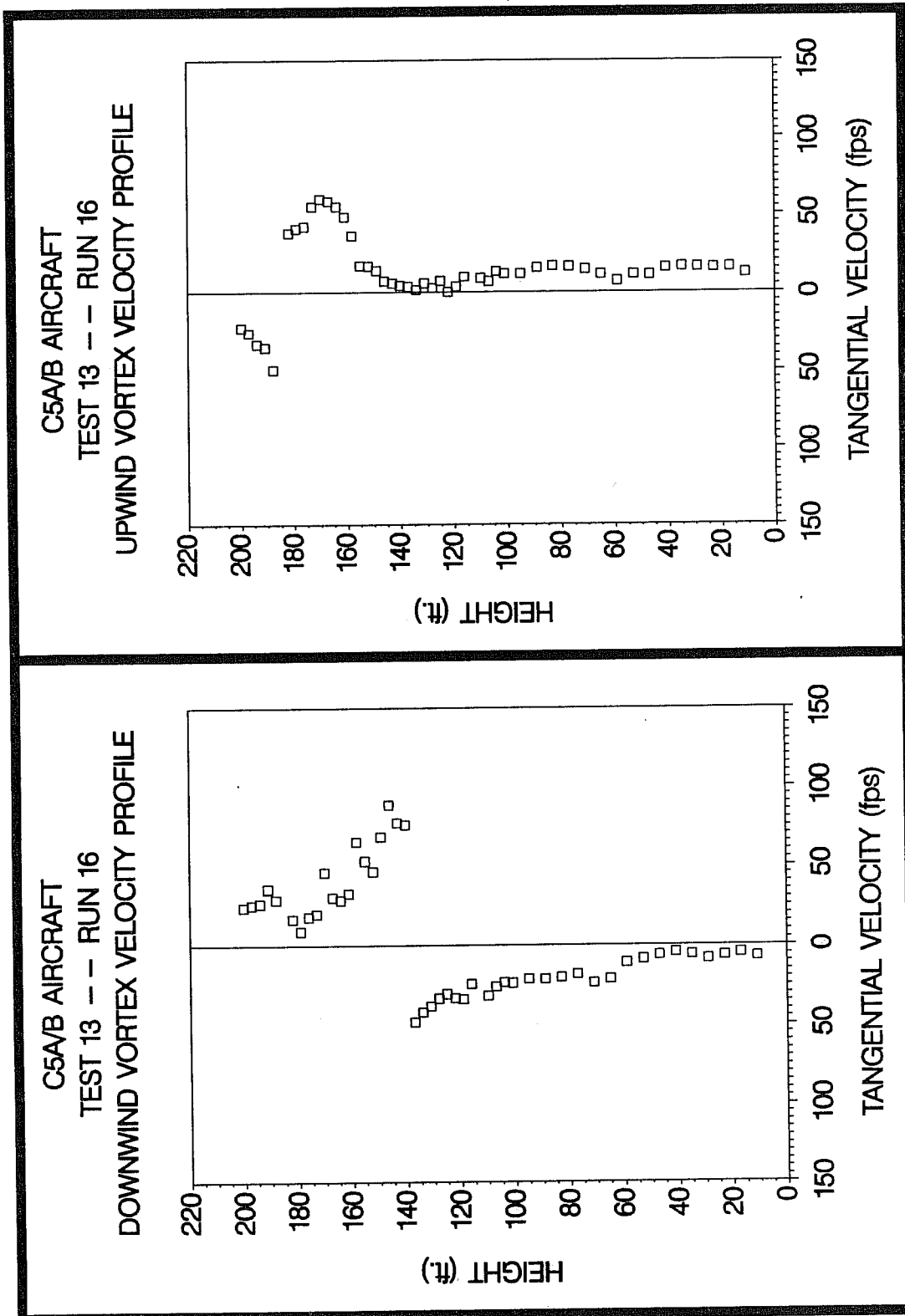


Figure C-164. C5A/B upwind (top) and downwind (bottom) vortex tangential velocity profile at maximum intensity from Test 13, Run 16, ambient wind speed=29.9 fps,  $\delta_F=80\%$ , IAS=160 knots, GW=(N/A)k lbs. Ages, radii, and velocities of the vortex cores are (N/A) and (N/A) sec., (N/A) and (N/A) ft., and 49.4 and 75.5 fps, respectively.